Mission-Oriented Seismic Research Program

Annual Report

2005

M-OSRP

University of Houston

Sponsors and Advisory Board representatives

Tier I

Amerada Hess ..... Jacques Leveille
Anadarko ..... John Logel
BHP ..... Mike Richardson
BP ..... Uwe Albertin
ChevronTexaco ..... Debbie Bones, Joseph Higginbotham
ConocoPhillips ..... Douglas Foster, Robert Stolt
Devon Energy ..... Kenneth Beeney
ENI-Agip ..... Michele Buia
ExxonMobil ..... Peter Traynin
Geotrace Technologies ..... Jaime Stein
GX Technology ..... Nick Bernitsas
IBM ..... Tom McClure
Petrobras ..... Ricardo Rosa Fernandes
PGS ..... Ruben Martinez
Shell ..... Jonathan Sheiman
Statoil ..... Lasse Amundsen
WesternGeco ..... Luis Canales

Tier II

Panorama Technologies ..... Bee Bednar
Stochastic Systems ..... Suresh Thadani

M-OSRP Personnel

Faculty

Lasse Amundsen (Statoil) ..... Adjunct Professor (Physics)
Douglas J. Foster (ConocoPhillips) ..... Adjunct Professor (Physics)
Kristopher A. Innanen ..... Assistant Professor (Physics)*
Robert G. Keys (ExxonMobil) ..... Adjunct Professor (Physics)
Jacques Leveille (Amerada Hess) ..... Adjunct Professor (Physics)
Ken H. Matson (BP) ..... Adjunct Associate Professor (Physics)
Bogdan Nita (Montclair State University) ..... Adjunct Assistant Professor (Physics)
Jon Sheiman (Shell) ..... Adjunct Professor (Physics)
Robert H. Stolt ..... Adjunct Professor (Physics)
T. Hing Tan (Shell) ..... Adjunct Professor (Physics)
Arthur B. Weglein ..... Cullen Distinguished Professor (Physics)
Daniel Whitmore (ConocoPhillips) ..... Adjunct Professor (Physics)

*Postdoctoral Fellow, University of British Columbia, Until Sept. 2005

Ph.D. Students

Walter Kessinger ..... Geosciences
Fang Liu ..... Physics
Einar Otnes ..... Petroleum Engineering and Applied Geophysics*
Adriana Citlali Ramírez ..... Physics
Haiyan Zhang ..... Physics
Jingfeng Zhang ..... Physics
Shansong Jiang ..... Physics
Jose Eduardo Lira ..... Geosciences†

Recent Alumni

Zhiqiang Guo ..... Geosciences
Francisco Miranda ..... Physics
Simon A. Shaw ..... Geosciences

Administrative Support

Jennifer Chin-Davis ..... Business Administrator
Nguyen Tran ..... Program Accountant
Jessica Maldonado ..... Program Coordinator
Joseph Ghobrial, Andrew Fritz, Jimy Chang ..... Computer/IT Support
Alex Garbino ..... Webmaster

*Norwegian University of Science and Technology, Statoil Fellow 2004-2005
†Petrobras, Brazil

Table of Contents

Introduction and Overview: MOSRP05

Introduction: defining and responding to pressing seismic challenges

In my view, a research program that addresses the most significant and pressing seismic challenges requires: (1) starting with a forthright, clear and candid view of the source of those challenges; (2) recognizing when and why current leading-edge seismic capability can fail; (3) identifying the actual prioritized limitations/impediments; and, what are secondary issues; and (4) determining the conceptual and practical limitations that caused other methods (that sought to respond to these same challenges to not reach their intended goals and objectives) and (5) be prepared to explain how your strategy recognizes and avoids the latter pitfalls.

A pressing challenge

Among the outstanding seismic exploration challenges faced by the petroleum industry is the inability to effectively remove multiples and image and invert seismic data for potential hydrocarbon targets at, and/or beneath, highly complex laterally and vertically heterogeneous, rapidly varying media and/or a rapidly varying and corrugated boundary.

Primaries and multiples: their different histories, status, and challenges

When addressing the complex, ill-defined, rapidly varying and inaccessible subsurface challenge, it is important for us to understand that the state of efficacy, and concomitant issues that need to be addressed today, are extremely different for removing multiples than for depth imaging and inverting primaries for target identification. Those differences arise from the very different historical starting points, subsequent record, and rate of progress in the evolution of seismic techniques for multiples and primaries. Primaries and multiples also involve very different degrees, ranges of issue, and distinct types of technical challenges, especially under complex conditions. As also expected, the priority and the form of the response to those challenges has been influenced by the history of petroleum industry trends and exploration and production focus and portfolios, and different types of plays.

In this Introduction to the M-OSRP 2005 Annual Report, we will overview our program, and its goals, technical strategy, and projects; and their progress, status and plans, and describe how our program and this report relates to each of these five (5) issues in the first paragraph. In addition, we describe how our projects, objectives and deliverables reflect and respond to those different types of challenges faced by processing multiples and primaries in seismic exploration. We provide, within the Report, the schedule of documented code delivery for both M-OSRP use and distribution to sponsors.

The inconsistent processing of primaries and multiples: circa 1980

The removal of multiples has a long seismic history. 25-30 years ago the work-horse standard methods were dominated in practice by algorithms based on: (1) a 1D earth model and statistical assumptions concerning primaries and multiples; or (2) a 1D earth model and velocity determination/estimation and discrimination filters. In that same time period, the imaging of primaries was being treated as a wave-field process, from multi-D reflectors beneath a multi-D subsurface, requiring an accurate multi-D velocity to achieve an accurate image. In contrast, methods using primaries for parameter estimation (e.g., AVO) and target identification from amplitude analysis assumed a homogeneous or 1D overburden and a single horizontal reflector model.

Before 1980, there was a clean and clear separation of interests and responsibilities: multiples were largely considered the domain and responsibility of those with an EE signal processing orientation, imaging primaries were for people comfortable with the wave equation, and amplitude analysis required: (1) knowledge of a linear approximate angle dependent reflection coefficient, (2) a strong aversion to multi-D wave theory, (3) and some familiarity with rock physics results. The fact that these three stages of processing, multiples, imaging, and amplitude analysis, were internally completely inconsistent and contradictory viewpoints within a single processing chain, gave little pause or concern.

Why multiple removal advanced first and fastest

The industry trend to deep water – even a horizontal deep water bottom, and a 1D subsurface – produced an immediate shut down in the statistics based demultiple methods. That multiple removal breakdown was exacerbated with any deviation from 1D, e.g., in the presence of a single dip in the water bottom. Hence, the industry trend to deep water brought a rejuvenated interest in new and more effective methods for removing multiples, first in deep water and then in 2D, 3D and complex difficult to define velocity models and subsurface conditions. With the development of the inverse scattering free surface removal and internal multiple attenuation methods in the early and mid 1990s the industry was first introduced to a new and inclusive de-multiple capability accommodating any depth of water (including deep water), and an arbitrarily complex and completely unknown subsurface. No velocity, no model type, no mapping of reflectors, no interpretive intervention.

Meanwhile, the basic conceptual state and vision behind the industry capability for imaging and inverting primaries today remains essentially what it was 25-30 years ago. There remains, in all current spatially accurate imaging methods, the requirement for a detailed and accurate velocity map to achieve that objective. The difficulty in satisfying that requirement and other challenges to current effective imaging will be described in a later section of this overview. Hence, in the past 25-30 years, multiples were 1D and needed a 1D velocity model, and primaries were multi-D and needed a multi-D velocity model. Today, multiples are multi-D and do not require a velocity and primaries remain with the model of 25-30 years past. Processing multiples have moved from behind to ahead of primaries in concept and capability.

For primaries, issues related to computational, turn around time, and limited data acquisition challenges have received the most attention, and those issues are critically important and certainly warrant attention. But progressing those issues alone will not result in an effective response. A

combination of a new imaging vision and capability, combined with a matching compute vision and progress in acquisition fidelity and availability, will be required.

25 years ago multiple removal lagged behind imaging primaries, now that is reversed – and it is time to close the gap

Given an appropriately recorded measured surface data, and an estimate of the source signature in water, and effective deghosting, there are field data tested inverse scattering methods for removing free surface multiples and attenuating internal multiples, available within our program, that can accommodate the most complex subsurface conditions, without any subsurface information, whatsoever. In contrast, given adequate and complete surface seismic measurements, and an estimate of the source signature in water, and an effective deghosting algorithm, there is no currently available and field data tested imaging and inversion algorithm that can reliably locate, delineate and defog the subsalt image. Our purpose is to close that gap, and to bring to the processing of primaries the same level of capability that has been earlier provided for multiples.

Developing new concepts and algorithms for not only attenuating (or reducing) but for eliminating or removing internal multiples, depth imaging and inverting primaries under complex circumstances and large target earth property changes are the programs central objectives. Advancing and satisfying the necessary data acquisition and/or reconstruction requirements, and source signature, and deghosting steps are essential prerequisities for this campaign to succeed. The individual contributions in this report address and progress these issues.

The first term of the inverse scattering series, consistent processing of primaries for depth imaging and AVO: 1981–1985

Inverse scattering, the inverse scattering series, and the inverse Born approximation were all first introduced and adapted to seismic exploration, starting about 25 years ago, to provide first and foremost a multidimensional direct inverse methodology. It was initially viewed as providing a first framework to progress, generalize and eventually extend and then merge two separate and previously disconnected lineages in the seismic processing of primaries: (1) imaging and (2) amplitude analysis. The concept of migration-inversion (M-I), or a generalized form of migration before inversion, derives from the first linear term in the inverse scattering series. If your method is restricted/confined to using only that single linear term; and, hence, accepting the inverse Born Approximation, you are assuming: (1) no multiples, (2) that an adequate velocity can be determined and (3) that changes in earth material properties are small enough to satisfy a linear relationship to a reflection coefficient. In contrast, if you use the entire Inverse-Scattering Series then none of those three limiting assumptions are present: (1) the input data are primaries and multiples, (2) no adequate velocity model is required as input or determined, and (3) no linear approximate relationship between reflection data and earth property changes is assumed.

That single term linear concept emerged and was developed in the early and mid 1980s, by (among others), Raz, Bleistein and Cohen, Clayton and Stolt, Stolt and Weglein, Coen, Gray, Foster, Hagin, Burridge, Beylkin, Coates, Anderson, Boyse, Keys, Tarantola, Beydoun, Cao, Ikelle, Keho, R. S. Wu, L. Huang, Miller, Oristaglio, Devaney, and Chapman and recently to 3D by S. Fomel. Those authors contributed concepts and methods that produced maps of spatial distributions of imaged

reflectors with an angle dependent point function providing a local angle dependent reflection coefficient with respect to the normal of a reflector. That output, in turn, provided the input for typically linear parameter estimation through a dip-recognizing and generalized AVO analysis - and that two step Migration-Inversion became understood as the required sequence consisting of, "where before what". Migration-Inversion shares with all migration methods the need for an accurate overburden velocity model. Using that single term linear approximate expression (also called the inverse Born approximation) we can derive: (1) Migration-Inversion, (2) Migration, (3) AVO, and (4) NMO-Stack. The demand for overburden information is higher in M-I than for migration since the image is no longer the end product but is now the input to subsequent amplitude analysis, to be literally and quantitatively interpreted as a reflection coefficient at depth, for subsequent linear or non-linear AVO. The two step migration followed by inversion had the advantage of producing a composite of parameter changes through the overburden before deciding on the model specific detail of the reflection process.

Given that overburden knowledge assumption, the above cited methods allowed, for the first time, a consistent multi-dimensional framework for reflector location and parameter estimation, automatically arranging for the amplitude analysis to be carried out with respect to the normal of the imaged reflector. We remind ourselves of that history both for the record; and, more importantly for the relevance and lessons gleaned for our research program and immediate upcoming plans.

As we know and have already noted, the industry trend to deep water in the 1980s resulted in a set of previously used demultiple methods to immediately shut down, and that combined with: (1) increased cost in exploring and drilling in deep water, and an associated lower tolerance for dry holes; and (2) the increased need and interest in exploring for complex and inaccessible targets, all combined to drive the need for higher technical efficacy. Methods for removing multiples and processing primaries were more frequently bumping up hard against their assumptions. That confluence of technical and economic factors motivated and supported the need for fundamental new seismic concepts and capability.

The inverse scattering series: a comprehensive theory for processing multiples and primaries: 1990–present

Weglein, Boyse and Anderson published a paper in 1981 on the inverse scattering series for seismic inversion. It seemed like a "formalism" and a framework, at best, at that earlier time when prestack time migration was considered to be pushing the envelope. However by the late 1980s and faced with the new E&P trends and challenges, it was decided to take a new look at the inverse scattering series (as the only direct multi-D inverse method) to examine its potential beyond only using the first linear term for Migration-Inversion, and advancing the processing of primaries and its concomitant restrictive assumptions of no multiples and adequate background information and velocity. Perhaps the non-linear inverse series as a whole might not make those limiting and restrictive assumptions. However, we need to remind ourselves that the single objective of the inverse scattering series, shared by all classic inverse methods, is to input data and then directly output the medium property configuration of the portion of the earth's subsurface under investigation.

The conditions that would allow for the convergence of the entire inverse scattering series in its pristine form turned out to be a complex issue, involving a numerical testing for the determination of convergence for the complete inverse series. The issue concerning the convergence of the entire

inverse series was first examined and tested by P. Carvalho and reported in his thesis (1992). For a one dimensional acoustic medium the entire series could input data with primaries and multiples and directly output the exact subsurface as a function of depth. However, those tests concluded that the contrast between actual and reference properties had to be less than about 11% to permit convergence. Hence, although the formalism of constructing terms in the series didn't require a velocity model, convergence of the series placed conditions on how far the unknown velocity could be from the reference. That disallowed the claim that the entire inverse scattering series did not require a velocity model for convergence, since convergence required a proximal velocity, and the ability to provide that level of velocity estimate was not easy in practice, and was at that earlier time (1990) often impeded by persistant and troublesome multiples. However, it is important to note that within its interval of convergence it was able to input all measured primary and multiply reflected data at once, and directly output the subsurface configuration without requiring any input velocity information, whatsoever.

As with all inverse methods that determine from seismic recorded data directly, and in one step, earth material property changes, there are issues of model type choice sensitivity and bandwidth that are experienced by the inverse scattering series when viewed in that single, one step, "all or nothing at all" mode.

There is a difference between the conditions for an overall series to be convergent and when terms in a series are useful, or when a subseries has more favorable characteristics. The harmonic series $1+1/2+1/3+1/4+1/5+\ldots$, is divergent, but the geometric series $1+1/2+1/4+1/8+\ldots=2$, is a subseries of the harmonic that is convergent. The WKBJ method is a useful result that derives from the first term of a divergent series. In contra-distinction there are convergent series where no finite number of terms produce useful results. Overall convergence of a series and the extraction of useful information from a series are two very different and distinct issues.

Inverse scattering isolated task specific subseries: navigating and negotiating the classic inversion impediments and producing a sequence of practical algorithms

The vision of: (1) a sequence of isolated task specific subseries, (2) model type independent subseries, and (3) purposeful perturbation ideas, were all new concepts brought to the inverse scattering series. This was an essential part of a strategy determined to seek to extract useful practical algorithms that would: (1) recognize and exploit all of the unique multi-dimensional direct inverse potential of the inverse scattering series, while (2) navigating, negotiating and addressing convergence, model type and bandwidth issues. The inability of earlier methods to effectively address the latter issues had derailed those initiatives. Recognizing the real problems, and designing a technical strategy to address those challenges that also acknowledges why earlier methods failed, has been the guiding philosophy in our history; and remains the driving force behind our program and plan.

Did the inverse scattering series have a set of sub-activities and sub-interests contained within its overall purpose, or was it solely driven by only a single isolated interest and objective, the classic target identification goal shared by all inverse methods, with all input data and all terms relentlessly and directly being treated as signal and used for and supporting that one objective? The former sub-activities inference was an intuitive guess that is central to our strategy; and our expectation of the existence of that set of useful subtexts has been justified to-date.

The removal of free surface multiples were by themselves a challenging and high priority issue, and hence, it was decided that the inverse scattering series would be examined to see if that event removal was something it might be interested in accomplishing; and, if so, then could that activity be isolated from other interests the inverse series was simultaneously pursuing. The idea was, perhaps those isolated interests would allow more favorable convergence and less stringent data completeness requirements, such as bandwidth, and perhaps would even automatically accommodate with a single unchanged algorithm a broad set of earth models. Those supposed interests of the inverse series might include: (1) removing free surface multiples; (2) removing internal multiples; (3) imaging primaries in space; and (4) the estimation of earth material property changes across those imaged reflectors.

The location of those isolated interests or tasks within the inverse scattering series is not trivial. In particular, in separating the latter three from each other can be quite daunting. There are forward series analogs that give strong suggestions for the symmetric inverse tasks. Providing diagrammatic interpretations of terms for creating and processing primaries and multiples has always played a major role in our history and current activity and plan. Several papers in this report by Innanen, and Ramírez and Otnes address and provide different important forward series insights. There are numerous papers that discuss forward and inverse processes on acoustic media. The history and contributors to these developments were reviewed in the Inverse Problems Topical Review in 2003, and several subsequent papers.

Order of tasks, bandwidth, model-type and the purposeful perturbation property

The inverse series does not perform its 4 tasks (as above) in this order, or in isolation, but actually performs them all at the same time as well as it can given the means at its disposal in any given order of term in the inverse series. However, there are terms that seem to be performing these tasks in combination, and other terms (or portions of terms) that seem to operate as though that task was the one and only task that ever needed to be performed. The latter isolated task contributions form the isolated task specific subseries. Why these tasks and that specific order of tasks? There are several good reasons, both historical and practical in nature. Free surface demultiple was first because when it is a problem, as for instance with a hard water bottom, it is the dominant problem and can swamp all other problems, with an R^2 compared to the internal multiple R^3. However, in deep water, and subsalt plays and onshore projects, internal multiples can and do dominate and can cause havoc.

In the presence of free surface and internal multiples, free surface multiples need to come out first, to satisfy internal demultiple algorithm assumptions. Bandwidth requirements are a critical factor as is algorithmic simplicity in deciding the order of tasks. The order of tasks: (1) free surface multiple removal; (2) internal multiple attenuation; (3) depth imaging primaries; and (4) estimating earth property changes across imaged reflectors, represent in that order a progression of less to more demand on bandwidth, and in particular the low end of the spectrum. The fourth task, estimating earth property changes, is the traditional inverse objective and its requirements are the most demanding. Solving these tasks in the indicated order reduces the difficulty and complexity of the next task isolated step, and the latter uses the previous accomplishment as a form of a-priori information to help keep its isolated focus. Accomplishing task 3, spatial reflector location, prior to task 4, parameter estimation, can allow the achievement of task 4, with extremely

bandlimited data, that is not achievable without task 3 preceding task 4. Another major hurdle besides bandwidth of single task inverse approaches that seek to directly go from data to identify earth material properties is the sensitivity to model type. The first two tasks involving multiple removal when accomplished with inverse scattering series methods are model type independent, and the third, spatial reflector location, appears able to be cast in a model type independent formalism, as well. Hence, three of the four tasks are less sensitive to missing bandwidth than parameter estimation, and furthermore accomplishing task three before task four mitigates that issue. Two of the tasks are model type independent, and the third is apparently, as well. Thus, not only are the isolated task specific inverse scattering subseries directly addressing the issues of processing in highly complex and inaccessible circumstances, without the need for subsurface information, they are, in addition, navigating and negotiating and mitigating the classic bandwidth and model type sensitivities. Another amazing benefit of the isolated task specific subseries methodology is its property of purposeful perturbation. The very first term in an isolated task specific subseries determines if the specific issue it is designed to address exists in your data, and it immediately determines whether its services are needed and shuts down before it even finishes computing the first term, if the data communicate that that problem is not in your data. For example, the internal multiple attenuator, the first term in an elimination series first determines if there are internal multiples, before proceeding to predicting and subtracting.

No purpose leads to no computation, and decides that quickly and produces the value zero before the very first term internal estimate completes its operation. Similarly for the imaging series, it first decides if there is an imaging problem, and before an integral is computed will send a message that your current velocity and imaging are in order, if that happens to be the case. And it only goes into action to correct a depth of a reflector after that determination is made for the need of its services. That theme is an isolated task specific series attribute–that a decision is first made if a task is needed, and that happens within and prior to the first linear step to address that task. That purposeful perturbation property is frankly an unanticipated and incredible property of the isolated task specific subseries concept and algorithms. Purposeful perturbation along with identifying the specific delivery of each term in the subseries adds incredible practical benefit, as well as mitigating issues of subseries convergence. When available, closed forms for an entire task specific subseries add tremendous additional practical impact, and allow the use of water speed reference, without concern for the cost and round-off errors incurred in computing large numbers of individual terms.

Perturbations change things from a reference value; purposeful perturbations decide if there is a need or purpose for that perturbation, and that decision is automatic within the linear perturbation step, before a first approximate perturbation is computed and takes place.

Inverse scattering series, iterative linear inverse, and global searching

The latter bandwidth and model type sensitivities and obstacles were among the factors contributing to the disappointment of the iterative linear and generalized inverse global full wave form “all at once” approach pursued by Tarantola and his colleagues and students in the 1980’s.

Inverse scattering series and DELPHI's feedback loop

The feedback loop methods developed by Berkhout, Verschuur and Delphi colleagues and students also represents a useful and worthwhile staged approach. However, the feedback method is not the inverse scattering series, nor does it correspond to the task specific subseries, for any one of the four tasks we listed above. The inverse scattering series can, in principle, not only attenuate but also remove internal multiples; and, not only image, but depth accurate image and invert primaries without knowing or determining the velocity model. That internal multiple removal and spatially accurate imaging is not achievable, in principle; and, hence, is precluded without the accurate velocity model in the Delphi feedback loop methodology. There are certain times when an internal multiple generator can be identified that the Delphi procedure provides an efficient and appropriate and effective choice. The Delphi group has also pioneered novel and worthwhile ways to use multiples for data extrapolation and enhanced imaging.

At this time the dominant view is the exclusive view that multiples are considered noise and primaries are signal; and, the use and inclusion of multiples is very much an embryonic and minority viewpoint. We would encourage keeping an open mind on the inclusive viewpoint, and there are certain achievements to-date. But the complexity of multiples and their propagation, make a general theory of imaging primaries and multiples even more demanding of a primary and multiple generating discontinuous overburden velocity model. Hence, that inclusive inmaging approach is pointed further in exactly the wrong direction for imaging beneath complex media, where we cannot find the primary velocity model and therefore a model for primaries and multiples is well beyond near term reach and determination.

In our strategy the inverse scattering series treats multiples unambiguously as coherent noise, to be removed before imaging primaries. Hence, when it comes to the most complex geology and difficult to interpret data, and interest in attenuating or removing maximum number and types of multiples, without any event picking, velocity or structural information or interpretive intervention–then the inverse scattering algorithms have since 1994, and remain today, the method of choice and without peer for efficacy and completeness. The internal multiple attenuation methods, are extended in this Report to internal multiple removal, since attenuation can sometimes be inadequate or insufficient, and hence a residual impediment in e.g., marine converted wave internal multiples, subsalt plays and onshore applications.

Superscripts, subscripts, and new concepts

Although we are focused on developing new practical methods that are effectively addressing pressing challenges on field data, much of our early embryonic research starts with simple 1-D acoustic models. The standard being applied here is that every new concept we pursue must be generalizable to the actual complex multi-D earth. And those steps from simple to added complexity are illustrated in this Report. However, if you cannot demonstrate how your new concept would work in a simple 1D acoustic world with perfect analytic data, then how do you expect it to be useful in the real world and field data. Take the simplest expression of the problem and test your concept. If the only way you can formulate your concept is with an obscure abstract notation and a blizzard of superscripts and subscripts, then, in my experience, it's probably not a new idea, but an old idea in a new fancy and obfuscating set of clothes. Different series methods have been advocated

(other than the inverse series, e.g. Bremmer series) with reported favorable convergence properties. However, that series requires detailed layer boundaries and velocities as input, and it is interesting, but largely irrelevant for the removal of multiples and imaging and inverting primaries under the pressing challenge represented by complex, ill-defined media.

Relevant rigor

The rigor we are most concerned about is the rigorous statement of the actual practical prioritized problem being addressed, and how the proposed method actually addresses outstanding issues, and has the potential to add value beyond current capability, and defining its place in the toolbox. New thinking rarely begins with rigorous math; you need a framework for rigor, and fundamentally new concepts and vision are by definition absent of a framework, and are most often intuitive in their embryonic early stages. Rigorous derivations of solutions to the wrong problems are interesting, but are, from our perspective, off target. Once you have developed new thinking, rigor then provides an understanding of the limits of algorithms and where further attention and progress will be needed. And further progress will always be needed. The relevant issue and objective is providing capability beyond current capability, not perfection, nor exact methods, nor completeness. The latter are not achievable, but increased effectiveness, and associated reduced risk and increased reliability are reachable and realizable goals.

Practical pre-requisites for the isolated task specific subseries

The M-OSRP program recognizes the theoretical and practical prerequisites and assumptions required for the non-linear series to reach their potential, and takes ownership and responsibility for new and effective methods, discussed and developed in this report, that will maximally accommodate and satisfy those requirements. Among those requirements are: (1) data collected, and/or effectively reconstructed by extrapolation and interpolation methods consistent with 2D or 3D wave theory seismic processing, (2) estimation of the source signature in water, and (3) source and receiver deghosting.

Inside and outside the model

Whereas, our overall and dominant view is that major strides are accomplished by increasing deterministic realistic accommodation, we recognize that all models (starting with our own) are just that: models. Completeness of any model in the sense of matching reality is not achievable, but progress and improved reliable prediction and reduced risk come from increased reality and movement towards completeness. To be effective we need to recognize that gap between model and reality, and typically that realm falls into the regime of statistics. Adaptive methods and subtraction techniques that seek an objective function with a property that can be constructive, are often needed, necessary and usefully applied. Those techniques are worthwhile progressing and the report by Sam Kaplan and Kris Innanen represents a new and important advance in that arena.

Compute vision: flexible optimal algorithms to accommodate different distributed compute architectures

Sam Kaplan, working with Kris Innanen, and Billy Robinson (IBM), has provided an excellent set of well-documented codes, both of his own individual contribution, (free surface and internal demultiple algorithms) and high-grading the deliverables of other M-OSRP contributors, such as Z. Guo (wavelet); J. Zhang (deghosting); and F. Liu (finite difference modelling). Sam's compute vision and deliverable allows adjustment of the codes to fit the strengths and weaknesses of a specific compute architecture, e.g., accommodating different memory per node and speed between node configurations. Their contribution is not only impacting our current code deliverables, through extremely creative and innovative optimally reconfigured algorithms for critical compute time turn-around efficiency; and, in adittion allowing codes to be adjusted for different machines, but are also providing an invaluable platform for ongoing, and future M-OSRP algorithm development and code delivery.

Migration and velocity

We have written several papers and a SEG reprint volume with Bill Dragoset about the problems and challenges with removing multiples; and, hence, thought it might be worthwhile to spend a few moments on the imaging problem.

Let's begin with the statement of the problem. All current imaging methods require an adequate velocity model to achieve an adequate depth image. Imaging methods include: Kirchhoff (Schneider), Gaussian beam (R. Hill), finite difference (Claerbout), F-K (Stolt), phase shift (Gazdag), post stack finite difference (Larner et al.), p-tau (Stoffa), reverse-time (Whitmore, McMechan, Kosloff, Levin), phase-screen (R.S. Wu, L. Huang), common image gather (Rocca, Biondi, Fomel, Sava, Symes), CFP (Berkhout, Verschuur, Alai), CRS (Gelchinsky, Hubral) and weighted sum CRS (Keydar, Landa). Many of these references can be found in the text by Stolt and Benson (1986) or in a recent historical review of migration by Bee Bednar (2005).

The depth imaging methods cited above can be re-arranged and represented as a spectrum of various degrees of depth imaging effectiveness and capability. As capability increases, and wave-theoretical completeness in depth imaging algorithms improves, there has been a concomitant greater need, dependence and sensitivity for an accurate detailed velocity model. For instance, post-stack time, pre-stack Kirchhoff, Gaussian beam, finite difference, and pre-stack reversed time migration, represent an evolution of both increased imaging capability and velocity demand. This increasing high bar of velocity model need for depth imaging beneath highly complex media can rarely (if ever) be directly satisfied in practice for the more advanced imaging techniques to reach their potential and promise. Hence, in current industry practice a procedure is used that indirectly seeks to determine the image that a correct, accurate and detailed velocity would directly produce. The indirect procedure seeks to satisfy a property, or invariance, (e.g., horizontal common image gather), or optimal offset trajectory stack, associated with the image with the correct velocity. These indirect property satisfaction approaches represent (at best) a necessary condition that a correct image would satisfy. They are not necessary *and* sufficient for determining the velocity model, and this distinction is especially significant under complex geologic circumstances. In addition, although simple in concept, satisfying those imaging invariance criteria is often no easy matter. Also, in

general, many velocities can satisfy the necessary invariance or other property and/or condition; and, that set of velocities includes both the correct and a plethora of incorrect velocity models. There is a sense that these indirect methods are too blunt an instrument for the subtleties faced in highly complex imaging problems. Also, these indirect approaches often have ray-theoretic rather than wave theoretic underpinnings.

For all of these reasons the above cited imaging procedures can and will produce useful or erroneous imaging results with the correct or erroneous velocity models, respectively. And both can arise from an indirect method that satisfies the necessary criteria for an image with the correct velocity. Separately, it is worthwhile mentioning that there are methods seeking to produce a focused "image" and not a more demanding "depth-accurate image"; and those lower ambition imaging methods (as you would reasonably expect) would be less demanding of velocity information. Never-the-less, and in summary: behind each of the cutting edge depth-imaging methods (cited above) there resides the explicit algorithmic assumption and requirement for an adequate velocity model to produce an accurate depth image.

For balance, it is important to mention that there is of course a large literature and innumerable instances where current velocity analysis and imaging methods provide effective and useful results. And those successes are of course deserving of our recognition, appreciation and gratitude. However, our purpose here is to define and respond to pressing seismic challenges. Thus, our necessary emphasis and focus is on the assumptions behind current capability: to understand why they can and do sometimes fail, and through a clear view of the challenges we face to have a chance to derive methods that either improve current methods, or totally avoid those limiting assumptions; and, hence, have a chance to succeed when current methods fail.

There are several factors that contribute to produce seismic imaging failure. One contributor is the inability to directly or indirectly determine an adequate velocity model under complex geologic circumstances. Even with the exact velocity model, all current leading-edge imaging methods can fail. One need not seek very complicated velocity models to exhibit the latter failure, e.g., a simple homogeneous 2D acoustic model, with a single isolated homogeneous closed region above the target will suffice. In fact given two homogeneous half spaces connected by a single complex corrugated and diffraction generating boundary can cause imaging problems with the constant velocity given in the upper half space. The dry hole drilling rate in subsalt, sub basalt and subkarsted plays, and the current trend away from the technical challenges in the deep water, to onshore plays, and other areas of the world with heightened geopolitical uncertainty replacing technical risk, all speak to that reality.

In Figure 1, the recorded reflection primary event, e, is the composite of its subsurface experiences between the source and the receiver, and can be described as a downward propagation, D, a reflection, R, and an upward propagation, U:

$$e = DRU. \tag{1}$$

When the down-going wave, D, passes through the complex highly rugous top and base salt it has a complex effect on the character of the wave. Similarly for the upgoing wave, U, traveling upward from the reflector through the salt to the receiver. Therefore, the recorded event, e, has a complex character due to the complex downward and upward alterations the wave experiences in passing through four complex salt boundaries.

What's the problem? The problem is our inability to adequately – directly or indirectly – model and remove that complex salt boundary interaction and transmission influence from the recorded event's character. We instead remove a smoothed version of the boundary's complex nature, and the resulting too-simple removal of the complex down, D, and up, U, by simpler d and upward, u, results in

$$e = dR'u, \tag{2}$$

and the complexity that resides in the recorded event has nowhere to go but R'. Hence, the cloud or fog in the sub-salt image. R' is R plus all of the complexity that is the difference between U and u, and D and d, respectively. We recognize that this is a simple cartoon of what actually transpires, but it in fact captures the essence of the challenge. 3D issues and anisotropy are always relevant. But the essence, the highest-priority contribution to that complex imaging challenge is rapid heterogeneous media and rapidly changing boundaries. That failure can be illustrated and needs to be first addressed in 2D acoustic media. In addressing real world challenges it is essential to define the actual obstacle to effectiveness, and to study and being able to address the simplest incarnation and realization of that actual problem. If we cannot image and invert the simplest 2D acoustic example of that prioritized issue, why study large scale 3D elastic anisotropic models? It is, of course, important to assure that synthetic data modeling, e.g., with finite differences, have not inadvertently through sampling and resulting averaging replaced the problem of rapid medium and boundary variation we seek by a smooth medium that no longer represents the issue. Practical limitations of compute time and cost on modeling projects suggest the larger the model the more likely this smoothing. Accurately modeling and capturing that rapid change in the salt boundary in a 2D acoustic model is a good place to start. Even though every explorationist knows of imaging failures, it is rare to find mention or examples in the geophysical literature or presented at conferences. A most welcome exception was a recent workshop illustrating challenges and difficulties of subsalt imaging held in 2005 at CSM.

Responding to the imaging challenge

To address that seismic imaging challenge requires either: (1) a major new and improved and reliable velocity analysis method, and concomitant imaging algorithms; or (2) a fundamental new method to directly provide depth accurate imaging without knowing or determining the adequate velocity.

The inverse scattering task specific sub-series for depth imaging is a response in the second category. It satisfies each of the four criteria listed in the first paragraph of the Introduction. Inverse scattering theory is a form of perturbation theory; and, it relates differences in a medium and a perturbation of that medium, to the differences between the original medium's (reference) wavefield and the perturbed medium's wavefield. For our purposes the reference medium is chosen and the perturbed medium corresponds to the actual earth property configuration.

It is therefore reasonable in discussing scattering theory to begin by defining a reference medium, actual medium, reference wavefield (Green's function), actual wavefield as, L_0, L, G_0, G, respectively, and the equations they satisfy:

$$LG = \delta, \qquad L_0 G_0 = \delta \tag{3}$$

and

$$G - G_0 = \phi_s, \quad L_0 - L = V. \tag{4}$$

The inverse objective is to determine V from measurements of $(G - G_0) = D$. The solution for V is in the form of a series,

$$V = V_1 + V_2 + V_3 + ..., \tag{5}$$

where V_J is the portion of V that is Jth order in the measured data. This expansion leads to the inverse scattering series,

$$(G_0V_1G_0)_m = (G - G_0)_m = (\Psi_s)_m \tag{6}$$

$$(G_0V_2G_0)_m = (-G_0V_1G_0V_1G_0)_m \tag{7}$$

$$(G_0V_3G_0)_m = (-G_0V_1G_0V_1G_0V_1G_0 - G_0V_2G_0V_1G_0 - G_0V_1G_0V_2G_0)_m \tag{8}$$

$$\vdots,$$

where the subscript m refers to measured values.

The inverse scattering series has several useful properties:

1. Each term V_J is solved by inverting the same operator G_0.
2. All forms of non-linearity are accommodated: (i) the intrinsic, e.g., the relationship between a reflection coefficient and the changes in earth material properties, and, (ii) the circumstantial, non-linearities that arise in removing multiples or imaging and inverting primaries that depend on the level of (or lack of) available or achievable overburden information. The data determine whether the services of circumstantial non-linearity are necessary, and immediately shut down any computation for which there is no purpose. That is the essence of purposeful perturbation, an amazing property of isolated task specific inverse scattering subseries.
3. Distinct task specific subseries are identifiable, for removing free surface, internal multiples, and for locating and inverting primaries.
4. All of the task specific subseries are accomplished directly in terms of the data and a reference medium Green's function, assumed to be inadequate, and the reference medium is never updated or moved towards the actual.

To illustrate the common thread in this evolution: The removal of internal multiples, and the depth imaging of primaries are each accomplished by two distinct direct algorithms, that derive from their corresponding task specific subseries. Each algorithm depends on a different multiplicative communication between events in the data, and neither requires any subsurface information whatsoever. Figure 2 provides a cartoon of the events that non-linearly communicate in the Mississippi Canyon internal multiple field data example, Figure 3. Figure 4 illustrates the primary events that will non-linearly communicate to allow the subsalt image to correctly depth image without knowing or determining the velocity.

The reflected data that leaves the top and base salt combines with the water bottom primary, and the target primary, to output the spatial location of the subsalt target without knowing or determining anything whatsoever above the target. This capability derives from the same comprehensive

starting point that earlier produced free surface and internal multiple algorithms: The inverse scattering series (e.g., Weglein et al., 1997; 2003). The free surface and internal multiple algorithms never predict or determine the velocity model or the rugous top and base salt boundaries, and neither will these inverse scattering imaging subseries results. They share the property of neither needing nor producing the velocity model or interface boundaries to accomplish their objectives: removing multiples and imaging primaries. The complex and rugous top and base salt primaries are complex reflection events that directly communicate with the subsalt primary to directly locate and invert that target. The complexity and inaccessibility of the underlying salt model and boundary plays absolutely no role in these direct methods for multiples and primaries. A sampling of a few key milestone contributions in the evolution and development of those inverse scattering subseries for multiple removal and depth imaging and non-linear inversion and Q compensation methods are provided in the references. Among those pioneering contributors are: P. Carvalho, F. Araújo, R. Stolt, K. Matson, R. Coates, D. Foster, S. Shaw, F. Liu, H. Zhang, B. Nita, K. Innanen, R. Keys, A.C. Ramírez, S. Kaplan, Z. Guo, E. Otnes, and J. Zhang.

Imaging series history and background

In our history, we have published papers, Abstracts and Topical Reviews that provide a logic or more often a reasonableness and cogency to the fundamental new concepts and methods we are deriving, developing, testing and applying. I thought it might be useful to provide a brief history of the development of the imaging and inversion research campaign to provide a framework for what has transpired, what this Report represents; and where we are going from here.

In 1998-1999 a research group at ARCO consisting of: Foster, Matson, Corrigan, Shaw and Weglein, began examining the inverse series to locate and isolate tasks and activity associated with primaries, i.e.,: (1) depth imaging and (2) amplitude analysis, to determine changes in earth material properties. This was motivated by: (1) the need at ARCO for a new vision and capability for effective depth imaging in complex geologic environments; and, (2) an understanding that the inverse scattering series provided the potential of achieving all processing objectives without the need or determination of actual subsurface properties, including velocity. Weglein launched this fundamental research campaign based on his assumption and optimistic guess/expectation of the possibility of an isolated task specific algorithm within the inverse scattering series that would perform velocity independent accurate depth imaging activity. For Weglein this issue and objective was viewed as a natural and more ambitious and certainly more complicated next possible stage beyond the velocity independent multiple attenuation algorithms that he, along with: Carvalho, Araujo, Stolt, Matson and other colleagues and students pioneered, developed and then applied; and, that had a demonstrated significance, impact and positive record. Weglein viewed the tasks associated with primaries as imaging and inversion, and he wanted to separate, if possible, imaging from inversion, with the hope that the former might be less demanding– since the latter was anticipated to be the ultimate, traditional and most challenging in terms of data requirements, such as bandwidth and the anticipated need to predict (from surface data and without any subsurface information being input or determined)absolute local amplitude subsurface information, such as, for example, a reflection coefficient. Those are two distinct and serious and well understood issues (along with others, like model type sensitivity) for that high level of ambition.

We started with the simplest model that would allow an imaging problem, when imaging with the wrong velocity. We considered a 1D acoustic model with only velocity changing and two interfaces,

and we looked at the inverse scattering series with a constant background water velocity for that simple case. Doug Foster made a significant contribution towards task isolation by separating the second term in the inverse series into a two term expression. One term was readily recognized as the first non-linear step in direct non-linear inversion to determine medium properties, and the second was thought to be the origin of moving mislocated reflectors to their correct location. Matson and Foster led the effort to analyze and interpret the complicated third term in the inverse series, where now with three interactions between the data, other tasks were able to start to be addressed, including the attenuation of internal multiples.

That impression about the purpose of the two separate terms in the second term of the inverse series came from individually examining each of the two terms, the amplitude term was local and had a self interaction interpretation associated with amplitude, that would be needed at all interfaces to turn a reflection coefficient into a change in earth properties, starting with the first reflector. The second term had an integral that was new and only began in the second term and was interpreted as an interaction between separated events, and the integral was an indication that that term cared about duration of velocity error, and, hence it was postulated as being associated with the first contribution to correcting a mis-located interface. The latter reflector depth correction task first arises with a constant reference medium and a two interface model, and the second term in the inverse series has the wherewithal to begin to address that problem, through its ability to have two interactions of the data and the data, one where the event communicates to itself and other events without an integral, and the other where it communicates to another event through an integral. Amplitude issues including transmission coefficient error, are spatially local issues whereas depth correction cares about duration of the mistaken velocity, and requires an integral.

However, (when the analytic data for the simplest normal incident wave on a two interface acoustic model was inserted into the integral term in the second term in the inverse series) the latter interpretation and speculation was very hard to argue, explain or justify, let alone convince anyone as valid, since the term containing the integral predicted a contribution only at the wrong mislocated depth, and was in fact only non-zero at that incorrect depth. So how could that term with the integral correct the image when added to the incorrect image and move the incorrect image to where it belongs, since the incorrect image and the first correction were at precisely the same wrong location. There was genuine confusion and consternation within the ARCO group and some were pessimistic on the prospects of inverse series velocity independent imaging capability.

Weglein then recognized that the move from incorrect to correct would not occur in a single term shift, but rather in terms of a series, and in fact a cascaded series when the shift was expressed in terms of measured reflection data. The location only operation from incorrect to correct depth was viewed as a Taylor series of the difference between two Heaviside functions, expanded about the mislocated depth and as powers in the difference between actual and mislocated depth. Each successive term in this 1D depth imaging Taylor series contains one higher power of actual minus mislocated depth, and actual depth minus mislocated depth is in turn expressible as a Taylor series in reflection data. Taking a part of the shift or imaging series, by keeping only one leading linear term in the expansion of actual depth minus mislocated depth in terms of reflection data, then leads to an approximate imaging series in the data called the leading order imaging series. These are all simple 1D normal incidence only concepts, of mislocated reflectors being a shift from the correct reflector, and although we recognized that 2D and 3 D would be a much more complicated issue to define and address, it never-the-less provided a useful primitive launch into the imaging problem in its simplest incarnation. And, therefore, a reasonable place to start.

Higher order imaging series would take more than one leading term of actual minus mislocated depth expanded in terms of reflection data. Those early ideas, concepts and tests were published in several papers and Abstracts in 2000, 2001, 2003, 2004. Simon Shaw then discovered, developed and tested an algorithm representing a pattern of leading order contributions to the imaging capability within the inverse scattering series, for a normal incident wave on a 1D acoustic medium. That leading order imaging series was derived into a compact and closed form by Robert Keys. Simon Shaw then derived the non-trivial generalization of that imaging series for prestack data, and derived a closed form expression, as well. Simon demonstrated the ability of the imaging series to retain effectiveness absent zero frequency data; and, showed flat common image gathers at the correct depth without knowing or determining the velocity model(2004).

The leading order imaging series, is just that, leading order; and, as anticipated given ever larger contrast models and longer duration of velocity away from the reference value, they eventually went beyond the ability of that first order approximate imaging algorithm.

Several simultaneous further single steps beyond the leading order 1D prestack imaging method were launched from that pioneering and encouraging 1D leading order acoustic velocity only imaging contribution of Shaw, Keys et al. After each isolated issue is progressed and understood then a combination is collected within one or several algorithms to form a strategy towards field data application. Among the simultaneous steps taken were: (1) to remain in a 1D acoustic velocity only model but to go to higher order terms, (Shaw, Innanen, Nita et al.) (2) to stay in the same 1D acoustic model and capturing a leading order series of coupled location and amplitude tasks (Nita , Innanen et al.) , (3) to go to the much more complicated and challenging multi-parameter acoustic and elastic worlds, in prestack 1D, with linear and non-linear contributions for isolating location correction tasks from improved amplitude for target identification tasks (H. Zhang et al.); (4) to take the serious leap from 1D to 2D, starting with an acoustic velocity only medium, and identifying location and amplitude terms in that more complicated and relevant world (F. Liu et al.); (5) one more step in realism is taking the step to the 1d inelastic acoustic earth, where the tasks are, interface location and improved resolution without knowing or determining the velocity or Q model (K.Innanen et al.). Several related and significant contributions advanced these objectives, often with use of forward series analysis, analogs and insights that help steer the search and understanding of the mirror inverse series processes. Among the latter contributions are; (1) B. Nita et al. on prestack forward series, and asymptotic assumptions, postcritical reflections and head waves; (2) A. C. Ramírez et al. , new internal multiple removal concepts and algorithm, (3) A. C. Ramírez and E.Otnes, velocity and density forward series, diagramatic interpretation, and inverse implications; and (4) K. Innanen, forward series that include diffractions, for modeling and inverse implications.

Non-linear direct target identification: a new significant step forward

AVO has largely been a static model over the past 20 years, in terms of how earth elastic property and density changes are considered to be related to a plane wave reflection coefficient. It is often considered a tech service rather a research area in oil companies, and for good reason, since not very much new has been happening on the theory front to justify calling it a research activity. Two approaches today are: (1) the linear approximate form, or (2) the indirect model matching, of a plane wave Zoeppritz reflection coefficient form and with global search engines. The former

has serious issues since it is rare for petroleum targets to satisfy small contrast assumptions, and the latter is computationally taxing and sometimes has reported erroneous or ambiguous results. The global search methods often learn more about the properties of search engines than underlying physics, and are difficult to imagine generalizing to a pinch out trap, or a multi-D corrugated or set of dipping reflectors, or the fingering fluid interfaces in time lapse application. Progress has been reported relating elastic property and density changes and rock and fluid properties, in different exploration target settings, through a combination of empirical and theoretical studies. Progress is also worth noting in upscaling and mapping subresolution properties and reflections into an effective seismic response and signature.

The inverse scattering series provides a framework for direct multi-dimensional inversion, and tasks associated with that objective, without the traditional need for subsurface information. The inverse scattering series can be formulated for a 2D or 3D acoustic or elastic heterogeneous subsurface. Among those contributing to that effort and elastic multi-D framework are: Clayton and Stolt, Stolt and Weglein, and Matson et al., in 2D; and, Stolt recently extended those earlier elastic results to 3D. Stolt and co-workers were mainly focused on linear elastic formulations, and Matson et al. were interested in multiple removal for ocean bottom or on-shore application.

The first step into exploring the direct multi-parameter non-linear estimation of acoustic or elastic properties from the comprehensive multi-dimensional inverse scattering series framework, was initiated by H. Zhang et al. around 2002.

In my view Haiyan Zhang's breakthrough, impressive and significant research results on direct non-linear parameter estimation, represents a milestone and will energize and rejuvenate this field, and allow e.g., distinctions to be made by non-linear accurate elastic property estimates that are too close for linear estimates to reliably resolve. Analysis and examples are provided in this report addressing time lapse application where the issue is to distinguish pressure from fluid changes. The latter analysis and application was under the mentoring and guidance of Bob Keys, Doug Foster and Simon Shaw of ConocoPhillips. This effort is direct, and provides a first time framework for what data is required to consistently perform non-linear estimation, and what value can be derived from a compromised p-wave only acquisition. Future research will examine multi-D generalizations. Since this is task 4, parameter estimation activity, we anticipate this as a development tool at first pass, reflecting its need for input reflection coefficient information at the target. Inverse scattering series theory suggests that this non-linear direct parameter inversion ought to be achievable directly from surface reflection data.

We will examine the practical data requirements needed to match and achieve the latter theory promise, and, also determine wether first achieving depth imaging location can reduce bandwidth demand. However, the latter is not our next step; rather, we will first seek to apply this new and promising and efficient improved target predicting tool in a development setting.

Higher order imaging series and steps into 2D: towards accommodating greater realism

Following some early higher order imaging results and tests by Simon Shaw, Kris Innanen progressed and presented the higher order imaging and inversion capability within the 1D inverse series and tested his derived form with positive and encouraging results. Simultaneously and independently,

Fang Liu was pioneering the much more complicated, challenging and daunting inverse series for a laterally and vertically varying 2D earth. There are issues and challenges that have no 1D analog, e.g., misshapen and mislocated reflectors, diffractions, corrugated boundaries, pinchouts, cusps, rapid lateral velocity variation, near vertical salt flanks, and each has inverse series activity to respond, and that response is neither called upon nor needed in a 1D earth. Moving from 1D to 2D involves more than replacing z by x, z in 1D formulas. There are certain issues and terms in a multi-D inverse series imaging capability that have 1D analogs and other also critical factors that do not; and thelatter exist exclusively in a multi-D world. And both are critical to understand and utilize for practical impact and efficacy. Fang Liu's results and closed form relates to multi-D imaging terms with 1D analogs. Up-Down shift occurs in 1D and a laterally varying up-down shift occurs in 2D, and is the generalization of a 1-D capability. Fang also recognizes a term with no 1-D analog, and notes its interest in removing salt flank diffractions in his salt model, and helping image the dipping layer in his earlier 2D layer examples. We anticipate that many of the current prioritized pressing imaging challenges will require and benefit from 1D generalized and 2D exclusive imaging terms. That further capture of exclusive 2D activity is part of our current activity and plan.

Hence, imaging has many more issues and challenges to address in 2D. Fang Liu first developed a multi-D extension of the leading order 1D imaging series capability of Simon Shaw. Fang produced his first imaging without the velocity results on 2D models of moderate but serious and respectable difference between actual and reference velocity. Fang Liu's 2D imaging without the velocity drew significant positive industry interest and attention. However as expected his partial 2D leading order algorithm results on larger contrast models noticed a breakdown prompted by the large contrast models mislocated images communicating with images at larger times, or pseudo depths. Fang was aware of Innanen's 1D higher order result, but separately intuited a different closed form that allowed 2D higher order imaging contributions, by precluding communication with deeper events, and keeping the amplitude of the image unchanged. Fang's new formula was able to go much beyond the early smaller contrast models, that were accommodated by his leading order form, with 2D examples that included a salt model designed by Peter Traynin of ExxonMobil. There was a need to understand how Fan Liu's 2D higher order imaging formula could be derived from the inverse series. Fang Liu, in discussion with Jingfeng Zhang and Kris Innanen, was able to derive his 2D formula based on generalizing the 1D higher order analysis of Innanen, and setting a Jacobian to one that represented keeping the amplitude of the image unchanged. Jingfeng provided an insightful analysis to formalize and comprehend Fang Liu's original intuitive leap. Jingfeng's analysis is included in this report. This interconnected and highly interactive trajectory is often the path to new algorithms and deeper understanding.

Fang Liu et al. have taken us into the multi-D imaging world. His results are impressive and encouraging. The next steps are to include more taxing multi-D phenomena in model tests and capturing new and more multi-D comprehensive and inclusive imaging algorithms derived from the inverse series. Fang's imaging formula is derivable by extending an argument which is based upon and originating in 1D. However, his term:

$$-\frac{1}{2}\frac{\partial \alpha_1(x,z)}{\partial x}\int_{-\infty}^{z} du \int_{-\infty}^{u} \frac{\partial \alpha_1(x,v)}{\partial x} dv$$

is a fully 2D phenomena and has no 1D analog and cannot be derived from generalizing 1D derivations. That term is addressing among other 2D exclusive issues the diffractions off the salt flank,

and other lateral issues in his earlier dipping layer models. More terms without 1D analogs are needed to address the rapid varying boundaries, diffractions and lateral rapid velocity variations. Issues of imaging a reflector that is undulating, with a simple constant velocity above, is needing some constructive attention, as well.

Can the inverse series address the imaging challenge with a known constant overburden velocity but a complex rapidly varying boundary? Last but not least, what are the steps needed from where we are to where we need to be, to initiate the first imaging series algorithm field data test? What hierarchy of challenges should we define in this set of field data tests? We will discuss and address these matters in our last presentation, at our meeting, providing a summary overview and describing plans. These inverse scattering task separated subseries techniques are especially well-suited, and demonstrate their mettle in complex media: and, hence, represent a direct response to the pressing seismic processing challenge. The current effort is to bring the same level of effectiveness to seismic signal and information extraction from primaries, as was earlier provided to the removal of multiples. The inverse scattering series methods hold a place in the seismic toolbox reserved for processing data under the most complex and ill-defined subsurface conditions. The practical prerequisites and preprocessing steps are the same for the imaging series as for the multiple algorithms: e.g., adequate surface data, collected or extrapolated/interpolated, deghosting, and wavelet estimation.

L. Amundsen and his colleagues have recently published several papers with new important insights and perspectives. They recognize several forms derived by our earlier imaging series analysis as having a WKBJ-like phase character and they are able to produce those original imaging series 1D results without resorting to a series. That contribution provides an important insight and awareness that perhaps implicit assumptions equivalent to WKBJ are within our diagrammatic separation and selection of tasks in the imaging task separated series in 1D.

As we move forward into addressing further complicated multi-D imaging challenges, understanding 1D assumptions and insights within our current algorithmic state is essential in progressing ahead and beyond the known and into unchartered fully complex multi-dimensional imaging territory. The salt model synthetic results this year of Fang Liu et al., under the mentorship of Peter Traynin of ExxonMobil, are extremely encouraging, and would be considered positive with a traditional migration and an estimated velocity, and Fang Liu uses only water speed. Those results galvanize and energize us to capture further imaging capability within the series, and test ever more realistic models of imaging challenges.

Link to compute and acquisition

The mandate of M-OSRP is to provide fundamental new concepts and algorithms that address the pressing seismic challenges. Codes are generated for use by M-OSRP students and faculty, and then distributed to our sponsors. Although compute issues are not our central responsibility, a detached attitude to the compute challenges that our algorithms can represent would be both inappropriate and counter-indicated. Our algorithms need to be computable to be useful and relevant. When a 3-D free surface algorithm can take a major oil company six months to run, and the internal demultiple is well beyond that, then, simply delivering code is not sufficient to be taking responsibility to assure high impact. Sam Kaplan had led an effort to design the inverse scattering free surface and internal multiple algorithms to be both compute optimal and adaptable to different distributed compute architectures. He has been working closely with Billy Robinson of

IBM and Kris Innanen. IBM is loaning Cell processors to M-OSRP, for its use and the use by its sponsors. IBM is interested in feedback to help design the optimal seismic processing architecture. We would like to suggest that an M-OSRP Advisory Board Compute Sub-committee be formed to link to that issue.

Another related aspect of the M-OSRP program is the state and progress of seismic (and other) acquisition, and how that interfaces with, couples and leverages new M-OSRP processing algorithms. An M-OSRP Advisory Board Acquisition Sub-Committee could facilitate that communication, and perhaps help in arranging a research field experiment that could have specifications and an exploration target that could benefit from new M-OSRP processing capability.

Imaging plan

We recognize that the imaging problem is much more complicated than the multiple removal problem, and the latter was no walk in the park. Multiples need to be predicted and subtracted. In contrast, there are various tiers, or hierarchies, of complexity of issues in an imaging problem. Moving a clear but miss-located image to the right spatial location is one thing, and no easy task, but taking a subsalt fog into a clear and correctly located image is another thing entirely.

Our plan for the imaging project is to catalog a set of currently outstanding imaging challenges in terms of degree of complexity, and then move to field data with an algorithm anticipated to address that first level of challenge, learn about field data application for the imaging series concept, and then return to meet the next more demanding and difficult level and challenge. That set of learning curve steps was how 10-15 years ago we moved to field data application in our earlier work on free surface removal and internal multiple attenuation. Examples are presented in this Report that exemplify these demultiple and imaging algorithms, and their evolution; and, their prerequisites and open issues and plans are presented. This report describes the progress on all of the projects that connect to form the strategy we have described.

A list of topics and lead author contributors, 2005 software delivery and M-OSRP presenters at our Annual Meeting is below:

- Data reconstruction, A. C. Ramírez et al.
- Wavelet estimation, Z. Guo et al.
- Deghosting, J. Zhang et al.
- Free Surface Multiple Removal and field data test, 2D and towards 3D, S. Kaplan, K. A. Innanen et al.
- Internal Multiple Attenuation, 2D S. Kaplan (Coding/Adapting internal multiple algorithms for different distributed compute architectures)
- Internal Multiple Elimination 2D, A. C. Ramírez et al.
- ICA Adaptive Subtraction, S. Kaplan and K. Innanen
- Forward series for velocity and density: implications for the imaging problem, A. C. Ramírez and E. Otnes

- Forward series for 3D perturbations and series approximation of diffractions, K. Innanen
- Imaging conditions, B. Nita
- Inverse processing for Q compensation without knowing or determining Q, Innanen et al.
- Depth imaging without the velocity in multi-D, F Liu et al.
- Progressing imaging concepts and algorithms, F. Liu, J. Zhang, K. Innanen
- Acoustic Modeling, F. Lui, J. Zhang
- Non-linear direct AVO for acoustic and elastic media, H. Zhang et al.
- Non-liner direct AVO for time lapse application, distinguishing fluid from pressure change, H. Zhang et al.
- Overview and plan, A. Weglein

Summary

So in summary, the big picture is: (1) improve the removal of multiples, (2) better locate your target, (3) improve the target identification; and (4) the resolution of the target, and all without the traditional requirement of subsurface information typically required to achieve those objectives. To make it all work requires advancing one single set of prerequsities: data collection/reconstruction, wavelet estimation and deghosting.

The idea is to provide a consistent seismic processing chain, not for academic and/or mathematical rigor, but for effectiveness. To allow methods that depend on earlier steps and prerequisites, and to be assured that the satisfaction of those prerequisites is as complete and effective as the methods they are meant to serve. That consistency will best assure that the end product deliverables in the processing chain, can reach their practical potential as a response to the pressing challenges, and their place in the seismic toolbox.

This is an exciting time, progressing and going after the subsalt image. This is very much a team effort and the success of each link in the processing chain determines the success of subsequent steps. We appreciate the support, encouragement, opportunity and privilege to work together to pursue an effective and high impact response to our pressing seismic challenges.

Sincerely,
Art

Arthur B. Weglein

Acknowledgments

We are grateful to the sponsors of M-OSRP for supporting this research. Support from DOE Basis Energy Sciences award DE-FG02-05ER15697 and NSF CMG award DMS-0327778 are most gratefully acknowledged.

References

Araújo, F. V., Weglein, A. B., Carvalho, P. M. and Stolt, R. H., Inverse scattering series for multiple attenuation: an example with surface and internal multiples, 1994: 64th Ann. Internat. Mtg. Soc. Expl. Geophys., *Expanded Abstracts*.

Bednar, J. B., A brief history of seismic migration, 2005: Geophysics, **70**, P.3MJ–20MJ.

Carvalho, P. M., Weglein, A. B. and Stolt, R. H., Nonlinear inverse scattering for multiple suppression: application to real data: part I, 1992: 62nd Ann. Internat. Mtg. Soc. Expl. Geophys., *Expanded Abstracts*.

Innanen, K. A., Two non-linear forward and inverse approximations for wave fields in the presence of sustained medium perturbations, 2005: 75th Ann. Internat. Mtg. Soc. Expl. Geophys., *Expanded Abstracts*.

Innanen, K. A. and Weglein, A. B., Towards non-linear construction of a Q-compensation operator directly from measured seismic reflection data, 2005: 75th Ann. Internat. Mtg. Soc. Expl. Geophys., *Expanded Abstracts*.

Keys, R. G. and Weglein, A. B., Generalized linear inversion and the first Born theory for acoustic media, 1983: J. Math. Phys., **24**, 1444–9.

Liu, F., Weglein, A. B., Innanen, K. A. and Nita, B. G., Extension of the non-linear depth imaging capability of the inverse scattering series to multidimensional media: strategies and numerical results, 2005: 9th Ann. Cong. SBGf, *Expanded Abstracts*.

Matson, K., An inverse-scattering series method for attenuating elastic multiples from multicomponent land and ocean bottom seismic data, 1997: Ph.D. thesis, University of British Columbia.

Nita, B. G., Matson, K. H. and Weglein, A. B., Forward Scattering Series and Seismic Events: Far Field Approximations, Critical and Postcritical Events, 2004: SIAP, **64**, 2167–2185.

Ramírez, A. C. and Weglein, A. B., An inverse scattering internal multiple elimination method: beyond attenuation, a new algorithm and initial tests, 2005: 75th Ann. Internat. Mtg. Soc. Expl. Geophys., *Expanded Abstracts*.

Shaw, S. A., An inverse scattering series algorithm for depth imaging of reflection data from a layered acoustic medium with an unknown velocity model, 2005: Ph.D. thesis, University of Houston.

Stolt, R. H. and Benson, A. K., Seismic migration: Theory and practice, 1986: Geophysical Press, Volume **5**.

Weglein, A. B., Gasparotto, F. A., Carvalho, P. M. and Stolt, R. H., An inverse-scattering series method for attenuating multiples in seismic reflection data, 1997: Geophysics, **62**, 1975–1989.

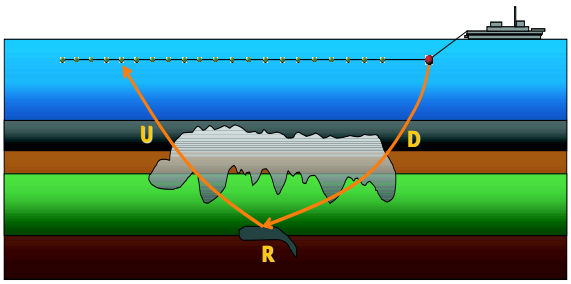

Figure 1: *Schematic model highlighting imaging challenges.*

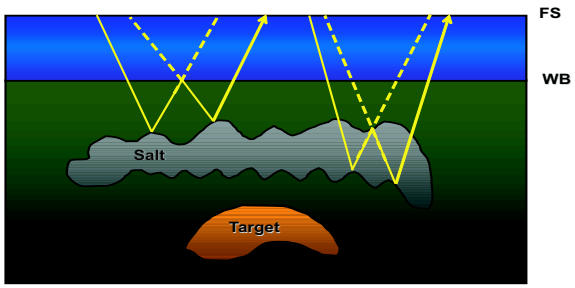

Figure 2: *Schematic illustrating the non-linear combination of data sub-events in inverse scattering series based multiple removal.*

Weglein, A. B., Araújo, F. V., Carvalho, P. M., Stolt, R. H., Matson, K. H., Coates, R., Foster, D. J., Shaw, S. A., and Zhang, H., Topical Review: Inverse-scattering Series and Seismic Exploration, 2003: Inverse Problems, **19**, R27–R83.

Zhang, H. and Weglein, A. B., The inverse scattering series for tasks associated with primaries: depth imaging and direct non-linear inversion of 1D variable velocity and density acoustic media, 2005: 75th Ann. Internat. Mtg. Soc. Expl. Geophys., *Expanded Abstracts*.

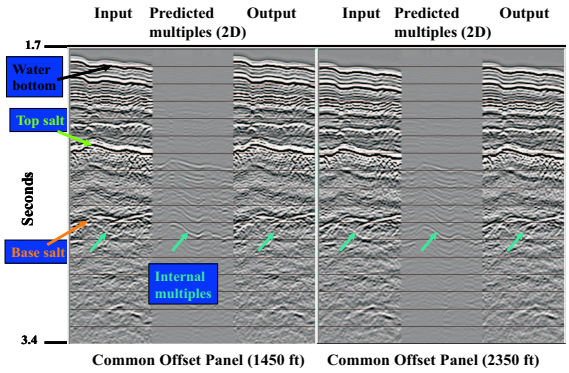

Figure 3: *Multiple removal: Mississippicanyon field data example.*

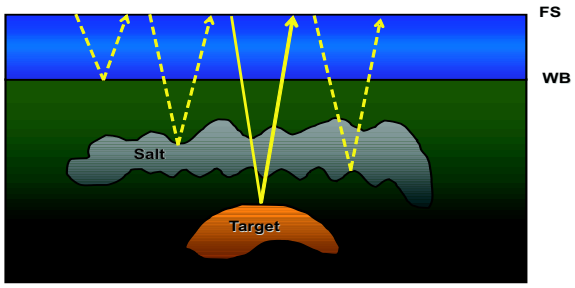

Figure 4: *Schematic illustrating the primaries involved in non-linear direct imaging for a sub-salt target.*

Near offset data extrapolation of primaries and multiples

Adriana Citlali Ramírez*[1], Arthur B. Weglein* and Ketil Hokstad †
*M-OSRP. Dept. of Physics, University of Houston, 77204-5005, USA
†Statoil Research Center, N-7005 Trondheim, Norway.

Abstract

We present a method that predicts water bottom primaries at near offsets. The concepts of limited aperture migration and inverse scattering are combined to develop a data driven theory for data reconstruction. Data extrapolation can be particularly challenging in shallow water, where early events of the recorded wavefield are mainly in the postcritical regime. For this kind of data, our results predict water bottom primaries with the correct travel time. When most of the data are precritical, the method accurately predicts primaries and multiples without the need for modeling or inverting for earth properties.

1 Introduction

The inverse scattering subseries formalism has acomplished the most comprehensive and accommodating methods to eliminate all multiples, withdrawing knowledge from the subsurface, but placing stringent requirements on wavelet estimation, deghosting and completeness of data collection and/or reconstruction. Near offset prediction, in particular, has represented a challenge for full wavefield seismic processing (e.g. demultiple, depth imaging).

Most of the current extrapolation methods are model type dependent and require a correct estimation of earth properties; or they are based on primary-processing techniques e.g. DMO (Hale, 1984), AMO (Baumstein, 2004). These methods only work accurately for primaries, and they are not designed to deal with postcritical data which are present in shallow water acquisitions. While these methods (within their own assumptions and resulting quality and properties of output) have been useful in addressing near-offset data extrapolation, they are not suited to provide a complete prerequisite satisfaction consistent with the demands of the later steps in data processing they are meant to serve. The potential of those full wavefield seismic processing tools are not close to being realized in practice with the existent extrapolation capability.

We use the aperture compensated migration/inversion method (Stolt and Benson, 1986; Wang, 1990) and concepts derived from inverse scattering to develop a data-driven theory for near-offset reconstruction. The prestack reflection data are imaged using a constant background velocity. This image is used as a model to generate the events that were not recorded. When the data are precritical, the method predicts primaries and multiples at near offsets with high accuracy. When the experiment contains mainly postcritical data, the method predicts water bottom primaries at the correct arrival time and other events are predicted with less accuracy.

*This work was done while working as a student intern at Statoil Research Center, Summer 2005.

2 Methodology

Data extrapolation is usually the first preprocessing step performed. Hence, the chosen extrapolation method must predict data with the events and characteristics of the recorded data. A method like this can be accomplished by combining the definitions and concepts for finite aperture migration introduced by Stolt and Benson (1986) and the concepts of inverse scattering introduced by Weglein et al. (1981).

The inverse scattering series processing methods can accommodate a complex multi-dimensional earth, without requiring any subsurface information. They only require measured reflection data, D, and the reference medium Green's function, G_0. We define the perturbation, V, as the difference between the reference and actual medium. The scattered field is the difference between the Green's functions in the actual and reference media, $\Psi_s = G - G_0$. We expand V in orders of measured data $V = \sum_{i=1}^{\infty} V_i$, where V_i is i^{th} order in the measured data. This expansion leads to the inverse scattering equations,

$$
\begin{aligned}
(G_0 V_1 G_0)_m &= (G - G_0)_m = (\Psi_s)_m && (1)\\
(G_0 V_2 G_0)_m &= (-G_0 V_1 G_0 V_1 G_0)_m && (2)\\
(G_0 V_3 G_0)_m &= (-G_0 V_1 G_0 V_1 G_0 V_1 G_0 - G_0 V_2 G_0 V_1 G_0 - \\
&\qquad G_0 V_1 G_0 V_2 G_0)_m && (3)\\
&\vdots,
\end{aligned}
$$

where the subscript m refers to measured values, $D = A \cdot (\Psi_s)_m$ and A is the source signature. The first inverse equation, (1), resembles the form of the Born approximation, $\Psi_s \approx G_0 V G_0$. Although they might look similar, they are in fact different. The first inverse equation is an exact equation for V_1 with the potential to work as an extrapolator of data. The main difference between equation (1) and the Born approximation is the substitution of V_1 in the first case and V in the second. The Born approximation, as its name states, is not exact and it cannot be used to accurately extrapolate data.

In equation (1), V_1 is the portion of V that is linear in the data. Its value is never assumed to be close to V, the real perturbation. Being linear in the data means that it is a direct data mapping that treats both, primaries and multiples, on equal footing.

Our method begins with equation (1) and solves for V_1 from D, with a compensation for the finite aperture of the prestack recorded data. We solve V_1 for a given earth model type, *e.g.*, acoustic, elastic or anelastic. The details of the data extrapolation method depend on the choice of parameters describing the model type. However, this choice does not require the correct model parameters, since the goal of extrapolation is to predict events that were not measured not to invert for the medium properties.

A 2-D constant density, variable velocity and acoustic model with free surface at $z = 0$ is defined by the wave equation

$$
\begin{aligned}
(\nabla^2 - \frac{1}{v(x,z)^2}\frac{\partial^2}{\partial t^2}) G(x,z|x_s,z_s;t) &= -\delta(t-t_s)\delta(x-x_s) \\
&\times[\delta(z-z_s) - \delta(z+z_s)],\ G = 0 \text{ for } t < t_s; \qquad (4)
\end{aligned}
$$

where $v(x,z)$ is actual velocity, and the subscript s refers to source position and time. The background model with free surface at $z=0$ is defined as

$$(\nabla^2 - \frac{1}{c_0}\frac{\partial^2}{\partial t^2})G_0(x,z|x_s,z_s;t) = -\delta(t-t_s)\delta(x-x_s) \times[\delta(z-z_s)-\delta(z+z_s)],\ G_0 = 0 \text{ for } t<t_s; \quad (5)$$

where c_0 is the constant reference velocity. From equations (4) and (5), the perturbation can be written as $V = k^2\alpha(x,z)$ where $k=\omega/c_0$ and $\alpha(x,z) = 1 - c_0^2/v(x,z)^2$. The series for V can then be expressed in a series for α, $V = \sum_{i=1}^{\infty} V_i = k^2 \sum_{i=1}^{\infty} \alpha_i$, and equation (1) becomes

$$D(x_g,z_g|x_s,z_s;\omega) = \int dx \int dz G_0(x_g,z_g|x,z;\omega)k^2\alpha_1(x,z) \times G_0(x,z|x_s,z_s;\omega), \quad (6)$$

where z_g and z_s are receiver and source depths, respectively. The souce signature is included in V_1. In the following, we are going to write $D(x_g,z_g|x_s,z_s;\omega)$ as $D(x_g|x_s;\omega)$ and its Fourier conjugates. The reference Green's function is

$$G_0(k_x,z|x',z';\omega) = \frac{e^{-ik_x x'}}{-2iq}(e^{iq|z-z'|} - e^{iq|z+z'|}), \quad (7)$$

where $q = sgn(\omega)\sqrt{\frac{\omega^2}{c_0^2} - k_x^2}$ is the vertical wave number, and k_x is the conjugate variable of x. We assume that α_1 is invariant with respect to x, i.e. $\alpha_1(x,z) = \alpha_1(z)$ and equation (6) becomes

$$D(k_{gx}|k_{sx}=k_{gx};\omega) = 2\pi\frac{\sin(\frac{k_z z_s}{2})\sin(\frac{k_z z_g}{2})}{k_z^2/4}\frac{\omega^2}{c_0^2}\alpha_1(k_z),$$

where $k_z = q_g + q_s = 2q_g$. The *sine* functions on the r.h.s. are known to be responsible for the removal of source and receiver ghosts (Krail and Shin, 1990; Weglein et al., 2003). For our purposes we want to preserve all the original characteristics of the recorded data in α_1, this will effect in a prediction of near offsets in agreement with the measured data. Hence, we include the *sine* functions in a more general parameter $\widetilde{\alpha_1(k_z)} = \alpha_1(k_z)\sin(\frac{k_z z_s}{2})\sin(\frac{k_z z_g}{2})$,

$$D(k_{gx};\omega) = 8\pi\frac{1}{k_z^2}\frac{\omega^2}{c_0^2}\widetilde{\alpha_1}(k_z). \quad (8)$$

The data have more degrees of freedom than $\widetilde{\alpha_1}$, leading to a non-unique solution of the problem. To perfect a migration/inversion, we would need an infinite receiver aperture. There are different ways to prevail over this situation and compensate for the limitations due to an incomplete acquisition. We choose to invert equation (8) with a weighted limited aperture migration/inversion technique (Stolt and Benson, 1986; Wang, 1990; Stolt, 2002), allowing us to exploit the extra degree of freedom the data have to attain a better solution.

The weighted limited aperture migration/inversion method can be expressed as

$$\widetilde{\alpha_1}(k_z) = \int dk_{gx} L(k_{gx},k_z)D(k_{gx};\omega), \quad (9)$$

$$\int dk_{gx} 2\pi\frac{\omega^2}{c_0^2}\frac{4}{k_z^2}L(k_{gx},k_z) = 1. \quad (10)$$

We perform an inverse Fourier transform over k_{gx} and k_z, change the order of integration and the variables from k_z to ω and k_{gx} to $\chi = \frac{c_0}{\omega} k_{gx}$,

$$\widetilde{\alpha_1}(z) = \frac{1}{2\pi} \int dx_g \int d\omega I(z|x_g;\omega) D(x_g;\omega), \tag{11}$$

$$I(z|x_g;\omega) = \int d\chi L(\frac{\omega}{c_0}\chi, 2\frac{\omega}{c_0}\sqrt{1-\chi^2}) \frac{2\omega}{c_0^2\sqrt{1-\chi^2}} \times e^{-i\frac{\omega}{c_0}(2z\sqrt{1-\chi^2}+\chi x_g)} \tag{12}$$

Assuming that the arbitrary weight function L varies slowly compared to the exponential, we solve equation (15) using steepest descents (Bleistein and Handelsman, 1986). For a stationary point χ_0 in a finite region $a < \chi_0 < b$,

$$I(z|x_g;w) = \int_a^b d\chi f(\chi) e^{i\omega g(\chi)};\ g'(\chi_0) = 0,\quad g''(\chi_0) \neq 0,$$

$$I(z|x_g;w) = \sqrt{\frac{2\pi i}{\omega g''(\chi_0)}} e^{i\omega g(\chi_0)} f(\chi_0) + \frac{1}{i\omega}\left[\frac{f(b)}{g'(b)} e^{i\omega g(b)} - \frac{f(a)}{g'(a)} e^{i\omega g(a)}\right]. \tag{13}$$

Hence,

$$I(z|x_g;w) = \sqrt{\frac{c_0\pi i}{\omega z}} \frac{4\omega z}{c_0^2} \left(\frac{2z}{r}\right)^{\frac{3}{2}} L(k_g x(\chi_0), kz(\chi_0)) e^{-i\omega\frac{r}{c_0}}$$
$$+ \frac{2}{ic_0}\left[\frac{L(k_{gx}(b), k_z(b))}{2z\chi(b) - x_g\sqrt{1-\chi(b)^2}} e^{-i\omega(t_b - \frac{1}{c_0}\frac{(x_g - x_b)x_b}{r_b})}\right]$$
$$- \frac{2}{ic_0}\left[\frac{L(k_{gx}(a), k_z(a))}{2z\chi(a) - x_g\sqrt{1-\chi(a)^2}} e^{-i\omega(t_a - \frac{1}{c_0}\frac{(x_g - x_a)x_a}{r_a})}\right], \tag{14}$$

where $t_b = \frac{r_b}{c_0},\ r_b = \sqrt{4z^2 + x_b^2},\ \chi_b = \frac{x_b}{r_b},\ t_a = \frac{r_a}{c_0},\ r_a = \sqrt{4z^2 + x_a^2},\ \chi_a = \frac{x_a}{r_a}$, and $\chi_0 = \frac{x_g}{r},\ r = \sqrt{4z^2 + x_g^2}$.

The first term on the r.h.s. of equation (14) is known as the stationary phase approximation. It is the leading order term of an asymptotic expansion. The second and third terms contain the contribution of the endpoints (χ_a and χ_b). The endpoints introduce noise to the image, $\widetilde{\alpha_1}$, producing diffraction-like events (Sun, 2002). If the aperture is positioned correctly with respect to the stationary point, then the endpoints contribution must be eliminated by introducing a taper function. The endpoints should be taken into account if the stationary point lies outside and far away of the migration aperture. Under the assumption that $\widetilde{\alpha}$ is invariant over the horizontal coordinates, all values in $\widetilde{\alpha_1}$ corresponding to the stationary point $\chi_0 = \frac{x_g}{r}$ are well positioned within the aperture. Hence, a taper function, B, with geometrical information about the aperture is included in the formalism as part of the arbitrary weight function (Stolt and Benson, 1986)

$$L(k_{gx}, k_z) = B(x_a, x_b, x_g - x_s) S(\frac{k_{gx}}{k_z}) F(\omega), \tag{15}$$

where k_{gx} and k_z are evaluated at the stationary point. This description of the weight function allows us to separate frequency from space variables at the stationary point. The simplest taper function is a neutralizer defined as

$$B(x_a, x_b, x_g - x_s)|_{x_s=0} = \begin{cases} 1 & \text{if } x_g \in (x_a, x_b) \\ 0 & \text{otherwise.} \end{cases} \tag{16}$$

Substitute the neutralizer into equation (15) and define $\beta = \frac{k_{gx}}{k_z}$, to find a solution for equation (10),

$$\int_{\beta_a}^{\beta_b} d\beta 2\pi(1 + 4\beta^2)S(\beta)F(\omega)k_z = 1, \tag{17}$$

where the limits of the integration are evaluated at the stationary point, *i.e.* $\beta_a = \frac{x_a}{4z}$, $\beta_b = \frac{x_b}{4z}$, representing the limits of the aperture that has been used.

Choose the arbitrary function $F(\omega) = \frac{c_0}{2\pi}\frac{1}{k_z}\frac{1}{\sqrt{1+4\beta^2}} = \frac{c_0}{4\pi}\omega^{-1}$, to take all the constants out of the integration, and find

$$S(\beta) = \frac{1}{\sqrt{1 + 4\beta^2}}\frac{1}{\beta_b - \beta_a}. \tag{18}$$

Replacing L by B, S and F, we obtain a formula for the limited aperture image of the data,

$$\widetilde{\alpha_1}(z) = \frac{1}{4\pi^2}\frac{1}{x_b - x_a}\int_{x_a}^{x_b} dx_g \, \frac{8z^2}{r^{3/2}} \times \int_{-\infty}^{\infty} d\omega \frac{\sqrt{2\pi i}}{\sqrt{c_0\omega}} e^{-i\omega\frac{r}{c_0}} D(x_g; \omega). \tag{19}$$

The limited aperture image, $\widetilde{\alpha_1}$, is equivalent to a linearized migration/inversion with background velocity, where the data contain all the original events and the source signature.

By definition a neutralizer is a taper function having all orders of partial derivatives. From the analysis of equation (14), we only need partial derivatives up to second order and the aperture correctly positioned so that the stationary point lies inside it. A taper function with derivatives up to second order can improve the migrated image by minimizing the edge effects. Hence, we can replace the neutralizer in equation (16) by a second order taper function (Fig.1) defined by the chosen aperture, N_1, and a subaperture, N_0. Inside the subaperture, N_0, the taper should be unity and then decrease smoothly from unity to zero at the limits of N_1. According to the theoretical guideline for the design of the migrated aperture given by Sun (2002), $N_0 = \frac{2}{3}N_1$. It is also possible to replace the neutralizer in equation (16) by a one-side Hanning or triangular window (Fig.2). The reason for keeping a neutralizer at the beginning of the aperture is that we are interested in prediction of near offsets, hence we want to keep all the contributions from the first recorded offsets. This is particularly helpful in shallow water acquisitions where most of the arrivals are postcritical, and the method benefits from any precritical information. If the taper is designed according to the criteria described above, the numerical results are slightly better with the Hanning window than the triangular one (Sun, 2002). Then, $B(x_a, x_b, x_g)$ can be any of these

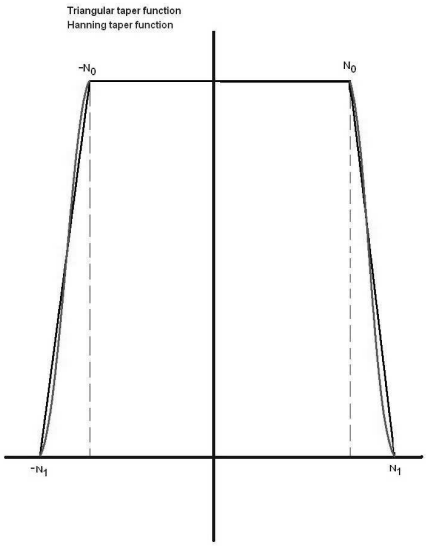

Figure 1: Hanning or triangular window.

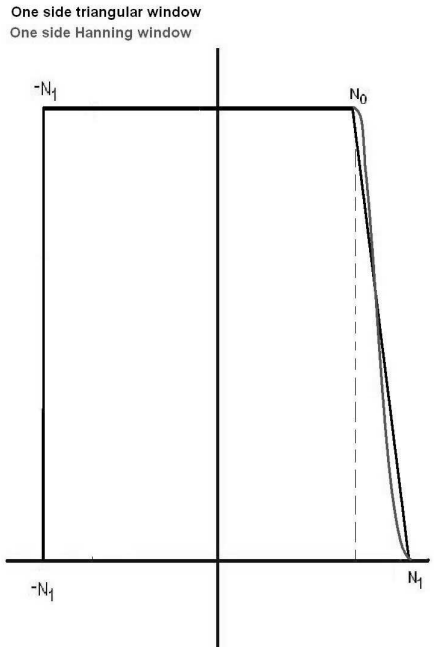

Figure 2: One side Hanning or triangular window

windows, and the limited aperture image of the data is given by

$$\widetilde{\alpha_1}(z) = \frac{1}{4\pi^2}\frac{1}{x_b - x_a}\int_{x_a}^{x_b} dx_g B(x_a, x_b, x_g)\frac{8z^2}{r^{3/2}} \times \int_{-\infty}^{\infty} d\omega \frac{\sqrt{2\pi i}}{\sqrt{c_0\omega}} e^{-i\omega\frac{r}{c_0}} D(x_g;\omega). \quad (20)$$

3 Data extrapolation

The data generation is performed by using the calculated image, $\widetilde{\alpha_1}$, as input to equation (8),

$$D(k_{gx};\omega) = 8\pi\frac{1}{k_z^2}\frac{\omega^2}{c_0^2}\widetilde{\alpha_1}(k_z),$$
$$D(x_g;t) = \int dk_{gx}\int d\omega\frac{4k^2}{k_z^2}e^{-i\omega t}\int dz e^{ik_z z}\widetilde{\alpha_1}(z).$$

The integral over k_{gx} is solved by the steepest descents method and a neutralizer. Due to the $1.5D$ assumption, the stationary point is always inside the aperture. Hence,

$$D(x_g;t) = \int dz\int d\omega 4\sqrt{\frac{-2\pi i\omega}{c_0}}e^{-i\omega t_r}\frac{\widetilde{\alpha_1}(z)}{2z}\sqrt{r}, \quad (21)$$

where $t_r = t - \frac{r}{c_0}$, and $t_r > 0$. We use equations (20) and (21) to generate the data shown in the 1.5D examples.

If the data used in this $1.5D$ formulation has a $3D$ source, it is possible to add an extra weight to the solution to obtain a better estimate of the amplitudes in the reconstructed data. The extra weight is usually related with geometrical spreading, and is given by $\frac{4z^2}{r^{3/2}}$. With this weight, the image and the extrapolator are written as:

$$\widetilde{\alpha_1}(z) = \frac{1}{4\pi^2}\frac{1}{x_b - x_a}\int_{x_a}^{x_b} dx_g B(x_a, x_b, x_g)\frac{32z^4}{r^{3/2}} \times \int_{-\infty}^{\infty} d\omega \frac{\sqrt{2\pi i}}{\sqrt{c_0\omega}} e^{-i\omega\frac{r}{c_0}} D(x_g;\omega),$$
$$D(x_g;t) = \int dz\int d\omega 4\sqrt{\frac{-2\pi i\omega}{c_0}}e^{-i\omega t}\frac{\widetilde{\alpha_1}(z)}{2zr}. \quad (22)$$

These equations are used in figure 5, where the data correspond to a single $2D$ line in a $3D$ acquisition.

4 2-D theory

The theory for data extrapolation introduced in the previous sections can be extended to attain the solution of a more realistic problem. Let's start with equation(6) in $3D$,

$$D(x_g, y_g, z_g|x_s, y_s, z_s;\omega) = \int dx\int dy\int dz\ G_0(x_g, y_g, z_g|x, y, z;\omega) \times\ V_1(x, y, z, \omega)G_0(x, y, z|x_s, y_s, z_s;\omega); \quad (23)$$

once more, z_g and z_s are the constant depths of source and receiver, and we are going to write $D(x_g, y_g, z_g|x_s, y_s, z_s; \omega)$ as $D(x_g, y_g|x_s, y_s; \omega)$. Now, assume that V_1 has a similar expression to the one in $2D$ but with lateral variations, *i.e.* $V_1 = k^2\alpha_1(x, y, z)$. Hence,

$$\begin{aligned} D(x_g, y_g|x_s, y_s; \omega) = & \int dx \int dz\ G_0(x_g, y_g, z_g|x, y, z; \omega)k^2\alpha_1(x, y, z) \\ & \times\ G_0(x, y, z|x_s, y_s, z_s; \omega), \\ D(k_{gx}, k_{gy}|k_{sx}, k_{sy}; \omega) = & \frac{sin(q_s z_s)sin(q_g z_g)}{q_g q_s} \int dx \int dy \int dz e^{-i(k_{gx}x+k_{gy}y)} \\ & \times\ e^{iq_g z}\frac{\omega^2}{c_0^2}\alpha_1(x, y, z)e^{i(k_{sx}x+k_{sy}y)}e^{iq_s z}, \end{aligned}$$

and

$$D(k_{gx}, k_{gy}|k_{sx}, k_{sy}; \omega) = \frac{1}{q_g q_s}\frac{\omega^2}{c_0^2}\widetilde{\alpha_1}(k_{gx} - k_{sx}, k_{gy} - k_{sy}, q_g + q_s), \tag{24}$$

$$\tag{25}$$

where

$$\begin{aligned} \widetilde{\alpha_1}(k_{gx} - k_{sx}, k_{gy} - k_{sy}, q_g + q_s) = & \alpha_1(k_{gx} - k_{sx}, k_{gy} - k_{sy}, q_g + q_s) \\ & \times\ sin(q_g z_g)sin(q_s, z_s) \end{aligned} \tag{26}$$

equation(24) is a three dimensional solution of migration/inversion. However, in many practical situations the earth is quasi-$2D$, and the data are collected along $2D$ line(s) with point sources ($2.5D$ problem). Assuming that $\widetilde{\alpha_1}$ is invariant in y direction (perpendicular to the seismic survey line) we may relate the point source to a line source, and use $2D$ theory. Thus, $\widetilde{\alpha_1}(x, y, z) = \widetilde{\alpha_1}(x, z)$, and $\widetilde{\alpha_1}(k_{gx} - k_{sx}, k_{gy} - k_{sy}, q_g + q_s) = 2\pi\delta(k_{gy} - k_{sy})\widetilde{\alpha_1}(k_{gx} - k_{sx}, q_g + q_s)$. Following the results from Stolt and Benson (1986); Wang (1990), the conversion from point source to line source leads to the following compensation,

$$\begin{aligned} D_{2.5}(x_g|x_s; t) &= \sqrt{t}D(x_g|x_s; t), \\ D_{2.5}(k_{gx}|k_{sx}; \omega) &= \sqrt{\frac{-i\omega}{\pi}}\frac{\omega^2}{c_0^3}\frac{\widetilde{\alpha_1}(k_m, k_z)}{q_g q_s}, \end{aligned} \tag{27}$$

where $k_m = k_{gx} - k_{sx}$ is the conjugate of the midpoint coordinate $x_m = \frac{x_g + x_s}{2}$ of the data and of the x coordinate in $\widetilde{\alpha_1}$.

The limited aperture migration/inversion method can be expressed in $2.5D$ as

$$\widetilde{\alpha_1}(k_m, k_z) = \int dk_h L(k_m, k_h, k_z)D(k_{gx}|k_{sx}; \omega), \tag{28}$$

$$\begin{aligned} \widetilde{\alpha_1}(x, z) = & \frac{1}{(2\pi)^2} \int dk_m \int dk_z \int dk_h e^{i(k_m x - k_z z)} L(k_m, k_h, k_z) \\ & \times \int dx_g \int dx_s e^{-i(k_{gx}x_g - k_{sx}x_s)} D(x_g|x_s; \omega), \end{aligned} \tag{29}$$

$$\int dk_h \sqrt{\frac{-i\omega}{2\pi}}\frac{\omega^2}{c_0^2 q_g q_s} L(k_m, k_h, k_z) = 1, \tag{30}$$

where $k_h = k_{gx} + k_{sx}$ is the conjugate of the half offset coordinate $x_h = \frac{x_g - x_s}{2}$.

Changing the order of the integrals and the integration variables from k_m, k_h and k_z to k_{gx}, k_{sx} and ω, respectively, yields

$$\widetilde{\alpha_1}(x,z) = \frac{1}{(2\pi)^2}\int dx_g \int dx_s \int d\omega I(x,z|x_g,x_s,\omega)D(x_g|x_s;\omega) \tag{31}$$

$$I(x,z|x_g,x_s,\omega) = \int dk_g \int dk_s e^{ik_{gx}(x-x_g)}e^{ik_z z}e^{-ik_{sx}(x_s-x)}\frac{\omega k_z L(k_m,k_h,k_z)}{c_0^2 q_g q_s}. \tag{32}$$

We use the stationary phase approximation to solve equation(32),

$$I(x,z|x_g,x_s,\omega) = \int_a^b dk_g e^{ig(k_{gx})}\int dk_s e^{ih(k_{sx})}f(k_{gx},k_{sx}); \tag{33}$$

$$g'(k_{gx0}) = h'(k_{sx0})0,\ g''(k_{gx0}) \neq 0,$$

$$h''(k_{sx0}) \neq 0,\ a < k_{gx0} < b;\ a < k_{sx0} < b;$$

$$I(x,z|x_g,x_s,\omega) = \sqrt{\frac{2\pi i}{g''(k_{gx0})}}\sqrt{\frac{2\pi i}{h''(k_{sx0})}}f(k_{gx0},k_{sx0})e^{i(g(k_{gx0}+h(k_{sx0})}; \tag{34}$$

where

$$k_{gx0} = \frac{\omega}{c_0}\frac{x_g - x}{r_g}, \qquad r_g = \sqrt{z^2 + (x_g - x)^2},$$

$$k_{sx0} = \frac{\omega}{c_0}\frac{x - x_s}{r_s}, \qquad r_g = \sqrt{z^2 + (x - x_s)^2}.$$

Thus,

$$I(x,z|x_g,x_s,\omega) = \frac{2\pi i z^2}{c_0^2}\frac{r_g + r_s}{r_g^{3/2} r_s^{3/2}}L(k_{m0},k_{h0},k_z), \tag{35}$$

where $k_{m0} = k_{gx0} - k_{sx0}$ and $k_{h0} = k_{gx0} + k_{sx0}$.

In agreement with the previous calculations, we define the arbitrary weight function to have a geometrical part related with the aperture in $2D$, and we separate space variables from frequency at the stationary points k_{gx0} and k_{sx0},

$$L(k_m,k_h,k_z) = B(h_a,h_b,x_g - x_s)S(\eta,\beta)F(\omega), \tag{36}$$

$$\beta = \frac{k_h}{k_z},\ \eta = \frac{k_m}{kz}$$

$$\int d\beta\sqrt{\frac{-i\omega}{\pi}}\frac{\omega^2}{c_0^3 q_g q_s}B(h_a,h_b,x_g - x_s)S(\eta,\beta)F(\omega) = 1, \tag{37}$$

where h_a and h_b represent offset coordinates at the limits of the aperture, $h_a = \frac{x_{ga} - x_{sa}}{2}$ and $h_b = \frac{x_{gb} - x_{sb}}{2}$.

Introducing a neutralizer,

$$B(h_a,h_b,x_g - x_s) = \begin{cases} 1 & \text{if } \frac{x_g - x_s}{2} \in (h_a,h_b) \\ \\ 0 & \text{, otherwise,} \end{cases} \tag{38}$$

and evaluating the variables β and η at the stationary points,

$$\beta_0 = \frac{(x_g - x)r_s + xr_g}{2r};\ r = r_g + r_s; \tag{39}$$

$$\eta_0 = \frac{(x_g - x)r_s - xr_g}{2r}; \tag{40}$$

$$h = \frac{x_g - x_s}{2} = z\beta\frac{1+\eta^2}{1-\eta^2\beta^2}, \tag{41}$$

we find,

$$\int_{\beta_a}^{\beta_b} d\beta\sqrt{\frac{-i\omega}{\pi}}\frac{\omega^2}{c_0^3 q_g q_s}S(\eta,\beta)F(\omega) = 1, \tag{42}$$

where,

$$\beta_i = \frac{\sqrt{(1+\eta_0^2)^2 + 4\eta_0^2 h^2/z^2} - (1+\eta_0^2)^2}{2\eta_0 h/z}, \tag{43}$$

i.e. the limits of the integral are evaluated at the boundaries of the aperture described by the neutralizer. Finally,

$$\widetilde{\alpha_1}(x,z) = \frac{-2\sqrt{2}z}{(2\pi)^2}\int_{x_{sa}}^{x_{sb}} dx_s \int_{x_s+2h_a}^{x_s+2h_b} dx_g \frac{r_g + r_s}{(r_g r_s)^{3/2}}\frac{1-\eta_0^2\beta_0^2}{\sqrt{1+\eta_0^2}\sqrt{1+\beta_0^2}}\frac{1}{\beta_a - \beta_b}$$
$$\times \int_{-\infty}^{\infty} d\omega \frac{e^{-\frac{3\pi}{4}-\omega t}}{\sqrt{2\pi\omega}} D(x_g, x_s, \omega), \tag{44}$$

is the limited aperture image of the data in $2.5D$. The extrapolation of the data is done by introducting $\widetilde{\alpha_1}$ into equation (24) and performing the appropriate Fourier transforms to bring the data back to space and time domain. It is also possible to use the stationary phase approximation to solve either the integral over ω or the integrals over k_{gx} and k_{sx}.

5 A single shot approximation

Dapeng Wang (1990) shows a method to find the limit of the finite aperture migration/inversion when the aperture is reduce to a single trace. Using reciprocity principles, we are going to use his idea to find the limit of $\widetilde{\alpha_1}(x,z)$ when the aperture of the data reduces to a single shot. We first, change the order of the integrals in equation (44),

$$\widetilde{\alpha_1}(x,z) = \frac{-2\sqrt{2}z}{(2\pi)^2}\int_{x_{ga}}^{x_{gb}} dx_g \frac{1}{r_g^{3/2}} \int_{x_g-2h_a}^{x_g-2h_b} dx_s \frac{r_g + r_s}{(r_s)^{3/2}}\frac{1-\eta_0^2\beta_0^2}{\sqrt{1+\eta_0^2}\sqrt{1+\beta_0^2}}\frac{1}{\beta_a - \beta_b}$$
$$\times \int_{-\infty}^{\infty} d\omega \frac{e^{-\frac{3\pi}{4}-\omega t}}{\sqrt{2\pi\omega}} D(x_g, x_s, \omega), \tag{45}$$

and take the *limit* of $x_s \to 0$, so that

$$lim|_{x_s\to 0}(\widetilde{\alpha_1}(x,z)) = \frac{-2\sqrt{2}z}{(2\pi)^2}\int_{x_{ga}}^{x_{gb}} dx_g \frac{r_g + r_s|_{x_s\to 0}}{(r_g r_s|_{x_s\to 0})^{3/2}}\frac{1-\eta_0^2|_{x_s\to 0}\beta_0^2|_{x_s\to 0}}{\sqrt{1+\eta_0^2|_{x_s\to 0}}\sqrt{1+\beta_0^2|_{x_s\to 0}}}$$
$$\times \frac{\triangle x_s \to 0}{\beta_a - \beta_b}\int_{-\infty}^{\infty} d\omega \frac{e^{-\frac{3\pi}{4}-\omega t}}{\sqrt{2\pi\omega}} D(x_g, x_s \to 0, \omega), \tag{46}$$

at the limit

$$\frac{\triangle x_s \to 0}{\beta_a - \beta_b} \to \frac{\partial x_s}{\partial \beta}$$
$$\frac{\partial x_s}{\partial \beta} = \frac{z r_s r^2}{(x^2 - x(x_g - x))r_g - r_g r_s r}. \tag{47}$$

The limited aperture image of the data for a single shot is given by

$$\begin{aligned}
\widetilde{\alpha_1}(x,z)|_{x_s=0} &= \int_{x_{ga}}^{x_{gb}} dx_g \frac{r}{(r_g r_s)^{3/2}} \frac{1-\eta_0^2\beta_0^2}{\sqrt{1+\eta_0^2}\sqrt{1+\beta_0^2}} \frac{z r_s r^2}{(-x(x_g-x)+x^2)r_g - r_g r_s r} \\
&\times \frac{-2\sqrt{2}z}{(2\pi)^2} \int_{-\infty}^{\infty} d\omega \frac{e^{-\frac{3\pi}{4}-\omega t}}{\sqrt{2\pi\omega}} D(x_g, x_s, \omega), \\
\widetilde{\alpha_1}(x,z)|_{x_s=0} &= \int_{x_{ga}}^{x_{gb}} dx_g \frac{r^3}{(r_g r_s)^{3/2}} \frac{\sqrt{1+\eta_0^2}\beta_0}{h\sqrt{1+\beta_0^2}} \frac{1}{(-x(x_g-x)+x^2)r_g - r_g r_s r} \\
&\times \frac{-2\sqrt{2}z^3}{(2\pi)^2} \int_{-\infty}^{\infty} d\omega \frac{e^{-\frac{3\pi}{4}-\omega t}}{\sqrt{2\pi\omega}} D(x_g, x_s, \omega).
\end{aligned} \tag{48}$$

The single shot approximation requires much less computational effort than the full $2.5D$ version presented in the previous section. It is a significant cost saving, allowing to compute each shot independently. Using a single shot per $2D$ line makes the extrapolation process become less expensive. Plus, it preserves the wavelet's shape (for a given shot) in the reconstructed traces.

6 Numerical Examples

In this section we present three numerical examples to test the $1.5D$ theory. Figure 3 shows a simple deep water test. The first reflector is at $500m$. The background velocity is $1500m/s$, and the the first layer's velocity $4000m/s$. The synthetic data are shown on the left, the r.h.s. shows the reconstructed near offsets ($0m$-$200m$.) using an aperture of 25 traces and receiver separation of $12.5m$. The result shows excellent agreement in amplitude, time and shape between the reconstructed traces and the original synthetic data.

A synthetic shallow water dataset is shown on the left of figure 4. The first reflector is at $100m$ and the second is at $310m$. The background velocity is $1500m/s$, the velocity in the second layer is $2850m/s$ and $6500m/s$ for the third layer. The data contain ghosts, headwaves, primaries and multiples. The data on the right show reconstructed near offsets ($0m$-$187.5m$) using an aperture of 15 traces. The results are accurate in time, but amplitudes are less accurate.

The example in figure 5, uses equations (22) where the data correspond to a single $2D$ line in a $3D$ acquisition. The left half of the figure is the data with the reconstructed near offsets using the $1.5D$ algorithm with geometrical weight, equations (22). The right half displays the original data. We observe that the prediction down to $1s$ is accurate. This is because the first reflectors that generate these data are laterally invariant and within the assumptions of the prediction formulas.

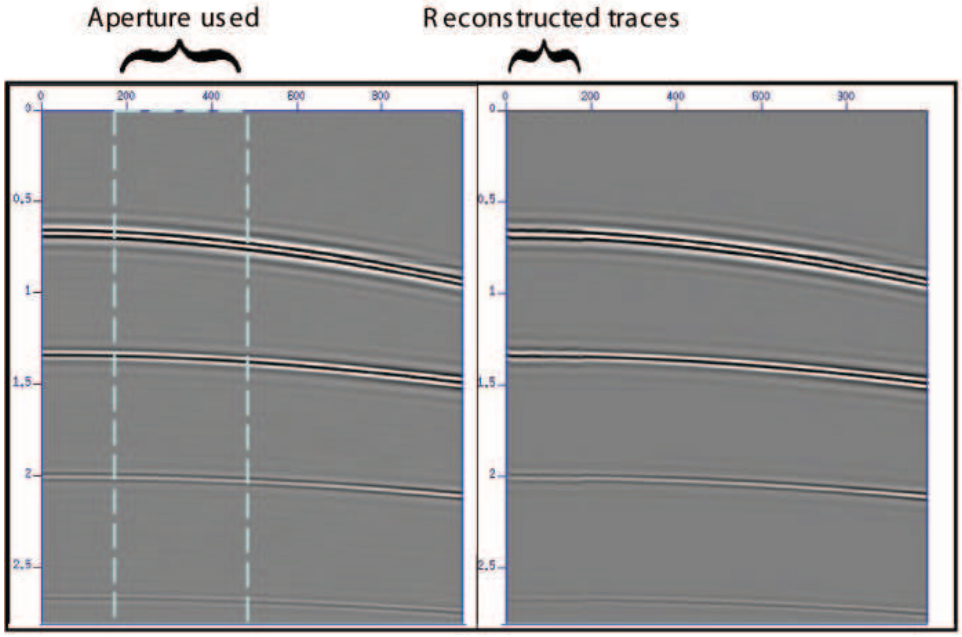

Figure 3: Deep water example.

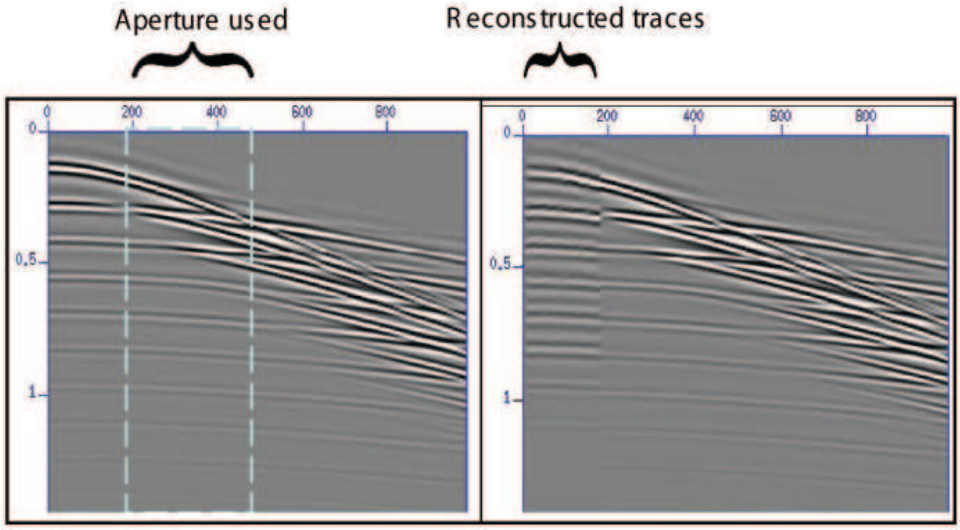

Figure 4: Shallow water example.

7 Conclusions

One of the most challenging problems in marine exploration is incomplete data coverage. In particular the problem of missing data at near offsets. Data extrapolation with the first inverse equation does not require *a priori* subsurface information, nor any preprocessing. Using V_1 gives an exact mathematical expression, while V leads to an approximation that is not a good estimate for either

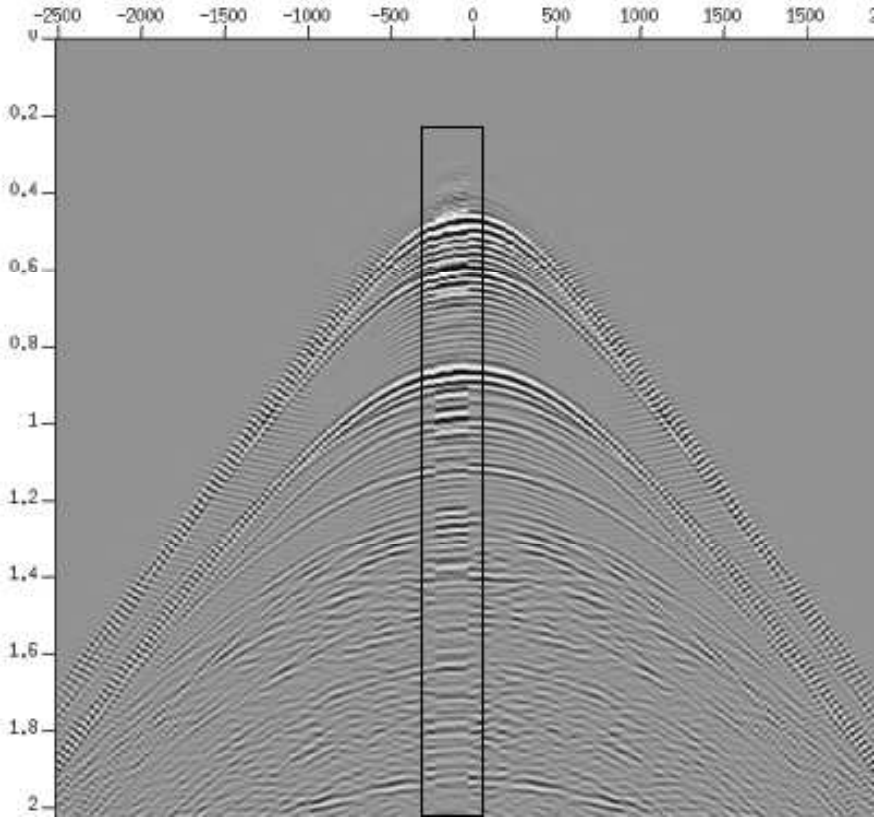

Figure 5: The reconstructed near offsets (using $1.5D$ method with extra weighting) are displayed within the rectangle.

primaries or multiples.

The near-offset reconstruction method presented in this work, uses only the first inverse equation. It is not a subseries of the inverse scattering series and it does not require any preprocessing. The first inverse equation gives a mathematical framework for data reconstruction because it represents an exact data mapping with no other assumptions. If we relax the interpretation of aperture migration as an earth property inversion and allow it to be the factor that sitting between two G_0's predicts all of your data; then having that factor we can evaluate the G_0's at the locations where the data were not measured and reconstruct it.

With the single shot approximation, the computational time and cost become negligible. It lowers the requirements and mathematically preserves the shape of the reconstructed traces with the raw data in each shot record. But, as an approximation it may lead to a less accurate prediction when the data comes from a more complex geology. This approximation is justified given moderate dips and refractors. Further testing needs to be done.

The full $2.5D$ data reconstruction method is being tested and extensions to $3D$ are being developed.

8 Acknowledgements

We would like to thank Statoil for the permission to publish this work. The first author acknowledges Statoil for the opportunity to work in this project, and thanks Roger Sollie and Einar Otnes for their encouragement of this research.

References

A. Baumstein. 3d inverse shot record dmo: A tool for shot-domain data regularization. *SEG Expanded Abstracts*, pages 2001–2004, 2004.

N. Bleistein and R. Handelsman. *Asymptotic expansions of integrals*. Dover, 2nd edition, 1986.

D. Hale. Dip-moveout by fourier transform. *Geophysics*, 49:741–757, 1984.

P. Krail and Y. Shin. Deconvolution of a directional marine source. *Geophysics*, 55:1542–1548, 1990.

R. H. Stolt. Seismic data mapping and reconstruction. *Geophysics*, 67:890–908, 2002.

R. H. Stolt and A. Benson. *Seismic migration*. Geophysical Press, 1986.

J. Sun. Limited-aperture migration. *Geophysics*, 65:584–593, 2002.

D. Wang. *Recovery of zero offset reflectivity from constant velocity aperture-compensated migration/inversion method*. PhD thesis, Univ. of Wyoming, 1990.

A. B. Weglein, F. V. Araujo, P. M. Carvalho, R. H. Stolt, K. H. Matson, R. T. Coates, D. Corrigan, D. J. Foster, S. A. Shaw, and H. Zhang. Topical review: Inverse scattering series and seismic exploration. *Inverse Problems*, 19:27–83, 2003.

A. B. Weglein, W. E. Boyse, and J. E. Anderson. Obtaining three-dimensional velocity information directly from reflection seismic data: an inverse scattering formalism. *Geophysics*, 46:1116–1120, 1981.

Application of the extinction theorem deghosting method to ocean bottom data

Jingfeng Zhang and Arthur B. Weglein

Abstract

As one of the pre-requisites for multiple removal, imaging and inversion, the effectiveness of deghosting affects the performance of its followed operations. The Extinction Theorem based deghosting method has been successfully applied on towed streamer data in last year's annual report. In that paper, the deghosted data were then processed using the inverse scattering series (ISS) free surface multiple removal (FSMR) algorithm, and it was shown that using deghosted data and the source wavelet, the ISS FSMR can predict the free surface multiples accurately both in time and amplitude. Thus, the ISS FSMR algorithm with appropriate wavelet and deghosting directly predicts and subtracts the free surface multiples without the need of adaptive subtraction. In practice, this will mitigate the need for adaptive subtraction; and its sometimes harmful application that can run at cross purposes to the underlying strength of the ISS FSMR method. In this paper, we apply the same deghosting algorithm on ocean bottom data. With source wavelet available, only pressure measurements have been used in the process of deghosting and this avoids the need for the troublesome vertical velocity measurements. Initial tests show that the deghosting results agree very well with the exact results calculated using the Cagniard-de Hoop method.

1 Introduction

In seismic exploration, a common sequence of data processing is source wavelet estimation, deghosting, free surface multiple removal, internal multiple removal, imaging and inversion. This sequence of processing steps is like a chain of tasks in the sense that the performance of the later operations could be affected by the former ones. As one of the pre-requisites for imaging and inversion, deghosting has received more and more attention recently. Part of the reason is that more and/or better information are expected to be extracted from the data at every processing stage (free surface and internal multiple removal, imaging and inversion). Deghosting could affect (sometimes critically) the performance of the above mentioned procedures. For example, deghosting is one of the pre-requisites for free surface multiple removal. Using adaptive subtraction, there are many situations where free surface multiple removal algorithm works well without deghosting. But for complex media, where severe overlapping can happen between primaries and multiples and adaptive subtraction has a difficult time, better prediction of multiples is very important and can be achieved using deghosted data. Also, ghost effects are angle dependent and thus, inversion such as AVO could be affected by ghost events. For some recently developed processing techniques such as imaging with reference medium velocity (e.g., Weglein et al., 2000, Shaw et al., 2003, Liu et al., 2005 and Innanen, 2005) and nonlinear inversion (Zhang and Weglein, 2005a), deghosting is a crucial step since those algorithms assume the data is fully deghosted and put a very high bar on the data quality.

The deghosting algorithm we derived is based on Green's/Extinction theorem and was firstly given by Weglein et al.(2002). We tested it on towed streamer data last year (Zhang and Weglein, 2005b)

and very good deghosting results were obtained. The deghosted data was then put into the ISS FSMR algorithm (Carvalho, 1992 and Weglein et al., 1997 and 2003) and accurate prediction of free surface multiples was obtained. Then the free surface multiples in the data were eliminated through a trivial subtraction instead of adaptive subtraction.

This year we test its application on ocean bottom data. Unlike the towed streamer case, point receivers are usually used on ocean bottom. So we don't need to test the receiver array effect. The deghosted results are compared with the exact one which is calculated using Cagniard-de Hoop method. Initial tests show that very good results can be obtained. We will not show the ISS FSMR results in this paper. But we would like to point out that the direct application of some surface multiple methods (e.g., Verschuur, 1991) on ocean bottom data will cause the predicted free surface multiple not having the correct arrival time, unless a separate data extrapolation has been performed on the seismic data in advance. The details will be discussed in the following sections.

In the next section, a brief review of the deghosting theory is provided. Then, numerical tests and acknowledgements are given.

2 Theory

Motivations and different methods about deghosting have been extensively discussed in literature (e.g., Schneider, 1964; Robertsson and Kragh, 2002; Weglein et al., 2002 and Amundsen et al., 2005). The deghosting method we used in this paper is firstly provided in Weglein et al., (2002). The receiver side deghosting formula is:

$$P^{\mathrm{up}}(\mathbf{r},\mathbf{r}_s,\omega)=\int\limits_{MS}\Big(P(\mathbf{r}',\mathbf{r}_s,\omega)\frac{\partial G_0^+(\mathbf{r},\mathbf{r}',\omega)}{\partial z'}-G_0^+(\mathbf{r},\mathbf{r}',\omega)\frac{\partial P(\mathbf{r}',\mathbf{r}_s,\omega)}{\partial z'}\Big)d\mathbf{S}'. \tag{1}$$

A similar operation performed on the source side removes the source side ghosts. Clearly, we need both the wave field and its vertical derivative to perform deghosting. With ocean bottom data, both measurements are available. However, there are several reasons not to directly use both measurements in Eq.1. The first reason is the different instrument response factor. On ocean bottom, the pressure/wavefield and its vertical derivative are measured by hydrophone and geophone respectively. Usually the instrument response factors of the two kinds of equipment are different. To achieve better processing results such as the integration in Eq.1, it is necessary to calibrate the two response factors which is not an easy task. The second reason is that the vertical derivative of the measurements can be inaccurate due to the loose attachment of the geophone to the ocean bottom. The last reason is that geophone measurements are usually very noisy. In this paper, we calculate the vertical derivative of the wavefield using the triangle relationship among the source wavelet $A(\omega)$, wavefield (P) and its vertical derivative ($\frac{dP}{dz}$) in the frequency-wavenumber domain (Weglein and Secrest, 1990 and Amundsen, 2001):

$$\frac{dP(k_x,z',x_s,z_s,\omega)}{dz} = \frac{A(\omega)e^{ik_xx_s}(e^{-ik_zz_s}-e^{ik_zz_s})}{e^{-ik_zz'}-e^{ik_zz'}}-ik_zP(k_x,z',x_s,z_s,\omega)\frac{e^{-ik_zz'}+e^{ik_zz'}}{e^{-ik_zz'}-e^{ik_zz'}}, \tag{2}$$

where $k_z=\sqrt{k^2-k_x^2}$. The advantage of this method is that the obtained $\frac{dP}{dz}$ will naturally have the same instrument response factor as P, as long as the source wavelet ($A(\omega)$) is obtained from methods based on hydrophone measurements.

The disadvantage of using Eq.2 is the unstable spectral division. Whenever the denomenator approaches zero, the numerical division is usually unstable. For large cable depths, i.e., big z', the denomenator is often zero. In our numerical calculation, we only calculate the values of $\frac{dP(k_x,z',x_s,z_s,\omega)}{dz}$ at those k_x where the absolute value of the denomenator is far from zero (e.g., > 0.3). Then the values of $\frac{dP(k_x,z',x_s,z_s,\omega)}{dz}$ at those unstable points will be interpolated using cubic spline interpolation. As shown in the next section, the initial results are satisfactory, but there are still some artifacts that need to be removed. How these artifacts are removed/attenuated is the subject of future work.

3 Numerical tests

The numerical tests are based on a simple 1D acoustic model. Using the Cagniard-de Hoop method, we generate synthetic data for the model in Fig.1. The source wavelet is a Ricker wavelet. The advantage of the Cagniard-de Hoop method is that we can accurately calculate any specific event we are interested in so that we can compare it with the results predicted by our deghosting algorithms.

In Fig.2, we illustrate the primary, its ghosts, and their summation. Apparently, the summation of these events are very different than the primary. Most importantly, the receiver ghost and the source-receiver ghost arrive significantly later than the primary and its source ghost, due to the big depth of the receivers. Let's explain in detail each event in Fig.3. The direct wave (Event (a)) arrives at exactly the same time as the primary (Event (b)). The only difference is that the former one does not hit the earth while the latter one hits the earth first then is recorded by the hydrophone. Similarly, the receiver ghost of the primary (Event (c)) arrives exactly at the same time as the first order free surface multiple (Event (d)) and the source-receiver ghost of the primay (Event (e)) arrives exactly at the same time as the source ghost of the first order free surface multiple (Event (f)).

If we simply convolve the ocean bottom data with itself to predict free surface multiples, the arrival time of the predicted first order free surface multiple will be *very* different from the actual one. So a separate data extrapolation operation to move the data from ocean bottom to the free surface is needed in order to ensure that the predicted free surface multiple has approximately the right arrival time. This step is performed naturally in the inverse scattering series based free surface multiple removal method.

In the following, we will present the receiver side deghosted result for the data that contain only primary and its ghosts. The data that contain direct wave and surface multiple events will be tested in the future.

In Fig.4, the deghosting results at four offsets are compared with the exact deghosting results and the data before deghosting. After receiver side deghosting the later event has been removed while the earlier events (primary and its source ghost) are kept. The source ghost can be further removed by a source side deghosting and the test is currently underway. There are two possible reasons for the artifacts in Fig.4 (e.g., at around 0.1s in (a)). The first one is due to the spectrum division in Eq. 2 which generates some errors. The other one is the error introduced because of limited aperture in the Fourier transform over space.

4 Conclusions

Using an Extinction theorem based deghosting algorithm, we have performed receiver side deghosting on ocean bottom data. Instead of requiring the difficult to accurately measure vertical derivative of the wavefield, it is calculated through the triangle relationship using the source wavelet and the pressure wavefield. The results are encouraging and further data tests and comparisons are underway.

5 Acknowledgements

We thank M-OSRP colleagues Kristopher A. Innanen and Fang Liu for helpful discussions. Adriana Ramirez, Haiyan Zhang and Sam Kaplan are thanked for their help in preparing this report. We are grateful to the support from the sponsors of M-OSRP. We have been partially funded by and are grateful for NSF-CMG award DMS-0327778 and DOE Basic Sciences award DE-FG02-05ER15697.

References

L. Amundsen. Elimination of free-surface related multiples without need of the source wavelet. *Geophysics*, 66:327–341, 2001.

L. Amundsen. Rough-sea deghosting of streamer seismic data using pressure gradient approximations. *Geophysics*, 50, 2005.

P. M. Carvalho. *Free-surface multiple reflection eliminatioin method based on nonlinear inversion of seismic data*. PhD thesis, Universidade Federal da Bahia, 1992.

K. A. Innanen and A. B. Weglein. Simultaneous imaging and inversion with the inverse scattering series. In *Proceedings of the Eighth International Congress of the SBGf and Fifth Latin American Geophysical Conference*, 2003.

F. Liu, B. G. Nita A. B. Weglein, and K. A. Innanen. Inverse scattering series for vertically and laterally varying media: application to velocity independent depth imaging. In *M-OSRP Annual Report*, 2005.

A. C. Ramírez and A. B. Weglein. An inverse scattering internal multiple elimination method: beyond attenuation, a new algorithm and initial tests. In *75th Ann. Internat. Mtg. Soc. Expl. Geophys.*, 2005.

Robertsson and Kragh. Rough sea deghosting uing a single streamer and a pressure gradient approximation. *Geophysics*, 67(5):783–805, 2002.

W. A. Schneider, K. L. Larner, J. P. Burg, and M. M. Backus. A new data processing technique for the elimination of ghost arrivals on reflection seismograms. *Geophysics*, 29(5):783–805, 1964.

S. A. Shaw, A. B. Weglein, D. J. Foster, K. H. Matson, and R. G. Keys. Isolation of a leading order depth imaging series and analysis of its convergence properties. In *M-OSRP Annual Report*, pages 157–195, 2003.

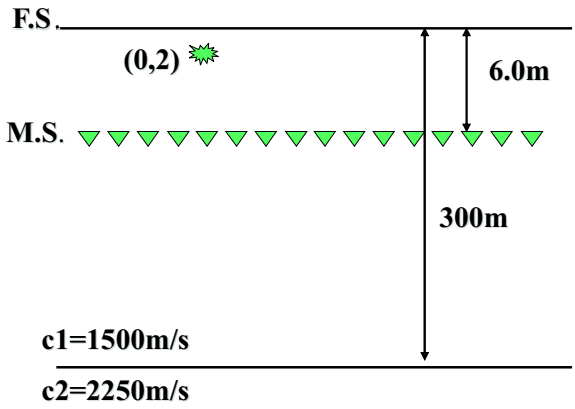

Figure 1: One dimensional acoustic constant density medium.

D. J. Verschuur. *Surface-related multiple elimination: an inversion approach*. PhD thesis, Delft University of Technology, 1991.

A. B. Weglein, K. H. Matson, D. J. Foster, P. M. Carvalho, D. Corrigan, and S. A. Shaw. Imaging and inversion at depth without a velocity model. In *70th SEG abstract*.

Arthur B. Weglein, Fernanda V. Araújo, Paulo M. Carvalho, Robert H. Stolt, Kenneth H. Matson, Richard T. Coats, Dennis Corrigan, Douglas J. Foster, Simon A. Shaw, and Haiyan Zhang. Inverse scattering series and seismic exploration. *Inverse Problems*, (19):R27–R83, 2003.

Arthur B. Weglein, Fernanda Araújo Gasparotto, Paulo M. Carvalho, and Robert H. Stolt. An inverse-scattering series method for attenuating multiples in seismic reflection data. *Geophysics*, 62(6):1975–1989, November-December 1997.

H. Zhang and A. B. Weglein. The inverse scattering series for tasks associated with primaries: depth imaging and direct non-linear inversion of 1d variable velocity and density acoustic media. In *75th Ann. Internat. Mtg. Soc. Expl. Geophys., Expanded Abstracts*, pages 1705–1708, 2005a.

Jingfeng Zhang and Arthur B. Weglein. Extinction theorem deghosting method using towed streamer pressure data: Analysis of the receiver array effect on deghosting and subsequent free surface multiple removal. In *SEG/Houston 2005 Annual Meeting*, pages 2095–2100, 2005b.

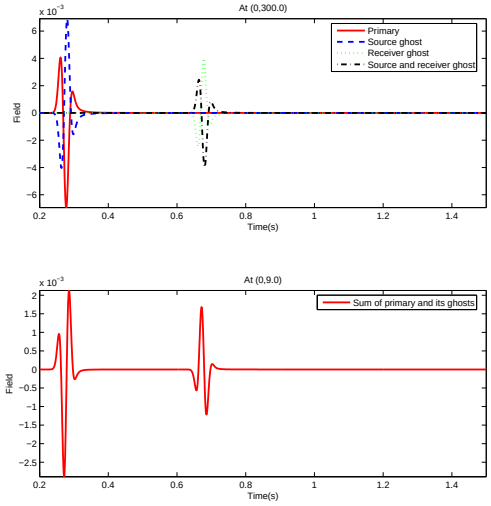

Figure 2: Top: Each specific event; Bottom: The summation of each event.

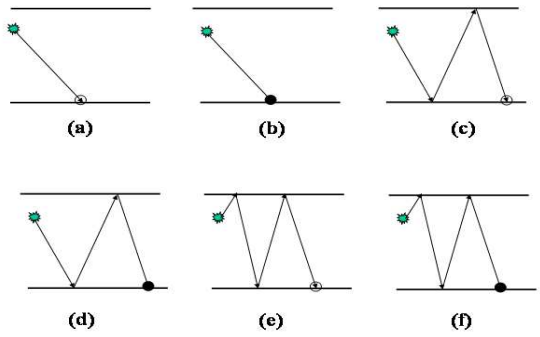

Figure 3: Empty circle means the wave does not hit the earth and solid circle means the wave hit the earth and then reflected upward and recorded by the receiver. (a): The direct wave; (b) The primary; (c) The receiver ghost of the primary; (d) The first order free surface multiple; (e) The source-receiver ghost of the primary and (f) The source ghost of the first order free surface multiple.

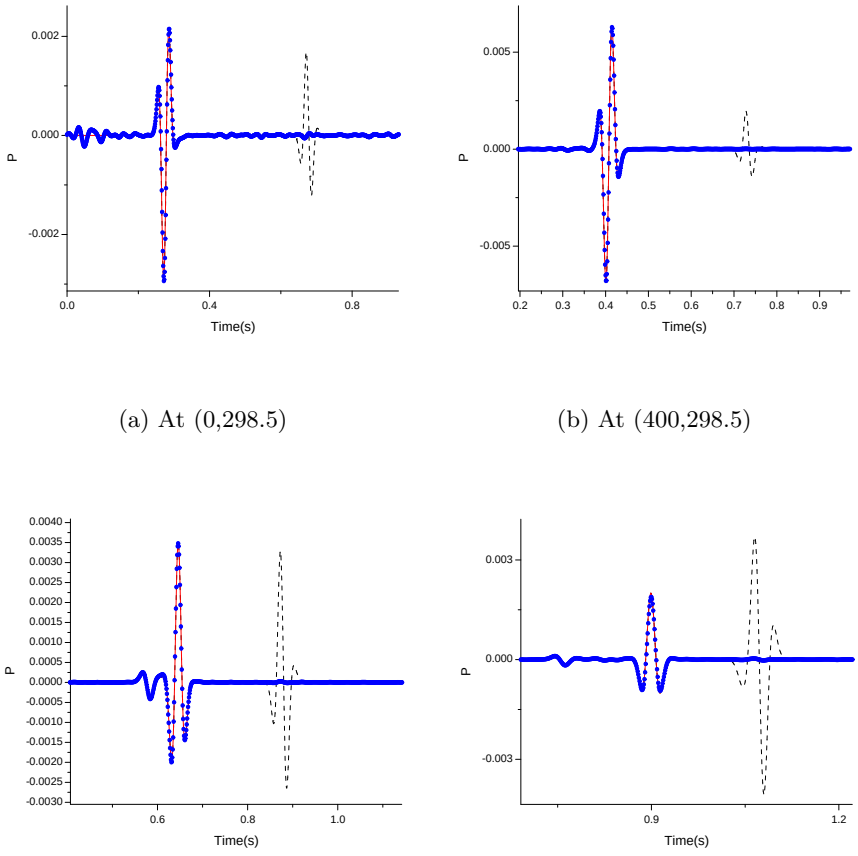

(a) At (0,298.5)

(b) At (400,298.5)

(c) At (800,298.5)

(d) At (1200,298.5)

Figure 4: Red solid: Exact receiver side deghosted results; Blue dots: Calculated deghosting results; Black dash: Total data before deghosting.

Forward scattering series for 2-parameter acoustic media: analysis and implications to the inverse scattering task specific subseries

Adriana Citlali Ramírez* and Einar Otnes †
*M-OSRP. Dept. of Physics, University of Houston, 77204-5005, USA
†Statoil Research Center, N-7005 Trondheim, Norway.

Abstract

We study the 2-parameter acoustic Born series for an actual medium with constant velocity and a density distribution. Using a homogeneous background we define a perturbation, the difference between actual and reference medium*, which exhibits an anisotropic behavior due to the density distribution. For an actual medium with a constant velocity, the reference velocity can be selected so that the waves in the actual medium travel with the same speed as the waves in the background medium. Scattering theory decomposes the actual wave field into an infinite series where each term contains the perturbation and the propagators in the background medium. Hence, in this formalism, all propagations occur in the background medium and the actual medium is included only through the perturbations, which scatters the propagating waves. The density-only perturbation has an isotropic and an anisotropic component. The anisotropic component is dependent on the incident direction of the propagating waves and behaves as a *purposeful perturbation* in the sense that it annihilates the part of the Born series that acts to correct the time to build the actual wave field, an unnecessary activity when the reference velocity is equal to the one in the actual medium. This means that the forward series is not attempting to correct for an issue that does not exist. We define the purposeful perturbation concept as the intrinsic knowledge of precisely what a given term is designed to accomplish. This is a remarkable behavior for a formalism that predicts the scattered wave field with an infinite series. At each order of approximation the output of the series is consistent with the fact that the time is correct because the velocity is always constant. In the density-only perturbation, the forward series only seeks to predict the correct amplitudes. Finally, we extend the analysis to a wave propagating in a medium where both density and velocity change. By selecting a convenient set of parameters, we find a conceptual framework for the multiparameter Born series. This framework provides an insightful analysis that can be mapped and applied to the concepts and algorithms of the inverse scattering series.

1 Introduction

In recent years, the inverse scattering series has proven to be a good framework for solving the free surface and internal multiple problem from surface seismic (Weglein et al., 1981, 1997) without the need for a velocity model. Recently, the inverse scattering series has given results which indicate that it can also be a good framework for doing imaging and inversion without a velocity model (Weglein et al., 2003; Shaw, 2005; Liu et al., 2005b,a; Zhang and Weglein, 2005). Shaw (2005) showed that a 1D earth can be imaged without the velocity model. Later, Liu et al. (2005b)

This work was done while working as a visiting faculty at M-OSRP, Dept. of Physics, University of Houston, in 2004.

*We use *background medium* and *reference medium* interchangeably. No distinction is intended between them.

showed some early examples where the inverse scattering series is also able to image a 2D earth without the velocity model.

In the above references, it is assumed that the inverse scattering series can be divided into different subseries, where each subseries is responsible for solving a single task of the inverse problem (Weglein et al., 2003). These single tasks are divided into the tasks which are common in standard seismic processing workflow:

- Free surface multiple removal
- Internal multiple removal
- Imaging
- Inversion for earth parameters

In addition, the inverse scattering series will contain terms that contribute to solve more than a single task. These terms are omitted in the framework suggested by Weglein et al. (2003).

In this paper we study the forward scattering series (also known as Born or Neumann series) in order to identify or shed light on which terms in the inverse scattering series are important for doing imaging. Matson (1996) showed analytically for the 1D one parameter acoustic wave equation the validity of the ideas and concepts introduced by Weglein et al. (1981, 1997, 2003) and used in the developent of inverse scattering processing methods (see for example Weglein et al. (2003)). The mathematical analysis and study of the forward series and its relation with seismic events was revisited by Nita et al. (2004) and by Innanen and Weglein (2003), the latter work included absorption and velocity changes in the transmission analysis of the forward series. We will extend Matson's original analysis by studying how the forward scattering series builds up the solution of the two parameter acoustic wave equation from a homogenous background. We will see that the terms containing a velocity perturbation are the terms that contribute to construct the correct time for the wave traveling in the actual medium.

The density perturbation will only contribute to building up the correct amplitude response of the actual wave field.

In the first section, we introduce the Lippmann-Schwinger equation and the forward scattering series used in this paper, which is constructed from the two-parameter acoustic wave equation. It also gives an introduction to how we choose to interpret each term in the series.

In the second section, we study the simple case of a 1D acoustic medium where only density changes. We show that the forward series does not calculate terms contributing to correcting the time of the actual wave field. Then, we extend the analysis to allow for an actual medium in which both parameters, velocity and density, change. In this case, we identify a special parametrization which helps us in interpreting the tasks of each term in the forward series. Hence, it is important to note that the interpretation of the tasks which each term in the forward series does is dependent of the choice of parameters used.

In the last part of this work, we present an analysis of the framework introduced in the first two sections. The relations between the forward and inverse scattering series are studied. Even if these two series have completely different tasks to solve, symmetry relations between them can be

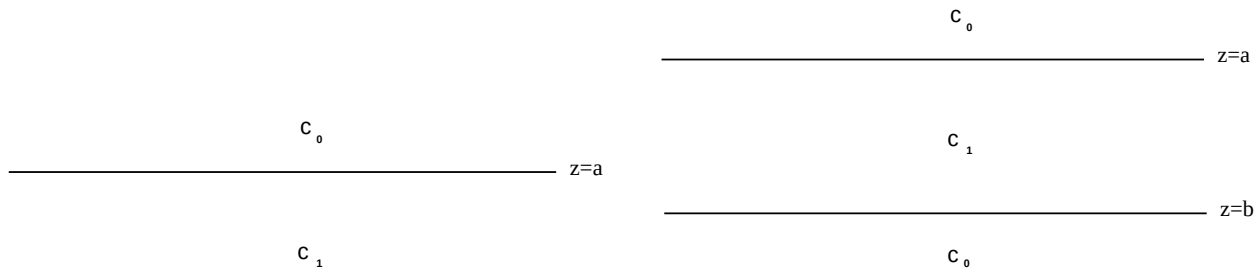

(a) Half space (b) One Layer

Figure 1: The Figure displays the two models used by Matson (1996).

found. Both the forward and the inverse series can be written as a sum of diagrams, i.e. Feynman diagrams. By studying the series and its diagrams it is found that the time corrector diagrams, which resembles a transmission-like event, in the forward series correspond with the depth corrector diagrams in the inverse scattering series. In addition, it is found that diagrams that resemble a reflection like event in forward series correspond to a self-interaction like diagram in the inverse series. Both these diagrams are responsible for correcting the amplitudes of the actual wave field or the medium properties, respectively. It is also found that both forward and inverse series utilizes the concept of purposeful perturbation, i.e. that the series know a priori that there is no series to sum if the task is not required. Each term in the task-specific subseries returns zero.

In the concluding section we sum up the results obtained throughout the paper.

2 The Lippmann-Schwinger equation

The purpose of forward scattering series is to find the wave field produced by a localized source and propagated through a certain medium. The forward series constructs the solution by adding an infinite number of terms, each one corresponding to propagations in the reference medium separated by different orders of scattering interactions with a point scatterer earth model.

We present a brief background to scattering theory and forward scattering series, following the development provided in Stolt and Weglein (1985); Matson (1996, 1997); Innanen and Weglein (2003); Nita et al. (2004) wherein further detail, contributors and references can be found.

A simple, yet insightful, problem to consider is scattering from a half space where only the velocity is allowed to change, like the one shown in Fig.1a. This model has been studied by Matson (1996, 1997) and Nita et al. (2004), and led to a clear comprehension of the unique properties in the formulation of the forward series that can be used to understand and work with the inverse scattering series and its subseries. We want to build a similar understanding by considering another simple case in scattering theory: scattering from a half space where only the density is allowed to change. We then extend this analysis to a change in both, density and velocity.

For a model with velocity and density distributions, Fig.2, which are constant over intervals and

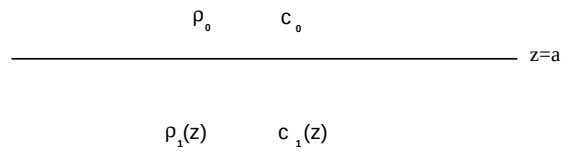

Figure 2: Model with a velocity and density distributions.

discontinuous at the interval boundaries, the actual medium satisfies the acoustic wave equation,

$$\left(\nabla \cdot \frac{1}{\rho(\boldsymbol{x})}\nabla + \frac{\omega^2}{\rho(\boldsymbol{x})c^2(\boldsymbol{x})}\right) P(\boldsymbol{x}|\boldsymbol{x'};\omega) = \delta(\boldsymbol{x}-\boldsymbol{x'}), \tag{1}$$

where $P(\mathbf{x}|\mathbf{x}';\omega)$ is the actual pressure field at point $\mathbf{x}$ and frequency ω due to a source located at $\mathbf{x}'$ ignited at $t=0$; $\rho(\mathbf{x})$ is the density distribution and $c(\boldsymbol{x})$ is the velocity distribution.

The reference medium will be chosen as a homogeneous whole space satisfying the acoustic wave equation,

$$\left(\nabla \cdot \frac{1}{\rho_0}\nabla + \frac{\omega^2}{\rho_0 c_0^2}\right) G_0(\boldsymbol{x}|\boldsymbol{x'};\omega) = \delta(\boldsymbol{x}-\boldsymbol{x'}), \tag{2}$$

where $G_0(\mathbf{x}|\mathbf{x}';\omega)$ is the causal free space Green's function.

The velocity and density distributions in Eq.(1) can be written in a convenient form, described by a constant reference velocity c_0 and density ρ_0, and their corresponding perturbations, $\alpha(\mathbf{x})$ and $\beta(\mathbf{x})$, so that

$$\frac{1}{c(\mathbf{x})^2} = \frac{1}{c_0^2}\left(1-\alpha(\mathbf{x})\right), \tag{3}$$

$$\frac{1}{\rho(\mathbf{x})} = \frac{1}{\rho_0}\left(1-\beta(\mathbf{x})\right). \tag{4}$$

The perturbation, V, is the difference between the reference and actual medium properties defined by the wave equation operators in Eq.(1) and Eq.(2),

$$\begin{aligned} V(\boldsymbol{x};\omega) &= \nabla\frac{1}{\rho_0}\nabla + \frac{\omega^2}{\rho_0 c_0^2} - \left(\nabla \cdot \frac{1}{\rho(\boldsymbol{x})}\nabla + \frac{\omega^2}{\rho(\boldsymbol{x})c^2(\boldsymbol{x})}\right) \\ &= \nabla \cdot \left(\frac{1}{\rho_0} - \frac{1}{\rho(\boldsymbol{x})}\right)\nabla + \omega^2\left(\frac{1}{\rho_0 c_0^2} - \frac{1}{\rho(\boldsymbol{x})c^2(\boldsymbol{x})}\right) \\ &= \frac{1}{\rho_0}\nabla \cdot \beta(\boldsymbol{x})\nabla + \frac{\omega^2}{\rho_0 c_0^2}\left(1-(1-\beta(\boldsymbol{x}))(1-\alpha(\boldsymbol{x}))\right). \end{aligned} \tag{5}$$

Using G_0 as the reference wave field we can write the Lippmann-Schwinger equation,

$$P(\mathbf{x}|\mathbf{x}';\omega) = G_0(\mathbf{x}|\mathbf{x}';\omega) + \int_{-\infty}^{\infty} G_0(\mathbf{x}|\mathbf{x}';\omega)V(\mathbf{x}';\omega)P(\mathbf{x}|\mathbf{x}';\omega), \tag{6}$$

or in operator form,

$$P = G_0 + G_0 V P, \tag{7}$$

which is an integral equation corresponding to Eq.(1) and its physical boundary conditions (G_0 is a causal Green's function and V contains the properties of the actual medium). The Lippman-Schwinger equation is a mathematical identity that describes the relationship between two wave fields, G_0 and P. The two wave fields satisfy two different wave equations. The fields are connected through common boundary conditions, the difference in the wave equation operators, V, and sources. A formal solution to the Lippman-Schwinger equation can be found through a series expansion,

$$\begin{aligned} P &= G_0 + G_0 V P \\ &\quad \Updownarrow \\ P &= (I - G_0 V)^{-1} G_0 \\ &= (I + G_0 V + G_0 V G_0 V + G_0 V G_0 V G_0 V + \cdots) G_0 \\ &\equiv P_0 + P_1 + P_2 + \cdots , \end{aligned} \tag{8}$$

where $P_0 = G_0$. The forward scattering series, Eq.(8), gives a solution for the actual wave field, P, in terms of the reference wave field, G_0, and the perturbation operator, V. So, in principle, by summing an infinite number of terms which involves the reference wave field and the perturbation, it is possible to model the actual wave field, P, with correct phase and amplitude. In other words, the forward series is able to predict the correct amplitude and phase of a wave field by letting a reference wave field, with its own amplitude and phase, interact with the perturbation and after summing an infinite amount of terms.

Since the reference wave field, G_0, travels with a velocity given by the wave equation for the reference medium, it is obvious that the perturbation operator, V, is responsible for obtaining the correct time and amplitude of the actual wave field by interacting with the reference wave field. The perturbation operator is the only entity in the Born series that contain information about the actual medium. How this process is taking place is not obvious, and one of the main objectives of this paper is to show how the Born series obtain the correct phase and amplitude of the actual wave field by summing an infinite amount of terms in an acoustic model, i.e. with density and velocity contrasts.

Now, using the wave fields and perturbation defined in equations (2) - (5) we have the following representation of the Born series in equation (8),

$$\begin{aligned} P(\boldsymbol{x_g}|\boldsymbol{x_s}) = {} & G_0(\boldsymbol{x_g}|\boldsymbol{x_s}) \\ & + \int_{-\infty}^{\infty} d\boldsymbol{x} G_0(\boldsymbol{x_g}|\boldsymbol{x}) V(\boldsymbol{x}) G_0(\boldsymbol{x}|\boldsymbol{x_s}) \\ & + \int_{-\infty}^{\infty} d\boldsymbol{x} d\boldsymbol{x'} G_0(\boldsymbol{x_g}|\boldsymbol{x}) V(\boldsymbol{x}) G_0(\boldsymbol{x}|\boldsymbol{x'}) V(\boldsymbol{x'}) G_0(\boldsymbol{x'}|\boldsymbol{x_s}) \\ & + \int_{-\infty}^{\infty} d\boldsymbol{x} d\boldsymbol{x'} d\boldsymbol{x''} G_0(\boldsymbol{x_g}|\boldsymbol{x}) V(\boldsymbol{x}) G_0(\boldsymbol{x}|\boldsymbol{x'}) V(\boldsymbol{x'}) G_0(\boldsymbol{x'}|\boldsymbol{x''}) V(\boldsymbol{x''}) G_0(\boldsymbol{x''}|\boldsymbol{x_s}) \\ & + \cdots . \end{aligned} \tag{9}$$

We have omitted the frequency dependency for convenience.

The Born series can be interpreted as a sequence of infinitely many scattering processes, where the first term is the Green's function in the reference medium which represents a wave propagating in

the reference medium from the source at $\boldsymbol{x_s}$, directly to the measurement point, $\boldsymbol{x_g}$, as shown in Fig. 3a.

The second term in the Born series contains $V(\boldsymbol{x})$ sitting between two wave fields propagating in the reference medium. The wave field on the right represents a wave propagating in the reference medium from the source, $\boldsymbol{x_s}$, down to a scattering point at $\boldsymbol{x}$. The wave field is now scattered by the perturbation $V(\boldsymbol{x})$ before it propagates to the measurement described by the wave field on the left. The integration means that you sum over all scattering configurations you can possibly have with a given perturbation. This process is displayed in Fig. 3b with a single scattering diagram. Diagrams are tools of interpretation and analysis for both, the inverse and forward scattering series, that are equivalent to Feynman diagrams in quantum mechanics. They were first introduced and applied in exploration seismology by Weglein et al. (1981, 1997, 2003).

The third term represents a sum over waves which propagate in the reference medium and undergo two scattering interactions. Following this interpretation of the scattering process, each term in the Born series involves a series of propagations and interactions with points within the scattering region. See Fig. 3c.

A cartoon of the fourth term in the forward series which involves three scatterers is shown in Fig. 3d.

The perturbation operator in the Born series is responsible for scattering the incoming wave, i.e. giving it a new direction and amplitude. And since the perturbation operator is dependent on the model used, the scattering pattern is dependent on the medium. As already mentioned, it is the scatterer acting on the field in the reference medium which is responsible for generating the correct amplitude and exact phase of the actual wave field.

The perturbation operator contain the differences in medium properties which the two wave fields have experienced, e.g. density and velocity in the acoustic case. In the forward series the reference field interacts with the whole perturbation operator to generate the correct field. Intuitively, in a 1D acoustic world with constant velocity and a density distribution, one would expect this velocity to be responsible for giving the correct time of the actual wave field. And the task for the perturbation to create the correct amplitudes. This is not obvious and it is one of the main objectives of this paper to use a simple analytical model to study the behavior of the Born series and how it generates the output field in the acoustic case with changes in density only.

The reason we want to do this exercise is not to find a more efficient way to do forward modelling with the forward series, but to give us a guide to how we can solve the inverse problem, i.e. if we want to do imaging with the inverse scattering series, how should we select the model? Can we have a model type independent imaging algorithm? Is it sufficient with velocities only? Will the densities be necessary to consider? What about using the Lamé parameter, $\lambda = \rho c^2$? What is the best choice to do imaging? What are the implications to non-linear AVO based on inverse scattering? The exercise we do here will give us a hint about how to choose the best model parameters, using symmetry relations between the forward and inverse scattering series.

3 Analytical Examples

The perturbation operator in the Born series contain the differences in medium properties which the two wave fields have experienced, e.g. density and velocity in the acoustic case. In the forward

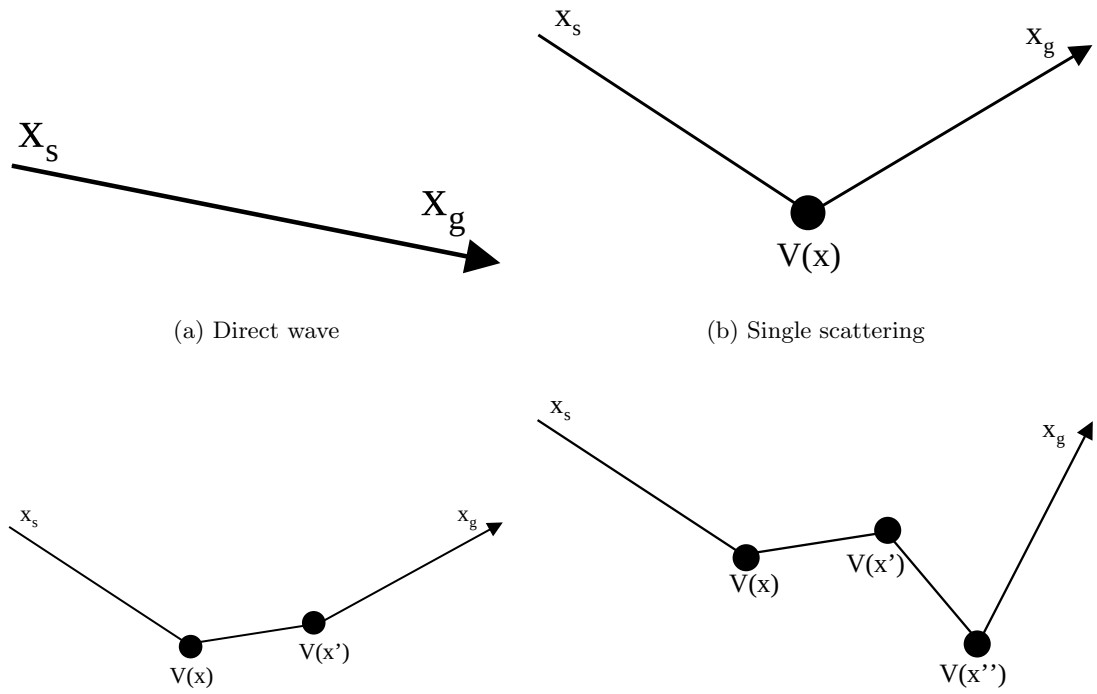

(a) Direct wave

(b) Single scattering

(c) Double scattering

(d) Triple scattering

Figure 3: The Figure displays the first four terms in the Born series, where (a) shows the direct wave propagating from source to receiver; (b) a propagation from source down to the scattering point, $\boldsymbol{x}$, and propagation to receiver; (c) a propagation from source down to the scattering point, $\boldsymbol{x}$, propagation from $\boldsymbol{x}$ to $\boldsymbol{x'}$, and propagation to receiver; (d) a propagation from source down to the scattering point, $\boldsymbol{x}$, propagation from $\boldsymbol{x}$ to $\boldsymbol{x'}$, propagation from $\boldsymbol{x'}$ to $\boldsymbol{x''}$, and propagation to receiver.

series the reference field interacts with the whole perturbation operator to generate the actual field. Intuitively, in a 1D acoustic world with constant velocity and changing densities, one would expect this velocity to be responsible for the prediction of the correct time of the actual wave field. And the task for the perturbation and all non-linear forward series activity is to correct the amplitudes. How this accurs is not obvious and in this section we will go through some analytical examples in a 1D model with a single interface to demonstrate how the forward series generates the actual wave field.

3.1 A 1D earth with constant velocity and changing densities.

There are some questions we want to answer: What happens if the perturbation operator only contains a difference in the densities? In that case we know that the reference wave field has the same time behavior as the actual wave field and there is no reason for the forward series to correct the time. How does the series accomplish this? Will it add and subtract non-zero terms an infinite number of times gradually converging to zero, or will it know from the first term that there is no time to be corrected? In order to answer these questions, we will study a simple acoustic 1D model with a single interface where the velocity is constant over the interface and the density changes. The model is displayed in Fig. (4).

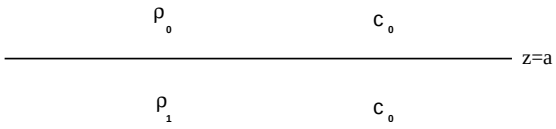

Figure 4: Model with constant velocity and density perturbation.

In a medium with constant velocity, the actual medium satisfies the acoustic wave equation in equation (1), with $c(\mathbf{x}) = c_0$, and the reference medium satisfies equation (2). The perturbation is in this case given by

$$V = \frac{\omega^2\beta(\mathbf{x})}{\rho_0 c_0^2} + \frac{\partial}{\partial \mathbf{x}}\frac{\beta(\mathbf{x})}{\rho_0}\frac{\partial}{\partial \mathbf{x}}, \tag{10}$$

which is equation (5), with $\alpha(\mathbf{x})$ set to zero. In 1D, the perturbation will depend on depth only, and the perturbation for the model in Fig. (4) is given by

$$\begin{aligned} V =& \frac{\omega^2\beta(z)}{\rho_0 c_0^2} + \frac{\partial}{\partial z}\frac{\beta(z)}{\rho_0}\frac{\partial}{\partial z} \\ =& \frac{\omega^2\beta H(z-a)}{\rho_0 c_0^2} + \frac{\beta}{\rho_0}\frac{\partial}{\partial z}H(z-a)\frac{\partial}{\partial z}, \end{aligned} \tag{11}$$

where $H(z-a)$ is the unit step or Heaviside function.

We are going to define the first term on the right hand side of the perturbation in equation (11) as isotropic and the second term, containing the gradients, as anisotropic. The isotropic part is similar in form and behaviour, to the velocity perturbation that Matson (1996) used in his work

which is the perturbation in equation (5) with $\beta(\boldsymbol{x}) = 0$ and $\alpha(\boldsymbol{x}) = \alpha H(z-a)$. The isotropic part depends on the background velocity and treats all directions with equal weighting. The anisotropic part depends only on the density, and it has two gradients. These gradients, will generate factors that depend on the direction of the incident reference wave field.

In a 1D homogenous earth, the solution to the wave equation in equation (2) is

$$G_0(z|z_s;\omega) = \rho_0 \frac{e^{ik|z-z_s|}}{2ik}, \tag{12}$$

where $k = \frac{\omega}{c_0}$. Note that G_0 has the correct time since the velocity in the reference medium, c_0, agrees with the velocity in the actual medium. Hence, the travel time prediction is correct at the first term, $P_0 = G_0$, in the forward series. And we would expect it to remain correct at every order of approximation of the wavefield, P_i, since each term propagates with the actual velocity.

The forward series has terms, which we represent with transmission-like diagrams Fig. (6), that add to generate the correct arrival time of the scattered wavefield. The reference Green's function, G_0, travels with the correct velocity in a forward series where the perturbation is due to a change in density properties only. Hence, the task of the forward series will be to construct the correct amplitude of the wavefield and to leave the time unchanged.

In the following examples, based on the model in Fig. (4), the perturbation in equation (11) and the reference wave field in equation (12) will be used.

3.1.1 Transmission Case

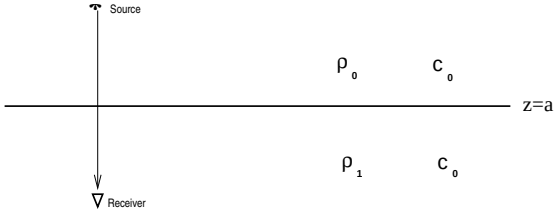

Figure 5: Transmission case with constant velocity.

We start off by considering the transmitted wave field, i.e. the actual wave field calculated below the interface at $z = a$.

We solve for the transmitted wave field whose source-receiver configuration is shown in Fig. (5). Starting with the first order approximation in the Born series, equation (9), we have

$$\begin{aligned} G_0 V G_0 &= \int_{-\infty}^{\infty} \rho_0 \frac{e^{ik|z_g-z|}}{2ik} \left(\frac{\omega^2 \beta H(z-a)}{\rho_0 c_0^2} \right) \rho_0 \frac{e^{ik|z-z_s|}}{2ik}\, dz \\ &\quad + \int_{-\infty}^{\infty} \rho_0 \frac{e^{ik|z_g-z|}}{2ik} \left(\frac{\beta}{\rho_0} \frac{\partial}{\partial z} H(z-a) \frac{\partial}{\partial z} \right) \rho_0 \frac{e^{ik|z-z_s|}}{2ik}\, dz, \qquad (13) \\ &= I_1 + I_2, \qquad (14) \end{aligned}$$

where,

$$I_1 = \frac{-1}{4}\int_a^{z_g} \frac{\beta}{\rho_0}\rho_0 e^{ik(z_g-z)}\rho_0 e^{ik(z-z_s)}\ dz - \frac{1}{4}\int_{z_g}^{\infty} \frac{\beta}{\rho_0}\rho_0 e^{ik(z-z_g)}\rho_0 e^{ik(z-z_s)}\ dz, \tag{15}$$

and

$$I_2 = -\frac{1}{4k^2}\int_a^{\infty} \frac{\beta}{\rho_0} sgn(z_g - z) ik\rho_0 e^{ik|z_g-z|} ik\rho_0 e^{ik(z-z_s)}\ dz, \tag{16}$$

$$I_2 = -\frac{i^2}{4}\int_a^{z_g} \frac{\beta}{\rho_0}\rho_0 e^{ik(z_g-z)}\rho_0 e^{ik(z-z_s)}\ dz - \frac{i^2}{4}\int_{z_g}^{\infty} \frac{\beta}{\rho_0}(-1)\rho_0 e^{ik(z-z_g)}\rho_0 e^{ik(z-z_s)}\ dz. \tag{17}$$

We can represent the terms in equation (15) and (17) with transmission-like and reflection-like diagrams as shown in Fig.(6), and note that the transmission-like terms cancel out. Thus,

$$G_0VG_0 = I_1 + I_2 = \frac{-\beta}{2}\int_{z_g}^{\infty} \rho_0 e^{2ikz} e^{ik(-z_g-z_s)}\ dz,$$

$$G_0VG_0 = \frac{\beta}{2}\frac{\rho_0 e^{ik(z_g-z_s)}}{2ik}. \tag{18}$$

This result shows that the first order approximation to the Born series in this simple model generates a wave which travels with the correct velocity c_0 from the source at z_s down to the receiver at z_g below the interface.

We have seen earlier that the isotropic part of the density perturbation has the exact same form as the velocity perturbation. This means that considering only the isotropic part of the density perturbation, the first order approximation to the Born series will try to correct the time of the actual wave field as well as the amplitude. This is not correct in the constant velocity case. The gradients in I_2, have a directionality feature. This feature plays a major and important role for how this particular forward series behaves. It is responsible for selecting the terms that contribute to the amplitude prediction of the scattered wavefield and cancelling the terms, whose task are to correct the arrival time.

The anisotropic part of the density perturbation (the one involving $\frac{\partial}{\partial \mathbf{x}}\frac{\beta(\mathbf{x})}{\rho_0}\frac{\partial}{\partial \mathbf{x}}$) acts as the exact negative of the time correction part of the isotropic density perturbation, i.e. the equations eliminate the integrals dependent on the depth difference $(z_g - a)$ at every order of approximation. This is due to the *signum* function in equation (16) that derives from the gradient operation on the reference wavefield. When the reference wavefield leaves the perturbation going downwards, the sign function gives a -1 which eliminates the integrals where $a < z < z_g$.

The depth difference factor, $(z_g - a)$, contained in the forward series was identified by Matson (1996); Innanen and Weglein (2003) to be a part of a Taylor series of an exponential function that corrects the arrival time of the predicted wave field to generate the actual scattered wave field. This exponential was identified as a time corrector whose 1^{st} order diagrammatic represention is shown in Fig.(6)a. For the model we are considering, the action of the time correctors are not needed,

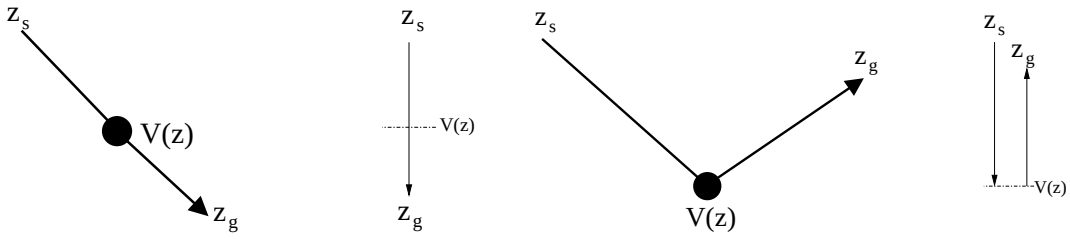

(a) Transmission-like diagram (b) Reflection-like diagram

Figure 6: The Figure displays the diagrams representing the time and the amplitude correction parts of the forward series in $1D$: (a) Shows a time-corrector diagram. Downward propagation from source to the scattering point z and to the receiver. (b) Shows an amplitude corrector diagram. Downward propagation from source to the scattering point, z and upward propagation to the receiver.

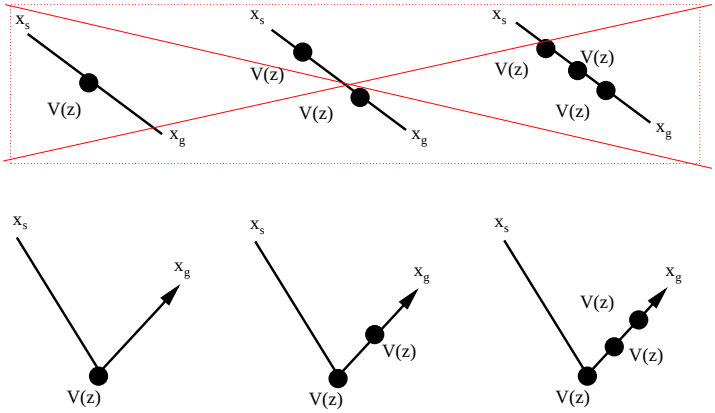

Figure 7: The density-only perturbation is a purposeful perturbation. The diagrams on the top are time correctors; since their action is not needed in this example, the forward series cancels them out.

hence the anisotropic part of the density perturbation anihilates the time correction contributions.

The density-only perturbation exhibits the feature of a purposeful perturbation. Its only task is to correct the amplitude of the predicted transmitted wave field order by order in the perturbation. It does not allow the creation of time corrector diagrams because their action is not needed. So we end up with the addition of amplitude correctors diagrams as shown in Fig.7.

Calculating the higher order terms of the Born series in equation (9) using the same approach as

in equation (18), we obtain

$$\begin{aligned} G_0 &= \frac{\rho_0 e^{ik(z_g-z_s)}}{2ik} \\ G_0VG_0 &= \frac{\beta}{2}\frac{\rho_0 e^{ik(z_g-z_s)}}{2ik} \\ G_0VG_0VG_0 &= \frac{\beta^2}{4}\frac{\rho_0 e^{ik(z_g-z_s)}}{2ik} \\ G_0VG_0VG_0VG_0 &= \frac{\beta^3}{8}\frac{\rho_0 e^{ik(z_g-z_s)}}{2ik} \\ G_0VG_0VG_0VG_0VG_0 &= \frac{\beta^4}{16}\frac{\rho_0 e^{ik(z_g-z_s)}}{2ik} \\ &\vdots \end{aligned} \tag{19}$$

From equation (19), we see that each term in the forward series has a common factor, G_0, which is the direct wave from the source to the receiver, travelling with the actual velocity. The terms in the forward series differ only in the amplitudes. Summing all these terms gives us the Born series representation of actual transmitted wavefield,

$$\begin{aligned} P &= G_0 + G_0VG_0 + G_0VG_0VG_0 + G_0VG_0VG_0VG_0 + \cdots \\ P(z_g > a|z_s;k) &= \left(1 + \frac{\beta}{2} + \frac{\beta^2}{4} + \frac{\beta^3}{8} + \frac{\beta^4}{16} + \cdots\right)\frac{\rho_0 e^{ik(z_g-z_s)}}{2ik}. \end{aligned} \tag{20}$$

The forward series does its job given the tools at its disposal. The perturbation has the correct information of the change in parameters, including the exact depth where the density changed and the knowledge of the constant velocity throughout the whole medium. Each order of approximation in the forward series provides the correct wave type, *i.e.* a transmitted wave with the correct arrival time, G_0. However, the amplitude of the transmitted wave is incorrect at each order, and it requires an infinite number of terms to be corrected.

We have yet to establish the connection between the Born series representation of the actual wave field and the analytical solution to the wave equation for the model in Fig. (4) given by

$$P(z_g > a|z_s;k) = T_{01}\frac{\rho_0 e^{ik(z_g-z_s)}}{2ik}, \tag{21}$$

where the transmission coefficient, T_{01}, is

$$T_{01} = \frac{2c_1\rho_1}{c_1\rho_1 + c_0\rho} = \frac{2\rho_1}{\rho_1 + \rho_0} = \frac{\frac{2\rho_0}{1-\beta}}{\frac{\rho_0}{1-\beta} + \rho_0} = \frac{2}{2-\beta} = \frac{1}{1-\frac{\beta}{2}}.$$

Hence, the transmission coefficient can be represented as a geometrical series

$$\frac{1}{1-\frac{\beta}{2}} = 1 + \frac{\beta}{2} + \frac{\beta^2}{4} + \frac{\beta^3}{8} + \frac{\beta^4}{16} + \cdots. \tag{22}$$

Comparing the geometrical series in equation (22) with the sum of terms in equation (20), we see that the forward series predicts the correct transmitted wave field.

3.1.2 Reflection Case

Now, we consider the case where we locate the receiver above the perturbation. Hence, we will obtain a reflected wave field which has interacted with the perturbation and a direct wave which has propagated directly from the source to the receiver without interacting with the perturbation. In this case, the Green's functions in the integrals in equation (9) propagating from the source to the first scattering potential and the wave propagating from the last scatterer back to the receiver will not have absolute values since $z_g < a$ and $z_s < a$. Hence, calculating the forward series yields the same amplitude coefficients as in equation (19). The difference is in the phase of the direct wave compared to the scattered wave. The direct wave, G_0, forms an event by itself; it has only traveled in the reference medium and is therefore correct.

The reflection coefficient is formed from the scattered waves, the part of the wave that has interacted with the perturbation. Hence, we have two events, the direct arrival plus the reflected wave

$$P(z_g < z|z_s;k) = \frac{\rho_0 e^{ik(z_g - z_s)}}{2ik} \tag{23}$$

$$+ \left(\frac{\beta}{2} + \frac{\beta^2}{4} + \frac{\beta^3}{8} + \frac{\beta^4}{16} + \cdots\right) \frac{\rho_0 e^{2ika} e^{ik(-z_g - z_s)}}{2ik}. \tag{24}$$

In order to compare the forward series solution of the wave equation with the analytical solution, we expand the reflection coefficient in a Taylor series,

$$R_{01} = \frac{c_0\rho_1 - c_0\rho_0}{c_0\rho_1 + c_0\rho_0} = \frac{\rho_1 - \rho_0}{\rho_1 + \rho_0} = \frac{\frac{\frac{\rho_0}{1-\beta} - \rho_0}{1-\beta}}{\frac{\rho_0}{1-\beta} + \rho_0} = \frac{\rho_0\beta}{2\rho_0 - \rho_0\beta} = \frac{\beta}{2-\beta}$$

$$= \frac{\beta}{2} + \frac{\beta^2}{4} + \frac{\beta^3}{8} + \frac{\beta^4}{16} + \cdots. \tag{25}$$

Comparing the Taylor series expansion of the reflection coefficient, R_{01}, with the coefficient series in front of the second term in equation (24), we find that the forward series predicts the actual reflected wave field recorded above the perturbation.

3.2 Two parameters, both density and velocity changes

How will the forward series act when we allow the two acoustic parameters to change?

In this section we will study the model in Fig. (2) which involves the same 1D model structure studied in the previous section, but now we will let both velocity and density change over the interface. We will calculate the transmitted wave field below the interface.

We use the 1D version of the perturbation given in equation (5). In the case for a single interface model, in a 1D medium, the perturbation in equation (5) can be written as

$$V = \frac{\omega^2}{\rho_0 c_0^2}\left[\alpha H(z-a) + \beta H(z-a) + \alpha\beta H(z-a)\right] + \frac{\beta}{\rho_0}\frac{\partial}{\partial z} H(z-a)\frac{\partial}{\partial z}. \tag{26}$$

For mathematical convenience, we will introduce a new parameter, χ, defined as $\chi = \alpha(1-\beta)$. Using this definitition together with $k^2 = \omega^2/c_0^2$ we obtain

$$V = \frac{k^2(\beta+\chi)H(z-a)}{\rho_0} + \frac{\beta}{\rho_0}\frac{\partial}{\partial z}H(z-a)\frac{\partial}{\partial z}. \tag{27}$$

The selection of these parameters is very important for an easier interpretation of each term and its task in the forward series. If we had chosen to introduce the bulk modulus which involves both the density and the velocity, the forward series could not be divided into task specific subseries. An analogous choice of parameters, density and velocity, in the inverse scattering series for parameter estimation has shown to be a convenient and transparent selection which eliminates the problem of linear "leaking" between linear property change predictions. The special parameters, density and velocity, were identified in the inverse series by Zhang and Weglein (2005).

In the 2-parameters acoustic wave equation, velocity and density are independent of each other. We found that velocity and density are the parameters that lead to a clear and transparent understanding of the different tasks performed by the forward series. The introduction of the parameter χ is convenient, because χ contains the portion of the perturbation associated with velocity which only acts as an isotropic part of the perturbation. Hence, χ represents an isotropic only part of the two parameter acoustic perturbation. On the other hand, β appears in both parts (isotropic and anisotropic) of the perturbation, and it is exactly the same perturbation as the one in the density-only case as seen in equation (11). The fact that we can separate the density-only part of the perturbation from the velocity dependent part, allows us to use the results, analysis and conclusions we obtained in the previous sections to understand and make inferences about the more general 2-parameter acoustic case currently studied. The first order approximation to the transmitted field is easily calculated using equation (18),

$$G_0VG_0 = \rho_0\frac{e^{ik(z_g-z_s)}}{2ik}\left(\frac{\chi}{4} - \frac{2ik\chi(z-a)}{4} + \frac{\beta}{2}\right). \tag{28}$$

The parameterization that we chose allows us to infer that the forward series is going to decide of whether the purpose of a given computation is overall necessary or not in the same clear way as it did in the density-only perturbation case. Equation (28), gives a transmitted-type wave field multiplied by the coefficient

$$\left(\frac{\chi}{4} - \frac{2ik\chi(z-a)}{4} + \frac{\beta}{2}\right). \tag{29}$$

The first and third term in equation (29) have a similar form, while the second term is multiplied by the depth difference between the position where the perturbation started (at the interface in the model) and the scatterer. The isotropic part of the perturbation contains χ which in turn contains the depth of the velocity change and the value of that change. It will be integrated with a factor $(z-a)$, which is dependent of depth. The depth difference is the best estimate of the correct arrival time that the first order approximation of the forward series can make. The factor $(z-a)$ is the depth that the wave traveled in the medium whose velocity is not the background one. The knowledge of this depth will create the correct time. The term $\frac{2ik\chi(z-a)}{4}$ in equation (29)is the linear term in a Taylor series expansion for an exponential function which is responsible for correcting the travel time of the reference wave towards the travel time of the actual wave field.

Hence, the second term on the right hand side of equation (29) corresponds to the output of a time corrector, while the first and third terms are amplitude correctors.

The second order approximation is given by

$$\begin{aligned}
G_0VG_0VG_0 &= \int_{-\infty}^{\infty} \frac{\rho_0 e^{ik|z_g-z|}}{2ik}\left(\frac{\omega^2(\chi+\beta)H(z-a)}{\rho_0 c(z)^2} + \frac{\beta}{\rho_0}\frac{\partial}{\partial z}H(z-a)\frac{\partial}{\partial z}\right) \\
&\quad \times \rho_0 \frac{e^{ik(z-z_s)}}{2ik}\left(\frac{\chi}{4} - \frac{2ik\chi(z-a)}{4} + \frac{\beta}{2}\right)\, dz \\
G_0VG_0VG_0 &= \int_{a}^{\infty} \frac{\rho_0 e^{ik|z_g-z|}}{-4} e^{ikz}e^{-ikz_s}\,(\chi+\beta)\left(\frac{\chi+2\beta}{4} - \frac{2ik\chi(z-a)}{4}\right)\, dz \\
&\quad + \int_{a}^{\infty} \frac{\rho_0 e^{ik|z_g-z|}}{-4k^2} e^{ikz}e^{-ikz_s}\,(sgn(z_g-z)ik\beta H(z-a)) \\
&\quad \times \left(ik\left(\frac{\chi+2\beta}{4} - 2ik(z-a)\frac{\chi}{4}\right) - 2ik\frac{\chi}{4}\right)\, dz. \qquad (30)
\end{aligned}$$

Expanding the absolute values of the Green's functions propagating from the source to a scatterer, we obtain

$$\begin{aligned}
G_0VG_0VG_0 &= \int_{a}^{z_g} \left[(\chi+\beta)\frac{\chi+2\beta-2ik\chi(z-a)}{4} - \beta\frac{-\chi+2\beta-2ik\chi(z-a)}{4}\right] \\
&\quad \times \frac{-\rho_0 e^{ik(z_g-z_s)}}{4}\, dz \\
&\quad + \int_{z_g}^{\infty} \left[(\chi+\beta)\frac{\chi+2\beta-2ik\chi(z-a)}{4} + \beta\frac{-\chi+2\beta-2ik\chi(z-a)}{4}\right] \\
&\quad \times \frac{-\rho_0}{4} e^{2ikz}e^{ik(z_g+z_s)}\, dz \qquad (31)
\end{aligned}$$

The integral in equation (31) where $a < z < z_g$ is the time corrector. The second integral corresponds to an amplitude corrector. In the first integral, the terms containing only β cancel out, while all the terms containing the velocity perturbation χ give a contribution,

$$\begin{aligned}
G_0VG_0VG_0 &= \left[\frac{\chi^2}{8} + \frac{\beta\chi}{4} + \frac{\beta^2}{4} - 2ik\left(\frac{\chi^2}{8} + \frac{3\beta\chi}{8}\right)(z-a) + (ik)^2\frac{\chi^2}{8}(z-a)^2\right] \\
&\quad \times \frac{\rho_0}{2ik} e^{ik(z_g-z_s)}. \qquad (32)
\end{aligned}$$

The density-only part of the perturbation does not give any contribution to time correctors. From equations (28) and (32) we see that all terms involving the density-only part of the perturbation, β, multiplied by the time correction factor, or depth difference, $(z-a)$, have vanished. This is the same effect as seen in the density-only case studied in section (3.1.1) which showed that the isotropic and anisotropic parts containing the time correctors cancel for each term in the series. The only parts that survive, are the terms responsible for amplitude corrections and the nonlinear terms coupled with the velocity term, χ, which are responsible of correcting the travel time and amplitudes.

The higher order terms of the forward series are calculated in the same manner as shown for the

first two terms. Summing all terms in the forward series yields

$$\begin{aligned} P(z_g > a|z_s;k) = (&\left[\frac{\chi}{4} + \frac{\chi^2}{8} + \frac{\beta}{2} + \frac{\beta^2}{4} + \frac{\beta^3}{8} + \frac{\beta\chi}{4}\frac{\beta\chi^2}{8} + \frac{3\beta^2\chi}{16} + \cdots\right] \\ &- 2ik(z-a)\left[\frac{\chi}{4} + \frac{\chi^2}{8} + \frac{3\chi^3}{32} + \frac{3\beta\chi}{8} + \frac{3\beta\chi^2}{16} + \frac{5\beta^2\chi}{16} + \cdots\right] \\ &- k^2(z-a)^2\left[\frac{\chi^2}{8} + \frac{3\chi^3}{32} + \frac{5\chi^2\beta}{16} + \frac{9\chi^4}{128} + \cdots\right] \\ &+ 2ik^3\left[\frac{\chi^3}{96} + \frac{\chi^4}{96} + \frac{7\chi^3\beta}{192} + \cdots\right])e^{ik(z_g - z_s)}. \end{aligned} \tag{33}$$

The transmission coefficient for this model is,

$$T_{01} = \frac{2c_1\rho_1}{c_1\rho_1 + c_0\rho} = \frac{2}{1 + (1-\beta)\sqrt{(}1-\alpha)},$$

using $\chi = -\alpha\beta + \alpha$, we find

$$\begin{aligned} \alpha &= \frac{\chi}{1-\beta}, \\ \gamma &= \frac{k_0}{k_1} = \sqrt{1-\alpha}. \end{aligned} \tag{34}$$

With these definitions, we perform a Taylor expansion of T_{01}, α and γ, in terms of the parameters χ and β, and compare them with the terms in equation (33), to obtain

$$\begin{aligned} P(z_g > a|z_s;k) =& T_{01}\frac{\rho_0}{2ik}e^{ik(z_g - z_s)}(1 - 2ik(1-\gamma)(z-a) - \frac{1}{2}4k^2(1-\gamma)^2(z-a)^2 \\ &+ \frac{1}{6}ik^3(1-\gamma)^3(z-a)^3 + \cdots) \\ P(z_g > a|z_s;k) =& T_{01}e^{ik(z_g - z_s)}e^{-ik(z_g - a)(1-\gamma)} \\ P(z_g > a|z_s;k) =& T_{01}e^{ik_1(z_g - a)}\frac{\rho_0}{2ik}e^{i(a - z_s)}. \end{aligned} \tag{35}$$

Again, the forward series predicts the actual wavefield recorded at a received located inside the perturbation.

4 Analysis

In the history of scattering series in exploration seismology, the study of the forward series has created a framework to build analogies and symmetries with the inverse scattering series (Weglein et al., 2003; Nita et al., 2004). However, the forward and the inverse series have very different objectives; the forward series uses the reference wave field and a perturbation to build the actual wave field, while the inverse series constructs the perturbation using the reference and the measured values of the actual wave field. Hence, the forward and inverse are not inverse in the standard mathematical sense, e.g. a matrix and its inverse. In other words, the forward series produces

the wave field order by order in the perturbation, while the inverse series (and its task specific suberies) does not annihilate the wave field, it uses order by order the measured values of the actual wave field together with the reference wave field to predict the perturbation from the earth that created it, the actual earth. The inverse scattering series currently provides a comprehensive multidimensional method for inversion, that allows to achieve different objectives, e.g., free-surface and internal multiple elimination, and depth structure maps and parameter estimation or non-linear AVO, all achieved sequentially with distinct algorithms corresponding to task specific subseries.

In a series approach, like this, a reasonable question to ask is how many terms would be required in practice to achieve an appropriate level of effectiveness towards the construction on the wave field with the forward series or the specific task associated with the inverse scattering subseries (Weglein et al., 1997, 2003). As we showed in the previous sections, the forward series takes a decision of whether the purpose of a given computation is overall necessary or not. The forward series gives a clear signal of this decision by not attempting to solve an issue that doesn't exist. That decision occurs at the first approximate step to address that specific issue. For the two parameter acoustic case we have identified special parameters in such a way that we are able to divide the forward scattering series into two task specific subseries, where one subseries is responsible for generating the time of the actual wave field, and the other is responsible for generating the correct amplitudes. When there is no velocity difference between the actual and the reference medium, the subseries responsible for time corrections is non-existent. It does not merely add up to zero, but it is zero from the start. The forward series tells us that it is not necessary to calculate this subseries. This is an example of purposeful perturbation. In other words, if a time issue does not exist, the subseries for correcting the time does not exist either and the first term in that subseries signals whether there is or is no issue to be addressed.

The powerful concept of purposeful perturbation was developed in the context of inverse scattering task-specific subseries, where several examples can be found (Weglein et al., 2003). Among the identified processes, purposeful perturbation occurs for the free-surface and internal multiple elimination series. The free-surface multiple elimination series eliminates an order of free-surface multiples with the corresponding term in the series; it has an understanding of the specific purpose of each term within the overall task (Carvalho, 1992). As long as you have source and receivers between a reflector and a free-surface, you will always have free-surface multiples, hence the free-surface multiple elimination series will always have a contribution. It cannot be zero because your data have all orders of multiples, the series will eliminate the free-surface multiples order by order and it will know and reveal what has and has not been accomplished for a given number of terms computed.

In an earth that only has a single reflector, the internal multiple attenuation algorithm(Araújo, 1994), as well as the elimination series and its leading order closed form algorithm, will be computed as zero without the necessity of computing the three or more integrals involved. The intrinsic knowledge of the algorithm will decide that a single reflector cannot create an internal multiple, and it will stop its whole machinery. This a clear statement of purposeful perturbation. It agrees with the fact that for this hypothetical case there is only one primary or one transmitted event and no multiples can be created or eliminated.

What basically happens in each task-specific subseries is that specific non-linear interactions take place between events in the data as a whole. The data times data communication allow free-surface and internal multiple prediction or accurate depth imaging to take place without an accurate

velocity model.

In the subseries for imaging at depth without an accurate velocity (Shaw, 2005; Liu et al., 2005b), the first term is the current standard migration performed with a reference velocity. It places each event exactly where that input reference velocity dictates. The second term in the inverse series, has integral terms represented by the separate diagram and non-integral terms represented in the diagrams by self interactions. The separate diagrams have the task of moving the incorrectly imaged events resulting from the linear migration step towards their correct spatial location. There is a non-linear dependence on the data, allowing non-linear interactions (*e.g.*, multiplication) between primary events from different reflectors. In these interactions, the primaries are enable to determine the accuracy of the input velocity. If the reference velocity is not precise for one or more events, then the troubled events will receive information via specific non-linear interacions with the shallower events to help moving the deeper events towards their correct location. When the reference velocity is consistent with the actual velocity, then there is no depth to correct and the first term in the imaging series, represented by a separate diagram, will be zero. The first separated diagram immediately and unambiguously judges the adequacy of the input velocity in an analogy with the transmission-like forward series diagram that is zero when the reference velocity is equal to the actual one.

The behavior of the imaging series has a clear symmetry with the 2-parameter acoustic forward series. When the density is the only parameter changing across the interfaces, there is no time to correct and there are no time corrector or transmission-like diagrams. Furthermore, at each step in the forward series the decision is taken and returns an unambiguous zero for any time corrector diagram, and there are no mixed diagrams allowed, only the amplitude diagrams are computed. This is not the case when the velocity is allowed to change. If the reference velocity is inadequate, an extra part of the perturbation is alive, and the time corrector diagrams are computed order by order in the perturbation giving the possibility to have specific (time or amplitude) and mixed diagrams.

Another important example of purposeful perturbation, that can be studied together with the results of this paper is in the 2-parameter inversion subseries for primaries (Zhang and Weglein, 2005). The term containing $\int(\alpha_1 - \beta_1)$ exists to correct depth imaging for incorrect input velocity, but first determines whether its function is required by a conversation between all the primaries about the adequacy of the velocity expressed through $\alpha_1 - \beta_1$. When the reference velocity is adequate, $\alpha_1 - \beta_1$ will be computed as zero. When the velocity is determined to be inadequate, the same term returns a value an sets the whole target identification subseries machinery to work. Furthermore, in our analytic examples, we identified a special parametrization in terms of density and velocity perturbations (β and χ) which helps us in interpreting the tasks of each term in the forward series. The same parameters, density and velocity, have been used as "special parameters" for inversion (Zhang and Weglein, 2005), showing that the common problem of linear "leaking" between linear property change predictions is addressed by an appropriate selection of parameters in the series. Hence, it is important to note that the interpretation and transparency of the tasks which each term in the forward series does is dependent of the choice of parameters used.

5 Conclusions

The inverse scattering series is a mathematical formalism pursued to process and invert seismic data; it is the only known method for multidimensional direct inversion. A critical concept in the progress of the algorithms based on inverse scattering is the idea of task separation (Weglein et al., 1997, 2003). Understanding the behavior of every term in the inverse series benefits the task separation approach. Experience shows that two mappings are required, one associating nonperturbative description of seismic events with their forward scattering series description and a second relating the construction of events in the forward to their treatment in the inverse scattering series (Nita et al., 2004).

In a multiparameter world, there are more issues in constructing and processing data. Modeling data with the forward series is a mathematical exercise performed with the goal of creating a framework for the processing of data with task specific inverse subseries. The theoretical analysis of the 1-parameter, acoustic, forward series performed originally by Matson (1996) gave a mathematical validation to some of the ideas and concepts used and developed to deal with the inverse series and its subseries (Weglein et al., 1981, 1997, 2003). The forward series is a formalism that creates the actual wave field order by order in an infinite series in terms of G_0 and V. Creating an issue (*i.e.* propagation in constant velocity and density distribution) in the data through a forward series with G_0 and V has a suggestion of how that issue is addressed in the inverse sense in terms of G_0 and D, which affects directly the imaging and the parameter estimation series.

In this paper we introduced a mathematical description and an analysis of the 2-parameter acoustic forward series. The main result comes from the analysis of a model where only the density was allowed to change. The density only perturbation has two parts in this scattering description. The first part behaves isotropically, its behavior is the same as the one for a model with constant density and changes in velocity (Matson, 1996, 1997; Innanen and Weglein, 2003; Nita et al., 2004). The second part behaves anisotropically; it has a directionality given by the gradients in its analytic form. These gradients inside the anisotropic part of the perturbation care of the direction from the source, or the last scatterer, and the direction going out from that source or scatterer. This anisotropic behavior cancels out all the time corrector contributions by giving the exact negative of the time corrector output of the isotropic part of the density perturbation. Leaving us with a double contribution of the reflection like diagrams, which build the correct amplitude of the scattered wave field, i.e. the transmission and reflection coefficients. When the velocity was allowed to change, the time corrector diagrams are alive. The transparency of the task that each diagram has is closely related with the chosen parameters defining the perturbation.

Acknowledgements

The authors thank Arthur B. Weglein who made invaluable contributions to this work. He helped us to understand the meaning of our results and encouraged us to write this paper.

We are grateful to the sponsors of M-OSRP for their support and helpful discussions. Einar Otnes would like to thank Statoil for financial support during his stay at M-OSRP in 2004.

References

F. V. Araújo. *Linear and nonlinear methods derived from scattering theory: backscattered tomography and internal multiple attenuation, PhD thesis*. PhD thesis, Universidad Federal da Bahía, Brazil, 1994.

P. M. Carvalho. *Free-surface multiple reflection elimination method based on nonlinear inversion of seismic data: Ph.D. thesis*. PhD thesis, Universidad Federal da Bahía, Brazil, 1992.

K. A. Innanen and A. B. Weglein. Construction of absorptive/dispersive wave fields with the forward scattering series. *Journal of Seismic Exploration*, 12:259–282, 2003.

F. Liu, S.H. Shaw, H. Zhang, K. Innanen, Z. Guo, J. Zhang, A. C. Ram´rez, D. Foster, K. Matson, R. Keys, F. Araújo, P. Carvalho, P. Traynin, R. Stolt, S. Kaplan, and A. B. Weglein. A response to the most pressing seismic e&p challenges: imaging and inversion beneath a complex, multi-dimensional ill-defined overburden. volume Society of Exploration Geophysicists International Exposition and Seventy-Fifth Annual Meeting, Houston, TX, USA, 2005a.

F. Liu, A.B. Weglein, K.A. Innanen, and B.G Nita. Extension of the non-linear depth imaging capability of the inverse scattering series to multidimensional media: strategies and numerical results. Salvador, Brazil, 2005b.

K. Matson. The relationship between scattering theory and the primaries and multiples of reflection seismic data. *Journal of Seismic Exploration*, 5, 1996.

K. Matson. *An inverse scattering series method for attenuating elastic multiples from multicomponent land and ocean bottom seismic data*. PhD thesis, The University of British Columbia, 1997.

B. G. Nita, K. H. Matson, and A. B. Weglein. Forward scattering series and seismic events: Far field approximations, critical and postcritical events. *Society for Industrial and Applied Mathematics*, 64(6):21672185, 2004.

S. A. Shaw. Some remarks on the leading order imaging series algorithm for depth imaging when the velocity model is unknown. Technical report, M-OSRP. University of Houston, April 2005.

R. H. Stolt and A. B. Weglein. Migration and inversion of seismic data. *Geophysics*, 50:2458–2472, 1985.

A. B. Weglein, F. V. Araujo, P. M. Carvalho, R. H. Stolt, K. H. Matson, R. T. Coates, D. Corrigan, D. J. Foster, S. A. Shaw, and H. Zhang. Topical review: Inverse scattering series and seismic exploration. *Inverse Problems*, 19, 2003.

A.B. Weglein, F. V. Araujo Gasparotto, P. M. Carvalho, and R. H. Stolt. An inverse-scattering series method for attenuating multiples in seismic reflection data. *Geophysics*, 62, 1997.

A.B. Weglein, W.E. Boyse, and J.E. Anderson. Obtaining three-dimensional velocity information directly from reflection seismic data: an inverse scattering formalism. *Geophysics*, 46, 1981.

H. Zhang and A.B. Weglein. The inverse scattering series for tasks associated with primaries: depth imaging and direct non-linear inversion of 1d variable velocity and density acoustic media. pages 1705–1708, 2005.

Non-linear forward scattering series expressions for and relations between reflected primary and transmitted direct wavefield events

Kristopher A. Innanen

Abstract

Forward scattering series approximations of two important types of measured wavefield event (given a homogeneous acoustic reference media and an "actual medium" represented by a P-wave velocity distribution with potentially strong spatial heterogeneity), are proposed. These approximations, for reflected primary wavefields and transmitted direct wavefields, are expressible in series form given a 2D or 3D medium, and in either series or closed-form given a 1D medium; in both series and closed-form they can be shown to be closely related through a quasi-linear mathematical construction. The 1D closed forms are principally used in this paper to provide a framework to analyze the behavior of the 2D/3D series forms; in all three dimensions light is shed not only on this modelling framework but many of our prototype inverse scattering series processing algorithms. Importantly, all of these subseries can be seen to act toward the creation of, effectively, new transmission-only Green's functions that are highly non-linear in the perturbation. This remains true in 1D and in 2D/3D, however, the latter cannot (without further restrictions) be collapsed to closed form.

1 Introduction

This paper concerns the construction of tools for understanding wave fields that propagate through complex heterogeneous media before they are measured.

The forward scattering series is an infinite series representation of a Green's function for wave propagation in a given medium, in terms of (1) a Green's function for wave propagation in a reference medium, and (2) a perturbation that accounts for the difference between the two media. Given a simple reference medium (in this paper, for instance, a homogeneous, acoustic, constant density medium is utilized) and the perturbation as input, the forward scattering series labors to compute the wavefield due to the original, "actual", medium.

This formalism can therefore be regarded as a machine for forward modelling, although, to be sure, an impractical one in the absence of further analysis and manipulation. Furthermore, the inverse scattering series, a theory for the order-by-order construction of the perturbation directly in terms of measured values of wavefield data, whose relevance to issues of reflection seismic imaging and target identification has been discussed elsewhere (e.g., Weglein, 1981; Weglein et al., 1997; Weglein et al., 2003), shares a high degree of symmetry with the forward series. As such, insight into the behavior of one tends to afford equivalent insight into the other. The various motivations for the developments described in this paper all have their roots in one or other of the above statements.

More specifically, this paper describes a program for manipulation of the forward scattering series to isolate the construction of the *primaries* and *direct waves* of reflection- and transmission-type source/receiver configurations. The wavefield signal returning from a reflection-type experiment (and the wavefield signal arriving from a transmission-type experiment) involves characteristic

echoes, or events, that are due to rapid spatial variations in the underlying (or intermediary) medium parameters. *Primaries* in a reflection-type experiment are events due to wave energy that has undergone no reverberation during its propagation down-and-back in the subsurface. *Multiples* are events corresponding to wave energy that has experienced some degree of reverberation; in a stratified medium multiples are events due to wave energy that has experienced at least one downward reflection during its propagation history. This wave energy is relatively complicated to describe in terms of medium parameters, and hence, in spite of recent and developing frameworks for using multiples in imaging and inversion problems, effort typically is expended to eliminate them from a recorded data-set, leaving primaries as the de facto signal. Weglein and Dragoset (2005) have recently edited a literature overview, conceptual background, and basic discussion of the categorization and processing of such events. *Direct waves* have slightly altered descriptions for reflection- or transmission-type experiments: in a reflection-type experiment the direct wave is that portion of the wavefield that has had no interaction with the subsurface structure, whereas in a transmission-type experiment the direct wave has interacted with the medium structure of interest but has not undergone any reverberative propagation. Direct waves of transmission-type are information bearing with respect to the medium structure; for this reason I consider this latter form only in what follows.

In the language of scattering theory, none of these events have an exact definition, so understanding the construction of a specified event of reflection- or transmission-type in terms of the combination of (1) a given reference medium, and (2) a subset of forward scattering series terms, is a matter for analysis, intuition, and approximation. To cite a well-known example: given a reference medium that is equal to the actual medium up to a specified (low) level of smoothness, such that the responsibility of the perturbation is therefore to capture the rapid, transitory "reflectivity" of the medium, the first-order term of the forward scattering series can be considered a useful approximation of the primaries of a reflected wavefield. An accumulation of discrepancies between the smooth reference medium and the smooth component of the actual medium contributes to an accumulation of error in this approximation. In constructing primaries due to a scattering potential that is structurally complex across many scales, with a highly simplified, perhaps homogeneous, reference medium, generally one encounters large errors in the linear primaries approximation.

To construct any event in a wavefield using scattering theory, in principle the full infinite forward scattering series is needed. Anything less than that is in some sense an approximation, and the main question becomes one of assessing its accuracy, which may be very high. The onset of inaccuracy in the aforementioned linear approximation of primaries simply implies that with the given combination of reference medium and perturbation, higher-order terms in the series are beginning to demand inclusion. And, unfortunately, that useful prescription for the accurate, though approximate, construction of specific events (reflected primaries) with specific series terms (the single linear term), is lost also, and is relegated to an *a priori* unknown set of mathematical terms and activities within the entire series.

How the forward scattering series constructs seismic reflection events, in the absence of an accurate reference medium, has been investigated by Matson (1996; 1997), Innanen and Weglein (2003), Nita et al. (2004) and Ramirez and Otnes (2006) for sets of single-interface and/or single layer Earth models that are depth-varying and piecewise constant. Innanen (2005) has posited two non-linear expressions that approximate reflected primaries due to arbitrary depth-varying acoustic media in both series and closed-form, given a homogeneous reference, and demonstrated that this approximation may be directly inverted to create an algorithm for imaging and inversion of

primaries. Numerical comparison of these non-linear wavefield constructions to analytically-derived "perfect data" (using a restricted set of models for which analytic data may be written down) clearly shows that the identified and separated sub-terms of the forward scattering series (1) work to construct only reflected primaries, and (2) compute to a high degree of accuracy the phase and amplitude of those events. One of the results of the current paper is a framework for the extension of those essentially stratified-medium manipulations to media with perturbation structure that varies in three dimensions.

In addition to allowing itself to be compartmentalized into components that construct the primary part of the reflected wavefield and/or the direct part of the transmitted wavefield, this non-linear series framework allows partial constructions of the former (reflected primary) to be expressed in terms of partial constructions of the latter (transmitted direct) in a number of related ways. This is an edifying result, in that it bridges the two developments; additionally, in speaking to the constructibility of reflection data from transmission data, it bears resemblance, but in a modelling sense, with the literature on interferometry and daylight imaging (Claerbout, 1968; Wapenaar, 2003; Schuster et al., 2004). Away from the modelling framework, basic theory exists highlighting the relationship between the inverse scattering series and the construction of the wavefield (transmitted and otherwise) everywhere in a scattering medium directly in terms of reflection data measured outside of the scattering medium (Weglein et al., 2006).

In the forthcoming development attention is restricted to scattering media in which a homogeneous, acoustic, constant density reference medium is perturbed by an alteration to the wavespeed that may vary in three dimensions. (The analysis is repeated thereafter for the simpler case of layered medium perturbations.) In that milieu, expressions are first derived for the first three orders of the forward scattering series three times: once with sources/receivers positioned to mimic a reflection geometry, and twice with transmission geometries. These expressions illustrate the core mathematical mechanisms associated with the generation of the full wavefields: primaries, direct waves, multiples etc. The next step is to extend to multiple dimensions the idea of constraining the reflection scattering integrals to approximate only primaries (Innanen, 2005). This turns out to be a straightforward extension *if* the correct domains are chosen. In addition, a conceptually similar set of constraints on the transmission scattering integrals are proposed as a means to approximate the direct wavefields. The result is a set of the lowest three orders of three distinct series for event approximation, one for reflected primaries and two for transmitted direct waves ("upward" and "downward"); the patterns needed to write down the n'th order terms of each are clear after three orders are explicitly given. In fact, those patterns may be used to postulate recursive forms for each of these series. The next step is to demonstrate that two transmitted wavefield series terms (at, say, n'th and m'th order) may be "stitched" together via a quasi-linear construction, to recreate the series term for a part of the associated reflected wavefield at $(m+n+1)$'th order. This whole development is then repeated for a depth-varying (1D as opposed to 3D) perturbation, and it is shown that, since closed- *and* series-forms are available in the 1D regime for each of the wavefield event approximations, the transmitted and reflected approximations may be once again related via a quasi-linear scattering construction, both order-by-order, and in total.

2 Terminology

Wave equations appropriate for acoustic waves propagating through media with fixed density and (sometimes) variable wavespeed are considered; a homogeneous reference medium with wavespeed c_0 has an associated Green's function satisfying

$$\left[\nabla_g^2 + \frac{\omega^2}{c_0^2}\right] G_0(\mathbf{x_g}|\mathbf{x_s};\omega) = \delta(\mathbf{x_g} - \mathbf{x_s}), \tag{1}$$

where

$$\begin{aligned} \mathbf{x_g} &= (x_g, y_g, z_g), \\ \mathbf{x_s} &= (x_s, y_s, z_s); \end{aligned} \tag{2}$$

a medium with a wavespeed varying in three dimensions is also considered, in which the appropriate Green's function satisfies

$$\left[\nabla_g^2 + \frac{\omega^2}{c^2(\mathbf{x_g})}\right] G(\mathbf{x_g}|\mathbf{x_s};\omega) = \delta(\mathbf{x_g} - \mathbf{x_s}); \tag{3}$$

here $\mathbf{x_g}$ is the spatial location of the receiver, $\mathbf{x_s}$ is the spatial location of the source, and ω is the angular temporal frequency. Defining a perturbation on the reference medium wavespeed

$$\alpha(\mathbf{x}) = 1 - \frac{c_0^2}{c^2(\mathbf{x})} \tag{4}$$

and substituting for $c^2(\mathbf{x})$ in equation 3, the two Green's functions are combined to form the Lippmann-Schwinger or scattering equation:

$$G(\mathbf{x_g}|\mathbf{x_s};\omega) = G_0(\mathbf{x_g}|\mathbf{x_s};\omega) + \int_{-\infty}^{\infty} d\mathbf{x}' G_0(\mathbf{x_g}|\mathbf{x}';\omega) k^2 \alpha(\mathbf{x}') G(\mathbf{x}'|\mathbf{x_s};\omega). \tag{5}$$

This gives rise, through back-substitution, to the representation of the Green's function for the variable medium in terms of the Green's function for the homogeneous reference medium and the perturbation α,

$$G(\mathbf{x_g}|\mathbf{x_s};\omega) = G_0(\mathbf{x_g}|\mathbf{x_s};\omega) + G_1(\mathbf{x_g}|\mathbf{x_s};\omega) + G_2(\mathbf{x_g}|\mathbf{x_s};\omega) + ..., \tag{6}$$

known as the forward scattering series or Born series. The individual terms of the series G_n can be considered n'th order in α, the repository for medium information, and are, to give the first- and second-order terms explicitly,

$$G_1(\mathbf{x_g}|\mathbf{x_s};\omega) = \int_{-\infty}^{\infty} d\mathbf{x}' G_0(\mathbf{x_g}|\mathbf{x}';\omega) k^2 \alpha(\mathbf{x}') G_0(\mathbf{x}'|\mathbf{x_s};\omega), \tag{7}$$

and

$$G_2(\mathbf{x_g}|\mathbf{x_s};\omega) = \int_{-\infty}^{\infty} d\mathbf{x}' G_0(\mathbf{x_g}|\mathbf{x}';\omega) k^2 \alpha(\mathbf{x}') \int_{-\infty}^{\infty} d\mathbf{x}'' G_0(\mathbf{x}'|\mathbf{x}'';\omega) k^2 \alpha(\mathbf{x}'') G_0(\mathbf{x}''|\mathbf{x_s};\omega). \tag{8}$$

G_n is the component of the wavefield that is mathematically equivalent to a field (1) interacting n times with scatterers of size α, and (2) propagating directly between each scatterer through the

reference medium via G_0. In this domain the scatterers (e.g., $\alpha(\mathbf{x}')$ and $\alpha(\mathbf{x}'')$ at second order) are separated in space from each other in all three coordinate directions (two lateral, x, y, and one vertical, z) explicitly.

A preferential coordinate direction (depth, z) rates focused attention. In seismology this is because depth is the coordinate along which no or few measurements are possible; in more general terms it is sufficient to stipulate that the preferential axis be that which is perpendicular to the measurement surface. The lateral directions, x and y, may be rendered implicit in the scattering interactions with certain Fourier transforms. To accomplish these, the Fourier transform conventions

$$\begin{aligned} f(k_{x_g}, k_{y_g}) &= \int_{-\infty}^{\infty} dx_g \int_{-\infty}^{\infty} dy_g e^{-ik_{x_g}x_g - ik_{y_g}y_g} f(x_g, y_g), \\ f(x_g, y_g) &= \left(\frac{1}{2\pi}\right)^2 \int_{-\infty}^{\infty} dk_{x_g} \int_{-\infty}^{\infty} dk_{y_g} e^{ik_{x_g}x_g + ik_{y_g}y_g} f(k_{x_g}, k_{y_g}) \end{aligned} \tag{9}$$

are followed for transformation of lateral receiver coordinates, and the opposite conventions,

$$\begin{aligned} f(k_{x_s}, k_{y_s}) &= \int_{-\infty}^{\infty} dx_s \int_{-\infty}^{\infty} dy_s e^{ik_{x_s}x_s + ik_{y_s}y_s} f(x_s, y_s), \\ f(x_s, y_s) &= \left(\frac{1}{2\pi}\right)^2 \int_{-\infty}^{\infty} dk_{x_s} \int_{-\infty}^{\infty} dk_{y_s} e^{-ik_{x_s}x_s - ik_{y_s}y_s} f(k_{x_s}, k_{y_s}), \end{aligned} \tag{10}$$

are followed for lateral source coordinates. Certain combinations of angular frequency and lateral wavenumbers are interpretable through their dispersion relations as being depth wavenumbers; a sign is chosen for these and they are given the denotation q, e.g.,

$$\begin{aligned} q_g &\equiv \operatorname{sgn}(\omega) \left[\frac{\omega^2}{c_0^2} - k_{x_g}^2 - k_{y_g}^2\right]^{1/2}, \\ q_s &\equiv \operatorname{sgn}(\omega) \left[\frac{\omega^2}{c_0^2} - k_{x_s}^2 - k_{y_s}^2\right]^{1/2}, \\ q_n &\equiv \operatorname{sgn}(\omega) \left[\frac{\omega^2}{c_0^2} - k_{xn}^2 - k_{yn}^2\right]^{1/2}. \end{aligned} \tag{11}$$

The wavefield event approximations will in later sections be expressed in the wavenumber domain k_{x_g}, k_{y_g}, k_{x_s}, k_{y_s} for the lateral coordinates, the angular frequency domain ω, and for fixed source and receiver depths z_g and z_s. These latter depths are essentially parameters, changed, at most, to be consistent with reflection or transmission experimental configurations. In the forward scattering series terms in equations 7–8 (and at all higher orders) these choices for output domain will alter the "leftmost" and "rightmost" reference Green's functions; all interior Green's functions remain fully in the space domains. For homogeneous reference media the solutions are straightforwardly expressible in wavenumber-space domains as:

$$\begin{aligned} G_0(k_{x_g}, k_{y_g}, z_g | x', y', z'; \omega) &= e^{-ik_{x_g}x' - ik_{y_g}y'} \frac{e^{iq_g|z_g - z'|}}{i2q_g} \\ G_0(x', y', z' | k_{x_s}, k_{y_s}, z_s; \omega) &= e^{ik_{x_s}x' + ik_{y_s}y'} \frac{e^{iq_s|z' - z_s|}}{i2q_s}, \end{aligned} \tag{12}$$

and in the space domain as

$$G_0(x', y', z'|x'', y'', z''; \omega) = \left(\frac{1}{2\pi}\right)^2 \int_{-\infty}^{\infty} dk_{x_1} \int_{-\infty}^{\infty} dk_{y_1} e^{ik_{x_1}(x'-x'')} e^{ik_{y_1}(y'-y'')} \frac{e^{iq_1|z'-z''|}}{i2q_1}. \quad (13)$$

Expressing the elements of the scattering series terms in this way, especially in bilinear form as in equation 13 above, will allow the depth coordinate z to be treated preferentially, and will allow meaningful wavefield "events" to be categorized in terms of scattering geometries specific to the depth axis.

I also use boldface as a convenience to describe multiple dimensionality in the wavenumber domain, but importantly, these are lateral wavenumbers only, and hence are two-dimensional vectors:

$$\begin{aligned} \mathbf{k_g} &= (k_{x_g}, k_{y_g}), \\ \mathbf{k_s} &= (k_{x_s}, k_{y_s}), \\ \mathbf{k_n} &= (k_{x_n}, k_{y_n}), \end{aligned} \quad (14)$$

etc. These will occur in dot products with lateral space vectors that also require further definition,

$$\begin{aligned} \widetilde{\mathbf{x}}_\mathbf{g} &= (x_g, y_g), \\ \widetilde{\mathbf{x}}_\mathbf{s} &= (x_s, y_s), \\ \widetilde{\mathbf{x}}_\mathbf{n} &= (x_n, y_n), \end{aligned} \quad (15)$$

but that in return render the expression of the interior and "leftmost" and "rightmost" Green's functions of any series term compactly and with distinct treatment of the depth variable z, viz.

$$\begin{aligned} G_0(\mathbf{k_g}, z_g|\mathbf{x}'; \omega) &= e^{-i\mathbf{k_g}\cdot\widetilde{\mathbf{x}}'} \frac{e^{iq_g|z_g-z'|}}{i2q_g}, \\ G_0(\mathbf{x}'|\mathbf{k_s}, z_s; \omega) &= e^{i\mathbf{k_s}\cdot\widetilde{\mathbf{x}}'} \frac{e^{iq_s|z'-z_s|}}{i2q_s}, \end{aligned} \quad (16)$$

and

$$G_0(\mathbf{x}'|\mathbf{x}''; \omega) = \left(\frac{1}{2\pi}\right)^2 \int_{-\infty}^{\infty} d\mathbf{k_1} e^{i\mathbf{k_1}\cdot(\widetilde{\mathbf{x}}'-\widetilde{\mathbf{x}}'')} \frac{e^{iq_1|z'-z''|}}{i2q_1}. \quad (17)$$

3 Forward scattering series terms for reflected and transmitted wave fields

Here, after writing down general forward scattering series terms corresponding to three distinct experimental geometries (upward transmitted, downward transmitted, and reflected), constraints on the scattering integrals within each term of the forward scattering series are imposed based on relative scattering geometries in the depth coordinate. These constraints lead to expressions that isolate the construction of two kinds of meaningful seismic events: reflected primaries and transmitted direct waves.

3.1 Scattering series terms for a transmission-like geometry

In this section the source depth is fixed to be shallower than the receiver depth, and the depth support of the scatterers α is restricted to lie between them. The resulting series terms G_n are renamed T_n^D to signify the n'th order term for the "downward transmitted" wavefield (schematically illustrated for a perturbation varying in 2D in Figure 1). At first order this produces, first generally,

$$T_1(\mathbf{k_g}, z_g|\mathbf{k_s}, z_s; \omega) = \int_{-\infty}^{\infty} d\mathbf{x}' G_0(\mathbf{k_g}, z_g|\mathbf{x}'; \omega) k^2 \alpha(\mathbf{x}') G_0(\mathbf{x}'|\mathbf{k_s}, z_s; \omega), \tag{18}$$

and following the source/receiver restrictions,

$$T_1^D(\mathbf{k_g}, z_g|\mathbf{k_s}, z_s; \omega) = -\frac{1}{4} e^{iq_g z_g - iq_s z_s} \frac{k^2}{q_g q_s} \int_{z_s}^{z_g} dz' e^{-i(q_g - q_s)z'} \alpha(\mathbf{k_g} - \mathbf{k_s}, z'). \tag{19}$$

Similarly, at second order,

$$\begin{aligned} T_2(\mathbf{k_g}, z_g|\mathbf{k_s}, z_s; \omega) = &\int_{-\infty}^{\infty} d\mathbf{x}' G_0(\mathbf{k_g}, z_g|\mathbf{x}'; \omega) k^2 \alpha(\mathbf{x}') \\ &\times \int_{-\infty}^{\infty} d\mathbf{x}'' G_0(\mathbf{x}'|\mathbf{x}''; \omega) k^2 \alpha(\mathbf{x}'') G_0(\mathbf{x}''|\mathbf{k_s}, z_s; \omega), \end{aligned} \tag{20}$$

and

$$\begin{aligned} T_2^D(\mathbf{k_g}, z_g|\mathbf{k_s}, z_s; \omega) = &-\frac{i}{8} e^{iq_g z_g - iq_s z_s} \frac{k^4}{q_g q_s} \left(\frac{1}{2\pi}\right)^2 \int_{-\infty}^{\infty} \frac{d\mathbf{k_1}}{q_1} \\ &\times \int_{z_s}^{z_g} dz' \int_{z_s}^{z_g} dz'' e^{-iq_g z'} e^{iq_1|z' - z''|} e^{iq_s z''} \\ &\times \alpha(\mathbf{k_g} - \mathbf{k_1}, z') \alpha(\mathbf{k_1} - \mathbf{k_s}, z''), \end{aligned} \tag{21}$$

and at third order

$$\begin{aligned} T_3^D(\mathbf{k_g}, z_g|\mathbf{k_s}, z_s; \omega) = &\frac{1}{16} e^{iq_g z_g - iq_s z_s} \frac{k^6}{q_g q_s} \left(\frac{1}{2\pi}\right)^4 \int_{-\infty}^{\infty} \int_{-\infty}^{\infty} \frac{d\mathbf{k_1} d\mathbf{k_2}}{q_1 q_2} \\ &\times \int_{z_s}^{z_g} dz' \int_{z_s}^{z_g} dz'' \int_{z_s}^{z_g} dz''' e^{-iq_g z'} e^{iq_1|z' - z''|} e^{iq_2|z'' - z'''|} e^{iq_s z'''} \\ &\times \alpha(\mathbf{k_g} - \mathbf{k_1}, z') \alpha(\mathbf{k_1} - \mathbf{k_2}, z'') \alpha(\mathbf{k_2} - \mathbf{k_s}, z'''). \end{aligned} \tag{22}$$

(The alterations to the depth integral limits are permissible because of the chosen depth support of α.) Stopping here, not because three orders are deemed to be sufficient to approximate the actual wavefield (quite the opposite: in studies of the inverse scattering series, which involves similar term by term behavior to the forward case, it has been pointed out in theory (Stolt and Jacobs, 1981) and in numerical application (Shaw et al., 2004; Shaw, 2005; Innanen, 2003; Innanen et al., 2006) that often many tens of terms are needed; this series in its most stripped down form resembles a polynomial approximation of an exponential function), but because the patterns arising in increasing order are reasonably clear, the source and receiver depths are next reversed, to generate an "upward transmitted" configuration. Similarly to the downward case:

$$T_1^U(\mathbf{k_g}, z_g|\mathbf{k_s}, z_s; \omega) = -\frac{1}{4} e^{-iq_g z_g + iq_s z_s} \frac{k^2}{q_g q_s} \int_{z_g}^{z_s} dz' e^{i(q_g - q_s)z'} \alpha(\mathbf{k_g} - \mathbf{k_s}, z'), \tag{23}$$

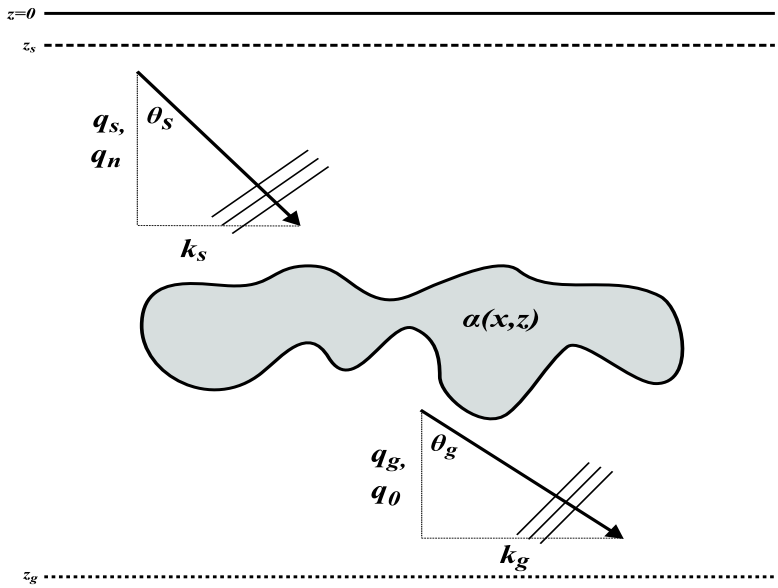

Figure 1: *A conceptual depiction in 2D of the transmission-type source/receiver/scatterer configuration. At a fixed depth z_s a source plane wave with the frequency $\omega = kc_0$ (and characterized by any one of the lateral wavenumber k_s, the source angle θ_s, or the depth wavenumber q_s) originates and propagates into the scattering region, interacts, and a receiver plane wave with the same frequency (and characterized by any one of k_g, θ_g, or q_g) returns to the fixed receiver depth z_g. In these notes particular use is made of the depth wavenumber. In the n'th order portion of the wave field there arises an ordered set of depth wavenumbers, and it is convenient to express the source depth wavenumber as the n'th in that set, and the receiver depth wavenumber as the zero'th in that set.*

$$T_2^U(\mathbf{k_g}, z_g|\mathbf{k_s}, z_s; \omega) = -\frac{i}{8} e^{-iq_g z_g + iq_s z_s} \frac{k^4}{q_g q_s} \left(\frac{1}{2\pi}\right)^2 \int_{-\infty}^{\infty} \frac{d\mathbf{k_1}}{q_1} \times \int_{z_g}^{z_s} dz' \int_{z_g}^{z_s} dz'' e^{iq_g z'} e^{iq_1|z'-z''|} e^{-iq_s z''} \times \alpha(\mathbf{k_g} - \mathbf{k_1}, z')\alpha(\mathbf{k_1} - \mathbf{k_s}, z''), \tag{24}$$

and

$$T_3^U(\mathbf{k_g}, z_g|\mathbf{k_s}, z_s; \omega) = \frac{1}{16} e^{-iq_g z_g + iq_s z_s} \frac{k^6}{q_g q_s} \left(\frac{1}{2\pi}\right)^4 \int_{-\infty}^{\infty} \int_{-\infty}^{\infty} \frac{d\mathbf{k_1} d\mathbf{k_2}}{q_1 q_2} \times \int_{z_g}^{z_s} dz' \int_{z_g}^{z_s} dz'' \int_{z_g}^{z_s} dz''' e^{iq_g z'} e^{iq_1|z'-z''|} e^{iq_2|z''-z'''|} e^{-iq_s z'''} \times \alpha(\mathbf{k_g} - \mathbf{k_1}, z')\alpha(\mathbf{k_1} - \mathbf{k_2}, z'')\alpha(\mathbf{k_2} - \mathbf{k_s}, z'''). \tag{25}$$

The series $\sum T_n^D$ and $\sum T_n^U$, when convergent, create all relevant components of a transmitted wavefield (upward or downward as the case may be). This must include portions of the solution that correspond to any "event", however it is defined or otherwise recognized. In transmitted wavefields these events include the direct wave, and multiples, events corresponding to energy that has reverberated, in the depth coordinate, within the scattering portion of the medium.

3.2 Scattering series terms for a reflection-like geometry

If the source and receiver depths are fixed to both exist at depths less than the depth-support of the scattering medium α, the resulting expressions will be consistent with a reflection experiment and geometry (schematically illustrated for a perturbation varying in 2D in Figure 2). Fixing them as such and renaming the series terms R_n, again to third order the expressions

$$R_1(\mathbf{k_g}, z_g|\mathbf{k_s}, z_s; \omega) = \int_{-\infty}^{\infty} d\mathbf{x}' G_0(\mathbf{k_g}, z_g|\mathbf{x}'; \omega) k^2 \alpha(\mathbf{x}') G_0(\mathbf{x}'|\mathbf{k_s}, z_s; \omega), \tag{26}$$

$$R_1(\mathbf{k_g}, z_g|\mathbf{k_s}, z_s; \omega) = -\frac{1}{4} e^{-iq_g z_g - iq_s z_s} \frac{k^2}{q_g q_s} \int_{-\infty}^{\infty} dz' e^{i(q_g + q_s)z'} \alpha(\mathbf{k_g} - \mathbf{k_s}, z'), \tag{27}$$

and

$$R_2(\mathbf{k_g}, z_g|\mathbf{k_s}, z_s; \omega) = \int_{-\infty}^{\infty} d\mathbf{x}' G_0(\mathbf{k_g}, z_g|\mathbf{x}'; \omega) k^2 \alpha(\mathbf{x}') \times \int_{-\infty}^{\infty} d\mathbf{x}'' G_0(\mathbf{x}'|\mathbf{x}''; \omega) k^2 \alpha(\mathbf{x}'') G_0(\mathbf{x}''|\mathbf{k_s}, z_s; \omega), \tag{28}$$

$$R_2(\mathbf{k_g}, z_g|\mathbf{k_s}, z_s; \omega) = -\frac{i}{8} e^{-iq_g z_g - iq_s z_s} \frac{k^4}{q_g q_s} \left(\frac{1}{2\pi}\right)^2 \int_{-\infty}^{\infty} \frac{d\mathbf{k_1}}{q_1} \times \int_{-\infty}^{\infty} dz' \int_{-\infty}^{\infty} dz'' e^{iq_g z'} e^{iq_1|z'-z''|} e^{iq_s z''} \times \alpha(\mathbf{k_g} - \mathbf{k_1}, z')\alpha(\mathbf{k_1} - \mathbf{k_s}, z''), \tag{29}$$

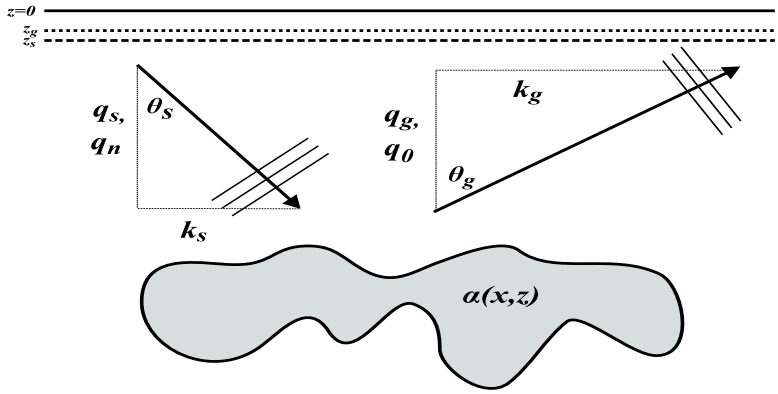

Figure 2: *A conceptual depiction in 2D of the reflection-type source/receiver/scatterer configuration. At a fixed depth z_s a source plane wave with the frequency $\omega = kc_0$ (and characterized by any one of the lateral wavenumber k_s, the source angle θ_s, or the depth wavenumber q_s) originates and propagates into the scattering region, interacts, and a receiver plane wave with the same frequency (and characterized by any one of k_g, θ_g, or q_g) returns to the fixed receiver depth z_g. In these notes particular use is made of the depth wavenumber. In the n'th order portion of the wave field there arises an ordered set of depth wavenumbers, and it is convenient to express the source depth wavenumber as the n'th in that set, and the receiver depth wavenumber as the zero'th in that set.*

and finally

$$\begin{aligned} R_3(\mathbf{k_g}, z_g|\mathbf{k_s}, z_s; \omega) = \frac{1}{16} e^{-iq_g z_g - iq_s z_s} \frac{k^6}{q_g q_s} \left(\frac{1}{2\pi}\right)^4 \int_{-\infty}^{\infty}\int_{-\infty}^{\infty} \frac{d\mathbf{k_1} d\mathbf{k_2}}{q_1 q_2} \\ \times \int_{-\infty}^{\infty} dz' \int_{-\infty}^{\infty} dz'' \int_{-\infty}^{\infty} dz''' e^{iq_g z'} e^{iq_1|z'-z''|} e^{iq_2|z''-z'''|} e^{iq_s z'''} \\ \times \alpha(\mathbf{k_g} - \mathbf{k_1}, z')\alpha(\mathbf{k_1} - \mathbf{k_2}, z'')\alpha(\mathbf{k_2} - \mathbf{k_s}, z'''), \end{aligned} \tag{30}$$

are produced. As in the case of the transmitted geometries, a convergent series $\sum R_n$ must produce all expected reflected wavefield events, including energy that has, within some reasonable standard for categorization, propagated "down-and-back" once only, forming a set of events known as primaries, and energy that has reverberated in the depth coordinate (forming multiples).

4 Approximations of the transmitted-direct and reflected-primary wave fields

In a potentially complicated multidimensional medium, concepts of "direct" and "primary" wavefield events, in regular use in exploration seismology, have the tendency to lose the straightforward meaning available to them in, say, a stratified medium. This is especially true when their description is to be in terms of scattering, in which even core concepts such as "reflection" are not elements but only results of the theory.

Nevertheless distinctions with respect to the categorization of an event as a primary or a multiple (i.e., a reverberation) are at the heart of processing methods based on the inverse scattering series (Weglein et al., 1997; Weglein et al., 2003), and specific methodologies have required a standard for determining whether or not a series term or part thereof is geared towards action on a primary only (e.g., Weglein et al., 2002; Shaw et al., 2004; Innanen, 2003; Liu et al., 2005; Zhang and

Weglein, 2005). The intuition leading to such standards has been aided by a study of the creation of primaries with the forward scattering series. The developments of Matson (1996) and others have guided the inverse approaches by suggesting which series terms act to create which wavefield events. More recently, a more general set of expressions, for the reflected primaries associated with an arbitrary layered acoustic medium, have been proposed. Partitioning of the forward scattering series based on *relative geometry of scattering interactions* gives rise to these expressions for the primaries, and the primaries only, of the reflected wavefield over a layered perturbation. Analysis and numerics of the layered case provide evidence that a certain brand of series partitioning does indeed produce accurate approximations of the phase and amplitude of such primaries (Innanen, 2005). Those encouraging results for layered media have been built upon here.

The complexities involved in extension of these series methods beyond 1D are not trivial (as Liu et al. (2005) have certainly shown for the direct imaging problem). In the layered case, *depth* is the coordinate along which the "relative geometry of scattering interactions" is determined; enumeration of the overall number of direction changes along this axis forming the main criterion. One of the main contributions of this paper is to advocate as full a retention of that approach as the multidimensional case will allow. It turns out that a lateral wavenumber representation permits the continued use of this criterion without any serious conceptual changes. The generalization then still amounts to a retention of terms with suitable scattering geometries in depth, but now as part of an integral over plane wave components.

4.1 Constraining the scattering integrals to approximate the direct component of the transmitted wave field

Equations 20–22 are to third order terms expressing a transmission-like wavefield through a heterogeneous perturbation that is assumed to lie between the source and receiver. The aim in this paper is to extract only that component of the full solution that corresponds to the direct wave, i.e., a single event that has propagated directly through the intermediate structure, suffering no reverberation.

This is accomplished through the retention of terms with suitable scattering geometry. The scattering integrals have been manipulated such that depth z is the only explicit space variable remaining whose geometry may be considered. Extracting these depth integrals from their corresponding wavefield series terms, we have

$$\begin{aligned}
\mathrm{ID}_1 &= \int_{z_s}^{z_g} dz' e^{-iq_g z'} \alpha(\mathbf{k_g} - \mathbf{k_s}, z') e^{iq_s z'} \\
\mathrm{ID}_2 &= \int_{z_s}^{z_g} dz' e^{-iq_g z'} \alpha(\mathbf{k_g} - \mathbf{k_1}, z') \int_{z_s}^{z_g} dz'' e^{iq_1|z'-z''|} \alpha(\mathbf{k_1} - \mathbf{k_s}, z'') e^{iq_s z''} \\
\mathrm{ID}_3 &= \int_{z_s}^{z_g} dz' e^{-iq_g z'} \alpha(\mathbf{k_g} - \mathbf{k_1}, z') \int_{z_s}^{z_g} dz'' e^{iq_1|z'-z''|} \alpha(\mathbf{k_1} - \mathbf{k_2}, z'') \\
&\quad \times \int_{z_s}^{z_g} dz''' e^{iq_1|z''-z'''|} \alpha(\mathbf{k_2} - \mathbf{k_s}, z''') e^{iq_s z'''},
\end{aligned} \tag{31}$$

etc. Clearly the nature of these expressions will change depending on the relative magnitudes of the depths of the contributing scattering interactions z', z'', z''', etc.; Figure 3 illustrates the four

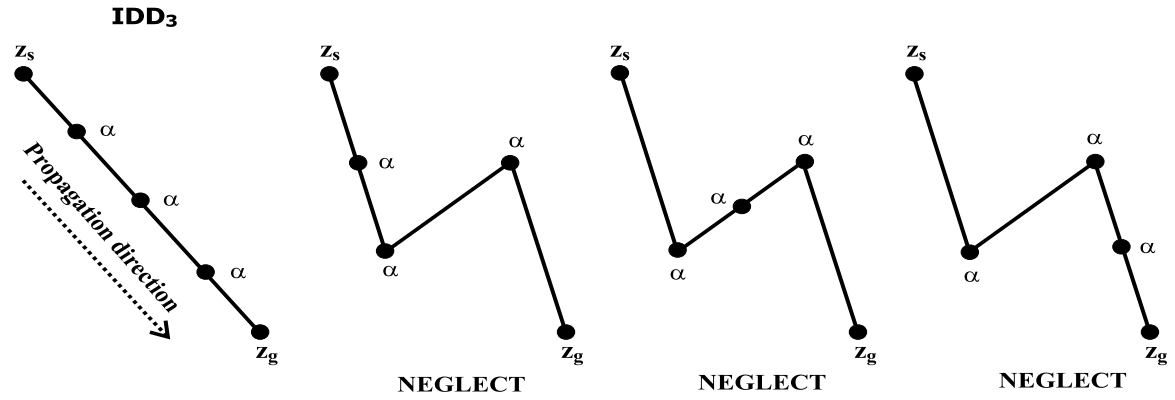

Figure 3: *Four diagrams illustrating the four contributions to the third-order transmission-like scattering integral. All but the first scattering contribution have geometries consistent with reverberation, i.e., transmitted multiples, and so are neglected in an approximation of the direct wave. The remaining contribution involves no "turn-around" point.*

permutations of third-order scattering interactions in depth. Some of the series terms at third order appear to correspond to reverberative paths of wave energy. This correspondence is used to constrain the integrals, the hypothesis being that eliminating contributions from this reverberative diagram-type will mean eliminating the creation of reverberative events. It is important to emphasize that the retention/rejection of scattering contributions at only a given order, say third order, will only eliminate the third order component of a multiple, which is itself at best only a poor approximation of the actual event; a large number of terms, at each order invoking such constraints, are necessary for the scheme to bear fruit. This is a comment that is conceptually very much aligned with the introductory descriptions in this paper, but it now appears to have produced a contradiction: if this third-order contribution, in spite of its diagrammatical resemblance to a reverberative event, is itself dissimilar to the *actual* multiple event in the wavefield solution, what reason is there to think that it has any role, let alone a key role, in the construction of the actual event we wish to suppress in a primary or direct wave approximation? The answer lies in the pathology of the forward scattering series, which is to use the lowest-order, or most primitive event approximations, as seeding points about which to expand the actual event in series. For instance, a multiple that has a single downward reflection, or one that reverberates once only, has its first and most primitive approximation appear at third order (e.g., Matson, 1996). At subsequent orders (and, in fact, represented by similar diagrams) are contributions to a correction of this linear event approximation. In general, the n'th order term in the forward scattering series involves contributions that are: first-order approximations of an event that has undergone n actual reflections, second-order approximations of an event that has undergone $n-1$ actual reflections, third-order approximations of an event that has undergone $n-2$ actual reflections, etc., and, finally, n'th order approximations of an event that has undergone a single actual reflection (viz., a primary). In other words, even at low order such geometrical (or diagrammatical) analysis of scattering interactions can reveal to what event any term is making its largest contribution. The subsequent rejection of "reverberating" seeding points is justifiably deemed to result in the rejection of reverberating components of the full solution. Doing so for the first three orders results in a new set of scattering

integrals that correspond to the zeroing of reverberative series contributions (see Figure 1):

$$\begin{aligned}
\mathrm{IDD}_1 &= \int_{z_s}^{z_g} dz' e^{i(q_s-q_g)z'} \alpha(\mathbf{k_g}-\mathbf{k_s}, z') \\
\mathrm{IDD}_2 &= \int_{z_s}^{z_g} dz' e^{i(q_1-q_g)z'} \alpha(\mathbf{k_g}-\mathbf{k_1}, z') \int_{z_s}^{z'} dz'' e^{i(q_s-q_1)z''} \alpha(\mathbf{k_1}-\mathbf{k_s}, z'') \\
\mathrm{IDD}_3 &= \int_{z_s}^{z_g} dz' e^{i(q_1-q_g)z'} \alpha(\mathbf{k_g}-\mathbf{k_1}, z') \int_{z_s}^{z'} dz'' e^{i(q_2-q_1)z''} \alpha(\mathbf{k_1}-\mathbf{k_2}, z'') \\
&\times \int_{z_s}^{z''} dz''' e^{i(q_s-q_2)z'''} \alpha(\mathbf{k_2}-\mathbf{k_s}, z''').
\end{aligned} \tag{32}$$

Substituting these back into the expressions for the transmitted wavefield results in order-by-order expressions for the "downward" transmitted direct wave:

$$\begin{aligned}
T_1^{DD}(\mathbf{k_g}, z_g|\mathbf{k_s}, z_s; \omega) &= -\frac{1}{4} e^{iq_g z_g - iq_s z_s} \frac{k^2}{q_g q_s} \\
&\times \int_{z_s}^{z_g} dz' e^{i(q_s-q_g)z'} \alpha(\mathbf{k_g}-\mathbf{k_s}, z'),
\end{aligned} \tag{33}$$

$$\begin{aligned}
T_2^{DD}(\mathbf{k_g}, z_g|\mathbf{k_s}, z_s; \omega) &= -\frac{i}{8} e^{iq_g z_g - iq_s z_s} \frac{k^4}{q_g q_s} \left(\frac{1}{2\pi}\right)^2 \int_{-\infty}^{\infty} \frac{d\mathbf{k_1}}{q_1} \\
&\times \int_{z_s}^{z_g} dz' e^{i(q_1-q_g)z'} \alpha(\mathbf{k_g}-\mathbf{k_1}, z') \\
&\times \int_{z_s}^{z'} dz'' e^{i(q_s-q_1)z''} \alpha(\mathbf{k_1}-\mathbf{k_s}, z''),
\end{aligned} \tag{34}$$

$$\begin{aligned}
T_3^{DD}(\mathbf{k_g}, z_g|\mathbf{k_s}, z_s; \omega) &= \frac{1}{16} e^{iq_g z_g - iq_s z_s} \frac{k^6}{q_g q_s} \left(\frac{1}{2\pi}\right)^4 \int_{-\infty}^{\infty} \int_{-\infty}^{\infty} \frac{d\mathbf{k_1} d\mathbf{k_2}}{q_1 q_2} \\
&\times \int_{z_s}^{z_g} dz' e^{i(q_1-q_g)z'} \alpha(\mathbf{k_g}-\mathbf{k_1}, z') \\
&\times \int_{z_s}^{z'} dz'' e^{i(q_2-q_1)z''} \alpha(\mathbf{k_1}-\mathbf{k_2}, z'') \\
&\times \int_{z_s}^{z''} dz''' e^{i(q_s-q_2)z'''} \alpha(\mathbf{k_2}-\mathbf{k_s}, z'''),
\end{aligned} \tag{35}$$

etc. Repeating this process with the "upward" transmitted wavefield, through construction and re-substitutions of similar (but "upward" propagating) scattering integral components IDU_n, results in

$$\begin{aligned}
T_1^{DU}(\mathbf{k_g}, z_g|\mathbf{k_s}, z_s; \omega) &= -\frac{1}{4} e^{-iq_g z_g + iq_s z_s} \frac{k^2}{q_g q_s} \\
&\times \int_{z_g}^{z_s} dz' e^{i(q_g-q_s)z'} \alpha(\mathbf{k_g}-\mathbf{k_s}, z'),
\end{aligned} \tag{36}$$

$$T_2^{DU}(\mathbf{k_g}, z_g|\mathbf{k_s}, z_s; \omega) = -\frac{i}{8} e^{-iq_g z_g + iq_s z_s} \frac{k^4}{q_g q_s} \left(\frac{1}{2\pi}\right)^2 \int_{-\infty}^{\infty} \frac{d\mathbf{k_1}}{q_1} \times \int_{z_g}^{z_s} dz' e^{i(q_g - q_1)z'} \alpha(\mathbf{k_g} - \mathbf{k_1}, z') \times \int_{z'}^{z_s} dz'' e^{i(q_1 - q_s)z''} \alpha(\mathbf{k_1} - \mathbf{k_s}, z''), \tag{37}$$

and

$$T_3^{DU}(\mathbf{k_g}, z_g|\mathbf{k_s}, z_s; \omega) = \frac{1}{16} e^{-iq_g z_g + iq_s z_s} \frac{k^6}{q_g q_s} \left(\frac{1}{2\pi}\right)^4 \int_{-\infty}^{\infty} \int_{-\infty}^{\infty} \frac{d\mathbf{k_1} d\mathbf{k_2}}{q_1 q_2} \times \int_{z_g}^{z_s} dz' e^{i(q_g - q_1)z'} \alpha(\mathbf{k_g} - \mathbf{k_1}, z') \times \int_{z'}^{z_s} dz'' e^{i(q_1 - q_2)z''} \alpha(\mathbf{k_1} - \mathbf{k_2}, z'') \times \int_{z''}^{z_s} dz''' e^{i(q_2 - q_s)z'''} \alpha(\mathbf{k_2} - \mathbf{k_s}, z'''), \tag{38}$$

etc. Summing $\sum_n T_n^{DD}$ and $\sum_n T_n^{DU}$ are postulated to form approximations of these wavefield components.

4.2 Constraining the scattering integrals to approximate the primary component of the reflected wave field

As with the transmitted case, the reflected primary components of the full reflected wavefield series expressions are isolated by a retention/rejection programme on the scattering integrals. In the case of the reflected primaries, only the terms for which the linear (single scattering) term is a seed point about which to expand in series are retained. Figure 4 illustrates the three, of four, third-order terms for which this is the case. Retention of only this type of term produces a subseries that, like the transmission case, follows straightforward mathematical patterns; in fact, the terms seeding the construction of multiples are responsible for the greatest mathematical complexities encountered in this three-dimensional single parameter acoustic framework. The raw scattering integrals,

$$\begin{aligned} \mathrm{IR}_1 &= \int_{-\infty}^{\infty} dz' e^{i(q_g + q_s)z'} \alpha(\mathbf{k_g} - \mathbf{k_s}, z') \\ \mathrm{IR}_2 &= \int_{-\infty}^{\infty} dz' e^{iq_g z'} \alpha(\mathbf{k_g} - \mathbf{k_1}, z') \int_{-\infty}^{\infty} dz'' e^{iq_1|z' - z''|} \alpha(k_1 - k_s, z'') e^{iq_s z''} \\ \mathrm{IR}_3 &= \int_{-\infty}^{\infty} dz' e^{iq_g z'} \alpha(\mathbf{k_g} - \mathbf{k_1}, z') \int_{-\infty}^{\infty} dz'' e^{iq_1|z' - z''|} \alpha(\mathbf{k_1} - \mathbf{k_2}, z'') \\ &\quad \times \int_{-\infty}^{\infty} dz''' e^{iq_2|z'' - z'''|} \alpha(\mathbf{k_2} - \mathbf{k_s}, z''') e^{iq_s z'''}, \end{aligned} \tag{39}$$

are manipulated and replaced with portions thereof. In the reflected primary case, the linear term produces the seeds for all primaries, and, in fact, approximates them all (albeit poorly). The task of all subsequent retained terms is to correct the phase and amplitude errors of these proto-events.

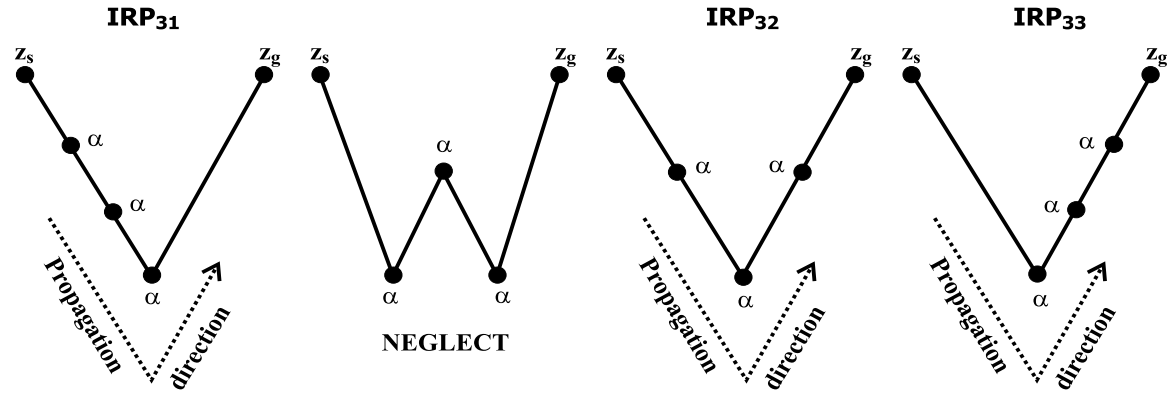

Figure 4: *Four diagrams illustrating the four contributions to the third-order scattering integral. In modelling primaries, the second scattering contribution, whose geometry is "multiple-like" (and all such contributions at higher order) are neglected. The remaining contributions involve a single "turn-around" point; in each case (at third order) the other two scattering interactions are transmission like and involve no change in propagation direction.*

This retention/rejection scheme when applied to first and second-orders suggests the replacement of IR_1 and IR_2 with partial integrals IRP_1 and IRP_2 respectively, where

$$\mathrm{IRP}_1 = \int_{-\infty}^{\infty} dz' e^{i(q_g+q_s)z'} \alpha(\mathbf{k_g} - \mathbf{k_s}, z'), \tag{40}$$

and

$$\begin{aligned} \mathrm{IRP}_2 = &\int_{-\infty}^{\infty} dz' e^{i(q_g+q_1)z'} \alpha(\mathbf{k_g} - \mathbf{k_1}, z') \int_{-\infty}^{z'} dz'' e^{i(q_s-q_1)z''} \alpha(\mathbf{k_1} - \mathbf{k_s}, z'') \\ &+ \int_{-\infty}^{\infty} dz' e^{i(q_g-q_1)z'} \alpha(\mathbf{k_g} - \mathbf{k_1}, z') \int_{z'}^{\infty} dz'' e^{i(q_1+q_s)z''} \alpha(\mathbf{k_1} - \mathbf{k_s}, z''). \end{aligned} \tag{41}$$

The same scheme at third-order requires three contributions such that IR_3 may be replaced with IRP_3:

$$\mathrm{IRP}_3 = \mathrm{IRP}_{31} + \mathrm{IRP}_{32} + \mathrm{IRP}_{33}, \tag{42}$$

where

$$\begin{aligned} \mathrm{IRP}_{31} = &\int_{-\infty}^{\infty} dz' e^{i(q_g+q_1)z'} \alpha(\mathbf{k_g} - \mathbf{k_1}, z') \int_{-\infty}^{z'} dz'' e^{i(q_2-q_1)z''} \alpha(\mathbf{k_1} - \mathbf{k_2}, z'') \\ &\times \int_{-\infty}^{z''} dz''' e^{i(q_s-q_2)z''} \alpha(\mathbf{k_2} - \mathbf{k_s}, z'''), \end{aligned} \tag{43}$$

$$\begin{aligned} \mathrm{IRP}_{32} = &\int_{-\infty}^{\infty} dz' e^{i(q_g-q_1)z'} \alpha(\mathbf{k_g} - \mathbf{k_1}, z') \int_{z'}^{\infty} dz'' e^{i(q_1+q_2)z''} \alpha(\mathbf{k_1} - \mathbf{k_2}, z'') \\ &\times \int_{-\infty}^{z''} dz''' e^{i(q_s-q_2)z''} \alpha(\mathbf{k_2} - \mathbf{k_s}, z'''), \end{aligned} \tag{44}$$

and

$$\begin{aligned} \mathrm{IRP}_{33} = &\int_{-\infty}^{\infty} dz' e^{i(q_g-q_1)z'} \alpha(\mathbf{k_g} - \mathbf{k_1}, z') \int_{z'}^{\infty} dz'' e^{i(q_1-q_2)z''} \alpha(\mathbf{k_1} - \mathbf{k_2}, z'') \\ &\times \int_{z''}^{\infty} dz''' e^{i(q_2+q_s)z''} \alpha(\mathbf{k_2} - \mathbf{k_s}, z'''). \end{aligned} \tag{45}$$

Substituting these portions of the scattering integral back into the full expressions for the reflected wavefield series terms is suggested as contributing to an order-by-order primary approximation with terms R_n^P, where at the first order

$$R_1^P(\mathbf{k_g}, z_g|\mathbf{k_s}, z_s; \omega) = -\frac{1}{4} e^{-iq_g z_g - iq_s z_s} \frac{k^2}{q_g q_s} \int_{-\infty}^{\infty} dz' e^{i(q_g+q_s)z'} \alpha(\mathbf{k_g} - \mathbf{k_s}, z'), \tag{46}$$

at second order

$$R_2^P = R_{21}^P + R_{22}^P, \tag{47}$$

where

$$\begin{aligned} R_{21}^P(\mathbf{k_g}, z_g|\mathbf{k_s}, z_s; \omega) = -\frac{i}{8} e^{-iq_g z_g - iq_s z_s} \frac{k^4}{q_g q_s} \left(\frac{1}{2\pi}\right)^2 \int_{-\infty}^{\infty} \frac{d\mathbf{k_1}}{q_1} \\ \times \int_{-\infty}^{\infty} dz' e^{i(q_g+q_1)z'} \alpha(\mathbf{k_g} - \mathbf{k_1}, z') \\ \times \int_{-\infty}^{z'} dz'' e^{i(q_s-q_1)z''} \alpha(\mathbf{k_1} - \mathbf{k_s}, z''), \end{aligned} \tag{48}$$

and

$$\begin{aligned} R_{22}^P(\mathbf{k_g}, z_g|\mathbf{k_s}, z_s; \omega) = -\frac{i}{8} e^{-iq_g z_g - iq_s z_s} \frac{k^4}{q_g q_s} \left(\frac{1}{2\pi}\right)^2 \int_{-\infty}^{\infty} \frac{d\mathbf{k_1}}{q_1} \\ \times \int_{-\infty}^{\infty} dz' e^{i(q_g-q_1)z'} \alpha(\mathbf{k_g} - \mathbf{k_1}, z') \\ \times \int_{z'}^{\infty} dz'' e^{i(q_1+q_s)z''} \alpha(\mathbf{k_1} - \mathbf{k_s}, z''); \end{aligned} \tag{49}$$

meanwhile at third order

$$R_3^P = R_{31}^P + R_{32}^P + R_{33}^P, \tag{50}$$

where

$$\begin{aligned} R_{31}^P(\mathbf{k_g}, z_g|\mathbf{k_s}, z_s; \omega) = \frac{1}{16} e^{-iq_g z_g - iq_s z_s} \frac{k^6}{q_g q_s} \left(\frac{1}{2\pi}\right)^4 \int_{-\infty}^{\infty} \int_{-\infty}^{\infty} \frac{d\mathbf{k_1} d\mathbf{k_2}}{q_1 q_2} \\ \times \int_{-\infty}^{\infty} dz' e^{i(q_g+q_1)z'} \alpha(\mathbf{k_g} - \mathbf{k_1}, z') \\ \times \int_{-\infty}^{z'} dz'' e^{i(q_2-q_1)z''} \alpha(\mathbf{k_1} - \mathbf{k_2}, z'') \\ \times \int_{-\infty}^{z''} dz''' e^{i(q_s-q_2)z''} \alpha(\mathbf{k_2} - \mathbf{k_s}, z'''), \end{aligned} \tag{51}$$

and

$$\begin{aligned} R^P_{32}(\mathbf{k_g}, z_g|\mathbf{k_s}, z_s; \omega) = \frac{1}{16} e^{-iq_g z_g - iq_s z_s} \frac{k^6}{q_g q_s} \left(\frac{1}{2\pi}\right)^4 \int_{-\infty}^{\infty}\int_{-\infty}^{\infty} \frac{d\mathbf{k_1} d\mathbf{k_2}}{q_1 q_2} \\ \times \int_{-\infty}^{\infty} dz' e^{i(q_g - q_1)z'} \alpha(\mathbf{k_g} - \mathbf{k_1}, z') \\ \times \int_{z'}^{\infty} dz'' e^{i(q_1 + q_2)z''} \alpha(\mathbf{k_1} - \mathbf{k_2}, z'') \\ \times \int_{-\infty}^{z''} dz''' e^{i(q_s - q_2)z''} \alpha(\mathbf{k_2} - \mathbf{k_s}, z'''), \end{aligned} \tag{52}$$

and finally

$$\begin{aligned} R^P_{33}(\mathbf{k_g}, z_g|\mathbf{k_s}, z_s; \omega) = \frac{1}{16} e^{-iq_g z_g - iq_s z_s} \frac{k^6}{q_g q_s} \left(\frac{1}{2\pi}\right)^4 \int_{-\infty}^{\infty}\int_{-\infty}^{\infty} \frac{d\mathbf{k_1} d\mathbf{k_2}}{q_1 q_2} \\ \times \int_{-\infty}^{\infty} dz' e^{i(q_g - q_1)z'} \alpha(\mathbf{k_g} - \mathbf{k_1}, z') \\ \times \int_{z'}^{\infty} dz'' e^{i(q_1 - q_2)z''} \alpha(\mathbf{k_1} - \mathbf{k_2}, z'') \\ \times \int_{z''}^{\infty} dz''' e^{i(q_2 + q_s)z''} \alpha(\mathbf{k_2} - \mathbf{k_s}, z''') \end{aligned} \tag{53}$$

are the three term portions given explicitly. To summarize, through what is essentially an ansatz regarding the chief mechanisms of construction of primaries and direct waves in reflected and transmitted configurations respectively in scattering theory, prescriptions have been presented for media describable as variations in P-wave velocity on a homogeneous background, or reference, medium for both these types of wavefield event. The remainder of the development in this paper is largely variations on this theme, such that, for instance, these approximations may be more readily computed and/or understood analytically.

4.3 Recursive forms

In the last part of this paper I will demonstrate the cumulative activity of an (effectively) infinite number of such series terms when the medium varies in the depth coordinate only. Unfortunately such summed closed-forms do not appear to be readily derivable for media that vary in two or three dimensions, a fact which, in practice, means a greater computational burden in using these expressions. However, although closed-forms are not available, recursive forms are. In other words, although it may be necessary to calculate the n'th term in the series derived above, the n'th term can be written as a relatively simple operation on the $n-1$'th term, potentially a significant lightening of the computational burden.

I will demonstrate with the downward transmitted direct wavefield. The upward transmitted direct wavefield follows immediately, and, as I will demonstrate in the next section, order-by-order relations can be derived between these two sets of transmitted direct wavefield series terms and the reflected primary series terms. So to have this one quantity is to have all three. An appeal, then,

is made to portions of equations 33–35 (omitting momentarily pre-factors common to each term), re-written with the "source" index s set to n and the "receiver" index g set to 0:

$$\widetilde{T}_1^{DD}(\mathbf{k_0}, z_g|\mathbf{k_1}, z_s; \omega) = \frac{ik^2}{2}\frac{1}{q_1}\int_{z_s}^{z_g} dz' e^{i(q_1-q_0)z'}\alpha(\mathbf{k_0}-\mathbf{k_1}, z'), \tag{54}$$

$$\begin{aligned}\widetilde{T}_2^{DD}(\mathbf{k_0}, z_g|\mathbf{k_2}, z_s; \omega) = &\left(\frac{ik^2}{2}\right)^2\frac{1}{q_2}\int_{z_s}^{z_g} dz'\left(\frac{1}{2\pi}\right)^2\int_{-\infty}^{\infty}\frac{d\mathbf{k_1}}{q_1}e^{i(q_1-q_0)z'}\alpha(\mathbf{k_0}-\mathbf{k_1}, z') \\ &\times\int_{z_s}^{z'} dz'' e^{i(q_2-q_1)z''}\alpha(\mathbf{k_1}-\mathbf{k_2}, z''),\end{aligned} \tag{55}$$

$$\begin{aligned}\widetilde{T}_3^{DD}(\mathbf{k_0}, z_g|\mathbf{k_3}, z_s; \omega) = &\left(\frac{ik^2}{2}\right)^3\frac{1}{q_3}\int_{z_s}^{z_g} dz'\left(\frac{1}{2\pi}\right)^2\int_{-\infty}^{\infty}\frac{d\mathbf{k_1}}{q_1}e^{i(q_1-q_0)z'}\alpha(\mathbf{k_0}-\mathbf{k_1}, z') \\ &\times\int_{z_s}^{z'} dz''\left(\frac{1}{2\pi}\right)^2\int_{-\infty}^{\infty}\frac{d\mathbf{k_2}}{q_2}e^{i(q_2-q_1)z''}\alpha(\mathbf{k_1}-\mathbf{k_2}, z'') \\ &\times\int_{z_s}^{z''} dz''' e^{i(q_3-q_2)z'''}\alpha(\mathbf{k_2}-\mathbf{k_3}, z''').\end{aligned} \tag{56}$$

In these forms the patterns underlying a recursion are visible. In fact it is true that:

$$\begin{aligned}\widetilde{T}_2^{DD}(\mathbf{k_0}, z_g|\mathbf{k_2}, z_s; \omega) &= \frac{ik^2}{8\pi^2}\int_{z_s}^{z_g} dz'\int_{-\infty}^{\infty}\frac{d\mathbf{k_1}}{q_1}e^{i(q_1-q_0)z'}\alpha(\mathbf{k_0}-\mathbf{k_1}, z')\widetilde{T}_1^{DD}(\mathbf{k_1}, z'|\mathbf{k_2}, z_s; \omega), \\ \widetilde{T}_3^{DD}(\mathbf{k_0}, z_g|\mathbf{k_3}, z_s; \omega) &= \frac{ik^2}{8\pi^2}\int_{z_s}^{z_g} dz'\int_{-\infty}^{\infty}\frac{d\mathbf{k_1}}{q_1}e^{i(q_1-q_0)z'}\alpha(\mathbf{k_0}-\mathbf{k_1}, z')\widetilde{T}_2^{DD}(\mathbf{k_1}, z'|\mathbf{k_3}, z_s; \omega),\end{aligned} \tag{57}$$

etc., or, more generally,

$$\widetilde{T}_n^{DD}(\mathbf{k_0}, z_g|\mathbf{k_n}, z_s; \omega) = \frac{ik^2}{8\pi^2}\int_{z_s}^{z_g} dz'\int_{-\infty}^{\infty}\frac{d\mathbf{k_1}}{q_1}e^{i(q_1-q_0)z'}\alpha(\mathbf{k_0}-\mathbf{k_1}, z')\widetilde{T}_{n-1}^{DD}(\mathbf{k_1}, z'|\mathbf{k_n}, z_s; \omega). \tag{58}$$

Summing these together and recalling that the largest-indexed lateral wavenumber is interpreted as a source lateral wavenumber $\mathbf{k_s}$, and the smallest-indexed lateral wavenumber is interpreted as the receiver lateral wavenumber $\mathbf{k_g}$, results in:

$$T^{DD}(\mathbf{k_g}, z_g|\mathbf{k_s}, z_s; \omega) = -\frac{e^{iq_g z_g - iq_s z_s}}{i2q_g}\sum_{i=1}^{\infty}\widetilde{T}_i^{DD}(\mathbf{k_g}, z_g|\mathbf{k_i}, z_s; \omega), \tag{59}$$

which, with equation 58 and the stopping criterion

$$\widetilde{T}_0^{DD}(\mathbf{k_1}, z'|\mathbf{k_1}, z_s; \omega) = \left(\frac{1}{2\pi}\right)^{-2}\delta(\mathbf{k_1}-\mathbf{k_s}), \tag{60}$$

is a recursive prescription for computing this transmitted wavefield through a perturbation that varies in three dimensions.

5 Relations between transmitted-direct and reflected-primary wave field series terms

The expressions developed in previous sections for transmitted-direct wavefields and reflected-primary wavefields, some specifically suited for computation and some less so, are approximations that required a scattering-theoretic definition of primaries and direct waves to be chosen. For instance, the reflected primary approximation is the cumulative effect of all scattering interactions in which there is a single direction change in the (potentially legion) scattering interactions within a term. This ansatz, in fact, underlies (although in a processing/inversion, not modelling, sense) all developing algorithms for direct non-linear reflector location (e.g., Weglein et al., 2002; Shaw et al., 2004; Shaw, 2005; Liu et al., 2004; Liu et al., 2005; Innanen et al., 2004; Innanen et al., 2006). Part of the value of a focused study of the forward series construction of events is that it tells us precisely what subsequent primary-processing (imaging and inversion) algorithms *think these events are*. In this section and in the next (in which the same expressions are reduced to 1D medium variation), I discuss implications along these lines. In this section it is shown, for instance, that the scattering-based primary approximation posited here and by Innanen (2005) – and the one underlying the above-referenced imaging prototype algorithms – sees a primary as a "stitching together" of transmitted-direct wavefields whose propagation is non-linearly related to the perturbation.

The diagrams describing ascending orders of transmitted direct-wavefield approximation (Figure 3), and the diagrams describing ascending orders of reflected primary wavefield approximation (Figure 4), suggest a straightforward theme for relating these quantities. Viz., the reflected primary term of fifth order, say, in which there is a single transmission-like scattering interaction on the "down" leg, a single scattering interaction in which the direction of propagation changes (by the definition of the primary approximation scheme), and three transmission-like scattering interactions on the "up" leg, might be posited to be representable as a quasi-linear construction involving a first order "downward" transmitted series term and a third-order "upward" transmitted series term. In pseudo-mathematics, this R_5 component would be related to $T_3 k^2 \alpha T_1$. This equivalence turns out to be precisely the case; I demonstrate with third-order terms of the series for the three wavefield types. The demonstration is illustrated in Figure 5. The only extra complexity is that, since the transmitted direct wavefields have so far been expressed in the k_g, k_s, ω domains, to include them within a quasi-linear construction will require several inverse Fourier transforms. First, consider the zero'th order upward transmitted direct wavefield and the second order downward (the former being the simple homogeneous Green's function, the latter having been derived in section 3.1):

$$\begin{aligned} T_0^{DU}(\mathbf{k_g}, z_g|\mathbf{x}';\omega) &= G_0(\mathbf{k_g}, z_g|\mathbf{x}';\omega) \\ &= e^{-i\mathbf{k_g}\cdot\tilde{\mathbf{x}}'}\frac{e^{iq_g(z'-z_g)}}{i2q_g}, \end{aligned} \tag{61}$$

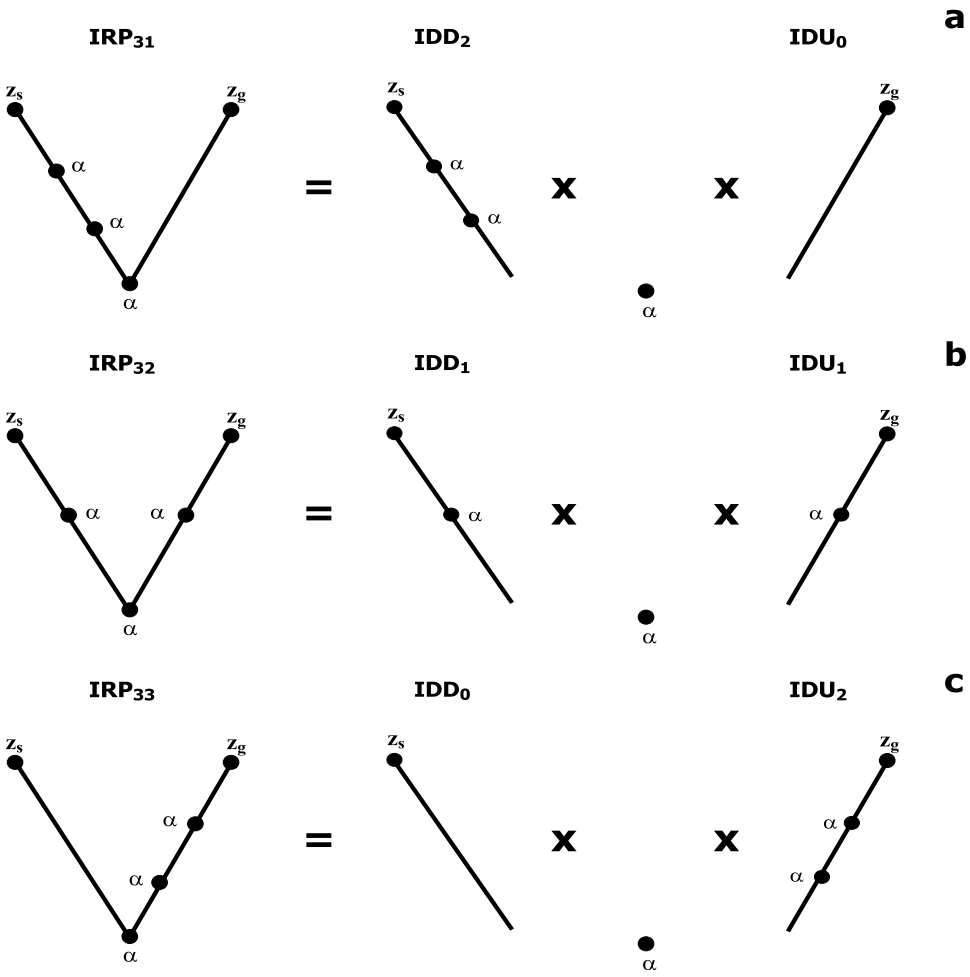

Figure 5: *Illustration of the relationships between transmitted-direct and reflected-primary wavefield expressions order-by-order. A quasi-linear construction involving the n'th order downward transmitted wavefield term and the m'th order upward transmitted term produces one of the contributing terms to the $m+n+1$'th reflected primary term. Illustrations (a)–(c) conceptually demonstrate this construction for the three components of the third-order reflected primary expression.*

and

$$\begin{aligned} T_2^{DD}(\mathbf{x}'|\mathbf{k_s}, z_s; \omega) &= \left(\frac{1}{2\pi}\right)^2 \int_{-\infty}^{\infty} d\mathbf{k'_g} e^{i\mathbf{k'_g}\cdot\widetilde{\mathbf{x}}'} T_2^{DD}(\mathbf{k'_g}, z'|\mathbf{k_s}, z_s; \omega) \\ &= \frac{i}{8} e^{-iq_s z_s} \frac{k^4}{q_s} \left(\frac{1}{2\pi}\right)^4 \int_{-\infty}^{\infty}\int_{-\infty}^{\infty} \frac{d\mathbf{k'_g} d\mathbf{k'_1}}{q'_g q_1} e^{i\mathbf{k'_g}\cdot\widetilde{\mathbf{x}}'} e^{iq'_g z'} \\ &\times \int_{z_s}^{z'} dz'' e^{i(q_1 - q_g)z''} \alpha(\mathbf{k_g} - \mathbf{k_1}, z'') \\ &\times \int_{z_s}^{z''} dz''' e^{i(q_s - q_1)z'''} \alpha(\mathbf{k_1} - \mathbf{k_s}, z'''). \end{aligned} \tag{62}$$

Conjoining these two quantities in the proposed quasi-linear construction results in

$$\begin{aligned} &\int_{-\infty}^{\infty} d\mathbf{x}' T_0^{DU}(\mathbf{k_g}, z_g|\mathbf{x}'; \omega) k^2 \alpha(\mathbf{x}') T_2^{DD}(\mathbf{x}'|\mathbf{k_s}, z_s; \omega) \\ &= \frac{1}{16} e^{-iq_g z_g - iq_s z_s} \frac{k^6}{q_g q_s} \left(\frac{1}{2\pi}\right)^4 \int_{-\infty}^{\infty}\int_{-\infty}^{\infty} \frac{d\mathbf{k_1} d\mathbf{k_2}}{q_1 q_2} \\ &\times \int_{-\infty}^{\infty} dz' e^{i(q_g + q_1)z'} \alpha(\mathbf{k_g} - \mathbf{k_1}, z') \\ &\times \int_{-\infty}^{z'} dz'' e^{i(q_2 - q_1)z''} \alpha(\mathbf{k_1} - \mathbf{k_2}, z'') \\ &\times \int_{-\infty}^{z''} dz''' e^{i(q_s - q_2)z''} \alpha(\mathbf{k_2} - \mathbf{k_s}, z'''). \end{aligned} \tag{63}$$

Notice that this is exactly equivalent to the third-order component R_{31}^P of the reflected primary approximation in equation 51. In other words,

$$R_{31}^P(\mathbf{k_g}, z_g|\mathbf{k_s}, z_s; \omega) = \int_{-\infty}^{\infty} d\mathbf{x}' T_0^{DU}(\mathbf{k_g}, z_g|\mathbf{x}'; \omega) k^2 \alpha(\mathbf{x}') T_2^{DD}(\mathbf{x}'|\mathbf{k_s}, z_s; \omega). \tag{64}$$

Using similar manipulations it may be similarly shown that, indeed,

$$R_{32}^P(\mathbf{k_g}, z_g|\mathbf{k_s}, z_s; \omega) = \int_{-\infty}^{\infty} d\mathbf{x}' T_1^{DU}(\mathbf{k_g}, z_g|\mathbf{x}'; \omega) k^2 \alpha(\mathbf{x}') T_1^{DD}(\mathbf{x}'|\mathbf{k_s}, z_s; \omega), \tag{65}$$

and

$$R_{33}^P(\mathbf{k_g}, z_g|\mathbf{k_s}, z_s; \omega) = \int_{-\infty}^{\infty} d\mathbf{x}' T_2^{DU}(\mathbf{k_g}, z_g|\mathbf{x}'; \omega) k^2 \alpha(\mathbf{x}') T_0^{DD}(\mathbf{x}'|\mathbf{k_s}, z_s; \omega), \tag{66}$$

hold also, as do similar constructions at all orders. In fact in general the N'th order reflected primary approximation is the sum of contributions from component transmission series terms whose combined order is $N-1$. To wit:

$$\begin{aligned} &R_N^P(\mathbf{k_g}, z_g|\mathbf{k_s}, z_s; \omega) \\ &= \sum_{n=0}^{N-1} \int_{-\infty}^{\infty} d\mathbf{x}' T_n^{DU}(\mathbf{k_g}, z_g|\mathbf{x}'; \omega) k^2 \alpha(\mathbf{x}') T_{N-n-1}^{DD}(\mathbf{x}'|\mathbf{k_s}, z_s; \omega). \end{aligned} \tag{67}$$

This result has practical and conceptual consequences. First, conceptually, and as mentioned above, it underlines the meaning of this view, or model, of what a primary is in the language of scattering theory; the result of a direct propagation down, transmitting non-linearly through the perturbed medium, a single direction-changing scattering interaction, followed by a direct propagation up again non-linearly through the overlying perturbation. Having designed the reflected primary approximation with this thought in mind, it is perhaps not such a remarkable result, but that idea followed from a view of the *totality* of the transmitted direct wavefield, not its order-by-order representation. The order-by-order connectivity of the transmitted direct and reflected primary wavefield approximations is less obviously true, at any rate to the eye of the author.

From a practical standpoint, it means that the recursive forms devised in section 4.3 for application to the direct transmitted wavefield approximation are immediately applicable also to the reflected primary case. This is an attractive prospect in that it permits potentially tractable forms for forward construction of primaries through complex 2D and 3D overburdens, and furthermore its lessons (e.g., Innanen, 2005) should contribute to the casting of the non-linear direct processing algorithms applied to the same problem (in the vein of Liu et al. (2005) and elsewhere in this report).

6 Reduction to the case of depth-variable (1D) media: series and closed forms

Beyond the conceptual "reasonableness" of the diagrammatic interpretation that spawned them, there exists little by way of proof that these non-linear event approximations do what they are claimed to do. This can be mitigated if we reduce them such that they need accommodate only depth-varying media, in which case these series may be summed to closed-form and analyzed for an understanding of (1) convergence and (2) what these terms are converging to. Practical and numerical use is also made of such depth-varying forms later in this report (Innanen, 2006).

The new milieu will be to consider line sources and receivers over a medium whose P-wave velocity may vary arbitrarily in depth. To begin, a refinement of the independent variables of the modelled reflection/transmission experiments is needed. Reducing variability to a single lateral dimension (x), the space vectors are redefined as

$$\begin{aligned} \mathbf{x_g} &= (x_g, z_g), \\ \mathbf{x_s} &= (x_s, z_s), \\ \mathbf{x}' &= (x', z'), \end{aligned} \tag{68}$$

As such a fully descriptive wave experiment can be chosen to involve a single receiver location $\mathbf{x_g}$, source plane waves characterized by lateral wavenumber k_s and frequency ω (or the angle $\theta = \cos^{-1} q_s/k$ these plane waves make with respect to the z axis), and the fixed source depth z_s. The scattered, reference, and actual wavefields are therefore

$$G_S(\mathbf{x_g}|k_s, z_s; \omega) = \int_{-\infty}^{\infty} d\mathbf{x}' G_0(\mathbf{x_g}|\mathbf{x}'; \omega) k^2 \alpha(z') G(\mathbf{x}'|k_s, z_s; \omega), \tag{69}$$

where $k = \omega/c_0$, and the series terms G_n are

$$G_1(\mathbf{x_g}|k_s, z_s; \omega) = \int_{-\infty}^{\infty} d\mathbf{x}' G_0(\mathbf{x_g}|\mathbf{x}', z', \omega) k^2 \alpha(z') G_0(\mathbf{x}'|k_s, z_s; \omega), \tag{70}$$

at first order,

$$G_2(\mathbf{x_g}|k_s,z_s;\omega)=\int_{-\infty}^{\infty}d\mathbf{x}'G_0(\mathbf{x_g}|\mathbf{x}',\omega)k^2\alpha(z')\int_{-\infty}^{\infty}dx''G_0(\mathbf{x}'|\mathbf{x}'',\omega)k^2\alpha(z'')G_0(\mathbf{x}''|k_s,z_s;\omega), \quad (71)$$

at second order, and so on. The depth-variable medium perturbation α reduces to

$$\alpha(z)=1-\frac{c_0}{c^2(z)}, \quad (72)$$

and the forward scattering series for the scattered field is

$$G_S(\mathbf{x_g}|k_s,z_s;\theta)=G_1(\mathbf{x_g}|k_s,z_s;\theta)+G_2(\mathbf{x_g}|k_s,z_s;\theta)+G_3(\mathbf{x_g}|k_s,z_s;\theta)+..., \quad (73)$$

where, with reference Green's functions substituted, the terms are given by

$$\begin{aligned}
G_1(\mathbf{x_g}|k_s,z_s;\theta)&=-\frac{1}{4\cos^2\theta}e^{ik_sx_g}\int_{-\infty}^{\infty}dz'e^{iq_s|z_g-z'|}\alpha(z')e^{iq_s|z'-z_s|},\\
G_2(\mathbf{x_g}|k_s,z_s;\theta)&=\frac{i2q_s}{16\cos^4\theta}e^{ik_sx_g}\int_{-\infty}^{\infty}dz'e^{iq_s|z_g-z'|}\alpha(z')\int_{-\infty}^{\infty}dz''e^{iq_s|z'-z''|}\alpha(z'')e^{iq_s|z''-z_s|},\\
G_3(\mathbf{x_g}|k_s,z_s;\theta)&=-\frac{(i2q_s)^2}{64\cos^6\theta}e^{ik_sx_g}\int_{-\infty}^{\infty}dz'e^{iq_s|z_g-z'|}\alpha(z')\int_{-\infty}^{\infty}dz''e^{iq_s|z'-z''|}\alpha(z'')\\
&\quad\times\int_{-\infty}^{\infty}dz'''e^{iq_s|z''-z'''|}\alpha(z''')e^{iq_s|z'''-z_s|},
\end{aligned} \quad (74)$$

etc. Because in the 3D case a representation in which depth was the only space coordinate explicitly active in the scattering process was deliberately chosen, these terms, for which depth is the only space coordinate at all the scattering process, may be acted upon with exactly the same strategy in order to approximate transmitted-direct and reflected-primary wavefields.

6.1 Transmitted direct wave approximations

The "transmitted downward" wavefield is found by computing the series form of the full wavefield with source above and receiver below the depth support of the perturbation:

$$\begin{aligned}
T_1^D(\mathbf{x_g}|k_s,z_s;\theta)&=-\frac{1}{4\cos^2\theta}e^{ik_sx_g}e^{-iq_s(z_s-z_g)}\int_{-\infty}^{\infty}dz'\alpha(z'),\\
T_2^D(\mathbf{x_g}|k_s,z_s;\theta)&=\frac{i2q_s}{16\cos^4\theta}e^{ik_sx_g}e^{-iq_s(z_s-z_g)}\int_{-\infty}^{\infty}dz'e^{-iq_sz'}\alpha(z')\int_{-\infty}^{\infty}dz''e^{iq_s|z'-z''|}\alpha(z'')e^{iq_sz''},\\
T_3^D(\mathbf{x_g}|k_s,z_s;\theta)&=-\frac{(i2q_s)^2}{64\cos^6\theta}e^{ik_sx_g}e^{-iq_s(z_s-z_g)}\int_{-\infty}^{\infty}dz'e^{-iq_sz'}\alpha(z')\int_{-\infty}^{\infty}dz''e^{iq_s|z'-z''|}\alpha(z'')\\
&\quad\times\int_{-\infty}^{\infty}dz'''e^{iq_s|z''-z'''|}\alpha(z''')e^{iq_sz'''},
\end{aligned} \quad (75)$$

and the direct component is achieved through a constraining of the scattering integrals as in section 4.1, such that at first-order there is no change, at second-order

$$T_2^{DD}(\mathbf{x_g}|k_s,z_s;\theta)\equiv\frac{i2q_s}{16\cos^4\theta}e^{ik_sx_g}e^{-iq_s(z_s-z_g)}\int_0^{z_g}dz'\alpha(z')\int_0^{z'}dz''\alpha(z''), \quad (76)$$

and at third-order

$$T_3^{DD}(\mathbf{x_g}|k_s,z_s;\theta) \equiv -\frac{(i2q_s)^2}{64\cos^6\theta}e^{ik_sx_g}e^{-iq_s(z_s-z_g)}\int_0^{z_g}dz'\alpha(z')\int_0^{z'}dz''\alpha(z'')\int_0^{z''}dz'''\alpha(z'''), \quad (77)$$

etc. In fact in general an (immediately) recursive form of the multidimensional downward transmitted direct wavefield reduced to 1D is straightforward:

$$\begin{aligned} T_N^{DD}(\mathbf{x_g}|k_s,z_s;\theta) &= \frac{e^{ik_sx_g}e^{-iq_s(z_s-z_g)}}{i2q_s}\left(-\frac{i2q_s}{4\cos^2\theta}\right)^N\Phi_N(z_g), \\ \Phi_i(z) &= \int_0^z\alpha(z')\Phi_{i-1}(z')dz', \\ \Phi_0(z) &\equiv 1. \end{aligned} \quad (78)$$

For the upward transmitted direct wavefield the expression is slightly altered:

$$\begin{aligned} T_N^{DU}(\mathbf{x_g}|k_s,z_s;\theta) &= \frac{e^{ik_sx_g}e^{iq_s(z_s-z_g)}}{i2q_s}\left(-\frac{i2q_s}{4\cos^2\theta}\right)^N\Phi_N(z_s), \\ \Phi_i(z) &= \int_0^z\alpha(z')\Phi_{i-1}(z')dz', \\ \Phi_0(z) &\equiv 1. \end{aligned} \quad (79)$$

6.2 Reflected primary field in 1D

The multi-dimensional reflected primary wavefield approximation likewise reduces straightforwardly, first with the full reflected wavefield:

$$\begin{aligned} R_1(\mathbf{x_g}|k_s,z_s;\theta) &= -\frac{1}{4\cos^2\theta}e^{ik_sx_g}e^{-iq_s(z_g+z_s)}\int_{-\infty}^{\infty}dz'e^{iq_sz'}\alpha(z')e^{iq_sz'}, \\ R_2(\mathbf{x_g}|k_s,z_s;\theta) &= \frac{i2q_s}{16\cos^4\theta}e^{ik_sx_g}e^{-iq_s(z_g+z_s)}\int_{-\infty}^{\infty}dz'e^{iq_sz'}\alpha(z')\int_{-\infty}^{\infty}dz''e^{iq_s|z'-z''|}\alpha(z'')e^{iq_sz''}, \\ R_3(\mathbf{x_g}|k_s,z_s;\theta) &= -\frac{(i2q_s)^2}{64\cos^6\theta}e^{ik_sx_g}e^{-iq_s(z_g+z_s)}\int_{-\infty}^{\infty}dz'e^{iq_sz'}\alpha(z')\int_{-\infty}^{\infty}dz''e^{iq_s|z'-z''|}\alpha(z'') \\ &\quad\times\int_{-\infty}^{\infty}dz'''e^{iq_s|z''-z'''|}\alpha(z''')e^{iq_sz'''}, \end{aligned} \quad (80)$$

and subsequently (via scattering integral constraints identical to those of section 4.2) the primary approximation is given, at second-order, as

$$\begin{aligned} R_2^P(\mathbf{x_g}|k_s,z_s;\theta) &= \frac{i2q_s}{16\cos^4\theta}e^{ik_sx_g}e^{-iq_s(z_g+z_s)}\int_{-\infty}^{\infty}dz'\underbrace{e^{i2q_sz'}\alpha(z')}_{\text{turn-around}}\underbrace{\left(\int_0^{z'}dz''\alpha(z'')\right)}_{\text{transmission down}} \\ &\quad+\frac{i2q_s}{16\cos^4\theta}e^{ik_sx_g}e^{-iq_s(z_g-z_s)}\int_{-\infty}^{\infty}\underbrace{\left(\int_0^{z'}dz''\alpha(z'')\right)}_{\text{transmission up}}\underbrace{e^{i2q_sz'}\alpha(z')}_{\text{turn-around}}, \end{aligned} \quad (81)$$

where the roles of the transmission-like entities are highlighted, and at third-order

$$\begin{aligned}
R_3^P(\mathbf{x_g}|k_s,z_s;\theta) = \frac{(i2q_s)^2}{64\cos^6\theta}e^{ik_sx_g}e^{-iq_s(z_g+z_s)} \\
\times\Bigg[\int_{-\infty}^{\infty}dz'e^{iq_sz'}\int_0^{z'}dz''e^{iq_s(z'-z'')}\alpha(z'')\int_0^{z''}dz'''e^{iq_s(z''-z''')}\alpha(z''') \\
+\underbrace{\int_{-\infty}^{\infty}dz'e^{iq_sz'}\int_0^{z'}dz''e^{iq_s(z'-z'')}\alpha(z'')\int_{z''}^{\infty}dz'''e^{iq_s(z'''-z'')}\alpha(z''')}_{\text{NEGLECT}} \\
+\int_{-\infty}^{\infty}dz'e^{iq_sz'}\int_{z'}^{\infty}dz''e^{iq_s(z''-z')}\alpha(z'')\int_{z''}^{\infty}dz'''e^{iq_s(z'''-z'')}\alpha(z''') \\
+\int_{-\infty}^{\infty}dz'e^{iq_sz'}\int_{z'}^{\infty}dz''e^{iq_s(z''-z')}\alpha(z'')\int_{z''}^{\infty}dz'''e^{iq_s(z'''-z'')}\alpha(z''')\Bigg],
\end{aligned} \tag{82}$$

where the reverberative element of the scattering integral has been shown explicitly (and labelled for rejection from this approximation). With similar highlighting of the transmission-like quantities internal to this approximation, the third-order primary approximation terms are

$$\begin{aligned}
R_3^P(\mathbf{x_g}|k_s,z_s;\theta) = \frac{(i2q_s)^2}{64\cos^6\theta}e^{ik_sx_g}e^{-iq_s(z_g+z_s)} \\
\times\Bigg[\int_{-\infty}^{\infty}dz'\underbrace{e^{i2q_sz'}\alpha(z')}_{\text{turn-around}}\underbrace{\left(\int_0^{z'}dz''\alpha(z'')\int_0^{z''}dz'''\alpha(z''')\right)}_{\text{transmission down}} \\
+\int_{-\infty}^{\infty}dz'\underbrace{\left(\int_0^{z'}dz''\alpha(z'')\right)}_{\text{transmission up}}\underbrace{e^{i2q_sz'}\alpha(z')}_{\text{turn-around}}\underbrace{\left(\int_0^{z'}dz''\alpha(z'')\right)}_{\text{transmission up}} \\
+\int_{-\infty}^{\infty}dz'\underbrace{\left(\int_0^{z'}dz''\alpha(z'')\int_0^{z''}dz'''\alpha(z''')\right)}_{\text{transmission up}}\underbrace{e^{i2q_sz'}\alpha(z')}_{\text{turn-around}}\Bigg].
\end{aligned} \tag{83}$$

In general, then, again a recursive form for this reduction to 1D of the multi-dimensional reflected primary approximation is straightforward:

$$\begin{aligned}
R_N^P(\mathbf{x_g}|k_s,z_s;\theta) &= \frac{e^{ik_sx_g}e^{-iq_s(z_g+z_s)}}{i2q_s}\left(-\frac{i2q_s}{4\cos^2\theta}\right)^N\int_{-\infty}^{\infty}dz'\sum_{i=1}^{N}\Phi_i(z')e^{i2q_sz'}\alpha(z')\Phi_{N-i}(z), \\
\Phi_i(z) &= \int_0^z\alpha(z')\Phi_{i-1}(z')dz', \\
\Phi_0(z) &\equiv 1.
\end{aligned} \tag{84}$$

6.3 Transmission-reflection relations in 1D

The order-by-order transmission-reflection relations derived in section 5 also reduce to much simpler forms in the 1D case, both now involving the simpler recursive forms expressed by the function Φ. Consider the orders A, B, and C, where we stipulate that $A = B + C + 1$. Writing the reflected primary approximation series to order A, the downward transmitted direct wave approximation to order B, and the upward transmitted direct wave approximation to order C produces

$$\begin{aligned}
R_A^P(\mathbf{x_g}|k_s, z_s; \theta) &= \frac{e^{ik_s x_g} e^{-iq_s(z_g+z_s)}}{i2q_s} \left(-\frac{i2q_s}{4\cos^2\theta}\right)^A \int_{-\infty}^{\infty} dz' \sum_{i=0}^{A-1} \Phi_i(z') e^{i2q_s z'} \alpha(z') \Phi_{A-i}(z), \\
T_B^{DD}(x_g^D, z_g|k_s, z_s; \theta) &= \frac{e^{ik_s x_g} e^{-iq_s(z_s-z_g)}}{i2q_s} \left(-\frac{i2q_s}{4\cos^2\theta}\right)^B \Phi_B(z_g), \\
T_C^{DU}(x_g^U, z_g|k_s, z_s; \theta) &= \frac{e^{ik_s x_g} e^{iq_s(z_s-z_g)}}{i2q_s} \left(-\frac{i2q_s}{4\cos^2\theta}\right)^C \Phi_C(z_s), \\
\Phi_i(z) &= \int_0^z \alpha(z') \Phi_{i-1}(z') dz', \\
\Phi_0(z) &\equiv 1.
\end{aligned} \tag{85}$$

As in the multidimensional case, the quasi-linear combination of the T_B^{DD} and T_C^{DU} is of interest, and is found to be:

$$\begin{aligned}
&\int_{-\infty}^{\infty} dz' T_C^{DU}(\mathbf{x_g}|k_s, z'; \theta) k^2 \alpha(z') T_B^{DD}(x_g, z'|k_s, z_s; \theta) \\
&= \frac{e^{ik_s(x_g^D + x_g^U)} e^{-iq_s(z_g+z_s)}}{i2q_s} \left(-\frac{i2q_s}{4\cos^2\theta}\right)^{B+C+1} \int_{-\infty}^{\infty} dz' \Phi_C(z') e^{i2q_s z'} \alpha(z') \Phi_B(z').
\end{aligned} \tag{86}$$

Noting that the exponent in the integral pre-factor is A, consider next the sum of all combinations of B and C for which this $B + C + 1$ remains constant:

$$\frac{e^{ik_s(x_g^D + x_g^U)} e^{-iq_s(z_g+z_s)}}{i2q_s} \left(-\frac{i2q_s}{4\cos^2\theta}\right)^A \int_{-\infty}^{\infty} dz' \sum_{i=0}^{A-1} \Phi_i(z') e^{i2q_s z'} \alpha(z') \Phi_{A-i}(z'). \tag{87}$$

This expression is of the form of the reflected primary approximation series term at order A. In terms of the orders of the transmitted direct wave approximations, this may be written in general as

$$R_{B+C+1}^P(x_g^U + x_g^D, z_g|k_s, z_s; \theta) = \sum_{n=1}^{B+C} \int_{-\infty}^{\infty} dz' T_n^{DU}(x_g^U, z_g|k_s, z'; \theta) k^2 \alpha(z') T_{B+C-n}^{DD}(x_g^D, z'|k_s, z_s; \theta). \tag{88}$$

Notice that, because this 1D reduction involves space-domain receiver variables, account is taken for any chosen offset between the lateral position of the receiver of the downward transmitted direct wave and the receiver of the upward transmitted direct wave.

6.4 Closed-forms and associated reflection-transmission relations

The most compelling reason to reduce the multidimensional expressions for reflected primary and transmitted direct wavefields to media that vary in depth only is that closed-forms are available: this is the greatest source of evidence that the series terms (as chosen through the scattering-geometry based retention/rejection program) do in fact result in plausible and useful approximations of the desired wavefield events. The closed-forms arise in 1D because the nested integrals over the perturbation (which arise for media in all dimensions) in this case simplify. In fact, they simplify to the point where, e.g., a twice-nested integral is equivalent to a single integral to the second power. Consider Φ_2, the core element of the scattering integrals of all three approximations at second order:

$$\begin{aligned}\Phi_2(z) &= \int_0^z \alpha(z')\Phi_1(z')dz' \\ &= \int_0^z \frac{d\Phi_1}{dz'}\Phi_1(z')dz' \\ &= \frac{1}{2}\int_0^z \frac{d}{dz'}\left[\Phi_1(z')\right]^2 dz' \\ &= \frac{1}{2}\Phi_1^2(z').\end{aligned} \tag{89}$$

This pattern repeats, so that in general:

$$\Phi_n(z) = \frac{1}{n!}\left(\int_0^z \alpha(z')dz'\right)^n. \tag{90}$$

Making this substitution in all terms of the upward transmitted direct series approximation results in:

$$\begin{aligned}T^{DU}(\mathbf{x_g}|k_s, z_s; \theta) &= \sum_{n=0}^{\infty} T_n^{DU}(\mathbf{x_g}|k_s, z_s; \theta) \\ &= \frac{e^{ik_s x_g} e^{iq_s(z_s - z_g)}}{i2q_s} \sum_{n=0}^{\infty}\left(-\frac{i2q_s}{4\cos^2\theta}\right)^n \Phi_n(z_s) \\ &= \frac{e^{ik_s x_g} e^{iq_s(z_s - z_g)}}{i2q_s} \sum_{n=0}^{\infty}\frac{1}{n!}\left(-\frac{iq_s}{2\cos^2\theta}\int_0^{z_s}\alpha(z')dz'\right)^n \\ &= \frac{e^{ik_s x_g} e^{iq_s(z_s - z_g)}}{i2q_s} e^{-\frac{iq_s}{2\cos^2\theta}\int_0^{z_s}\alpha(z')dz'},\end{aligned} \tag{91}$$

likewise with the downward transmitted direct series approximation:

$$T^{DD}(\mathbf{x_g}|k_s, z_s; \theta) = \frac{e^{ik_s x_g} e^{-iq_s(z_s - z_g)}}{i2q_s} e^{-\frac{iq_s}{2\cos^2\theta}\int_0^{z_g}\alpha(z')dz'}, \tag{92}$$

and, finally, the reflected primary series approximation:

$$\begin{aligned}
R^P(\mathbf{x_g}|k_s,z_s;\theta) &= \sum_{n=0}^{\infty} R_n^P(\mathbf{x_g}|k_s,z_s;\theta) \\
&= \frac{e^{ik_s x_g} e^{-iq_s(z_g+z_s)}}{i2q_s} \sum_{n=0}^{\infty} \left(-\frac{i2q_s}{4\cos^2\theta}\right)^n \int_{-\infty}^{\infty} dz' \sum_{i=1}^{n} \Phi_i(z') e^{i2q_s z'} \alpha(z') \Phi_{n-i}(z) \\
&= \frac{e^{ik_s x_g} e^{-iq_s(z_g+z_s)}}{i2q_s} \sum_{n=0}^{\infty} \left(-\frac{i2q_s}{4\cos^2\theta}\right)^n \int_{-\infty}^{\infty} dz' \sum_{i=1}^{n} \frac{[\Phi_1(z')]^i}{i!} e^{i2q_s z'} \alpha(z') \frac{[\Phi_1(z)]^{n-i}}{(n-i)!} \\
&= \frac{e^{ik_s x_g} e^{-iq_s(z_g+z_s)}}{i2q_s} \int_{-\infty}^{\infty} dz' e^{i2q_s z'} \sum_{n=0}^{\infty} \left(-\frac{i2q_s}{4\cos^2\theta}\Phi_1(z')\right)^n \alpha(z') \left(\sum_{i=0}^{n} \frac{1}{n!(n-i)!}\right) \\
&= \frac{e^{ik_s x_g} e^{-iq_s(z_g+z_s)}}{i2q_s} \int_{-\infty}^{\infty} dz' e^{i2q_s \left[z' - \frac{1}{2\cos^2\theta}\int_0^{z'} \alpha(z'')dz''\right]} \alpha(z').
\end{aligned} \tag{93}$$

The aim of these series, replete with nested integrals of the perturbation, becomes more transparent: the terms are working to generate a specific non-linear activity involving the perturbation, that in 1D amounts to placing it in the argument of a complex exponential. From this vantage point up in the exponential, so to speak, the perturbation has the wherewithal to affect the phase and amplitude of the (1D) wavefield. In the 3D situation essentially the same activity is occurring, but with an exponential phase term at each juncture in the nested integrals (see equations 57–58 for example), which halts the straightforward collapse of these terms to closed form, but which, through the difference in depth wavenumbers before and after the scattering interaction, may account for propagation through a multidimensional overburden.

Moreover, the reflection-transmission relations may be expressed in closed-form also:

$$\begin{aligned}
&\int_{-\infty}^{\infty} dz' T^{DU}(x_g^U, z_g|k_s, z';\theta) k^2 \alpha(z') T^{DD}(x_g^D, z'|k_s, z_s;\theta) \\
&= \int_{-\infty}^{\infty} dz' \left[\frac{e^{ik_s x_g^U} e^{iq_s(z'-z_g)}}{i2q_s} e^{-\frac{iq_s}{2\cos^2\theta}\int_0^{z'} \alpha(z'')dz''}\right] k^2 \alpha(z') \left[\frac{e^{ik_s x_g^D} e^{-iq_s(z_s-z')}}{i2q_s} e^{-\frac{iq_s}{2\cos^2\theta}\int_0^{z'} \alpha(z'')dz''}\right] \\
&= -\frac{i2q_s}{4\cos^2\theta} \frac{e^{ik_s(x_g^U+x_g^D)} e^{-iq_s(z_g+z_s)}}{i2q_s} \int_{-\infty}^{\infty} dz' e^{i2q_s\left[z' - \frac{1}{2\cos^2\theta}\int_0^{z'} \alpha(z'')dz''\right]} \alpha(z') \\
&= -\frac{i2q_s}{4\cos^2\theta} R^P(x_g^U + x_g^D, z_g|k_s, z_s;\theta).
\end{aligned} \tag{94}$$

This suggests that the desired outcome of the "there and back" retention/rejection scheme, which is difficult to validate in the fully multidimensional case, has been realized. The reflected primary approximation is enacted through a non-linear transmitted direct wavefield propagating downward to the target, scattering, and propagating as a non-linear transmitted direct wavefield upward to the receiver. The non-linearity in the nested integrals is effecting to propagate the wavefield through an overburden not included in the reference medium. In 1D this amounts to the creation of new, transmission-only, Green's functions T^{DD} and T^{DU} between which a scattering interaction takes place. In multiple dimensions a similar process is taking place but in a manner that (presently) can only be represented as a series.

7 Conclusions

A combination of constrained scattering geometry, source/receiver locations, and Green's functions in bilinear form, may be used to produce an approximation of two important and related types of wavefield event using the forward scattering series. The approximation is specifically designed to operate given any level of spatial variability in the wavespeed in a constant density acoustic medium, and a homogeneous reference medium.

The aims are twofold: first, recent research suggests that the mechanisms of construction of primaries with the forward series leads – directly and/or indirectly – to the forms for processing and inversion of the same wavefield component in the inverse scattering series. Second, a volume scattering model of primaries reflected from, and direct waves transmitted through, multidimensional structure may be a useful addition to a wave-theoretic forward modelling toolbox.

Order-by-order and (for 1D media) in closed-form the two wavefield types are seen to be closely related in this approximation. Furthermore – and of most interest for computational purposes – the 2D/3D forms, which require a series, can at least be written recursively. That is, the 100th term may require computation but it may be computed as a reasonable straightforward set of operations upon the 99th term.

Computation of these terms (for forward modelling purposes), and direct inversion of these terms (for direct non-linear processing of reflection data) are the subjects of current and ongoing research.

References

Claerbout, J. F., 1968, Synthesis of a layered medium from its acoustic transmission response: Geophysics, **33**, 204–209.

Innanen, K. A., 2003, Methods for the treatment of acoustic and absorptive/dispersive wave field measurements: Ph.D. Thesis, University of British Columbia.

Innanen, K. A. and A. B. Weglein, 2003, Construction of absorptive/dispersive wave fields with the forward scattering series: *Journal of Seismic Exploration*, **12** 259–282.

Innanen, K. A., 2005, Two non-linear forward and inverse approximations for wavefields in the presence of sustained medium perturbations: *75th Ann. Internat. Mtg. Soc. Expl. Geophys.*

Innanen, K. A., 2006, The forward scattering series and diffractions: non-linear series expressions for wavefields reflecting from 2D medium structure: *MOSRP-05 Annual Report (this report).*

Innanen, K. A., B. G. Nita and A. B. Weglein, 2006, Analytical and numerical aspects of the processing of reflected seismic primaries with the inverse scattering series: *submitted to Geophysical Journal International.*

Liu, F., Weglein, A. B., Innanen, K. A. and Nita, B. G., 2005, Extension of the non-linear imaging capability of the inverse scattering series to multidimensional media: strategies and numerical

results: *Proceedings of the Ninth International Congress of the SBGf and Sixth Latin American Geophysical Conference, Salvador de Bahia, Brazil.*

Matson, K. H., 1996, The relationship between scattering theory and the primaries and multiples of seismic data: *Journal of Seismic Exploration*, **5** 63–78.

Matson, K. H., 1997, An inverse scattering series method for attenuating elastic multiples from multicomponent land and ocean bottom seismic data, *PhD Thesis*, University of British Columbia.

Nita B.G., Matson K.H. (BP), Weglein A.B., 2004, Forward scattering series and seismic events: far field approximations, critical and postcritical events, *SIAM J. Appl. Math., Vol. 64, No. 6*, pp. 2167-2185

Nita B.G. and Weglein A.B., 2004, Imaging with tau versus t: implications for the inverse scattering internal multiple attenuation algorithm, *SEG Expanded Abstracts, 74th Annual Meeting of the Society of Exploration Geophysicists*, Denver, Colorado.

Ramirez, A. C., and Otnes, E., 2006, Forward scattering series for 2-parameter acoustic media: analysis and implications to the inverse scattering task specific subseries, *M-OSRP05 Annual Report*, This report.

Schuster, G. T., J. Yu, J. Sheng, and J. Rickett, 2004, Interferometric/daylight seismic imaging: Geophysical Journal International, **157**, 838–852.

Shaw, S. A., Weglein, A. B., Foster, D. J., Matson, K. H., and Keys, R. G., 2004, Isolation of a leading order depth imaging series and analysis of its convergence properties for a 1D acoustic medium: *Journal of Seismic Exploration 13*, (2004): 99-120.

Shaw, S. A., 2005: An inverse scattering series algorithm for depth imaging of reflection data from a layered acoustic medium: Ph.D. Thesis, University of Houston.

Stolt, R. H. and Jacobs, B., 1981, An approach to the inverse seismic problem: Stanford Exploration Project Report, **25**, 121–132.

Wapenaar, C. P. A., 2003, Synthesis of an inhomogeneous medium from its acoustic transmission response: Geophysics, **68**, pp. 1756–1759.

Weglein, A. B., W. E. Boyse, and J. E. Anderson, 1981, Obtaining three-dimensional velocity information directly from reflection seismic data: an inverse scattering formalism: Geophysics, **46**, pp. 1116–1120.

Weglein, A. B., F. A. Gasparotto, P. M. Carvalho, and R. H. Stolt, 1997, An inverse scattering series method for attenuating multiples in seismic reflection data: Geophysics, **46**, pp. 1975–1989.

Weglein, A. B., Foster, D. J., Matson, K. H., Shaw, S. A., Carvalho, P. M., and Corrigan, D., 2002, Predicting the correct spatial location of reflectors without knowing or determining the precise

medium and wave velocity: initial concept, algorithm and analytic and numerical example: *Journal of Seismic Exploration*, **10**,.

Weglein, A. B., Araujo, F. A., Carvalho, P. M., Stolt, R. H., Matson, K. H., Coates, R., Corrigan, D., Foster, D. J., Shaw, S. A., and Zhang, H. 2003, Topical Review: Inverse-scattering Series and Seismic Exploration. *Inverse Problems 19*, R27–R83.

Weglein, A. B., B. G. Nita, K. A. Innanen, E. Otnes, S. A. Shaw, F. Liu, H. Zhang, A. C. Ramírez, J. Zhang, G. L. Pavlis, and C. Fan, 2006, Using the inverse scattering series to predict the wavefield at depth and the transmitted wavefield without an assumption about the phase of the measured reflection data or back-propagation in the overburden: Geophysics, *accepted for publication*.

Weglein, A. B., and W. Dragoset, 2005, Multiple attenuation: Society of Exploration Geophysicists Reprint Series.

Zhang, H., and Weglein, A. B., 2005, The inverse scattering series for tasks associated with primaries: depth imaging and direct non-linear imaging of 1D variable velocity and density acoustic media: *75th Ann. Internat. Mtg. Soc. Expl. Geophys.*

The forward scattering series and diffractions: non-linear series and closed-form expressions for wavefields reflecting from 2D medium structure

Kristopher A. Innanen

Abstract

In this paper, previously discussed non-linear expressions for wavefield events that are reflected from and transmitted through multidimensional, unincorporated, medium structure (*unincorporated* meaning not included in the reference medium) are further developed. The simplicity of the non-linear expressions when this unincorporated part of the medium is restricted to variation in depth only is leveraged to investigate the activity of the forward scattering series in producing wavefields that have interacted with – nevertheless– multidimensional target structure. To be specific, a summation of forward scattering series terms (i.e., a closed-form) is proposed that, to an acceptable level of accuracy, models diffracted wavefield reflections. This occurs through a program of retention of series terms that are non-linear in the depth-dependent component of the perturbation, and linear in the multidimensional, or diffractive, component.

1 Introduction

Earlier in this report (Innanen, 2006) a set of expressions and relations within the forward scattering series were postulated for approximating reflected primaries and transmitted direct waves in media that vary in three dimensions; closed-form expressions and relations applicable to media that vary in the depth dimension only were also derived. It is an inconvenient fact that the forward scattering series expressions for "interesting" wave fields, that interact with media with 2D/3D structure, require a series, while the eminently computable and interpretable forward series closed-forms involve the construction of wave fields that have propagated through highly restricted (1D) media. An example of a wavefield component that exists in 2D and 3D but not in 1D is a diffraction – an important and highly visible part of most reflection seismograms.

In this paper I propose a forward scattering series framework for the construction of inherently multidimensional events, such as diffractions, that with certain approximations may yet capitalize on the closed-forms available to the 1D case. The framework makes a distinction between parts of a medium that can be considered "targets" and parts that can be considered "overburden" *while retaining them both in the perturbation part of the medium decomposition.* It turns out that if we assume the overburden to vary in depth only, we can use the closed-form machinery of the 1D non-linear forward scattering series terms to create approximations of wavefields reflected from targets that have 2D structure. The point of this would be twofold: first, guide the identification of inverse scattering series terms that concern themselves with the processing of diffractive primaries; second, investigate the applicability of the forward scattering series, a volume scattering formalism for forward modelling markedly different from, say, finite difference and reflectivity methodologies.

The non-linear terms of the forward scattering series that are concerned with the construction of primaries labor to accommodate deviations of the actual medium from the reference medium. In particular, non-linear series activity is heightened in describing the effect of regions of sustained,

large deviation. Small, transitory deviations, or perturbations (see, e.g., the medium structure illustrated in Figure 1), are often well-described with the linear term of the forward scattering series. Targets beneath an overburden with sustained deviations from the reference medium aggravate the error in this linear approximation. Forward scattering subseries primary approximations of Innanen (2005; 2006) were developed to address these circumstances. In those references, we find that a fully 1D overburden and target structure admits primary approximation subseries of the forward scattering series that have closed-forms. Meanwhile, a fully 3D overburden and target structure requires, for forward scattering subseries approximations to accomplish the same goal, a series that as yet has no closed-form. Since, however, the non-linear activity exists in large part to take account of the overburden, the simplicity of the 1D problem is transferred into (non-collapsible) complexity in the multi-dimensional case in large part because of the onset of lateral variability in the overburden. Which leads to the question: therefore, can we not, given a predominantly 1D overburden and targets with multi-dimensional but small-contrast and non-spatially sustained structure, formulate a non-linear primary approximation that has a closed-form? A quantitative answer to that question – in the affirmative – is the subject of the balance of this paper.

2 Terminology

A single-parameter 2D acoustic constant density medium is considered, in which the reference medium is chosen to be a homogeneous wholespace characterized by wavespeed c_0. The reference and the actual media are therefore assumed to be described by the wave equations

$$\left[\nabla_g^2 + \frac{\omega^2}{c_0^2}\right] G_0(x_g, z_g|x_s, z_s; \omega) = \delta(x_g - x_s)\delta(z_g - z_s), \tag{1}$$

and

$$\left[\nabla_g^2 + \frac{\omega^2}{c^2(x,z)}\right] G_0(x_g, z_g|x_s, z_s; \omega) = \delta(x_g - x_s)\delta(z_g - z_s), \tag{2}$$

where x_g, z_g are the lateral and vertical coordinates of the observation point and x_s, z_s are the coordinates of the source point. The Green's functions for the reference medium are straightforwardly given in various useful domains by

$$\begin{aligned} G_0(k_g, z_g|x', z'; k) &= e^{-ik_g x'} \frac{e^{iq_g|z_g - z'|}}{i2q_g}, \\ G_0(x', z'|k_s, z_s; k) &= e^{ik_s x'} \frac{e^{iq_s|z' - z_s|}}{i2q_s}, \\ G_0(x', z'|x'', z''; k) &= \left(\frac{1}{2\pi}\right) \int_{-\infty}^{\infty} dk_1 e^{ik_1(x' - x'')} \frac{e^{iq_1|z' - z''|}}{i2q_1}, \end{aligned} \tag{3}$$

where q_n is a depth wavenumber defined by $k = \omega/c_0$ and a given lateral wavenumber k_n:

$$q_n^2 = k^2 - k_n^2. \tag{4}$$

The actual medium, characterized by the wavespeed distribution $c(x, z)$, is expressed in terms of the reference medium, in which waves behave as per eqn. (2), and the perturbation

$$\alpha(x, z) = 1 - \frac{c_0^2}{c^2(x, z)}. \tag{5}$$

At points during this development it will be useful to restrict the actual medium to have variability only in the vertical (depth) coordinate direction: $c = c(z)$.

An approximation to the scattered field ($\psi = G - G_0$) is generated in these notes order by order in α, i.e., as the series

$$\psi = \psi_1 + \psi_2 + \psi_3 + ..., \tag{6}$$

in which ψ_n is considered to be that portion of the wave field that is n'th order in the perturbation. The developments of the following section start from this point, making use of the constraints of the scattering integrals that are discussed specifically by Innanen (2006) and that also underlie (and are predated by) the manipulations of the inverse scattering series for task-separated primary processing (e.g., Weglein et al., 2003).

3 Modelling diffractions beneath a 1D perturbed overburden

A 1D medium, i.e., one that varies in depth only, produces a highly redundant reflection wave experiment; to wit, all source and receiver pairs that have the same lateral separation produce the same result. In previous 1D developments this was handled by considering experiments with sources everywhere and a single receiver (which permitted the use of plane incident waves), but could equivalently have been expressed vice versa, i.e., as an experiment with a single source and receivers everywhere (and therefore expressed in coordinates k_g, x_s). Here a 1D medium is considered for sources *and* receivers everywhere for purposes that will become clearer in the following section; hence, the redundancy of the experiment appears much more explicitly in the modelling equations.

3.1 An approximation of reflected primaries for depth-variable perturbations

Considering the wave field in conjugate lateral coordinates k_g and k_s, the first three terms in the full forward scattering series for a homogeneous reference medium with depth-varying perturbations on the wavespeed are

$$\psi_1(k_g, z_g|k_s, z_s; k) = \int_{-\infty}^{\infty} dx' \int_{-\infty}^{\infty} dz' G_0(k_g, z_g|x', z'; k) k^2 \alpha(z') G_0(x', z'|k_s, z_s; k), \tag{7}$$

$$\begin{aligned} \psi_2(k_g, z_g|k_s, z_s; k) = &\int_{-\infty}^{\infty} dx' \int_{-\infty}^{\infty} dz' G_0(k_g, z_g|x', z'; k) k^2 \alpha(z') \\ &\times \int_{-\infty}^{\infty} dx'' \int_{-\infty}^{\infty} dz'' G_0(x', z'|x'', z''; k) k^2 \alpha(z'') G_0(x'', z''|k_s, z_s; k), \end{aligned} \tag{8}$$

and

$$\begin{aligned} \psi_3(k_g, z_g|k_s, z_s; k) = &\int_{-\infty}^{\infty} dx' \int_{-\infty}^{\infty} dz' G_0(k_g, z_g|x', z'; k) k^2 \alpha(z') \\ &\times \int_{-\infty}^{\infty} dx'' \int_{-\infty}^{\infty} dz'' G_0(x', z'|x'', z''; k) k^2 \alpha(z'') \\ &\times \int_{-\infty}^{\infty} dx''' \int_{-\infty}^{\infty} dx''' G_0(x'', z''|x''', z'''; k) k^2 \alpha(z''') G_0(x''', z'''|k_s, z_s; k). \end{aligned} \tag{9}$$

Placing the source and receiver depths on the same side (above) the depth-support of the perturbation, a series expression for the reflected wavefield is created. Applying the constraints to the depth integrals that isolate primary-like scattering geometries (Innanen, 2006), and calling these primaries R_n, results in, to third order,

$$R_P^1(k_g, z_g|k_s, z_s; k) = -\delta(k_g - k_s)\int_{-\infty}^{\infty} dz' \frac{e^{iq_g z'}}{i2q_g} k^2 \alpha(z') \frac{e^{iq_s z'}}{i2q_s}, \tag{10}$$

$$\begin{aligned} R_P^2(k_g, z_g|k_s, z_s; k) =& \frac{i}{2}\delta(k_g - k_s)\int_{-\infty}^{\infty} dz' \frac{e^{iq_g z'}}{i2q_g} k^2 \alpha(z') \frac{e^{iq_s z'}}{i2q_s} \left(q_s \frac{\int_0^{z'} \alpha(z'')dz''}{q_s^2/k^2} \right) \\ &+ \frac{i}{2}\delta(k_g - k_s)\int_{-\infty}^{\infty} dz' \frac{e^{iq_g z'}}{i2q_g} \left(q_g \frac{\int_0^{z'} \alpha(z'')dz''}{q_g^2/k^2} \right) k^2 \alpha(z') \frac{e^{iq_s z'}}{i2q_s}, \end{aligned} \tag{11}$$

and

$$\begin{aligned} R_P^3(k_g, z_g|k_s, z_s; k) =& -\frac{1}{4}\delta(k_g - k_s)\int_{-\infty}^{\infty} dz' \frac{e^{iq_g z'}}{i2q_g} k^2 \alpha(z') \frac{e^{iq_s z'}}{i2q_s} \left(q_s \frac{\int_0^{z'} \alpha(z'')dz''}{q_s^2/k^2} \right)^2 \\ &- \frac{1}{4}\delta(k_g - k_s)\int_{-\infty}^{\infty} dz' \frac{e^{iq_g z'}}{i2q_g} \left(q_g \frac{\int_0^{z'} \alpha(z'')dz''}{q_g^2/k^2} \right) k^2 \alpha(z') \frac{e^{iq_s z'}}{i2q_s} \left(q_s \frac{\int_0^{z'} \alpha(z'')dz''}{q_s^2/k^2} \right) \\ &- \frac{1}{4}\delta(k_g - k_s)\int_{-\infty}^{\infty} dz' \frac{e^{iq_g z'}}{i2q_g} \left(q_g \frac{\int_0^{z'} \alpha(z'')dz''}{q_g^2/k^2} \right)^2 k^2 \alpha(z') \frac{e^{iq_s z'}}{i2q_s}. \end{aligned} \tag{12}$$

Within the scattering integral however the source and receiver depth wavenumbers q_g and q_s are explicitly present, and this will be key in the next section to accord to the mathematics the ability to create expressions for diffractions.

In the closed-forms derived previously, the depth wavenumbers q_s (from the source) and q_g (to the receiver) were merged into the single "two-way" wavenumber $2q_s$; here they are kept separate. The reduction to closed-form therefore is slightly complicated by the presence of both these wavenumbers in the mathematics. However, considering two Taylor's series expansions, the first being

$$\begin{aligned} &\exp\left(-\frac{iq_g}{2\cos^2\theta_g} \int_0^z \alpha(z'')dz'' \right) \\ &= 1 + \left(-\frac{iq_g}{2\cos^2\theta_g} \int_0^z \alpha(z'')dz'' \right) + \frac{1}{2!}\left(-\frac{iq_g}{2\cos^2\theta_g} \int_0^z \alpha(z'')dz'' \right)^2 + \frac{1}{3!}\left(-\frac{iq_g}{2\cos^2\theta_g} \int_0^z \alpha(z'')dz'' \right)^3 + ..., \end{aligned} \tag{13}$$

and the second being

$$\begin{aligned} &\exp\left(-\frac{iq_s}{2\cos^2\theta_s} \int_0^z \alpha(z'')dz'' \right) \\ &= 1 + \left(-\frac{iq_s}{2\cos^2\theta_s} \int_0^z \alpha(z'')dz'' \right) + \frac{1}{2!}\left(-\frac{iq_s}{2\cos^2\theta_s} \int_0^z \alpha(z'')dz'' \right)^2 + \frac{1}{3!}\left(-\frac{iq_s}{2\cos^2\theta_s} \int_0^z \alpha(z'')dz'' \right)^3 + ..., \end{aligned} \tag{14}$$

and in particular noting the forms that appear due to their product:

$$\begin{aligned}
&\exp\left(-\frac{iq_g}{2\cos^2\theta_g}\int_0^z \alpha(z'')dz''\right)\exp\left(-\frac{iq_s}{2\cos^2\theta_s}\int_0^z \alpha(z'')dz''\right)\\
&=1+\left(-\frac{iq_s}{2\cos^2\theta_s}\int_0^z \alpha(z'')dz''\right)+\left(-\frac{iq_g}{2\cos^2\theta_g}\int_0^z \alpha(z'')dz''\right)+\frac{1}{2!}\left(-\frac{iq_g}{2\cos^2\theta_g}\int_0^z \alpha(z'')dz''\right)^2\\
&\quad+\left(-\frac{iq_s}{2\cos^2\theta_s}\int_0^z \alpha(z'')dz''\right)\left(-\frac{iq_g}{2\cos^2\theta_g}\int_0^z \alpha(z'')dz''\right)+\frac{1}{2!}\left(\frac{iq_s}{2\cos^2\theta_s}\int_0^z \alpha(z'')dz''\right)^2+...,
\end{aligned} \tag{15}$$

the emergent patterns are readily applied to the expressions in equations (10)–(12), leading to a closed-form for the sum over an infinite number of these primary generating terms $R_P = R_P^1 + R_P^2 + R_P^3 + ...$:

$$R_P(k_g, z_g|k_s, z_s; k) = \delta(k_g - k_s)\int_{-\infty}^{\infty} dz' \frac{e^{iq_g\left[z'-\frac{1}{2\cos^2\theta_g}\int_0^{z'}\alpha(z'')dz''\right]}}{i2q_g}k^2\alpha(z')\frac{e^{iq_s\left[z'-\frac{1}{2\cos^2\theta_s}\int_0^{z'}\alpha(z'')dz''\right]}}{i2q_s}. \tag{16}$$

In its present form this expression does exactly the same job as the previous version of the closed-form reflected primary approximation. This version forms the basis for the diffracted primary approximation.

3.1.1 Post-critical phenomena

An interesting and important aspect of this approximation is that it will involve a new and unusual "choice of solutions" beyond the critical angle, never encountered in the linear problem. Post-critical refers to combinations of k, k_g and k_s for which q_g or q_s are imaginary; wave solutions must be chosen such that in these regimes an evanescent, or vanishing, wavefield exists. The wrong choice leads to an increase without bound of the post-critical wavefield amplitudes during propagation.

We have seen that the cumulative effect of the non-linear terms of the forward scattering series is to alter the argument of the exponentials with a factor that depends both on q_g and/or q_s and the integral of the perturbation, which at a given z value can be either positive or negative, depending on the relative sizes of the actual and reference medium wavespeeds. The overall sign of the argument may therefore in general be expected to toggle positive and negative over the support of a given model. Since the [correct] decay or [incorrect] growth of the solution relies on it being one or the other, left to its own devices, this non-linear expression would likely experience instability. This may be a further example of the convergence problems already detected for the forward scattering series at and beyond the critical angle (Nita et al., 2004).

There would appear to be two ways to proceed. First, as is often done in any case, the post-critical components of the wavefield could simply be avoided in all calculations. Since the physical solution always decays, these components are generally small. On the other hand, we are always justified in choosing the correct of two solutions, hence, in any calculation, replacing $\int_0^z \alpha(z')dz'$ with $\left[\text{sgn}\left(\int_0^z \alpha(z')dz'\right)\right]\int_0^z \alpha(z')dz'$, *for post-critical angles only*, should bear fruit. To put it into words, simply because the non-linear terms are lengthening rather than shortening the propagation

time of an event in accordance with the sign of the perturbation, does not suggest that at post-critical angles the field should do anything but decay. We must expect similar considerations to be in play in the absorptive/dispersive problem also.

3.2 Reflected primaries expressions for moderate- and large-contrasts

In addition to using the expression for reflected primaries over a 1D perturbation given in equation 16, which is the forward analog to the "leading order" reflector location (and amplitude correction) primary processing subseries of the inverse scattering series, a generalization incorporating "high order" terms of the forward scattering series may be made using the same argument as those made by Innanen (2005). Let us consider the leading order version, as derived in the previous section, to be appropriate for media with "moderate" contrasts in the perturbation, and re-write it as

$$R_P^M(k_g, z_g|k_s, z_s; k) = \delta(k_g - k_s) \int_{-\infty}^{\infty} dz' \frac{e^{iq_g\left[z' + Z^{\rm MU}(z',\alpha,\theta_g)\right]}}{i2q_g} k^2 \alpha(z') \frac{e^{iq_s\left[z' + Z^{\rm MD}(z',\alpha,\theta_s)\right]}}{i2q_s}, \tag{17}$$

in which the cumulative effect of the non-linearity in α is contained in the functions $Z^{\rm MD}(z', \alpha, \theta_s)$ and $Z^{\rm MU}(z', \alpha, \theta_g)$, which are given by

$$Z^{\rm MU}(z', \alpha, \theta) = \frac{1}{2\cos^2\theta} \int_0^{z'} \alpha(z'')dz'' \tag{18}$$

As is developed and capitalized on by Innanen (2005) and Liu et al. (2005), this "Z" may be adapted to accommodate "large" contrasts, thus resulting in a further approximation of the reflected primaries:

$$R_P^L(k_g, z_g|k_s, z_s; k) = \delta(k_g - k_s) \int_{-\infty}^{\infty} dz' \frac{e^{iq_g\left[z' + Z^{\rm LU}(z',\alpha,\theta_g)\right]}}{i2q_g} k^2 \alpha(z') \frac{e^{iq_s\left[z' + Z^{\rm LD}(z',\alpha,\theta_s)\right]}}{i2q_s}, \tag{19}$$

in which

$$Z^{\rm LU}(z', \alpha, \theta) = \frac{1}{2\cos^2\theta} \int_0^{z'} \frac{\alpha(z'')}{1 - \frac{1}{4}\alpha(z'')} dz''. \tag{20}$$

There are reasons to use both of these expressions: the leading order (or moderate contrast) Z function will produce an expression with error at large contrast, but it is the result of a series that converges for any α at a finite frequency. Meanwhile, the high order (or large contrast) Z function produces results that maintain accuracy over a larger range of contrasts, provided those contrasts are such that $|\alpha/4| < 1$, to ensure convergence. In the numerical results in this paper I use the large contrast expression.

3.3 A "non-linear overburden, linear diffractor" approximation

The reflected primary results in the previous section are attractively compact, but, as stated, apply to media whose variation is in depth only. Let us next apply these ideas to a forward scattering series framework in which a wavefield is generated that is non-linear in certain components of the

medium but linear in others in a way that permits multi-D wavefields to be created using our previous 1D mathematical machinery.

Consider a velocity perturbation on a homogeneous reference medium that has a component with vertical variation only and a component that varies both vertically and horizontally. In other words, consider a perturbation

$$\alpha(x,z) = A(z) + B(x,z), \tag{21}$$

wherein, for example, $A(z)$ could be considered an overburden overlying a scattering body, or target, $B(x,z)$ (e.g., Figures 1-2). Placing this form into the first order term of the forward scattering series with reflection-like source/receiver depths results in

$$\begin{aligned} R^1(k_g|k_s;k) &= \int_{-\infty}^{\infty} dz' \int_{-\infty}^{\infty} dx' e^{-ik_g x'} \frac{e^{iq_g z'}}{i2q_g} k^2 \alpha(x',z') e^{ik_s x'} \frac{e^{iq_s z'}}{i2q_s} \\ &= -\frac{k^2}{q_g q_s} \int_{-\infty}^{\infty} dz' e^{i(q_g+q_s)z'} \left[A(z') + \int_{-\infty}^{\infty} dx' e^{i(k_s-k_g)x'} B(x',z') \right], \end{aligned} \tag{22}$$

or

$$\begin{aligned} R^1(k_g|k_s;k) = &- \delta(k_g-k_s) \frac{k^2}{q_g q_s} \int_{-\infty}^{\infty} dz' e^{i(q_g+q_s)z'} A(z') \\ &- \frac{k^2}{q_g q_s} \int_{-\infty}^{\infty} dz' e^{i(q_g+q_s)z'} B(k_g-k_s,z'). \end{aligned} \tag{23}$$

Comparing equation 23 with equation 10 the result can be seen to be the sum of (1) the linear part of a series exactly like that of the fully 1D case, but now involving the "overburden" $A(z)$ instead of the full $\alpha(z)$, and (2) the linear part of the reflection from the vertically- and laterally-varying "target" component B. We know that proceeding with only A results in a closed-form solution, and we know that proceeding with only B results in more complex forms at high orders.

At high order we encounter terms that are, loosely, quadratic in α, then cubic in α, and so forth, hence, for an α that has two additive components A and B the first few terms (of either the full forward scattering series or the reflected primary approximation derived from it) will involve the following combinations of these components:

$$\begin{aligned} &\underbrace{A}_{\text{ovrbrdn.}} + \underbrace{B}_{\text{ovrbrdn. + targ.}} \\ &\underbrace{A^2}_{\text{ovrbrdn.}} + \underbrace{AB}_{\text{ovrbrdn. + targ.}} + B^2 \\ &\underbrace{A^3}_{\text{ovrbrdn.}} + \underbrace{A^2B}_{\text{ovrbrdn. + targ.}} + B^2A + A^3 \\ &\underbrace{A^4}_{\text{ovrbrdn.}} + \underbrace{A^3B}_{\text{ovrbrdn. + targ.}} + A^2B^2 + AB^3 + B^4 \\ &\ldots \quad . \end{aligned} \tag{24}$$

Let these terms be a set from which we allow ourselves to selectively retain and/or reject any desired element in order to attain our goals. For instance, if we were to retain only the first (leftmost) column of these terms and reject all others, the primary approximation would be insensitive to

the "target" component B, and would return a reflected primary approximation whose events would correspond to an experiment in which $A(z)$ represented the only medium variation, and this approximation would have a closed-form as in, e.g., equation 19. Note that the series terms have had to do two things in creating this closed form: they needed α to non-linearly produce exponential functions to alter the phase and amplitude of the linear wavefield approximation, and they needed α to remain in the integrand to be acted upon by these exponential functions. In the sense of the descriptive scheme of equation 24, these two things occur as follows: the set of terms $A + A^2 + A^3 + A^4 + ...$ has one A taken out of each term, $A(1 + A + A^2 + A^3 + ...)$, after which the bracketed activity works to create the exponential functions, leaving the remaining A to be acted on by them.

Consider next the result of retaining only the *second* column of contributions to the reflected primary approximation series in equation 24. In it the target component $B(x, z)$ is incorporated but only once per term: $B+BA+BA^2+BA^3+...$ etc. Notice that this lets B act in the second capacity as described above, that is, schematically, it is separable from the herd: $B(1 + A + A^2 + A^3 + ...)$. This subgroup of forward scattering series terms will work to create non-linear corrections to the propagation of an event through a depth-varying medium, by creating the exact exponential functions used in the fully 1D case. However, these corrective functions will act on the 2D target B only.

The consequence of retaining this subset of terms is straightforward. Non-linearity is to be accounted for in the depth-varying (overburden) component of the medium only; the target component, which may vary in two dimensions, is only linearly accounted for. These circumstances are acceptable if the target has the same characteristics that make any linear approximation acceptable: it is of low contrast and is not spatially sustained. If that is the case, the non-linear forward scattering series approximation for the wavefield reflected from the target given by a perturbation $B(x, z)$ that underlies the perturbation $A(z)$,

$$R_{Df}(k_g|k_s;k) = \int_{-\infty}^{\infty} dz' \frac{e^{iq_g\left[z'-Z^{\mathrm{LU}}(z',A,\theta_g)\right]}}{i2q_g} k^2 B(k_g - k_s, z') \frac{e^{iq_s\left[z'-Z^{\mathrm{LD}}(z',A,\theta_s)\right]}}{i2q_s}, \qquad (25)$$

where the Z functions are as given in section 3.2, is an accurate one.

4 Numerical examples

Equation 25 is a 2D prescription for modelling of the reflected primaries from an diffractive target ($B(x, z)$) that underlies a depth-dependent overburden $A(z)$ with sustained spatial support *without* including the latter in the reference medium. The prescription takes on some of the qualities of a modelling scheme that *has* included the overburden in the reference medium. To wit, the exponential functions take on aspects of two new transmitting Green's functions accounting for the perturbation. This resemblance technically holds, but becomes far less apparent in more complex multidimensional environments however, for which a series is required (Innanen, 2006). In this section I demonstrate the numerical behavior of this prescription.

Figure 1 is an illustration of the 2D target component of the perturbation $B(x, z)$, corresponding to a spatially-varying structure with a constant deviation of 0.2 away from the reference, in total (Figure 1a) and in detail (Figure 1b). The target is a heterogeneous set of diffracting bodies between 40 and

80m deep and extending approximately 30m about the chosen lateral origin. Figure 2 illustrates the same target now overlain by the depth dependent overburden $A(z)$, which is chosen to be a set of two layers, of increased wavespeed (4500m/s and 6500m/s in contrast to the reference wavespeed of 1500m/s), with a layer thickness of 10m each.

The prescription in equation 25 is carried out on both input models, leading to an expression in the k_{x_g}, k_{x_s}, ω domain. This is inverse Fourier transformed into the x_g, x_s, t domain, and three shot records are displayed in each of Figures 3 and 4. These correspond to shot locations $x_s = -16.0$m, $x_s = 0.0m$, and $x_s = 16.0$m in Figures 3 and 4a, b, and c respectively.

The delay and move-out alterations to the complex target response, expected in this example involving a large intermediary velocity increase, is the most noticeable effect.

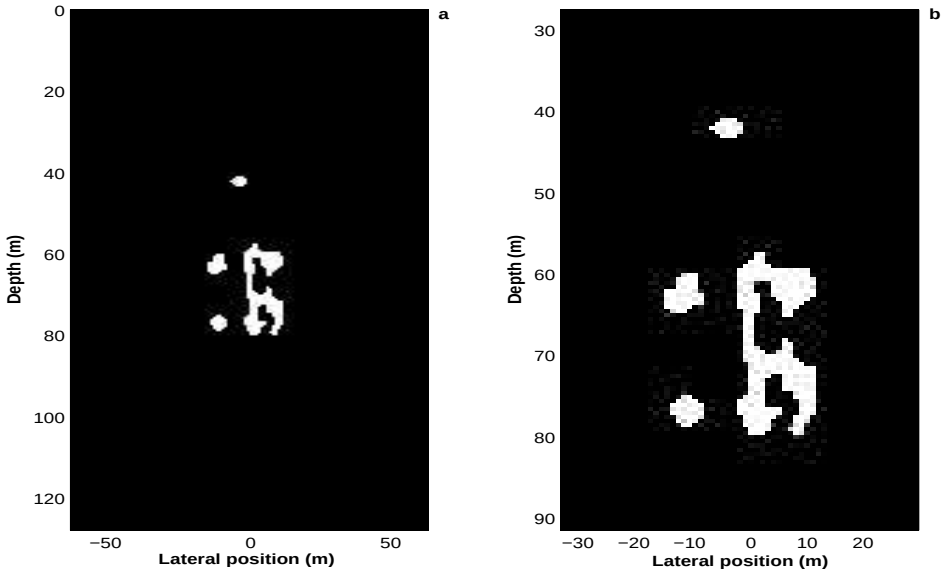

Figure 1: *Diffracting scatterers model in the absence of an overburden: (a) in full, and (b) in detail.*

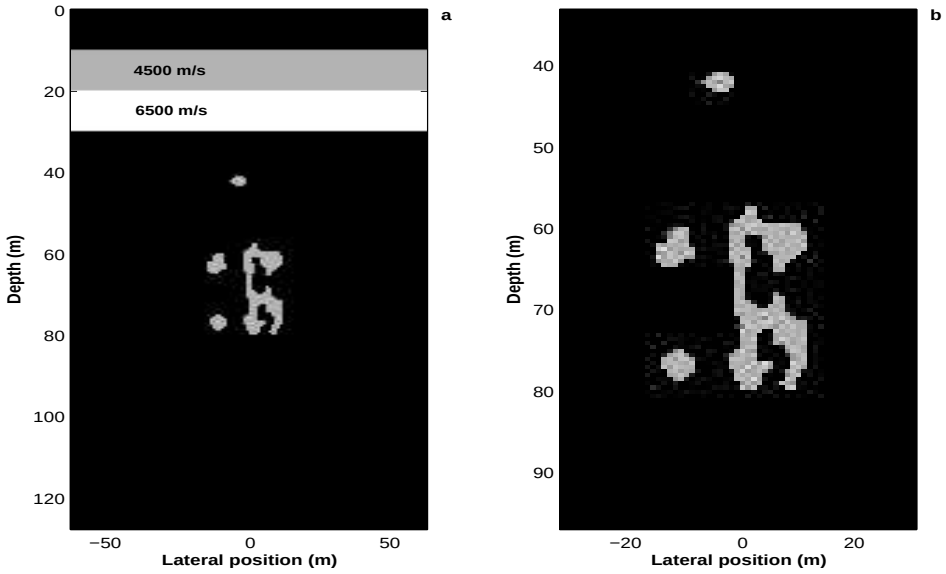

Figure 2: *Diffracting scatterers model in the presence of a two layer overburden: (a) in full, and (b) in detail.*

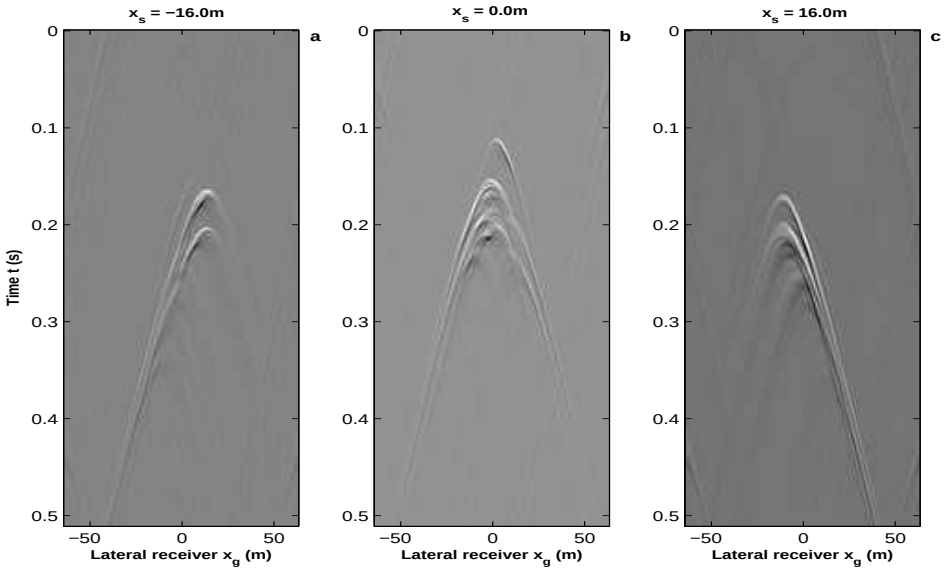

Figure 3: *Three shot records associated with the "no overburden" example (Figure 1): (a) $x_s = 16m$ to the left of center of the scatterer model, (b) $x_s = 0m$ directly above the scatterer model, and (c) $x_s = 16m$ to the right of center of the scatterer model.*

5 Conclusions

General series expressions for direct transmitted wavefields and reflected primary wavefields propagating through multidimensional perturbations (that are, i.e., unincorporated in the background

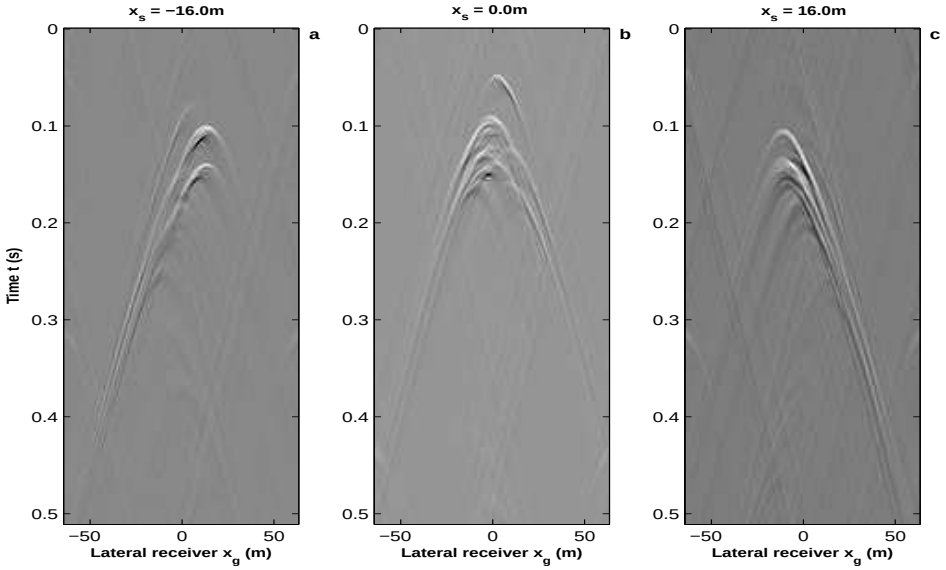

Figure 4: *Three shot records associated with the "with overburden" example (Figure 2): (a) $x_s = 16m$ to the left of center of the scatterer model, (b) $x_s = 0m$ directly above the scatterer model, and (c) $x_s = 16m$ to the right of center of the scatterer model.*

reference medium), have been developed in this report (Innanen, 2006). Elsewhere (Innanen and Weglein, 2006), we demonstrate the salutary effect of manipulating series expressions such that some components of the perturbation are acted on linearly and some non-linearly.

In the latter reference we find it useful to selectively apply linear or non-linear processing with respect to specific *parameters* of the perturbation. In this paper we find it useful to selectively apply linear and/or non-linear computations to model components with specific *spatial dimensionality*. The ability to act with these related kinds of linear/non-linear selectivity would appear to be one of the greatest strengths of the forward and inverse scattering series.

The linear/non-linear selectivity is here used to approximate diffractive wavefield events that have a 1D overburden in their propagation history not included in the reference medium. Numerical investigation appears to confirm the accuracy of these expressions, taking the diffractions and operating on them non-linearly in the perturbation such that their phase (visible in their arrival times and move-out patterns) alter as expected given the unincorporated overburdens.

A rapidly computable expression such as this may be a useful tool for forward modelling and/or as a driver for an indirect inverse procedure, or (of more interest for this program) either conceptually informing the derivation of direct inverse procedures (as did Matson (1996) and others), or perhaps forming a forward scattering series primary approximation that may be directly inverted order-by-order as discussed by Innanen (2005). In all likelihood these two latter approaches will result in very similar direct inversion prototype algorithms that have the wherewithal – should they exist – to non-linearly process diffractions.

Given the insight into the forward problem derived here, is there anything we can now say, anticipating the nature of these postulated direct inverse processing algorithms? Consider the activity seen thus far, in, e.g., equation 25, first imagining $A(z) = 0$. An intercept time and move-out pattern is

established with the "double square root" operators in the argument of the exponential (involving q_s and q_g), that is by assumption acceptably accurate when there exists no unincorporated overburden. The non-zero perturbation conjoins with and alters the components of this double square root, altering the existing intercept time and move-out pattern. Hence, it is reasonable to assume that a direct processing procedure, deriving from the inverse scattering series, acting on such diffractions, would involve a collapsing of wave energy in accordance with a correction of the zero-perturbation double square root operators. The corrections would be driven by data self-interaction, which in the inverse direction takes the place of the perturbation self-interaction of the forward scattering series. Given previous experience with the symmetry of the forward and inverse scattering series, that a corresponding inverse procedure would have these properties seems highly likely, but that remains a subject of current and future research.

6 Acknowledgements

The author is grateful to the sponsors and personnel of M-OSRP, especially Sam T. Kaplan for his futile attempt to teach me C++ in time to try the numerics presented herein. So it's back to matlab for me and apologies and thanks to Sam. I have been partially funded by and am grateful for NSF-CMG award DMS-0327778 and DOE Basic Sciences award DE-FG02-05ER15697.

7 References

Innanen, K. A., 2005, Two non-linear forward and inverse approximations for wavefields in the presence of sustained medium perturbations: *75th Ann. Internat. Mtg. Soc. Expl. Geophys.*

Innanen, K. A., 2006, Non-linear forward scattering series expressions for and relations between reflected primary and transmitted direct wavefield events: *MOSRP-05 Annual Report (this report).*

Liu, F., Weglein, A. B., Innanen, K. A. and Nita, B. G., 2005, Extension of the non-linear imaging capability of the inverse scattering series to multidimensional media: strategies and numerical results: *Proceedings of the Ninth International Congress of the SBGf and Sixth Latin American Geophysical Conference, Salvador de Bahia, Brazil.*

Matson, K. H., 1996, The relationship between scattering theory and the primaries and multiples of seismic data: *Journal of Seismic Exploration*, **5** 63–78.

Nita, B. G., Matson, K. H. and Weglein, A. B., 2004, Forward scattering series and seismic events: far field approximations, critical and postcritical events. *SIAM*, **Vol. 64 Is. 6**, 2167–2185.

Weglein, A. B., Araujo, F. A., Carvalho, P. M., Stolt, R. H., Matson, K. H., Coates, R., Corrigan, D., Foster, D. J., Shaw, S. A., and Zhang, H. 2003, Topical Review: Inverse-scattering Series and Seismic Exploration. *Inverse Problems 19*, R27–R83.

Accurate implementation of the wavelet in finite-difference modelling

Fang Liu and Arthur Weglein

Abstract

As we develop direct non-linear imaging and target identification methods based on the inverse scattering series (as well as other series based processing methods), which are ambitious in the sense of data interrogation, tools for testing and validation of these methods become increasingly important. For example, as methods are extended to multiple dimensions, we require forward modelling tools that provide a wave-accurate set of multidimensional input synthetic data. This paper outlines some issues encountered when utilizing finite difference schemes to provide such tools, and some strategies for overcoming them. We discuss: (1) a straightforward quality control method for finite-difference modelling, (2) accurate inclusion of the source signature in more flexible locations, especially in the presence of a free-surface and (3) the physical meaning of a discontinuous model, implemented in multi-dimensional array.

1 Introduction

This Annual Report comprises recent developments in the development of a comprehensive and direct wave-theoretic approach to the seismic inverse problem, largely based on the task-separated inverse scattering series. In the last two years or so, extensions of prototype algorithms along these lines have included (1) to multiparameter acoustic, elastic, and viscoacoustic media, (2) to multidimensional media, and (3) to large contrast media. As we develop direct non-linear imaging and target identification methods based on the inverse scattering series (as well as other series based processing methods), which are ambitious in the sense of data waveform interrogation, tools for testing and validation of these methods become increasingly important. Specifically, as methods are extended to multiple dimensions, we require forward modelling tools that provide a wave-accurate set of input synthetic data. This paper outlines some issues encountered when utilizing finite difference schemes to provide such tools, and some strategies for overcoming them.

Forward modelling is a mature topic in exploration seismology. For non-constant media, especially media with lateral variations, an analytic solution to the wave-equation is very difficult to obtain. Alford et al. (1974) introduced a finite-difference approximation to acoustic differential equations and demonstrated its usefulness as applied to exploration seismology. Later effort included the use of specific boundary conditions to minimize boundary artifacts (Reynolds, 1978), generalization of the acoustic scheme to full-elastic (Kelly et al., 1976), improvement of the accuracy of the spatial derivatives by means of both the Fourier transform (Kosloff and Baysal, 1982) and higher-order evaluation (Dablain, 1986).

This article discusses several issues in finite difference modelling. In particular, it discusses the physical meaning of the finite-difference approximation for discontinuous media and the accurate implementation of the wavelet. A constant density acoustic medium is considered.

A finite difference approximation of the wave-equation is a kind of digitization of the original problem. Compared with reflectivity and Cagniard-de Hoop method (discussed by J. Zhang in this

report), the finite-difference method has the ability to handle lateral variations in the medium; however, it does not have the analytic accuracy of those other methods. In particular, the accuracy of the approximation depends strongly on the digitation interval.

Current seismic imaging algorithms take advantage of knowledge of subsurface velocity structure to place events at their correct spatial locations. The most important aspect of the data contributing to the success of these algorithms is therefore the correct arrival time. In comparison, the waveform of the events are much less critical. This is no longer true for the prototype methods based on the inverse scattering series, where not only time information, but exact and complete waveform information is much preferred.

In this paper we first derive some analytic solutions for wavefields in media without lateral variations, and introduce a set of tools for validation of the amplitudes generated by finite difference approximations of these same wavefields. These tools are first used to demonstrate some weaknesses in pre-packaged finite difference modellers, after which some strategies for FD parameter choice are discussed which circumvent the weaknesses.

2 Analytic solutions for media without lateral variations

After the geological model is identified, modelling parameters must be chosen: $\triangle x$ (the sampling rate in the x-direction), $\triangle z$ (the sampling rate in the z-direction), $\triangle t$ (the sampling rate in time), and the source signature. By source signature, we mean the spectral content of the wavefield leaving the source (the "wavelet in the water", in other words). This is different from the reflected waveforms read from the seismograph (in 1D, 2D, and 3D). It is important to emphasize this, because common practice in exploration seismology is to compute the synthetic seismogram by convolving the wavelet with the reflection coefficient sequence.

The 2D wave-equation with a vertically-varying medium velocity $c(z)$ is:

$$\left(\frac{\partial^2}{\partial x^2}+\frac{\partial^2}{\partial z^2}-\frac{1}{c^2(z)}\frac{\partial^2}{\partial t^2}\right)\phi(x,z,t)=\delta(x-x_s)\delta(z-z_s)A(t), \tag{1}$$

where (x_s, z_s) is the spatial location of the source, and $A(t)$ is the source signature (or wavelet).

We can apply a Fourier transform $\int_{-\infty}^{\infty} dx e^{-ikx}$ to both sides of the equation, at which point, defining $\widetilde{\phi}(k,z,t)=\int_{-\infty}^{\infty} dx e^{-ikx}\phi(x,z,t)$, we have:

$$\left(\frac{\partial^2}{\partial z^2}-\frac{1}{c^2(z)}\frac{\partial^2}{\partial t^2}-k^2\right)\widetilde{\phi}(k,z,t)=e^{-ikx_s}\delta(z-z_s)A(t).$$

If we define $P(z,t)=\widetilde{\phi}(0,z,t)=\int_{-\infty}^{\infty} dx\phi(x,z,t)$, i.e., summing the readings from all receivers together, we have:

$$\left(\frac{\partial^2}{\partial z^2}-\frac{1}{c^2(z)}\frac{\partial^2}{\partial t^2}\right)P(z,t)=\delta(z-z_s)A(t).$$

$P(z,t)$, the result of summing the wave-field over all receivers, exactly satisfies the 1D wave-equation (2). The solution, as derived in the next section and expressed in (3) and (4), for a homogeneous medium $c(z) \equiv c_0$, would therefore be:

$$P(z,t) = -\frac{2}{c_0} \int_{-\infty}^{t-|z-z_s|/c_0} du A(u).$$

This "summing over receivers" logic has been described by many authors; it seems many have come to similar results using different approaches. This simple sum, transforming the problem to 1D if the Earth has no lateral variations, eliminates spherical divergence and the angle-dependency of the amplitude of the seismic events.

For several simple models without lateral variation, the analytic solutions can be derived by matching the boundary conditions. They are very useful in quality control. A straightforward quality control procedure that would validate the choice of modelling parameters: $\triangle x$, $\triangle z$, $\triangle t$, and source signature is to try them on the 1D model, sum the recording from all receivers as we have just discussed, then compared with analytic 1D solutions. We begin with a derivation of several such solutions.

2.1 Solution for homogeneous medium

Let us illustrate the wavelet issue in the simplest 1D case, where a source is ignited at $z = z_s$,

$$\left(\frac{\partial^2}{\partial z^2} - \frac{1}{c(z)^2}\frac{\partial^2}{\partial t^2}\right) P(z,t) = \delta(z - z_s)A(t), \tag{2}$$

where $A(t)$ is the source term expressed in the time domain. Because the source explodes at $z = z_s$, if the medium is homogeneous water: $c(z) \equiv c_0$, let's assume the form of the solution is causal:

$$P(z,t) = f\left(t - |z - z_s|/c_0\right). \tag{3}$$

Our solution (3) expresses a wave propagating outward from the source location $z = z_s$ with velocity c_0. A recording device (phone) at any fixed location $z = z_0$ will record a time series prescribed by $f\left(t - |z_0 - z_s|/c_0\right)$. So it will record a single event in the form $f(t)$ shifted by the amount $|z_0 - z_s|/c_0$. If the phone will record the waveform of the source, $f(t)$ should be proportional to $A(t)$. If this is not true, that means a phone will never record the form of the source no matter how close it is to the source, contrary to our intuitive concepts.

Obviously, for whatever f, our solution (3) satisfies the wave-equation (2) when $z \neq z_s$, since for this case the wave-equation is homogeneous.

Let's then consider the source point, following the usual technique dealing with the singularity $\delta(z - z_s)$ at $z = z_s$, we consider the integral of equation (2) across the following two points $z = z_s - \varepsilon$ and $z = z_s + \varepsilon$,

$$\int_{z_s-\varepsilon}^{z_s+\varepsilon} dz \left(\frac{\partial^2}{\partial z^2} - \frac{1}{c_0^2}\frac{\partial^2}{\partial t^2}\right) P(z,t) = \int_{z_s-\varepsilon}^{z_s+\varepsilon} dz \delta(z - z_s)A(t) = A(t).$$

Let us take a close look at the left-hand-side of the equation above: if ε is approximately 0, the second term $\int_{z_s-\varepsilon}^{z_s+\varepsilon} dz \frac{\partial^2}{\partial t^2} P(z,t)$ will approach 0 if f is continuous. But the first term will produce:

$$\int_{z_s-\varepsilon}^{z_s+\varepsilon} dz \frac{\partial^2}{\partial z^2} P(z,t) = \left[\frac{\partial}{\partial z} f(t-|z-z_s|/c_0) \right]_{z=z_s-\varepsilon}^{z=z_s+\varepsilon} = f'(t-\varepsilon/c_0) \left(\frac{-1}{c_0} - \frac{1}{c_0} \right) \longrightarrow -\frac{2}{c_0} f'(t),$$

so we have the following relation:

$$-\frac{2}{c_0} f'(t) = A(t).$$

This demonstrates that the general solution of the equation above is:

$$f(t) = C - \frac{c_0}{2} \int_{-\infty}^{t} A(u) du,$$

where C is an arbitrary constant. Further, considering the boundary condition at $t = -\infty$, we know that before the source is ignited, the receiver shouldn't receive any waveform. So we have: $f(-\infty) = 0$, and hence $C = 0$ in the equation above. The physical solution of f would be:

$$f(t) = -\frac{c_0}{2} \int_{-\infty}^{t} A(u) du. \tag{4}$$

A special situation appears when the source term in equation (2) is $A(t) = \delta(t)$, in which case we have:

$$f(t) = -\frac{c_0}{2} \int_{-\infty}^{t} A(u) du = -\frac{c_0}{2} \int_{-\infty}^{t} \delta(u) du = -\frac{c_0}{2} H(t).$$

We next substitute the solution above in (3), and find the causal Green's function for homogeneous medium in 1D (Morse and Feshbach, 1953, p. 843, equation (7.3.16)):

$$G_0(z, z_s, t) = -\frac{c_0}{2} H(t - |z - z_s|/c_0).$$

2.2 Solution for model with 1 reflector

We next repeat this process for a model with a little more complexity:

$$c(z) = \begin{cases} c_0 & z \le z_1 \\ c_1 & z > z_1 \end{cases} \tag{5}$$

where z_1 is the depth of the only reflector in the model. We assume the source located strictly inside the first medium: $z_1 > z_s$. Then

$$P(z,t) = \begin{cases} f\left(t - |z - z_s|/c_0\right) + R * f\left(t - (2z_1 - z - z_s)/c_0\right) & z < z_1 \\ T * f(t - (z_1 - z_s)/c_0 + (z - z_1)/c_1) & z > z_1 \end{cases}, \tag{6}$$

where $R = (c_1 - c_0)/(c_1 + c_0)$ is the reflection coefficient of the single interface in the medium, and $T = 1 + R = 2c_1/(c_1 + c_0)$ is the corresponding transmission coefficient. The solution expressed in equation (6) satisfies the wave-equation (2) in the medium defined by equation (5).

For the first layer, $z < z_1$, the solution consists of 2 parts: the direct wave $f\left(t - |z - z_s|/c_0\right)$ and reflected wave $R * f\left(t - |z + z_1 - z_s|/c_0\right)$. The direct wave will satisfy the inhomogeneous wave-equation. The reflected wave satisfy the corresponding homogeneous wave-equation. Introduction of the reflected wave will make sure the sum will satisfy the inhomogeneous wave-equation, just as the direct-wave alone.

For the second layer, the source is outside the medium, $z_1 > z_s$, and the wave-equation in this medium is homogeneous. That's why the transmitted wave in the form $T * f(t - |z_1 - z_s|/c_0 + (z - z_1)/c_1)$ will satisfy the wave-equation in this layer.

The waveform and amplitude of the reflected and transmitted waves are determined by matching the boundary condition at $z = z_1$, the continuity of the wave-field $P(z,t)|_{z=z_1}$ and its derivative over z, $\partial P(z,t)/\partial z|_{z=z_1}$. It's easy to prove that the solution expressed in equation (6) satisfies the boundary condition (continuity of wave-field and its derivative over z) for all time.

2.3 Solution for model with 2 reflectors

For a model with 2 layers:

$$c(z) = \begin{cases} c_0 & z \le z_1 \\ c_1 & z_2 > z > z_1 \\ c_2 & z > z_2 \end{cases}, \tag{7}$$

where z_1 is the depth of the first reflector, and z_2 is the depth of the second reflector. We assume the source is located strictly inside the first medium: $z_1 > z_s$. Following the discussions above, we

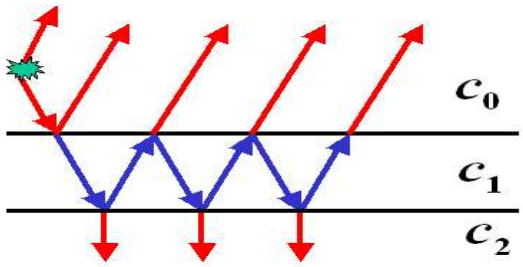

,

can write the solution in the first medium ($z < z_1$):

$$\begin{aligned} P(z,t) = f\left(t - |z - z_s|/c_0\right) + R_1 f\left(t - (2z_1 - z - z_s)/c_0\right) \\ + R_2' f\left(t - (2z_1 - z - z_s)/c_0 + 2(z_2 - z_1)/c_1\right) \\ + \sum_{n=1}^{\infty} R_2' \left[-R_1 R2\right]^n f\left(t - (2z_1 - z - z_s)/c_0 + 2(n+1)(z_2 - z_1)/c_1\right), \end{aligned} \tag{8}$$

where $R_1 = \frac{c_1 - c_0}{c_1 + c_0}$ is the reflection coefficient of the first reflector, $R_2 = \frac{c_2 - c_1}{c_2 + c_1}$, is the reflection coefficient of the second reflector, and $R_2' = R_2 * (1 - R_1^2)$ is the product of R_2 and the cumulative transmission lose of the layers above.

In the solution above, the first term is the direct wave, the second and third terms are primaries from the first and second reflectors, respectively. The remaining terms are internal multiples bouncing between the only 2 reflectors in the model.

2.4 Solution for model with free-surface and 1 reflector

Let's consider a problem with free-surface:

$$c(z) = \begin{cases} 0 & z < z_f \\ c_0 & z_f \le z < z_1 \\ c_1 & z > z1 \end{cases} \tag{9}$$

where z_f is the depth of the free-surface, and z_1 is the depth of the only reflector below the free-surface. Assuming that the source is located between the free-surface and the water-bottom: $z_f < z_s < z_1$, we simply write the solution down:

$$P(z,t) = \begin{cases} 0 & z \le z_f \\ \phi^{\mathtt{ini}} + \sum_{n=1}^{\infty} \left\{ \phi_n^{\uparrow\uparrow} + \phi_n^{\uparrow\downarrow} + \phi_n^{\downarrow\uparrow} + \phi_n^{\downarrow\downarrow} \right\} & z_f < z < z_1 \\ \sum_{n=1}^{\infty} \left\{ \psi_n^{\uparrow} + \psi_n^{\downarrow} \right\} & z > z_1 \end{cases}, \tag{10}$$

where various terms are defined in the table below. This solution satisfies the inhomogeneous wave-equation in water, and the homogeneous wave-equation below the water bottom.

$\phi^{\mathtt{ini}} = f\left(t - \frac{\lvert z-z_s\rvert}{c_0}\right) - f\left(t - \frac{z-2z_f+z_s}{c_0}\right)$	$\lambda_n = 2n(z_1 - z_f) + z_s,\ \mu_n = \lambda_n - 2\left(z_s - z_f\right)$
$\phi_n^{\uparrow\uparrow} = (-R)^n f\left(t - \frac{\lambda_n - z}{c_0}\right)$	$\phi_n^{\downarrow\uparrow} = -(-R)^n f\left(t - \frac{\mu_n - z}{c_0}\right)$
$\phi_n^{\uparrow\downarrow} = -(-R)^n f\left(t - \frac{\lambda_n + z - 2z_f}{c_0}\right)$	$\phi_n^{\downarrow\downarrow} = (-R)^n f\left(t - \frac{\mu_n + z - 2z_f}{c_0}\right)$
$\psi_n^{\uparrow} = (T/R) * (-R)^n f\left(t - \frac{\lambda_n - z_1}{c_0} - \frac{z-z_1}{c_1}\right)$	$\psi_n^{\downarrow} = -(T/R) * (-R)^n f\left(t - \frac{\mu_n - z_1}{c_0} - \frac{z-z_1}{c_1}\right)$

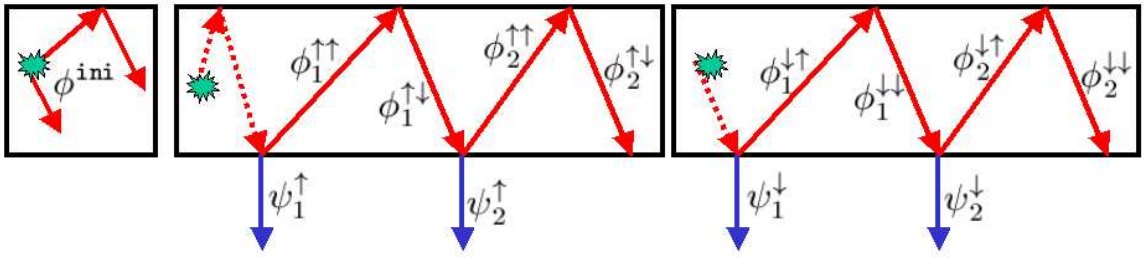

The free-surface boundary-condition: $P(z,t)|_{z=0} \equiv 0$ is satisfied by the following cancellations: (1) 2 terms in $\phi^{\mathtt{ini}}$: $\left[f(t - \frac{|z-z_s|}{c_0}) - f(t - \frac{z+z_s-2z_f}{c_0})\right]_{z=z_f} = 0$. (2), for $n = 1, 2, \cdots$, we have: $\left[\phi_n^{\uparrow\uparrow} + \phi_n^{\uparrow\downarrow}\right]_{z=z_f} = 0$, $\left[\phi_n^{\downarrow\uparrow} + \phi_n^{\downarrow\downarrow}\right]_{z=z_f} = 0$.

It is somewhat tedious to verify the boundary condition at level $z = z_1$ because there are a large number of events. Some level of efficiency derives from classifying them into groups, in which each

group contains an incident wave, a reflection, and a transmission (the groups are displayed in the table below), and noting that each group share a same common amplitude factor (denoted as A_0) and arrival time at the interface (denoted as θ_0).

Group	A_0	$\theta_0 * c_0$
$\left\{\phi_{n-1}^{\uparrow\downarrow}, \phi_n^{\uparrow\uparrow}, \psi_n^{\uparrow}\right\}$	$-(-R)^{n-1}$	$2(n-1)(z_1-z_f)+z_1+z_s-2z_f$
$\left\{\phi_{n-1}^{\downarrow\downarrow}, \phi_n^{\downarrow\uparrow}, \psi_n^{\downarrow}\right\}$	$(-R)^{n-1}$	$2(n-1)(z_1-z_f)+z_1-z_s,$

where the proofs of the phase are:

$$\begin{array}{lll} \lambda_{n-1}+z_1-2z_f & =2(n-1)(z_1-z_f)+z_1+z_s-2z_f & =\lambda_n-z_1 \\ \mu_{n-1}+z_1-2z_f & =2(n-1)(z_1-z_f)+z_1-z_s & =\mu_n-z_1. \end{array}$$

By $\phi_0^{\uparrow\downarrow}$, we mean the second part of $\phi^{\texttt{ini}}$: $\phi_0^{\uparrow\downarrow} \stackrel{\text{def}}{=} -f\left(t-\frac{z-2z_f+z_s}{c_0}\right)$. By $\phi_0^{\downarrow\downarrow}$, we mean the down-going portion of the first half of $\phi^{\texttt{ini}}$: $\phi_0^{\downarrow\downarrow}=f\left(t-\frac{z-z_s}{c_0}\right)$ (which holds only for $z>z_s$).

With the notations above, we can generally express each group as:

Incidence	Reflection	Transmission
$A_0 f\left(t-\theta_0-\frac{z-z_1}{c_0}\right)$	$A_0 R f\left(t-\theta_0+\frac{z-z_1}{c_0}\right)$	$A_0 T f\left(t-\theta_0-\frac{z-z_1}{c_1}\right)$

At the boundary $z=z_1$, the continuity of the wave-field and its derivative over z is proved by:

$$\begin{array}{lcl} 1+R=T & \Longrightarrow & \{\texttt{Incidence}+\texttt{Reflection}\}_{z=z_1^-} = \{\texttt{Transmission}\}_{z=z_1^+}, \\ -\frac{1}{c_0}+\frac{R}{c_0}=-\frac{T}{c_1} & \Longrightarrow & \frac{\partial}{\partial z}\{\texttt{Incidence}+\texttt{Reflection}\}_{z=z_1^-} = \frac{\partial}{\partial z}\{\texttt{Transmission}\}_{z=z_1^+}. \end{array}$$

In marine exploration, the receiver-line is normally below the source: $z_g>z_s$. In this case, the total recorded wave-field from the receivers can be expressed as

$$\begin{aligned} P(z_g,t) =& f\left(t-\frac{z_g-z_s}{c_0}\right)-f\left(t-\frac{z_g-2z_f+z_s}{c_0}\right)+\sum_{n=1}^{\infty}\left\{\phi_n^{\uparrow\uparrow}+\phi_n^{\uparrow\downarrow}+\phi_n^{\downarrow\uparrow}+\phi_n^{\downarrow\downarrow}\right\}_{z=z_g} \\ =& f(t-t_0)-f(t-[t_0+\tau_s]) \\ &+\sum_{n=1}^{\infty}(-R)^n\left\{f(t-t_n)-f(t-[t_n+\tau_s])-f(t-[t_n+\tau_g])+f(t-[t_n+\tau_s+\tau_g])\right\}, \end{aligned}$$

where $\tau_s=2(z_s-z_f)/c_0$, $\tau_g=2(z_g-z_f)/c_0$, $t_n=\frac{z_g-z_s}{c_0}+2n\frac{z_1-z_f}{c_0}$.

We note that for the direct-wave (the portion with 0 power of R), the ghosting process resembles a "finite-difference", applied once. But for reflected wave information (the portion with non-zero power of R), the ghosting process looks like a "finite-difference" applied twice, with unequal steps (first with step τ_s, then with τ_g), as described by:

$$\begin{aligned} &\texttt{If we define operator :}\quad \wp^a f(t)=f(t)-f(t-a) \\ &\texttt{We have :}\quad [\wp^{\tau_g}[\wp^{\tau_s}]]\, f(t-t_n)= \\ &\{f(t-t_n)-f(t-[t_n+\tau_s])-f(t-[t_n+\tau_g])+f(t-[t_n+\tau_s+\tau_g])\}. \end{aligned}$$

If the step becomes very small, the finite-difference operation will approach a derivative operation, and the "finite-difference twice" operation similar to taking the derivative twice. For example, if

the original wavelet is a Gaussian, the ghosting effect will make each event look like a Ricker (the second-order derivative of a Gaussian).

Without ghosts, each event has the form $f(t-t_n)$, where $n=0$ is for a primary, and $n=1$ is for the first order free-surface multiple. But the presence of the source and receiver ghost, changes its form to $f(t-t_n)-f(t-t_n-\tau_g)-f(t-t_n-\tau_s)+f(t-t_n-\tau_g-\tau_s)$.

We next study the change in its frequency content. Defining $g(t)=f(t-t_n)$, and its spectrum $\widetilde{G}(\omega)$, we have

$$\begin{aligned}
&f(t-t_n)=g(t)\longleftrightarrow\widetilde{G}(\omega)\\
&f(t-t_n)-f(t-t_n-\tau_g)-f(t-t_n-\tau_s)+f(t-t_n-\tau_g-\tau_s)\\
&=g(t)-g(t-\tau_g)-g(t-\tau_s)+g(t-\tau_g-\tau_s)\\
&\longleftrightarrow\widetilde{G}(\omega)\left(1-e^{-i\omega\tau_g}\right)\left(1-e^{-i\omega\tau_s}\right).
\end{aligned}$$

The spectrum of each event is multiplied by $\left(1-e^{-i\omega\tau_g}\right)\left(1-e^{-i\omega\tau_s}\right)$. Because both $\left(1-e^{-i\omega\tau_g}\right)$ and $\left(1-e^{-i\omega\tau_s}\right)$ approach 0 linearly when $\omega\rightarrow 0$, multiplying $\left(1-e^{-i\omega\tau_g}\right)\left(1-e^{-i\omega\tau_s}\right)$ will cause the spectrum to attenuate quadratically when $\omega\rightarrow 0$, just as in the previous argument.

For this simple model, after the direct wave, the reflection and its multiples are periodic. If we define: $u_n(t)=\left\{\phi_n^{\uparrow\uparrow}+\phi_n^{\uparrow\downarrow}+\phi_n^{\downarrow\uparrow}+\phi_n^{\downarrow\downarrow}\right\}$, we have that $u_n(t)=-R*u_n(t-2(z_1-z_f))$, in which the period is $2(z_1-z_f)$. *This result can be used to verify the quality of the finite-difference modelling.*

3 Finite-difference approximation of the wave-equation

Let us next generate the finite difference approximations that will be used for numerical modelling, in particular demonstrating the negative effect of incorrect implementation of the source. Consider the wave-equation for a constant-density acoustic medium:

$$\left(\frac{\partial^2}{\partial x^2}+\frac{\partial^2}{\partial z^2}-\frac{1}{c^2(x,z)}\frac{\partial^2}{\partial t^2}\right)\phi(x,z,t)=\delta(x)\delta(z-z_s)A(t), \tag{11}$$

and the finite-difference approximation of the left-hand-side (**?**, p. 836, equation (8)):

$$\begin{aligned}
&P(m\triangle x,n\triangle z,(l+1)\triangle t)-(2-5\gamma^2)P(m\triangle x,n\triangle z,l\triangle t)+P(m\triangle x,n\triangle z,(l-1)\triangle t)\\
&-\frac{4\gamma^2}{3}\left[\begin{array}{c}P((m+1)\triangle x,n\triangle z,l\triangle t)+P((m-1)\triangle x,n\triangle z,l\triangle t)\\+P(m\triangle x,(n+1)\triangle z,l\triangle t)+P(m\triangle x,(n-1)\triangle z,l\triangle t)\end{array}\right]\\
&+\frac{\gamma^2}{12}\left[\begin{array}{c}P((m+2)\triangle x,n\triangle z,l\triangle t)+P((m-2)\triangle x,n\triangle z,l\triangle t)\\+P(m\triangle x,(n+2)\triangle z,l\triangle t)+P(m\triangle x,(n-2)\triangle z,l\triangle t)\end{array}\right],
\end{aligned} \tag{12}$$

where m, n, and l are the indices of the wave-field in x, z, and t, respectively, $\gamma=c(x,z)\frac{\triangle t}{\triangle x}$, and the digitization interval in x and z direction are set to be equal, $\triangle x=\triangle z$.

If the source term of equation (11) is zero, equation (12) can be used to calculate the future wave-field $P(m\triangle x,n\triangle z,(l+1)\triangle t)$ from the neighboring grids from current time $l\triangle t$ and previous time

$(l-1)\triangle t$.

$$
\begin{aligned}
P(m\triangle x, n\triangle z, (l+1)\triangle t) &= (2-5\gamma^2)P(m\triangle x, n\triangle z, l\triangle t) - P(m\triangle x, n\triangle z, (l-1)\triangle t) \\
&+ \frac{4\gamma^2}{3}\left[\begin{array}{c} P((m+1)\triangle x, n\triangle z, l\triangle t) + P((m-1)\triangle x, n\triangle z, l\triangle t) \\ +P(m\triangle x, (n+1)\triangle z, l\triangle t) + P(m\triangle x, (n-1)\triangle z, l\triangle t) \end{array}\right] \\
&- \frac{\gamma^2}{12}\left[\begin{array}{c} P((m+2)\triangle x, n\triangle z, l\triangle t) + P((m-2)\triangle x, n\triangle z, l\triangle t) \\ +P(m\triangle x, (n+2)\triangle z, l\triangle t) + P(m\triangle x, (n-2)\triangle z, l\triangle t) \end{array}\right].
\end{aligned} \tag{13}
$$

Next, we illustrate the source issue by testing the finite difference modelling code from a third-party package. In this case, the only parameters we used as input are listed in fig 1. From its documentation, we know that it implements the Ricker wavelet (the second derivative of Gaussian). We only specify the geological model and spatial sampling rate: $\triangle x = \triangle z = 5(m)$, and give the program the maximal freedom to determine the other critical parameters such as peak frequency, sampling rate in time: $\triangle t$. Although the 3^{rd}-party program applies transparent boundary conditions to

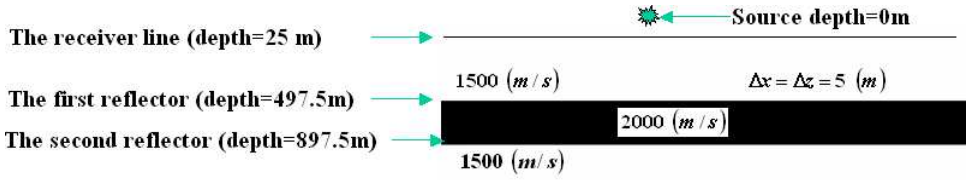

Figure 1: The geological model and modelling parameter for a 3^{rd}-party finite-difference program

minimize the boundary artifacts, we have avoided that issue entirely by making the model sufficiently large (width=$15000m$, height=$5000m$) that the receivers will not receive the unwanted boundary-artifacts from the top, bottom, left of right edges. From figure 2, we see that although

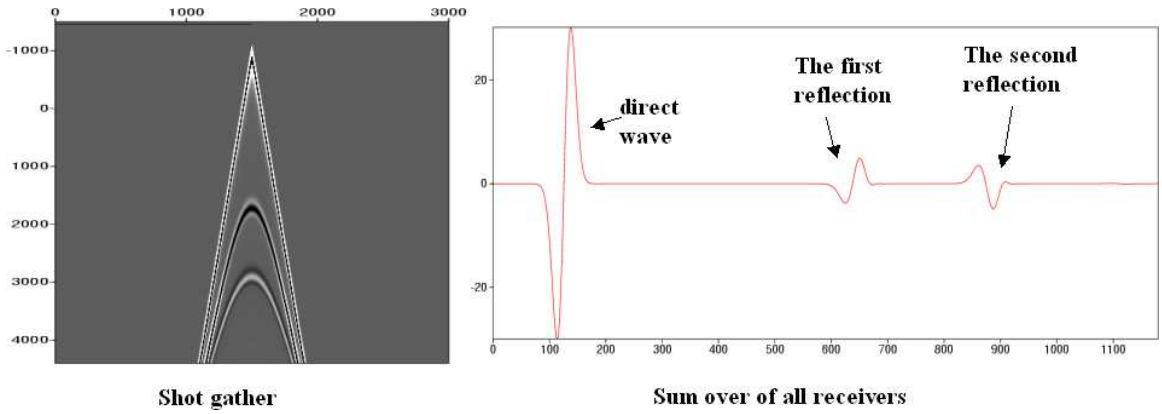

Figure 2: Left: the finite-difference modelling results using the 3^{rd}-party code and the model displayed in Figure 5. The vertical axis is the index of samples, it can be linear transformed to time. Right: the sum of the recordings from all the receivers in the left.

the linear travel time of the direct wave, and the hyperbolic arrival-time of various reflections are accurate, the sum over all receivers shows some unwanted phenomena: the wave-form of the second reflection deviates significantly from the integral of the wavelet (the first derivative of Gaussian).

The positive portion of the second reflector is significantly smaller than the negative half*.

The example above illustrates the importance of implementing the source signature accurately to the waveform modelling. We next propose a means for accurate implementation of the source in arbitrary locations.

We assume that after a certain time T_M, the source has become weak enough to be ignored. After T_M, the wave-equation (1) can be considered homogeneous, hence we may use the homogeneous scheme in equation (12) to propagate to the next time-step. All we need is to have the wave-field at time T_M and $T_M - \triangle t$. If we assume the medium is homogeneous within a certain distance from the source, and T_M is small enough that outside a circular region (denoted as $\mathbb{O}$), the energy of the wave can be neglected, we can calculate the analytic wave-field inside $\mathbb{O}$, once at the moment T_M, and once at the moment $T_M - \triangle t$.

Figure 3 shows two analytic wave-fields using equation (9) from **?** † and wavelet shown in figure 4.

Compared with straightforward digitization of the source, one advantage of implementing the source as pre-calculated analytic wave-fields is that the source can be emplaced very flexibly in space, either coincident with the grid or anywhere in between. In computing the pre-calculated wave-field, we only need to know its distance to each grid. If the source is implemented by straightforward digitization, any source deviating from the grid point will be invisible to the finite-difference formalism.

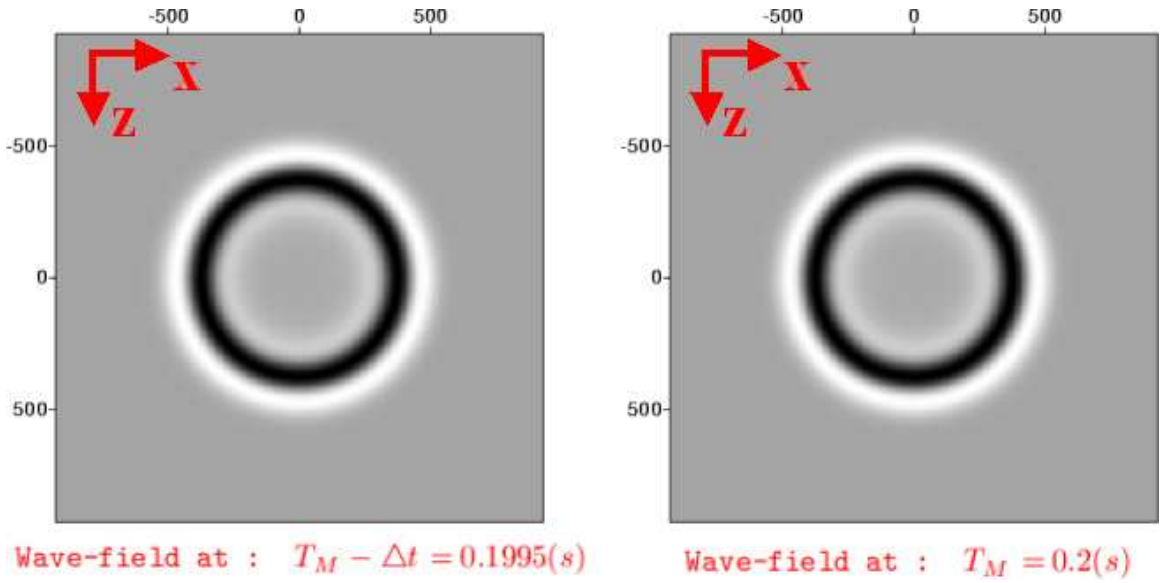

Figure 3: The pre-calculated wave-fields at $T_M - \triangle t$ and T_M

We apply the pre-calculated wave-fields displayed in figure 3 to the geological model displayed in figure 4, using a wavelet as displayed in figure 4. The other parameters are: $\triangle x = \triangle z = 5(m)$, $\triangle t = 0.5(ms)$. Equation (13) was applied to update the wave-fields at the next moment. The final results were displayed in figure 5. We next apply the quality control procedure. First all

*The first derivative of Gaussian is an odd function, its positive portion should have the same shape and size as the negative portion.

† "The $F(\omega)$ in equation (9) of **?** should be considered as the Fourier transform of A(t) (our source signature)"

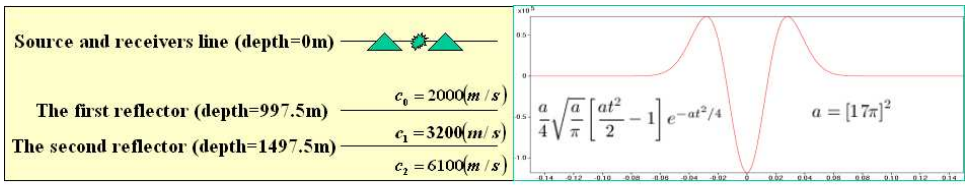

Figure 4: Left: the geological model. Right: source signature (wavelet).

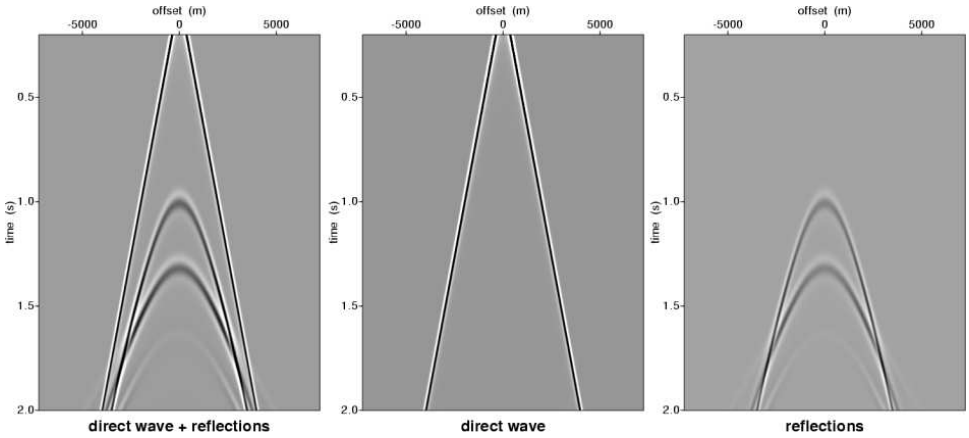

Figure 5: Finite-difference modelling results starting from analytic wave-fields at $t = 0.2s$

traces in the rightmost panel in figure 5 are summed together to form a single trace, as shown by the red curve in figure 6. The desired "actual" sum can be calculated from the reflection data for the models with 2 layers to have: equation (8). Here only the 2 primary reflections are available (corresponding to the second and third term in equation (6)), hence we have the quality control formula:

$$\frac{R_1 f\left(t-t_1\right)+R_2' f\left(t-t_2\right)+R_3' f(t-t_3)}{5} \tag{14}$$

where

$$f(t) = -\frac{c_0}{2}\int_{-\infty}^{t} A(u)du = -\frac{c_0}{2}\frac{a}{4}\sqrt{\frac{a}{\pi}}te^{-at^2/4}$$

$$t_1 = (2z_1 - z - z_s)/c_0, \quad t2 - (2z_1 - z - z_s)/c_0 + 2(z_2 - z_1)/c_1, \quad t3 - (2z_1 - z - z_s)/c_0 + 4(z_2 - z_1)/c_1$$

$$R_1 = \frac{c_1 - c_0}{c_1 + c_0}, \quad R_2 = \frac{c_2 - c_1}{c_2 + c_1}, \quad R_3 = \frac{c_3 - c_2}{c_3 + c_2}, \quad R_2' = \left(1 - R_1^2\right) R2, \quad R_3' = R_2' * (-R_1 R_2)$$

From figure 6, we feel confident about the implementation and frequency content of the wavelet, $\triangle x$, $\triangle z$, and $\triangle t$ since the sum of all receivers perfectly recover the 1D experiment.

Figure 7 compares different digitized "interpretations" of z_1, which will affect the result of the analytic solution (equation 14). The velocity model is stored in a 2-dimensional array. We illustrate the issue of interpretation with the following example. We ignore the dimension of the array

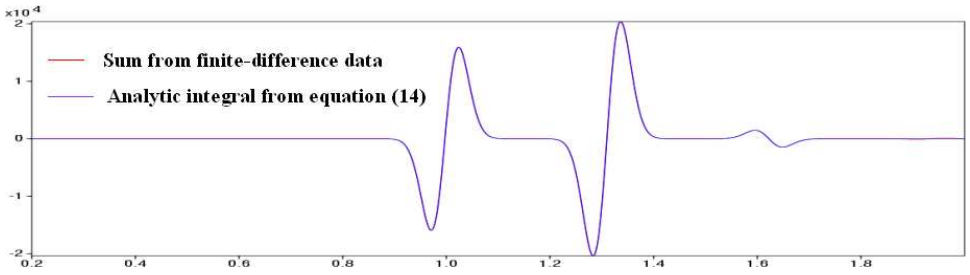

Figure 6: Comparison of the sum over all receivers from the finite-difference data with the analytic solution (equation-14). The first curve is almost completely covered by the second, they agree with each other very well.

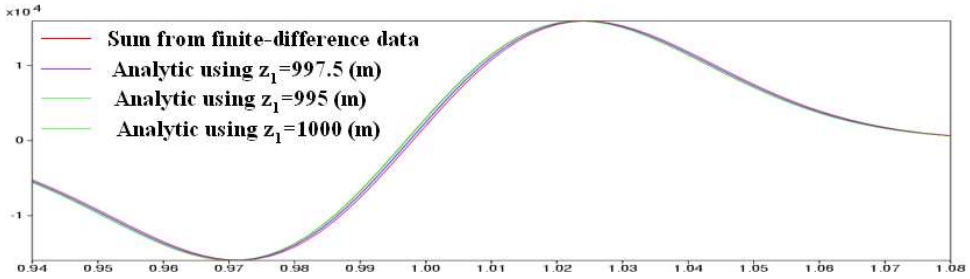

Figure 7: Comparison of the analytic solutions (equation-14) using different interpretation of z_1. The interpretation using $z_1 = 997.5(m)$ agrees with finite-difference data. This implies that the interface in the velocity should be interpreted as in the middle between discontinuous values.

corresponding to the x-direction, and only consider the dimension corresponding to depth, denoting the array as $c[i]$, $i = 0, 1, 2, \cdots$.

The physical meaning of $c[i]$ is the velocity at depth $i * \triangle z$. In this case we have, $c[0] = c[1] = \cdots = c[199] = c_0$, $c[200] = c[201] = \cdots = c_1$, so we know the velocity at $995m$ is c_0, and the velocity at $1000m$ is c_1. Where, then, should the interface be? A natural answer would be: in the middle of $995m$ and $1000m$, or equivalently at $997.5m$. This is emphasized here because it is natural to interpret the depth of the reflector either as $995m$ or as $1000m$.

This is important when it comes to modelling the free-surface. If we define the grid points as 0, $\triangle z$, $2\triangle z$, $\cdots$, the free-surface can only be defined somewhere in the middle of the grids. As a result, we cannot define a free-surface at $0m$, contrary to one of the most commonly used conventions in our geography and geology. We test the free-surface modelling with the geological model and

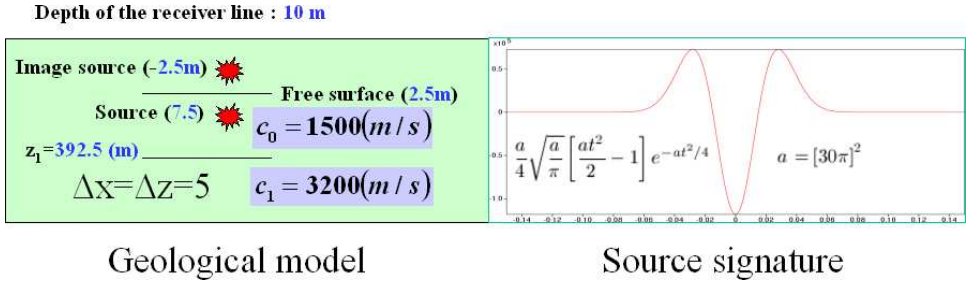

Figure 8: The geological model and modelling parameters

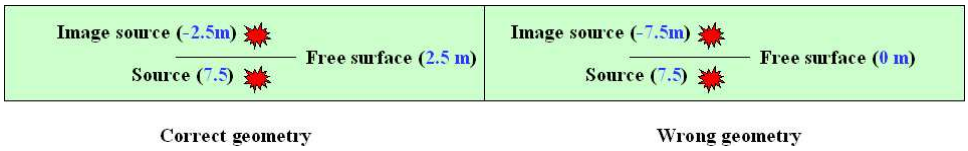

Figure 9: 2 different interpretation lead to slightly different geometries for the position of the image source. Left: correct interpretation $z_f = 2.5m$. Right: wrong interpretation $z_f = 0m$

modelling parameters displayed in figure 8. Notice that the interpretation of the depth of the free-surface is at $2.5m$ (the left half of figure 9 contains greater detail). It is all too easy to use the wrong interpretation, which is shown in the right half of figure 9; for these two interpretations, the pre-calculated wave-fields look very similar, as shown in figure 10, as do the final modelling results in figure 11. However, upon summations of all traces together to recover 1D experiment (i.e., our

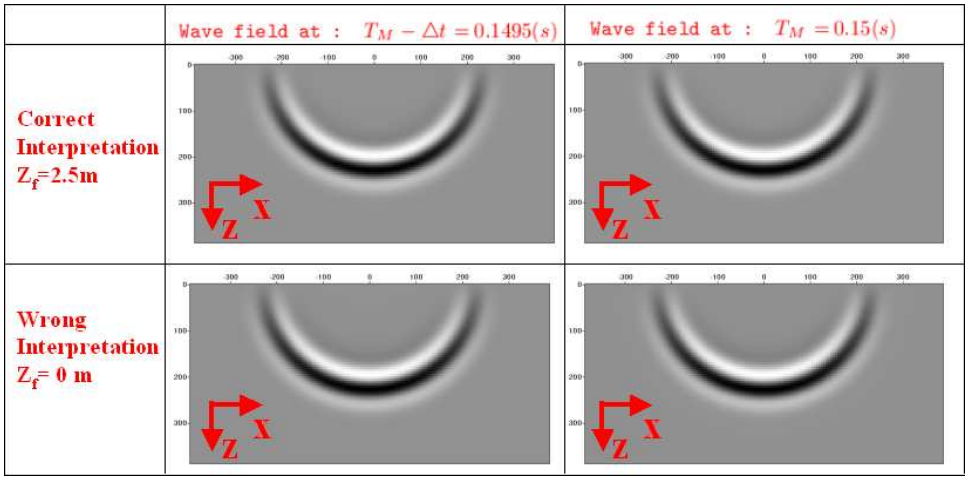

Figure 10: 2 sets of pre-calculated wave-fields computed using different interpretations. These 2 sets looked very similar

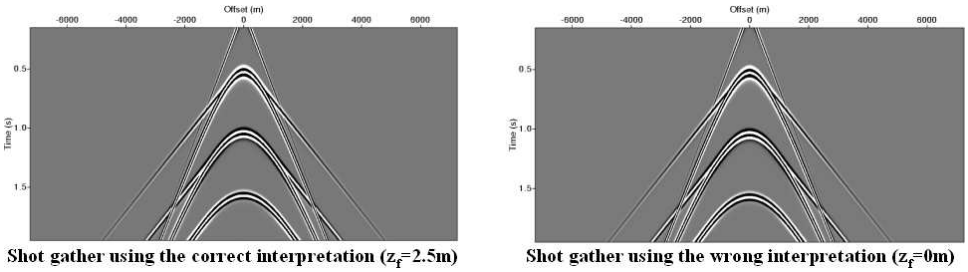

Figure 11: Comparison of modelling results using different interpretations, the left uses the correct interpretation, the right uses wrong interpretation. These 2 sets looked very similar and the difference are subtle.

quality control methodology), decidedly non-negligible differences arise (see figure 12).

We take this as evidence of (1) the importance of sensitive quality control methods for validation of modelled waveform amplitudes, and (2) the importance (demonstrated via (1)!) of a correct digital assignment of depths to the model.

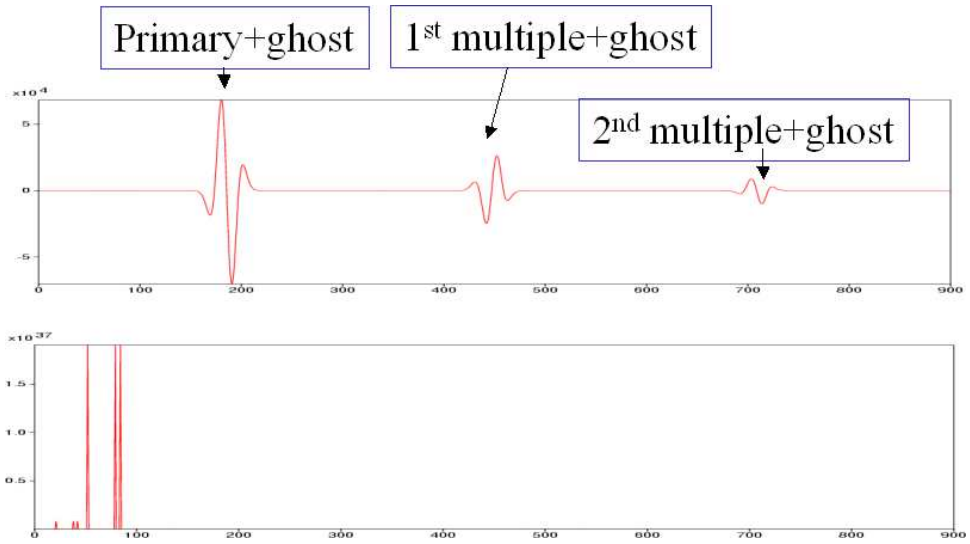

Figure 12: Comparison of the sum of the all traces in the shot gather. These 2 sums looked very different. Top, the free-surface is correctly interpreted. Bottom, the free-surface depth is interpreted $2.5(m)$ away from its true location. It's very obvious that the error caused by wrong interpretation can be easily caught by this quality control method although the shot gathers looks very similar

4 Conclusion

As we develop direct non-linear imaging and target identification methods based on the inverse scattering series (as well as other series based processing methods), which are ambitious in the sense of data waveform interrogation, tools for testing and validation of these methods become increasingly important. Specifically, as methods are extended to multiple dimensions, we require forward modelling tools that provide a wave-accurate set of input synthetic data. This paper outlines some issues encountered when utilizing finite difference schemes to provide such tools, and some strategies for overcoming them.

Importantly, we discuss means by which the source signature can be implemented accurately in an arbitrary position in finite difference modelling. We illustrate the importance of the physical meaning of a discontinuous medium in finite difference formalism, as a jump in the middle of discontinuous numerical values. Finally, we demonstrate that summing all traces together can serve as a sensitive method for quality control of the choice of finite-difference parameters.

Acknowledgements

All M-OSRP colleagues were thanked for the efforts in proof-reading the manuscript. We are very grateful for the informative discussions with Jingfeng Zhang, Shansong Jiang. All M-OSRP sponsors were acknowledged for the support. We have been partially funded by and are grateful for NSF-CMG award DMS-0327778 and DOE Basic Sciences award DE-FG02-05ER15697.

References

R. M. Alford, K. R. Kelly, and D. M. Boore. Accuracy of finite-difference modeling of the acoustic wave equation. *Geophysics*, 39(06):834–842, 1974.

M. A. Dablain. The application of high-order differencing to the scalar wave equation. *Geophysics*, 51(01):54–66, 1986.

K. R. Kelly, R. W. Ward, S. Treitel, and R. M. Alford. Synthetic seismograms - A finite-difference approach. *Geophysics*, 41(01):2–27, 1976.

D. D. Kosloff and E. Baysal. Forward modeling by a Fourier method. *Geophysics*, 47(10):1402–1412, 1982.

P. M. Morse and H. Feshbach. *Methods of theoretical physics*. McGraw-Hill Book Co., 1953.

A. C. Reynolds. Boundary conditions for the numerical solution of wave propagation problems. *Geophysics*, 43(06):1099–1110, 1978.

A note on data modelling using the Cagniard-de Hoop method

Jingfeng Zhang and Arthur B. Weglein

Abstract

Data modelling for a 1D layered medium using the Cagniard-de Hoop method is discussed. In particular a 1D acoustic model and data generated and then used in a deghosting algorithm.

1 Introduction and motivation

Data forward modelling is a very important topic in seismic exploration. It is crucial for new algorithm validation and forward model-matching techniques. Data with higher quality help to more correctly evaluate the effectiveness of the algorithm and give better model-matching prediction results. For most conventional seismic processing techniques, arrival time of a seismic event is much more important than the amplitude. Thus, the modelled data fidelity might be held to a lower standard. However, there are some (recently developed) algorithms that fully employ the amplitude information as well as the arrival time of the signal. In that case, the fidelity of the synthetic data is more important in order to give better assessment of the algorithms. Some examples of those algorithms are deghosting (Weglein et al., 2002; Zhang and Weglein, 2005b), inverse scattering series (ISS) based free surface multiple removal (Weglein et al., 1997), internal multiple attenuation (Weglein et al., 1997) and elimination (Ramirez and Weglein, 2005), imaging with reference medium velocity (Shaw et al., 2004; Liu et al., 2005; Innanen and Weglein, 2003) and nonlinear inversion techniques (Zhang and Weglein, 2005a). The above listed algorithms work like a chain of tasks in the sense that the performance of the latter ones will be affected by the former ones. And each algorithm is fully wave-theoretic, requiring wavefield data, synthetic or otherwise, to proceed.

There are many methods to generate seismic data. For complex media, where an analytic solution is not available, methods such as finite difference and finite element are the usual choice. For 1D layered media, where analytic solutions can be found, methods such as reflectivity (Kennett, 1983) and Cagniard-de Hoop (de Hoop and van der Hijden, 1983; Aki and Richards, 2002) have the opportunity to generate data either more efficiently or with better quality. The advantages and disadvantages of each method will not be elaborated in this paper. For the validation of the deghosting algorithm, the Cagniard-de Hoop method is the best choice.

First, data generated in a 1D medium will suffice, so the major drawback of the Cagniard-de Hoop method is not relevant here. Second, we may benefit from a powerful property of the method: the ability to calculate individual wavefield events. The first step in Extinction theorem deghosting is receiver side deghosting; after that, source side deghosting is performed. As in any other numerical processing routine, quality control of the results of each step is worthwhile. For instance, after receiver side deghosting, the data are supposed to contain the signal and its source side ghost. It would be valuable to have the exact results for comparison. Based on generalized ray theory, Cagniard-de Hoop method enables us to calculate the field due to each specific event. So it is straightforward to calculate the data that only contain the signal and the source ghost. Finite

difference methods, on the other hand, don't have this ability. The last reason is that, at least for a one parameter (velocity) 1D acoustic medium, the Cagniard-de Hoop method can produce "perfect" data in the sense that the wavefield is calculated through an integration of a regular integrand over a finite range. Just like the numerical integration of $sin(x)$ from 0 to π, we can get the result as accurate as we want, up to the limit of the computer.

In the following section, after some introductory words about data modelling for 1D layered media, the analytic Green's function in space-time domain will be listed directly for a one interface model and a line source. Then two comments are made on the numerical evaluations. Finally, we present the data generated for a simple acoustic model.

2 Theory

The 2D acoustic constant density wave equation is

$$\nabla^2 P(x,z,x_s,z_s,t) - \frac{1}{c^2}\frac{\partial^2}{\partial t^2}P(x,z,x_s,z_s,t) = A(t)\delta(x-x_s)\delta(z-z_s), \tag{1}$$

where $A(t)$ is the source wavelet and we assume the line source is at position (x_s, z_s) and goes off at $t = 0$. The solution can be easily obtained if we can solve the corresponding Green's function equation:

$$\nabla^2 G(x,z,x_s,z_s,t) - \frac{1}{c^2}\frac{\partial^2}{\partial t^2}G(x,z,x_s,z_s,t) = \delta(t)\delta(x-x_s)\delta(z-z_s), \tag{2}$$

since

$$P(x,z,x_s,z_s,t) = \int_0^t A(t-\tau)G(x,z,x_s,z_s,\tau)d\tau. \tag{3}$$

So now the problem is how to solve Eq.2. One way is to perform Fourier transforms over x and t on Eq.2, so that

$$\frac{d^2}{dz^2}G(k_x,z,x_s,z_s,\omega) + q^2 G(k_x,z,x_s,z_s,\omega) = \delta(z-z_s), \tag{4}$$

where $q^2 = \frac{\omega^2}{c^2} - k_x^2$. Clearly Eq.4 is essentially a 1D wave equation. Its analytical solution $G(k_x,z,x_s,z_s,\omega)$ is not difficult to find for a simple 1D layered medium. We can obtain $G(x,z,x_s,z_s,t)$ through inverse Fourier transform over ω and k_x. This is essentially the way that the Reflectivity method works. The associated difficulty of this method relates to the infinite integral range and irregular integrand.

Instead of performing Fourier transform over x and t on Eq.2, Cagniard-de Hoop method performs a Laplace transform over t and a Fourier transform over x:

$$\int_{-\infty}^{\infty} e^{-ik_x x}dx \int_0^{\infty} e^{-st}dt, \tag{5}$$

where s is real and positive, then Eq.2 becomes

$$\frac{\partial^2}{\partial z^2}G(k_x,z,s) - n^2 G(k_x,z,s) = \delta(z-z_s), \tag{6}$$

where $n^2 = k_x^2 + \frac{s^2}{c^2}$ and for convenience, we have omitted variables x_s and z_s in G. Once we find the solution for $G(k_x, z, s)$, we have

$$G(x, z, s) = \frac{1}{2\pi} \int_{-\infty}^{\infty} G(k_x, z, s) e^{ik_x x} dk_x. \tag{7}$$

Until now, this procedure is very similar with the Reflectivity method, except the fact that s instead of $-i\omega$ is being used. Noticing that

$$G(x, z, s) = \int_0^{\infty} G(x, z, t) e^{-st} dt, \tag{8}$$

The Cagniard-de Hoop method analytically manipulates Eq.7 into the form of Eq.8 and recognizes the expression for $G(x, z, t)$ by just looking at the new transformed integrand! The whole work is done without actually carrying out any numerical integrations! Cagniard proved that the obtained solution is in fact the physical solution we are looking for. The derivation details have been given in literature and will be omitted here. Instead, we will directly list the solutions for a one interface constant density acoustic model with velocities c_0 and c_1 above and below the reflector (at z_d) respectively.

The direct wave Green's function is

$$G(x, z, t) = \frac{-1}{2\pi} \frac{H(t - R_0/c_0)}{\sqrt{t^2 - R_0^2/c_0^2}}; \tag{9}$$

the pre-critical reflection Green's function is

$$G(x, z, t) = \frac{-1}{2\pi} Re\grave{P}\acute{P} \frac{H(t - R/c_0)}{\sqrt{t^2 - R^2/c_0^2}}; \tag{10}$$

and the post-critical reflection Green's function (if it exists) is

$$G(x, z, t) = \frac{-1}{2\pi} Im\grave{P}\acute{P} \frac{H(t - t_h) - H(t - R/c_0)}{\sqrt{R^2/c_0^2 - t^2}} + \frac{-1}{2\pi} Re\grave{P}\acute{P} \frac{H(t - R/c_0)}{\sqrt{t^2 - R^2/c_0^2}}, \tag{11}$$

where

$$\begin{aligned}
R_0 &= \sqrt{x^2 + (z - z_s)^2}; \\
t_h &= \frac{x}{c_1} + |z + z_s - 2z_d| \sqrt{c_0^{-2} - c_1^{-2}}; \\
\grave{P}\acute{P} &= \frac{\eta_0 - \eta_1}{\eta_0 + \eta_1}; \qquad (12) \\
\eta_i &= \sqrt{c_i^{-2} - p^2}, \text{where } i = 0, \text{or } 1; \qquad (13) \\
p &= \begin{cases} \frac{xt - |z + z_s - 2z_d| \sqrt{R^2/c_0^2 - t^2}}{R^2} & t \le \frac{R}{c_0} \\ \frac{xt + i|z + z_s - 2z_d| \sqrt{t^2 - R^2/c_0^2}}{R^2} & t \ge \frac{R}{c_0} \end{cases}; \qquad (14) \\
R &= \sqrt{x^2 + (z + z_s - 2z_d)^2}.
\end{aligned}$$

The above results can be easily generalized to the case that the free surface is present and multi-layer medium. $\grave{P}\acute{P}$ is the plane wave reflection coefficient for compressional wave and t_h is the

arrival time of the head wave. There are two comments that we would like to make in this note. The first one is that, in order to perform the convolution in Eq.3 properly, it is convenient to use integration by parts to deal with the spike in the above Green's functions. For example, we can calculate the direct wave in the following way:

$$\begin{aligned} P(x,z,x_s,z_s,t) &= \int_0^t A(t-\tau)G(x,z,x_s,z_s,\tau)d\tau \\ &= \frac{-1}{2\pi}\int_{\frac{R_0}{c_0}}^t A(t-\tau)\frac{1}{\sqrt{\tau^2-R_0^2/c_0^2}}d\tau \\ &= \frac{-1}{2\pi}\int_{\frac{R_0}{c_0}}^t A(t-\tau)\frac{1}{\tau}d\sqrt{\tau^2-R_0^2/c_0^2} \\ &= \frac{-1}{2\pi}A(t-\tau)\frac{1}{\tau}\sqrt{\tau^2-R_0^2/c_0^2}\Big|_{\tau=\frac{R_0}{c_0}}^t \\ &\quad -\frac{-1}{2\pi}\int_{\frac{R_0}{c_0}}^t \sqrt{\tau^2-R_0^2/c_0^2}\Big[\frac{-A(t-\tau)}{\tau^2}+\frac{1}{\tau}A(t-\tau)\Big]d\tau. \end{aligned} \tag{15}$$

The above integration is regular and easy to calculate. For the first term in Eq.11, we might just need to change variable t to $\frac{R}{c_0}\sin(\theta)$. The second point we would like to make relates to a mistake we made before. Variable η in Eq.13 is complex in general. It seems convenient to calculate its value using the the square root subroutine for complex number in Fortran or C. However, this might lead to a mistake. The reason is that, for example, when the argument under the square root is negative pure real, there are two possible values for η. The intrinsic subroutine might choose the positive one. This is unfortunately not correct in this case. Actually, we have to use the negative pure imaginary value. The argument is that the values of η and p are supposed to be continuous with continuously increasing t. When t changing from $t \leq \frac{R}{c_0}$ to $t \geq \frac{R}{c_0}$, p picks up a (small) positive imaginary value which causes η having a negative (might not be small) imaginary part. Obviously, in order to make η change continuously, we need to make sure that the pure negative value is used for η when p is real. The consequence of not doing so will be illustrated in the next section.

3 Examples

In this section, we present the data generated using Cagniard-de Hoop method for an acoustic model (Fig.1). The model has a free surface at $z = 0$ and a reflector at $300m$ below which is a homogeneous half space. The source is at $(0, 7m)$ and the cable is at $9m$. We use a Ricker wavelet with a dominant frequency of 25Hz (Fig.2).

Primaries and their ghosts at pre-critical (Fig.3) and post-critical (Fig.4) offsets are compared with each other. Not surprisingly, the primary arrives first and its source-receiver ghost arrives the latest. Also the summation of primary and its ghosts tends to have more polarity changes than any of its components.

The data for $(0, 4.5s)$ and $(0, 5000m)$ are generated (Fig.5). The data contain primaries, one to fourth order free surface multiples and their ghosts. The direct wave and its ghost have not been included. The data generated without taking care of the sign of η is presented in Fig.6. It seems

that there is no big difference. But only the data in Fig.5 are the real physical wave field. Very good deghosting results are obtained when using the correct data set (Fig.7). The reflections at the right boundary in Fig.7 are due to limited offset aperture. Problematic results are produced (Fig.8) using the data in Fig.6. Besides the boundary reflections, there are also some artifacts reflections arise where headwaves start to appear. These unexpected artifacts are the consequences of using data in Fig.6.

4 Acknowledgements

We would like to thank Adrian de Hoop (Delft University of Technology) for providing helpful literatures. Hing Tan (Shell) is thanked for intriguing comments. Fang Liu, Bogdan Nita (Montclair State University), Simon Shaw (ConocoPhillips) and Kris Innanen are thanked for helpful discussions. Haiyan Zhang and Sam Kaplan are thanked for their help in writing this report. M-OSRP sponsors are appreciated for their supports. We have been partially funded by and are grateful for NSF-CMG award DMS-0327778 and DOE Basic Sciences award DE-FG02-05ER15697.

References

K. Aki and P. G. Richards. *Quantitative Seismology*. University Science Books, 2nd edition, 2002.

A. T. de Hoop and J. H. M. T. van der Hijden. Generation of acoustic waves by an impulsive line source in a fluid/solid configuration with a plane boundary. *J. Acoust. Soc. Am.*, 74:333–342, 1983.

K. A. Innanen and A. B. Weglein. Simultaneous imaging and inversion with the inverse scattering series. In *Proceedings of the Eighth International Congress of the SBGf and Fifth Latin American Geophysical Conference*. SBGf, 2003.

B. L. N. Kennett. *Seismic wave propagation in stratified media*. Cambridge University Press, 1983.

F. Liu, A. B. Weglein, B. G. Nita, and K. A. Innanen. Inverse scattering series for vertically and laterally varying media: application to velocity independent depth imaging. *M-OSRP Annual Report*, 4, 2005.

Adriana C. Ramirez and Arthur B. Weglein. An inverse scattering internal multiple elimination method: Beyond attenuation, a new algorithm and initial tests. *M-OSRP Annual Report*, 4, 2005.

S. A. Shaw, A. B. Weglein, D. J. Foster, K. H. Matson, and R. G. Keys. Isolation of a leading order depth imaging series and analysis of its convergence properties. *Journal of Seismic Exploration*, 2:157–195, November 2004.

A. B. Weglein, F. A. Gasparotto, P. M. Carvalho, and R. H. Stolt. An inverse-scattering series method for attenuating multiples in seismic reflection data. *Geophysics*, 62(6):1975–1989, 1997.

A. B. Weglein, S. A. Shaw, K. H. Matson, J. L. Sheiman, R. H. Stolt, T. H. Tan, A. Osen, G. Correa, K. A. Innanen, Z. Guo, and J. Zhang. New approaches to deghosting towed-streamer and ocean-bottom pressure measurements. In *72nd Annual Internat. Mtg., Soc. Expl. Geophys., Expanded Abstracts*, pages 1016–1019. Soc. Expl. Geophys., 2002.

H. Zhang and A. B. Weglein. The inverse scattering series for tasks associated with primaries: Depth imaging and direct non-linear inversion of 1d variable velocity and density acoustic media. In *75th Annual Internat. Mtg., Soc. Expl. Geophys., Expanded Abstracts*, pages 1705–1708. Soc. Expl. Geophys., 2005a.

J. Zhang and A. B. Weglein. Extinction theorem deghosting method using towed streamer pressure data: Analysis of the receiver array effect on deghosting and subsequent free surface multiple removal. In *75th Annual Internat. Mtg., Soc. Expl. Geophys., Expanded Abstracts*, pages 1705–1708. Soc. Expl. Geophys., 2005b.

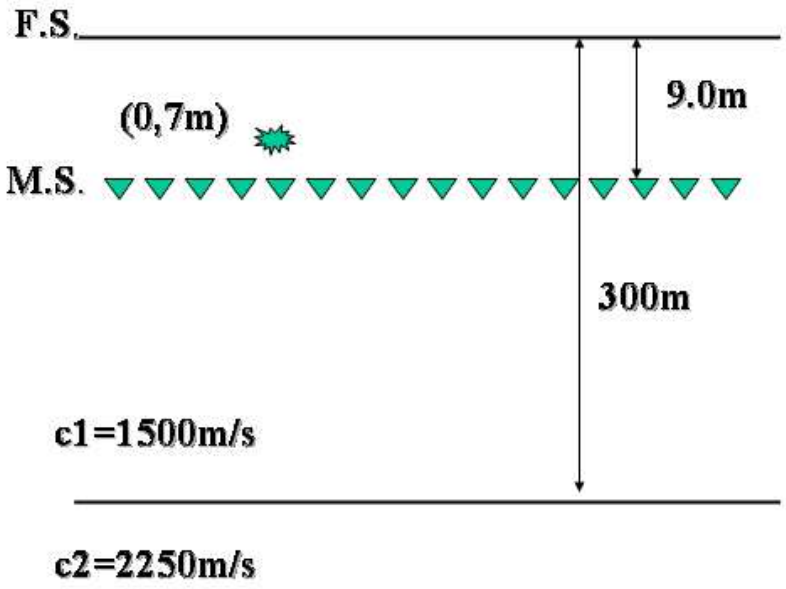

Figure 1: Constant density acoustic model.

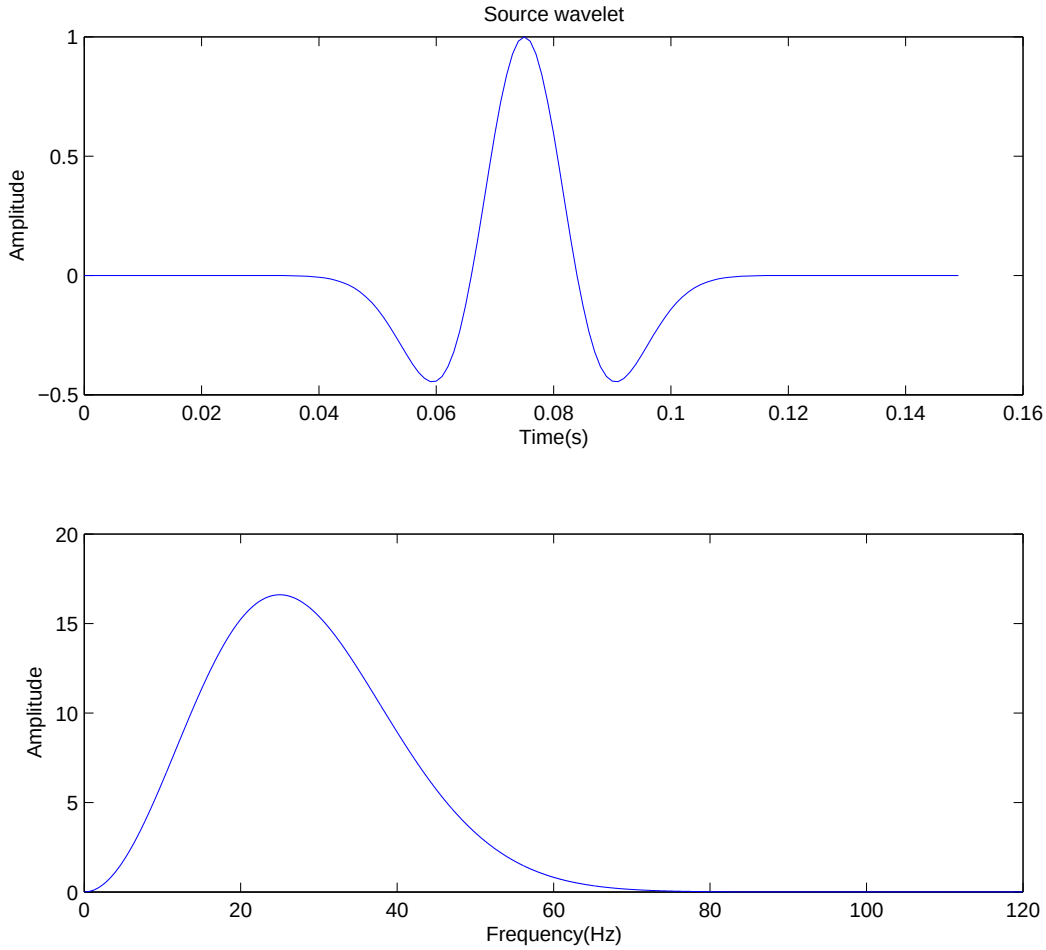

Figure 2: Ricker source wavelet.

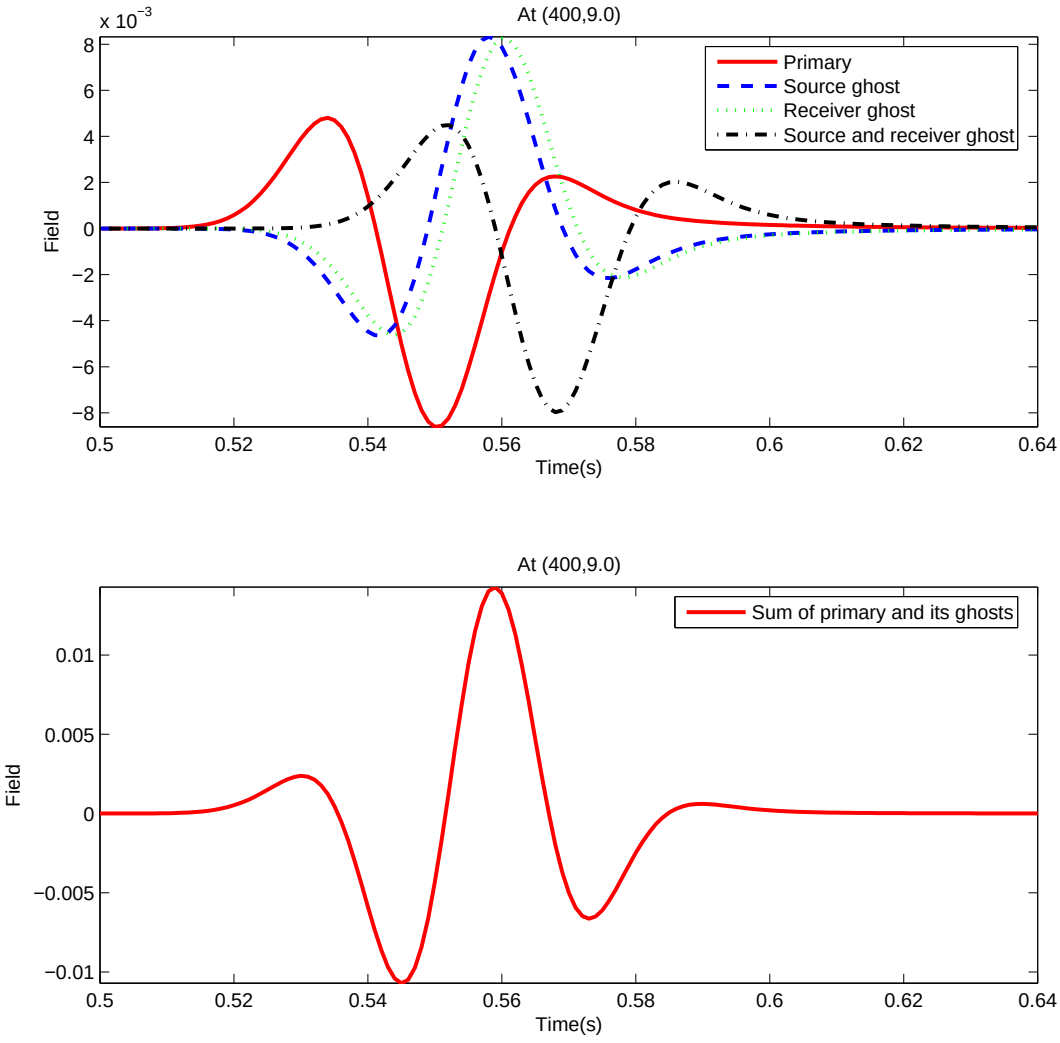

Figure 3: Wave field at (400,9m). Top: four components of the data; Bottom: Summation of the data.

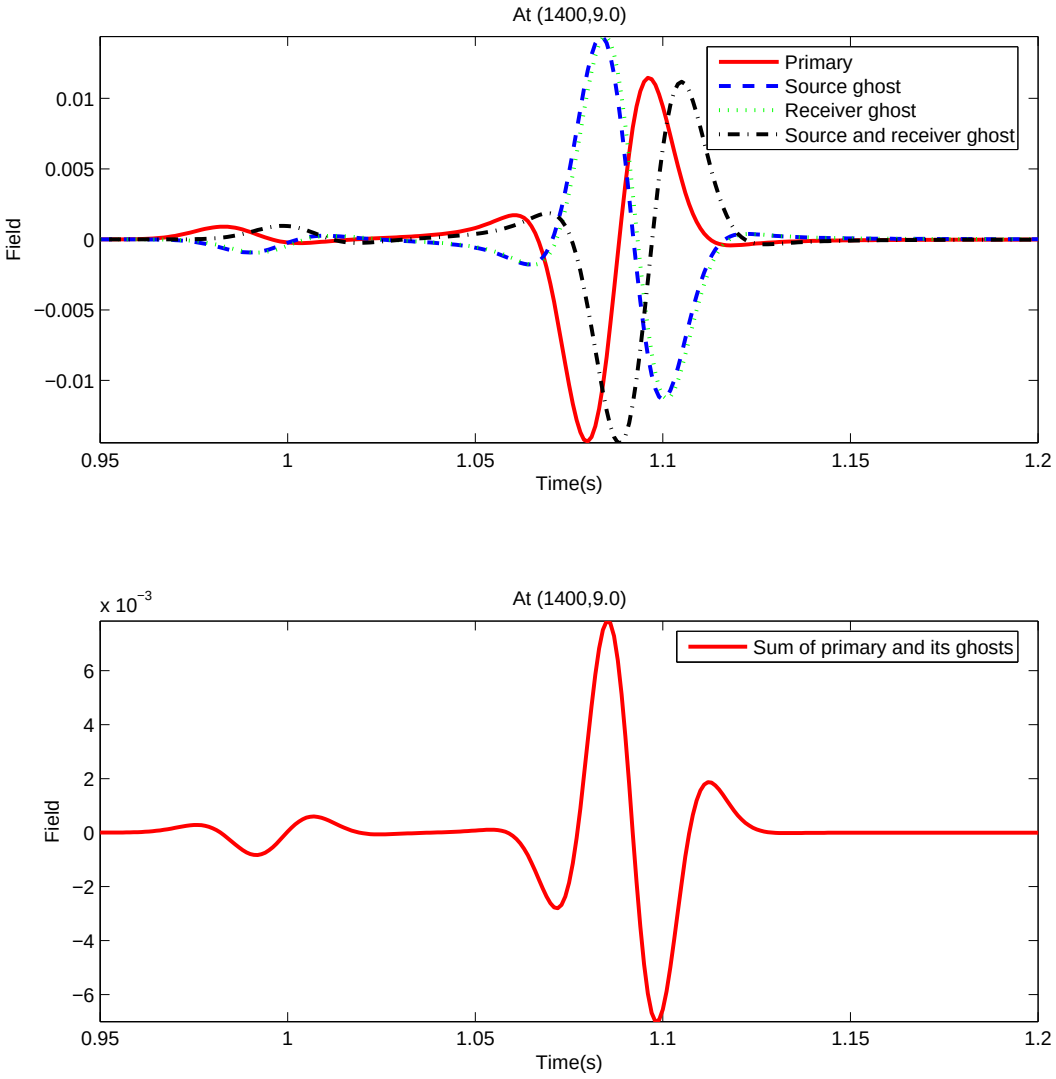

Figure 4: Wave field at large offset (1400,9m). Top: four components of the data; Bottom: Summation of the data.

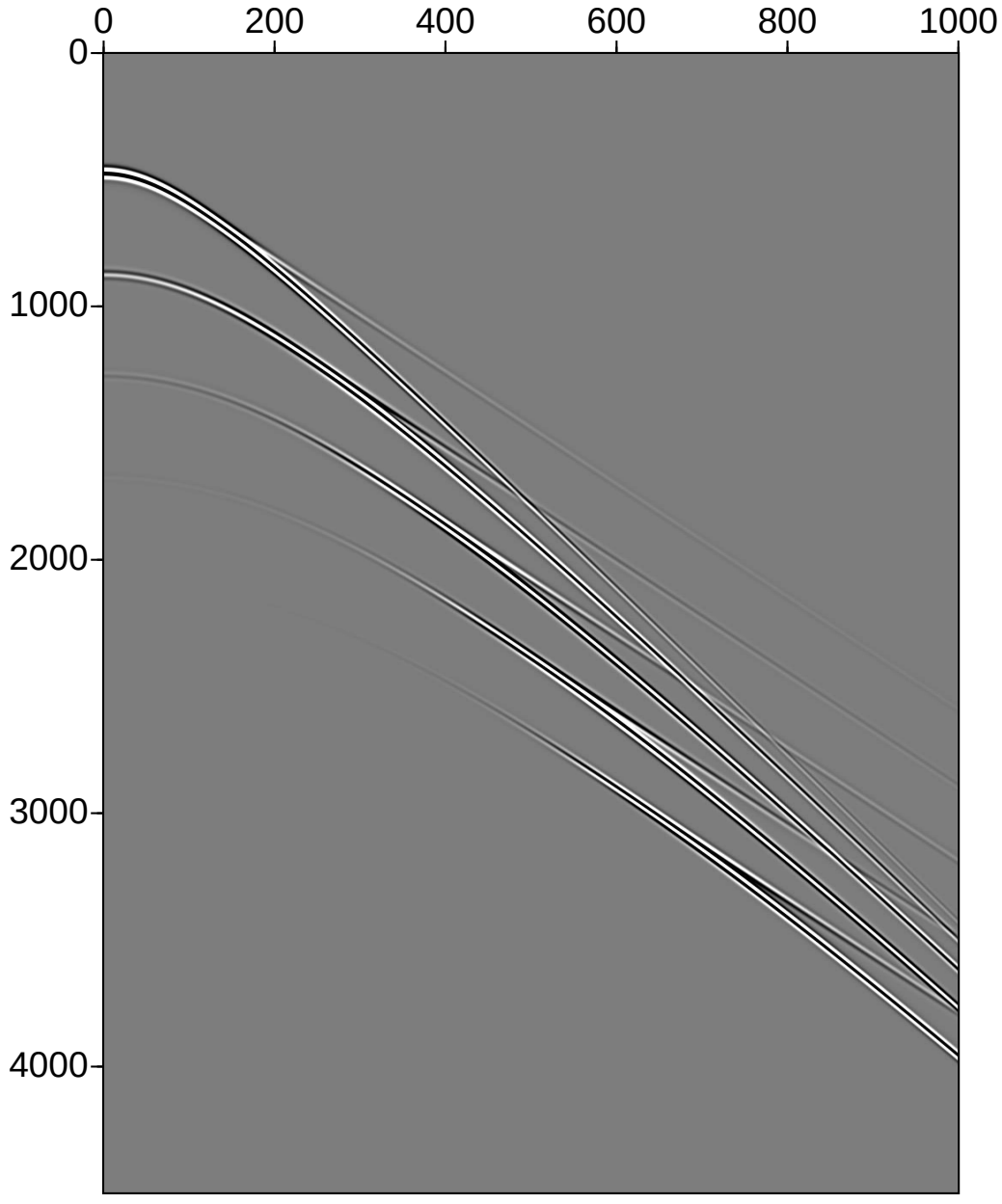

Figure 5: Total correct data generated.

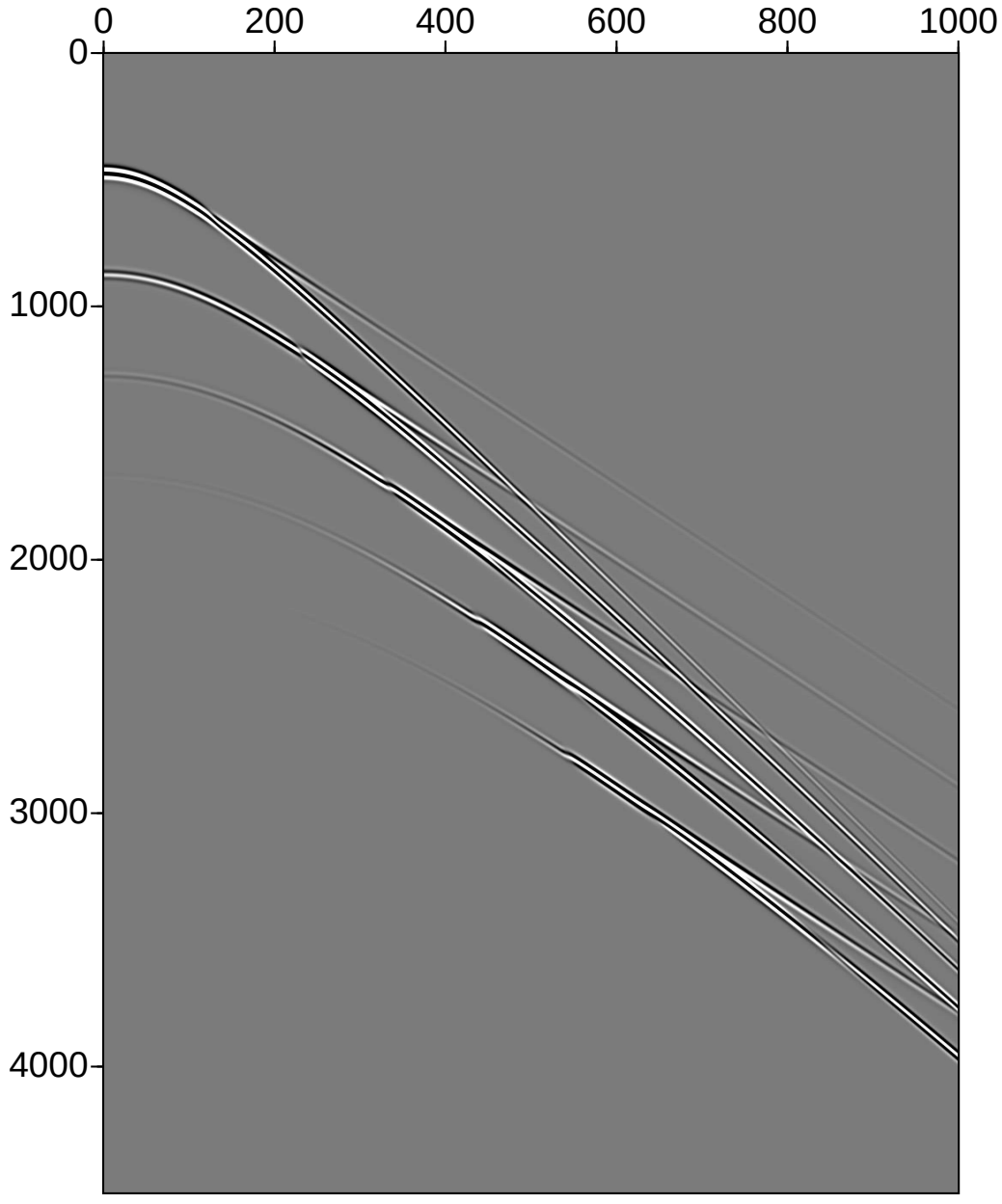

Figure 6: Total incorrect data generated.

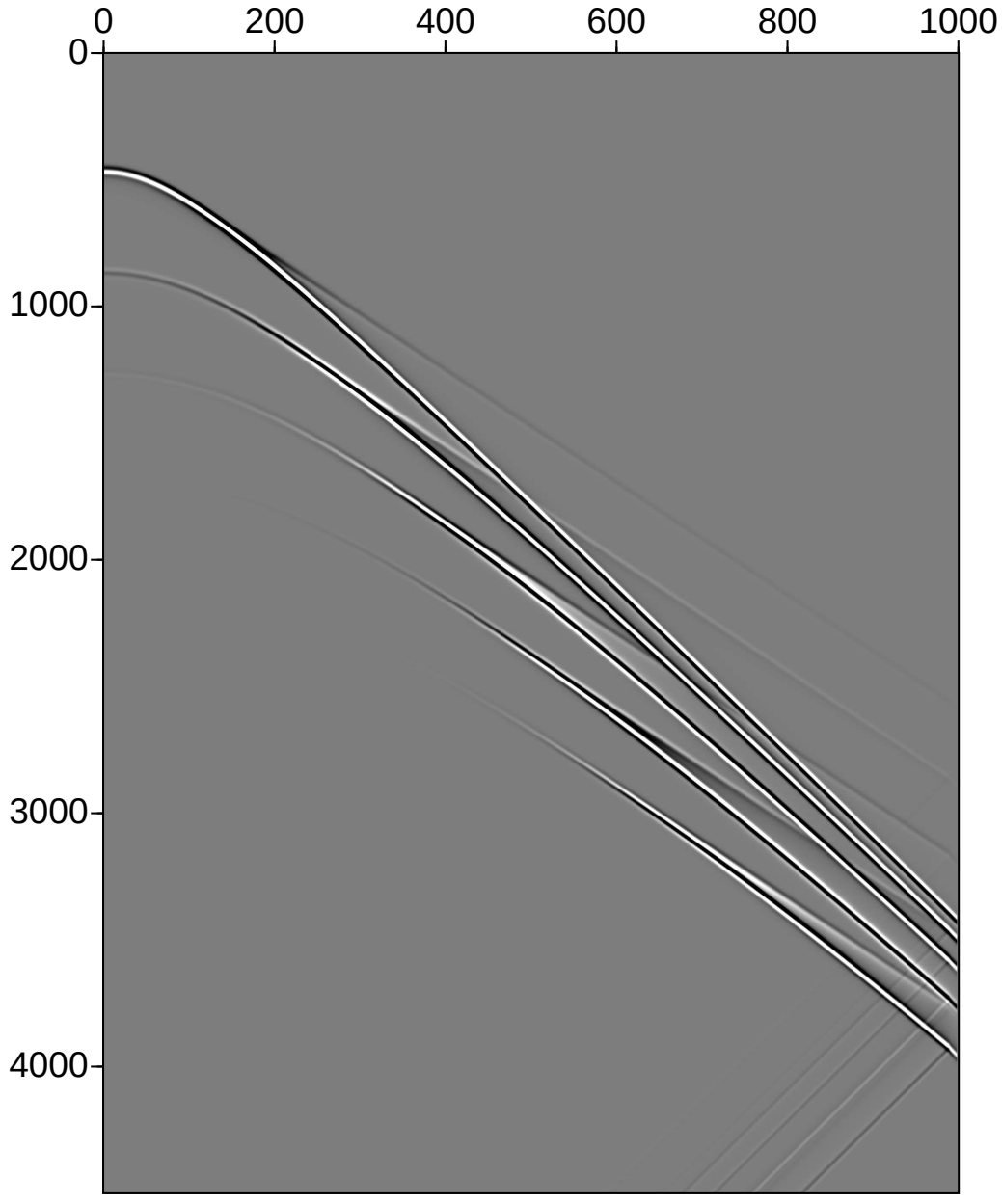

Figure 7: Deghosting result using correct data in Fig.5.

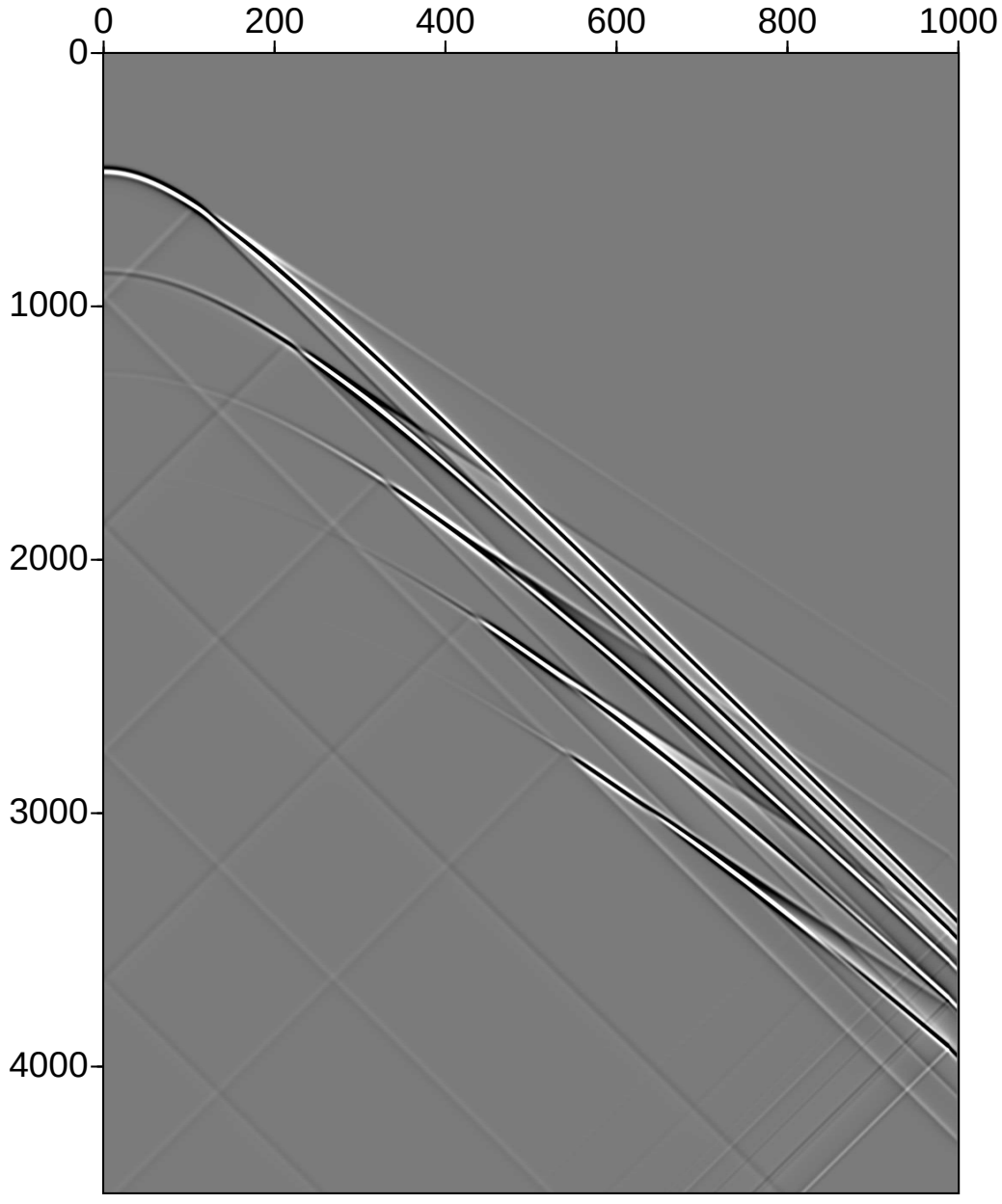

Figure 8: Deghosting result using incorrect data in Fig.6.

Updates to internal and free surface multiple coding projects

Sam T. Kaplan, Kristopher A. Innanen and Arthur B. Weglein

Abstract

We outline changes to the implementation of the 2D M-OSRP internal multiple attenuation (IMA) algorithm, and introduce an implementation of the 2D free surface multiple elimination (FSME) algorithm. We use the IMA algorithm's need for only the non-evanescent portion of the wavefield to minimize its required computer memory. In addition, we update our load-balancing scheme for the IMA algorithm by finding a smaller subset of the algorithm to use as a basis for computation. The 2D FSME algorithm is presented (1) for when the distance between adjacent shots is equal to the distance between adjacent geophones, and (2) for the case in which these distances differ.

1 Introduction

The purpose of this short note is two-fold. First, we outline optimizations and changes made to the M-OSRP internal multiple attenuation (IMA) algorithm (Kaplan et al., 2004), and second we introduce the M-OSRP free surface multiple elimination (FSME) algorithm. Both of these computer programmes are the end products of M-OSRP's ongoing coding project. Our goals are to both deliver software for application to real data (e.g., Kaplan et al., 2005b), and for use as a basis of ongoing research (e.g., Kaplan and Innanen, 2005).

In addition to the IMA algorithm announced at the 2004 M-OSRP annual meeting, we are currently working on and testing a separate IMA algorithm for large distributed computing systems (Kaplan et al., 2005a). Our hope is that this will pave the way for three dimensional implementations of the algorithm. None-the-less, there are updates to the 2004 two dimensional algorithm that we wish to share, and do so in this note. The changes allow for more efficient use of computer memory, and better load balancing on distributed systems.

Our two dimensional FSME code implements the algorithm presented in Weglein et al. (2003). Like its IMA counter-part, it is designed to run on distributed computing systems. The FSME algorithm is most readily understood when the lateral distance between shots is equal to the lateral distance between receivers. Here, we note our method for allowing shot spacing and receiver spacing to differ. This is particularly important for real data applications.

2 Internal multiple attenuation code optimizations

We made two notable changes to the M-OSRP IMA code since its release shortly after the 2004 annual meeting. First, we take advantage of the algorithm's requirement for only the non-evanescent portion of the wavefield to reduce its memory foot-print; and second, we use an analysis of the IMA equations that is more suitable for their load-balancing on a distributed system.

The first change, reduction in the memory foot-print of the algorithm, we find through simple analysis of the dispersion relation. We write the IMA algorithm in two dimensions:

$$b_{3IM}(k_{gx}, k_{sx}, \omega) = \frac{1}{(2\pi)^2} \int_{-\infty}^{\infty} \rho(k_1, k_2, k_{gx}, k_{sx}, \omega) dk_1 dk_2 \tag{1}$$

where

$$\rho(k_1, k_2, k_{gx}, k_{sx}, \omega) = \int_{-\infty}^{\infty} b_1(k_1, k_2, z_1) e^{-i(k_{1z}+k_{2z})z_1} \left[\int_{z_1+\epsilon}^{\infty} b_1(k_{gx}, k_1, z_2) e^{i(k_{gz}+k_{1z})z_2} dz_2 \right] \cdot \left[\int_{z_1+\epsilon}^{\infty} b_1(k_2, k_{sx}, z_2) e^{i(k_{2z}+k_{sz})z_2} dz_2 \right] dz_1 \tag{2}$$

In equations (1) and (2), b_{3IM} is the internal multiple attenuator with dimensions of receiver- and source-side wavenumbers (k_{gx} and k_{sx}) and frequency ω, and b_1 is un-collapsed Stolt (constant wavespeed) migrated data where z_1 is pseudo-depth. We relate pseudo-depth to two way travel time t using constant wavespeed c_0 (usually waterspeed) such that $z_1 = t/(2c_0)$. We define ϵ to be some small positive constant that ensures that b_{3IM} contains only internal multiples, and does not also contain primary events. Finally, we note that the dispersion relation, the central tool of our ensuing analysis, relates the vertical wavenumbers k_{1z}, k_{2z}, k_{gz} and k_{sz} to their horizontal counter-parts. In particular, we have

$$\begin{aligned} k_{1z} &= -\, sgn(\omega) \sqrt{\frac{\omega^2}{c_0^2} - k_1^2} & \qquad k_{2z} &= -\, sgn(\omega) \sqrt{\frac{\omega^2}{c_0^2} - k_2^2} \\ k_{gz} &= -\, sgn(\omega) \sqrt{\frac{\omega^2}{c_0^2} - k_{gx}^2} & \qquad k_{sz} &= -\, sgn(\omega) \sqrt{\frac{\omega^2}{c_0^2} - k_{sx}^2}. \end{aligned} \tag{3}$$

The non-evanescent portion of the wavefield is defined by purely real vertical wavenumbers, and it is this portion of the wavefield that the IMA algorithm uses in its computation. Hence, we define a domain of non-evanescence, and store the corresponding portion of b_1 in the computer's memory. In particular, we see from the dispersion relations that the domain of interest is

$$D = \{(k_{gx}, k_{sx}, k_1, k_2) | -\frac{\omega}{c_0} \leq \{k_{gx}, k_{sx}, k_1, k_2\} \leq \frac{\omega}{c_0}\}$$

and is illustrated in Figure 1. Making note of this domain before reading b_1 from disk allows for the efficient use of the computer's memory.

The second change, improved load balancing, we find by noting that each realization of ρ in equation (2) requires the same amount of computation; hence, we count the number of realizations of ρ, and then divide these realizations evenly amongst the processing units on a many-CPU computer (see Kaplan et al. (2005a) for further details).

3 Free surface multiple algorithm, field data issues

The FSME algorithm presented in Weglein et al. (2003) is

$$D^{fs} = D_1 + D_2 + \cdots \tag{4}$$

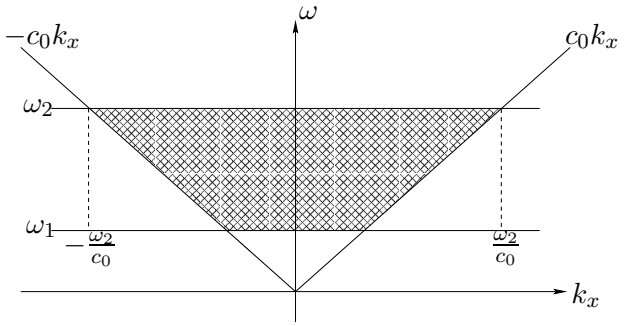

Figure 1: We plot the domain of non-evanescence for the IMA algorithm. We say that ω_1 is the minimum frequency that we compute in b_{3IM} and, likewise, ω_2 is the maximum computed frequency in b_{3IM}.

where in two dimensions,

$$D_n(k_x, z|k_{sx}, z_s; \omega) = \frac{i}{M\pi} \int_{-\infty}^{\infty} k_0' e^{-ik_0'(z+z_s)} D_{n-1}(k_x', z|k_{sx}, z_s; \omega) D_1(k_x, z|k_x', z_s; \omega) dk_x', \quad (5)$$

$k_0' = sgn\sqrt{\omega^2/c_0^2 - k_x'}$, and c_0 is the wavespeed between the measurement surface z and the free surface. M is frequency distribution of the source wavelet.

Unlike the IMA algorithm, FSME is straight-forward to implement in a parallel architecture. This is because the algorithm works frequency-by-frequency, and we make a load balanced implementation by evenly dividing these frequencies amongst the nodes of the computer.

Our 2D implementation of FSME allows for some of the peculiarities of real data. In particular, it lets the distance between consecutive shots differ from the distance between consecutive receivers. Since equation (5) operates in the wave-number domain, we can choose its parameters independently from their real domain counter-parts. In particular, we note that

$$\Delta k_{gx} = \frac{2\pi}{N_g \Delta x_g} \qquad \Delta k_{sx} = \frac{2\pi}{N_s \Delta x_s}$$

where Δx_g is the geophone sampling interval, Δx_s is the shot sampling interval, Δk_{gx} is the geophone wavenumber sampling interval and Δk_{sx} is the shot wavenumber sampling interval. Also, we assume that x_s and x_g are sampled on a square grid, and that N_g and N_s are the number of shots and receivers, respectively, on the grid. An inspection of equation (5) reveals the need for $\Delta k_{sx} = \Delta k_{gx}$. If $\Delta x_s = \Delta x_g$, then this need is easily satisfied by $N_g = N_s$. In the usual case where $\Delta x_s > \Delta x_g$, we write

$$N_g = N_s \left(\frac{\Delta x_s}{\Delta x_g} \right) \quad (6)$$

so that

$$\Delta k_{gx} = \frac{2\pi}{N_g \Delta x_g} = \frac{2\pi}{N_s (\Delta x_s / \Delta x_g) \Delta x_g} = \frac{2\pi}{N_s \Delta x_s} = \Delta k_{sx}.$$

Hence, given a number of shots N_s, we zero-pad the geophone dimension out to a total of N_g samples, according to equation (6).

Of course, the zero-padding governed by equation (6) does not change the Nyquist wavenumbers. For the case of $\Delta x_s > \Delta x_g$, we note that $k_{gn} > k_{sn}$ where k_{gn} and k_{sn} are Nyquist wavenumbers

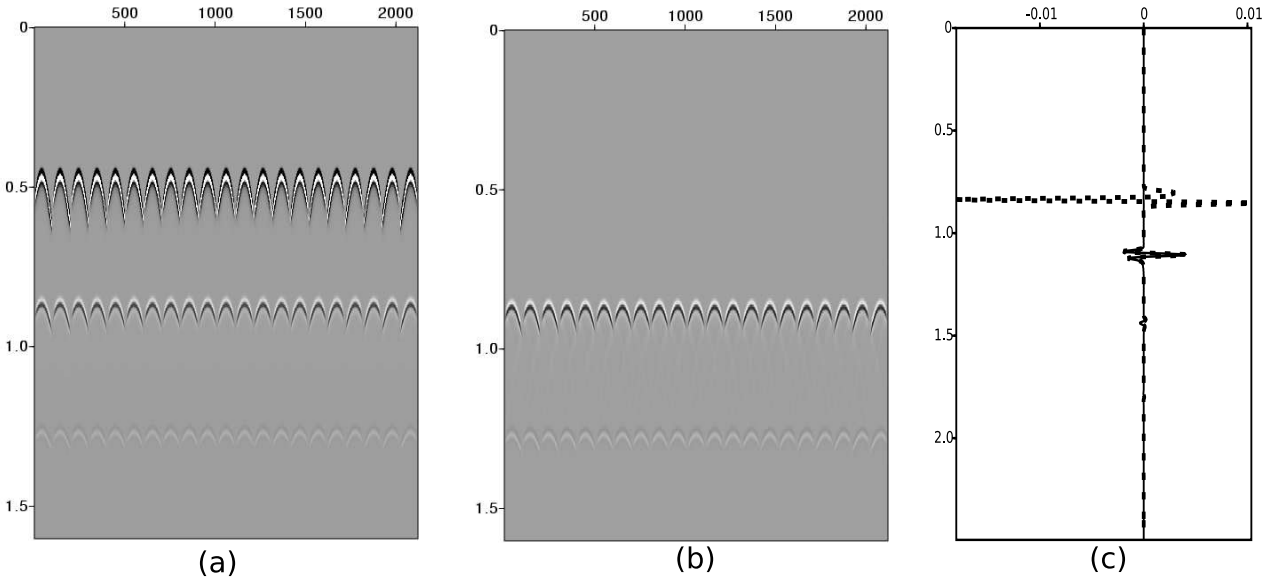

Figure 2: We illustrate the 2D FSME algorithm for data with $\Delta x_s = \Delta x_g = 10m$. From left to right, we plot (a) synthetic data acquired from a 2D survey over a 1D earth with a single reflector; hence, the data contains one primary event and two free surface multiples; (b) the free surface multiple prediction evaluated for the first two terms in equation (4); and, (c) a data trace (thick dashed line) taken from (a) and its corresponding prediction (solid line). Notice that, as expected, we find both amplitude and phase of the first two orders of free surface multiples.

for geophone and shot dimension respectively. Hence, to satisfy the requirements of equation (5), we must truncate $D_1(k_{gx}, k_{sx}, \omega)$ so that $k_{gx} < k_{sn}$. Of course this reduces the information in both wavenumber dimensions to the extent of the Nyquist wavenumber in the shot dimension.

4 Free surface multiple algorithm, synthetic example

In this section, we apply FSME to synthetic data. The data is deghosted (Zhang and Weglein, 2005), has a know source wavelet, and is from a 2D acquisition geometry and a 1D earth model. However, we emphasize that the algorithm is fully 2D. Here, we show examples for both $\Delta x_s = \Delta x_g$ and $\Delta x_s \neq \Delta x_g$.

First, Figure 2 shows our example for $\Delta x_s = \Delta x_g = 10m$. Figure 2a plots the shot gathers and Figure 2b the corresponding second order prediction $D^{fs} = D_2 + D_3$. Figure 2c plots a single trace from the data (thick dashed line), and the corresponding second order prediction (solid line). Notice that with deghosted data and full knowledge of the source wavelet, the algorithm finds both phase and amplitude of the multiple events. Second, Figure 3 shows the same example, but for $\Delta x_s = 20m$ and $\Delta x_g = 10m$.

5 Discussion

In this short note, we briefly summarize updates made to the M-OSRP 2D IMA implementation, and introduce the M-OSRP 2D FSME algorithm. The implementation of the latter is largely

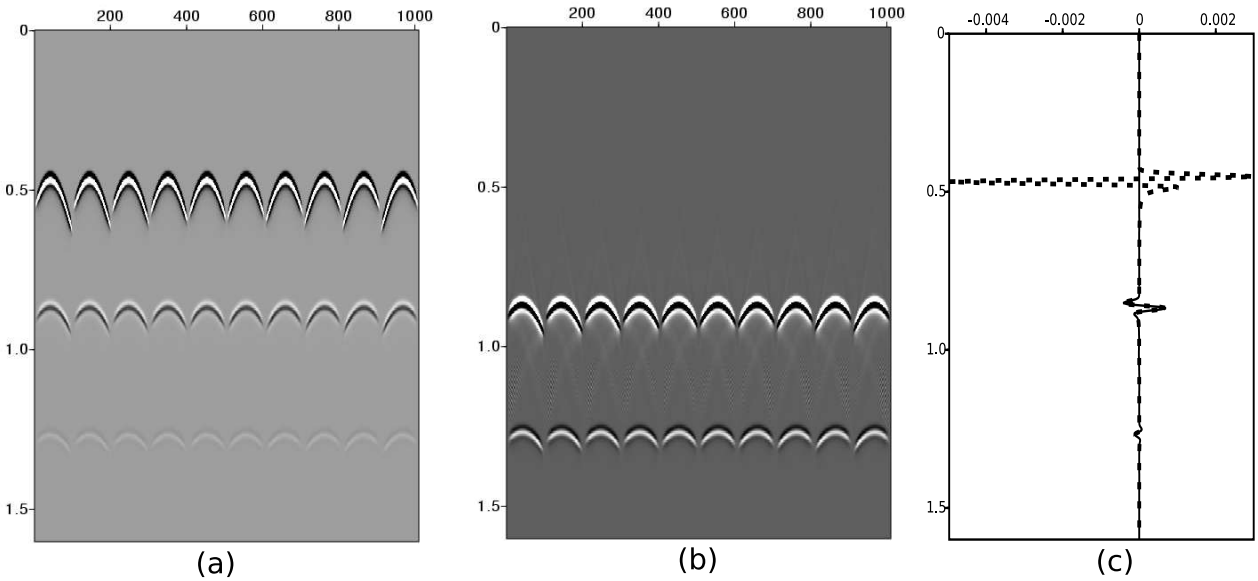

Figure 3: We illustrate the 2D FSME algorithm for data with $\Delta x_s = 20m$ and $\Delta x_g = 10m$. From left to right, we plot (a) synthetic data similar to what is shown in Figure 2; (b) the free surface multiple prediction computed using the first two terms in equation (4); (c) a data trace (thick dashed line) taken from (a) and its corresponding prediction (solid line).

straight-forward; but, here we make note of the case where $\Delta x_s \neq \Delta x_g$, and provide an implemented method for dealing with this situation directly within the algorithm. This is important for field data, and may also be useful in a three dimensional version of the algorithm.

Acknowledgements

We thank the M-OSRP sponsors and personnel for their support. In particular, we acknowledge Jingfeng Zhang and Simon Shaw for providing useful synthetic data sets, and helpful discussions.

References

Sam T. Kaplan and Kristopher A. Innanen. Adaptive subtraction of free surface multiples through order-by-order prediction, matching filters and independent component analysis. In *Mission-Oriented Seismic Research Program (M-OSRP) Annual Report*, 2005.

Sam T. Kaplan, Kristopher A. Innanen, Einar Otnes, and Arthur Weglein. Internal multiple attenuation code-development and implementation. In *Mission-Oriented Seismic Research Program (M-OSRP) Annual Report*, pages 83–102, 2004.

Sam T. Kaplan, Billy Robinson, and Kristopher A. Innanen. Optimizing internal multiple attenuation algorithms for large distributed computing systems. In *Mission-Oriented Seismic Research Program (M-OSRP) Annual Report*, 2005a.

Sam T. Kaplan, J. K. Welford, and Kristopher A. Innanen. A collaborative application of the free-surface multiple elimination code and adaptive subtraction: 2d field data over variable ocean bottom topography. In *Mission-Oriented Seismic Research Program (M-OSRP) Annual Report*, 2005b.

Arthur B. Weglein, Fernanda V. Araújo, Paulo M. Carvalho, Robert H. Stolt, Kenneth H. Matson, Richard T. Coats, Dennis Corrigan, Douglas J. Foster, Simon A. Shaw, and Haiyan Zhang. Inverse scattering series and seismic exploration. *Inverse Problems*, (19):R27–R83, 2003.

Jingfeng Zhang and Arthur B. Weglein. Extinction theorem deghosting method using towed streamer pressure data: Analysis of the receiver array effect on deghosting and subsequent free surface multiple removal. In *SEG/Houston 2005 Annual Meeting*, pages 2095–2100, 2005.

Optimizing internal multiple attenuation algorithms for large distributed computing systems

Sam T. Kaplan, Billy Robinson, Kristopher A. Innanen and Arthur B. Weglein

Abstract

We build a version of the internal multiple attenuation algorithm for large scale distributed computing systems. Given large enough amounts of data, the internal multiple attenuation algorithm is extremely costly, requiring computers that can deliver significant FLOPS (performance). The algorithm is also costly in terms of its memory requirements in that any realization of its output requires a scan over all realizations of its input. Unfortunately, this causes a dilemma, as the computers that offer the greatest performance are typically distributed systems (e.g., IBM BlueGene) that contain many, but limited, memory spaces. Our proposed algorithm takes advantage of the sum total of resources of the distributed system (both processing and memory), while allowing for the memory limitations of its individual components.

1 Introduction

The internal multiple attenuation (IMA) algorithm presented in Weglein et al. (1997) along with the variation shown in Kaplan et al. (2004) estimate seismic events that have experienced at least one downward reflection from a buried reflector in the earth (i.e. internal multiples). The implementation of internal multiple attenuation yields a computationally expensive algorithm. The issues are two-fold. (1) The number of operations required to compute the internal multiple attenuator is large, thus requiring a computer capable of large numbers of floating point operations per second (FLOPS); and (2) any given realization of the attenuator requires a scan over all realizations of input data, thus a successful implementation needs a computer algorithm that has fast access to the entirety of the input data set.

In this paper, we consider the implementation of the IMA algorithm on a distributed computing system. These systems consist of multiple computers (nodes) that communicate data to each other over a network. Each node may have slim resources with respect to to both storage and FLOPS; but, the sum total of resources in the distributed system is what makes it an appealing tool for the IMA algorithm. The IBM BlueGene architecture is one such example of a distributed computer, and one such instance of this architecture is the BlueGene/L computer at the Lawrence Livermore National Laboratory consisting of 65,536 nodes and 33 Tera-bytes of random access memory (512 Mega-bytes per node). To take advantage of a distributed system such as this, the IMA algorithm needs to cope with the limitations of the individual nodes while taking advantage of their abundance. In particular, we need to evenly and efficiently distribute the algorithm's task amongst the multitude of nodes.

To motivate the requirement of developing an IMA algorithm for a large distributed system, we start with an analysis of its computational complexity. Next, we perform an analysis of the IMA equations suitable for our need to divide their task into thousands of sub-tasks. Further, we find that because the algorithm requires multiple scans over input data, the storage and communication of these input data to the individual nodes is a significant burden to the algorithm. We utilize reciprocity to reduce this communication burden, and provide an algorithm that is potentially capable of scaling with the size of the distributed system.

2 The IMA algorithm

In this section, we do not pretend to give a complete explanation of internal multiple attenuation. Rather, we present, for reference, a synopsis of the IMA equations which are used as the basis for our subsequent analysis. We encourage the interested reader to see Weglein et al. (1997, 2003) and Kaplan et al. (2004) for further details.

For two dimensions, the internal multiple attenuator can be written as (Kaplan et al., 2004)

$$b_{3IM}(k_{gx},k_{sx},\omega) = \frac{1}{(2\pi)^2}\int_{-\infty}^{\infty}\int_{\infty}^{\infty}\int_{-\infty}^{\infty} b_1(k_1,k_2,z_1)e^{-i(k_{1z}+k_{2z})z_1} \cdot \left[\int_{z_1+\epsilon}^{\infty} b_1(k_{gx},k_1,z_2)e^{i(k_{gz}+k_{1z})z_2}dz_2\right]\left[\int_{z_1+\epsilon}^{\infty} b_1(k_2,k_{sx},z_2)e^{i(k_{2z}+k_{sz})z_2}dz_2\right]dz_1dk_1dk_2 \quad (1)$$

where b_{3IM} is the internal multiple attenuator with dimensions of receiver- and source-side wave numbers (k_{gx} and k_{sx}) and frequency ω, and b_1 is Stolt (constant wavespeed) migrated data in dimensions of source- and receiver-side wave numbers and pseudo-depth z. We relate pseudo-depth to two way travel time t using a constant wavespeed c_0 (usually waterspeed) such that $z = t/(2c_0)$. Further, we note that k_{1z}, k_{2z}, k_{gz} and k_{sz} are vertical wavenumbers and are related to their horizontal counter-parts through the ubiquitous dispersion relation. In particular, we have

$$k_{1z} = -\,sgn(\omega)\sqrt{\frac{\omega^2}{c_0^2}-k_1^2} \qquad k_{2z} = -\,sgn(\omega)\sqrt{\frac{\omega^2}{c_0^2}-k_2^2}$$
$$k_{gz} = -\,sgn(\omega)\sqrt{\frac{\omega^2}{c_0^2}-k_{gx}^2} \qquad k_{sz} = -\,sgn(\omega)\sqrt{\frac{\omega^2}{c_0^2}-k_{sx}^2}. \quad (2)$$

Lastly, we define ϵ to be some small positive constant that ensures that b_{3IM} contains only internal multiples, and does not also contain primary events.

Our analysis of equation (1) proceeds in two stages. Next, we will analyze its complexity, and then we build an algorithm suitable for large distributed systems.

3 IMA algorithmic complexity

The effort required to make a working IMA algorithm for a large distributed computing system is not trivial. Here, we motivate the need for this work through an analysis of the computational cost of the algorithm. In particular, we find a strategy for counting its number of floating point operations. This serves as a litmus test for both the viability of the algorithm, and for the size of problem (data set) that it can reasonably cope with. We compare the complexity of the algorithm (floating point operations) to a computer's FLOPS (performance) to give an estimate of execution time.

To facilitate the required analysis of the IMA algorithm, we define

$$\begin{aligned} f(k_1,k_2,\omega,z) &= b_1(k_1,k_2,z)e^{-i(k_{1z}+k_{2z})z} \\ g(k_{gx},k_1,\omega,z) &= b_1(k_{gx},k_1,z)e^{i(k_{gz}+k_{1z})z} \\ h(k_2,k_{sx},\omega,z) &= b_1(k_2,k_{sx},z)e^{i(k_{2z}+k_{sz})z} \end{aligned}$$

and

$$\rho(k_1,k_2,k_{gx},k_{sx},\omega)=\int_{-\infty}^{\infty}f(k_1,k_2,\omega,z_1)\left[\int_{z_1+\epsilon}^{\infty}g(k_{gx},k_1,\omega,z_2)dz_2\right]\left[\int_{z_1+\epsilon}^{\infty}h(k_2,k_{sx},\omega,z_2)dz_2\right]dz_1 \tag{3}$$

so that equation (1) becomes

$$b_{3IM}(k_{gx},k_{sx},\omega)=\frac{1}{(2\pi)^2}\int_{-\infty}^{\infty}\int_{-\infty}^{\infty}\rho(k_1,k_2,k_{gx},k_{sx},\omega)dk_1dk_2. \tag{4}$$

The number of floating point operations required to compute any single realization of ρ is constant. Therefore, ρ is a useful construct for our subsequent analysis.

We define

$$\rho_f(N_z,N_\epsilon)=[\rho(k_1,k_2,k_{gx},k_{sx},\omega)]\quad\forall\{k_1,k_2,k_{gx},k_{sx},\omega\}$$

to be the number of floating point operations required to evaluate ρ for any single realization of $\{k_1,k_2,k_{gx},k_{sx},\omega\}$ where N_z is the size of the pseudo-depth dimension in the input data b_1. Also, $N_\epsilon\Delta z=\epsilon$ where Δz is the sampling interval in pseudo-depth. Later, we will present two strategies for evaluating ρ_f. But first, we use it to formulate an expression for the algorithmic expense of the IMA algorithm.

The expression for the internal multiple attenuator in equation (4) is evaluated in the computer using a Riemann sum. However, this mathematical convenience is complicated by the separation of the wavefield into its evanescent and non-evanescent constituents, and in particular by the fact that the IMA algorithm concerns itself with only the non-evanescent portion (the non-evanescent portion being defined by purely real vertical wave numbers). We refer to the dispersion relations in equation (2) to find the domain of interest:

$$D=\{(k_{gx},k_{sx},k_1,k_2)|-\frac{\omega}{c_0}\le\{k_1,k_2,k_{gx},k_{sx}\}\le\frac{\omega}{c_0}\},$$

and compute b_{3IM} by the Riemann sum so that equation (4) becomes

$$\begin{aligned}b_{3IM}(k_k,k_l,\omega_m) &= \frac{1}{2\pi}\sum_{k_i\in D}\sum_{k_j\in D}\rho(k_i,k_j,k_k,k_l,\omega_m)\quad,\quad k_k\in D,k_l\in D\\ &= \frac{1}{2\pi}\sum\sum_{i,j=I_1(m)}^{I_2(m)}\rho(k_i,k_j,k_k,k_l,\omega_m)\quad,\quad k,l\in[I_1(m)\dots I_2(m)]\end{aligned} \tag{5}$$

where

$$I_1(m)=I(-\frac{\omega_m}{c_0})\qquad\qquad I_2(m)=I(\frac{\omega_m}{c_0}) \tag{6}$$

and I is some operator that maps to appropriate indices in the Riemann sum. We count the number of summation operations in equation (5) to find that the total number of floating point operations used to compute b_{3IM} is

$$b_{3IMf}(M_1,M_2,N_z,N_\epsilon)=[b_{3IM}(k_k,k_l,\omega_m)]=\sum_{m=M_1}^{M_2}(I_2(m)-I_1(m))^4\rho_f(N_z,N_\epsilon). \tag{7}$$

where M_1 and M_2 bound the computed temporal frequencies in b_{3IM}; that is, $N_\omega = M_2 - M_1 + 1$ where N_ω is the number of realizations of ω in b_{3IM}. Equation (7) is our desired result except that the value of ρ_f is still unknown. We proceed to evaluate ρ_f using two methods. First, we make a simple count of the number of operations used to compute ρ_f which produces a lower bound ρ_{f1}. Next, we use a computer to evaluate realizations of ρ in order to obtain a second estimate of ρ_f which we call ρ_{f2}. This second estimate should provide more accuracy, and should be corroborated by its lower bound ρ_{f1}.

3.1 Counting floating point operations in ρ

In order to find ρ_{f1}, we evaluate equation (3) using a Riemann sum. First we write,

$$G_i(g(k_{gx}, k_1, \omega, z)) = g_{i+N_\epsilon} + g_{i+1+N_\epsilon} + \cdots + g_{N_z} \quad (8)$$

$$H_i(h(k_2, k_{sx}, \omega, z)) = h_{i+N_\epsilon} + g_{i+1+N_\epsilon} + \cdots + h_{N_z} \quad (9)$$

where $g_i = g(k_{gx}, k_1, \omega, z_i)$, $h_i = h(k_2, k_{sx}, \omega, z_i)$. Then, using equations (8) and (9), and letting $n = N_z - N_\epsilon$, we write the Riemann sum for equation (3):

$$\rho(k_1, k_2, k_{gx}, k_{sx}, \omega) = \sum_{i=1}^{n} f(k_1, k_2, \omega, z_i) G_i(g(k_{gx}, k_1, \omega, z)) H_i(h(k_2, k_{sx}, \omega, z)). \quad (10)$$

To analyze the computational complexity of a single realization of ρ, we perform our analysis in four steps. We find a lower bound on the total number of floating point operations required to evaluate (1) $f(k_1, k_2, \omega, z_i)$, (2) $G_i(g(k_{gx}, k_1, \omega, z))$ and (3) $H_i(h(k_2, k_{sx}, \omega, z))$ for all possible values of i. (4) We use the results from steps (1)-(3) in our analysis of equation (10) to find the total number of floating point operations required to compute a single realization of ρ. In what follows, we assume that additions and multiplications of real numbers count for one floating point operation each. Complex addition costs two floating point operations, complex multiplication six floating point operations, and cosine and sine functions are each equivalent to forty floating point operations.

First, we compute all realizations of f in equation (10) by defining

$$e_n = e^{-i(k_{1z}+k_{2z})z_n} \qquad \Delta e = e^{i(k_{1z}+k_{2z})\Delta z} \quad (11)$$

and using the recursion defined by the equations,

$$f(k_1, k_2, \omega, z_n) = b_1(k_1, k_2, z_n)e_n \qquad e_i = e_{i+1}\Delta e \qquad f(k_1, k_2, \omega, z_i) = b_1(k_1, k_2, z_i)e_i \quad (12)$$

for $i = (n-1), (n-2), \ldots, 1$. A simple and rough analysis of equation (11) reveals one addition, two multiplications, two sine functions and two cosine functions for a total of 163 floating point operations. A rough analysis of equation (12) gives $2n$ complex multiplications for a total of $12n$ floating point operations. Hence, for the computation of f, the total floating point operations is approximately given by

$$f_f = 163 + 12n. \quad (13)$$

Next, we compute all realizations of G in equation (10) by defining e_{N_z} and redefining Δe such that,

$$e_{N_z} = \exp(i(k_{gz} + k_{1z})z_{N_z}) \qquad \Delta e = \exp(-i(k_{gz} + k_{1z})\Delta z) \quad (14)$$

and note the recursive formulation for G_i,

$$G_{N_z} = g_{N_z} = b_1(k_{gx}, k_1, z_{N_z})e_{N_z} \quad e_i = e_{i+1}\Delta e \quad G_i = G_{i+1} + g_i = G_{i+1} + b_1(k_{gx}, k_1, z_i)e_i \quad (15)$$

where $i = (N_z - 1), (N_z - 2), \ldots, N_\epsilon$. A simple and rough analysis of equation (14) reveals, as before, 163 floating point operations. A similar analysis of equation (15) gives $2n$ complex multiplications and n complex additions for a total of $14n$ floating point operations. An equivalent analysis holds for the complexity of H, so that

$$G_f = H_f = 163 + 14n. \quad (16)$$

Finally, we use f_f (equation (13)), G_f and H_f (equation (16)) and equation (10) to find the total number of floating point operations for a single realization of ρ:

$$\rho_{f1} = f_f + G_f + H_f + 14n = 489 + 54n. \quad (17)$$

We emphasize that equation (17) represents a lower bound on the number of floating point operatons required to compute a single realization of ρ. A more studious count of the operations is beyond the scope of this paper. In fact, the next section of our paper uses an alternate method to count floating point operations, and equation (17) is used to validate the ensuing result.

3.2 Measuring floating point operations in ρ

In the previous section, we performed an analysis to find a lower bound on the number of floating point operations required to compute ρ. Further, we noted previously that because ρ has constant computational complexity, it is a useful construct in our broader analysis. Here, we evaluate the computational complexity of ρ using the internal clock of a personal computer. The analysis proceeds in two steps. First, we measure the number of compute cycles required to compute one floating point operation. Then, we find the number of compute cycles required to compute one realization of ρ. Combining this information provides us with the number of floating point operations required to compute ρ.

To find the number of compute cycles required to compute one floating pint operations op_F, we implement the following pseudo-code:

```
start = clock();
for i=1...N, do y = x + x
end = clock();
op_F = (end - start)/N;
```

On a Pentium 4 personal computer, $op_F = 6 \times 10^{-10}$. In a similar fashion, we compute the number of clock cycles required to compute a single realization of $\rho(k_1, k_2, k_{gx}, k_{sx}, \omega)$, op_ρ. Then, the effective number of floating point operations is given by the ratio of these two values. That is, $\rho_{f2} = op_\rho / op_F$. We tabulate the results for various values of N_z and N_ϵ in Table 1.

$N_z - N_\epsilon$ (pseudo-depth samples)	flops (ρ_{f1})	effective flops (ρ_{f2})
146	8,373	12,650
206	11,613	18,800
256	14,313	22,460

Table 1: The number of floating point operations required in the computation of a single realization ρ is a function of the number of samples recorded in pseudo-depth ($n = N_z - N_\epsilon$). The second column is computed using equation (17), and the third column is computed using the internal clock of a personal computer.

3.3 2D example

Using the framework presented in the previous two sections, we find the required floating point operations for a particular two dimensional data set. In particular, we choose a data set with 100 shots, 100 receivers, 1000 pseudo-depth points (n), and 1000 output frequencies in b_{3IM}. We choose a reference wavespeed c_0 of $2000m/s$ and a sampling interval in time of $.001s$. Using these parameters we find $\rho_{f1} \approx 70,000$, and a total of $b_{3IMf} \approx 3 \times 10^{15}$ floating point operations. For comparison, the BlueGene/L computer at the Lawrence Livermore National Laboratory is capable of 50×10^{12} FLOPS. Hence, an efficient implementation of the algorithm should run in around one minute.

It is important to note that because of evanescence (equation (6)), the computational cost increases greatly with increased realizations of output frequencies in b_{3IM}. Thus, at the expense of accuracy, one can always choose a smaller number of output frequencies which in turn gives a much smaller computational cost.

3.4 3D examples

Much of the analysis presented in the previous sections is also applicable to three dimensional data. The only difference is equation (7) which becomes,

$$b_{3IMf}(M_1, M_2, N_z, N_\epsilon) = [b_{3IM}(k_k, k_l, \omega_m)] = \sum_{m=M_1}^{M_2} (I_2(m) - I_1(m))^8 \rho_f(N_z, N_\epsilon). \qquad (18)$$

Once again, this formulation can be used to determine appropriate parameters for a data set given the available FLOPS. The requirements of the 3D algorithm are considerable. Indeed, using parameters similar to the preceding 2D example (with 100 shots/receivers in each dimension), we find approximately 10^{23} required floating point operations. Of course, smaller experiments could achieve reasonable run times; but, it, never-the-less, may prove useful to investigate approaches that constrain the parameters of the three dimensional model.

4 IMA algorithm for distributed systems

The analysis in the previous section should convince the reader of the need for large distributed computing systems when implementing IMA. However, the difficulty of implementing the algorithm

on a distributed system, alluded to in our introduction, is due to the inherent requirements of b_{3IM}. We know that each node on the system has a small amount of memory, and so can only store a small portion of b_1. Further, we know that to execute the algorithm (equation (1)), the various realizations of b_1 must be convolved and correlated with each other. This means that a massive amount of communication between nodes is required. The goal of this section is to formulate the problem to both allow for its solution on a distributed system, and to attempt to minimize the amount of communication required for this solution. To that end, we must (1) find a way to compute something useful with little data, (2) find a way to efficiently communicate these data to the same memory space where the computation can be performed, and (3) efficiently communicate the result of this computation to a location on the distributed system where it can be appropriately used.

We recall our definition of ρ (equation (3)) for $2D$ IMA which allows us to compute a single realization of ρ with access to, at most, three traces. For convenience, we repeat this equation here:

$$\rho(k_1, k_2, k_{gx}, k_{sx}, \omega) = \int_{-\infty}^{\infty} f(k_1, k_2, \omega, z_1) \left[\int_{z_1+\epsilon}^{\infty} g(k_{gx}, k_1, \omega, z_2) dz_2 \right] \left[\int_{z_1+\epsilon}^{\infty} h(k_2, k_{sx}, \omega, z_2) dz_2 \right] dz_1 \tag{19}$$

where f is a function of $b_1(k_1, k_2, z)$, g is a function of $b_1(k_{gx}, k_1, z)$, and h is a function of $b_1(k_2, k_{sx}, z)$. Hence, we see, quite simply, that any single realization of ρ is computed with at most three traces. We choose to design our algorithm around this central idea, setting aside a portion of nodes on the distributed system for the task of computing realizations of ρ. Further, we recall that the computational complexity of any realization of ρ is constant. Thus, it is a simple matter to evenly divide the computation amongst the nodes of the computer. Given that a particular node, then, is required to compute some number of realizations of ρ, we are tasked with sending it the required traces, and collecting, from the node, its computed realization of ρ.

With this in mind, we divide the nodes in the distributed computing system into three groups. (1) We designate a group of nodes (*compute nodes*) responsible for computing some subset of the realizations of ρ. (2) We designate a group of nodes (*data nodes*) for storing the input b_1, and, when needed, sending appropriate portions of its data to the compute nodes. Due to the size of seismic data in both 2D and 3D surveys, it is more than likely that multiple nodes are required to store these data. (3) We designate a group of nodes (*collection nodes*) for storing the output of the algorithm b_{3IM}, for collecting the realizations of ρ from the compute nodes, and for making appropriate summations over the realizations of ρ. Again, given the size of b_{3IM} it is most likely that multiple nodes will be required for storing this information. A schematic of the algorithm is shown in Figure 1, and we proceed to analyze its various components.

4.1 Data nodes

We assign a total of n_d data nodes, and partition $b_1(k_g, k_s, z)$ amongst these nodes so that each one holds a number of geophone gathers. That is, the i^{th} node holds $n_{gd}(i) = N_i(n_g/n_d)$ gathers where n_g is the total number of geophone gathers, and N_i is an operator that deals with the remainder in the division, ensuring that $n_{gd}(i)$ is always an integer value. If this division does have a remainder, then the n_d^{th} data node is tasked with these remaining gathers. We define the i^{th} node's subset of geophone gathers as

$$b_1(i) = b_1(k_g(i), k_s, z) \quad , \quad k_g(i) \in [k_{gd}^1(i), k_{gd}^2(i)] \quad , \quad k_{gd}^1(i+1) = k_{gd}^2(i) + \Delta k_g.$$

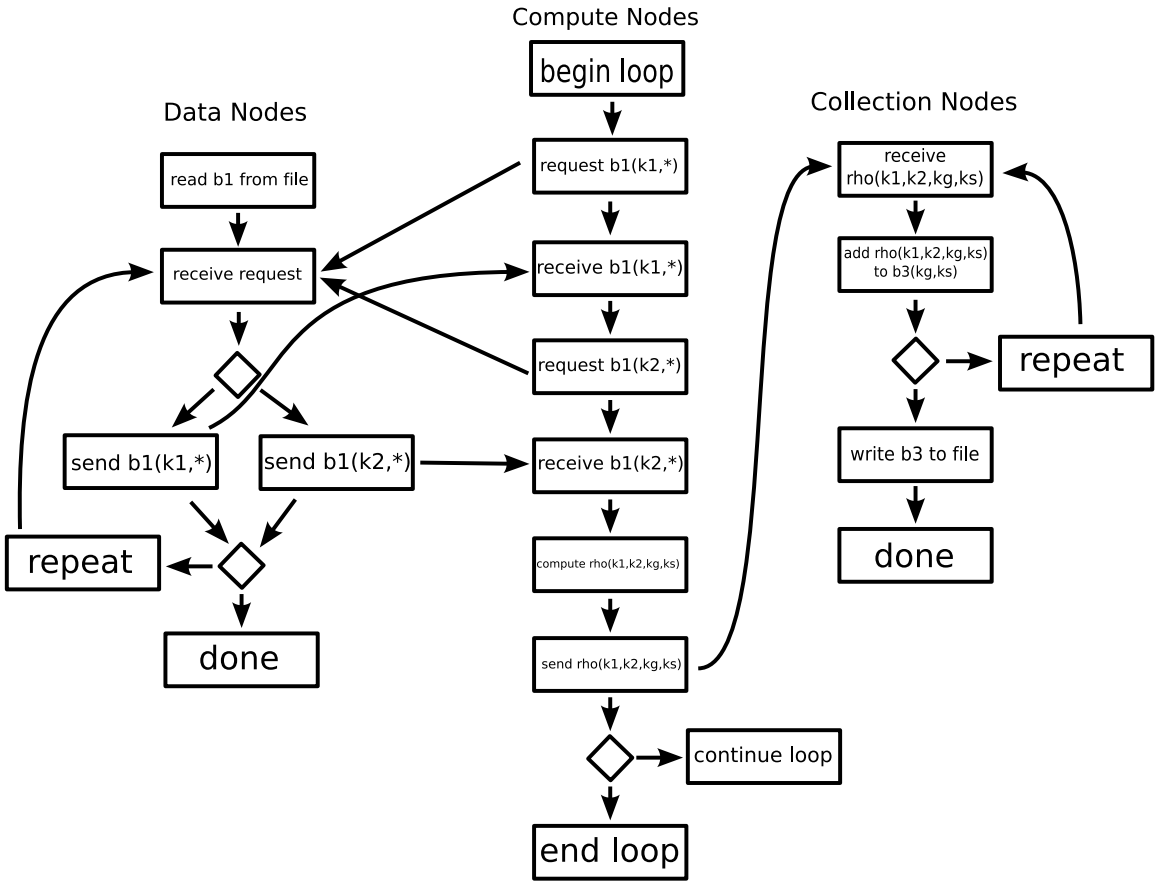

Figure 1: A rough schematic of internal multiple attenuation algorithm designed for a distributed computing system. The algorithm is divided into three parts consisting of data nodes (left side), compute nodes (middle) and collection nodes (right side).

We must choose n_d to be sufficiently large so that there is adequate memory on each data node for storing their subset of geophone gathers.

Aside from storing their assigned geophone gathers, each data node waits to receive a signal from a compute node. This signal will ask for a particular geophone gather which the data node will, then, send across the network of the distributed system to the waiting compute node. The data node will repeat this process until its data is no longer required by any compute nodes. A schematic of the algorithm run on each compute node is shown on the left side of Figure 1.

4.2 Collection nodes

We assign a total of n_c collection nodes, and partition $b_{3IM}(k_g, k_s, \omega)$ amongst these nodes so that each one holds a number of geophone gathers. Like the data nodes, the i^{th} collection node holds $n_{gc}(i) = N_i(n_g/n_c)$ gathers where n_g is the total number of geophone gathers. We define the i^{th} node's subset of geophone gathers as

$$b_{3IM}(i) = b_{3IM}(k_g(i), k_s, \omega) \quad , \quad k_g(i) \in [k^1_{gc}(i), k^2_{gc}(i)] \quad , \quad k^1_{gc}(i+1) = k^2_{gc}(i) + \Delta k_g.$$

In analogy to the data nodes, we must choose n_c large enough so that there is adequate memory on each collection node for holding their subset of geophone gathers.

Aside from storing their assigned portions of b_{3IM}, each collection node waits to receive realizations of ρ from a compute node. Once received, it adds these realizations to its portion of b_{3IM} according to equation (5), waits for the next computed realization of ρ, and repeats this process until all realizations of ρ are accounted for. A schematic of the algorithm run on each collection node is shown on the right side of Figure 1.

4.3 Compute nodes

We make each compute node responsible for an equal number of realizations of ρ. The particular subset that a compute node is responsible for is found by simply counting the total number of realizations of ρ (equation (7)), and dividing this result by the number of compute nodes. The algorithm on any given compute node loops through its assigned realizations of ρ, requesting suitable portions of b_1 from data nodes. A schematic of the algorithm run on each compute node is shown in the middle portion of Figure 1.

Whenever a compute node requests a portion of b_1 from a data node, it must wait for that data to be sent across the network. This can severely hamper the scaling characteristics of the algorithm. That is, the algorithm may slow down due to massive amounts of information (b_1) transmitted across the network. To circumvent this problem, we assume that each compute node has enough memory to hold at least two receiver gathers. This allows us to use reciprocity to minimize the data transfer of b_1 across the network. In particular, we note that reciprocity gives the relation

$$b_1(k_1, k_2, z) = b_1^*(k_2, k_1, z)$$

where $*$ denotes the complex conjugate. Hence, storing, on the compute node, a geophone gather $b_1(k_1, k_2, z)$ (i.e., a single realization of the geophone wavenumber k_1 and all realizations of the shot

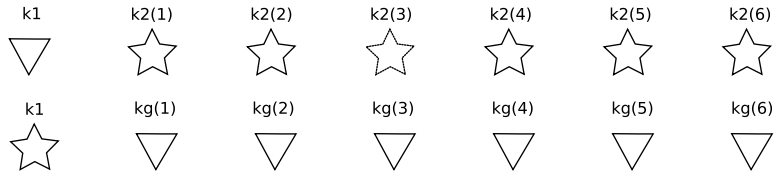

Figure 2: A schematic of reciprocity which we use to illustrate a component of the compute nodes' algorithms. The top row illustrates a geophone gather with geophone wavenumber $k1$ and shot wavenumbers $k2(1)$, $k2(2)$, etc. The bottom row illustrates the equivalent information stored in a shot gather with shot wavenumber k_1, and geophone wavenumbers $kg(1) = k2(1)$, $kg(2) = k2(2)$, etc.

wavenumber k_2), gives immediate knowledge of the shot gather $b_1(k_g, k_1, z)$ (i.e., a single realization of the shot wavenumber k_1 and all realizations of the geophone wavenumber k_g). Figure 2 shows a simple schematic of this idea.

Due to this reciprocal relation, we are, despite the third order nature of the algorithm, able to collect only two geophone gathers from the data nodes, to effect knowledge of (1) $b_1(k_1, k_2, z)$, (2) $b_1(k_g, k_1, z)$ and (3) $b_1(k_2, k_s, z)$ for one realization of k_1, and all k_2 and k_g in (1) and (2); and for one realization of k_2, and all realizations of k_s in (3). Once a compute node has this information, it can compute its corresponding realizations of ρ, and send them to the appropriate collection nodes. It may be the case that the required data are already on the compute node. In this case, the request to the data node is skipped. Moreover, if computer memory is available, we allow compute nodes to hold many receiver gathers. This allows the algorithm to operate efficiently on a wide range of hardware.

5 BlueGene/L experiments

We test our implementation of the 2D IMA algorithm using up to, and including, 1024 central processing units (nodes) on an IBM BlueGene/L machine with each node addressing 256 Mega-bytes of random access memory *. Here, we show three experiments to illustrate the algorithms scaling characteristics on distributed computing systems. In all three experiments, the 2D input $b_1(k_{gx}, k_{sx}, z_1)$ to the algorithm is built from 81 shots each with 81 geophones. Each trace has 300 samples in pseudo-depth. The original $t - x$ data is generated using a finite-difference algorithm.

The experiments are summarized in Tables 2 through 4. In each of these three experiments, we compute several instances of the same b_{3IM} where in each subsequent execution of the program, we increase the number of compute nodes. Ideally, the run-time of the program should be inversely proportional to the number of compute nodes. To see whether or not this is true, we use ratios of run-times, labelled *normalized run time* in Tables 2 through 4. For example, experiment 1a in Table 2 computes $b_{3IM}(k_{gx}, k_{sx}, \omega)$ for 60 realizations of ω, and uses 3 data nodes, 3 collection nodes and 1 compute node. Meanwhile, experiment 1b computes the same portion of b_{3IM}, but with 8 compute nodes. The normalized run time for experiment 1b is the ratio of the run time for

*In actuality, The BlueGene machine that we use has two central processing units on each node, and a total of 512 Mega-bytes of memory per node. However, each processor has access to only half of that memory. For our purposes, we refer to each of these single-processor/single-memory units as nodes, even though they are physically grouped in pairs.

experiment 1a to that of experiment 1b. Likewise, for experiment 1c, the normalized run time is the ratio of the run time for experiment 1a to that of experiment 1c, and so on. Therefore, ideal scaling of the IMA algorithm is evidenced by a one-to-one relation between the number of compute nodes and the normalized run time. The results of the first experiment, shown in Table 2, illustrate an ideal (linear) scaling of the algorithm for up to 64 compute nodes.

The second experiment, summarized by Table 3, computes $b_{3IM}(k_{gx}, k_{sx}, \omega)$ for 120 realizations of ω. Like experiment 1, we use 3 data nodes and 3 collection nodes. We note that using 512 compute nodes in experiment 2c gives a normalized run time of 453.2, and shows a slight degradation in performance. Running the algorithm with 1024 compute nodes in experiment 2d gives a normalized run time of 405.4 which, without doubt, confirms the problem. However, experiment 3 in Table 4 shows that this scalability degradation has a simple remedy.

The reason for the poor scaling result illustrated by experiment 2 is due to the relation between the many compute nodes (1024) and the few collection nodes (3). Due to the BlueGene architecture, after a compute node sends its computed realizations of ρ to the collection node, it must wait for confirmation that the collection node has, in fact, received these same realizations. If many compute nodes are sending realizations of ρ to few collection nodes, then we observe compute nodes spending a significant amount of time waiting for their confirmation. We test a solution to this problem in experiment 3 where we increase the number of collection nodes from 3 to 8, thereby reducing the workload for each individual collection node, and reducing the confirmation time for the compute nodes. The results of our third experiment are detailed in Table 4, where a quick comparison of the normalized run time and the number of compute nodes reveals, as expected, much improved scaling of the algorithm.

6 Discussion

The internal multiple attenuation algorithm yields a computationally expensive algorithm. In this paper, we quantify the cost of the two and three dimensional forms of the algorithm, motivating the need for its implementation on large distributed computing systems. With this motivation firmly in place, we explained our 2D implementation which uses the immense cumulative resources of a distributed computer while allowing for its particular local limitations. Namely, its lack of memory per node.

While the discussion in this paper surrounds a 2D algorithm, many of the ideas should be easily extended to three dimensions. That is, we think of the 2D version of the algorithm as both a useful entity in itself, and as a precursor to its 3D counter-part. The basic premises of the 2D algorithm, and in particular the use of ρ, remain applicable in three dimensions, and the success that we see in our 2D distributed systems implementation of the algorithm should translate to an analogous 3D algorithm.

Acknowledgements

We thank M-OSRP sponsors and personnel for their continued support. In particular, we acknowledge Einar Otnes for many interesting discussions, and IBM for the ongoing use of a BlueGene/L

machine. Some of the authors have been supported by and express their gratitude to NSF-CMG award DMS-0327778 and DOE Basic Sciences award DE-FG02-05ER15697.

References

Sam T. Kaplan, Kristopher A. Innanen, Einar Otnes, and Arthur Weglein. Internal multiple attenuation code-development and implementation. In *Mission-Oriented Seismic Research Program (M-OSRP) Annual Report*, pages 83–102, 2004.

Arthur B. Weglein, Fernanda V. Araújo, Paulo M. Carvalho, Robert H. Stolt, Kenneth H. Matson, Richard T. Coats, Dennis Corrigan, Douglas J. Foster, Simon A. Shaw, and Haiyan Zhang. Inverse scattering series and seismic exploration. *Inverse Problems*, (19):R27–R83, 2003.

Arthur B. Weglein, Fernanda Araújo Gasparotto, Paulo M. Carvalho, and Robert H. Stolt. An inverse-scattering series method for attenuating multiples in seismic reflection data. *Geophysics*, 62(6):1975–1989, November-December 1997.

	data nodes	collection nodes	compute nodes	run time (sec)	norm. run time
exp. 1a	3	3	1	887.9	1
exp. 1b	3	3	8	111.9	8.0
exp. 1c	3	3	32	28.1	31.6
exp. 1d	3	3	64	14.2	62.6

Table 2: We run experiments on an IBM BlueGene/L machine to compute 64 output frequencies in b_{3IM}. In each subsequent experiment, we increase the number of compute nodes, up to a total of 64. The final column (normalized run time) provides a metric of the algorithm's success, and is the ratio of its compute time to the compute time of experiment 1a. Perfect scaling would show a one-to-one relation between the number of compute nodes and the normalized run time.

	data nodes	collection nodes	compute nodes	run time (sec)	norm. run time
exp. 2a	3	3	8	3404.0	8.0
exp. 2b	3	3	64	429.6	63.4
exp. 2c	3	3	512	60.1	453.2
exp. 2d	3	3	1018	67.2	405.4

Table 3: We run a second set of experiments similar to Table 2, except with 120 output frequencies in b_{3IM}, and a maximum of 1018 compute nodes. Notice that the normalized run time indicates poor scaling for 512 and more compute nodes. The results in Table 4 address this problem.

	data nodes	collection nodes	compute nodes	run time (sec)	norm. run time
exp. 3a	8	8	256	9039.2	256.0
exp. 3b	8	8	512	4756.5	497.6
exp. 3c	8	8	1008	2436.5	971.4

Table 4: We run a third set of experiments similar to Tables 2 and 3, except with 512 output frequencies in b_{3IM} and maximum of 1008 compute nodes. Notice that compared to Table 3, we have increased the number of collection nodes, from 3 to 8. This change addresses the scaling issue shown in Table 3, as the normalized run time indicates good scaling of the algorithm.

Adaptive subtraction of free surface multiples through order-by-order prediction, matching filters and independent component analysis

Sam T. Kaplan and Kristopher A. Innanen

Abstract

We present a three stage algorithm for adaptive subtraction of free surface multiples, a processing step made necessary in the free-surface multiple elimination method, for example, by the absence of any of its deterministic prerequisites (knowledge of source wavelet, deghosted data, etc.). First, we construct multiple orders from the free surface multiple prediction formula. Each order contains unique information about the data. Second, we use the full recording duration of any given data trace to construct filters that attempt to match the data and the multiple predictions. This filter produces good phase results, but because of the order by order nature of the free surface algorithm, results that are still insufficient for straightforward subtraction. Instead, third, we construct, trace-by-trace, a mixing model where the mixtures are the data trace and its orders of multiple predictions. Corresponding to the mixtures, there are sources and a mixing process, both of which we find through a blind source separation technique, in particular by employing independent component analysis. One of the recovered sources is the desired signal. That is, it is the data without free surface multiples. This side-steps the subtraction inherent to most adaptive subtraction methods, and instead separates the desired signal from the free surface multiples.

1 Introduction

Given certain prerequisites, the free surface multiple elimination (FSME) algorithm presented in Weglein et al. (1997, 2003) provides a perfect prediction of all orders of free surface multiples. The prerequisites for the algorithm are data without ghosts, and knowledge of the source wavelet. While both of these requirements have published methods, their current applicability to real data is still under development. For example, algorithms that estimate the source wavelet require either regularization (Guo et al., 2003), or specific acquisition geometries (Weglein and Secrest, 1990). Additional factors contributing to errors in the prediction may include 2D algorithms applied to data with 3D effects, errors in the source and receiver depths, etc. (Abma et al., 2005). Adaptive subtraction is a statistical technique used to compensate for these errors.

In this paper, we propose an adaptive subtraction algorithm that we exercise on input from the free surface multiple prediction presented in Weglein et al. (1997, 2003), but our algorithm is made in the absence of deghosting and/or wavelet estimation. The algorithm proceeds in three stages. 1) We compute several orders of the free surface multiple prediction while ignoring the algorithm's rigorous requirements for deghosting and source wavelet knowledge. 2) For each trace, a matching filter is computed and applied to both data and free surface multiple predictions. This filter partially compensates for our already mentioned lack of rigour in the application of the free surface multiple algorithm. 3) We use the filtered data and multiple estimates to set up and solve a blind source separation problem (BSS). The source components of the BSS problem are computed

using independent component analysis (ICA), and are the separated orders of free surface multiples and the desired separated primaries.

The BSS approach avoids the problem of matching noise to signal by replacing the subtraction step with a separation step. Another attempt to treat the problem with separation rather than subtraction is presented in Lu and Mao (2005) who use a geometric ICA algorithm, a parametrized model (amplitude and phase-shift), and windowed sections of the data. In this paper, we drop these assumptions/requirements in favour of more information (multiple orders of free surface multiple predictions).

We readily (and eagerly) admit that ideally the processing of seismic data would require no adaptive subtraction step. That is, the physics of the wave equation should ultimately produce algorithms that meet all of the requirements for the prediction and straight forward subtraction of free surface multiples. In the mean time for our imperfect world, we accept the need for practical and interesting statistical methods.

2 Free surface multiple algorithm

The goal of this paper is, of course, to remove free surface events from seismic data. The method that we use employs both physics and information theory. In this section, we concern ourselves with the former through the application of the FSME algorithm. Our partial application of the FSME algorithm results in several orders of predictions of free surface multiples. While it is not immediately obvious why all of these orders of predictions should be computed, we assure the reader that it is exactly this abundance of information that we later take advantage of in our BSS/ICA formulation.

The FSME algorithm of Weglein et al. (1997, 2003) stems from an analysis of the wave equation which in two dimensions is

$$\mathcal{L}[G_0(x,z|x_s,z_s;\omega)] = \left(\frac{\partial^2}{\partial x^2}+\frac{\partial^2}{\partial z^2}+\frac{\omega^2}{c_0^2}\right) G_0(x,z|x_s,z_s;\omega) = M\delta(x-x_s)\left[\delta(z-z_s)-\delta(z+z_s)\right] \tag{1}$$

where M is the time distribution of the source, and $\delta(x-x_s)\delta(z-z_s)$ and $\delta(x-x_s)\delta(z+z_s)$ model a point source and the free surface respectively. The solution G_0 is valid for an acoustic half-space with wavespeed c_0. We find a solution $\psi(x,z,t)$ valid in an arbitrary medium through scattering theory. In particular, the forward scattering series is

$$\psi_s = G_0VG_0 + G_0VG_0VG_0 + G_0VG_0VG_0VG_0 + \cdots \tag{2}$$

where $\psi_s = \psi - G_0$ is the scattered wavefield in a medium defined by the reference wavespeed c_0 and an arbitrary model perturbation (scattering potential) represented by $V(x,z)$. Meanwhile, the inverse series is written as

$$V = V_1 + V_2 + V_3 + \cdots \quad . \tag{3}$$

where V_n is n^{th} order in the data. Substituting (3) into (2) gives

$$\begin{aligned} \psi_s &= (G_0V_1G_0) + [G_0V_2G_0 + G_0V_1G_0V_1G_0 + G_0V_3G_0 + G_0V_2G_0V_1G_0 \\ &\quad + G_0V_1G_0V_2G_0 + G_0V_1G_0V_1G_0V_1G_0 + \cdots] \\ &= (G_0V_1G_0) + \phi \end{aligned} \tag{4}$$

where $\phi = 0$, and by equating like orders in equation (4), we see that

$$\begin{aligned} 0 &= G_0V_2G_0 + G_0V_1G_0V_1G_0 \quad (5)\\ 0 &= G_0V_3G_0 + G_0V_2G_0V_1G_0 + G_0V_1G_0V_2G_0 + G_0V_1G_0V_1G_0V_1G_0 \quad (6)\\ &\cdots \quad . \end{aligned}$$

To build the free surface multiple elimination algorithm, we define G_0^d and G_0^{fs} such that $G_0 = G_0^d + G_0^{fs}$, $\mathcal{L}[G_0^d] = M\delta(x - x_s)\delta(z - z_s)$, and $\mathcal{L}[G_0^{fs}] = -M\delta(x - x_s)\delta(z + z_s)$. Next, we define V_n^{fs} in terms of ψ_s^{fs} and G_0^d to build the desired portion of equation (4),

$$\psi_s^{fs} = G_0^dV_2^{fs}G_0^d + G_0^dV_3^{fs}G_0^d + \cdots \quad . \quad (7)$$

Each term in equation (7) is recursively built from its preceding term using the properties of the scattering series illustrated in equations (5) and (6). In particular, we have for the second order terms (equation (5)),

$$(G_0^d + G_0^{fs})V_2(G_0^d + G_0^{fs}) = -(G_0^d + G_0^{fs})V_1G_0V_1(G_0^d + G_0^{fs}) \quad (8)$$

Left and right multiplying equation (8) by $(G_0^d + G_0^{fs})^{-1}$ and G_0^d gives

$$G_0^dV_2^dG_0^d + G_0^dV_2^{fs}G_0^d = -G_0^dV_1G_0^dV_1G_0^d - G_0^dV_1G_0^{fs}V_1G_0^d \quad (9)$$

where, we note that

$$G_0^dV_2^{fs}G_0^d = -G_0^dV_1G_0^{fs}V_1G_0^d \quad (10)$$

is the first term in equation (7). All subsequent terms in equation (7) are computed recursively from the preceding terms. For example, we consider the second term in equation (7) which is found through due consideration of the third order terms in the inverse scattering series (equation (6)). In particular, we have

$$\begin{aligned} G_0V_3G_0 &= -G_0V_2G_0V_1G_0 - G_0V_1G_0V_2G_0 - G_0V_1G_0V_1G_0V_1G_0\\ &= -G_0V_2G_0V_1G_0 - G_0V_1G_0V_2G_0 + G_0V_2G_0V_1G_0\\ &= -G_0V_1G_0V_2G_0. \end{aligned}$$

Using a simple analogy to our derivation of equation (10), it can be shown that

$$G_0^dV_3^{fs}G_0^d = -G_0^dV_1G_0^{fs}V_2^{fs}G_0^d$$

is the second term in equation (7), and in general the n^{th} term is

$$G_0^dV_n^{fs}G_0^d = -G_0^dV_1G_0^{fs}V_{n-1}^{fs}G_0^d. \quad (11)$$

For convenience, we define $D_1 = \psi_s = G_0^dV_1G_0^d$ and $D_n = G_0^dV_n^{fs}G_0^d$, $n = 2, 3, \ldots$ where D_1 is the de-ghosted seismic data. Following substitution of the appropriate Green's functions and some algebra, we find (Weglein et al., 1997, 2003)

$$D_n(k_x, z|k_{sx}, z_s; \omega) = \frac{i}{M\pi}\int_{-\infty}^{\infty} k_0' e^{-ik_0'(z+z_s)} D_{n-1}(k_x', z|k_{sx}, z_s; \omega)D_1(k_x, z|k_x', z_s; \omega)dk_x' \quad (12)$$

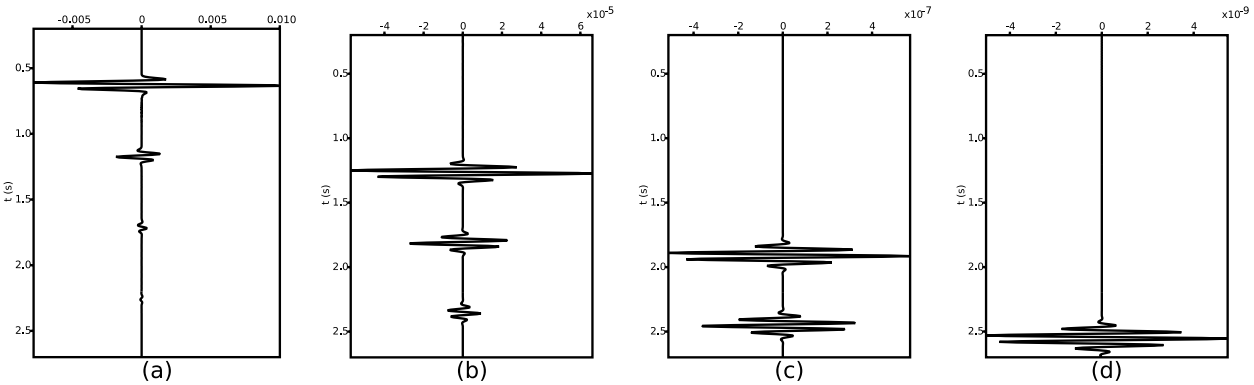

Figure 1: We use a finite difference algorithm to generated a single shot gather for an acoustic and 1D earth model consisting of a single reflector at a depth of $400m$. We place both the source and receivers at a depth of $10m$. Figure (a) plots the zero offset trace of the shot gather. (b)-(d) plot our estimates of D_2 through D_4, and are computed with $M = 1$ in equation (12) and without removing the ghost from the data so that we are using an approximation to D_1.

(more details can be found in Appendix A) where equation (7) becomes

$$\psi_s^{fs} = D_2 + D_3 + \cdots \tag{13}$$

and is the free surface multiple predictor.

To illustrate the properties of each D_n in equation (13), we consider the example in Figure 1. We use a finite difference algorithm to generate a single shot gather from a 1D earth model consisting of a single reflector at a depth of $400m$. Hence, the data contains one primary event and several orders of free surface multiples. Both the source and receivers are placed at a depth of $10m$, and we do not perform any deghosting step. Figure 1a shows the shot gather's zero-offset trace. Figures 1b-d show D_n for $n = 2, 3, 4$ and are computed with $M = 1$ in equation (12). Because of our neglect of the wavelet and ghosts, each subsequent D_n is altered by convolution with an effective wavelet that precludes the direct subtraction of $D_2 + D_3 + D_4$ from the data D_1.

3 Matching filter

The FSME algorithm has created series terms D_n that, with all prerequisites supplied, are ready for subtraction from the data. In the absence of some or all prerequisites, a situation assumed in this paper, we instead treat these D_n as linear mixtures of primaries and free surface multiples, to be separated via ICA. However, the raw FSME output is not yet ready to be considered in such a linear mixture; it requires a preprocessing step, in the form of a matching filter, to be applied to all but one D_n. Once the filters are suitably applied to all but the highest order of free surface multiple prediction, we have data appropriate for the BSS/ICA step of the algorithm.

We proceed using matrix analysis, and say that the vector $\mathbf{d}_n$ is a single trace of D_n and match $\mathbf{d}_n$ to $\mathbf{d}_{n+1}$ using a smallest energy criteria. In particular, we construct a convolution matrix $\mathbf{H}_n$ from $\mathbf{d}_n$, and find the matching filter,

$$\mathbf{m}^* = arg\,\underset{\mathbf{m}}{min}\left[\frac{1}{2\sigma_n^2}||\mathbf{d}_{n+1} - \mathbf{H}_n\mathbf{L}\mathbf{m}||_2^2 + \frac{1}{2\sigma_m^2}||\mathbf{m}||_2^2\right], \tag{14}$$

where σ_n and σ_m are the standard deviations of the noise and matching filter respectively, and $\mathbf{L}$ is a zero-padding operator which allows us to choose the length of the matching filter. In general, the matching filter should be at least as long as the recording duration of a single event in the data. After some calculus, we find that equation (14) evaluates to

$$\mathbf{m}^* = \left(\mathbf{L}^T\mathbf{H}_n^T\mathbf{H}_n\mathbf{L} + \frac{\sigma_n^2}{\sigma_m^2}\mathbf{I}\right)^{-1}\mathbf{L}^T\mathbf{H}_n^T\mathbf{d}_{n+1}, \tag{15}$$

where $\mathbf{I}$ is the identity matrix.

It is important to note the direction in which the matching filter is computed and applied. For example, we apply the filter to $\mathbf{d}_1$ in an attempt to match $\mathbf{d}_2$:

$$\mathbf{m}^* = \left(\mathbf{L}^T\mathbf{H}_1^T\mathbf{H}_1\mathbf{L} + \frac{\sigma_n^2}{\sigma_m^2}\mathbf{I}\right)^{-1}\mathbf{L}^T\mathbf{H}_1^T\mathbf{d}_2,$$

rather than applying it to $\mathbf{d}_2$ to try to match $\mathbf{d}_1$:

$$\mathbf{m}^* = \left(\mathbf{L}^T\mathbf{H}_2^T\mathbf{H}_2\mathbf{L} + \frac{\sigma_n^2}{\sigma_m^2}\mathbf{I}\right)^{-1}\mathbf{L}^T\mathbf{H}_2^T\mathbf{d}_1.$$

The order matters because of the obvious need for a well posed inverse in equation (15), and the order determines what information goes into the matrix to be inverted. For illustration, we again consider the data from Figure 1a which is also plotted in Figure 2a. First, we compute the filter by matching the data $\mathbf{d}_1$ to the first order prediction $\mathbf{d}_2$. The resulting filter is shown in Figure 2e, and the result of applying the filter to $\mathbf{d}_1$ is plotted in Figure 2c. Figure 2f shows the filter found by matching the first order prediction $\mathbf{d}_2$ to the data $\mathbf{d}_1$, and Figure 2d shows the application of the filter to $\mathbf{d}_2$. The reason for the ill-favoured results in Figures 2d and 2f are most readily understood in the frequency domain. Figures 2g and 2h plot the amplitude spectra of $\mathbf{d}_1$ and $\mathbf{d}_2$ respectively. Due to the convolution in the prediction algorithm (equation (12)), $\mathbf{d}_1$ has a larger cut-off frequency than $\mathbf{d}_2$, hence the spectral division of $\mathbf{d}_2$ by $\mathbf{d}_1$ is well-posed, whereas the spectral division of $\mathbf{d}_1$ by $\mathbf{d}_2$ is ill-posed. Since the inversion in equation (15) is the time domain equivalent of this spectral division, the choice of order is clear.

The matching filter $\mathbf{m}^*$, or its real analysis counter-part $m^*(t)$, does not prepare the predictions for direct subtraction, rather it can be shown that

$$\begin{aligned} m^* * D_1 &= (m^* * P) + (m^* * M_1) + \cdots + (m^* * M_{n-1}) \\ D_2 &= c_2(m^* * M_1) + c_3(m^* * M_2) + \cdots + c_n(m^* * M_{n-1}) \end{aligned}$$

where P are the primary events in the data, M_i are the i^{th} order free surface multiples, and $c_i \neq 1$ for $i = \{2, n\}$. The reasons for this are two-fold. First, the cost function is effected by the primary event in D_1 which is non-existence in D_2; second, the multiple prediction algorithm introduces unique error factors into each order of free surface multiple. The existence of these non-unity factors is why a direct subtraction is impossible. One solution to this problem is the application of a short filter in a moving window where each window is assumed to contain only one order of free surface multiple. The development of the BSS/ICA formulation is aimed at side-stepping the one major pitfall of this windowed approach, which is its tendency to transform data noise into

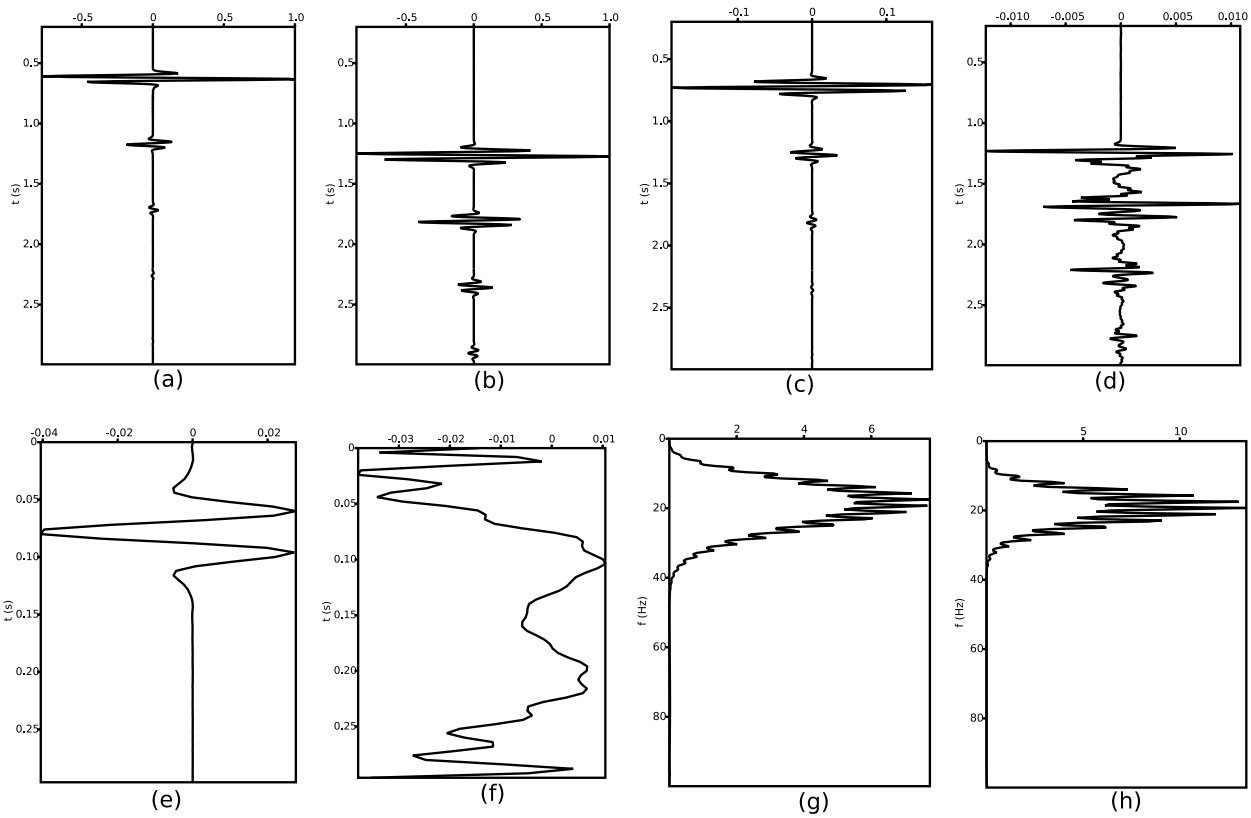

Figure 2: We illustrate the importance of order when building the matching filter (equation (15)). Figure (a) is a single data trace $\mathbf{d}_1$, and (b) is the corresponding first order free surface prediction $\mathbf{d}_2$. Figures (g) and (h) are, respectively, the amplitude spectra of $\mathbf{d}_1$ and $\mathbf{d}_2$ (notice the broader spectrum of $\mathbf{d}_1$). Figure (e) is the filter built to match $\mathbf{d}_1$ to $\mathbf{d}_2$. The application of the filter is in (c), and gives the desired result. Meanwhile, (f) is the filter built to match $\mathbf{d}_2$ to $\mathbf{d}_1$. The application of the filter to $\mathbf{d}_2$ is in (d), and not surprisingly yields a poor result.

signal, damaging primaries. We also note the application of m^* to the desired signal P, and the subsequent need to deconvolve its effect which will be done in the next section.

In this section, we have explicitly shown the construction of a matching filter which is applied to D_1 to match D_2. This can be extended so that, in general, D_i is matched to D_j where $j > i$. Anon, we use this idea to formulate the adaptive subtraction problem in the context of BSS/ICA.

4 BSS and ICA for free surface predictions

Independent component analysis is a technique for performing blind source separation (e.g., Hyvärinen et al., 2001). It considers a model in which sources are combined to produce mixtures, and uses concepts from information theory to simultaneously find both the sources and the process by which the sources are mixed. It turns out that, after application of the matching filters, the data and free surface predictions can be thought of as the mixtures in this mixing model. The sources in the mixing model are the individual orders of free surface multiples and the primaries. For our purpose, we are able to assume a linear mixing model with equal numbers of sources and mixtures. Indeed,

the goal of this section is to set up an appropriate mixing model which is solved by ICA, and then to isolate the portion of the ICA solution that corresponds to the primary events in the data. That is, rather than performing a subtraction to remove the free surface multiples, we perform a separation to extract the desired signal.

As mentioned, we formulate our ICA model by assuming a linear combination of n sources, producing n mixtures. This, obviously, means that we need to consider a linear system with n equations. In particular, we have

$$\begin{aligned} x_1(t) &= c_{11}s_1(t) + c_{12}s_2(t) + \cdots c_{1n}s_n(t) \quad (16)\\ x_2(t) &= c_{21}s_1(t) + c_{22}s_2(t) + \cdots c_{2n}s_n(t) \\ &\cdots \\ x_n(t) &= c_{n1}s_1(t) + c_{n2}s_2(t) + \cdots c_{nn}s_n(t) \quad (17) \end{aligned}$$

where $x_i(t)$ are mixtures and $s_i(t)$ are sources. For parsimony, we can write equations (16)-(17) in their matrix-vector form so that

$$\mathbf{x}(t) = \mathbf{A}\mathbf{s}(t)$$

where $\mathbf{x}^T(t) = [\ x_1(t) \quad x_2(t) \quad \cdots \quad x_n(t)\ ]$ and $\mathbf{s}^T(t) = [\ s_1(t) \quad s_2(t) \quad \cdots \quad s_n(t)\ ]$ are random vectors, and

$$\mathbf{A} = \begin{bmatrix} c_{11} & c_{12} & \cdots & c_{nn} \\ c_{21} & c_{22} & \cdots & c_{2n} \\ \cdots & & & \\ c_{n1} & c_{n2} & \cdots & c_{nn} \end{bmatrix}$$

is called the mixing matrix. The goal of ICA is to, given the mixtures $\mathbf{x}(t)$, find a matrix $\mathbf{B}$ such that $\mathbf{y}(t) = \mathbf{B}\mathbf{x}(t)$ and $\mathbf{y}(t) = \mathbf{P}\mathbf{s}(t)$ where $\mathbf{P}$ is a linear operator that is allowed to swap and scale the elements of $\mathbf{s}(t)$. When the elements of $\mathbf{y}(t)$ satisfy this relation, they are called independent components. That is, independent components are scaled and permuted versions of the sources. In effect, this means that ICA finds two unknowns in one equation.

We will not explain the full details of the ICA theory in this paper. The interested reader is referred to Hyvärinen et al. (2001) and Kaplan (2003) for more information. In short, the ICA algorithm works by using the statistics of the random vector $\mathbf{y}(t)$, and the ubiquitous central limit theorem which allows us to say that the components of $\mathbf{y}(t)$ are independent components exactly when they are maximally non-Gaussian. In general, one can use an estimate of negentropy to quantify Gaussianity. For the purpose of this paper, we use the Gram-Charlier expansion for this estimate (e.g., Kendall and Stuart, 1977).

To make appropriate use of ICA, we must first coax our adaptive subtraction problem into the discussed mixing matrix form. To do this, we use the matching filters that we constructed in the previous section. As before, we let P be the primary events in D_1 (with or without ghosts), and M_i be the i^{th} order free surface multiple, and write

$$\begin{aligned} m_1 * D_1 &= (m_1 * P) + (m_1 * M_1) + \cdots + (m_1 * M_{n-1}) \quad (18)\\ m_2 * D_2 &= c_{22}(m_1 * M_1) + \cdots + c_{2n}(m_1 * M_{n-1}) \\ m_3 * D_3 &= c_{33}(m_1 * M_2) + \cdots + c_{3n}(m_1 * M_{n-1}) \\ &\cdots \\ D_n &= c_{nn}(m_1 * M_{n-1}) \quad (19) \end{aligned}$$

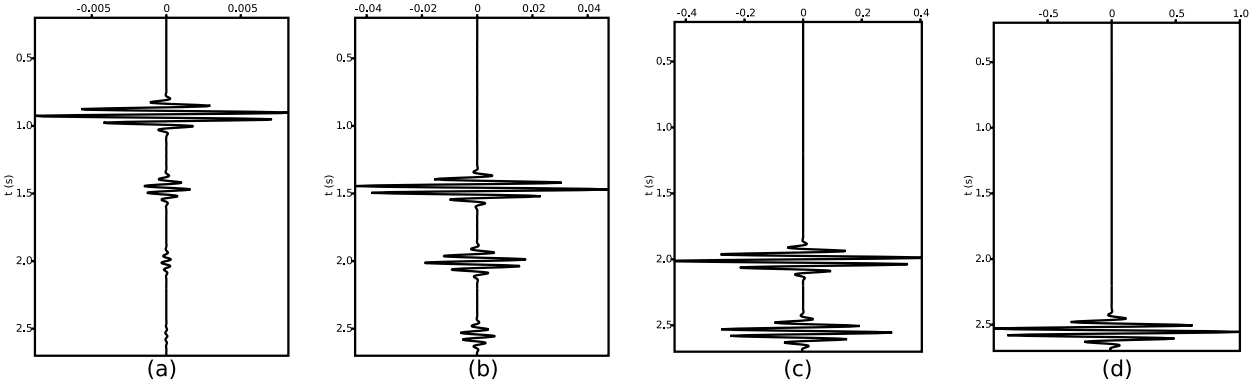

Figure 3: We plot $m_i * D_i$ for $i = 1 \ldots n$ for D_i in Figure 1. From left to right, we plot (a) $m_1 * D_1$, (b) $m_2 * D_2$, (c) $m_3 * D_3$, and (d) D_4. These are the four mixtures used in the ICA mixing model.

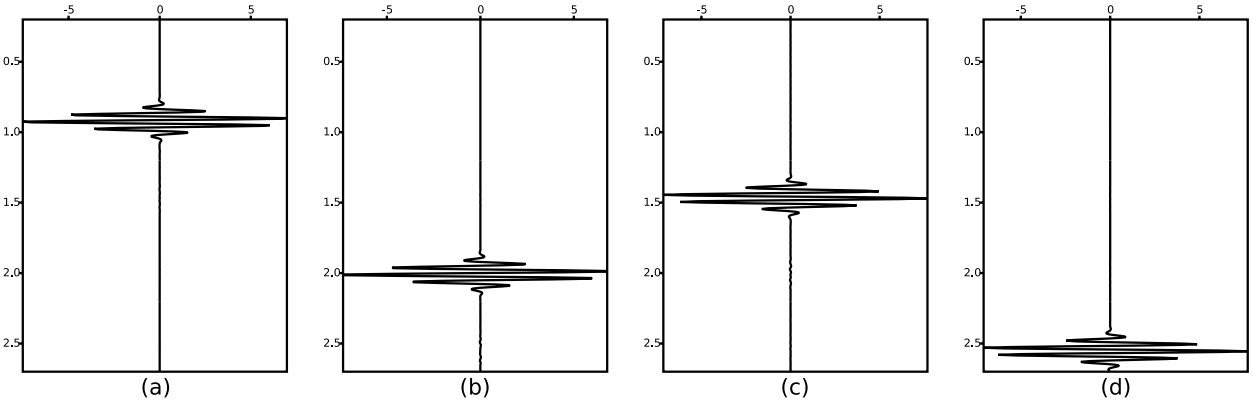

Figure 4: We plot the four independent components recovered from the application of ICA to the mixtures plotted in Figure 3. Notice that (a) is the desired result (the primary event).

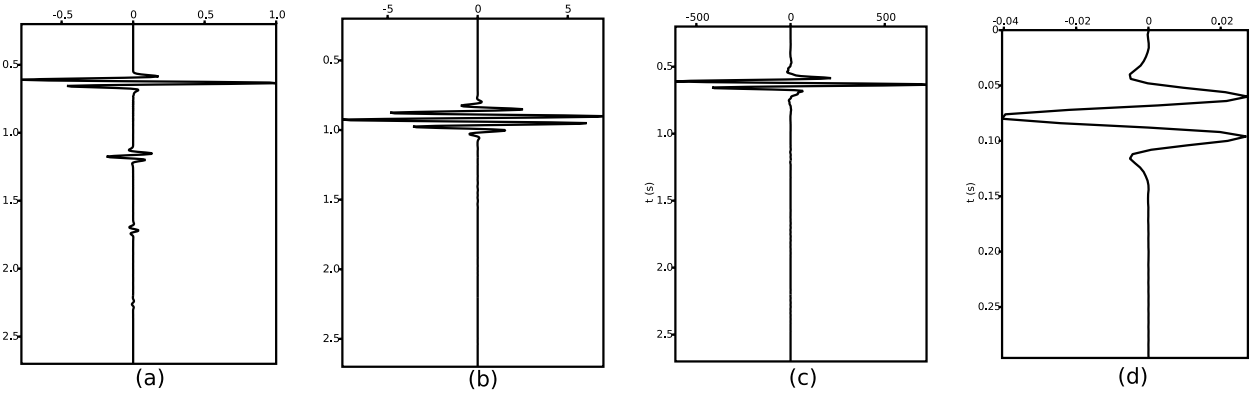

Figure 5: From left to right, we plot (a) the original data trace, (b) the recovered independent component that correlates best with the primary event. (c) the recovered independent component after deconvolution with its matching filter m_1, and (d) the matching filter m_1^*.

where D_i, $i = 2 \dots n$ are the free surface multiple predictions computed using equation (12) and $M = 1$, and m_i are matching filters. With a bit of thought, we observe that

$$m_i = m_{i+1} * m_i^* \tag{20}$$

where m_i^* is the filter matching $m_{i+1}D_i$ to $m_{i+1}D_{i+1}$. To illustrate this, we consider Figure 3. Figure 3d is D_4. Figure 3c is $m_3 * D_3$ where $m_3 = m_3^*$, matching D_3 to D_4. Next, Figure 3b is $m_2 * D_2$ where $m_2 = m_3 * m_2^*$. Finally, Figure 3a is $m_1 * D_1$ where $m_1 = m_2 * m_1^*$. This may seem like a complicated set of steps, but we point out that it is merely the application of a sequence of simple matching filters. In essence, these matching filters are sequentially allowing for the convolution effects of the free surface algorithm.

Once the matching filters are applied, we are ready to form the mixing problem for ICA. First, the mixtures $\mathbf{x}$ are

$$\mathbf{x}^T(t) = \left[\begin{array}{cccc} m_1(t) * D_1(t) & \cdots & m_{n-1}(t) * D_{n-1}(t) & D_n(t) \end{array} \right].$$

Our example in Figure 3 illustrates $n = 4$ mixtures. Second, the unknown sources $\mathbf{s}$ for ICA are

$$\mathbf{s}^T(t) = \left[\begin{array}{ccccc} m_1(t) * P(t) & m_1 * M_1(t) & \cdots & m_1 * M_{n-1} \end{array} \right],$$

and finally the unknown mixing matrix is

$$\mathbf{A} = \begin{bmatrix} 1 & 1 & 1 & \cdots & 1 & 1 \\ 0 & c_{22} & c_{23} & \cdots & c_{2(n-1)} & c_{2n} \\ 0 & 0 & c_{33} & \cdots & c_{3(n-1)} & c_{3n} \\ & & & \cdots & & \end{bmatrix}.$$

For example, we consider again the data in Figure 3 which are the mixtures for our ICA model. After running ICA, we recover the independent components in Figure 4. Rember that the independent components are a perturbed and scaled version of the sources, and one of the sources is the desired result, $m_1 * P$. The correct independent component is found through simple application of a correlation operator. In this case, Figure 4a is $m_1 * P$.

We conclude this section with a summary of the example that we have followed through Figures 1-4. The summary is shown in Figure 5. First, we computed the matching filters m_i to match D_i to D_{i+1}. The matching filter m_1^* for our example is plotted in Figure 5d. Once the matching filter was applied, we used ICA to find the desired source $m_1 * P$, which in this case contains the one primary event (Figure 5b). The original data is shown in Figure 5a, and after deconvolution with m_1, we get the final result (the recovered primary) in Figure 5c.

5 Example

While the example presented in the previous section served its purpose to explain our algorithm, it is overtly simple. In this section, we show a slightly more complex example. The model consists of two reflectors, the first at $400m$ and the second at $1300m$. Both source and receivers are placed at a depth of $10m$. As before, we produce a single shot gather using finite difference modeling, and corrupt it with additive Gaussian random noise in order to test the robustness of our method. The

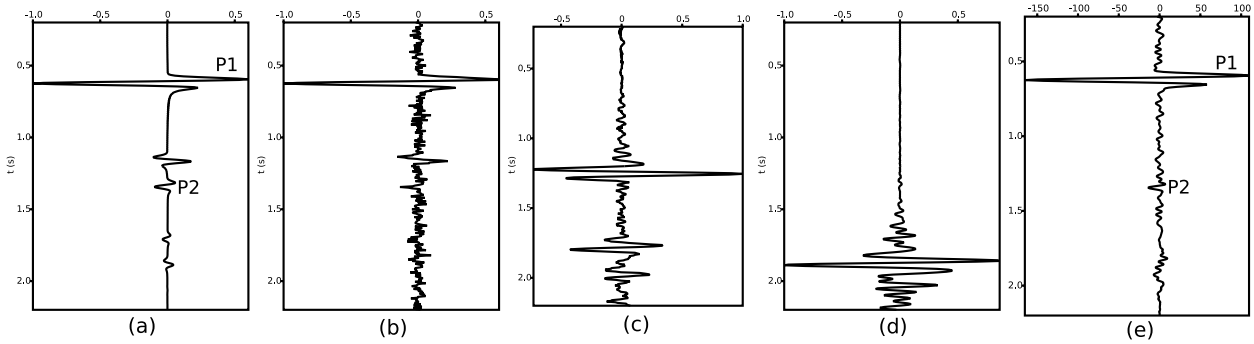

Figure 6: In this example we consider an 1D earth with two reflectors. We generated the data using acoustic finite differencing with source and receivers at depths of $10m$. Figure (a) plots the noise free zero-offset trace, and (b) plots the same zero-offset trace with additive Gaussian noise. Figures (c) and (d) plot, respectively, D_2 and D_3 from the noisy data in (b). Finally, (e) plots the recovered independent component after deconvolution with the matching filter. Notice that both primary events (labelled P1 and P2) are preserved.

zero-offset trace is plotted in Figure 6b (its noise free version is plotted in Figure 6a). The free surface multiple predictions D_i, $i = 2, 3$ are plotted in Figures 6c-d. We then apply the matching filters, and the subsequent ICA step and deconvolution to find the result in Figure 6e. Notice that we have done a reasonable job in removing all free surface multiple energy while retaining the low amplitude primary event from the second reflector.

6 Discussion

This paper proposes an adaptive subtraction algorithm specifically suited for free surface multiples. In particular, we consider the case where we lack knowledge of the source wavelet and/or where the data contains ghosts. The algorithm works in stages. First, we find multiple terms in the free surface multiple prediction series; second, for each data trace we find filters that make a best (in an $L2$ sense) match between the data and the computed terms in the series; and third, we apply ICA to separate free surface multiple energy from the desired signal. In doing so, we replace the subtraction step with a separation step, and avoid the problem of fitting noise to signal.

Of course, we acknowledge that in an ideal world, the free surface elimination algorithm would require only straight forward subtraction, and the adaptive component of the algorithm would be rendered useless by complete use of the physics. Never-the-less, the statistical methods that result from our lack of adherence to the physics are both interesting and fruitfull.

Further, we concede that the matching filter in our algorithm will likely experience difficulties where there are crossing events in the data. However, there are potential solutions to this problem. First, we note that the computation of the matching filter could be augmented with a reference model taken from near-by traces that lack crossing events. Currently we, in effect, use a zero reference model for the matching filter. Second, we could incorporate statistical information about the trace to aid in the building of the matching filter. Namely, the known sparseness of the reflectivity series. These are certainly interesting topics, and are possibilities for future research.

Acknowledgements

We wish to thank Dr. Art Weglein and the M-OSRP sponsors for their encouragement and support. We, in particular, thank Dr. Simon Shaw for his contributions to our understanding of adaptive subtraction algorithms. In addition, we thank Dr. Kim Welford for many useful and encouraging conversations, and tempering us to the reality of real data; and lastly, we thank Dr. Tad Ulrych and Dr. Ken Matson for many enlightening and interesting ICA discussions. Some of the authors have been supported by and express their gratitude to NSF-CMG award DMS-0327778 and DOE Basic Sciences award DE-FG02-05ER15697.

References

Ray Abma, Nurul Kabir, Ken H. Matson, Scott Mitchell, Simon A. Shaw, and Bill McLain. Comparisons of adaptive subtraction methods for multiple attenuation. *The Leading Edge*, 24(3): 277–280, March 2005.

Zhiqiang Guo, T. Hing Tan, and Arthur B. Weglein. Wavelet estimation below towed streamers. *Mission-Oriented Seismic Research Program Annual Report*, pages 21–29, 2003.

Aapo Hyvärinen, Juha Karhunen, and Erkki Oja. *Independent Component Analysis*. Adaptive and Learning Systems for Signal Processing, Communications, and Control. John Wiley & Sons, Inc., 2001.

Sam T. Kaplan. Principal and independent component analysis for seismic data. Master's thesis, University of British Columbia, April 2003.

Maurice Kendall and Alan Stuart. *The Advanced Theory of Statistics*, volume 1. MacMillan Publishing Co., Inc., 1977.

Wenkai Lu and Feng Mao. Adaptive multiple subtraction using independent component analysis. *The Leading Edge*, 24(3):282–284, March 2005.

Arthur B. Weglein, Fernanda V. Araújo, Paulo M. Carvalho, Robert H. Stolt, Kenneth H. Matson, Richard T. Coats, Dennis Corrigan, Douglas J. Foster, Simon A. Shaw, and Haiyan Zhang. Inverse scattering series and seismic exploration. *Inverse Problems*, (19):R27–R83, 2003.

Arthur B. Weglein, Fernanda Araújo Gasparotto, Paulo M. Carvalho, and Robert H. Stolt. An inverse-scattering series method for attenuating multiples in seismic reflection data. *Geophysics*, 62(6):1975–1989, November-December 1997.

Arthur B. Weglein and Bruce G. Secrest. Wavelet estimation for a multidimensional acoustic earth model. *Geophysics*, 55(7):902–913, July 1990.

A Free surface multiple elimination algorithm details

In the body of the paper, we derived the free surface multiple elimination algorithm in equation (11) in terms of Green's functions and scattering potential V. Then, we wrote down the explicit form of the two dimensional algorithm in equation (12). Here we flush out some of the details that allow us to move from the general form in equation (11) to the particular 2D form in equation (12).

From the 2D wave equation (equation (1)), we derive the following forms of G_0^d and G_0^{fs} that are useful in the derivation of the free surface multiple attenuation algorithm.

$$G_0^d(x,z|x_s,z_s;\omega) = -\frac{M}{N^2}\int_{-\infty}^{\infty} e^{ik_x(x-x_s)}\frac{i\pi}{k_0}e^{-ik_0|z-z_s|}dk_x \tag{21}$$

$$G_0^d(k_x,z|x_s,z_s;\omega) = -\frac{M}{N}e^{-ik_x x_s}\frac{i\pi}{k_0}e^{-ik_0|z-z_s|} \tag{22}$$

$$G_0^d(x,z|k_{sx},z_s;\omega) = -\frac{M}{N}e^{ik_{sx}x}\frac{i\pi}{k_{s0}}e^{-ik_{s0}|z-z_s|} \tag{23}$$

$$G_0^{fs}(x,z|x_s,z_s;\omega) = \frac{M}{N^2}\int_{-\infty}^{\infty} e^{ik_x(x-x_s)}\frac{i\pi}{k_0}e^{-ik_0|z+z_s|}dk_x \tag{24}$$

We used the following definitions in deriving (21)-(24).

$$k_0 = \sqrt{\frac{\omega^2}{c^2}-k_x^2}$$

$$k_{s0} = \sqrt{\frac{\omega^2}{c^2}-k_{sx}^2}.$$

In addition, we use the following Fourier conventions for time, shot and receiver coordinates. First we note our convention for time.

$$F(\omega) = \mathcal{F}\{f(t)\} = \int_{-\infty}^{\infty} f(t)e^{-i\omega t}dt$$

$$f(t) = \mathcal{F}^{-1}\{F(\omega)\} = \frac{1}{N}\int_{-\infty}^{\infty} F(\omega)e^{i\omega t}d\omega$$

and next for the receiver coordinate.

$$F(k_x) = \mathcal{F}\{f(x)\} = \int_{-\infty}^{\infty} f(x)e^{-ik_x x}dx$$

$$f(x) = \mathcal{F}^{-1}\{F(k_x)\} = \frac{1}{N}\int_{-\infty}^{\infty} F(k_x)e^{ik_x x}dk_x$$

and, lastly, for the shot coordinate.

$$F(k_{sx}) = \mathcal{F}\{f(x_s)\} = \int_{-\infty}^{\infty} f(x_s)e^{ik_{sx}x_s}dx_s$$

$$f(x_s) = \mathcal{F}^{-1}\{F(k_{sx})\} = \frac{1}{N}\int_{-\infty}^{\infty} F(k_{sx})e^{-ik_{sx}x_s}dk_{sx}.$$

The factor N balances the Fourier transform pair and in the continuous domain is, of course, 2π. Now, we can apply our Green's functions to equation (11) to find equation (12). First,

$$\begin{aligned} D_n(k_x, z|k_{sx}, z_s; \omega) &= \int_{-\infty}^{\infty}\int_{-\infty}^{\infty} G_0^d(k_x, z|x', z'; \omega) V_n(x', z') G_0^d(x', z'|k_{sx}, z_s; \omega) dx' dz' \\ &= -\frac{M^2}{N^2}\frac{\pi^2}{k_0 k_{s0}} e^{i(k_0 z + k_{s0} z_s)} \int_{-\infty}^{\infty}\int_{-\infty}^{\infty} e^{-ik_0 z'} e^{-ik_x x'} V_n(x', z') e^{ik_{sx} x'} e^{-ik_{s0} z'} dx' dz' \end{aligned} \quad (25)$$

Second,

$$\begin{aligned} D_n(k_x, z|k_{sx}, z_s; \omega) &= -\int_{-\infty}^{\infty}\int_{-\infty}^{\infty} G_0^d(k_x, z|x', z'; \omega) V_1(x', z') \int_{-\infty}^{\infty}\int_{-\infty}^{\infty} G_0^{fs}(x', z'|x'', z''; \omega) \\ &\quad \times V_{n-1}(x'', z'') G_0^d(x'', z''|k_{sx}, z_s; \omega) dx'' dz'' dx' dz' \\ &= i\frac{M^3}{N^4}\frac{\pi^3}{k_0 k_{s0}} e^{i(k_0 z + k_{s0} z_s)} \int_{-\infty}^{\infty} \frac{1}{k_0'} \int_{-\infty}^{\infty}\int_{-\infty}^{\infty} e^{-ik_0 z'} e^{-ik_x x'} V_1(x', z') e^{ik_x' x'} e^{-ik_0' z'} \\ &\quad \times \int_{-\infty}^{\infty}\int_{-\infty}^{\infty} e^{-ik_0' z''} e^{-ik_x' x''} V_{n-1}(x'', z'') e^{ik_{sx} x''} e^{-ik_{s0} z''} dx'' dz'' dx' dz' dk_x'. \end{aligned} \quad (26)$$

Substituting (25) into (26), and choosing to evaluate the integrals at the measurement and shot depths (z and z_s) gives

$$D_n(k_x, z|k_{sx}, z_s; \omega) = \frac{i}{M\pi} \int_{-\infty}^{\infty} k_0' e^{-ik_0'(z+z_s)} D_{n-1}(k_x', z|k_{sx}, z_s; \omega) D_1(k_x, z|k_x', z_s; \omega) dk_x'$$

which is the same as equation (12).

A collaborative application of the free-surface multiple elimination code and adaptive subtraction: 2D field data over variable ocean bottom topography

Sam T. Kaplan, J. Kim Welford[1] and Kristopher A. Innanen
[1] *Dept. of Earth Sciences, Memorial University of Newfoundland*

Abstract

An inter-institution collaboration between the University of Houston and Memorial University of Newfoundland (MUN) has guided free-surface multiple elimination (FSME) code alterations specifically geared to immediate field data application, both in the main algorithm implementation and in the design of adaptive subtraction schemes. In this paper we (1) describe the scientific goals of the MUN-based SCREECH project and the associated field data set, including all preprocessing, (2) the application of the altered FSME code and internal adaptive subtraction technology, and (3) illustrate and discuss the results.

1 Introduction

In this paper we apply, to 2D field data example, the free surface multiple prediction implementation (Kaplan et al., 2005), and the adaptive subtraction scheme presented in Kaplan and Innanen (2005). Opportunity has allowed the application of this research to real data be an inter-institution collaboration between M-OSRP and Memorial University of Newfoundland (MUN) in Canada.

We begin by describing the scientific goals of the MUN-based SCREECH project, in particular those goals currently impeded by coherent noise in the form of free-surface multiples. We then enumerate the pre-processing steps accomplished prior to application of the field data ready demultiple algorithm. The issues remaining after pre-processing – those to be handled on the M-OSRP side, so to speak – include free surface multiple elimination which we explore in the two aforementioned stages: first, the application of the free surface multiple prediction; and second, the application of the adaptive subtraction algorithm.

2 Free-surface multiples as an impediment to the scientific goals of the SCREECH project

Offshore Newfoundland is an ideal natural research laboratory for investigating the fundamental processes of continental extension, rifting, the opening of ocean basins and the related development of sedimentary basins. Oil and gas discoveries in the basins offshore Newfoundland have also served to enhance interest in developing a more complete understanding of the region. In 2000, Memorial University, along with international partners, acquired seismic profiles offshore Newfoundland as part of the Study of Continental Rifting and Extension on the Eastern Canadian Shelf project (SCREECH). These profiles extended from the continental shelf, across the rifted margin, to oceanic crust. The deep water data have been analyzed, in 2000, to constrain drill sites for the Ocean Drilling Project (ODP). The data acquired over the continental shelf have, in contrast, not been

fully processed or analyzed, as they suffer from contamination by (largely ocean-bottom related) free-surface multiples. Due to the variable topography of the ocean bottom, the interference of successive multiple wave trains and the dominance of the multiples over subtler reflections from within the crust, conventional methods of suppressing these water bottom multiples have proved less than satisfactory. The consensus continues to be that an adequate and interpretable image of the extended margin will benefit from, if not require, a more complete removal of this coherent noise.

2.1 SCREECH project details

In 2000, a joint US-Canadian-Danish collaborative project between Woods Hole Oceanographic Institution, the University of Wyoming, the Danish Lithosphere Centre, Dalhousie University and Memorial University of Newfoundland acquired a series of seismic profiles offshore Newfoundland as part of the Study of Continental Rifting and Extension on the Eastern Canadian Shelf (SCREECH). The main scientific focus of this collaboration was to better characterize the origin of the crust in the Newfoundland basin. Both refraction/wide-angle seismic reflection and near-vertical multichannel seismic reflection profiles were acquired, extending from the continental shelf, across the rifted margin, to known oceanic crust beyond. For this study, the MUN group is focusing on one line of the multichannel seismic reflection component, which extends from the continental shelf across the Flemish Pass and Beothuk Knoll, down the continental slope and into deeper ocean (Fig. 1). While the ocean-ward portion of Line 2 was previously investigated to tie in with the results from Leg 210 of the International Ocean Drilling Project (ODP), the land-ward portion of the line has not previously been examined.

3 The SCREECH field data-set and pre-processing

In this section we enumerate details of the data set, and its preparation for the application of FSME.

3.1 Acquisition

The acquisition details for the SCREECH multichannel seismic reflection experiment are outlined in Table 1. The multichannel seismic reflection data collected for the SCREECH experiment were of hight quality, however data collected over the shallowest portions of the continental shelf were contaminated with significant free-surface multiple energy (Figs. 2, 3). Due to the variable bathymetry of the shelf, attempts at removing this energy using predictive deconvolution, the parabolic Radon transform and f-k methods produced less than satisfactory results.

3.2 Pre-processing

The FSME algorithm (Weglein et al., 1997) requires as complete a measurement of the wavefield as possible, and, ideally, knowledge of the source wavelet. In order to satisfy the former requirement, the one-sided gathers generated during the marine seismic survey is expanded into two-sided gathers

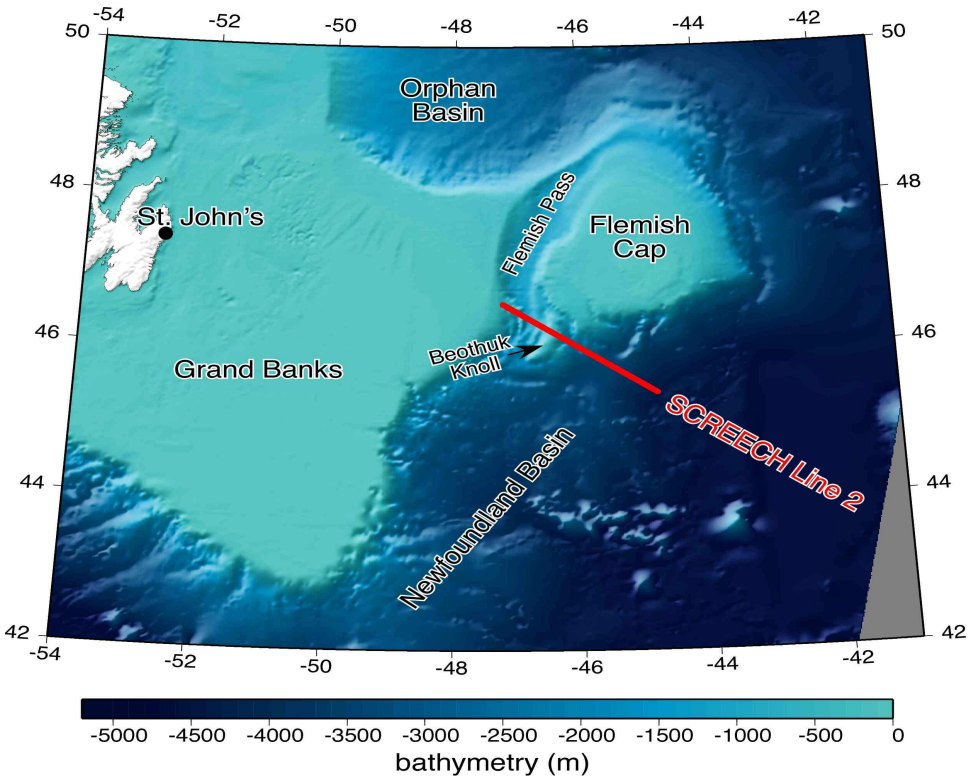

Figure 1: *Bathymetry map for offshore eastern Newfoundland. The section of SCREECH Line 2 considered in this study is overlain in red. Important bathymetric features are labelled in black.*

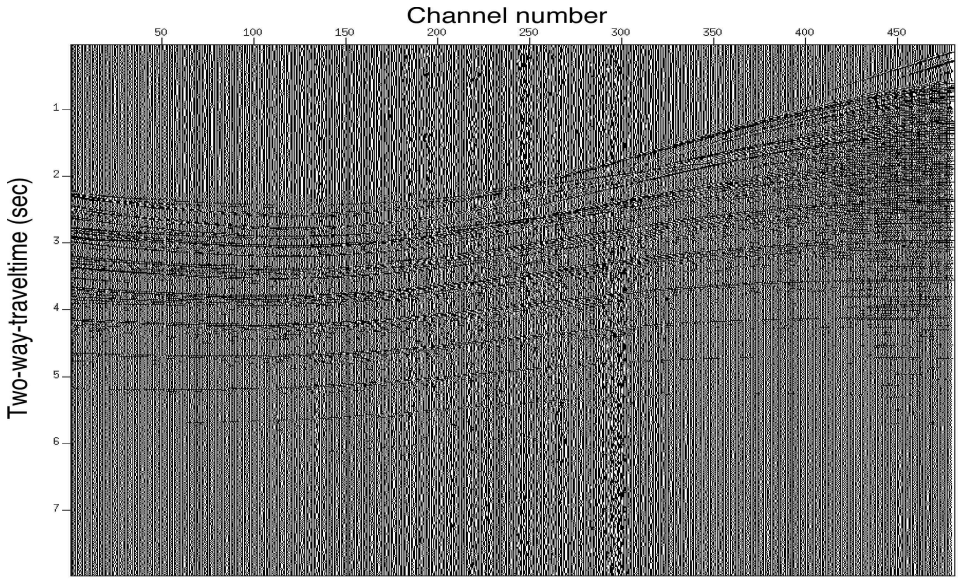

Figure 2: *Raw shot gather collected along SCREECH Line 2. Only the first 8 seconds of two-way-traveltime are displayed to highlight the presence of free-surface multiple energy.*

Table 1: Acquisition parameters for the SCREECH experiment

Source	20 gun, 8540 cu.in. (140 L) airgun array
Shot spacing	50 m
Shot depth	7.5 m
Number of receivers along streamer	480
Receiver spacing along streamer	12.5 m
Streamer depth	7.5 m
Near-trace offset	181.65 m
Far-trace offset	6169.15 m
Sampling rate	4 ms
Trace length	16320 ms
Number of samples per trace	4081

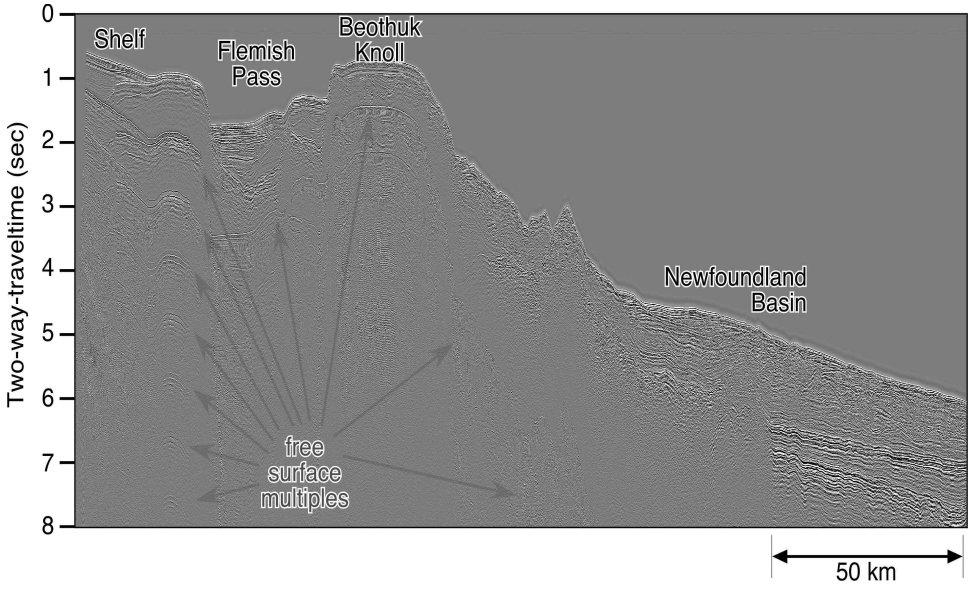

Figure 3: *Brute stack of SCREECH Line 2 without any attempts at free-surface multiple removal. Only the first 8 seconds of two-way-traveltime are displayed to highlight the presence of free-surface multiple energy.*

(described below). In lieu of the latter requirement an extra adaptive subtraction step was employed to complete the de-multiple processing. Below we describe the generation of the necessary two-sided gathers for the SCREECH data-set.

Generating receiver gathers from shot gathers

Receiver gathers are first constructed to assist in the reciprocity-based simulation of a two-sided acquisition; the idea will be to re-associate shot points with receiver points and vice versa. The tendency of cable feathering and slight boat path deviations to cause shot and receiver locations to imperfectly overlap was compensated-for as follows. For every output shot point, each shot gather was scanned to determine the nearest receiver (to a threshold of 24.9 m, half the shot spacing).

For the traces at these receiver locations, the output shot ID was assigned as a receiver ID, and traces from receivers beyond 24.9m of shot locations were removed. Given the survey's average shot spacing of 50 m and average receiver spacing of 12.5 m, this step resulted in the preservation of only every 4th trace. The remaining traces were re-sorted using the receiver ID numbers that had been stored in their headers. Traces with the same receiver ID formed a receiver gather.

Exploiting reciprocity to form two-sided gathers

The receiver gathers generated from the previous step are, by reciprocity, equivalent to the shot gathers that would have been generated had the streamer preceded the boat during the SCREECH experiment. Transforming these receiver gathers into shot gathers simply involves switching the sign of the offset and reassigning the shot and receiver header ID numbers; merging the two sets of gathers produced two-sided gathers. They are, however, not yet ready for input into the FSME algorithm, since (1) there are four times as many traces on one side than the other and (2) the trace spacing is large across zero offset.

Balancing and interpolating the two-sided gathers

In order to balance the number of traces for each side of the two-sided gathers, dummy traces were inserted into the right side of each gather at missing offset locations. To insert data into these dummy traces, the gathers were first NMO corrected using a constant velocity of 1475 m/s to flatten out the free-surface multiples. Next, data were interpolated into the dummy traces using the TRINTERP module from the Globe Claritas seismic processing package which operates as follows:

1. The log of the Fast Fourier Transform (FFT) of each live trace is computed.
2. Across a range of live traces (two in this case), the log of the FFT of each dummy trace in between is interpolated by computing a least squares polynomial fit of arbitrary order (second in this case) for each individual frequency. A lower order polynomial fit is sought if an internal chi-square criteria is not met.
3. The interpolated log of the FFT of the dummy trace is transformed into a seismic trace.

Once the dummy traces in a gather had all been interpolated, the NMO correction was removed and the original non-interpolated traces were re-inserted into the gathers.

Spanning zero offset

At this point, the two-sided gathers contained a total of 960 traces with 480 on each side. While the traces within each side maintained a trace spacing of 12.5 m, the trace gap across zero offset spanned 363.3 m (twice the survey's shortest offset of 181.65 m). By inserting an extra 14 dummy traces either side of zero offset, maintaining a trace spacing of 12.5 m between them, the trace gap across zero offset was reduced to 13.3 m. While slightly larger than the survey trace spacing of 12.5 m, no further trace spacing normalization was performed in order to ensure that the maximum number

of original non-interpolated traces were involved in the multiple prediction. The interpolation of the additional dummy traces was undertaken using the same method as outlined in the previous step only this time the polynomial fit was computed across four live traces. The resulting fully interpolated two-sided shot gather containing 988 traces is shown in Fig. 4.

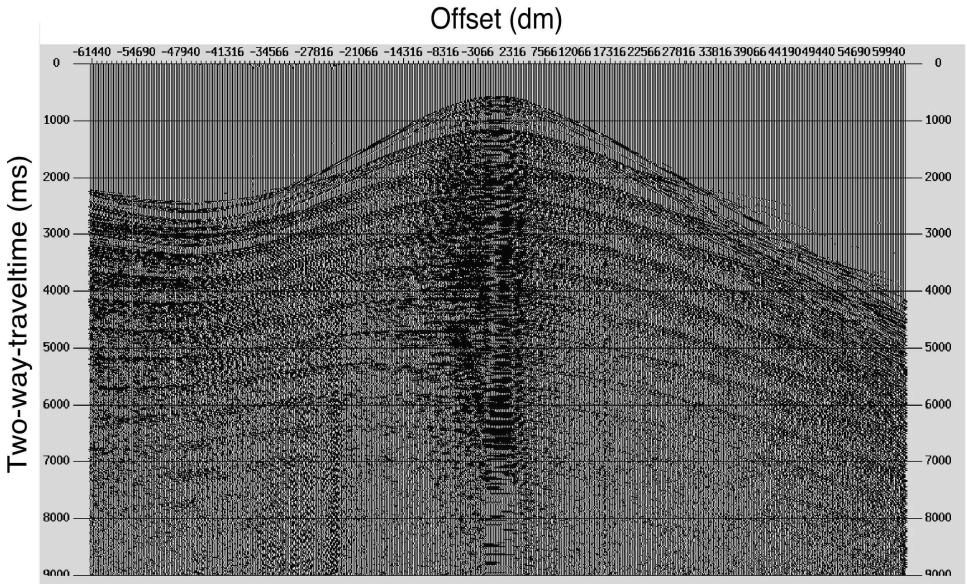

Figure 4: *Interpolated two-sided shot gather. Only the first 9 seconds of two-way-traveltime are displayed to highlight the presence of free-surface multiple energy.*

Muting of direct wave

The final step in the preparation of the SCREECH data for the multiple prediction was the muting of the direct wave. This was achieved by picking a two-sided symmetric mute function for every 50th shot gather and interpolating the mute function across the intervening gathers.

Data subset selection for algorithm testing and validation

As a first test of the inverse scattering series free-surface multiple prediction method, only a subset of the SCREECH data was used. This subset was selected such that the shots and receivers spanned the same range of x locations. Given the 50 m shot spacing and 12.5 m receiver spacing, a file containing 32 shot gathers spanned 128 receiver locations with gathers ranging from right-sided to two-sided to left-sided (Fig. 2). The temporal extent of the data was limited to 8 seconds two-way-traveltime where the free-surface multiples dominated.

4 Free surface multiple prediction, multiple orders

To predict the free surface multiples corresponding to the 2D prestack data in Fig. 2, we use the implementation of the free surface multiple prediction method described in Kaplan et al. (2005).

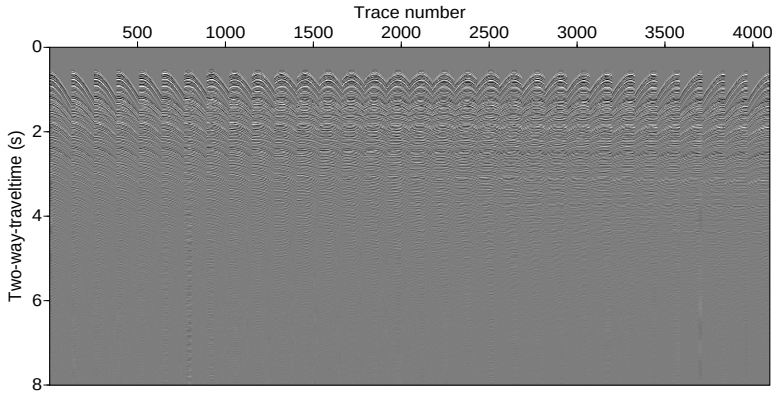

Figure 5: *Range of gathers used for inverse scattering series free-surface multiple prediction method. A percentile clip of 97 has been applied to the data to enhance the reflections.*

This algorithm, in turn, implements the method described in Weglein et al. (2003) for multiple orders of predictions; but, in addition allows for differing shot and receiver spacings (an obvious requirement for the SCREECH data). In our usage of the algorithm we neglect wavelet estimation and deghosting. This results in an imperfect prediction, and prevents their immediate subtraction from the data; but, allows for a real data test of the adaptive subtraction algorithm described in Kaplan and Innanen (2005). Here, we perform this test on the first 2.3 seconds of data, and display the results of the application of adaptive subtraction to this real data example for a single shot gather.

To satisfy the requirements of our adaptive subtraction method, we compute the first two orders of prediction corresponding to the data in Fig. 2. To compensate for edge effects in the prediction, due to limited aperture of the data, we apply a dip filter (*sudipfilt* from the Seismic Unix processing package) to the raw prediction results, plotting the results in Fig. 6. Despite the best efforts of the dip-filter, we find that the edge effects adversely effect the adaptive subtraction at large offsets.

The adaptive subtraction scheme is summarized in Fig. 7 where we illustrate the procedure, and show its results for a single shot gather and the first 2.3 seconds of data. We plot the shot gather in Fig. 7a and its first two orders of prediction in Figs. 7b and 7c, respectively. The data, and the two orders of prediction are used as input to the adaptive subtraction algorithm that, in turn, produces its estimate of the free surface multiple attenuated data in Fig. 7d. Fig. 7e and 7f plot the data and attenuated data for a single trace. Notice that we have done a reasonable job in attenuated the multiples while preserving the two visible primary events (labelled P1 and P2), the first of which is the water bottom, and the second of which is the base of a thin veneer of sediments on the continental shelf.

5 Discussion

This paper represents a collaboration of M-OSRP and MUN to process a portion of the SCREECH data for further academic analysis and interpretation. To this point it has given us, through the challenges of real data, the opportunity to test and further our implementations of free surface multiple prediction (Kaplan et al., 2005) and adaptive subtraction (Kaplan and Innanen, 2005).

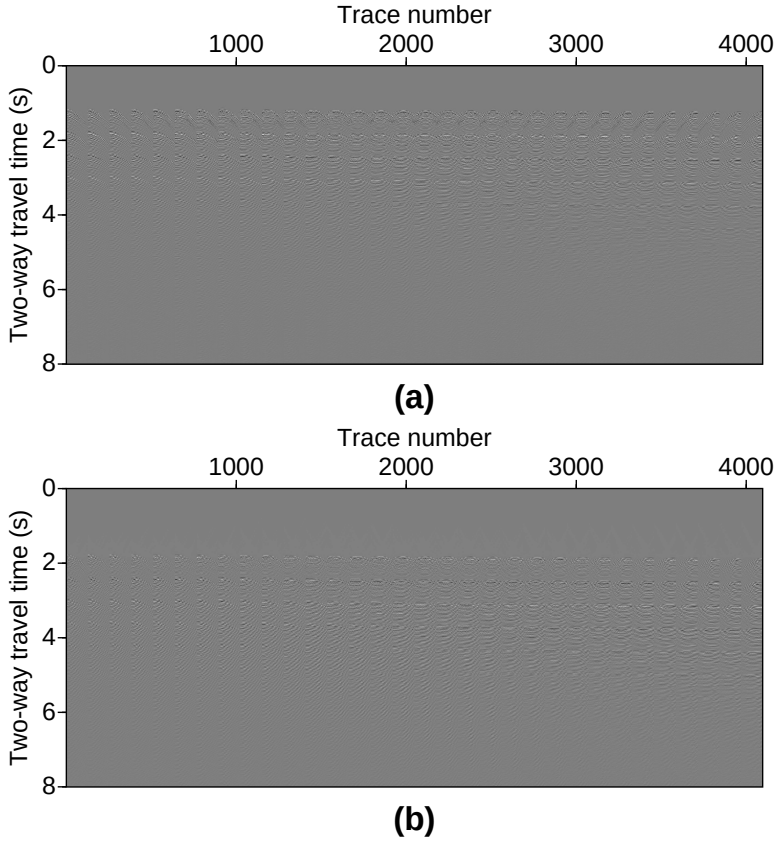

Figure 6: *Inverse scattering series free-surface multiple prediction example. We plot the first two orders of multiple predictions corresponding to the range of gathers in Fig. 2. (a) the first order prediction. (b) the second order prediction. These orders of prediction are subsequently used in an adaptive subtraction scheme, the results of which, we summarize in Fig. 7.*

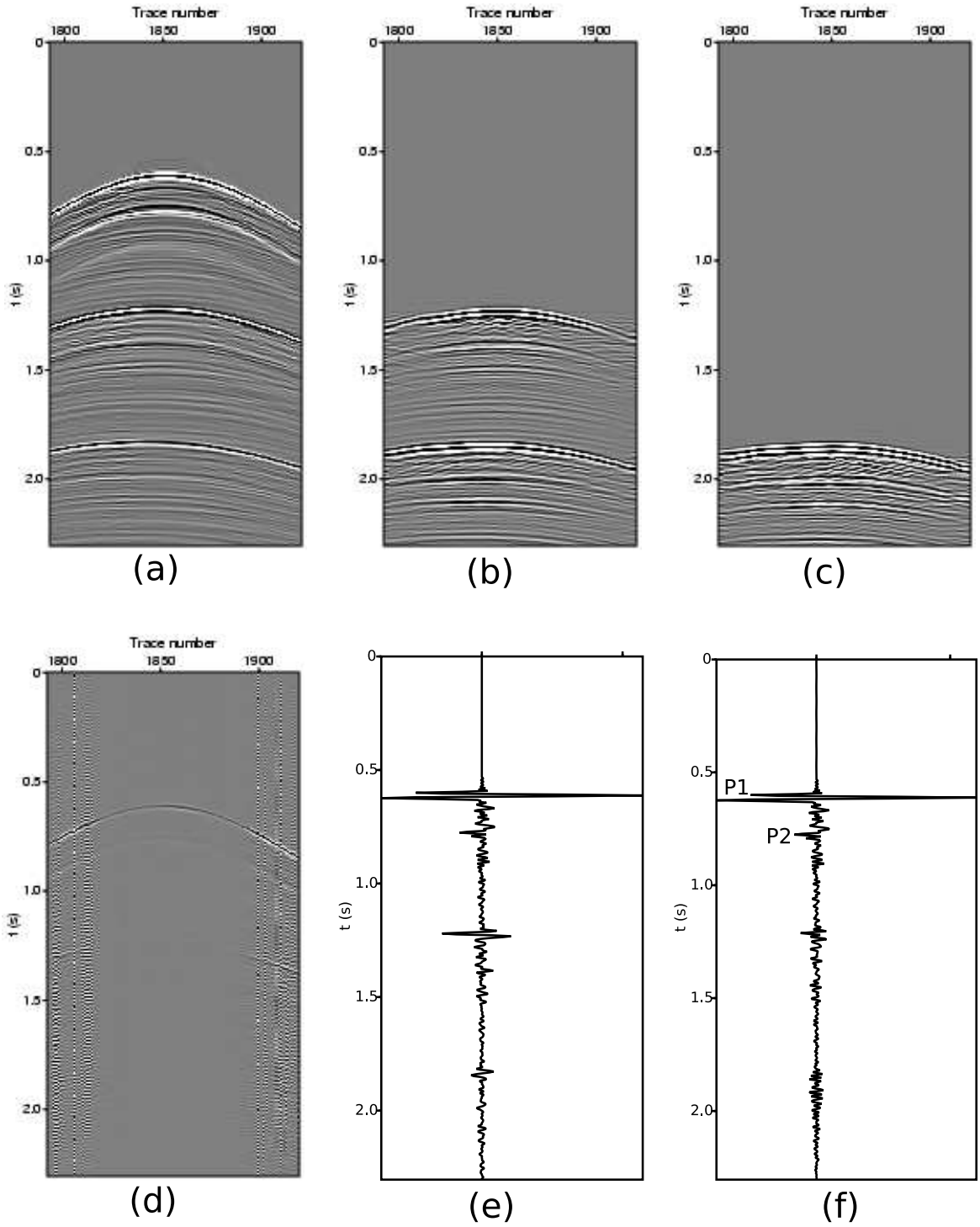

Figure 7: *Inverse scattering series free-surface multiple prediction example. (a) A single shot gather taken from Fig. 2; (b) first order term in the prediction series; (c) second order term in the prediction series; (d) The shot gather in (a) after our adaptive subtraction procedure; (e) trace number 1850 taken from (a); (f) trace number 1850 taken from (d). In (a)-(d), a percentail clip of 98 has been applied to the data to enhance reflections. We associate the difficulties at the large offsets of the shot gather, apparent in (d), to artifacts in the prediction (due to edge effects).*

A second goal is to, of course, sufficiently process the data for its subsequent interpretation. The methods employed in this paper show a measure of success and point to further research. In particular, we see the need to deal with artifacts in the free surface multiple algorithm for aperture limited data that improve on the simple dip filtering performed in this paper.

6 Acknowledgements

We thank M-OSRP sponsors and personnel for their ongoing support. In particular, we thank Dr. Simon Shaw for his adaptive subtraction efforts. In addition, we thank Jeremy Hall, and the PanAtlantic Petroleum Systems Consortium for their support of the MUN research group. Some of the authors have been supported by and express their gratitude to NSF-CMG award DMS-0327778 and DOE Basic Sciences award DE-FG02-05ER15697.

References

Sam T. Kaplan and Kristopher A. Innanen. Adaptive subtraction of free surface multiples through order-by-order prediction, matching filters and independent component analysis. In *Mission-Oriented Seismic Research Program (M-OSRP) Annual Report*, 2005.

Sam T. Kaplan, Kristopher A. Innanen, and Arthur B. Weglein. Updates to M-OSRP internal and free surface multiple coding projects. In *Mission-Oriented Seismic Research Program (M-OSRP) Annual Report*, 2005.

Arthur B. Weglein, Fernanda V. Araújo, Paulo M. Carvalho, Robert H. Stolt, Kenneth H. Matson, Richard T. Coats, Dennis Corrigan, Douglas J. Foster, Simon A. Shaw, and Haiyan Zhang. Inverse scattering series and seismic exploration. *Inverse Problems*, (19):R27–R83, 2003.

Inverse scattering internal multiple elimination: leading order and higher order closed forms

Adriana Citlali Ramírez and Arthur B. Weglein

Abstract

Internal multiples are events in the measured wave field that have experienced at least two upward reflections and one downward reflection in the subsurface. Internal multiples are distinguished from primaries because the latter events had experienced only one upward reflection. The objective of internal multiple elimination using only recorded data (measured values of the scattered field) and information about the reference medium is achievable through the inverse scattering task specific subseries formalism. The first term in the subseries of the first order internal multiple elimination series is an attenuator, which predicts the correct travel time and an amplitude always less than the true internal multiples' amplitude. The higher order terms in the elimination series corrects the amplitude predicted by the attenuator moving the algorithm towards an eliminator. The main contributing terms in this series are identified as terms in a subseries with nonlinear self-interactions at the generating reflector (where the downward reflection of the first order internal multiple took place), adding this subseries we obtain a leading order closed form that eliminates all internal multiples generated at the first reflector and improves the attenuation of the remaining multiples. A second subseries corrects the attenuation due to information on the overburden of the generating reflector. The main part of this second subseries is summed to find a higher order closed form that eliminates the internal multiples generated at the second reflector and further improves the reduction of all internal multiples. A prestack form of the algorithm, which can be extended to a multidimensional form, is given for the leading order subseries and its closed form.

1 Introduction

The inverse scattering series is the only multidimensional direct inversion procedure that can accommodate a geologically complex earth without requiring knowledge of the subsurface properties.

Seismic exploration is an inverse problem. The seismic data are inverted for the properties of the medium that created them. In exploration seismology, the medium properties correspond to the characteristics of the earth's subsurface, and include the spatial location of the reflectors as well as the density and elastic properties of the layers between reflectors.

In practice, seismic data are described as a set of waves reflected and/or transmitted within these reflectors. A catalog of these events (Weglein et al., 2003) can be separated in two event categories:

1. Events that did not interact with the earth. This category includes the direct arrival, and the wave that went from the source up to the free surface, reflects from that surface and then propagated directly to the receiver.

2. Events that interacted with the earth, which are further separated into:
   (a) Events that began as a wave moving upwards, leaving the source and/or ended traveling downwards when they arrived to the receiver. The events in this category are known as ghosts.
   (b) Events that began as a wave moving downwards, leaving the source and ended traveling upwards when they arrived at the receiver. These events are further catalogued by the number and location of their reflections.
      i. Events with one upward reflection are called primaries.
      ii. Events with more than one upward reflection are called multiples. Multiples are further divided into events that have experienced the free surface, and those that have not: The former are called free surface multiples and the latter are called internal multiples.

The seismic data processing is usually accomplished in a sequence of steps. e.g., seismic data reconstruction and regularization, source wavelet deconvolution, removal of free surface multiples, removal/attenuation of internal multiples, depth imaging or migration and inversion for changes in earth properties. The standard practice is to perform these steps in a specific order because each step is a pre-processing condition for the next procedure.

Among all the mathematical theory dedicated to develop algorithms to perform these steps, the inverse scattering series processing methods are the only ones that provide a comprehensive multidimensional framework for seismic inversion capable of dealing with geological complex media and rapid variations in earth properties. The strategy used is to find and isolate subseries of the complete inverse scattering series with task specific purposes analogous to the ordinary seismic processing steps (Weglein et al., 1981, 2003). To this date, these task specific subseries had been successfully isolated and used to deal with the removal of free surface multiples and the attenuation of internal multiples. Encouraging research and tests towards inverse scattering depth imaging and parameter estimation has being developed and is being studied by Shaw (2005); Liu et al. (2005); Zhang and Weglein (2005) among others.

The removal of free surface and internal multiples is a prerequisite for all processing methods for primaries. The current high-water-mark of multiple removal techniques is the inverse scattering free surface eliminator, and internal multiple attenuator, pioneered by Carvaho et al and Araujo et al, respectively. Our overall purpose here is to place internal multiples and free surface multiples on the same footing, with algorithmic capability within your seismic toolbox to reach that same level of elimination effectiveness when you deem that necessary and indicated. There are circumstances when: (1) free surface multiples are a problem and internal multiples are not;(2) internal multiples are a problem and free surface multiples are not (e.g., very deep water and on-shore); (3) both types of multiple are a problem; (4) internal multiple identification or attenuation are sufficient; and (5) when a residual left from internal multiple attenuation is a challenge and impediment to effective and reliable prediction. Which of these circumstances you are facing depends on the details of the geology and the logic behind the play, and the level of ambition and demands of your processing and exploration objectives.

Among the circumstances when internal multiple elimination would provide added-value above that provided by an attenuator for towed streamer marine data are: (1) converted wave internal

multiples;(2) proximal or interfering primaries and internal multiples at the target;(3) reducing the burden on adaptive subtraction to account for missing deterministic predictive capability. We anticipate that internal multiple elimination will place greater demands on preprocessing steps such as data collection and wavelet estimation; and we simultaneously progress those issues to match that requirement. However, the methods presented here never move from not needing to needing subsurface information when we progress from attenuate to eliminating internal multiples. The last comment further separates the inverse scattering multiple removal capability from the feedback loop internal multiple concept.

The research described in this report does not concern with the attenuation but the elimination of internal multiples. The difference between attenuation and elimination of a seismic event or set of events in the data is that attenuation refers to the amplitude reduction of that event in the seismic data and elimination refers to a complete removal of the amplitude of that event or set of events from the data. The first research efforts to address the complete removal of internal multiples from marine seismic data, without destroying primary reflections and with absolutely no knowledge of the subsurface were done by Ramírez and Weglein (2005a).

Internal multiple elimination may be seen as a step that removes an identified coherent noise from the recorded data. We called it coherent noise because most algorithms for imaging and parameter estimation assume that the data have been preconditioned by removing all multiples (free-surface and internal, see for example Carvalho and Weglein (1994); Araújo et al. (1994)).

This work represents progress in the identification, analysis and mathematical manipulation of higher order terms in the series for internal multiple elimination, where the first term is an attenuator (Araújo, 1994). These higher order terms add their contribution to the attenuator to improve its effectiveness towards a complete elimination of internal multiples in the data.

2 Background

The inverse and forward scattering series are perturbation theories. Scattering theory does not have description of events in the seismic way (in terms of boundaries and reflections). The study of the forward scattering series and its analogies with the inverse series has led to a scattering description for the construction of seismic events that is used to process them with inverse scattering task specific subseries. The forward scattering series describes the creation of events in terms of a reference Green's function and a perturbation, which contains the information of the earth properties. The processing of seismic events, with the inverse scattering subseries, is done with the same reference Green's function and the measured data. The inverse scattering data processing benefits from the description and understanding derived from the forward series.

The forward scattering series, as studied by Matson (1996); Nita et al. (2004); Innanen and Weglein (2003), describes events by an infinite series of terms. Each term is defined by propagators in the reference medium interacting, a certain amount of times, with the perturbation. These terms are added up to create a certain event that corresponds to a seismic event. Hence, in scattering theory, a primary can interact more than once with the perturbation. The concepts derived from the inverse scattering theory and the intuition provided by Weglein et al. (1981, 1997) as well as the

framework given by the mathematical study of the forward series (Matson, 1996), showed that the first order approximation in the construction of a primary in the forward series is located at the first term, which is linear in the perturbation. The processing of a primary starts at the first term in the inverse series, which is linear in the data. That same intuition, concepts and mathematical analysis, Matson (1996) and Weglein et al. (2003) made clear that the beginning of the creation of an internal multiple to be a part of the third term in the forward series. The third term is third order in the perturbation and contains three interactions of the reference Green's function with the perturbation. Araújo (1994) and Weglein et al. (1997) found the piece of the third term in the inverse series, third order in the data, that starts processing internal multiples and leads to an algorithm that exactly predicts the travel time of internal multiples and approximately estimates their amplitude. The approximate amplitude has a value always less than the actual. We call *attenuator* this first order term in the processing of internal multiples (Araújo, 1994).

The attenuator has proven to be the high-water-mark processing algorithm towards identification and attenuation of internal multiples. It is the most comprehensive method in the industry. Weglein et al. (2003) made an analytical study, extended by Ramírez and Weglein (2005b), of this term. These studies helped to determine the attenuator's degree of effectiveness. A $1D$ expression that shows the exact amount of attenuation the algorithm achieves (for each kind of first order internal multiple) was obtained. The first order internal multiples were cataloged, for the purposes of this analysis, by the place where their downward reflection occurred. Please note that this definition and analytic study of the attenuation algorithm was performed with the only purpose of understanding the inner workings of the algorithm. The internal multiple attenuator algorithm does not require any knowledge of the subsurface properties, neither the distinction between internal multiples, nor the knowledge of the location where the downward reflection took place. The internal multiple algorithm is a non-linear data driven algorithm that only requires a reference Green's function and the data. The study of the properties of the internal multiple algorithm shed light on the location and isolation of the higher order terms in the internal multiple elimination series, which were identified and first studied in (Ramírez and Weglein, 2005a) and a leading order closed form was found and used in the initial tests.

3 Internal Multiple Elimination

The third term in the inverse scattering series: $(G_0V_1G_0V_1G_0V_1G_0)$ contains the leading order contribution for the removal series of 1^{st} order internal multiples. This leading order term is the internal multiple attenuator. Let's assume that the actual medium varies only in depth. The $1D$ earth and normal incidence wave version (Weglein et al., 2003) of the first order internal multiple attenuator is

$$b_1(k) = D(\omega), \tag{1}$$

$$b_3^{IM_1}(k) = \int_{-\infty}^{\infty} dz_1 e^{ikz_1} b_1(z_1) \int_{-\infty}^{z_1-\epsilon_2} dz_2 e^{-ikz_2} b_1(z_2) \int_{z_2+\epsilon_1}^{\infty} dz_3 e^{ikz_3} b_1(z_3), \tag{2}$$

where $k = 2\frac{\omega}{c_0}$ is the vertical wave number, $D(\omega)$ is the temporal Fourier transforms of the measured scattered field (data), and the superscript IM_1 refers to the $1st$ order internal multiple elimination series.

A simple procedure to use and understand the attenuation algorithm in a $1D$ layered medium is to send a normal incident spike wave and record the data, D, or scattered field at the receiver position. Perform a temporal Fourier transform to take the data to ω space. Use the constant reference velocity, c_0, to define the vertical wave number as $k_z = k = \frac{2\omega}{c_o}$, and change the variable ω in $D(\omega)$ to k, which defines $b_1(k) = D(k)$. Perform a second Fourier transform that brings $b_1(k)$ to pseudodepth z (the pseudodepth is defined in the reference medium as $z = \frac{c_0 t}{2}$). Introduce $b_1(k)$ into equation(2) and obtain a first order internal multiple prediction.

The attenuation algorithm prediction is performed by a nonlinear combination of three sets of data. This nonlinear combination predicts the travel time of the true internal multiple in the data. The amplitude prediction is an estimate of the true internal multiple's amplitude. The estimate is always less than the actual amplitude and the error is a factor known as the attenuation factor of the predicted internal multiple (Ramírez and Weglein, 2005a),

$$(AF_{P.IM})_j = \begin{cases} T_{01}T_{10} & \text{for } j = 1 \\ \\ \Pi_{i=1}^{j-1}\left(T^2_{i\ i-1}T^2_{i-1\ i}\right)T_{j\ j-1}T_{j-1\ j} & \text{for } 1 < j < J \end{cases} \tag{3}$$

where j represents the interface where the downward reflection took place, $T_{j-1\ j}$ and $T_{j\ j-1}$ are the transmission coefficients going down and up through the interface j, respectively, and J is the total number of interfaces in the model. The interfaces are numbered with integers, starting with the shallowest location. In a single layer medium, the first order internal multiple has an amplitude of $-T_{01}R_2R_1R_2T_{10}$ (see Figure(1)) and $b_3^{IM_1}$ predicts a first order internal multiple with an amplitude of $T_{01}T_{10}R_2R_1R_2T_{10}T_{01}$. In agreement with equation (3), the attenuation factor of the predicted internal multiple is $T_{01}T_{10}$. The attenuation factor, equation(3), is affected by the history of the event down to and including only the depth of the shallowest reflection, independent of the place where the two upward reflections occurred.

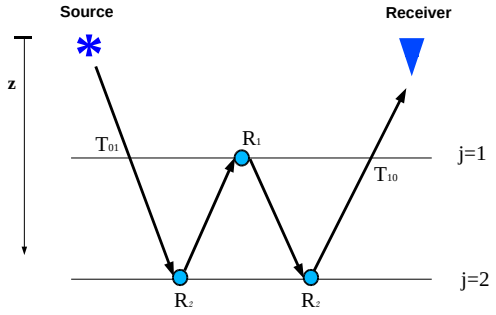

Figure 1: First order internal multiple with downward reflection at $j = 1$.

The terms in the elimination series use the data to predict multiples and remove them from the data itself. This removal is highly accurate and it does not affect the primaries in the data, it only acts on internal multiples. The first order internal multiple elimination series starts with $b_3^{IM_1}$. Since $b_3^{IM_1}$ has estimated the internal multiple amplitude attenuated by a factor of $(AF_{P.IM})_j$, the

purpose of the higher order terms in the elimination series is to remove the effect of the attenuation factor. The higher order terms improve the effectiveness of the attenuator, towards the objective of completely subtract the amplitude of multiples within the data. In order to achieve an elimination method, the inverse scattering subseries for internal multiples elimination should be able to predict the true amplitude for these events by correcting the attenuation factor in equation (3).

In the attenuator's prediction, the factor that multiplies the internal multiples generated at the first reflector*, $(IM)_{j=1}$, is $T_{01}T_{10}$. This attenuation factor corresponds to the first term in the Taylor expansion of $T_{01}T_{10}\left(\frac{1}{T_{01}T_{10}}\right) = 1$,

$$\begin{aligned} T_{01}T_{10}\left(\frac{1}{T_{01}T_{10}}\right) &= T_{01}T_{10}\frac{1}{(1-R_1^2)} \\ &= T_{01}T_{10}\left(1 + R_1^2 + R_1^4 + R_1^6 + \cdots\right). \end{aligned} \tag{4}$$

In the attenuator's prediction, the factor $(T_{01}T_{10})^2T_{12}T_{21}$ that multiplies the internal multiples generated at the second reflector, $(IM)_{j=2}$, corresponds to the first term in the more complicated geometric series for:

$$\begin{aligned} \frac{(T_{01}T_{10})^2T_{12}T_{21}}{(T_{01}T_{10})^2T_{12}T_{21}} &= (T_{01}T_{10})^2T_{12}T_{21}\frac{1}{(1-R_1^2)^2(1-R_2^2)}, \\ &= (T_{01}T_{10})^2T_{12}T_{21}\left(1 + 2R_1^2 + R_2^2 + 3R_1^4 + 2R_2^2R_1^2 + R_2^4 + \cdots\right). \end{aligned} \tag{5}$$

Adding these higher order terms in the elimination series builds a sum of amplitude corrections that improves the subtraction of internal multiples from the data. The higher order terms generate amplitude factors that corresponds to the higher order terms in these Taylor expansions, equations (4) and (5). The higher order amplitude corrections are given by algorithms, found in the internal multiple elimination series $b_3^{IM_1} + b_5^{IM_1} + b_7^{IM_1} + \cdots$ (Ramírez and Weglein, 2005a), that only required measured values of the scattered field and the reference Green's function.

The second term in the elimination series, ${b_5}^{IM_1}$, resides within the fifth term in the inverse series. It is the first step to move the attenuation algorithm towards an elimination of 1^{st} order internal multiples, and it is given by

$$\begin{aligned} b_5^{IM_1}(k) = &\int_{-\infty}^{\infty} dz e^{ikz} b_1(z) \\ &\times \int_{-\infty}^{z-\epsilon} dz' e^{-ikz'} \left[b_1(z')^3 + 2\, b_1(z') \int_{-\infty}^{z'-\epsilon} dz'''\, b_1(z''')^2 \right] \\ &\times \int_{z'+\epsilon}^{\infty} dz'' e^{ikz''} b_1(z''). \end{aligned} \tag{6}$$

The second term in the 1^{st} order internal multiple elimination series can be separated in two parts,

*We define the generating reflector of a first order internal multiple as the reflector where the downward reflection took place.

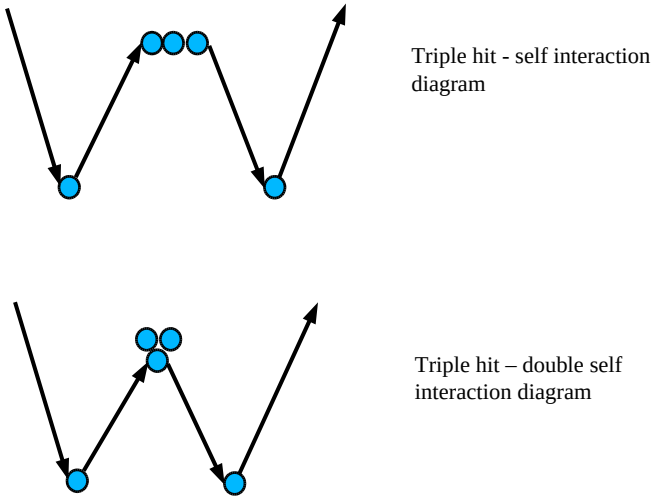

Figure 2: Diagrams for $b_{51}^{IM_1}$ (upper figure) and $b_{52}^{IM_1}$ (lower figure).

and represented with the diagrams in Figure(2),

$$b_{51}^{IM_1}(k) = \int_{-\infty}^{\infty} dz e^{ikz} b_1(z) \times \int_{-\infty}^{z-\epsilon} dz' e^{-ikz'} b_1(z')^3 \int_{z'+\epsilon}^{\infty} dz'' e^{ikz''} b_1(z''), \tag{7}$$

$$b_{52}5^{IM_1}(k) = \int_{-\infty}^{\infty} dz e^{ikz} b_1(z) \times \int_{-\infty}^{z-\epsilon} dz' e^{-ikz'} 2\ b_1(z') \int_{-\infty}^{z'-\epsilon} dz'''\ b_1(z''')^2 \int_{z'+\epsilon}^{\infty} dz'' e^{ikz''} b_1(z''). \tag{8}$$

Both diagrams affect 1^{st} order internal multiples, with the following particular characteristics:

1. The diagram located at the top of Figure(2) corresponds to equation (7) and it belongs to a series that eliminates all 1^{st} order internal multiples that were downward reflected at the shallowest reflector. This term combines nonlinearly five sets of data to give higher order amplitude information and the correct time. The three hits in the diagram indicate triple self interaction at the generating reflector. Hence, the extra amplitude information given by the self-interacting data corresponds to powers of the reflection coefficient of each generating reflector. The analysis of the properties of this term, using its diagram representation and numerical example, showed that it is the main contribution of $b_5^{IM_1}$ to the elimination of internal multiples. Its mathematical representation resembles the one of the attenuator, which is the leading order term of the series by itself. We can add the attenuator diagram, the triple self-interacting diagram, and the corresponding diagram in each higher order term in the elimination series, $b_7^{IM_1} + b_9^{IM_1} + b_{11}^{IM_1} + \cdots$, where the number in the subscript refers to the number of times the data is nonlinearly combined with itself. The leading order terms are represented with the diagrams shown in Figure(3). The sum of these diagrams leads to

the leading order closed form term

$$b_{LO}^{IM_1} = \int_{-\infty}^{\infty} dz e^{ikz} b_1(z) \times \int_{-\infty}^{z-\epsilon} dz' e^{-ikz'} \left(\frac{1}{1 - b_1(z')^2} \right) b_1(z') \int_{z'+\epsilon}^{\infty} dz'' e^{ikz''} b_1(z''). \quad (9)$$

This equation is the infinite sum of the leading order subseries of the inverse scattering internal multiple elimination series in a closed form term, $b_{LO}^{IM_1}$. The leading order eliminator of internal multiples, $b_{LO}^{IM_1}$, eliminates all 1^{st} order internal multiples with generated at the shallowest reflector without requiring a-priori information, nor a velocity model. It is all done in terms of the effective data, b_1, and the reference velocity contained in $k = \frac{2\omega}{c_0}$. Furthermore, the leading order eliminator helps to better attenuate all the internal multiples with downward reflections at deeper reflectors.

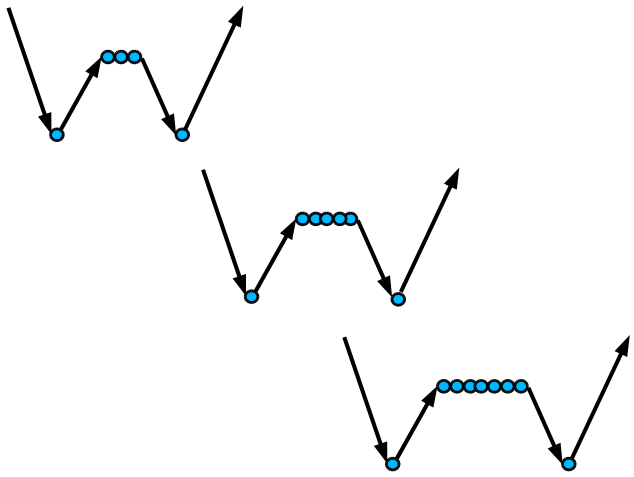

Figure 3: Leading order diagrams.

2. The diagram located at the bottom of Figure(2) represents equation(8), which contains $2b_1(z') \int_{-\infty}^{z'-\epsilon} dz''' \; b_1(z''')^2$ in the middle integral. The data in the middle integral, represented in the middle part of the diagram, has two self-interacting data above the generating reflector. The double self interaction gives extra amplitude information of any interface above the reflector where the downward reflection took place. Since it gives second order corrections for the overburden of the generating reflector, it only acts on internal multiples downward reflected at interfaces below the shallowest reflector. It doesn't act on the internal multiples generated at the shallowest reflector, which are completely eliminated with the leading order closed form term in equation (9). The double self-interacting diagram further attenuates all 1^{st} order internal multiples generated at deeper reflectors[†]. It starts the subseries of the internal multiple elimination series that complements the action of the terms contained in

[†]Where deeper refers to all reflector located below the shallowest one.

the leading order $b_{LO}^{IM_1}$. The main part of these second subseries can be summed in a higher order closed form term,

$$b_{HO}^{IM_1} = \int_{-\infty}^{\infty} dz e^{ikz} b_1(z) \int_{-\infty}^{z-\epsilon} dz' e^{-ikz'} \frac{2G_1(z') \int_{-\infty}^{z'-\epsilon} dz''' \; J(z''')}{1 - \int_{-\infty}^{z'} dz''' \; J(z''')} \int_{z'+\epsilon}^{\infty} dz'' e^{ikz''} b_1(z''). \tag{10}$$

$$J(z''') = \frac{b_1(z''')^2}{1 - b_1(z''')^2} \tag{11}$$

$$G_1(z') = \frac{b_1(z')}{1 - b_1(z')^2} \tag{12}$$

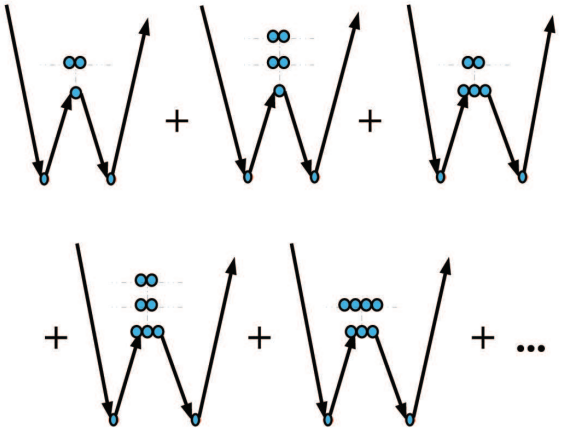

Figure 4: Higher order diagrams.

Some of the diagrams included in this closed form are shown in Figure 4. Equation (10) is the infinite sum of the main terms in the higher order subseries of the internal multiple elimination series in a closed form term, $b_{HO}^{IM_1}$. The higher order eliminator, applied after the leading order, improves the reduction of the remaining multiples. It is including diagrams that have extra data self-interactions above the generating reflector. The reason it is not including all the higher order terms is because, these terms in the inverse series for internal multiple elimination have different integer weights, which means that a specific higher order diagram is required to act more than ones in the removal process. From the form of equation (10), the closed form only contains a weighting factor of 2 (please refer to the middle integral) in agreement to the weighting factor needed by equation 8. The first term included in the higher order closed form corresponds to equation 8, which represented in the first diagram in Figure 4.

An elimination algorithm for internal multiples based on inverse scattering series has the potential of removing difficult internal multiples, leaving all primaries unaffected. Although the internal multiple amplitudes are reduced by the attenuator, $b_3^{IM_1}$, and substantially reduced (and a subset is eliminated) by the leading order closed form, $b_{LO}^{IM_1}$, there is in some cases an observable residual

that can be further attenuated with the action of the higher order closed form, $b_{HO}^{IM_1}$. The higher order closed form term of the internal multiple elimination series complements the elimination of the amplitude of the remaining internal multiples by adding nonlinear contributions in terms of nonlinear combinations of data and a reference Green's function. The combination of the leading order closed form with the higher order closed form term gives an improved algorithm for the removal of internal multiples.

4 $2D$ extension of the algorithm

In the theory presented in the previous section, no assumptions about the earth below the receivers are made, this characteristic makes it ideal for addressing one of the current challenges in exploration seismology: removing multiples, locating and identifying targets in highly complex medium, when the velocity model is unobtainable. Hence, the extension to a multidimensional earth is a necessary step.

The attenuation algorithm for a $2D$ earth, presented in Araújo (1994); Weglein et al. (1997) and Weglein et al. (2003), is

$$b_1(k_g, k_s, q_g + q_s) = -2iq_s D(k_g, k_s, \omega), \tag{13}$$

$$\begin{aligned} b_3^{IM_1}(k_g, k_s, q_g + q_s) = \frac{1}{(2\pi)^2} \int_{-\infty}^{\infty} dk_1 e^{iq_1(x_s - x_g)} \int_{-\infty}^{\infty} dk_2 e^{iq_2(\epsilon_g - \epsilon_s)} \\ \times \int_{-\infty}^{\infty} dz_1 e^{i(q_g+q_1)z_1} b_1(k_g, -k_1, z_1) \\ \times \int_{-\infty}^{z_1-\epsilon_2} dz_2 e^{i(-q_1-q_2)z_2} b_1(k_1, -k_2, z_2) \\ \times \int_{z_2+\epsilon_1}^{\infty} dz_3 e^{i(q_2+q_s)z_3} b_1(k_2, -k_s, z_3), \end{aligned} \tag{14}$$

where ω represents the temporal frequency, c_0 is the acoustic velocity of water; k_g and k_s are the horizontal wave numbers corresponding to receiver and source coordinates: x_g and x_s, respectively; the 2-D wave vectors: $\mathbf{k}_g = (k_g, -q_g)$ and $\mathbf{k}_s = (k_s, q_s)$ are constrained by $|\mathbf{k}_g| = |\mathbf{k}_s| = \frac{\omega}{c_0}$; the vertical wave numbers are $q_g = sgn(\omega)\sqrt{(\frac{\omega}{c_0})^2 - {k_g}^2}$ and $q_s = sgn(\omega)\sqrt{(\frac{\omega}{c_0})^2 - {k_s}^2}$, and ϵ_i is a small positive parameter chosen to insure that the relations $z_1 > z_2$ and $z_3 > z_2$ are satisfied.

In equations (18) and (19), the effective data $b_1(k_g, k_s, q_g + q_s)$ is defined as a source obliquity factor times the $2D$ measured values of the scattered field, D. The variable z is the Fourier conjugate to the sum of the vertical wave numbers, $k_z = -(q_g + q_s)$.

As we show in $1D$, the second term in the 1^{st} order internal multiple elimination series can be

separated in two equations. In $2D$, the first equation is

$$b_{51}^{IM_1}(k_g,k_s,q_g+q_s) = \frac{1}{(2\pi)^2}\int_{-\infty}^{\infty} dk_1 e^{iq_1(x_s-x_g)} \int_{-\infty}^{\infty} dk_2 e^{iq_2(\epsilon_g-\epsilon_s)} \times \int_{-\infty}^{\infty} dz_1 e^{i(q_g+q_1)z_1} b_1(k_g,-k_1,z_1) \times \int_{-\infty}^{z_1-\epsilon_2} dz_2 e^{i(-q_1-q_2)z_2} \left[b_1(k_1,-k_2,z_2)\right]^3 \times \int_{z_2+\epsilon_1}^{\infty} dz_3 e^{i(q_2+q_s)z_3} b_1(k_2,-k_s,z_3), \tag{15}$$

$$\tag{16}$$

which have the same diagrammatic representation as shown in Figure(2). Studying the higher order terms in the inverse scattering internal multiple elimination series in a multidimensional model type independent form, we find that the form of the terms with self-interacting data at the generating reflector conserves the properties and characteristics found in the simple $1D$ case. Analogous to the $1D$ case, the first term in the leading order elimination series is the attenuator, equation 19, and the second term is given by equation 15. The next terms in the leading order series have the form:

$$b_{51}^{IM_1}(k_g,k_s,q_g+q_s) = \sum_{J=1}^{\infty} \frac{1}{(2\pi)^2}\int_{-\infty}^{\infty} dk_1 e^{iq_1(x_s-x_g)} \int_{-\infty}^{\infty} dk_2 e^{iq_2(\epsilon_g-\epsilon_s)} \times \int_{-\infty}^{\infty} dz_1 e^{i(q_g+q_1)z_1} b_1(k_g,-k_1,z_1) \times \int_{-\infty}^{z_1-\epsilon_2} dz_2 e^{i(-q_1-q_2)z_2} \left[b_1(k_1,-k_2,z_2)\right]^J \times \int_{z_2+\epsilon_1}^{\infty} dz_3 e^{i(q_2+q_s)z_3} b_1(k_2,-k_s,z_3), \tag{17}$$

We can add the leading order terms in the multidimensional case to a closed form, which is given by,

$$b_1(k_g,k_s,q_g+q_s) = -2iq_s D(k_g,k_s,\omega), \tag{18}$$

$$b_3(k_g,k_s,q_g+q_s) = \frac{1}{(2\pi)^2}\int_{-\infty}^{\infty} dk_1 e^{iq_1(x_s-x_g)} \int_{-\infty}^{\infty} dk_2 e^{iq_2(\epsilon_g-\epsilon_s)} \times \int_{-\infty}^{\infty} dz_1 e^{i(q_g+q_1)z_1} b_1(k_g,-k_1,z_1) \times \int_{-\infty}^{z_1-\epsilon_2} dz_2 e^{i(-q_1-q_2)z_2} \frac{b_1(k_1,-k_2,z_2)}{1-b_1(k_1,-k_2,z_2)^2} \times \int_{z_2+\epsilon_1}^{\infty} dz_3 e^{i(q_2+q_s)z_3} b_1(k_2,-k_s,z_3), \tag{19}$$

This is a $2D$ model type independent leading order elimination algorithm for internal multiples. The leading order eliminator is a data-driven algorithm written in terms of effective data b_1 (see equation (18)). The leading order closed form, $b_{LO}^{IM_1}$, gives the main contribution towards eliminating internal multiples. It completely removes all 1^{st} order internal multiples generated at the first

reflector and improves the attenuation of the remaining multiples. Leading order as an eliminator means it eliminates a class of internal multiples and further attenuates the rest. In a $2D$ medium, the multiples that have no cumulative transmission error (the ones with downward reflection at the shallowest reflector) are eliminated by the algorithm in equation 19, $b_1 + b_{LO}^{IM_1}$. The higher order closed form is being examined for a $2D$ extension. It is not always possible to generalize a $1D$ closed form to $2D$; an algorithm in $2D$ have more variables and different dependencies than the same algorithm in $1D$. However, we are studying the $2D$ expressions for the higher order terms in the elimination series. For a multidimensional world, the leading order eliminator provides the removal of all first order internal multiples generated at the first reflector and effectively attenuates the rest of the multiples.

Numerical Example

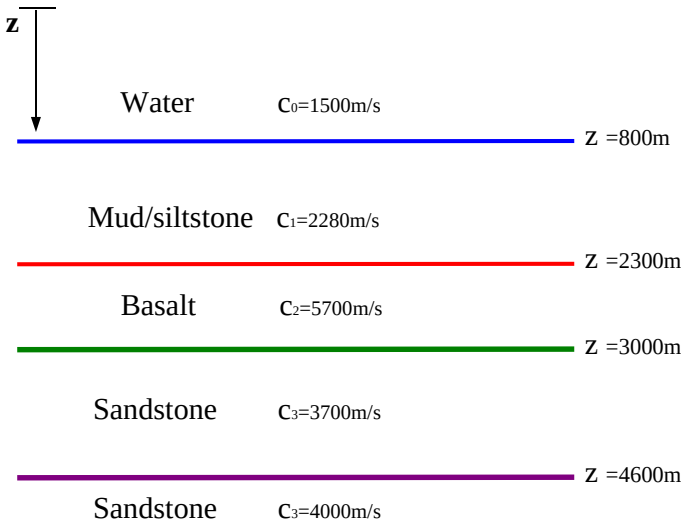

Figure 5: 1D model.

To test the performance of the internal multiple elimination given

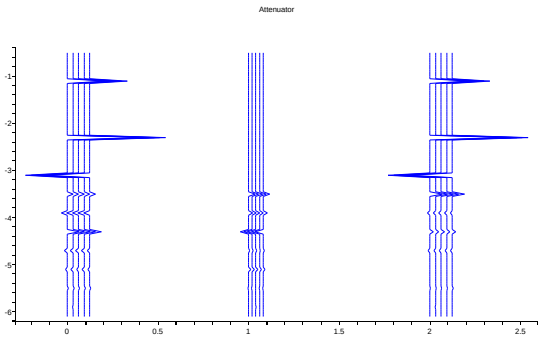

Figure 6: Attenuation of internal multiples with $b_3^{IM_1}$.

by the action of the leading order and the higher order closed forms, $b_{LO}^{IM_1} + b_{HO}^{IM_1}$, we use a 1D model, Figure 5, and a spike wave to generate synthetic data. This example was used to illustrate the performance of the leading order closed form term in Ramírez and Weglein (2005a), we now want to see if the residual multiples can be further eliminated by the addition of the higher order term. In this model, the reflectors depths were selected to have a negative interference between the first water bottom multiple and the primary reflected at the deepest reflector, both arriving at $3.5s$. The event at $3.5s$ (the interference between a multiple and a primary) has an amplitude of 0.0311 in the data.

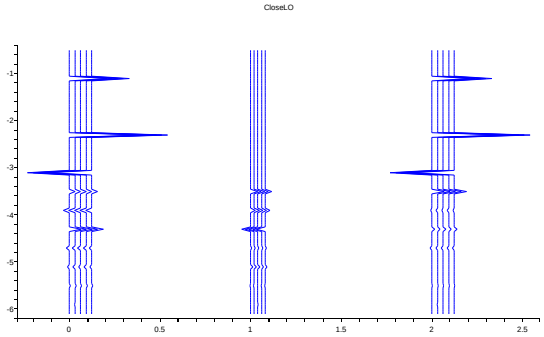

Figure 7: Elimination of water bottom internal multiples with $b_{LO}^{IM_1}$.

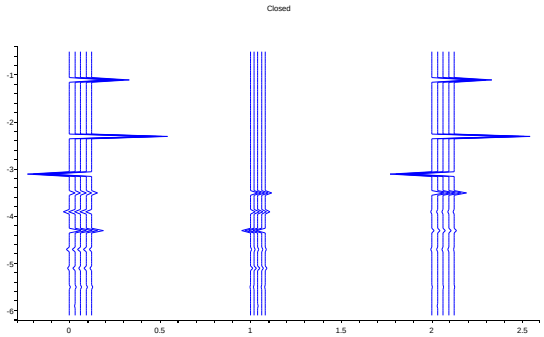

Figure 8: Elimination of water bottom internal multiples with $b_{LO}^{IM_1} + b_{HO}^{IM_1}$.

In Figure 6 we have data with primaries and 1^{st} order internal multiples (on the leftmost traces). The inner traces are the output of the attenuator, it gives the first order estimate of the amplitude (with opposite sign) and the correct time prediction. The traces on the right side of Figure 6 are the primaries and the residual multiples after adding $b_1 + b_3^{IM_1}$. The amplitude at $3.5s$, after attenuating the multiple is 0.0657. On the left side of Figure 7 we show the same data, the inmost traces are the output of $b_{LO}^{IM_1}$. On the right side of Figure 7 the multiples generated at the shallowest reflector were removed, the output traces are primaries and small residual of multiples with transmission error above the depth of their downward reflection, after adding the data to the leading order eliminator, $b_1 + b_{LO}^{IM_1}$. The amplitude at $3.5s$, after eliminating the water bottom multiple is 0.0686, corresponding to the true amplitude of the primary reflected at the fourth interface.

The interfering internal multiple has been eliminated. On the left side of Figure 8 we show the

same data, the inmost traces are the output of $b_{LO}^{IM_1} + b_{HO}^{IM_1}$. On the right side of Figure 8, the multiples generated at the shallowest reflector have been removed and the remaining multiples were attenuated a little bit more. However, since we had a negative interference between a multiple and a primary, and the primaries are the subevents responsible of the amplitude prediction in the algorithm, we observe that the improvement provided by $b_{HO}^{IM_1}$ is minimum compared with the effect of $b_{LO}^{IM_1}$ in the elimination. In other words, it has been shown that the attenuator (see for example Weglein et al. (2003); Nita and Weglein (2005)) and the leading order eliminator (Ramírez and Weglein, 2005a) that the internal multiples are constructed by considering three effective data sets b_1 and searching for a set of events which satisfy the lower-higher-lower relationship in their pseudo depths. Having found those events, the algorithms combine their amplitudes and phases in a non-linear sense. The nonlinear combination of phases gives the travel time prediction, which perfectly agrees with the actual travel time.

If the amplitude of an event in the data is affected by interference with another event, it will also affect the effectiveness of the prediction. However, the interfering events did not confuse or damage the main output of these algorithms, i.e. all the first order internal multiples were predicted with the correct travel time. In this example, the higher order closed form made an improvement. The higher order closed form, which is applied after the leading order, captures some of the remaining terms in the series but not all of them. This algorithm also predicts the exact travel time of the internal multiples and gave extra amplitude information to move towards the goal of elimination. It gave extra contributions to remove the residual multiples (left after the action of b_{LO}^{IM}). However, this contribution was smaller, compared to the reduction the same algorithm provides when there is no interference. I n comparison with the action of the leading order eliminator on multiples generated at the shallowest reflector, the higher order outcome is small; but its contribution has a positive impact. The derivation and objective of the new algorithm is to add value and go beyond the capability of the internal multiple attenuator.

There is an important subset of first order internal multiples that is now eliminated, and other internal multiples are reduced beyond attenuation. The former subset in practice can often be the most significant from a practical field viewpoint. The removal automatically eliminates those multiples that have their first reflection at the shallowest reflector, the water bottom, in marine exploration, and degree of addition benefit beyond that to shallower multiples depends on the detail of the specific situation. The water bottom property is neither required nor determined for this eliminator algorithm, nor is information below the water bottom input to provide that ancillary benefit. The degree of the latter secondary benefit will vary but is always present. These examples exemplify these benefits and characteristics of the new algorithm. The fact that the new algorithm is not at all more expensive than the attenuator is worth noting. The sensitivity of the new algorithm for input wavelet information will be examined in a future contribution, but new direct methods such as, e.g., Guo et al. (2005) and over under cable advances will allow e.g. Weglein and Secrest (1990) are anticipated to match that need.

Let's observe the output of a different example, shown in Figure 9. On the left side of Figure 10, the traces are data with primaries and 1^{st} order internal multiples, the traces in the middle are the output of the attenuator and the traces on the right are the residual after adding $b_1 + b_3^{IM_1}$.

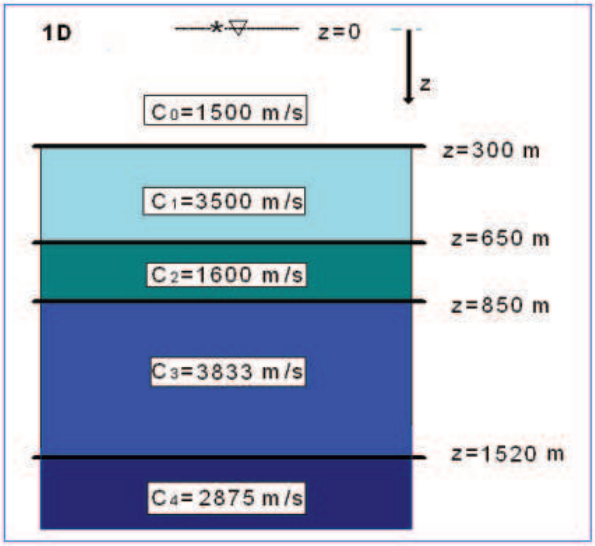

Figure 9: 1D model.

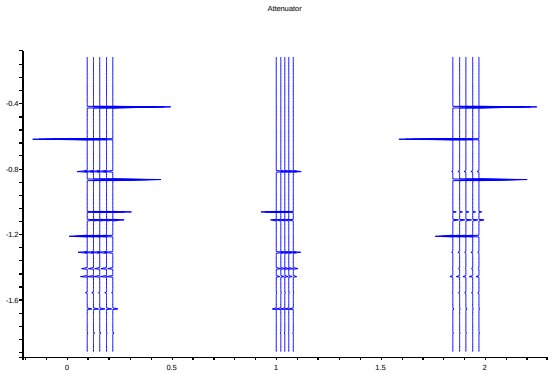

Figure 10: Attenuation of internal multiples with $b_3^{IM_1}$.

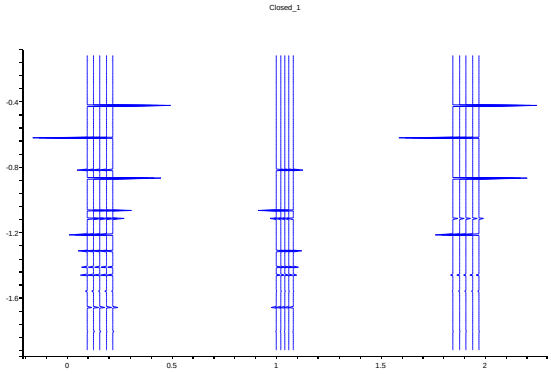

Figure 11: Elimination of water bottom internal multiples with $b_{LO}^{IM_1}$

On the left side of Figure11 we observe the data with primaries and first order internal multiples. The inner traces are the output of the leading order closed form, $b_{LO}^{IM_1}$, it leaves all primaries

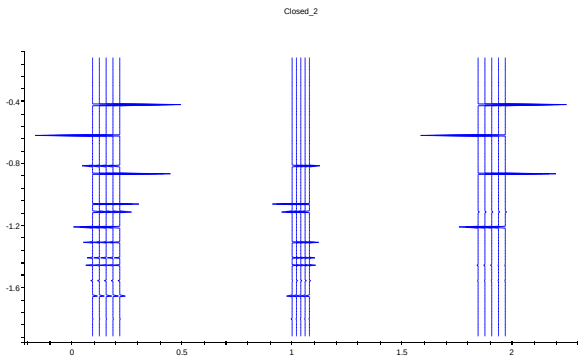

Figure 12: Elimination of water bottom internal multiples with $b_{LO}^{IM_1} + b_{HO}^{IM_1}$

unaffected and eliminates the internal multiples generated at the first reflector; the traces on the right side are the primaries and the residual multiple after adding $b_1 + b_{LO}^{IM_1}$. In Figure 10, the traces on the left show the same data, the traces in the middle are the output of the leading order closed form plus the higher order closed form, and the traces on the right are the residual after adding $b_1 + b_{LO}^{IM_1} + b_{HO}^{IM_1}$. We observe that the higher order closed form has improved the removal of internal multiples.

Conclusions

In many circumstances the first order term in the inverse scattering internal multiple series, known as the attenuator, provides an effective solution (Weglein et al., 2003). It predicts the correct arrival time and attenuates the amplitude of the internal multiples in the data. However, there are situations for towed streamer pressure measurements where either the residual can be far from small (*e.g.* converted wave internal multiples) or where a small residual interferes with a target primary, and the latter is itself small. In these cases, the attenuation is not enough and we need to seek for algorithms that provide an elimination of these events in the data.

This work shows progress in the identification, analysis and mathematical manipulation of higher order terms in the series for internal multiple elimination, where the first term is an attenuator (Araújo, 1994). These higher order terms in the series add higher order contributions to the attenuator to improve its effectiveness towards an elimination of internal multiples. The algorithm presented is based on inverse scattering, and it goes further in the removal of first order internal multiples. Two closed forms were obtained and used in examples. The first one, adds the leading order terms elimination subseries and it is an algorithm that completely eliminates all first order internal multiples generated at the first reflector. The second closed form adds the main contribution of the higher order terms. It shows a better estimate of the amplitudes and provides an improvement towards the elimination of 1^{st} order internal multiples. In this theory, no assumptions about the earth below the receivers are made.

The examples presented in this report, show value when going further in the inverse series for 1^{st} order internal multiple elimination. However, they show that the effectiveness of the higher order closed form can be affected by interference of the events in the data, decreasing its extra

contribution. This is due to the fact that the elimination algorithms use events in the data to obtain the travel time and amplitude of the internal multiples. If a primary in the data is interfering with a multiple, then it appears to have an amplitude different to the actual one. Hence, when it is used as a subevent in the multiple elimination algorithm, the amplitude prediction is also affected by that interference.

The analytic study of the multiple elimination algorithms were performed with the only purpose of understanding the inner workings of the algorithm. The internal multiple elimination algorithm does not require any knowledge of the subsurface properties, neither the distinction between internal multiples, nor the knowledge of the location where the downward reflection took place. The internal multiple algorithm is a non-linear data driven algorithm that only requires a reference Green's function and the data.

The extension to a multidimensional earth was achieved for the leading order closed form term. The leading order eliminator provides the removal of all first order internal multiples generated at the shallowest reflector and effectively attenuates the rest of the multiples. The extension to a multidimensional earth of the higher order terms as well as extensions of definitions is our current subject of study.

Acknowledgments

We acknowledge and thank the sponsors and members of M-OSRP for the support of this research. We have been partially funded by and are grateful for NSF-CMG award DMS-0327778 and DOE Basic Sciences award DE-FG02-05ER15697.

References

F. V. Araújo. *Linear and non-linear methods derived from scattering theory: backscattering tomography and internal-multiple attenuation.* PhD thesis, Universidade Federal da Bahia, Brazil, 1994. in Portuguese.

F. V. Araújo, A. B. Weglein, P. M. Carvalho, , and R. H Stolt. Inverse scattering series for multiple attenuation: An example with surface and internal multiples. *SEG Expanded Abstracts, 1039-1041*, 1994.

P.M. Carvalho and A.B. Weglein. Wavelet estimation for surface multiple attenuation using a simulated annealing algorithm. *Expanded Abstr., 64th Ann. Internat. SEG Mtg., Los Angeles*, 1994.

Z. Guo, A. B. Weglein, and T.H. Tan. Using pressure data on the cable to estimate the seismic wavelet. *SEG Expanded Abstracts, 2390-2393*, 2005.

K A Innanen and A B Weglein. Viscoacustic born series continued: toward scattering-based q compensation/estimation. Technical report, M-OSRP 2002 annual report, 2003.

F. Liu, A.B. Weglein, K.A. Innanen, and B.G Nita. Extension of the non-linear depth imaging capability of the inverse scattering series to multidimensional media: strategies and numerical results. SEGf (Sociedade Brasileira de Geofísica) Expanded Abstracts, 2005.

K. Matson. The relationship between scattering theory and the primaries and multiples of reflection seismic data. *Journal of Seismic Exploration*, 5, 1996.

B. G. Nita, K. H. Matson, and A. B. Weglein. Forward scattering series and seismic events: Far field approximations, critical and postcritical events. *Society for Industrial and Applied Mathematics*, 64(6):21672185, 2004.

B. G. Nita and A. B. Weglein. Inverse scattering internal multiple attenuation algorithm in complex multi-d media: the pseudodepth/vertical-time monotonicity condition and higher order dimension analytic analysis. Technical report, M-OSRP. University of Houston, April 2005.

A. C. Ramírez and A.B. Weglein. An inverse scattering internal multiple elimination method: Beyond attenuation, a new algorithm and initial tests. *SEG Expanded Abstracts.*, pages 2115–2118, 2005a.

A. C. Ramírez and A.B. Weglein. Progressing the analysis of the phase and amplitude prediction properties of the inverse scattering internal multiple attenuation algorithm. *J. of Seismic Expl.*, 13:283–301, 2005b.

S. A. Shaw. Some remarks on the leading order imaging series algorithm for depth imaging when the velocity model is unknown. Technical report, M-OSRP. University of Houston, April 2005.

A. B. Weglein, F. V. Araujo, P. M. Carvalho, R. H. Stolt, K. H. Matson, R. T. Coates, D. Corrigan, D. J. Foster, S. A. Shaw, and H. Zhang. Topical review: Inverse scattering series and seismic exploration. *Inverse Problems*, 19:27–83, 2003.

A. B. Weglein, F. V. Araujo Gasparotto, P. M. Carvalho, and R. H. Stolt. An inverse-scattering series method for attenuating multiples in seismic reflection data. *Geophysics*, 62(6):1975–1989, 1997.

A. B. Weglein, W. E. Boyse, and J. E. Anderson. Obtaining three-dimensional velocity information directly from reflection seismic data: an inverse scattering formalism. *Geophysics*, 46:1116–1120, 1981.

A. B. Weglein and B.G. Secrest. Wavelet estimation for a multidimensional acoustic or elastic earth. *Geophysics, 55, no. 7, 902-913*, 1990.

H. Zhang and A.B. Weglein. The inverse scattering series for tasks associated with primaries: depth imaging and direct non-linear inversion of 1d variable velocity and density acoustic media. In *SEG Technical Program Expanded Abstracts*, pages 1705–1708. SEG, 2005.

A comparison of the imaging conditions and principles in depth migration algorithms

Bogdan G. Nita, Department of Mathematical Sciences, Montclair State University

Abstract

Seismic migration/inversion is presently the most used method for determining the structure and properties of the sub-surface in seismic exploration for hydrocarbons. Roughly speaking, determining the location of abrupt changes in medium's parameters involves, in one form or another, an imaging principle which can simply be stated by equating a component, or the full value of the travel-time t, with zero. Depending on the domain of definition of the imaged data, i.e. space-frequency or wavenumber-frequency, the imaging step has different implications, capabilities and produces different results. We analyze this principle for the depth migration procedures and point out that the space-frequency algorithms imply a total travel-time condition $t = 0$ while the wavenumber-frequency algorithms imply vertical intercept time condition $\tau = 0$. We present two analytic examples of the most common migration algorithms for both domains, i.e. $f-k$ migration for the wavenumber-frequency and Kirchhoff for the space-frequency algorithms, and discuss the implications of these differences.

1 Introduction

Seismic migration represents the shifting and focusing of the recorded reflections to their true position thus creating an image of the sub-surface under investigation. Most of the depth migration algorithms can be viewed as a two-step procedure in which the geophysical data is first downward-extrapolated to any depth and then imaged to its correct location by using an imaging principle. Depending on the domain in which the second step (imaging) is performed the algorithms can be divided into two broad categories: 1. space-frequency algorithms e.g. Kirchhoff (Schneider, 1978), 15° finite differences (Claerbout, 1981) etc. and 2. wavenumber-frequency algorithms e.g. phase-shift migration (Gazdag, 1978), $f-k$ migration (Stolt, 1978) etc. In this paper we compare the imaging step involved in these two types of algorithms and point out that the imaging condition in the space-frequency domain amounts to imposing a zero total travel time condition $t = 0$, while the imaging condition in the wavenumber-frequency domain amounts to imposing zero vertical intercept time condition $\tau = 0$. The two categories of migration algorithms have been illustrated through numerical results extensively in the literature, see e.g. Yilmaz (2001). Rather than providing redundant numerical instances, we find it useful to present two analytic examples which show some of the similarities and differences between the two types of algorithms. Given the wide application of the migration algorithms, it is important to have a good grasp and understanding of the mathematics and physics associated with their formulation. This in turn leads to a better understanding of their capability and consequently to the development of more accurate and complete imaging methods. This research impacts not only the migration methods but also other algorithms which implicitly use an imaging principle in their formulation, e.g. inverse

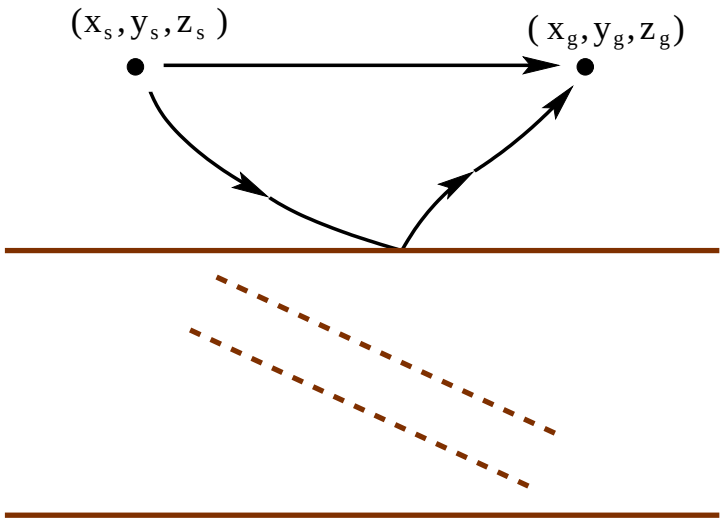

Figure 1: A typical seismic experiment over a multi-dimensional earth.

scattering methods and in particular internal multiple attenuation and imaging algorithms (see Weglein et al., 2003). We begin by describing the relationship between spherical waves and their Fourier planewave decomposition and concentrate on understanding the geometry and elements of one planewave component. We then briefly review two of the most common migration algorithms representative for the wavenumber-frequency and space-frequency domains, namely $f-k$ migration and Kirchhoff migration. We finally provide analytic examples for acoustic 1.5-D models emphasizing the imaging step in each of the two procedures. Conclusions are drawn in the last section.

2 Spherical waves and Fourier planewave decomposition

A typical seismic experiment involves man-made sources, of acoustic or elastic disturbances, and receivers, to capture these disturbances after traveling through the earth and interacting with different internal structures (see Figure 1). For a 3-dimensional acoustic inhomogeneous medium, with sources and receivers located on the earth surface at $z_s = z_g = 0$, and with the horizontal coordinates $\mathbf{x_s} = (x_s, y_s)$ and $\mathbf{x_g} = (x_g, y_g)$ respectively, the propagation of the waves through the medium is described by the Helmoltz equation

$$\nabla^2 P - \frac{1}{c^2}\frac{\partial^2 P}{\partial t^2} = -4\pi\delta(\mathbf{x_g} - \mathbf{x_s})\delta(t) \tag{1}$$

where P represents an acoustic wave propagating through an inhomogeneous medium whose spatially varying velocity is given by the function c. The homogeneous space ($c = c_0$) solution or the direct arrival can be described by

$$P_h(\mathbf{x_g}, 0, \mathbf{x_s}, 0, \omega) = \frac{e^{i\omega\frac{R}{c_0}}}{R} \tag{2}$$

where $R = \|\mathbf{x_g} - \mathbf{x_s}\| = \sqrt{(x_g - x_s)^2 + (y_g - y_s)^2}$ represents the distance between the source and receiver. Solutions corresponding to other arrivals can be obtained by adding boundary conditions describing the internal structure of the medium under investigation. For each abrupt change in the medium parameter, or interface, the incoming wave is broken down into a reflected and a transmitted wave, which satisfy the continuity conditions with regards to pressure and displacement. The recorded data

$$D(\mathbf{x_g}, \mathbf{x_s}, \omega) = P(\mathbf{x_g}, 0, \mathbf{x_s}, 0, \omega) \tag{3}$$

consists in all possible sesmic arrivals which result from such internal interactions.

Equation (1) can also be solved using Fourier transform methods (see e.g., Aki and Richards, 2002) to obtain the solutions in the Weyl integral form. The homogeneous solution will then have the form

$$P_h(\mathbf{x_g}, 0, \mathbf{x_s}, 0, \omega) = \frac{1}{2\pi i} \int_{-\infty}^{\infty} d\mathbf{k_g} \int_{-\infty}^{\infty} d\mathbf{k_s} \frac{e^{i(\mathbf{k_g}\cdot\mathbf{x_g} - \mathbf{k_s}\cdot\mathbf{x_s})}}{k_z} \tag{4}$$

where $\mathbf{k_g} = (k_{xg}, k_{yg})$, $\mathbf{k_s} = (k_{xs}, k_{ys})$ and we used different sign convention for the Fourier transform over the source and receiver coordinates. Here $k_z = q_s + q_g$ with q_s and q_g being the vertical source and receiver wavenumbers respectively, satisfying the dispersion relationships

$$q_g^2 + \|\mathbf{k_g}\|^2 = q_s^2 + \|\mathbf{k_s}\|^2 = \omega^2/c_0^2. \tag{5}$$

This solution can be interpreted as a continuous summation over all planewaves described by the horizontal wavenumbers $\mathbf{k_g}$ and $\mathbf{k_s}$. Each individual planewave satisfies the Fourier transformed Helmoltz equation and, in the presence of boundary condition, can be interpreted as the medium response to incoming planewaves. The data in this case will be the set of collected planewave events on the measurement surface and will be expressed through

$$\tilde{D}(\mathbf{k_g}, \mathbf{k_s}, \omega). \tag{6}$$

It is not difficult to see that the relationship between D and $\tilde{D}$ is

$$D(\mathbf{x_g}, \mathbf{x_s}, t) = \int_{-\infty}^{\infty} d\omega \int_{-\infty}^{\infty} d\mathbf{k_g} \int_{-\infty}^{\infty} d\mathbf{k_s} e^{-i(\omega t - \mathbf{k_g}\cdot\mathbf{x_g} + \mathbf{k_s}\cdot\mathbf{x_s})} \tilde{D}(\mathbf{k_g}, \mathbf{k_s}, \omega). \tag{7}$$

Notice that, to construct the point-source/point-receiver response, all the horizontal wavenumbers dependent planewave components are needed. The same is not true, for example, for a ray approximation where each event in the point-source/point-receiver response is approximated by one ray-like diagram. In the next section we discuss one planewave component and look at its geometry, propagation and ways of characterizig its turning point or reflection from an interface.

3 The geometry of planewaves

Figure 2 shows a planewave component with the typical quantities attached to it, i.e. the angle of incidence θ, the ray perpendicular to the wavefront indicating the direction of propagation, the velocity of propagation of the planewave c_0 and the vertical and horizontal intercept velocities c_v and c_h. The intercept velocities are dependent on the incidence angle θ and usually are larger than

c_0 (with the exception of vertical or horizontal propagation in which case one of them is equal to c_0 and the other is zero) and for oblique incidence have the expressions

$$c_h = \frac{c_0}{\sin\theta} \tag{8}$$

and

$$c_v = \frac{c_0}{\cos\theta}. \tag{9}$$

The quantities $\frac{1}{c_h}$ and $\frac{1}{c_v}$ and called the horizontal and vertical slowness respectively and are denoted by p and q. The wavefront of the planewave can be viewed as an infinite line in the $z-x$ domain having the equation

$$z = z_0 - x\tan\theta \tag{10}$$

where z_0 is the intercept between the front of the planewave and the vertical axis. To indicate that the planewave is moving downward it is necessary to have only this z-intercept advance on the vertical axis as

$$z = c_v t - x\tan\theta, \tag{11}$$

where t is the traveltime, or

$$z = c_0\frac{t}{\cos\theta} - x\tan\theta. \tag{12}$$

Solving for the total travel-time from equation (12) we find

$$t = z\frac{\cos\theta}{c_0} + x\frac{\sin\theta}{c_0}. \tag{13}$$

The quantity

$$\tau_s = z\frac{\cos\theta}{c_0} \tag{14}$$

is called the vertical intercept time and has the units of time (seconds). The subscript s indicates the fact that the quantity is specific to the source-reflector leg. A similar expression, possibly with a different reflection angle, can be written for τ_g, the vertical time for the reflector-receiver leg. The total vertical time for the planewave seismic event is defined as

$$\tau = \tau_s + \tau_g. \tag{15}$$

In terms of the vertical time τ_s and the horizontal slowness p defined above equation (13) can now be re-written as

$$t = \tau_s + xp. \tag{16}$$

Equation (13) describes the time at which the planewave will pass any (x,z) point in the 2-dimensional plane. To describe the time shift of this planewave as it moves along its ray from the source to the receiver, we represent the planewave as

$$\phi = e^{-i\omega(t-t_0)} = e^{-i\omega(t-z\frac{\cos\theta}{c_0}-x\frac{\sin\theta}{c_0})}. \tag{17}$$

A similar expression can be written for the reflector-to-receiver leg of the planewave propagation. Comparing this relation with the kernel of the Fourier transform in the expression (7) we discover the relations between the horizontal wavenumbers and the incidence angle

$$\sin\theta = \frac{\|\mathbf{k_s}\|}{\omega/c_0} \tag{18}$$

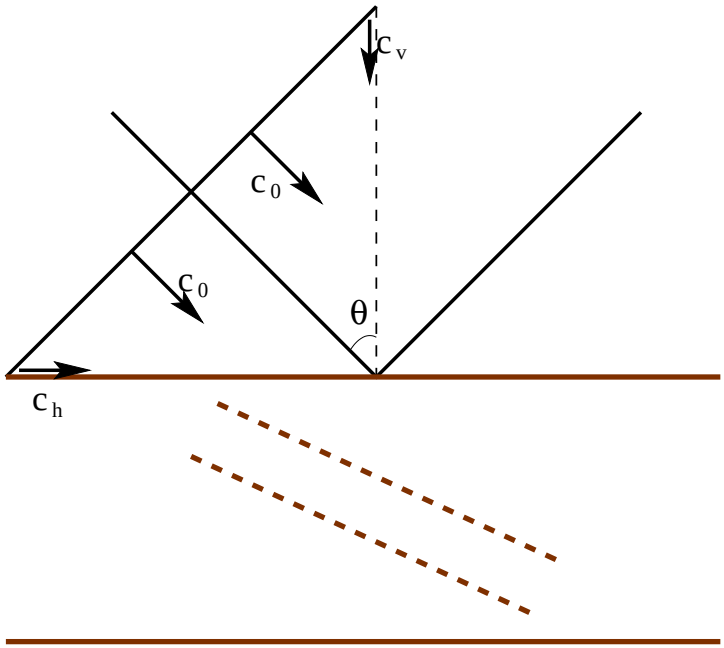

Figure 2: A plane wave component: downgoing ray and wavefront.

and

$$\cos\theta = \frac{q_s}{\omega/c_0}. \tag{19}$$

Eliminating the angle between equations (19) and (14) we find

$$\tau_s = z\frac{q_s}{\omega}. \tag{20}$$

Similarly for the reflection-receiver leg we can write

$$\tau_g = z\frac{q_g}{\omega} \tag{21}$$

or, after adding the two equations

$$\tau = \frac{k_z z}{\omega}. \tag{22}$$

As expected, the vertical intercept time of a planewave is only dependent on the vertical wavenumber k_z, the depth coordnate z and the frequency ω.

The importance of equation (22) comes from the fact that the expression $k_z z$ is the phase used to downward extrapolate planewave components in wavenumber-frequency seismic depth migration. Such a relation shows that the time component which varies in the downward extrapolation step is the vertical intercept time and it also offers a hint for interpreting the integration over frequency in the imaging principle. This concept along with the imaging conditions in wavenumber-frequency and space-frequency domains will be discussed in the following sections.

4 Pre-stack depth migration algorithms

We start with the data set $D(\mathbf{x_g}|\mathbf{x_s};t)$ depending on the source and receiver horizontal coordinates $\mathbf{x_s} = (x_s, y_s)$ and $\mathbf{x_g} = (x_g, y_g)$ and the total travel-time t measured from the source's explosion. For simplicity we assume that both sources and receivers are located on the earth's surface at depth $z = 0$. The data can then be represented as a wavefield P such that

$$P(\mathbf{x_g}, 0|\mathbf{x_s}, 0; t) = D(\mathbf{x_g}|\mathbf{x_s}; t). \tag{23}$$

To downward extrapolate this wave field we first Fourier transform it to the wavenumber-frequency domain

$$P(\mathbf{k_g}, 0|\mathbf{k_s}, 0; \omega) = \int d\mathbf{x_g} d\mathbf{x_s} dt e^{i(\omega t - \mathbf{k_g}\cdot\mathbf{x_g} + \mathbf{k_s}\cdot\mathbf{x_s})} P(\mathbf{x_g}, 0|\mathbf{x_s}, 0; t), \tag{24}$$

where we used different sign conventions for Fourier transforms over source and receiver coordinates. In the formula above $\mathbf{k_g} = (k_{xg}, k_{yg})$ and $\mathbf{k_s} = (k_{xs}, k_{ys})$ are the horizontal wavenumbers associated with the source and receiver horizontal positions $\mathbf{x_s}$ and $\mathbf{x_g}$ respectively. The effect of these transformations is a mono-chromatic planewave decomposition of the recoded signal. The quantity $P(\mathbf{k_g}, 0|\mathbf{k_s}, 0; \omega)$ can be viewed as the medium's response, recorded on the measurement surface, due to a set of planewaves characterized by the frequency ω and the horizontal wavenumbers $\mathbf{k_s}$ (from the source surface to the reflector) and $\mathbf{k_g}$ (from the reflector to the measurement surface). The wavefront of any such planewave is an infinite plane in the xyz space whose upward or downward propagation is described by the advance of the $z-$intercept on the vertical axis. In other words, in the wavenumber-frequency domain, the phase of any event will account only for this up-down propagation. As a consequence, the planewave response can be downward extrapolated by using a phase-shift operator on the vertical component only

$$P(\mathbf{k_g}, z|\mathbf{k_s}, z; \omega) = P(\mathbf{k_g}, 0|\mathbf{k_s}, 0; \omega) e^{ik_z z} \tag{25}$$

where, as before, $k_z = q_s + q_g$ and q_s and q_g are the medium dependent vertical source and receiver wavenumbers respectively. As emphasized earlier, since the only space component that varies in the downward extrapolation process is the z-intercept, it is clear that the only variable time component is the vertical intercept time τ (see equation (22))

$$\tau = k_z z/\omega. \tag{26}$$

Summing over all frequency components, by performing either an integral over ω, (Gazdag, 1978), or over k_z, (Stolt, 1978), while the data is in the wavenumber-frequency domain is thus equivalent to a vertical intercept time $\tau = 0$ imaging condition. The last step in the migration procedure is an inverse Fourier transform over the horizontal wavenumbers to convert the imaged data back to the space domain. The result of this transformation is an image, denoted I_1, of the subsurface

$$I_1(x, y, z) = \int d\mathbf{k_g} d\mathbf{k_s} e^{i(\mathbf{k_g} - \mathbf{k_s})\cdot\mathbf{x}} d\omega P(\mathbf{k_g}, z|\mathbf{k_s}, z; \omega). \tag{27}$$

where $\mathbf{x}$ denotes the horizontal position vector (x, y). The full migration procedure can hence be written as

$$I_1(x, y, z) = \int d\mathbf{k_g} d\mathbf{k_s} e^{i(\mathbf{k_g} - \mathbf{k_s})\cdot\mathbf{x}} d\omega e^{ik_z z} \int d\mathbf{x_g} d\mathbf{x_s} dt e^{i(\omega t - \mathbf{k_g}\cdot\mathbf{x_g} + \mathbf{k_s}\cdot\mathbf{x_s})} D(\mathbf{x_g}|\mathbf{x_s}; t). \tag{28}$$

To obtain a version of this migration procedure in the space-frequency domain we re-arrange the order of integration in formula (28) while keeping the data in the frequency domain to obtain

$$I_2(x,y,z) = \int d\mathbf{x_g} d\mathbf{x_s} d\omega D(\mathbf{x_g}|\mathbf{x_s};\omega) \int d\mathbf{k_g} d\mathbf{k_s} e^{i(k_z z - \mathbf{k_g}\cdot(\mathbf{x_g}-\mathbf{x}) + \mathbf{k_s}\cdot(\mathbf{x_s}-\mathbf{x}))}. \tag{29}$$

The last set of integrals over the horizontal wavenumbers is usually evaluated using a stationary phase approximation (see e.g., Bleistein and Hendelsman, 1975) to obtain an approximative migration formula commonly called Kirchhoff migration, see e.g. Schneider (1978) and Stolt and Benson (1986). Formula (29) describes a weighted summation along diffraction hyperbolas in the original data. Since the data is now in the space-frequency domain, the phase of each event must account for both vertical and lateral propagation. This implies that an integration over frequency is equivalent to a total travel-time, $t = 0$, imaging condition.

The re-arrangement of integrals and their calculation in a different order have a significant effect, producing a different result in the two migration versions, and consequently a different image. This can be easily seen from the dispersion relations (5). For the wavenumber-frequency migration described by formula (28), the integral over ω is performed while keeping the horizontal wavenumbers constant. In this case, we can think of $(\mathbf{k_g}, \mathbf{k_s}, \omega)$ or $(\mathbf{k_g}, \mathbf{k_s}, k_z)$ as independent variables. It also implies that the vertical wavenumber k_z varies as a function of ω when performing the imaging step while $\mathbf{k_g}$ and $\mathbf{k_s}$ remain constant. For the space-frequency migration described by formula (29) the inner most integrals in $\mathbf{k_g}$ and $\mathbf{k_s}$ are performed while keeping the frequency constant. This implies that $\mathbf{k_g}$, $\mathbf{k_s}$ and k_z are no longer independent and one has to consider k_z as a function of both $\mathbf{k_g}$ and $\mathbf{k_s}$. Approximating the inner most integral in equation (29) using high frequency approximations (as one usually does in Kirchoff migration) results in a ray-path assumption for the seismic events and imposes a well defined relationship between the wavenumbers and frequency. This relation is used when integrating over frequencies and hence performing the imaging step in the space-frequency migration. These concepts will be made clearer in the analytic examples discussed below.

Imaging with the vertical intercept time $\tau = 0$ and with total travel-time $t = 0$ and the relation with the inverse scattering internal multiple attenuation algorithm was discussed by Nita and Weglein (2004) and Nita and Weglein (2005). They show that 1. the constant velocity pre-stack migration built into the algorithm is using a $\tau = 0$ imaging condition and 2. the pseudo-depth monotonicity condition can be translated into vertical time monotonicity. Both conclusions, along with the present research, are significant in understanding the efficiency, capabilitites and limitations of the multiple attenuation algorithm and its different castings in other domains. The two analytic examples described below will further point out the advantages of using the $\tau = 0$ condition, or more generally, a wavenumber-frequency depth migration procedure.

5 Analytic example: wavenumber-frequency domain migration

Consider a one-dimensional model consisting of two half-spaces with the interface located at depth z_a (see Figure 3). The space-frequency domain data, $D(x_h;\omega)$, or the associated wavefield,

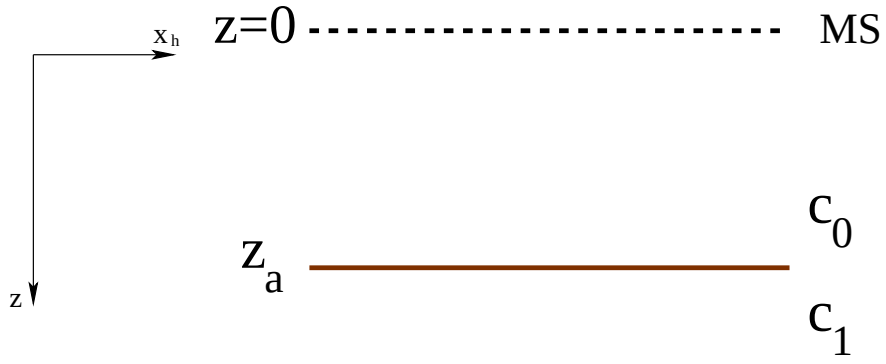

Figure 3: *The model for the analytic 1.5D example.*

$P(x_h, 0; \omega)$, for such an experiment can be expressed as

$$P(x_h, 0; \omega) = \frac{1}{2\pi} \int_{-\infty}^{\infty} dk_h \frac{R(k_h)}{ik_z} e^{ik_h x_h} e^{-ik_z z_a} \tag{30}$$

(see e.g., Aki and Richards, 2002), where R is the angle dependent reflection coefficient. Depending on the offset x_h this expression includes the primary (pre- or post-critical reflection) and the headwave. In applying the $f-k$ migration algorithm to the data, we make use of a slightly modified migration operator which is defined in terms of the time derivative of the space-time domain data rather than the data itself (see e.g. Stolt and Benson, 1986). In the frequency domain this amounts to multiplying by an $i\omega$ factor and hence use the modified data

$$P'(x_h, 0; \omega) = \frac{\omega}{2\pi} \int_{-\infty}^{\infty} dk_h \frac{R(k_h)}{k_z} e^{ik_h x_h} e^{-ik_z z_a}. \tag{31}$$

Fourier transforming over the space coordinate we obtain

$$P'(k_h, 0; \omega) = \frac{\omega}{k_z} R(k_h) e^{-ik_z z_a} \delta(k_g - k_s). \tag{32}$$

We next apply a phase-shift on both the source and receiver depth coordinates and obtain

$$P'(k_h, z; \omega) = \frac{\omega}{k_z} R(k_h) e^{ik_z (z - z_a)} \delta(k_g - k_s). \tag{33}$$

Notice that, consistent with the previous analysis, the phase of the events contains information only about vertical propagation (and hence vertical intercept time τ). Applying the imaging condition by integrating over frequency we find

$$I_1(k_h, z) = R(k_h) \delta(k_g - k_s) \int d\omega \frac{\omega}{k_z} e^{ik_z (z - z_a)}. \tag{34}$$

It is obvious at this point that the integral over ω will produce a delta like event at the correct depth z_a. However we can change the variable of integration from ω to k_z hence switching from

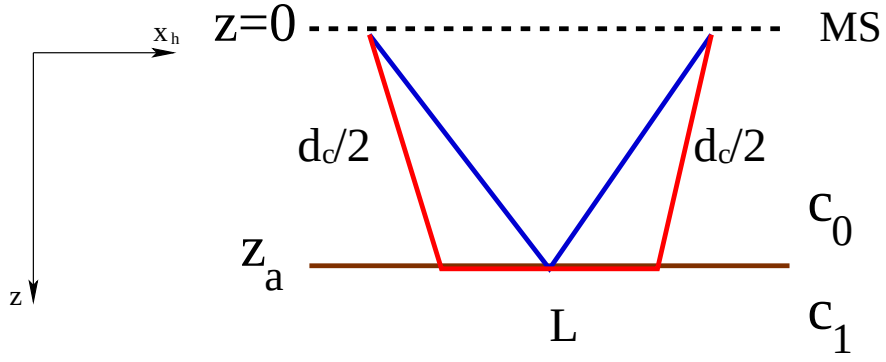

Figure 4: *Post-critical data consisting of a reflection and a headwave arrival.*

plain phase-shift migration to $f-k$ migration. The relationship between ω and k_z is

$$\omega = \frac{k_z c}{2}\sqrt{1+\frac{k_h^2}{k_z^2}} \tag{35}$$

and so we also have

$$\frac{\omega}{k_z}d\omega = \frac{c^2}{4}dk_z. \tag{36}$$

With this change of variable, and after integrating over k_z, the last integral becomes

$$I_1(k_h,z) = R(k_h)\delta(k_g-k_s)\frac{c^2}{4}\delta(z-z_a). \tag{37}$$

This last formula shows that the wavenumber-frequency domain migration procedure with the vertical intercept time $\tau=0$ imaging condition has placed the angle dependent reflection coefficient at the correct depth for all pre-critical, post-critical and critical events. An additional inverse Fourier transform may be performed to obtain the image in (x,z) space.

6 Analytic example: space-frequency domain migration

For the second example we use the same model described above (see Figure 3). As before we start with the data in the space-frequency domain

$$D(x_h,\omega) = \frac{1}{2\pi}\int_{-\infty}^{\infty} dk_h \frac{R(k_h)}{ik_z}e^{ik_h x_h}e^{-ik_z z_a}. \tag{38}$$

The integral above can be approximated using a stationary phase formula to obtain (see e.g. Aki and Richards, 2002)

$$D(x_h,\omega) = \frac{R(x_h)}{d_0}e^{-i\omega t_R} + A(x_h,\omega)e^{-i\omega t_H}. \tag{39}$$

In this equation the first term describes the seismic reflection and the second the headwave which exists for post-critical offsets only (see Figure 4). In the first term, the reflection coefficient R is a function of offset x_h, d_0 represents the total distance from the source to the reflector and to the receiver along a ray-like path and $t_R = d_0/c_0$ represents the total travel-time. In the second term A is an amplitude factor which has the approximate value

$$A(x_h, \omega) = \frac{i}{\omega} \frac{c_0^2}{\left(1 - c_0^2/c_1^2\right)} \frac{1}{r^{1/2} L^{3/2}}, \tag{40}$$

with L being the length of the propagation path of the headwave along the interface, and

$$t_H = d_c/c_0 + L/c_1, \tag{41}$$

is the total travel-time for the headwave arrival, with d_c being the total distance from the source to the interface and back to the receiver along the critical ray path (see Figure 4). Notice that in the expression (39), consistent with the previous analysis, the phase of each event contains information about the total travel-time of that arrival; this is a direct consequence of expressing the data in the space-frequency domain.

We next apply equation (29) to the data described by equation (39) and find

$$I_2(x_h, z) = \int dx_h d\omega D(x_h; \omega) \int dk_h e^{i(k_h x_h + k_z z)}. \tag{42}$$

Notice that k_z and k_h are no longer independent variables and, in fact, we can consider k_z to be a function of k_h described by the dispersion relations. The inner most integral is approximated using the stationary phase formula

$$\int dk_h e^{if(k_h)} \approx \sqrt{\frac{2\pi i}{f''(k_h^0)}} e^{if(k_h^0)} \tag{43}$$

where k_h^0 is the stationary point for $f(k_h)$ found by solving $f'(k_h) = 0$. For our discussion the function f is

$$f(k_h) = x_h k_h + z\sqrt{(\omega/c_0)^2 - k_h^2}. \tag{44}$$

Solving the equation $f'(k_h^0) = 0$ we find the stationary point k_h^0 to be

$$k_h^0 = \frac{\omega x_h}{c_0 d} \tag{45}$$

where $d = \sqrt{x_h^2 + z^2}$. The values of the function f and of its second derivative f'' at this stationary point are $f(k_h^0) = \frac{\omega}{c_0} d$ and $f''(k_h^0) = -\frac{c_0 d^3}{\omega z^2}$ respectively. Putting all these in formula (42) we find the inner most integral to be

$$\int dk_h e^{i(k_h x_h + k_z z)} \approx \frac{z}{d} \sqrt{\frac{2\pi\omega}{i c_0 d}} e^{i\frac{\omega}{c_0} d} \tag{46}$$

and so the image I_2 becomes

$$I_2(x_h, z) = \int dx_h d\omega D(x_h; \omega) \frac{z}{d} \sqrt{\frac{2\pi\omega}{i c_0 d}} e^{i\frac{\omega}{c_0} d}. \tag{47}$$

With the data given by equation (39) the migration procedure yields

$$I_2(x_h,z)=\int dx_h \frac{R(x_h)}{d_0}\frac{z}{d}\sqrt{\frac{2\pi}{ic_0 d}}\int d\omega\sqrt{\omega}e^{i\frac{\omega}{c_0}(d-d_0)}+\int dx_h \frac{z}{d}\sqrt{\frac{2\pi}{ic_0 d}}\int d\omega\sqrt{\omega}A(x_h,\omega)e^{i\omega\left(\frac{d}{c_0}-t_H\right)}. \tag{48}$$

The main conclusions inferred from the equation above are that, first, the integration over the frequency ω amounts to a total travel-time imaging condition $t=0$ and, second, the imaging step places the reflection at the correct and the headwave at the incorrect spatial location. Imaging with $t=0$ is a direct consequence of the domain of the imaged data, in this case space-frequency, and, even for simple cases, creates false images.

7 Conclusions

In this paper we discuss the application of the imaging principle in depth migration algorithms and its dependence on the domain in which it is applied. We show that an integration over the frequency amounts to a total travel-time $t=0$ condition when the data is in the space-frequency domain and to a vertical intercept time $\tau=0$ condition when the data is in the wavenumber-frequency domain. We describe two of the most common depth migration methods representative of the two imaging domains and show that even though their formulation is similar (compare equations (28) and (29)) involving, besides approximations, only a different integration order, the results can be very different. The two analytic examples we discuss emphasize one important distinction in their ability to handle refracted events (headwaves). This research provides new insights into the mathematical formulation and physical interpretation of depth migration algorithms. Understanding the differences and capabilities of the imaging principles is the key to developing more accurate and complete imaging methods. The results described in this paper impact not only the migration schemes but also others which use the imaging principle implicitly, e.g. inverse scattering methods and in particular the internal multiple attenuation algorithm.

Acknowledgments

This work was partially supported by NSF-CMG award DMS-0327778 and DOE Basic Sciences award DE-FG02-05ER15697. The author thanks Sam Kaplan for his suggestions in improving this manuscript. M-OSRP support is also gratefully acknowledged.

References

Keiti Aki and Paul G. Richards. *Quantitative Seismology.* Second Edition, University Science Books, 2002.

Norman Bleistein and Richard A. Hendelsman. *Asymptotic Expansions of Integrals.* Holt, Rinehart and Winston, 1975.

Jon Claerbout. *Fundamentals of geophysical data processing.* Blackwell Scientific Publications, Inc., 1981.

Jeno Gazdag. Wave equation migration with the phase-shift method. *Geophysics*, 43(7):1342–1351, 1978.

Bogdan G. Nita and Arthur B. Weglein. Imaging with $\tau = 0$ versus $t = 0$: implications for the inverse scattering internal multiple attenuation algorithm. *74th Annual International Meeting, SEG, Expanded Abstracts*, pages 1289–1292, 2004.

Bogdan G. Nita and Arthur B. Weglein. Inverse scattering internal multiple attenuations algorithm in complex multi-d media. Technical report, Mission Oriented Seismic Research Project, University of Houston, 2005.

William A. Schneider. Integral formulation for migration in two and three dimensions. *Geophysics*, 43(1):49–76, February 1978.

R. H. Stolt. Migration by fourier transform. *Geophysics*, 43(1):23–48, 1978.

Robert H. Stolt and Alvin K. Benson. *Seismic Migration: Theory and Practice*, volume 5 of *Seismic Exploration*. Geophysical Press, 1986.

Arthur B. Weglein, Fernanda V. Araújo, Paulo M. Carvalho, Robert H. Stolt, Kenneth H. Matson, Richard T. Coats, Dennis Corrigan, Douglas J. Foster, Simon A. Shaw, and Haiyan Zhang. Inverse scattering series and seismic exploration. *Inverse Problems*, (19):R27–R83, 2003.

Öz Yilmaz. *Seismic Data Analysis: Processing, inversion and Interpretation of Seismic Data.* Society of Exploration Geophysicists, 2001.

A sub-event interpretation of the non-linear equations of daylight imaging

Kristopher A. Innanen

Abstract

The underlying equations of daylight imaging (in particular of Claerbout, 1968), in addition to many variants of data-driven free-surface and internal multiple elimination methods, are non-linear, but low-order, in the input data. The latter are often discussed, both anecdotally and in the literature, within the framework of a sub-event interpretation, that links the events of the processing output (multiples) with the generative events of the processing input (primaries and lower-order multiples). Such an interpretation is possible and, in at least a heuristic way, valuable for the former also. For instance, early-time events of a reflected data set, constructed from non-linearly combined transmitted data sets, are seen to require "hidden" infinite series and the contribution of events spanning the full time of the input data.

1 Introduction

Many contemporary processing techniques for seismic data involve operations that are non-linear (although perhaps low-order) in the input data. For instance this is a hallmark of all flavors of free-surface multiple removal (e.g., Weglein et al., 1997; Verschuur et al., 1992), internal multiple attenuation (Weglein et al., 1997), and, furthermore, the interrelation of reflected and transmitted wave field responses that underlies the equations of acoustic daylight imaging (Claerbout, 1968; Wapenaar, 2003; Schuster, 2004; etc.). The multiple methods have benefited heuristically and practically by having had associated with them a "sub-event" interpretation (e.g., Weglein and Matson, 1998). An inter-data non-linearity within a processing routine means, in practice, a multiplicative combination of the amplitudes of events in the data, and a summed combination of the phases of these events. The phase of a first-order free-surface multiple, for instance, is constructible via the sum of the phases of two primaries. The consideration of non-linear processing algorithms as such contributes to an intuitive understanding of their behavior. Furthermore, an elucidation of the sub-event model with simple analytical examples goes even further to this end; the sub-event and 1D normal incidence, single-layer analytic example of Weglein and Matson has been sufficient to capture much of the core behavior of the full theory of internal multiple attenuation (discussed in greater detail by, e.g., Nita and Weglein, 2005).

A sub-event interpretation of the equations of daylight imaging, similar to that of the multiple methods, is possible; in fact, as I demonstrate in this note, it is not unreasonable to think of these equations themselves as being a different kind of non-linear "multiple method". The result is a heuristic model for the mechanics by which specific subsets of the events in a transmitted seismic data set may non-linearly interact to produce specific reflection events. Beyond this, I will point out at least one aspect of these equations that may not be immediately obvious from a study of the mathematics of the construction in the absence of such a heuristic.

2 Reflected and transmitted data over a single layer

To begin with I consider two data sets arising from a plane source normally incident upon a single layer, the top interface of which is chosen to be coincident with the receiver. The interfaces are considered to be step changes in impedance, the exact nature of which is not relevant to the phase issues at hand, but which give rise to reflection coefficients that then appear in the data. A reflection data set is generated by placing the source plane such that it is coincident with the receiver plane, at the top interface of the layer (Figure 1); a transmission data set is generated by placing the source plane coincident with the bottom interface (Figure 2). Foregoing, as indicated, a particular consideration of the amplitudes as they relate to reflection/transmission coefficients, but labelling them unambiguously, the reflected data, transmitted data, and conjugate transmitted data, in the frequency domain, are given by

$$\begin{aligned} R(\omega) &= P_r e^{i2\frac{\omega}{c_1}z_1} + M_r^1 e^{i4\frac{\omega}{c_1}z_1} + M_r^2 e^{i6\frac{\omega}{c_1}z_1} + ... \\ T(\omega) &= D_t e^{i\frac{\omega}{c_1}z_1} + M_t^1 e^{i3\frac{\omega}{c_1}z_1} + M_t^2 e^{i5\frac{\omega}{c_1}z_1} + ... \\ T^*(\omega) &= D_t^* e^{-i\frac{\omega}{c_1}z_1} + M_t^{1*} e^{-i3\frac{\omega}{c_1}z_1} + M_t^{2*} e^{-i5\frac{\omega}{c_1}z_1} + ... \end{aligned} \tag{1}$$

Figure 1 illustrates the events that arise from these two experiments, in the former, a single primary followed by a train of "surface-related" reverberations, and in the latter, a single direct wave, again followed by a train of reverberations. Claerbout's equations of daylight imaging, and the surface-related multiple prediction/elimination equations, both reduce to very simple non-linear data computations in the presence of media/experimental configurations as simple as those undertaken here. The aim in this letter is to carry these calculations out and make what comments may be made.

3 Free-surface multiple prediction: sub-event data activity

I begin in this section by discussing the (well-known) sub-event interpretation of the free-surface multiple prediction algorithm in regular use (in its multidimensional forms, of course) in the industry. Most derivations of the methodology express the output (predicted) multiples as an infinite series in the input data (with primaries and multiples), truncated at the term that is second order in the data; a form of optimization then occurs to compensate for this truncation as well as, for instance, the lack of prior knowledge of the source wavelet (e.g., Verschuur, 1992). In the full wave-theory derivation behind the inverse scattering series approach (Weglein et al., 1997), with a prior estimate of the source wavelet and the computation of up to the n'th term in the series no subtraction process is required up to the n'th order multiple. The normally utilized second order truncation followed by optimization leads to the framework of "prediction and subtraction" tasks of surface-related multiple processing. In this note I pay no attention to the "subtraction" portion and focus entirely on the phase aspects of this brand of non-linear processing for second and third order series truncations. As such, the finished products of the non-linear processing are defined to be $M^{(2)}$, the nominally computed multiple prediction that is second order in the measured data, and $M^{(3)}$, the third-order term that is the data convolved with $M^{(2)}$. In the presence of a wavelet, which I do not consider here, these quantities are in error in amplitude and in phase.

At this near-trivial level of complexity, the first quantity of interest is simply the product of the reflected data with itself, thus:

$$\begin{aligned}
M^{(2)}(\omega) =& R(\omega)R(\omega) \\
=& \left[P_r e^{i2\frac{\omega}{c_1}z_1} + M_r^1 e^{i4\frac{\omega}{c_1}z_1} + M_r^2 e^{i6\frac{\omega}{c_1}z_1} + ...\right]^2 \\
=& P_r P_r e^{i4\frac{\omega}{c_1}z_1} + P_r M_r^1 e^{i6\frac{\omega}{c_1}z_1} + P_r M_r^2 e^{i8\frac{\omega}{c_1}z_1} + ... \\
&+ M_r^1 P_r e^{i6\frac{\omega}{c_1}z_1} + M_r^1 M_r^1 e^{i8\frac{\omega}{c_1}z_1} + ... \\
&+ M_r^2 P_r e^{i8\frac{\omega}{c_1}z_1} + ... \\
=& (P_r P_r) \underbrace{e^{i4\frac{\omega}{c_1}z_1}}_{\text{1st multiple}} + \left(P_r M_r^1 + M_r^1 P_r\right) \underbrace{e^{i6\frac{\omega}{c_1}z_1}}_{\text{2nd multiple}} + \left(P_r M_r^2 + M_r^1 M_r^1 + M_r^2 P_r\right) \underbrace{e^{i8\frac{\omega}{c_1}z_1}}_{\text{3rd multiple}} + ...,
\end{aligned} \tag{2}$$

meanwhile the second quantity is

$$\begin{aligned}
M^{(3)}(\omega) \approx& M^{(2)}(\omega)R(\omega) \\
=& \left[(P_r P_r)\, e^{i4\frac{\omega}{c_1}z_1} + \left(P_r M_r^1 + M_r^1 P_r\right) e^{i6\frac{\omega}{c_1}z_1} + \left(P_r M_r^2 + M_r^1 M_r^1 + M_r^2 P_r\right) e^{i8\frac{\omega}{c_1}z_1} + ...\right] \\
&\times \left[P_r e^{i2\frac{\omega}{c_1}z_1} + M_r^1 e^{i4\frac{\omega}{c_1}z_1} + M_r^2 e^{i6\frac{\omega}{c_1}z_1} + ...\right] \\
=& (P_r P_r P_r) \underbrace{e^{i6\frac{\omega}{c_1}z_1}}_{\text{2nd multiple}} + \left(P_r P_r M_r^1 + P_r M_r^1 P_r + M_r^1 P_r P_r\right) \underbrace{e^{i8\frac{\omega}{c_1}z_1}}_{\text{3rd multiple}} + ... \quad .
\end{aligned} \tag{3}$$

This second quantity is, ultimately, added to the first after weighting by (1) the inverse source wavelet and (2) an obliquity factor, if the wave-theory based algorithm (Weglein et al., 1997) is used; the full problem involves the construction and weighted addition of the full series $M^{(n)}$. The purpose here is to point out several facets of this term-by-term construction; these points will be set in contrast to the sub-event interpretation of the Claerbout equations in the next section. The points can be easily verified from inspection of equations (2) and (3), since the provenance of sub-event contributions is visible through the event amplitudes, which are "labelled".

1. *The multiple prediction $M^{(n)}$, as n grows, is the last term to include a contribution to the $n-1$'th order multiple (for instance, $M^{(3)}$ has no contribution at the phase of the first-order multiple). No finite-order multiple requires an infinite number of computed terms for its construction/elimination.*

2. *At any order, no contribution to any multiple prediction/elimination is an infinite series. Rather, at that n, the set of all sub-events whose sum-of-orders is equal are collected and summed to contribute to a specific multiple. Especially at low orders, this is generally a small selection of data events.*

4 Transmission-to-reflection response mapping: sub-event data activity

The Claerbout equations underlying acoustic daylight imaging, which in essence compute a reflection data set, as defined in the first section, from the cross-correlation of two transmission data

sets, have been extended to multiple dimensions through the use of reciprocity relations and certain assumptions regarding the phase of the recorded wave field (see previous references). There are mechanical similarities between this procedure and the surface multiple construction/elimination procedure discussed in the previous section. A sub-event interpretation of this mapping highlights these similarities, and also outlines some interesting differences.

There is no infinite series to be computed (i.e., approximated) in the transmission-to-reflection data mapping; the procedure requires a single second-order operation on the transmitted data. Using the data generated in section 2, the construction of the physically meaningful "side of the autocorrelation of the seismogram", (Claerbout, 1968), $R(\omega) = T(\omega)T^*(\omega)$, is, in detail,

$$
\begin{aligned}
T(\omega)T^*(\omega) = \quad & \left[D_t e^{i\frac{\omega}{c_1}z_1} + M_t^1 e^{i3\frac{\omega}{c_1}z_1} + M_t^2 e^{i5\frac{\omega}{c_1}z_1} + ...\right] \\
& \times \left[D_t^* e^{-i\frac{\omega}{c_1}z_1} + M_t^{1*} e^{-i3\frac{\omega}{c_1}z_1} + M_t^{2*} e^{-i5\frac{\omega}{c_1}z_1} + ...\right] \\
= \quad & D_t D_t^* e^{i0\frac{\omega}{c_1}z_1} + ... \\
& + M_t^1 D_t^* e^{i2\frac{\omega}{c_1}z_1} + M_t^{1*} M_t^1 e^{i0\frac{\omega}{c_1}z_1} + ... \\
& + M_t^2 D_t^* e^{i4\frac{\omega}{c_1}z_1} + M_t^2 M_t^{1*} e^{i2\frac{\omega}{c_1}z_1} + M_t^2 M_t^{2*} e^{i0\frac{\omega}{c_1}z_1} + ... \\
& + M_t^3 D_t^* e^{i6\frac{\omega}{c_1}z_1} + M_t^3 M_t^{1*} e^{i4\frac{\omega}{c_1}z_1} + M_t^3 M_t^{2*} e^{i2\frac{\omega}{c_1}z_1} + M_t^3 M_t^{3*} e^{i0\frac{\omega}{c_1}z_1} + ... \\
= \quad & \left(D_t D_t^* + M_t^{1*} M_t^1 + M_t^2 M_t^{2*} + M_t^3 M_t^{3*} + ...\right) \underbrace{e^{i0\frac{\omega}{c_1}z_1}}_{\text{direct wave}} \\
& + \left(M_t^1 D_t^* + M_t^2 M_t^{1*} + M_t^3 M_t^{2*} + ...\right) \underbrace{e^{i2\frac{\omega}{c_1}z_1}}_{\text{primary}} \\
& + \left(M_t^2 D_t^* + M_t^3 M_t^{1*} + ...\right) \underbrace{e^{i4\frac{\omega}{c_1}z_1}}_{\text{1st multiple}} \\
& + \left(M_t^3 D_t^* + ...\right) \underbrace{e^{i6\frac{\omega}{c_1}z_1}}_{\text{2nd multiple}} \\
& + ...
\end{aligned}
\tag{4}
$$

As in the case of the surface-related multiple prediction/elimination algorithm, the transmission sub-events that contribute to the creation of meaningful reflection events are discernable through their labels, e.g., D_t is the transmitted direct wave. With Figure 2 as a guide, the sub-event contribution scheme entailed by $T(\omega)T^*(\omega)$ is visible. All events with the same difference-in-order are combined, and these contribute to the construction of the reflection event at that difference-in-order. For instance, all multiples that differ by one order contribute to the construction of the first order data event, the reflected primary. The constructed primary has a "path" equivalent to that not shared by the two sub-event multiples. A similar commentary is made by Schuster et al. (2004) in the development of their interferometry equations. Remarks follow.

1. *Reverberations, or multiples, in the transmitted wave field are critical to the construction of every important event in the output reflected wave field, including the primaries (see the contributions to the primary in equation 4).*

2. *The full construction of each event, including the primary, requires an infinite series. The series for the primary, for instance, involves the product of all reverberation pairs whose order differs by unity (e.g., $M^{(2)}$ and $M^{(3)}$).*

5 Discussion and conclusions

In the transmission-to-reflection mapping, no series is computed. However, the construction of any reflected event requires an infinite series nonetheless, a series that is discernable through a sub-event interpretation. The most compelling of these is the construction of the single primary. The (non-normalized) amplitude of the primary is an infinite series, the summation of all orders of transmitted event combined with the next lower order. It is curious to think that the full construction of any primary, even those occurring at early times in the reflection response, requires in principle the processing and influence of the n'th and $n-1$'th transmitted multiple, events that both could occur at very late times in the data record. In other words, a sub-event interpretation demonstrates that there is – in principle – a time-aperture issue in the use of the transmission to reflection mapping. In general, also, all primaries are constructed through a retention and manipulation of transmitted multiples; Claerbout's equations are in a very real way an example of the prediction of primaries from multiples, a subject of current research that was accorded a session unto itself at the 2005 SEG meeting.

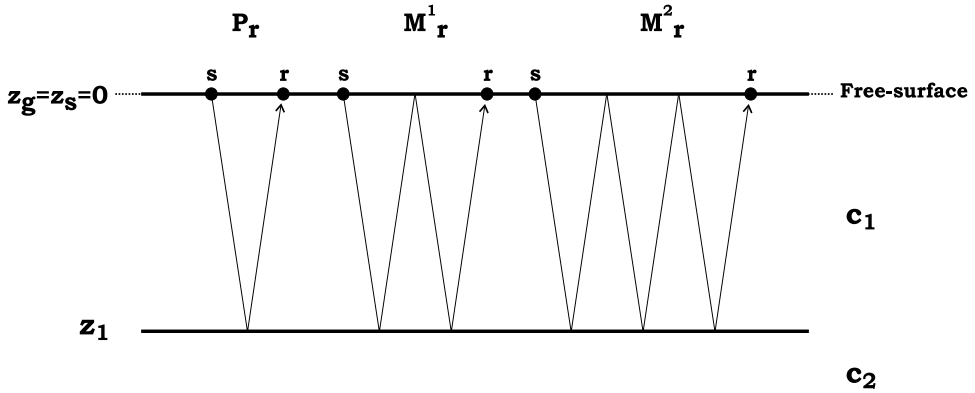

Figure 1: *Configuration for a reflection experiment over a single layer; two interfaces associated with impedance contrasts, a free-surface and a contrast in wavespeed from c_1 to c_2, are illustrated. All contributing propagation has been constrained to the c_1 medium. The source and receiver are collocated on the free-surface, and a downward-propagating normally incident wave field (the offset in the event diagrams is a convenience) results in a single primary followed by an infinite, diminishing, series of reverberations that are the 1D equivalent of surface-related multiples.*

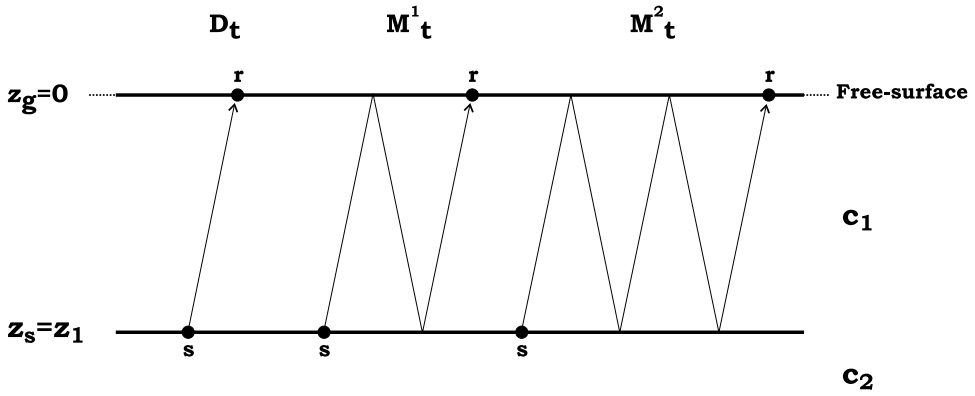

Figure 2: *Configuration for a transmission experiment through a single layer; two interfaces associated with impedance contrasts, a free-surface and a contrast in wavespeed from c_1 to c_2, are illustrated. All contributing propagation has been constrained to the c_1 medium.*

Acknowledgements

The author is grateful to the sponsors and personnel of M-OSRP, including and especially A. B. Weglein. I have been partially funded by and am grateful for NSF-CMG award DMS-0327778 and DOE Basic Sciences award DE-FG02-05ER15697.

References

Claerbout, J. F., 1968, Synthesis of a layered medium from its acoustic transmission response: Geophysics, **33**, 204–209.

Nita, B. and Weglein, A. B., 2006, Pseudo-depth/intercept-time monotonicity requirements in the inverse scattering algorithm for predicting internal multiple reflections, submitted to

Schuster, G. T., J. Yu, J. Sheng, and J. Rickett, 2004, Interferometric/daylight seismic imaging: Geophysical Journal International, **157**, 838–852.

Verschuur, D. J., Berkhout, A. J., and Wapenaar, C. P. A., 1992, Adaptive surface-related multiple elimination: Geophysics, **57**, 1166–1177.

Wapenaar, C. P. A., 2003, Synthesis of an inhomogeneous medium from its acoustic transmission response: Geophysics, **68**, pp. 1756–1759.

Weglein, A. B., F. A. Gasparotto, P. M. Carvalho, and R. H. Stolt, 1997, An inverse scattering series method for attenuating multiples in seismic reflection data: Geophysics, **46**, pp. 1975–1989.

Weglein, A. B., and Matson, K. H., 1998, Inverse scattering internal multiple attenuation: an analytic example and sub-event interpretation. *Mathematical Methods in Geophysical Imaging (Proc. SPIE vol. 3453).*

Using the inverse scattering series to predict the wavefield at depth and the transmitted wavefield without an assumption about the phase of the measured reflection data or back-propagation in the overburden

A. B. Weglein, B. G. Nita, K. A. Innanen, E. Otnes, S. A. Shaw, F. Liu, H. Zhang, A. C. Ramírez, J. Zhang, G. L. Pavlis, and C. Fan

Abstract

The inverse scattering series is the starting point for the derivation of a new set of approaches for predicting both the wavefield at depth in an unknown medium, and transmission data, from measured reflection data. We present a selection of these maps that differ in order (i.e., linear or non-linear), capability, and data requirements, which have their roots in the consideration of a data format known as the T-matrix, and which show to have direct applicability to the data construction techniques motivating this special issue. Of particular note, one of these, a construction of the wavefield at any depth (including the transmitted wavefield), order-by-order in the measured reflected wavefield, has an unusual set of capabilities (e.g., it does not involve an assumption regarding the minimum phase nature of the data, and is accomplished with processing in the simple reference medium only) and requirements (e.g., a suite of frequencies from surface data are required to compute a single frequency of the wavefield at depth when the subsurface is unknown). An alternate reflection-to-transmission data mapping, which does not require a knowledge of the wavelet, and in which the component of the unknown medium that is linear in the reflection data is used as a proxy for the component of the unknown medium that is linear in the transmission data, is also derivable from the inverse scattering series framework.

1 Introduction

There are many fields of non-destructive investigation, of which both exploration seismology and deep earth investigation are prime examples, whose aim in broad terms is to make inferences about the interior of an object from external measurements. Within the spheres of these two examples very different requirements on the type, extent and completeness of surface measurements may be encountered. These surface measurement requirements for determining target properties depend upon many factors, including: (1) the assumed ability (or inability) to estimate propagation properties in the medium that is above and/or surrounding a target, (2) whether or not that target overburden can be well-approximated (e.g., for the purpose of estimating the wavefield at depth) by a medium that supports only one-way or two-way propagation, (3) the level of ambition in "identification" of a target, e.g., whether the goal is a structure map of interfaces in their correct spatial location, excluding or including evanescent components, or the more ambitious estimation of earth property changes across those interfaces, and (4) whether or not the algorithm used for target location and identification requires or does not require information about medium properties between the target at depth and surface measurements.

The extent and completeness of recorded surface data is often determined by economic and/or natural acquisition constraints. An example of a natural constraint in whole earth investigation is

that the sources are, typically, only located at great depth (i.e., earthquake sources), whereas the receivers are on the surface. In exploration seismology, sources are man-made, and, along with all receivers, are located on or near the earth's surface; in this case natural constraints disallow sources or receivers to be placed at great depth, and economic constraints disallow arbitrarily finely-spaced and widely-ranging source/receiver positions on the surface.

There are several types of *data construction* activities, pursued in the seismology of exploration and production, that can assist in overcoming some of these constraints. Amongst them, (1) extrapolation and interpolation of surface reflection data, (2) mapping from reflection experiment data to transmission experiment data and vice-versa, and (3) mapping surface data to data at depth, the latter of which is an essential ingredient in wave-theoretic migration and migration-inversion algorithms. Taking a surface experiment and inferring another type of surface experiment (e.g., reflection-to-transmission or transmission-to-reflection) has several additional, specific motivations, including (1) allowing the direct use of mature subsurface determination methods that are not available for the measured data but that are available for the predicted data type, (2) increasing surface coverage for methods that require and/or benefit from both reflection and transmission data, (3) increasing the illumination of targets, and (4) allowing evanescent wave prediction in a stable and reliable manner.

The diminishment, in recent years, of the apparent separation between whole-earth and exploration seismology, given the differing experimental configurations and objectives of transmission- and reflection-type experiments (see, e.g., the AGU 2004 Session "Oil at the Core-Mantle Boundary? Bridging the Gap Between Exploration and Global Seismology" chaired by R. Snieder and S. A. Levin), has been influenced by data construction advancements, with the introduction of the daylight imaging method for a 1D medium by Claerbout (1968) and its later generalization to 3D acoustic or elastic media by Wapenaar (2003) and Wapenaar et al (2004). The method, based on reciprocity principles (see, e.g., Fokkema and Van den Berg, 1993; de Hoop and de Hoop, 2000), describes a way to relate reflection and transmission data, and, under certain conditions, to construct one from another. In essence, the method consists of crosscorrelating passive traces from two surface receivers, to create the reflection seismogram that would be computed at one of the locations if there was a source at the other. Claerbout's idea has since been rediscovered, extended and applied to numerous areas of interest, among them helioseismology (Duval et al., 1993; Rickett and Claerbout, 1999), ocean acoustics (Roux et al., 2004), ultrasonics (Larose et al., 2004; Malcolm et al., 2004; Weaver and Lobkis, 2004) and seismology (Snieder et al., 2002; Snieder, 2004; Wapenaar, 2004; Shapiro and Campillo, 2004; Shapiro et al., 2005; Sabra et al., 2005).

Building reflection data from transmission recordings and vice versa provides two kinds of benefit: first, as mentioned, a transmission experiment can be translated into a reflection experiment (and vice versa) and hence apply, to the problem at hand, a set of methods which is normally specific to the other geometry. Second, having both types of data (data from measurements and data from construction) allows the development/application of more complex methods for imaging and inversion which would require both. The relation between transmission and reflection seismograms is useful, for example, for seismic imaging of the Earth's interior, using passive recordings of noise sources located in the subsurface. Among the most notable extensions of the daylight imaging principle we mention the method of interferometric imaging (Schuster, 2001; Schuster et al., 2004) which broadens the previous concept to any number or distribution of sources and to arbitrary reflectivity distributions. Moreover, the method offers means to migrate free-surface and internal

multiples in the data together with the primaries (see, e.g., Sheng, 2001; Schuster et al., 2004), migrate transmitted waves and locate unknown sources in the subsurface from ambient noise or earthquakes recordings. Alternate descriptions include crosscorrelation migration (Schuster, 1999; Schuster and Rickett, 2000) or an extended form of auto-correlation migration (Schuster et al., 1997).

There are, furthermore, specific examples in which the ability to relate reflection and transmission data allows methods developed for one type of geometry to be applied to another problem. In a recent project sponsored by the National Science Foundation (NSF), a group from the University of Houston led by A.B. Weglein, together with a group from Indiana University led by G. Pavlis, has undertaken the task of translating some of the seismic exploration inverse scattering series methods and algorithms to the deep earth seismology problem. The first product of this collaboration was a method for separating the forward- and the back-scattered wavefields from earthquake recordings (Fan et al., 2006) which produced encouraging results on field data (Fan et al., 2005). A further notable method inspired by the daylight imaging principles with application to seismic exploration is the "virtual source method" (Bakulin and Calvert, 2004).

There is another and more recently understood benefit to predicting transmission data from reflection data. The inverse scattering series currently provides a comprehensive multidimensional direct inversion method that allows inverse objectives, e.g., free-surface and internal multiple removal, and depth structure maps and non-linear direct AVO to proceed, all without knowing or ever determining the actual properties that govern wave propagation in the subsurface. Those inverse tasks are achieved sequentially with distinct algorithms corresponding to task-specific subseries. In addition to being independent of any actual subsurface medium properties governing wave propagation, the free surface and internal multiple attenuation algorithms are independent of whether the earth is acoustic, elastic, heterogeneous, anisotropic or inelastic (see, e.g., Weglein et al., 2003); in other words, they are independent of model-type. Recently, a task specific subseries aimed at performing imaging, i.e., locating reflectors in space, has been identified and tested on analytic data for simple 1D-earth examples with encouraging results (see Weglein et al., 2001; Shaw and Weglein, 2003; Innanen, 2003; Shaw et al., 2004; Shaw, 2005). Liu et al. (2005a; 2005b) have very recently shown the first multidimensional acoustic examples of these methods for determining the correct spatial location of reflectors without knowing or determining the overburden velocity model. As the analysis of Weglein et al. (2000), with respect to the possibility and requirements for a model-type independent imaging algorithm, and the diagrams of Shaw et al. (2004), describing scattering interactions within the imaging subseries, show, a model-type independent algorithm would require both reflection and transmission data.

Reflection-to-transmission transformations (of importance, then, to the fundamental capability and concepts of velocity independent depth imaging) are, when task-separated imaging methods are not being considered, themselves provided by distinct methods derived from the inverse scattering series. By way of introducing this potential framework for data construction, the development of which being the central theme of this paper, we next highlight some relevant aspects of the daylight imaging data construction method.

The relation between the two data types is derived from reciprocity theorems of the correlation

type written for one-way wavefields (see, e.g., Wapenaar and Grimbergen 1996, Wapenaar, 2004)

$$\int\limits_{z_M=const.} d^2\mathbf{x}\left\{(P_A^+)^* P_B^+ - (P_A^-)^* P_B^-\right\} = \int\limits_{z_m=const.} d^2\mathbf{x}\left\{(P_A^+)^* P_B^+ - (P_A^-)^* P_B^-\right\}, \tag{1}$$

where P^+ and P^- are flux-normalized down-going and up-going wavefields, respectively. The derivation of equation 1 assumes that the medium is lossless and that evanescent components can be neglected and hence this equation can be viewed as an approximation rather than an exact relation.

The two states A and B can be chosen in different ways to derive relations between reflection and transmission responses (for a comprehensive description see Wapenaar et al. (2004)). Choosing both states A and B to represent experiments with the source located at depth $z_m - \epsilon$ in a homogeneous half space (see Figure 1), leads to a relationship which allows the construction of the transmission response from reflection data. Let the space coordinates of the sources be denoted by $\mathbf{x}_A$ and $\mathbf{x}_B$. The inhomogeneity $V(x, y, z)$ is located between depths z_m and z_M and the space beyond $z_M + \epsilon$ is assumed homogeneous. A receiver located at the same depth as the source with coordinates $\mathbf{x}$ would record the reflection response $R(\mathbf{x}, \mathbf{x}_A, \omega)$ while a receiver located deeper than z_M would record the transmission response $T(\mathbf{x}, \mathbf{x}_A, \omega)$. To obtain a relationship between the reflection and transmission responses R and T, the one-way reciprocity theorem of the correlation type, equation 1, is employed. With states A and B defined as above, we have the following. At depth z_m,

$$P_{A,B}^+(\mathbf{x}, \mathbf{x}_{A,B}, \omega) = \delta(x - x_{A,B})\delta(y - y_{A,B}) s_{A,B}(\omega), \tag{2}$$

$$P_{A,B}^-(\mathbf{x}, \mathbf{x}_{A,B}, \omega) = R(\mathbf{x}, \mathbf{x}_{A,B}, \omega) s_{A,B}(\omega), \tag{3}$$

where s represents the source signature. At depth z_M,

$$P_{A,B}^+(\mathbf{x}, \mathbf{x}_{A,B}, \omega) = T(\mathbf{x}, \mathbf{x}_{A,B}, \omega) s_{A,B}(\omega), \tag{4}$$

$$P_{A,B}^-(\mathbf{x}, \mathbf{x}_{A,B}, \omega) = 0. \tag{5}$$

Substituting these into equation 1 and dividing by $s_A^*(\omega) s_B(\omega)$ we find

$$\int\limits_{z_M} d^2\mathbf{x}\, T^*(\mathbf{x}, \mathbf{x}_A, \omega) T(\mathbf{x}, \mathbf{x}_B, \omega) + \int\limits_{z_m} d^2\mathbf{x}\, R^*(\mathbf{x}, \mathbf{x}_A, \omega) R(\mathbf{x}, \mathbf{x}_B, \omega) = \delta(\mathbf{x}_B - \mathbf{x}_A). \tag{6}$$

A similar equation can be written for the elastic case (see Wapenaar et al. (2004)). This relation provides amplitude information about the transmission response from recorded reflection data and vice versa. However, all the phase information is lost in this process and there is no unique way to recover it from this relation alone. Reconstructing the phase from the amplitude for a signal would require additional information which is sometimes provided by the minimum phase condition. For 1D acoustic media, Herman (1992) and Wapenaar and Herrmann (1993) describe the procedure of constructing the transmission response from reflection data. The procedure implicitly uses the fact that the transmission response for this type of medium is minimum phase, and hence its full phase can be reconstructed from amplitude information only. This property of the recorded wavefield depends on the medium that the wave propagates through; in general it is not satisfied. In other words, even when the source wavelet used in a seismic experiment is minimum phase,

the interaction with complex subsurface structures results in a non-minimum phase signal being recorded on the measurement surface. Different descriptions of minimum phase signals in the time and frequency domains, as well as properties of minimum phase media and reflection coefficients, have been collected by Nita and Weglein (2005). Bostock (2004) points out some of the cases in which the wavefield preserves the minimum phase property, namely for pre-critical intra-modal free surface reverberations and transmitted P-waves in weak to moderate contrast stratification with small horizontal wavenumbers. However, for general acoustic and elastic media and wavefield propagation with arbitrary horizontal wavenumber, the recorded signal will have a mixed phase character.

In this paper we present a new approach for obtaining data at depth from measured reflection data based on the inverse scattering series, that is fundamentally different from the daylight imaging approach. Our objective, having provided a brief overview of the current thinking behind reflection-to-transmission data prediction, is to present new, embryonic ideas concerning potential contributions of the inverse scattering series to the problem of constructing data that were not acquired from data that were acquired, and predicting the data both beneath and within the target medium. This involves two different approaches and extensions of previous ideas, one, a linear reflection-to-transmission map drawing from Stolt (2002), and the other, a construction of the wavefield at depth without the velocity model, drawing from Weglein et al. (2001). The exposition is somewhat involved, and so we include a table of symbols (Table 1) for reference.

The inverse scattering series, and hence this second approach, operates entirely in terms of a chosen reference medium, usually water in the marine case, and involves data operations adequate to image only through this reference medium. The former linear extrapolation and interpolation method derives from an exact linear relationship within the inverse scattering series, and equally accommodates primaries and multiples without requiring a velocity model for either type of event. The non-linear inverse-scattering wavefield at depth is obtained, in principle, as though an accurate, actual, complex velocity was known and a currently leading-edge linear migration technique was used, with neither the velocity nor the extra boundary measurements required for a discontinuous subsurface as with a conventional two-way wave migration. However, the cost in the inverse series depth imaging approach is that a suite of frequencies from the surface data is required to downward continue a single temporal frequency of the wavefield when the medium is unknown*.

An inverse scattering series framework for constructing the wavefield at depth and the transmission response from reflection data

In this section we describe the opportunity provided by the inverse scattering series for constructing, from reflection data, the actual wavefield at all depths, including the transmitted wavefield. The

*When the medium is known, one temporal frequency of surface data determines the same temporal frequency of the wavefield at depth (all current methods for constructing the wavefield at depth fall into this category, and can be viewed as following from Green's theorem, i.e., they are linear in the surface data). When the medium is unknown, the inverse scattering series prescribes a non-linear combination of surface data at a suite of frequencies to predict one given frequency of the wavefield at depth. These concepts and insights are the direct extension of lessons learned about temporal frequency requirements and linear/non-linear processes in the removal of free-surface and internal multiples (see, e.g., the Tutorial for chapters 4 and 5 in Weglein and Dragoset (2005)).

latter is achievable without requiring or determining the Earth material properties needed by linear Green's theorem based approaches. Early thinking on this approach for determining the wavefield at depth from the inverse scattering series was first described by Weglein et al. (2000). To describe this procedure we first introduce a data format known in the literature of scattering theory (e.g., Goldberger and Watson, 1964; Taylor, 1972) as the T-matrix, and the experiment that motivated that definition. We then describe the generalization of that experiment-motivated T-matrix definition and how that generalized T-matrix played a role in early inverse scattering series papers of Moses (1956), Razavy (1975), and Weglein et al. (1981). The relationship between seismic recorded data and a T-matrix format was presented by Weglein et al. (1981) and Stolt and Jacobs (1981). The challenge within the inverse scattering series that the presence of the full generalized T-matrix represented is then described and how those papers addressed that issue. In addressing that requirement for the complete T-matrix resides the kernel of a wavefield-at-depth concept and methodology. In fact, we show that satisfying the full off-shell T-matrix requirement, order-by-order in the measured data, as described by the classic inverse scattering series papers of Moses and Razavy cited above is equivalent to constructing the actual scattered, and total, wavefields at depth. This method will be available for marine applications involving acoustic, elastic and inelastic media, requiring only knowledge of the source signature in the water as input.

1.1 Background

Scattering theory is a form of perturbation analysis, in which a perturbation in the properties of a medium is related to a perturbation in a wavefield that experiences that medium. The original, unperturbed medium is typically labeled as the reference medium. The difference between the actual and reference media is characterized by the perturbation operator, and the corresponding difference between the actual and reference wavefields is called the scattered wavefield. Forward scattering takes as input the reference medium, the reference wavefield, and the perturbation operator, and outputs the actual wavefield. Inverse scattering takes as input the reference medium, the reference wavefield and values of the actual field on the measurement surface and outputs the difference between actual and reference medium properties through the perturbation operator. Inverse scattering theory methods typically assume the support of the perturbation to be on one side of the measurement surface. In seismic application, this condition translates to a requirement that the difference between actual and reference media be non-zero only below the source-receiver surface. Conversely, in seismic applications, inverse scattering methods require that the reference medium agrees with the actual at and above the measurement surface.

For the marine seismic application, the sources and receivers are located within the water column and the simplest reference medium (that satisfies the above stated conditions) is a half-space of water bounded by a free surface at the air-water interface. Since scattering theory relates the difference between actual and reference wavefields to the difference between their medium properties, it is reasonable that the mathematical description begin with the differential equations governing wave propagation in these media. Let

$$\mathbf{L}G = -\delta(\mathbf{r} - \mathbf{r}_s), \tag{7}$$

and

$$\mathbf{L}_0 G_0 = -\delta(\mathbf{r} - \mathbf{r}_s), \tag{8}$$

where $\mathbf{L}$, $\mathbf{L}_0$ and G, G_0 are the actual and reference differential operators and Green's functions, respectively, for a single temporal frequency, ω, $\delta(\mathbf{r}-\mathbf{r}_s)$ is the Dirac delta function, and $\mathbf{r}$ and $\mathbf{r}_s$ are the field point and source location, respectively. Equations 7 and 8 assume that the actual source and receiver signatures have been deconvolved. The quantities G and G_0 are the matrix elements of the Green's operators, $\mathbf{G}$ and $\mathbf{G}_0$, in the spatial coordinates and the temporal frequency domain; $\mathbf{G}$ and $\mathbf{G}_0$ themselves satisfy $\mathbf{LG} = -\mathbb{1}$ and $\mathbf{L}_0\mathbf{G}_0 = -\mathbb{1}$, where $\mathbb{1}$ is the unit operator. A further set of operators based on differences between these quantities are considered next:

$$\mathbf{V} \equiv \mathbf{L} - \mathbf{L}_0, \tag{9}$$

and

$$\mathbf{\Psi}_s \equiv \mathbf{G} - \mathbf{G}_0; \tag{10}$$

$\mathbf{V}$ is referred to as the perturbation operator and $\mathbf{\Psi_s}$ is the scattered field operator. The Lippmann-Schwinger equation is the fundamental equation of scattering theory, an operator identity that relates $\mathbf{\Psi}_s$, $\mathbf{G}_0$, $\mathbf{V}$ and $\mathbf{G}$ (Taylor, 1972):

$$\mathbf{\Psi}_s = \mathbf{G} - \mathbf{G}_0 = \mathbf{G}_0\mathbf{V}\mathbf{G} \ . \tag{11}$$

When the right-hand members of equations 7 and 8 include a wavelet, we re-express equation 11 as

$$\mathbf{P}_s = S(\omega)\mathbf{\Psi}_s = \mathbf{P} - \mathbf{P}_0 = \mathbf{G}_0\mathbf{V}\mathbf{P}, \tag{12}$$

where $\mathbf{P_0}$, $\mathbf{P}$ are the reference and actual wave operators respectively, and $\mathbf{G_0}$ is the causal reference Green's operator.

In the coordinate representation, equation 12, alternatively called the Scattering equation, is valid for all positions of $\mathbf{r}$ and $\mathbf{r}_s$ whether or not they are inside the support of $\mathbf{V}$. Examples of $\mathbf{L}$, $\mathbf{L_0}$, and $\mathbf{V}$ (when $\mathbf{P}$ corresponds to a pressure field) in an inhomogeneous, variable velocity constant density medium, are:

$$\begin{aligned} L &= \nabla^2 + \frac{\omega^2}{c^2(\mathbf{r})}, \\ L_0 &= \nabla^2 + \frac{\omega^2}{c_0^2}, \\ V &= L - L_0 = -k^2\alpha(\mathbf{r}), \end{aligned} \tag{13}$$

where $k = \omega/c_0$ and $\alpha = 1 - \frac{c_0^2}{c^2}$. For this model, equation 12 becomes, explicitly,

$$\begin{aligned} P(\mathbf{r},\mathbf{r}_s,\omega) &= P_0(\mathbf{r},\mathbf{r}_s,\omega) - \int G_0(\mathbf{r},\mathbf{r}',\omega)k^2\alpha(\mathbf{r}')P(\mathbf{r}',\mathbf{r}_s,\omega)d\mathbf{r}' \\ &= P_0(\mathbf{r},\mathbf{r}_s,\omega) - \int \frac{e^{ik|\mathbf{r}-\mathbf{r}'|}}{4\pi|\mathbf{r}-\mathbf{r}'|}k^2\alpha(\mathbf{r}')P(\mathbf{r}',\mathbf{r}_s,\omega)d\mathbf{r}'. \end{aligned} \tag{14}$$

We next proceed, using the above form as a starting point, to review and develop upon some of the key quantities used in the scattering description and formulation.

1.2 The T-matrix and the seismic wavefield

Let us consider the special case where a single frequency plane wave,

$$\frac{e^{i\mathbf{k}\cdot\mathbf{r}}}{(2\pi)^{3/2}}, \tag{15}$$

is incident upon a localized target, $\alpha(\mathbf{r})$, in which the support of α is within a sphere of radius R, and $\mathbf{k} = |\mathbf{k}|\hat{k} = \omega/c_0\hat{k}$. Consider measuring the wavefield at a position $\mathbf{r}$ in the far-field well beyond the support of α. For that experiment, the scattering equation becomes

$$P(\mathbf{r},\mathbf{k}) = \frac{e^{i\mathbf{k}\cdot\mathbf{r}}}{(2\pi)^{3/2}} - \frac{e^{ik|\mathbf{r}|}}{4\pi|\mathbf{r}|}\int e^{-ik\hat{r}\cdot\mathbf{r}'}k^2\alpha(\mathbf{r}')P(\mathbf{r}',\mathbf{k})d\mathbf{r}', \tag{16}$$

where we have substituted the far-field form of the Green's function:

$$\frac{e^{ik|\mathbf{r}-\mathbf{r}'|}}{4\pi|\mathbf{r}-\mathbf{r}'|} \approx \frac{1}{4\pi}\frac{e^{ik|\mathbf{r}|}}{|\mathbf{r}|}e^{-ik\hat{r}\cdot\mathbf{r}'}, \tag{17}$$

in propagating from the scattering point $\mathbf{r}'$ to the field point $\mathbf{r}$; $\hat{\mathbf{r}}$ is the unit vector in the direction of $\mathbf{r}$. In the far-field, P_s, from equation 12 (with $\mathbf{k}' \equiv k\hat{\mathbf{r}}$), becomes

$$P_s(\mathbf{r},\mathbf{k}) \approx -\frac{e^{ik|\mathbf{r}|}}{4\pi|\mathbf{r}|}\int e^{-i\mathbf{k}'\cdot\mathbf{r}'}k^2\alpha(\mathbf{r}')P(\mathbf{r}',\mathbf{k})d\mathbf{r}'. \tag{18}$$

This is an anisotropic spherical wave with an amplitude of

$$\int e^{-i\mathbf{k}'\cdot\mathbf{r}'}k^2\alpha(\mathbf{r}')P(\mathbf{r}',\mathbf{k})d\mathbf{r}', \tag{19}$$

that depends on $\alpha(\mathbf{r})$, the incident wave vector $\mathbf{k}$, and a vector, $\mathbf{k}'$, of the same magnitude, pointing in the direction of the observation point $\mathbf{r}$. The message of equation 18 is that in the far-field the scattered wave is a spherical wave with an angle-dependent amplitude that captures the properties of the actual (in general) extended target $\alpha(\mathbf{r})$.

The above observation motivates the definition of what is referred to as the T-matrix ('T' for *transition*; see, e.g., Taylor, 1972), a quantity relating the strength of the far-field scattered wave, in direction $\hat{\mathbf{r}} = \mathbf{k}'/|\mathbf{k}|$ to the wave vector $\mathbf{k}$:

$$T(\mathbf{k},\mathbf{k}') \equiv k^2\int \frac{e^{-i\mathbf{k}'\cdot\mathbf{r}'}}{(2\pi)^{3/2}}\alpha(\mathbf{r}')P(\mathbf{r}',\mathbf{k})d\mathbf{r}'. \tag{20}$$

In the experiment we use to motivate this definition, $\mathbf{k}$ and $\mathbf{k}'$ have the same magnitude ω/c_0. For the purposes of inverse scattering theory it is useful to generalize the T-matrix definition to

$$T(\mathbf{p},\mathbf{p}') \equiv \int \frac{e^{-i\mathbf{p}'\cdot\mathbf{r}'}}{(2\pi)^{3/2}}k^2\alpha(\mathbf{r}')P(\mathbf{r}',\mathbf{p})d\mathbf{r}', \tag{21}$$

where $\mathbf{p}$ and $\mathbf{p}'$ are two arbitrary vectors, unrelated to $\mathbf{k}$ in either magnitude or direction.

The data format represented by equation 20 is the standard found in the papers by Moses (1956) and Razavy (1975). It can, for instance, be interpreted for $\mathbf{k}' = \mathbf{k}$ and $\mathbf{k}' = -\mathbf{k}$ as the forward scattering amplitude and backscattering amplitude, respectively. The relationship between T-matrix incident plane wave, far-field measurements (equation 20) and reflection seismic data was first described by Weglein et al. (1981) and further analyzed and developed by Stolt and Jacobs (1981). In three dimensions, we have

$$e^{i(q_g z_g + q_s z_s)} \frac{T(\mathbf{k}';\mathbf{k})}{q_g q_s} = e^{i(q_g z_g + q_s z_s)} \frac{T(k_{gx}, k_{gy}, -q_g; k_{s_x}, k_{s_y}, q_s)}{q_g q_s} = \tilde{\phi}_s(k_{g_x}, k_{g_y}, z_g; k_{s_x}, k_{s_y}, z_s; \omega), \tag{22}$$

where k_{g_x}, k_{g_y} and k_{s_x}, k_{s_y} are the Fourier conjugates to x_g, y_g and x_s, y_s, the depth wavenumbers q_g and q_s are

$$\begin{aligned} q_g &= \operatorname{sgn}(\omega) \left[\left(\frac{\omega}{c_0} \right)^2 - k_{g_x}^2 - k_{g_y}^2 \right]^{1/2}, \\ q_s &= \operatorname{sgn}(\omega) \left[\left(\frac{\omega}{c_0} \right)^2 - k_{s_x}^2 - k_{s_y}^2 \right]^{1/2}, \end{aligned} \tag{23}$$

and z_g, z_s are, as earlier, the depths of the receiver and source respectively. $\tilde{\phi}_s$ is the seismic scattered (reflection) data due to a point source and measured at a point receiver. Beyond this, Weglein et al. (2003) have shown that the T-matrix expression $T(\mathbf{p}, \mathbf{k})$, where $\mathbf{k} = \omega/c_0 \hat{k} = (k_{s_x}, k_{s_y}, q_s)$ and $\mathbf{p}$ is an arbitrary three-dimensional vector unrelated to $\mathbf{k}$, can also be related to the seismic exploration experiment. For arbitrary $\mathbf{p}$, the 3D relationship between $\tilde{\phi}(\mathbf{p}, \mathbf{k})$ and $T(\mathbf{p}, \mathbf{k})$ is

$$\tilde{\phi}_s(p_x, p_y, p_z; k_{s_x}, k_{s_y}, q_s) = \tilde{\phi}_s(\mathbf{p}; k_{s_x}, k_{s_y}, q_s) = \frac{T(\mathbf{p}, \mathbf{k})}{k^2 - p^2 - i\varepsilon} \left(\frac{1}{q_s} \right), \tag{24}$$

where $\mathbf{p}$ is the 3D Fourier conjugate of the wavefield observation vector $\mathbf{r} = (x, y, z)$, which is not confined to the measurement surface $z = z_g$; further, the magnitude of $\mathbf{p}$ is unrelated to the magnitude or direction of $\mathbf{k}$. The interpretation that follows from equation 24 is that $T(\mathbf{p}, \mathbf{k})$ with $\mathbf{k} = \omega/c_0 \hat{k}$ and $\mathbf{p}$ arbitrary is equivalent to knowing the scattered field at all spatial locations (i.e., all x, y and all depths z) for a suite of single frequency experiments, at frequency ω, with sources located at (x_s, y_s, z_s). The variable $\mathbf{p}$ is the 3D conjugate of (x, y, z) in all 3D space, and $\mathbf{k}$ comes from a Fourier transform over single-frequency point sources on the surface. The inverse scattering series solution for $\alpha(\mathbf{r})$ is described in equations 20–22 of Weglein et al. (1981); further, the reader may wish to examine equations 32–40 of Weglein et al. (2003) for further discussion on what we next review.

To generate the inverse scattering series for the constant density variable velocity acoustic case, we first define the Fourier transform of $\alpha(\mathbf{r})$ as

$$W(\mathbf{k}) \equiv \int e^{2i\mathbf{k}\cdot\mathbf{r}'} \frac{\alpha(\mathbf{r}')}{(2\pi)^{3/2}} d\mathbf{r}'. \tag{25}$$

To determine $W(\mathbf{k})$ for all $\mathbf{k}$ is to determine the inverse solution for $\alpha(\mathbf{r})$. Equation 21 of Weglein et al. (1981) then relates $W(\mathbf{k})$ to the T-matrix quantities as

$$W(\mathbf{k}) = -\left(\frac{2}{\pi} \right)^{1/2} \frac{b(\mathbf{k})}{k^2} + k^2 \int \mathcal{T}^*(\mathbf{k}, \mathbf{q}) \mathcal{T}(-\mathbf{k}, \mathbf{q}) \left\{ \frac{H(k)}{q^2 - k^2 - i\varepsilon} + \frac{H(-k)}{q^2 - k^2 + i\varepsilon} \right\} d\mathbf{q}, \tag{26}$$

where

$$b(\mathbf{k}) = \frac{k^2\mathcal{T}(-\mathbf{k},\mathbf{k})}{\left(\frac{2}{\pi}\right)^{1/2}} = \tilde{\phi}_s(-k_{s_x},-k_{s_y},-q_s;k_{s_x},k_{s_y},q_s)q_g^2 e^{-iq_s(z_s+z_g)}, \tag{27}$$

and where $k^2\mathcal{T} \equiv T$ and $H(k)$ is the Heaviside step function. Note that the second term on the right-hand side of equation 26 requires $T(\mathbf{k},\mathbf{q})$ for all $\mathbf{q}$ for a given $\mathbf{k} = \omega/c_0\hat{k}$, $\mathbf{k} = (k_{s_x},k_{s_y},q_s)$, where $\mathbf{q}$ is an arbitrary 3D vector per its whole space integration, $\int d\mathbf{q}$.

Hence, the inverse scattering series solution in the Fourier domain can be interpreted as requiring the scattered field (and, hence, the entire wavefield) at all points in space, not only on the measurement surface. Included in that requirement on the right-hand side of equation 26 is $T(\mathbf{q},\mathbf{k})$ when $\mathbf{q} = \mathbf{k}$, or rather $T(\mathbf{k},\mathbf{k})$. The latter is the transmitted component of the scattered field.

Weglein et al. (2003) review the procedure first developed by Moses (1956) to address this "wavefield everywhere" requirement. The inverse scattering series produces all quantities associated with an unknown subsurface as a series order-by-order in the measured surface reflection data. The scattered (or total) wavefield at depth is no exception. In fact, the wavefield at depth is explicitly calculated, order-by-order, at each step within the calculation of $W(\mathbf{k})$, the Fourier transform of $\alpha(\mathbf{r})$,

$$W(\mathbf{k}) = W_1(\mathbf{k}) + W_2(\mathbf{k}) + W_3(\mathbf{k}) + ..., \tag{28}$$

and hence, through the inverse Fourier transform of W, the calculation of $\alpha(\mathbf{r})$. The relevant equation for wavefield construction is

$$T(\mathbf{p},\mathbf{k}) = T_1(\mathbf{p},\mathbf{k}) + T_2(\mathbf{p},\mathbf{k}) + T_3(\mathbf{p},\mathbf{k}) + ..., \tag{29}$$

where $T(\mathbf{p},\mathbf{k})$ is

$$T(p_x,p_y,p_z;k_{x_s},k_{y_s},q_s).$$

Weglein et al. (2000) demonstrate that the first order approximation to $T(\mathbf{p},\mathbf{k})$, i.e., $T_1(\mathbf{p},\mathbf{k})$, or $\tilde{\phi}_s$, at all depths requires all frequency components contained within the surface data to predict one frequency of $\tilde{\phi}_s$ at all depths. Hence the inverse scattering series allows one frequency of the wavefield at all depths in the Earth to be predicted as a series, order-by-order in the surface data, using all the frequency information therein. We describe this prediction in detail in the following section. That prediction of the scattered field at depth does not involve a back-propagation within the medium at depth; if the medium at depth is known, then one frequency on the surface predicts the scattered wavefield at depth at that frequency. This is a direct analog of the inverse scattering internal multiple attenuator (Weglein et al., 1997) where, absent of any subsurface information, a suite of frequencies of surface data are required to predict one frequency of the output.

The latter "one frequency in one frequency out" wavefield prediction, when the medium is known, derives from Green's theorem with Dirichlet, Neumann or Robin boundary conditions and is the theory underlying all current migration theory. The inverse scattering series predicts the wavefield at depth, including the transmitted wavefield, without knowing the medium, but all frequencies in the measured wavefield are required to produce a series solution for the wavefield at depth for any given frequency. The source signature in the reference medium is a pre-requisite for this and all such inverse methods. These concepts can be applied to all models that allow a perturbative expression.

Among the models accommodated are acoustic, elastic, and inelastic media. However, it appears that the specific detail of the wavefield construction will depend on the assumed model type. Transmission data can mitigate that model-type dependence for a wavefield at depth construction, whose purpose is to determine an accurate structural map.

2 Order-by-order computation of the wavefield at depth

The inverse scattering series, considered from the standpoint of the T-matrix, constructs the wavefield everywhere in the unknown medium, order-by-order in the scattered wavefield measured outside of that medium.

The wavefield at depth theory, as discussed by Weglein et al. (2000), is based on a constant density acoustic model of wave propagation. When the predicted wavefield is combined with a causality-based, small time imaging condition, its output is a reflectivity function map. Such an output quantity would correspond to an angle-dependent reflection coefficient, or scattering operator, for a specular or non-specular target, respectively (see, e.g., Weglein and Stolt, 1999). The act of locating the reflectors would be driven by an acoustic approximation, but the goal would be that the output nevertheless corresponds to the imaged wavefield associated with a more general, elastic or inelastic Earth.

The approach begins with the linear component of the inverse scattering series, in which $D = G_0 V_1 G_0$, and explicitly solves for V_1 from the data for a given earth model-type. For a constant density, variable velocity, acoustic model, the perturbation V can be written as in equation 13, as $V = -k^2\alpha(x,y,z)$ where $k = \omega/c_0$, c_0 is the constant reference velocity, and $\alpha(x,y,z)$ is the variation of the index of refraction. The linear relationship becomes

$$\alpha_1(p_{g_x} - p_{s_x}, p_{g_y} - p_{s_y}, -q_g - q_s) = \frac{4q_g q_s}{-k^2}\psi_s(p_{g_x}, p_{g_y}, z_g, p_{s_x}, p_{s_y}, z_s; \omega), \tag{30}$$

where $\psi_s(p_{g_x}, p_{g_y}, z_g, p_{s_x}, p_{s_y}, z_s; \omega)$ is the measured scattered field, i.e., the data D, due to a set of experiments with sources at (x_s, y_s, z_s) and receivers at (x_g, y_g, z_g). The quantities z_s, z_g are the constant depth of source and receiver, respectively; p_{g_x}, p_{s_x}, p_{g_y}, and p_{s_y} are the Fourier conjugates of x_g, x_s, y_g and y_s, and the vertical wave numbers are defined by

$$\begin{aligned} q_g &= \mathrm{sgn}(\omega)\left[\left(\frac{\omega}{c_0}\right)^2 - p_{g_x}^2 - p_{g_y}^2\right]^{1/2}, \text{and} \\ q_s &= \mathrm{sgn}(\omega)\left[\left(\frac{\omega}{c_0}\right)^2 - p_{s_x}^2 - p_{s_y}^2\right]^{1/2}. \end{aligned} \tag{31}$$

In contrast with equation 30, the first-order wavefield at depth is

$$\psi_s^{(1)}(p_{g_x}, p_{g_y}, p_{g_z}, p_{s_x}, p_{s_y}, p_{s_z}; \omega) = \frac{k^2\alpha_1(p_{g_x} - p_{s_x}, p_{g_y} - p_{s_y}, -p_{g_z} - p_{s_z})}{(p_{s_x}^2 + p_{s_y}^2 + p_{s_z}^2 - k^2 - i\epsilon)(p_{g_x}^2 + p_{g_y}^2 + p_{g_z}^2 - k^2 - i\varepsilon)}, \tag{32}$$

where $(p_{s_x}, p_{s_y}, p_{s_z})$, $(p_{g_x}, p_{g_y}, p_{g_z})$ are the conjugate variables to (x_s, y_s, z_s) and (x_g, y_g, z_g), respectively, and ε is a small positive parameter needed to ensure causal Green's functions. Equation 32

follows from the Lippmann-Schwinger equation by expanding each of ψ_s (at depth), V and G in orders of the surface data $(\psi_s)_m = D$ and then equating terms of equal order in D on both sides of the equation. The scattered wavefield ψ_s, in general, for any source and receiver position may be expressed as

$$\psi_s = G_0 k^2 \alpha \psi, \tag{33}$$

and α and ψ are expandable in terms of the data $(\psi_s)_m = D$:

$$\begin{aligned} \alpha &= \alpha_1 + \alpha_2 + \alpha_3 + ... \\ \psi &= \psi_0 + \psi_1 + \psi_2 + \psi_3 + ..., \end{aligned} \tag{34}$$

where

$$\begin{aligned} \psi_0 &= G_0, \\ \psi_s^{(1)} &= \psi_1 = G_0 k^2 \alpha_1 G_0, \\ \psi_s^{(2)} &= \psi_2 = G_0 k^2 \alpha_2 G_0 + G_0 k^2 \alpha_1 (\psi_1), \end{aligned} \tag{35}$$

etc. These equations are valid at all spatial locations, including in the medium, and they form the basis of the velocity-independent wavefield construction method. We point out that these equations are not the inverse scattering series equations. The latter are a relationship between the measured values of the wavefield and an order-by-order construction of α. Equations 35 represent something entirely different, an order-by-order construction of the wavefield, ψ_s, at depth. The procedure starts with α_1 determined by $(\psi_s)_m$, the measured values of ψ_s, followed by the substitution of α_1 into the expression for $\psi_s^{(1)}$. Then α_1, α_2 and ψ_1 are used to construct $\psi_s^{(2)}$, the second order approximation of the wavefield at depth. For sources and receivers at depth,

$$\begin{aligned} \psi_s &= \psi_s^{(1)} + \psi_s^{(2)} + \cdots \\ G &= G_0 + \psi_s, \end{aligned} \tag{36}$$

where $\psi_s^{(n)}(x_g, y_g, z_g, x_s, y_s, z_s; \omega)$ is the portion of the wavefield at depth that is n'th order in the measured data. Within equation 35 there is the opportunity to include only task-separated portions of α_2 rather than its entirety. The inclusion of only reflector location terms, or imaging terms within α_2 (as in Shaw et al., 2004), might be expected to produce a structurally accurate imaged wavefield, without computing the complete α_2. Whether the complete α_2, or a portion thereof, is computed and input into equation 35 as part of the construction of $\psi_s^{(2)}$, this predicted wavefield at depth (to second order) is never back-propagated through an actual, or updated, medium. All back-propagation occurs in the original, unchanged, reference medium. On the measurement surface (throughout this paper, brackets $(\cdot)_m$ indicate the quantity $\cdot$ evaluated on a measurement surface), these terms reduce to

$$\begin{aligned} (\psi_s)_m &= \left(\psi_s^{(1)}\right)_m \\ \left(\psi_s^{(2)}\right)_m &= \left(\psi_s^{(3)}\right)_m = \cdots = 0. \end{aligned} \tag{37}$$

In detail, the first-order field at depth in terms of the wavefield on the measurement surface is

$$\psi_s^{(1)}(p_{g_x}, p_{g_y}, p_{g_z}, p_{s_x}, p_{s_y}, p_{s_z}; \omega) = \frac{-4\frac{k^2 q_g' q_s'}{k_1^2}\left[\psi_s(p_{g_x}, p_{g_y}, q_g', p_{s_x}, p_{s_y}, q_s'; \omega_1)\right]_m}{(p_{s_x}^2 + p_{s_y}^2 + p_{s_z}^2 - k^2 - i\epsilon)(p_{g_x}^2 + p_{g_y}^2 + p_{g_z}^2 - k^2 - i\epsilon)}, \tag{38}$$

where

$$k_1 = \frac{\omega_1}{c_0},$$
$$q'_{g,s} = \mathrm{sgn}(\omega)\left[\frac{\omega_1^2}{c_0^2} - p_{g_x,s_x}^2 - p_{g_y,s_y}^2\right]^{1/2}, \tag{39}$$

and

$$\left(\frac{\omega_1}{c_0}\right)^2 = p_{s_x}^2 + p_{s_y}^2 + \left[\frac{p_{s_x}^2 + p_{s_y}^2 - p_{g_x}^2 - p_{g_y}^2 - (p_{s_z} - p_{g_z})^2}{2(p_{s_z} - p_{g_z})}\right]^2. \tag{40}$$

The quantity $\psi_s^{(1)}(x_g, y_g, z_g, x_s, y_s, z_s; \omega)$ for any (x_s, z_s) and (x_g, z_g), follows by inverse Fourier transforming equation 38. To find the first order estimate of the wavefield at all depths for a single frequency, ω, requires sweeping through surface data for all frequencies, ω_1, in order to fill the spectrum of the source and receiver depth variable's Fourier conjugates, p_{s_z} and p_{g_z}, respectively, for the left hand side of equation 38. That calculation provides the first order wavefield at depth without the velocity. The higher order computations of the wavefield at depth without the velocity follow directly from equations 35.

3 Analysis of a linear reflection-to-transmission mapping

In this section we consider an approximation to the reflection-to-transmission problem motivated by the order-by-order construction of the transmitted wavefield that is a natural by-product of the full inverse scattering series. We also consider a "linear-linear" mapping of reflected to transmitted wavefield data, and comment on its potential level of applicability and accuracy.

The fact that the first equation in the inverse scattering series, $D = G_0 k^2 \alpha_1 G_0$ (see Weglein et al., 2003) solves for a factor α_1 that treats all events on equal footing (whether they are primaries or multiples) is a deficit from an inversion point of view, but a definite asset from a data reconstruction point of view and objective. For the purpose of data reconstruction we suggest that the idea of (1) seeking to construct a (linear) Earth model, and then (2) using that Earth model to reconstruct data is overly restrictive. Rather, we view α_1 as a more general curve-fitting factor that is flexible enough to match the variability of the data. Adopting such a view provides a framework for the extrapolation of both primaries and multiples that does not include as input a knowledge of or determination of the actual medium velocity, while simultaneously maintaining a relatively simple linear form.

In this section we discuss and a linear map of reflected-to-transmitted data. We first present a form of the mapping for a single-parameter 3D acoustic model, then examine it for a 1D normal-incidence problem and carry out an initial analysis regarding accuracy.

3.1 A 3D single-parameter linear reflection-to-transmission mapping

We demonstrate the framework for a linear reflection-to-transmission mapping with a 3D, single-parameter scattering model that assumes medium wavespeed fluctuations away from a homogeneous

fluid reference medium with constant density. Data $D(x_g, y_g, z_g|x_s, y_g, z_s; \omega)$, corresponding to the measurement of a scattered field on a surface defined by fixed z_g (receiver depth) and z_s (source depth), and variable lateral receiver and source locations x_g, y_g and x_s, y_s (respectively) is related to the linear component of the single-parameter acoustic scattering potential $\alpha(x, y, z) = 1 - c_0^2/c^2(x, y, z)$, namely $\alpha_1(x, y, z)$, by

$$\begin{aligned} D(k_{g_x}, k_{g_y}, z_g|k_{s_x}, k_{s_y}, z_s; \omega) = \int_{-\infty}^{\infty} dx' \int_{-\infty}^{\infty} dy' \int_{-\infty}^{\infty} dz' G_0(k_{g_x}, k_{g_y}, z_g|x', y', z'; \omega) \\ \times k^2 \alpha_1(x', y', z') G_0(x', y', z'|k_{s_x}, k_{s_y}, z_s; \omega), \end{aligned} \tag{41}$$

in which the lateral coordinates x_g, y_g and x_s, y_g have been Fourier-transformed into their conjugate domain parameters k_{g_x}, k_{g_y} and k_{s_x}, k_{s_y} respectively, and the G_0's are 3D homogeneous acoustic Green's functions, given explicitly by

$$\begin{aligned} G_0(k_{g_x}, k_{g_y}, z_g|x', y', z'; \omega) &= -\frac{e^{-ik_{g_x}x' - ik_{g_y}y'}}{2\pi} \frac{e^{iq_g|z_g - z'|}}{i2q_g}, \\ G_0(x', y', z'|k_{s_x}, k_{s_y}, z_s; \omega) &= -\frac{e^{ik_{s_x}x' + ik_{s_y}y'}}{2\pi} \frac{e^{iq_s|z' - z_s|}}{i2q_s}. \end{aligned} \tag{42}$$

(The difference in sign on the source and receiver wavenumbers is due to different sign conventions in the Fourier transform.) We next fix the source location to be at depth z' such that $z' > z_s$ for all $\alpha_1(x', z') \neq 0$, which, in addition to the substitution of equations 42 into 41, leads to

$$\begin{aligned} D(k_{g_x}, k_{g_y}, z_g|k_{s_x}, k_{s_y}, z_s; \omega) &= \frac{1}{4\pi^2} \int_{-\infty}^{\infty} dx' \int_{-\infty}^{\infty} dy' \int_{-\infty}^{\infty} dz' \left[e^{-ik_{g_x}x' - ik_{g_y}y'} \frac{e^{iq_g|z_g - z'|}}{i2q_g} \right] \\ &\quad \times k^2 \alpha_1(x', y', z') \left[e^{ik_{s_x}x' + ik_{s_y}y'} \frac{e^{iq_s|z' - z_s|}}{i2q_s} \right] \\ &= -\frac{k^2}{16\pi^2 q_g q_s} e^{-iq_s z_s} \int_{-\infty}^{\infty} dz' e^{iq_g|z_g - z'|} e^{iq_s z'} \alpha_1(k_{g_x} - k_{s_x}, k_{g_y} - k_{s_y}, z'). \end{aligned} \tag{43}$$

Data corresponding to a reflection-like geometry (called, say, R) and a transmission-like geometry (T) derive from equation 43 simply by further fixing the receiver depths in each case to be, respectively, either smaller than all contributing z' values (z_g^R), or greater than all contributing z' values (z_g^T). Such data are then relatable, linearly, to portions of the scattering potential, let us say α_1^R and α_1^T respectively. The inverse scattering series could be solved for α order-by-order in either reflection or transmission data. In orders of reflected data $\alpha = \alpha_1^R + \alpha_2^R + ...$, and in orders of transmission data $\alpha = \alpha_1^T + \alpha_2^T + ...$; the first term in each of these two series correspond to

$$\begin{aligned} R(k_{g_x}, k_{g_y}, z_g^R|k_{s_x}, k_{s_y}, z_s; \omega) &= -\frac{k^2}{16\pi^2 q_g q_s} e^{-i(q_s z_s + q_g z_g^R)} \int_{-\infty}^{\infty} dz' e^{i(q_g + q_s)z'} \alpha_1^R(k_{g_x} - k_{s_x}, k_{g_y} - k_{s_y}, z'), \\ T(k_{g_x}, k_{g_y}, z_g^T|k_{s_x}, k_{s_y}, z_s; \omega) &= -\frac{k^2}{16\pi^2 q_g q_s} e^{-i(q_s z_s - q_g z_g^T)} \int_{-\infty}^{\infty} dz' e^{i(q_s - q_g)z'} \alpha_1^T(k_{g_x} - k_{s_x}, k_{g_y} - k_{s_y}, z'). \end{aligned} \tag{44}$$

Performing the Fourier transforms and solving for α_1^R, we have

$$\begin{aligned}
\alpha_1^R(k_{g_x}-k_{s_x},k_{g_y}-k_{s_y},-q_g-q_s) &= -\frac{4q_gq_s}{k^2}e^{i(q_sz_s+q_gz_g^R)}R(k_{g_x},k_{g_y},z_g^R|k_{s_x},k_{s_y},z_s;\omega),\\
T(k_{g_x},k_{g_y},z_g^T|k_{s_x},k_{s_y},z_s;\omega) &= -\frac{k^2}{4q_gq_s}e^{-i(q_sz_s-q_gz_g^T)}\alpha_1^T(k_{g_x}-k_{s_x},k_{g_y}-k_{s_y},q_g-q_s).
\end{aligned} \tag{45}$$

The idea here is to use the reflection-derived linear inverse α_1^R as computed in equation 45 to estimate the transmitted data, by substitution of α_1^R for α_1^T. It may be of particular interest to point out that this mapping is only possible in the case of a medium that has 2D or 3D variability. Notice that the linearized medium-transmitted wavefield relationship in equation 44 involves a Fourier transform over the depth z, in which the conjugate coordinate is the difference between source and receiver depth wavenumbers. In a 1D medium these depth wavenumbers are equal, and as such the integral captures only the DC component of the vertical wavenumber of α_1^T; in order to "fill the spectrum" of α_1^T with data information, we require a range of contributing $q_g - q_s$ values, which, again, are only present if the medium has lateral variability.

If a source wavelet, $S(\omega)$, is included in the physical description, then the P_0 and P are multiplied by $S(\omega)$, and $G_0(x',y',z',k_{s_x},k_{s_y},z_s;\omega)$ in equation 41 is replaced by $S(\omega)G_0(x',y',z',k_{s_x},k_{s_y},z_s;\omega)$ and equations 45 become

$$\begin{aligned}
S(k_{m_x},k_{m_y},k_{h_x},k_{h_y},k_z)\alpha_1^R(k_{m_x},k_{m_y},k_z) &= A^R(k_{m_x},k_{m_y},k_{h_x},k_{h_y},k_z)R(k_{m_x},k_{m_y},k_{h_x},k_{h_y},k_z)\\
S(k_{m_x},k_{m_y},k_{h_x},k_{h_y},k_z)\alpha_1^T(k_{m_x},k_{m_y},k_z) &= A^T(k_{m_x},k_{m_y},k_{h_x},k_{h_y},k_z)T(k_{m_x},k_{m_y},k_{h_x},k_{h_y},k_z),
\end{aligned} \tag{46}$$

where

$$A^R = -\frac{16\pi^2q_gq_s}{k^2}e^{i(q_sz_s+q_gz_g^R)}, \tag{47}$$

and

$$A^T = -\frac{16\pi^2q_gq_s}{k^2}e^{i(q_sz_s-q_gz_g^T)}, \tag{48}$$

are expressed as functions of k_{m_x}, k_{m_y}, k_{h_x}, k_{h_y} (the midpoint- and offset-conjugate variables, respectively), and depth wavenumber k_z. By simply defining

$$\alpha_1'^R(k_{m_x},k_{m_y},k_{h_x},k_{h_y},k_z) \equiv S(k_{m_x},k_{m_y},k_{h_x},k_{h_y},k_z)\alpha_1^R(k_{m_x},k_{m_y},k_z) = A^RR, \tag{49}$$

and

$$\alpha_1'^T(k_{m_x},k_{m_y},k_{h_x},k_{h_y},k_z) \equiv S(k_{m_x},k_{m_y},k_{h_x},k_{h_y},k_z)\alpha_1^T(k_{m_x},k_{m_y},k_z) = A^TT, \tag{50}$$

we generate a new mapping, in which $\alpha_1'^R$ is determined by the reflection data (including its wavelet), R, and the analytic form A^R. Then, $\alpha_1'^R$ is substituted into equation 50 to determine the transmitted field T including the wavelet. This scheme which only depends on $\alpha_1^R(k_{m_x},k_{m_y},k_z) = \alpha_1^T(k_{m_x},k_{m_y},k_z)$ (a conjecture to be fully examined in a future correspondence) does not in any way require knowledge of the wavelet, let alone its phase character. This wavelet independence is in contrast with the methods based on reciprocity theorems, as given in the Introduction of this paper.

3.2 Analysis of the linear reflection-to-transmission mapping in 1D

We examine the R to T linear map procedure described here for the case of a 1D[†] normally-incident acoustic plane wave on a delta-, or spike-like, velocity perturbation in a homogeneous reference medium. Figure 2 illustrates the 1D model and the two "experimental" configurations we analyze. With source fixed at the origin, $z_s = 0$, and field position at any depth z_g, and the delta-scatterer of amplitude λ placed at z_0, the full non-linear expression for the scattered field in terms of these elements is

$$\psi_s(z_g, z_s = 0, k) = \frac{\frac{k\lambda}{2i} e^{ik|z_g - z_0|} e^{ikz_0}}{1 - \frac{k\lambda}{2i}}. \tag{51}$$

This general expression is specified to correspond to data of either reflection- or transmission-type by setting the receiver at depths shallower or deeper than the scatterer (see Figure 2). These cases result in

$$\begin{aligned} R(z_g, k) &\equiv \psi_s(z_g < z_0, z_s = 0, k) = \frac{\frac{k\lambda}{2i} e^{i2kz_0} e^{-ikz_g}}{1 - \frac{k\lambda}{2i}}, \\ T(z_g, k) &\equiv \psi_s(z_g > z_0, z_s = 0, k) = \frac{\frac{k\lambda}{2i} e^{ikz_g}}{1 - \frac{k\lambda}{2i}}. \end{aligned} \tag{52}$$

Given a homogeneous reference medium characterized by wavespeed c_0, these data are related to their respective linear model components $\alpha_1^R(z)$ and $\alpha_1^T(z)$, using

$$\begin{aligned} R(z_g, k) &= \int_{-\infty}^{\infty} G_0(z_g|z';\omega) k^2 \alpha_1^R(z') \psi_0(z'|0;k) dz', \\ T(z_g, k) &= \int_{-\infty}^{\infty} G_0(z_g|z';\omega) k^2 \alpha_1^T(z') \psi_0(z'|0;k) dz'. \end{aligned} \tag{53}$$

Being sensitive to the relative depths of the source, receiver and integration variable z', the reflection and transmission configurations lead to quite different expressions; with $G_0(z_g|z';\omega) = (i2k)^{-1} \exp(ik|z_g - z'|)$ and $\psi_0(z'|0;k) = \exp(ikz')$ we have

$$\begin{aligned} \frac{2i}{k} R(z_g, k) e^{-ikz_g} &= \widetilde{\alpha}_1^R(-2k) \\ \frac{2i}{k} T(z_g, k) e^{-ikz_g} &= \widetilde{\alpha}_1^T(0), \end{aligned} \tag{54}$$

in which $\widetilde{\cdot}$ signifies that quantity in the conjugate (k) domain. The second equation makes it clear why we will, from here on, be forced to restrict ourselves to comments on the $k = 0$ component of the model. Substituting the analytic data in equations 52 into these formulas for the reflected and transmitted Born inverse approximations, and considering the reflected case at $k = 0$, we have

$$\begin{aligned} \widetilde{\alpha}_1^R(0) &= \lambda \\ \widetilde{\alpha}_1^T(0) &= \lambda. \end{aligned} \tag{55}$$

In other words, at the only k value for which comparable results are available for 1D analysis, $k = 0$, the component of the model that is linear in the reflected data and the component of the

[†]This obviously contravenes the requirement for lateral variability that we just mentioned; as a consequence, we shall only be able to analyze and compare the wavenumber $k = 0$ component of both linear model estimates.

model that is linear in the transmitted data are equal. This is an encouraging result, since we want the linear model component of one configuration to reproduce the data of the other configuration.

The linear method described in this section is based on several assumptions. At the outset is the assumption that an inverse scattering series solution is available in terms of either reflected or transmitted data. (By transmitted data we mean the transmitted portion of the scattered field.) The scattered field, and its transmitted and reflected portions, are all zero when the actual medium corresponds to the reference medium; also, in 2D and 3D the terms of the inverse scattering series may be constructed for both reflected and transmitted data. Hence, there is reason to believe that it is possible to expand the earth property perturbation in terms of either reflected or transmitted data. We further assume that the linear term in these two expansions are the same, or at least not too far apart. That is the key assumption in this linear reflection-to-transmission mapping procedure, and its validity and reasonableness is currently being examined.

If we can establish the validity of this assumption, we may find ourselves with a method of no small applicability, since there are *very few other* assumptions or approximations, linear or otherwise, in the expressions used for α_1^R and α_1^T in equations 44[‡]. Furthermore, since the reference medium is homogeneous, and is never altered or updated, all of the "migrations" of the linear inversion procedure require data only on one side of the closed volume where the wavefield is predicted, i.e., either reflected or transmitted data, independent of whether or not the actual medium supports two-way propagation.

In 1D we have benefited from the ability to consider this linear reflection-to-transmission map analytically, but as a result of this dimensional restriction we are restricted to the $k = 0$ portion of the spectrum of α_1^T. The last example in this section has demonstrated that the assumption $\alpha_1^R = \alpha_1^T$ is valid at this portion of the spectrum. The ability, encountered in 2D/3D cases, to actually construct the terms in the series, and fill the spectrum of the first linear estimate, is not an assurance that all is well with a series solution. However, constructibility supersedes convergence, stability, etc., as a necessary condition for considering a series approach and therefore we have an affirmative response to this important first question. We plan to test these ideas with 2D and 3D examples.

4 Discussion and conclusions

In this section we provide: (1) a perspective on the new approaches for the reflection-to-transmission mapping problem proposed in this paper; (2) a discussion on how these new approaches relate to the research program on task-separated subseries of the inverse scattering series, and to the migration-inversion philosophy and strategy, and (3) a set of open issues that will be addressed and developed, as part of our plan.

In the section on constructing the wavefield at depth, a general formula for $T(\mathbf{p}, \mathbf{q})$, for arbitrary $\mathbf{p}$, $\mathbf{q}$, and a fixed ω, is presented as a series in orders of the measured reflection data. Constructing this $T(\mathbf{p}, \mathbf{q})$ for all $\mathbf{p}$, $\mathbf{q}$ and for a fixed ω is equivalent to computing the scattered wavefield at any

[‡]These are exact equations relating the data to a specific linear approximate model component, but for our current purposes they are viewed as solutions for curve-fitting factors α_1^R and α_1^T.

source and receiver location in the subsurface. (The source and receiver positions are the conjugates of $\mathbf{p}$, $\mathbf{q}$ respectively; all $\mathbf{p}$, $\mathbf{q}$ are 2D or 3D vectors depending on the dimension of variation of the subsurface.) A subset of the formula for $T(\mathbf{p},\mathbf{q})$ at any $\mathbf{p}$, $\mathbf{q}$, namely that computed with (1) $|\mathbf{p}| = |\mathbf{q}| = |\mathbf{k}|$ and (2) the z components of $\mathbf{p}$ and $\mathbf{q}$ (i.e., p_z and q_z) equal to q_s and q_g respectively, is a series for the transmitted component of the scattered field. In 2D, for instance, where $k_{g_x} = k_g$ and $k_{s_x} = k_s$, the transmitted data is $T(k_g, q_g, k_s, q_s; \omega) = T_1(k_g, q_g, k_s, q_s; \omega) + T_2(k_g, q_g, k_s, q_s; \omega) + \ldots$; T_n is n'th order in the measured reflection data, which is $T(k_g, -q_g, k_s, q_s; \omega)$. This is a reflection-to-transmission data map in orders of the reflection data. In theory, it requires knowledge of the signature of the source wavelet, but it does not make any assumptions regarding this wavelet, and is not limited to wavelets or data with particular (minimum) phase properties. The latter, but not the former, is also a property of linear map method for R-to-T construction we have presented. Further examination of these ideas as to their practical implementation is under way.

In the recent work on the inverse scattering series for imaging and inverting primaries (Weglein et al., 2000; Weglein et al., 2001; Weglein et al., 2003; Shaw and Weglein, 2003; Innanen, 2003; Innanen and Weglein, 2003; Shaw et al., 2004; Shaw, 2005; Zhang and Weglein, 2005; Innanen, 2005; Liu et al., 2005a and 2005b) the location of structure is determined by following the action of the inverse series in taking data towards earth material property maps. The individual acoustic, elastic or anelastic properties are placed at the locations where they each, individually, experience a rapid variation; the values of the changes in those properties, at those interfaces, are also separately determined.

In the history of seismic migration and seismic inversion, there was a development (e.g., Stolt and Weglein, 1985) that took a different route to the location and parameter estimation problem. Rather than going directly from data to location and magnitude of Earth properties, it was suggested that there were conceptual and practical advantages to, first, downward continuing and imaging the wavefield to produce a structural map; second, recognizing that the amplitude of that imaged quantity is related to the local, angle-dependent reflection coefficient; and third, using that coefficient to determine changes in local earth material properties. Amongst the advantages of this two step approach, labeled Migration-Inversion, or migration before inversion, are: (1) the structural map does not require that one follow all the trials and tribulations of each earth property, changing its value as it finds its correct spatial location; (2) the *location* of reflectors may only depend on the velocity of wave propagation and not require each separate earth property to be defined; (3) the petroleum industry has a rich, mature and developed experience in locating structure using wavefield extrapolation and imaging techniques. Behind this philosophy is the view that location is governed principally by a transmission process that cares about the average velocity and its slowly varying components, and a reflection process, within the imaged amplitude, that cares about rapid local changes in earth properties.

Of course, all current migration and migration-inversion algorithms depend upon an adequate velocity model to determine structure. In this paper, the section on predicting the wavefield at depth without the velocity model is providing a first embryonic step toward a response to the migration-inversion strategy for locating structure followed by inversion, when the adequate velocity model is unavailable. There are many important targets e.g, beneath salt, basalt and karsted sediments where this lack of adequate velocity model availability is the norm, and without an effective, currently available solution. Our purpose is to have these research efforts and approaches reported here contribute towards and advance a practical response.

We anticipate a strategy and plan as follows: for subsalt plays with often ill-defined or nonexistent images at the target (with all current leading edge velocity analysis and imaging methods), it is reasonable to start by setting the goal as the determination of a well-defined accurate depth image, or structure map, temporarily neglecting the more ambitious earth property and rock and fluid prediction. For that objective, an imaging theory involving multi-dimensional heterogeneity in acoustic velocity only, i.e., the inverse scattering imaging subseries for determining the location of rapid changes governed by an acoustic medium (without requiring an adequate velocity model; see previous references) would be a good first step in moving towards a sub-salt field data test. Once the sub-salt target location issue is successfully addressed, the next level of ambition will arrive, i.e., to use the angle dependent amplitude of the structure map to determine the local earth mechanical and then rock and fluid properties. At that point, the idea of imaging the actual wavefield in depth without an adequate velocity model, as progressed in this paper, becomes relevant. Equations 35 and 38 are direct calculations of the wavefield at depth that nevertheless could benefit from task specific insights/algorithms (using, e.g., only the imaging terms) to provide a structural map from an imaged wavefield at depth. In this strategy we concentrate, as a first pass, on the acoustic location properties of the inverse scattering series, but anticipating that they will evolve into an imaged wavefield at depth procedure, to be viewed as a new task with its own task specific subseries. The task-separated stages of inversion will become: (1) removal of free surface multiples; (2) removal of internal multiples; (3) production of accurate angle dependent reflection coefficients (i.e., the scattering operator) at depth; and (4) estimation of earth material properties.

The inverse scattering series is a comprehensive theory and inversion methodology for removing multiples, and imaging and inverting primaries. The theory operates *directly* in terms of reflection data and an estimate of medium propagation properties, the latter of which is neither assumed to be adequate, nor ever changed (e.g., iterated) towards adequacy. Directness means that the theory provides algorithms that output the specific indicated inverse objective without the use of external measures of effectiveness, nor centering itself around the minimization of an objective function. As such, horizontal common image gathers, for instance, or any move-out trajectory or weighted sums thereof – criteria at the heart of many valuable and worthwhile processing methods – are not called upon, or required in these direct procedures. The construction of desired inverse quantities, using task-specific subseries and algorithms derived from the inverse scattering series, are distinct from methods based on such criteria precisely because of this directness. In this paper, we have described: (1) how velocity-independent imaging algorithms can benefit from the availability or prediction of transmission data; (2) how new concepts that originate from the inverse scattering series can contribute to the satisfaction of that transmission data interest, without the typical need for phase assumptions on the reflection data; finally and separately, (3) how the wavefield at all depths can be predicted without a back-propagation in the actual subsurface.

5 Acknowledgments

A.B. Weglein and B.G. Nita, and students C. Fan, H. Zhang and F. Liu gratefully acknowledge the partial support of NSF-CMG program under grant DMS-0327778. G. Pavlis was also supported by NSF-CMG grant number DMS-0327827. A. B. Weglein, B. G. Nita and K. A. Innanen, and students J. Zhang and A. C. Ramírez also gratefully acknowledge the partial support of DOE grant number DOE-De-FG02-05ER15697. M-OSRP sponsors are thanked for their support.

References

Bakulin, A. and R. Calvert, 2004, Virtual Source: new method for imaging and 4D below complex overburden: SEG Expanded Abstracts, 74th Annual Meeting, Denver, Colorado.

Bostock, M. 2004, Green's functions, source signatures, and the normalization of teleseismic wavefields: Journal of Geophysical Research B: Solid Earth, **109**, no.3, pp. B03303 1–15.

Claerbout, J. F., 1968, Synthesis of a layered medium from its acoustic transmission response: Geophysics, **33**, 204–209.

Duvall, T. L., S. M. Jefferies, J. W. Harvey and M. A. Pomerantz, 1993, Time-distance helioseismology: Nature, **362**, 430–432.

de Hoop, M. V. and A.T. de Hoop, 2000, Wavefield reciprocity and optimization in remote sensing: Proceedings of the Royal Society of London, Series A (Mathematical, Physical and Engineering Sciences), **456**, pp. 641–682.

Fan, C, G. L. Pavlis, A. B. Weglein, B. G. Nita 2005, Free Surface Effect and Separation of Teleseismic Waves: Transmission and Reflection, Primary vs Multiple: presented at 2005 AGU/SEG Joint meetings, New Orleans, LA.

Fan, C., G. L. Pavlis, A. B. Weglein, B. G. Nita, 2006, Exploiting the free surface effect to separate forward and back scattered teleseismic wavefields: this issue of Geophysics.

Fokkema, J. T., and P. M. Van den Berg, 1993, Seismic applications of acoustic reciprocity: Elsevier Scientific Publication Co.

Goldberger, M. L., and K. M. Watson, 1964, Collision theory: John Wiley and Sons.

Herman, G. C., 1992, Estimation of the inverse acoustic transmission operator of a heterogeneous medium directly from its reflection operator: Inverse Problems, **8**, 559–574.

Innanen, K. A., 2003, Methods for the treatment of acoustic and absorptive/dispersive wavefield measurements: Ph.D. Thesis, University of British Columbia, Vancouver, Canada.

Innanen, K. A. and A. B. Weglein, 2003, Simultaneous imaging and inversion with the inverse scattering series: SBGf 2003 (Sociedade Brasileira de Geofísica) Expanded Abstracts.

Innanen, K. A., 2005, Two non-linear forward and inverse wavefield approximations in the presence of sustained medium perturbations: Expanded Abstracts of the 2005 Technical Program of the Society of Exploration Geophysicists, Society of Exploration Geophysicists, Houston, TX, USA.

Kennett, B. L. N., K. Koketsu, A. J. Haines, 1990: Propagation invariants, reflection and transmission in anisotropic, laterally heterogeneous media, Geophys. J. Int., **103**, pp. 95–101.

Larose E., A. Derode, M. Campillo and M. Fink, 2004, Imaging from one-bit correlations of wideband diffuse wavefields: Journal of Applied Physics, **95**, 8393–8399.

Liu F, A. B. Weglein, K. A. Innanen and B.G. Nita, 2005a, Extension of the non-linear depth imaging capability of the inverse scattering series to multidimensional media: strategies and numerical results: SBGf (Sociedade Brasileira de Geofísica) Expanded Abstracts.

Liu, F., S. A. Shaw, H. Zhang, K. Innanen, Z. Guo, J. Zhang, A. C. Ramírez, D. Foster, K. Matson, R. Keys, F. Araujo, P. Carvalho, P. Traynin, P., R. Stolt, S. Kaplan, and A. B. Weglein, 2005b, A response to the most pressing seismic E&P challenges: imaging and inversion beneath a complex, multi-dimensional ill-defined overburden: Intel Viz Theater (presented by A. B. Weglein), Society of Exploration Geophysicists International Exposition and Seventy-Fifth Annual Meeting, Houston, TX, USA.

Malcolm, A. E., J. A. Scales, and B. A. van der Tiggelen, 2004, Retrieving the Green function from diffuse equipartitioned waves: Physical Review E, **70**, 015601(R).

Moses, H. E., 1956, Calculation of scattering potential from reflection coefficients: Physical Review, **102**, pp 559–567.

Nita, B. G. and A. B. Weglein, 2005, On acoustic reciprocity theorems and the construction of transmission response from reflection data: Mission-Oriented Seismic Research Program (M-OSRP) 2004 Annual Report pp. 271.

Razavy, M., 1975, Determination of the wave velocity in an inhomogeneous medium from reflection data: Journal of the Acoustical Society of America, **58**, 956–963.

Rickett, J., and J. Claerbout, 1999, Acoustic daylight imaging via spectral factorization: Helioseismology and reservoir monitoring: The Leading Edge, **18**, 957–960.

Roux, P., K.G. Sabra, W.A. Kuperman and A. Roux, 2005, Ambient noise crosscorrelation in free space: theoretical approach: Journal of the Acoustical Society of America, **117**, 79–84.

Sabra, K.G., P. Gerstoft, P. Roux, W.A. Kuperman and M. C. Fehler, 2005, Extracting time-domain Greens function estimates from ambient seismic noise: Geophysical Research Letters, **32**, doi: 10.1029/2004GL021862.

Schuster, G. T., 1999, Seismic interferometric imaging with waveforms, Utah Tomography and Modeling-Migration: Project Midyear Report, 121–130.

Schuster, G.T., Z. Liu and F. Followill, 1997, Migration of autocorrelograms: Expanded Abstracts of the 1997 Technical Program of the Society of Exploration Geophysicists with Biographies, pp. 1893–1896, Society of Exploration Geophysicists, Tulsa, OK.

Schuster, G. and J. Rickett, 2000, Daylight imaging in V(x, y, z) media, Utah Tomography and Modeling-Migration: Project Midyear Report and Stanford Exploration Project Midyear Reports, pp. 55–66.

Schuster, G. T., 2001, Theory of daylight/interferometric imaging: Tutorial: 63rd European Association of Exploration Geophysicists Annual Meeting, Extended Abstract, A032.

Schuster, G. T., J. Yu, J. Sheng, and J. Rickett, 2004, Interferometric/daylight seismic imaging: Geophysical Journal International, **157**, 838–852.

Shapiro, N. M. and M. Campillo, 2004, Emergence of broadband Rayleigh waves from correlations of the ambient seismic noise: Geophysical Research Letters, **31**, L07614.

Shapiro, N. M., M. Campillo, L. Stehly and M. H. Ritzwoller, 2005, High resolution surface wave tomography from ambient seismic noise: Science, **307**, 1615–1617.

Shaw, S. A. and A. B. Weglein, 2003, Imaging seismic reflection data at the correct depth without specifying an accurate velocity model: initial numerical examples of an inverse scattering subseries: Frontiers of remote sensing information processing, C.H. Chen (ed.), World Scientific Publishing Co.

Shaw, S. A., A. B. Weglein, D. J. Foster, K. H. Matson and R. G. Keys, 2004, Isolation of a leading order depth imaging series and analysis of its convergence properties: Journal of Seismic Exploration, **13** (2), pp. 99–120.

Shaw, S. A., 2005, An inverse scattering series algorithm for depth imaging of reflection data from a layered acoustic medium with an unknown velocity model: Ph.D. Thesis, University of Houston, Houston, TX, USA.

Sheng, J., 2001, Migration of multiples and primaries in CDP data by crosscorrelogram migration: Expanded Abstracts of the 2001 Technical Programme of the Society of Exploration Geophysicists, pp. 1297–1300, Society of Exploration Geophysicists, Tulsa, OK, USA.

Snieder, R., A. Gret, H. Douma and J. Scales, 2002, Coda wave interferometry for estimating nonlinear behavior in seismic velocity: Science, **295**, pp. 2253–2255.

Snieder, R., 2004, Extracting the Green's function from the correlation of coda waves: A derivation based on stationary phase: Physical Review E, **69**, 046610.

Stolt, R. H. and B. Jacobs, 1981, An approach to the inverse seismic problem: SEP Report 25, 121–132.

Stolt, R. H. and A. B. Weglein 1985, Migration and inversion of seismic data: Geophysics, **50**, pp. 2458–2472.

Stolt, R. H., 2002, Seismic data mapping and reconstruction: Geophysics **67**, 890–908.

Takenaka, H., B. L. N. Kennett, K. Koketsu, 1993, The integral operator representation of propagation invariants for elastic waves in irregularly layered media: Wave Motion, **17**, pp. 299–317.

Taylor, J. R., 1972, Scattering Theory: New York, Wiley.

Wapenaar, C. P. A. and F. J. Herrmann, 1993, True-amplitude migration taking fine-layering into account: Expanded Abstracts of the 1992 Technical Programme of the Society of Exploration Geophysicists, Society of Exploration Geophysicists.

Wapenaar, K. and J. L. T. Grimbergen, 1996, Reciprocity theorems for one-way wavefields: Geophysical Journal International, **127**, pp. 169–177.

Wapenaar, K., 2003, Synthesis of an inhomogeneous medium from its acoustic transmission response: Geophysics, **68**, pp. 1756–1759.

Wapenaar, K., 2004, Retrieving the elastodynamic Greens function of an arbitrary inhomogeneous medium by crosscorrelation: Physical Review Letters, **93**, 254–301.

Wapenaar, K., J. Thorbecke, and D. Draganov, 2004, Relations between reflection and transmission responses of three-dimensional inhomogeneous media: Geophysical Journal International, **156**, pp. 179–194.

Weaver, R.L., and O.I. Lobkis, 2004, Diffuse fields in open systems and the emergence of the Greens function: Journal of the Acoustical Society of America, **116**, 2731–2734.

Weglein, A. B., W. E. Boyse and J. E. Anderson 1981, Obtaining three-dimensional velocity information directly from reflection seismic data: an inverse scattering formalism: Geophysics, **46**, pp. 1116–1120.

Weglein, A. B., F. A. Gasparotto, P. M. Carvalho, and R. H. Stolt, 1997, An inverse scattering series method for attenuating multiples in seismic reflection data: Geophysics, **46**, pp. 1975–1989.

Weglein, A. B. and R. H. Stolt, 1999, Migration-inversion revisited: The Leading Edge, **18**, p. 950-975

Weglein, A. B. , K. H. Matson, D. J. Foster, P. M. Carvalho, D. Corrigan, S. A. Shaw, 2000, Imaging and inversion at depth without a velocity model: theory, concepts and initial evaluation: SEG Expanded Abstracts, 70th Annual Meeting of the Society for Exploration Geophysicists, Calgary, Canada.

Weglein, A. B., D. J. Foster, K. H. Matson, S. A. Shaw, P. M. Carvalho, and D. Corrigan, 2001, An inverse-scattering sub-series for predicting the spatial location of reflectors without the precise reference medium and wave velocity: SEG Expanded Abstracts, **20**, pp. 2108.

Weglein, A. B., F. V. Araújo, P. M. Carvalho, R. H. Stolt, K. H. Matson, R. T. Coates, D. Corrigan, D. J. Foster, S. A. Shaw, and H. Zhang, 2003, Inverse scattering series and seismic exploration: Inverse Problems, **19**, R27–R83.

Weglein, A. B., and W. Dragoset, 2005, Multiple attenuation: Society of Exploration Geophysicists Reprint Series.

Zhang, H. and A. B. Weglein, 2005, The inverse scattering series for tasks associated with primaries: depth imaging and direct non-linear inversion of 1D variable velocity and density acoustic media: Expanded Abstracts of the 2005 Technical Programme of the Society of Exploration Geophysicists, Society of Exploration Geophysicists, Houston, TX, USA.

Symbols	
$\mathbb{1}$	Unit operator
c, c_0	Actual, reference velocity
$\mathbf{G}$, $\mathbf{G_0}$	Actual, reference Green's operator
$\mathbf{k} = (\omega/c_0)\widehat{\mathbf{k}}$	Incident wave-vector
$\mathbf{k}' = \lvert\mathbf{k}\rvert\widehat{\mathbf{r}}$	A wave-vector directed towards observation point $\widehat{\mathbf{r}}$
$\widehat{\mathbf{k}}$	Unit vector in the direction of $\mathbf{k}$
(x_g, y_g, z_g)	Receiver coordinates
(x_s, y_s, z_s)	Source coordinates
k_{g_x}, k_{g_y}	Fourier conjugates to x_g, y_g
k_{s_x}, k_{s_y}	Fourier conjugate to x_s, y_s
k_{m_x}, k_{m_y}	Midpoint-conjugate variables
k_{h_x}, k_{h_y}	Offset-conjugate variables
$\mathbf{L}$, $\mathbf{L_0}$	Actual, reference differential operator
$\mathbf{P}$, $\mathbf{P}_0$	Actual, reference wave operator
$\mathbf{p} = (p_x, p_y, p_z)$	3D Fourier conjugate to $\mathbf{r} = (x, y, z)$
p_{g_x}, p_{s_x}, p_{g_y}, p_{s_y}	Fourier conjugates to x_g, x_s, y_g, y_s
p_{g_z}, p_{s_z}	Fourier conjugates to z_g, z_s
P^+, P^-	Flux-normalized down-going, up-going wavefields
q_g, q_s	Depth wave-numbers
R	Reflection response
$\mathbf{r}$, $\mathbf{r}'$, $\mathbf{r}_s$	Field point, scattering point, source point
s,$s_{A,B}$,s_A,s_B, $S(\omega)$	Source signature
T	Transmission response
$\mathbf{T}(\mathbf{k}, \mathbf{k}')$, $\mathbf{T}(\mathbf{p}, \mathbf{p}')$	T-matrix, generalized T-matrix
$\mathbf{V}$	Perturbation operator
$V(x, y, z)$	Inhomogeneity located between z_m and z_M
$W(\mathbf{k})$	Fourier transform of $\alpha(\mathbf{r})$
$\mathbf{x}_A$,$\mathbf{x}_B$	Spatial coordinates of the sources
z_0	The location of the delta-scatter
z_M, z_m	Upper, lower limit of inhomogeneity $V(x, y, z)$
$\alpha(\mathbf{r})$	Velocity perturbation
α_1^R	Reflection-derived linear inverse
α_1^T	Transmission-derived linear inverse
ω	Temporal frequency
Ψ_s	Scattered field operator
ψ_s, ϕ_s	Scattered wave fields
$\psi_s^{(n)}$ $n = 1, 2, \cdots$	The portion of the wavefield that is n-th order in the measured data
λ	The amplitude of the delta-scatter

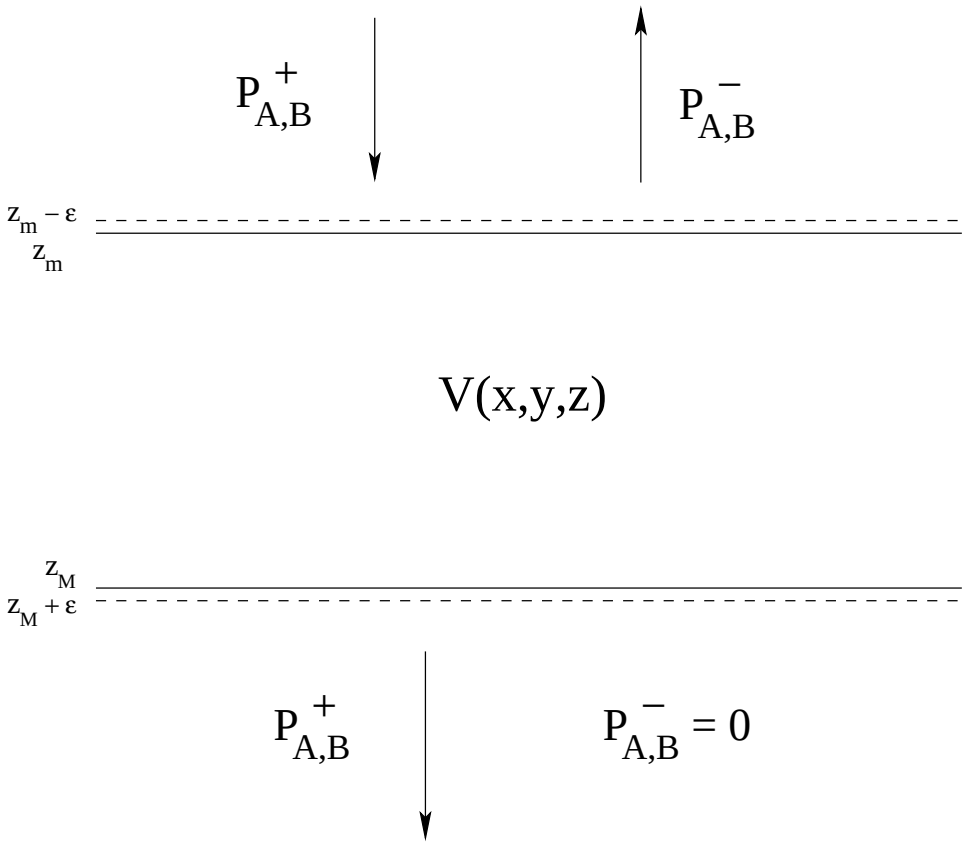

Figure 1: *The choice of acoustic states in an experiment without free surface and corresponding up-going and down-going wavefields.*

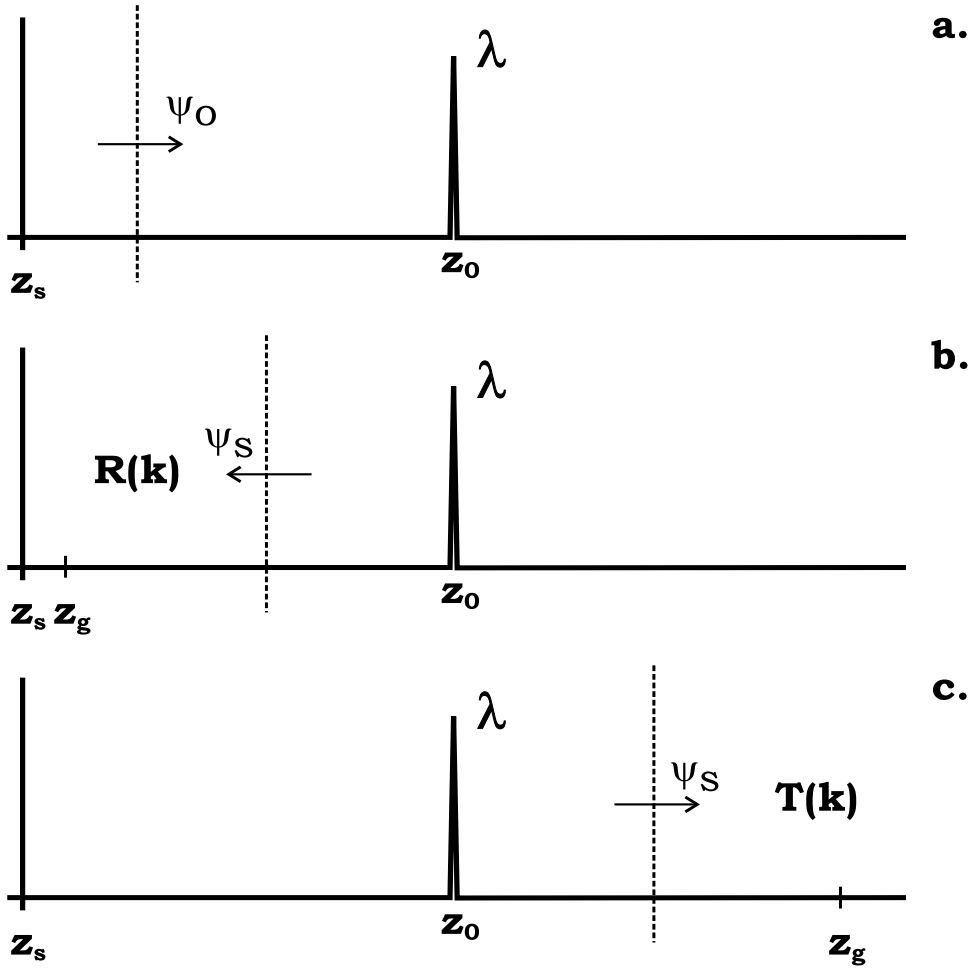

Figure 2: *Schematic illustration of the 1D delta-scatterer analytic framework. (a) The incident plane wave ψ_0 propagates toward the scatterer $\lambda\delta(z-z_0)$; (b) the reflection response with $z_g < z_0$; (c) the transmission response with $z_g > z_0$.*

Multi-dimensional seismic imaging using the inverse scattering series

Fang Liu, Arthur B. Weglein, Kristopher A. Innanen, Bogdan G. Nita

Abstract

The inverse scattering series (ISS) is a comprehensive theory for processing primaries and multiples without the traditional need for an adequate velocity model. Weglein et al. (2003), Shaw et al. (2003a), and Shaw (2005) describe an application of ISS that achieves accurate depth of the subsurface reflectors with no prior knowledge of subsurface velocity. However, this is essentially the 1D activity of a multidimensional theory. The work described in this paper is geared towards understanding and incorporating the ISS mechanisms that act directly on 2D/3D data to locate reflectors in 2D/3D space. Some of these mechanisms have 1D analogs, while others do not, in fact, we currently regard the lateral/vertical imaging problem as, loosely, a series expansion about the *vertical* problem, whose terms are most analogous to the depth-only 1D algorithms referenced above. In themselves these terms can be demonstrated to provide value as the basis for imaging algorithms. We do so in this paper, with a numerical application of the partial capture of 2D imaging terms on two synthetic models. We further present and discuss a low order term of the 2D-only ISS imaging subseries in terms of its expected activity, and describe in detail how the large-contrast form of the algorithm used in the numerical examples is derived from the inverse scattering series.

1 Introduction

The inverse scattering series is a direct, non-linear inverse procedure for the reconstruction of an unknown spatial distribution of multidimensional medium parameters in terms of only measurements of a reflected wave field. The history of its investigation as a tool for the processing and inversion of seismic data, and the development of the task-separated treatment of the ISS, is detailed by Weglein et al. (2003). The ISS had been cast to individually carry out what are externally defined to be classical objectives of seismic data processing and inversion: (1) elimination of free surface multiples, (2) attenuation of internal multiples, (3) location in depth of rapid variations of medium parameters (imaging), and (4) determination of the parameter changes at those locations (inversion). The ISS expands the desired output as an infinite series in terms of only the data and a chosen (often very simple) reference Green's function, thus each of the above tasks is additionally carried out without an accurate input velocity model.

In our current task-specific methods, terms from the inverse series with different purposes are identified and grouped together to form subseries. In this paper we study the components of the ISS whose purpose is specifically to obtain the location in depth of reflectors given only the data and a simple (and highly inaccurate) reference Green's function as input. For the numerical examples in this paper, we assume: the availability of the source wavelet, the the removal of ghosts and the free-surface multiples.

We work in the simplest framework that allows study of one new aspect of the problem or issue that is of interest, and has not yet been addressed. Ultimately, these issues (now understood) will be combined to achieve a processing tool of sufficient realism to be of practical application. In the research we describe herein, we move from 1D to multi-dimensional subsurface structure - a step that has a plethora of new issues and challenges to address beyond what is faced in a 1D medium. In this paper, we consider the idealized problem of non-linear, ISS-based imaging (Weglein et al. (2000); Shaw et al. (2003a)) in a constant-density acoustic medium, as described for the 1D prestack case by Shaw (2005), with the added complexity of lateral variability in the unknown medium parameter.

In this paper, we begin with a brief review of the ISS, followed by a discussion of a form of the linear inverse, given a line source in a homogeneous reference medium. The patterns of the imaging terms of the ISS are investigated; several second-order terms deemed to be responsible for 2D reflector location tasks are presented and described (see equation (7) and (8)).

The 2D imaging subseries is next discussed as a cascaded infinite series containing (1) leading order and portions of higher-order imaging contributions amounting to laterally varying 1D prestack forms, and (2) further ISS terms that have no 1D analogy. These latter terms only address issues that relate to 2D phenomena, e.g., lateral variations and diffractions. On the salt model tested here that term may be seen to initiate action to accomplish some combination of intrinsically 2D tasks (e.g., lateral shift, diffraction processing) without knowing the velocity model.

We illustrate with numerical examples, in particular carried out on the salt model, within a $k_h = 0$ setting (k_h is the offset-conjugate wavenumber; see Clayton and Stolt (1981) for more detailed definition) using a formula incorporating components (1) in the previous paragraph (i.e., in which a correction similar to the 1D normal incident case is performed at each lateral location). These include both leading and higher-order imaging subseries terms, the latter of which we show become quite pronounced for large contrast velocity models. We demonstrate the use of these 2D forms on two input models. The numerical tests of the higher-order imaging algorithm on data from these models is encouraging.

Appendix A provides a new understanding of the current task-isolated higher-order imaging series in relation to other high-order ISS primary processing mechanisms. Appendix B describes the ongoing development a more general framework for direct multidimensional imaging, i.e., in which $k_h \neq 0$.

2 Background

In operator form, the differential equations describing wave propagation in an actual and a reference medium can be written as

$$LG = -I \qquad L_0 G_0 = -I \tag{1}$$

where L, L_0 and G, G_0 are the actual and reference differential and Green's operators, respectively, for a single temporal frequency (ω) and I is the identity operator. The perturbation V is defined as $V = L_0 - L$. The Lippmann-Schwinger equation, $G = G_0 + G_0 V G$, may be expanded to form

the forward scattering series:

$$G - G_0 = G_0 V G_0 + G_0 V G_0 V G_0 + \cdots . \tag{2}$$

As detailed by Weglein et al. (2003), the representation of $V = V_1 + V_2 + V_3 + \cdots$ in equation (2) as an infinite series in orders of the measured scattered wave field $G - G_0$, gives rise to the ISS when like orders are equated:

$$\begin{array}{rcl} D &=& G - G_0 = G_0 V_1 G_0 \\ 0 &=& -G_0 V_2 G_0 - G_0 V_1 G_0 V_1 G_0 \\ 0 &=& -G_0 V_3 G_0 - G_0 V_1 G_0 V_2 G_0 - G_0 V_2 G_0 V_1 G_0 \\ && -G_0 V_1 G_0 V_1 G_0 V_1 G_0 \\ && \vdots \end{array} \tag{3}$$

etc. For a constant density acoustic reference medium characterized by wavespeed c_0, the relationship between the perturbation and the velocity is: $c_0^2 V/\omega^2 = \alpha(z)$, where $\alpha(z) = 1 - c_0^2/c^2(z)$. Through the use of a variety of changes of integration variable and instances of integration by parts, Shaw (2005) identifies a portion of the ISS sum $\alpha = \alpha_1 + \alpha_2 + \alpha_3 + \cdots$ that acts *only* to alter the locations of the discontinuities of the linear inverse α_1 from the wrong depth to the correct depth. First we consider the leading-order imaging subseries and its closed-form (c.f. Shaw et al. (2003a)):

$$\begin{array}{rl} \alpha_{IM}(z) &= \sum\limits_{n=0}^{\infty} \frac{(-1/2)^n}{n!} \alpha_1^{(n)}(z) \left(\int\limits_0^z \alpha_1(z')dz' \right)^n \\ &= \alpha_1 \left(z - \frac{1}{2} \int\limits_0^z \alpha_1(z')dz' \right) \end{array} \tag{4}$$

The terms in the series above were exposed and isolated after integration by parts. They have two characteristics: (1) a derivative of the linear inverse with respect to the coordinate in which the reflector location is being corrected, (2) weighted by a depth integral of the same linear inverse. We proceed with a study of related forms in the more complex 2D case.

2.1 Equations for multidimensional imaging

Equation (3) can be solved for 2D constant density acoustic media, in which the single perturbation parameter,

$$\alpha(x,z) = 1 - c_0^2/c^2(x,z), \tag{5}$$

is the essential quantity. In the ISS representation our objective is solved for as an infinite series, $\alpha(x,z) = \alpha_1(x,z) + \alpha_2(x,z) + \alpha_3(x,z) + \cdots$. The first term (linear inverse) is expressible in terms of the data via the solution of the first equation in (3) as Clayton and Stolt (1981):

$$\widetilde{\widetilde{\alpha}}_1(k_m, k_z) = -\frac{4k_z^2}{k_z^2 + k_m^2} \widetilde{\widetilde{D}} \left\{ k_m, \frac{c_0 k_z}{2} \sqrt{1 + \frac{k_m^2}{k_z^2}} \right\}, \tag{6}$$

in the midpoint conjugate (k_m) and depth conjugate (k_z) domains with the restriction $k_h = 0$ (for a more general framework, see Appendix B); the quantity $\widetilde{\widetilde{D}}$ as it appears is computed from wave

field information on the measurement surface:

$$\widetilde{\widetilde{D}}\left\{k_m,\omega\right\} = \int_{-\infty}^{\infty} dx_m \int_{-\infty}^{\infty} dt \int_{-\infty}^{\infty} dx_h e^{i(\omega t - k_m x_m)} D\left\{x_m + \frac{x_h}{2}, x_m - \frac{x_h}{2}, t\right\}$$

where the data in the integrand are considered in the source and receiver coordinates: $D(x_g, x_s, t)$. With this computation, in lateral and depth coordinates, of the linear inverse, we turn to the non-linear terms of the ISS, and express them as operations on $\alpha_1(x,z)$ in analogy to the 1D case, we also apply the integration-by-parts strategy to extract terms with the imaging-like aspect visible in equation (4). Solving the second equation in (3) for $\alpha_2(x,z)$, and manipulating the results accordingly, produces, amongst other terms (Liu et al. (2005b)):

$$\alpha_1(x,z) = -\frac{1}{2}\frac{\partial \alpha_1(x,z)}{\partial z}\int_0^z \alpha_1(x,z')dz', \quad \text{and} \tag{7}$$

$$\alpha_1(x,z) = -\frac{1}{2}\frac{\partial \alpha_1(x,z)}{\partial x}\int_0^z \int_0^{z'} \frac{\partial \alpha_1(x,z'')}{\partial x} dz'. \tag{8}$$

These two terms bear resemblance to the imaging terms in Shaw et al. (2003a). Equation (7) is an exact reproduction of the 1D depth imaging mechanism, involving a first derivative of α_1 with respect to depth weighted by the integral of α_1 down to that depth. The term in equation (8), meanwhile (with no analogous 1D term), has the expected hallmarks of a lateral corrector at second order, involving a first derivative with respect to the lateral coordinate, weighted by the depth integral of the rate of change of α_1. Notice that this term will vanish if the linear inverse does not vary laterally. We surmise that this term is the first in an infinite series correcting the lateral error in the linear inverse.

The above analysis leads to two main conclusions. First, the presence, in the multi-D case, of an exact reproduction of the 1D depth imaging engine, as terms that are zeroth order in $\partial\alpha_1/\partial x$ (and the tendency of the imaging terms of the ISS to behave like nested, or cascaded Taylors series), suggests that we consider the vertical and lateral imaging problem as being akin to a series expansion about the purely vertical imaging problem. Lateral corrector terms that are of low order should be effective when applied to problems involving slow lateral variability; rapid lateral variations will evidently require terms of higher-order in $\partial\alpha_1/\partial x$. Second, this re-appearance of the same patterns as those found in the 1D case allow for the same summations to closed-form that exists in 1D scenarios. Hence, the zeroth order lateral corrector, and a portion of leading order depth corrector expression for the 2D case is (c.f. equation (4)):

$$\alpha_{LOIS}(x,z) = \alpha_1\left(x, z - \frac{1}{2}\int_0^z \alpha_1(x,z')dz'\right). \tag{9}$$

We refer to the quantity above as "leading-order imaging subseries" (LOIS) to conform with descriptions of the 1D imaging algorithm. Leading order refers to the fact that the subseries coefficients are approximated as the integral of the first power of α_1 only (Shaw, 2005). Similarly, then, to the imaging mechanism of Shaw's analysis, equation (9) can achieve accurate depth imaging for media

of low- to moderate-velocity contrast. It is a depth corrector that involves the same engine as in the 1D case, but with a different quantity under scrutiny at each x.

We have had occasion to study idealized Earth models whose constrast levels have been of a size too large for the leading order mechanisms alone to be used; this has led to some effort at incorporation of high-order ISS reflector location terms, as part of a new partial higher-order imaging without inversion formula. The introduction to this Annual Report describes the development, context and motivation that lead Liu to this form; further, in Appendix A we show how a primitive result in this effort, that amounts to a 1D higher-order imaging and inversion algorithm, can lead to this form in that limited 1D environment, if a Jacobian is set to one. Liu has taken it through the large generalizing leap to the 2D case, and additionally generated an imaging without inversion formula, which, as a task-isolated form, is our objective. The imaging form is

$$\alpha_{HOIS}\left(x, z+\frac{1}{2}\int_0^z \frac{\alpha_1(x,z')}{1-0.25\alpha_1(x,z')}\right)=\alpha_1(x,z); \tag{10}$$

By comparing this expression to the leading order form, the effect of the higher order terms, (an alteration in the integrand), which will become significant for larger contrast media, are noticeable. We hereafter refer to this task-separated direct imaging formula as HOIS.

We next explore this new formula as applied to a set of acoustic models.

2.2 Numerical examples

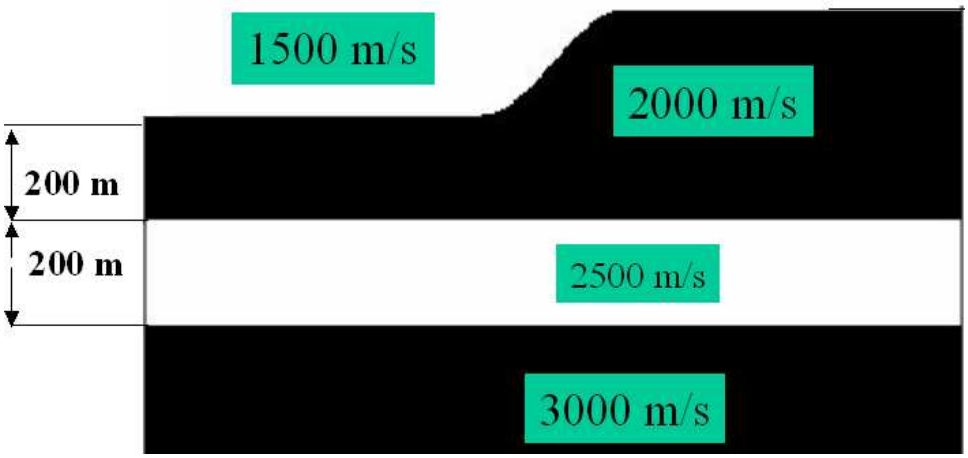

Figure 1: *The geometry and velocity distribution of geological model-1.*

We present two examples of the "low lateral order" 2D imaging algorithms of eqns (6) and (10). Fig 1 illustrates model 1 and Fig 2 shows a sample shot record from the synthetic data sets acquired from model 1. The data are created using a fourth-order finite difference scheme, with a temporal sampling rate of 2ms and a lateral spatial sampling rate of $5m$. The source signature is the first derivative of a Gaussian (peak frequency of $28Hz$). The resultant data are used as described above to compute the linear inverse associated with a homogeneous reference medium of wavespeed

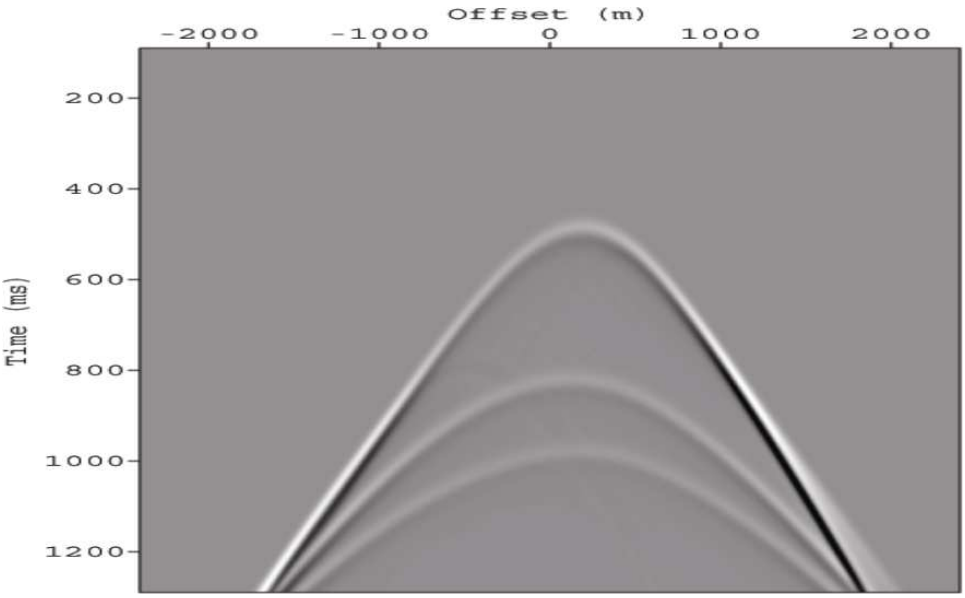

Figure 2: *A sample finite-difference synthetic shot gather acquired from model-1.*

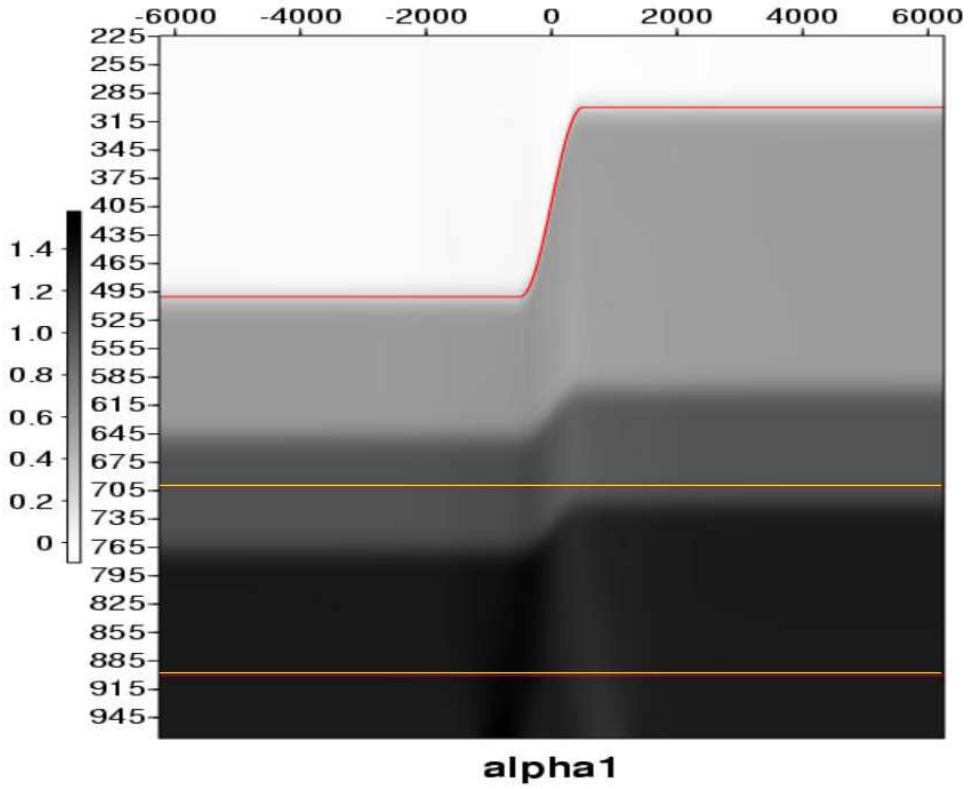

Figure 3: *Model 1 linear imaging results α_1, here only the water-bottom is correctly imaged by the water-speed.*

$c_0 = 1500m/s$. First, the linear term α_1 (Figure 3) is calculated from data according to equation (6), then the higher-order imaging subseries (Figure 4) is calculated via equation (10). In Figures 3 and 4 the colored lines are the benchmarks indicating the correct locations of three reflectors.

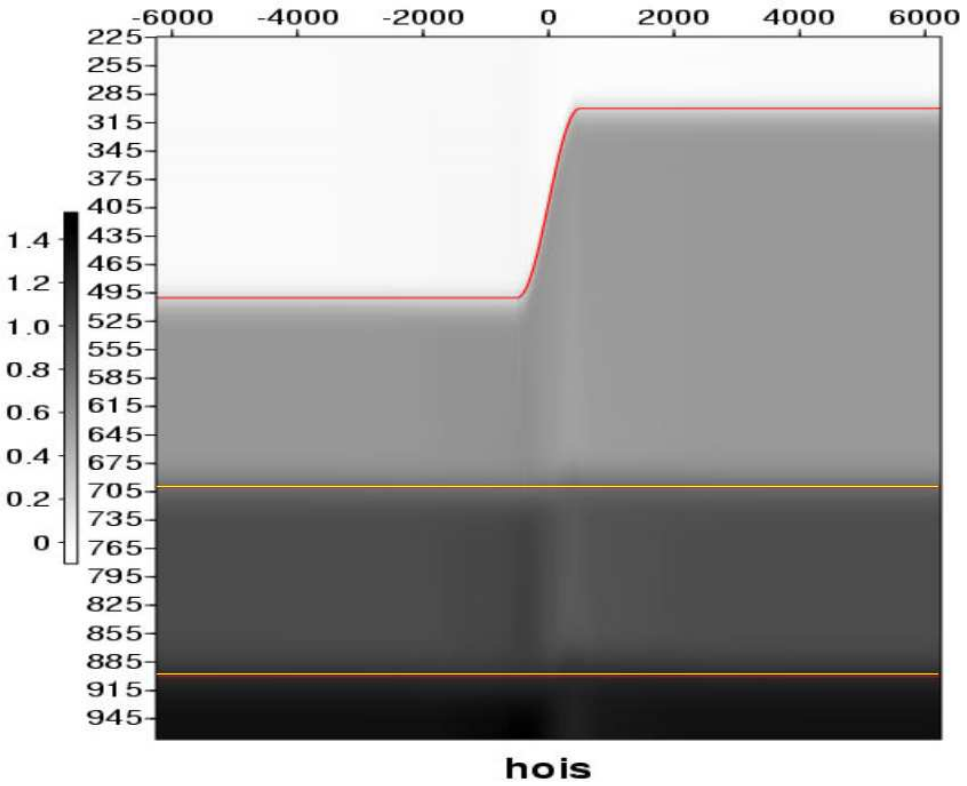

Figure 4: *Model-1 higher-order imaging subseries, here all reflectors were correctly imaged by an unchanged constant water-speed.*

Figure 5 shows the second model, obviously the lateral variation is greatly increased, and the contrast is also increased that the highest velocity is more than three times that of the reference velocity. The same finite-difference modeling algorithm is used to generate the shot gathers (see Figure 6). The the linear inverse in equation (6) is calculated with a whole space constant velocity $c_0 = 1500(m/s)$ and is shown in Figure 7. Its partial derivative with respect to depth is also taken and displayed in Figure 8.

The part of α_2 which is responsible for imaging, i.e., the term in equation (7), was shown in Figure 9. Even for this complicated geological model, its basic features remain the same: (1) where the water bottom is located, this term does not act. This makes sense as the water bottom has already been correctly imaged by water speed. *The inverse series does not act when it is not necessary*, a very important feature of purposeful perturbation. (2) Below the water bottom, this term is strong where there are reflectors in the linear image. The reflectors below the water bottom have activated this term, and will be moved.

After α_1 is calculated, the higher-order imaging subseries (see Figure 10) can be calculated; we note that the same unchanged reference velocity is used in every step.

The current higher-order imaging subseries, although very effective in moving reflectors to their actual locations, captured only the part of the imaging capability within ISS most pronounced for vertical variations. Other terms, for example, equation (8), which has no 1D analogy, will deal with imaging problems associated with fast lateral variations (for example, diffractions). This terms is

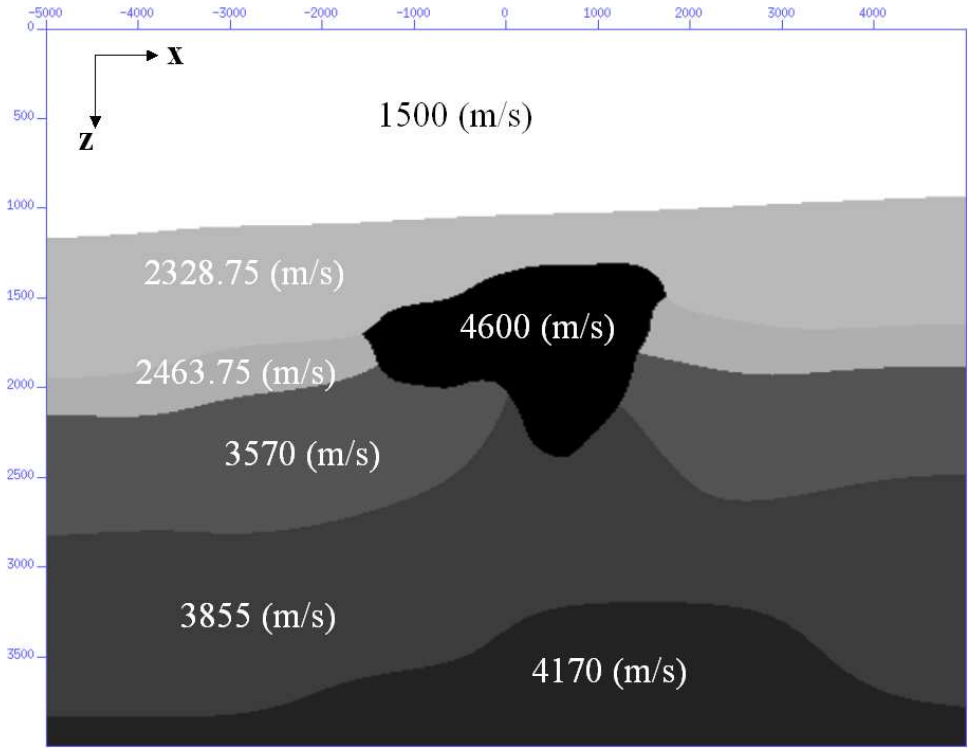

Figure 5: *The geometry and velocity of each layer in model-2.*

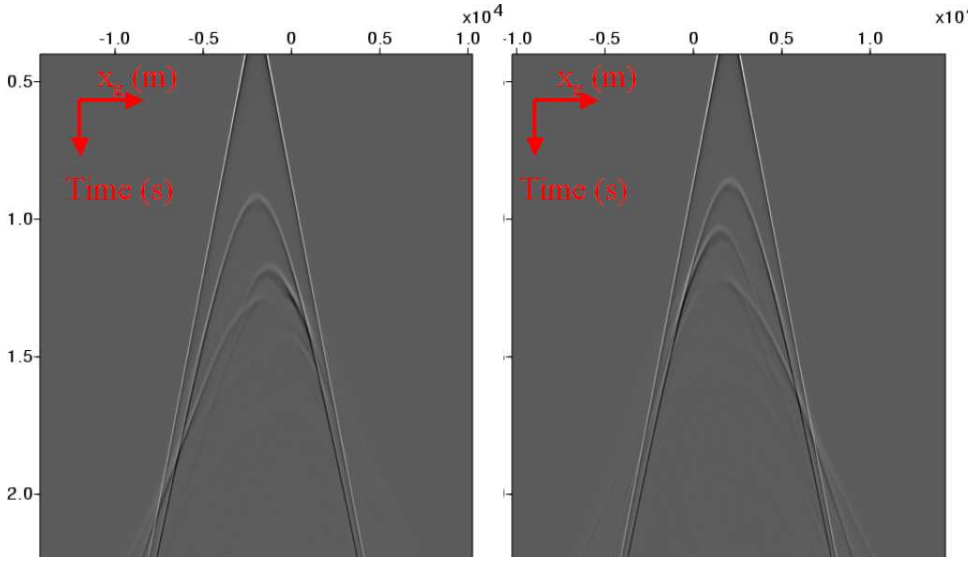

Figure 6: *Left: shot gather with $x_s = -2000(m)$. Right: shot gather with $x_s = 2000(m)$. In both shot gathers, conflicting hyperbolas are present which will cause ambiguities in velocity analysis.*

calculated and shown in Figure 12.

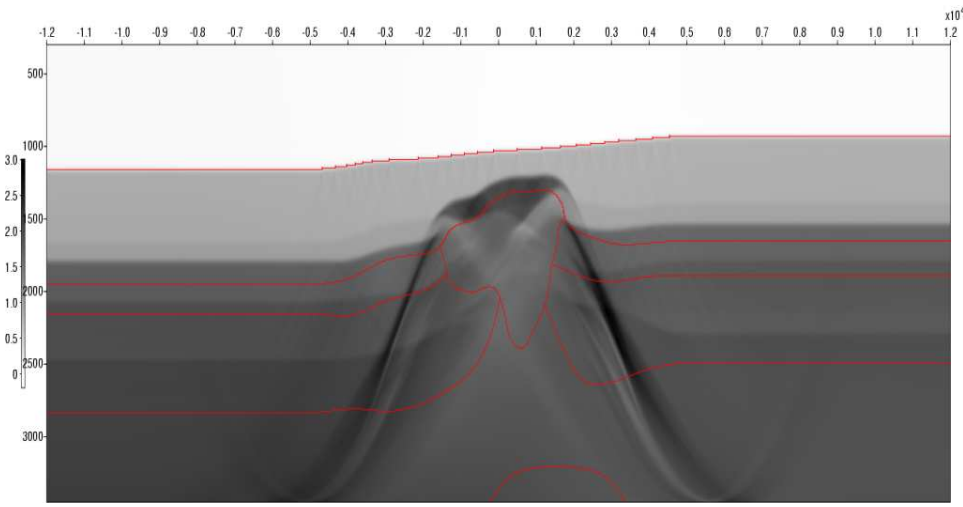

Figure 7: *Model 2 linear imaging results.*

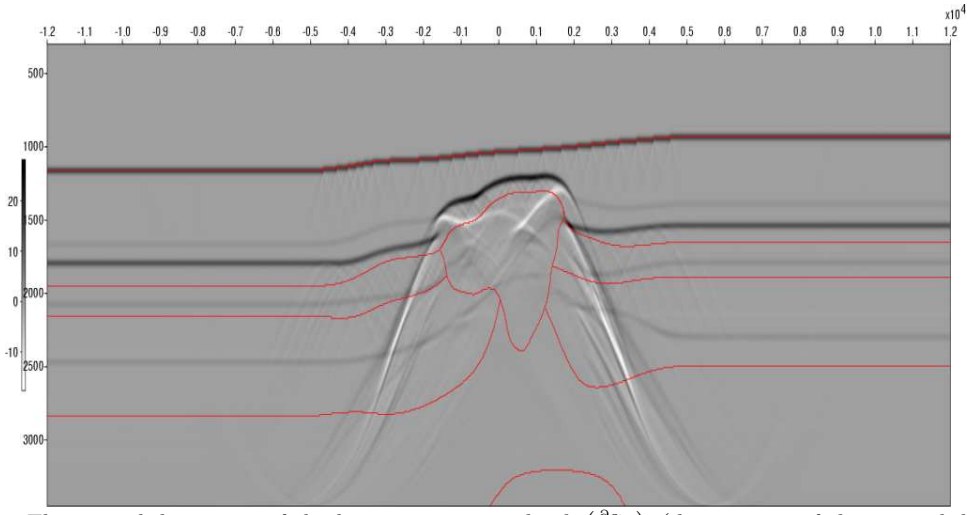

Figure 8: *The partial derivative of the linear term over depth* $\left(\frac{\partial \alpha_1}{\partial z}\right)$ *(the purpose of this partial derivative is to make the reflectors clearer in the section). The red lines are benchmarks indicating the actual geology. In the linear image, only the water bottom was correctly imaged by the whole-space water velocity. All other reflectors are in wrong locations. Diffractions below the water bottom was not collapsed because only the water velocity is used to do the migration. The bow-tie at the tip of the salt bottom was not properly untied because the inaccuracy of the reference velocity. The bottom reflector was more that* $1km$ *away from its correct locations.*

3 Conclusions

We present an extension of the velocity-independent imaging methods of the ISS to accommodate media that vary laterally as well as in depth. In spite of the added complexity of the ISS terms, the use of an integration-by-parts operation produces classes of terms that either generalize and become the laterally variable depth corrective terms of the 1D normal incidence case, or have the hallmarks of being part of a totally new laterally corrective mechanism. Both classes of terms call for specific and reasonably straightforward non-linear data activity, that we demonstrate encouraging numerical examples on 2D synthetic data. Ongoing research is geared towards finding and grouping

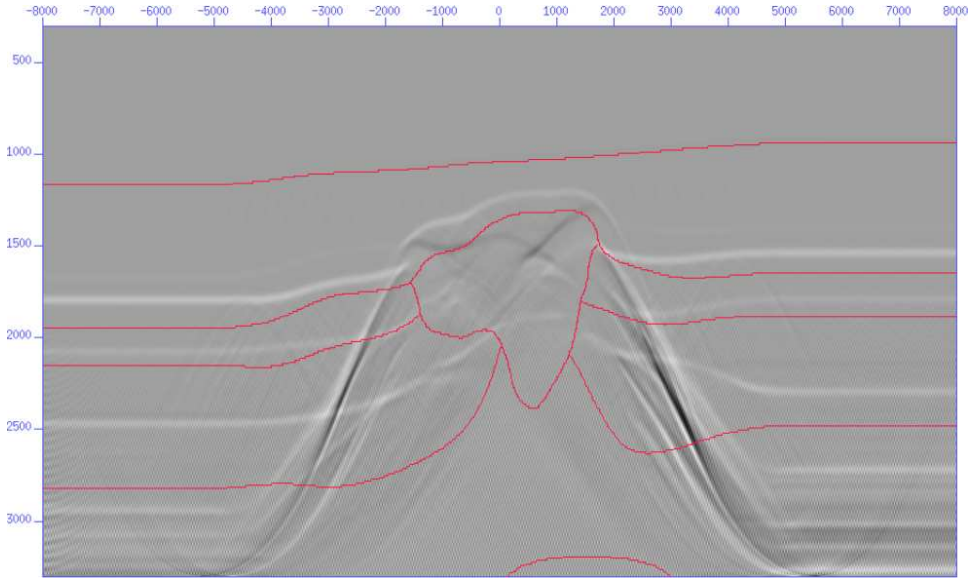

Figure 9: *The part of α_2 which is responsible for seismic imaging.*

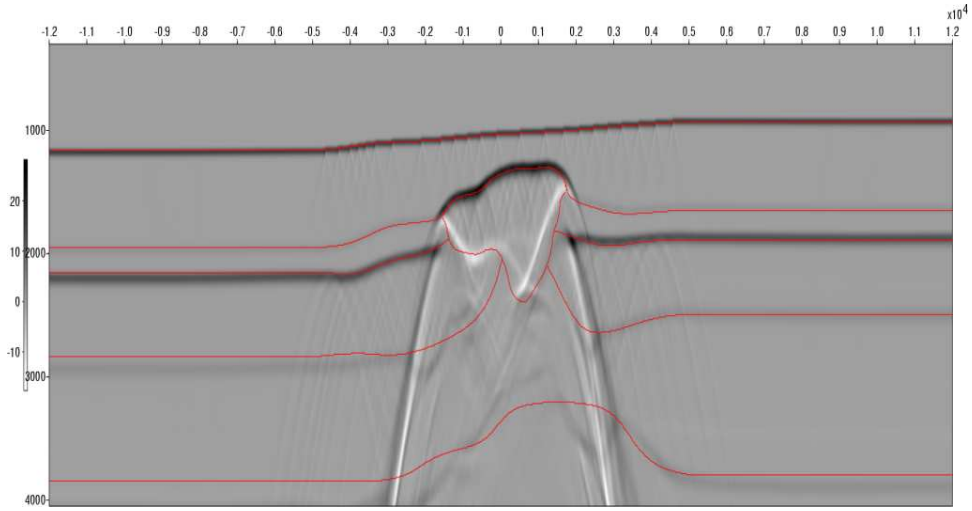

Figure 10: *Higher-order imaging subseries calculated using a constant, unchanged reference velocity (to make the reflectors clearer, the partial derivative over z is taken). The actual locations of the reflectors are indicated by red lines. The water bottom was not touched since it had already being correctly imaged by the water velocity. The second reflector (including the top salt) was correctly imaged. The third reflector (including the salt bottom was imaged very close to their actual locations. Outside the salt flank, the locations of the fourth reflector was also very close to its actual locations.*

terms which is more specific for large lateral variations, and studying the structure of the algorithm in a more general framework than restricting $k_h = 0$.

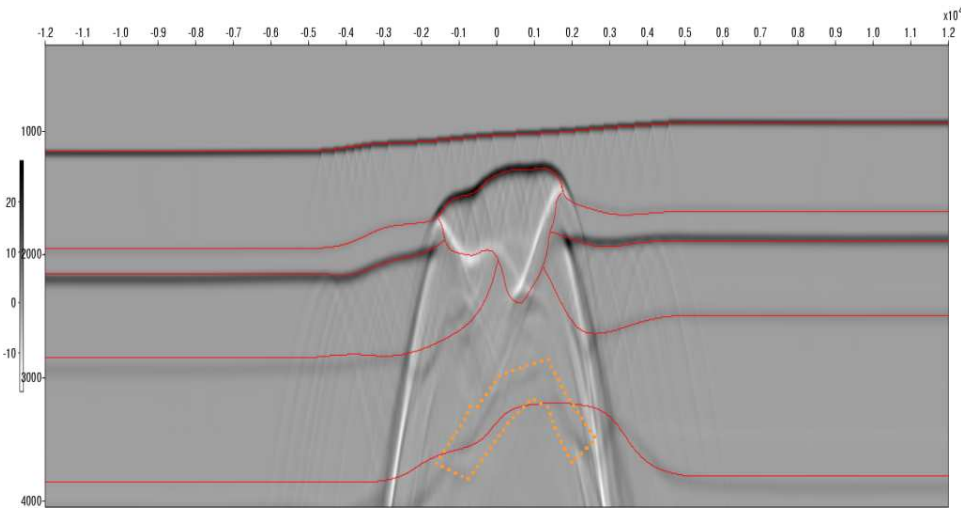

Figure 11: *Higher-order imaging subseries calculated using a constant, unchanged reference velocity (again, to make the reflectors clearer, the partial derivative over z is taken). A dashed polygon (in orange) was overlayed around the portion of the fifth reflector below the salt. The spatial location of the fifth reflector was much improved over the linear image: very close to its actual location on the right side of the salt, still visible below the salt, but the spatial error is larger in the left half of the model.)*

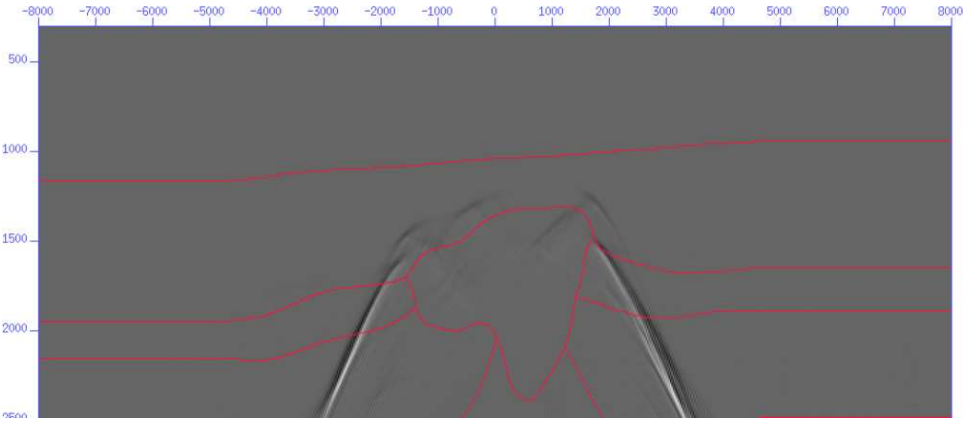

Figure 12: *The part of α_2 calculated by equation (??). This term vanishes for models with no lateral variation, and is very weak for the models with small lateral variation, but becomes pronounced for this model with large lateral variation. It is particularly strong where there is un-collapsed diffraction energy in the linear image. This low-order term alone is likely the starting point of a series meant to handle uniquely 2D phenomena.*

4 Acknowledgements

The Authors would like to recognize, acknowledge and express our deepest appreciation to Peter Traynin for his outstanding mentoring, instruction and guidance of Fang Liu during Fang's internship with ExxonMobil. Simon Shaw is thanked for his pioneering research and for sharing his deep understanding, keen insights; and, his constant encouragement. ExxonMobil is acknowledged for providing the salt model in numerical test. All M-OSRP members and sponsors are acknowledged. We have been partially funded by and are grateful for NSF-CMG award DMS-0327778 and DOE Basic Sciences award DE-FG02-05ER15697.

References

R. W. Clayton and R. H. Stolt. A Born-WKBJ inversion method for acoustic reflection data. *Geophysics*, 46(11):1559–1567, 1981.

K. A. Innanen. Reflector location using high-order inverse scattering series terms. *M-OSRP Annual Report*, 4, 2005.

F. Liu, A. B. Weglein, K. A. Innanen, and B. G. Nita. Extension of the non-linear depth imaging capability of the inverse scattering series to multidimensional media: strategies and numerical results. In *9th Ann. Cong. SBGF, Expanded Abstracts*. SBGf, 2005a.

F. Liu, A. B. Weglein, B. G. Nita, and K. A. Innanen. Inverse scattering series for vertically and laterally varying media: application to velocity independent depth imaging. *M-OSRP Annual Report*, 4, 2005b.

S. A. Shaw and A. B. Weglein. A leading order imaging series for prestack data acquired over a laterally invariant acoustic medium. Part I: Derivation and preliminary analysis. *M-OSRP Annual Report*, 3, 2004.

S. A. Shaw, A. B. Weglein, D. J. Foster, K. H. Matson, and R. G. Keys. Convergence properties of a leading order depth imaging series. In *73rd Annual Internat. Mtg., Soc. Expl. Geophys., Expanded Abstracts*, pages 937–940. Soc. Expl. Geophys., 2003a.

S. A. Shaw, A. B. Weglein, D. J. Foster, K. H. Matson, and R. G. Keys. Isolation of a leading order depth imaging series and analysis of its convergence properties. *M-OSRP Annual Report*, 2:157–195, 2003b.

Simon. A. Shaw. *An inverse scattering series algorithm for depth imaging from a layered medium with an unknown velocity model*. PhD thesis, University of Houston, 2005.

A. B. Weglein, F. V. Araújo, P. M. Carvalho, R. H. Stolt, K. H. Matson, R. T. Coates, D. Corrigan, D. J. Foster, S. A. Shaw, and H. Zhang. Inverse scattering series and seismic exploration. *Inverse Problems*, 19:R27–R83, 2003.

A. B. Weglein, K. H. Matson, D. J. Foster, P. M. Carvalho, D. Corrigan, and S. A. Shaw. Imaging and inversion at depth without a velocity model: Theory, concepts and initial evaluation. In *70th Annual Internat. Mtg., Soc. Expl. Geophys., Expanded Abstracts*, pages 1016–1019. Soc. Expl. Geophys., 2000.

H. Zhang and A. B. Weglein. Target identification using the inverse scattering series: data requirements for the direct inversion of large-contrast, inhomogeneous elastic media. *M-OSRP Annual Report*, 3, 2004.

Appendix A: new understanding of the intuitive leap made last year

In Liu et al. (2005b), the intuitive higher-order imaging subseries is provided without solid derivations. One big difference between this higher-order form and the leading-order imaging subseries (see Shaw et al., 2003a) is that, the moving term is applied to the left-hand-side of the equation rather than the right-hand-side. In this section, we indicate how this change is triggered by the inverse scattering series.

This section offers a demonstration of the equivalence between the intuitive higher-order imaging series (see Liu et al., 2005b, Liu et al., 2005a) and the reflector location behavior of a high order series coupling the imaging and inversion activity.

The closed-form of the the leading order imaging subseries (see Shaw et al. (2003b)) is

$$\alpha^{\mathrm{LOIS}}(z) = \alpha_1 \left(z - \frac{1}{2} \int_{-\infty}^{z} \alpha_1(u) du \right). \tag{11}$$

For a medium with small to moderate contrasts, the leading-order imaging subseries can achieve accurate depth imaging using a constant, unchanged reference velocity. As mentioned in Shaw (2005), it omits terms which will become significant for medium with large velocity contrast. To improve the imaging capabilities of the leading-order imaging subseries, two changes were arrived at. One of them arose from a consideration of the combined imaging and inversion capability of the ISS Innanen (2005), which we will refer to as

$$\alpha^{\mathrm{SII}}(z) = \int_{-\infty}^{\infty} e^{ikz} \left[\int_{-\infty}^{\infty} \exp\left(-ik\left[z' + Z(z')\right]\right) \alpha_1(z') dz' \right] dk, \tag{12}$$

and in which $Z(z')$ is defined as:

$$Z(z') = \frac{1}{2} \int_{-\infty}^{z'} \frac{\alpha_1(z'')}{1 - 0.25\alpha_1(z'')} dz''. \tag{13}$$

The other is the higher-order imaging subseries in Liu et al. (2005b), Liu et al. (2005a) (ignoring the x-dependency):

$$\alpha^{\mathrm{HOIS}} \left(z + \frac{1}{2} \int_{-\infty}^{z} \frac{\alpha_1(u)}{1 - 0.25\alpha_1(u)} du \right) = \alpha_1(z). \tag{14}$$

Equation (14) was reached by the observation that, the leading-order imaging subseries has the possibility of using the information below the reflector itself to decide the amount of moving. This is a violation the view that in the ISS *an event only communicates with the events above it to decide how it should be moved*. How can we avoid this behavior? A solution is to shift the non-linear operation to the other side of the equation with the sign reversed:

$$\alpha^{\mathrm{SLOIS}} \left(z + \frac{1}{2} \int_{-\infty}^{z} \alpha_1(u) du \right) = \alpha_1(z) \tag{15}$$

If the velocity contrast is very small, equation (15) is very close to equation (11), so the accuracy of the leading-order imaging subseries for small contrast is kept. Furthermore, this step forces the moving algorithm to rely solely on information from depths shallower than that being moved.

The high-order imaging and inversion subseries was proposed in Innanen (2005) in such a way that a geometric series in the data was incorporated under the integrand. This series, which was shown to be consistent to third order with all orders of moving term, was furthermore summed such that inside this integrand series could be expressed in closed-form. The integrand in fact changed from α_1 to $\frac{\alpha_1}{1-0.25\alpha_1}$. In Liu et al. (2005b), this modified moving term is plugged into equation (15) to have equation (14). The advantage of equation (14) is that, while the higher-order imaging capability is introduced, the task-separated nature of the series remained: the amplitude of α_1 was not modified. In Liu et al. (2005b), its effectiveness in moving all the reflectors to their actual locations with a constant, unchanged reference velocity is demonstrated. Here the equivalence of equation (12) and the intuitive equation (14) was provided as follows:

If the order of integration is changed, equation (12) becomes:

$$\begin{aligned}\alpha^{\mathrm{SII}}(z) &= \int_{-\infty}^{\infty} e^{ikz}\left[\int_{-\infty}^{\infty} \exp\left(-ik\left[z'+Z(z')\right]\right)\alpha_1(z')dz'\right]dk \\ &= \int_{-\infty}^{\infty} dz'\alpha_1(z')\int_{-\infty}^{\infty} dk\exp\left(-ik\left[z'+Z(z')-z\right]\right)dz'dk\end{aligned}$$

Noticing that the innermost integral in the equation above results in a δ-function, we have,

$$\alpha^{\mathrm{SII}}(z) = 2\pi\int_{-\infty}^{\infty} dz'\alpha_1(z')\delta\left(z'+Z(z')-z\right)$$

For simplicity, let's define a function,

$$f(z') = z' + Z(z'). \tag{16}$$

With the definition above, $\alpha^{\mathrm{SII}}(z)$ can be further expressed as,

$$\alpha^{\mathrm{SII}}(z) = 2\pi\int_{-\infty}^{\infty} dz'\alpha_1(z')\delta\left(f(z')-z\right)$$

The expression above can be simplified by changing the integration variable from z' to $u = f(z')$, and since $z' = f^{-1}(u)$, the expression above becomes,

$$\alpha^{\mathrm{SII}}(z) = 2\pi\int_{-\infty}^{\infty} df^{-1}(u)\alpha_1(f^{-1}(u))\delta\left(u-z\right)$$

$$\alpha^{\mathrm{SII}}(z) = 2\pi\int_{-\infty}^{\infty} \delta\left(u-z\right)\alpha_1(f^{-1}(u))\frac{\partial f^{-1}(u)}{\partial u}du$$

$$\alpha^{\mathrm{SII}}(z) = \alpha_1(f^{-1}(z)) * 2\pi\frac{\partial f^{-1}(z)}{\partial z}.$$

If we ignore the Jacobian term $2\pi\frac{\partial f^{-1}(z)}{\partial z}$, which affects the amplitude but not the location of the reflectors, we obtain,

$$\alpha^{\mathrm{SII}}(z) = \alpha_1(f^{-1}(z)).$$

Obviously, the equation above is equivalent to,

$$\alpha^{\mathrm{SII}}(f(z)) = \alpha_1(z).$$

Plug in the definition of f in equation (16), we have,

$$\alpha^{\mathrm{SII}}(z + Z(z)) = \alpha_1(z).$$

Substituting in the definition of $Z(z)$ in equation (13), the expression above become,

$$\alpha^{\mathrm{SII}}\left(z + \frac{1}{2}\int_{-\infty}^{z}\frac{\alpha_1(u)}{1-0.25\alpha_1(u)}du\right) = \alpha_1(z). \tag{17}$$

The expression above is identical to equation (14).

Appendix B: derivation of α_1 in a more general framework

Here we provides a more general framework (than $k_h = 0$) for inverse scattering series in the presence of lateral variation.

Let's consider a simplified seismic experiment in 2D where the elevation of the sources z_s and receivers z_g are fixed (see Figure 13). In this case, the seismic data should be considered as a function of three variables: the horizontal coordinates of the sources (x_s), the horizontal coordinates of the receivers (x_g), and time (t).

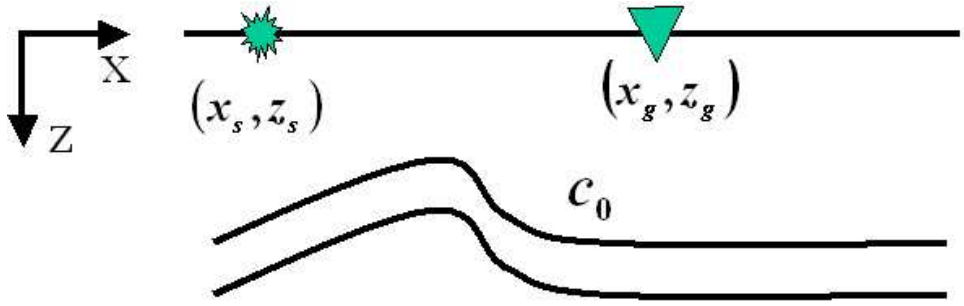

Figure 13: *A model with sources and receivers located at the same depth level: $z_g = z_s$. Free-surface is not considered because we assume the pre-processing had already eliminated its effects (ghosts and free-surface multiples).*

In many formalisms for seismic imaging, a certain model (often much simplified) is assumed for the derivation of the algorithm. For example, in the most popular constant-density acoustic model, only the velocity is assumed to be varying. If velocity is the only objective, the earth has only two degrees of freedoms: the horizontal coordinate x and the vertical coordinate z. Obviously there is one more freedom in the data than the objective function. The extra freedom must be reduced to reach an answer. In section (2.3), we discuss the differences between different reduction methods.

The wave-equation in seismic exploration can be expressed as

$$LG = -I, \tag{18}$$

where L is the differential operator associated with the actual medium velocity (c), G is the Green's function (or impulse response) for the actual medium. I is the identity operator. In ISS, we first solve another problem:

$$L_0 G_0 = -I, \tag{19}$$

where L_0 and G_0 are the differential operator and Green's function associated with the reference medium (usually a medium much simpler than the actual one), respectively.

The potential V is defined as the difference between the reference and actual differential operator $V = L_0 - L$. If velocity is the only varying parameter, V can be expressed as $V = (\omega/c_0)^2\alpha$, where ω is the temporary frequency and α is defined as $\alpha(x,z) = 1 - \frac{c_0^2(x,z)}{c^2(x,z)}$.

Equation (18) and (19) can be combined to have the Lippmann-Schwinger equation (Weglein et al., 2003):

$$GVG_0 = G - G_0 \tag{20}$$

In the left-hand-side of equation (20), both G and V are unknown, the right-hand-side is known only on the measurement surface where data is available. ISS is a perturbative solution to equation (20) by first solving:

$$G_0 V_1 G_0 = G - G_0. \tag{21}$$

Then the later terms are iteratively solved by setting terms with order higher than 1 to be zero (Weglein et al., 2003):

$$\begin{aligned} 0 &= G_0V_2G_0 + G_0V_1G_0V_1G_0 \\ 0 &= G_0V_3G_0 + G_0V_1G_0V_2G_0 + G_0V_2G_0V_1G_0 + G_0V_1G_0V_1G_0V_1G_0 \\ &\vdots \end{aligned} \tag{22}$$

For constant density acoustic model, the relationship between the data and the objective function α_1 can be expressed as (Clayton and Stolt, 1981, Liu et al., 2005b):

$$\widetilde{\widetilde{\alpha}}_1(k_g - k_s, q_g + q_s) = -4\frac{q_g q_s}{\omega^2/c_0^2}\widetilde{\widetilde{D}}\,(k_g, k_s, \omega) \tag{23}$$

where $\widetilde{\widetilde{\alpha}}_1$ is the double Fourier transform of $\alpha_1(x,z)$:

$$\widetilde{\widetilde{\alpha}}_1(k_m, k_z) = \int_{-\infty}^{\infty} dx e^{-ik_m x} \int_{-\infty}^{\infty} dz e^{ik_z z}\alpha_1(x,z)$$

and $q_g = \mathrm{sgn}(\omega)\sqrt{(\omega/c_0)^2 - k_g^2}$, $q_s = \mathrm{sgn}(\omega)\sqrt{(\omega/c_0)^2 - k_s^2}$. $\widetilde{\widetilde{D}}$ is triple Fourier transform of the data $D(x_g, x_s, t)$:

$$\widetilde{\widetilde{D}}\,(k_g, k_s, \omega) = \int_{-\infty}^{\infty} dx_g e^{ik_g x_g} \int_{-\infty}^{\infty} dx_s e^{-ik_s x_s} \int_{-\infty}^{\infty} dt e^{i\omega t} D(x_g, x_s, t)$$

Let's summarize all the variables and their corresponding Fourier conjugates in the table below:

Physical meaning	Variable name	Fourier conjugate
x-coordinate of the receiver	x_g	k_g
x-coordinate of the source	x_s	k_s
Time	t	ω
x-coordinate of the mid-point	$x_m = 0.5(x_g + x_s)$	$k_m = k_g - k_s$
Offset	$x_h = x_g - x_s$	$k_h = k_g + k_s$

By a simple transformation of coordinates, the data can be transformed to the mid-point x_m and offset x_h:

$$x_m = \frac{x_g + x_s}{2} \qquad\qquad x_h = x_g - x_s \tag{24}$$

$$\widetilde{\widetilde{\alpha}}_1(k_m, k_z) = -4\frac{q_g q_s}{\omega^2/c_0^2}\widetilde{\widetilde{D}}\left(k_m, k_h, k_z\right) \tag{25}$$

It's clear that there is one more freedom in data than the objective function. In Liu et al. (2005b), the extra degree of freedom is fixed by choosing the offset conjugate k_h to be zero.

The extra freedom in the data had been studied by Zhang and Weglein (2004), by fixing ratio between ω and $q_g = q_s$,

$$\begin{aligned} &q_g = q_s = \frac{\omega}{c_0}\cos(\theta), \qquad\qquad \text{where :} \qquad \theta = \text{constant}, \\ &k_g = k_s. \end{aligned} \tag{26}$$

Similar treatment can be found from the first equation in $\mathbf{P}_{161}$ by Shaw and Weglein (2004). The objective of this article is to generalize the works mentioned above to allow **both** lateral variations in the medium **and** extra freedom in the data. This extra freedom is crucial for studying other parameters (e.g. density variations).

To generalize equation (26), we define a fixed angle θ without restricting $k_g = k_s$:

$$k_g + k_s = 2\frac{\omega}{c_0}\sin\left(\theta\right). \tag{27}$$

And Liu et al. (2005b) can be considered as the special case of $\theta = 0$. With this data choice, the relationship in equation (14) of Liu et al. (2005b) can be generalized as:

$$k_h = k_g + k_s = 2\tfrac{\omega}{c_0}\sin\left(\theta\right) \qquad\qquad k_g - k_s = k_m \tag{28}$$

We will solve equation (23) under the constraint of equation (28). Equivalently speaking, for each k_m and ω, the corresponding vertical wave-number k_z can be calculated by:

$$k_z = q_g + q_s = \mathtt{sgn}(\omega)\sqrt{\left(\frac{\omega}{c_0}\right)^2 - \left(\frac{\omega}{c_0}\sin\left(\theta\right) + \frac{k_m}{2}\right)^2} + \mathtt{sgn}(\omega)\sqrt{\left(\frac{\omega}{c_0}\right)^2 - \left(\frac{\omega}{c_0}\sin\left(\theta\right) - \frac{k_m}{2}\right)^2}.$$

For fixed k_m and θ, let's consider the equation above as a function of ω:

$$k_z = \mathtt{sgn}(\omega)\sqrt{\left(\frac{\omega}{c_0}\right)^2 - \left(\frac{\omega}{c_0}\sin\left(\theta\right) + \frac{k_m}{2}\right)^2} + \mathtt{sgn}(\omega)\sqrt{\left(\frac{\omega}{c_0}\right)^2 - \left(\frac{\omega}{c_0}\sin\left(\theta\right) - \frac{k_m}{2}\right)^2} = \kappa(\omega). \tag{29}$$

For the same fixed k_m and θ, we can invert the relation above to express ω as a function of k_z:

$$\omega = \kappa^{-1}(k_z) = \frac{c_0 k_z}{2}\sqrt{\frac{k_z^2 + k_m^2}{k_z^2\cos^2(\theta) - k_m^2\sin^2(\theta)}} \tag{30}$$

With ω being defined in equation (30), our generalized formalism can be expressed as :

$$\begin{aligned}\widetilde{\widetilde{\alpha}}_1(k_m, k_z) &= -\frac{4q_g q_s}{\omega^2/c_0^2}\widetilde{\widetilde{D}}\left(\frac{\omega\sin(\theta)}{c_0} + \frac{k_m}{2}, \frac{\omega\sin(\theta)}{c_0} - \frac{k_m}{2}, \omega\right) \\ &= -\frac{4q_g q_s}{\omega^2/c_0^2}\int_{-\infty}^{\infty} dx_g e^{-ik_g x_g}\int_{-\infty}^{\infty} dx_s e^{ik_s x_s}\int_{-\infty}^{\infty} dt e^{i\omega t} D(x_g, x_s, t)\end{aligned} \tag{31}$$

Let's change the integration variable ($x_m = 0.5(x_g + x_s)$, $x_h = x_g - x_s$) :

$$\begin{aligned}&= -\frac{4q_g q_s}{\omega^2/c_0^2}\int_{-\infty}^{\infty} dx_m \int_{-\infty}^{\infty} dx_h e^{-ik_g[x_m + 0.5x_h]} e^{ik_s[x_m - 0.5x_h]}\int_{-\infty}^{\infty} dt e^{i\omega t} D(x_m + 0.5x_h, x_m - 0.5x_h, t) \\ &= -\frac{4q_g q_s}{\omega^2/c_0^2}\int_{-\infty}^{\infty} dx_m e^{-i(k_g - k_s)x_m}\int_{-\infty}^{\infty} dx_h e^{-i(k_g + k_s)x_h/2}\int_{-\infty}^{\infty} dt e^{i\omega t} D(x_m + 0.5x_h, x_m - 0.5x_h, t) \\ &= -\frac{4q_g q_s}{\omega^2/c_0^2}\int_{-\infty}^{\infty} dx_m e^{-ik_m x_m}\int_{-\infty}^{\infty} dx_h e^{-i\frac{\omega\sin(\theta)}{c_0}x_h}\int_{-\infty}^{\infty} dt e^{i\omega t} D(x_m + 0.5x_h, x_m - 0.5x_h, t) \\ &= -\frac{4q_g q_s}{\omega^2/c_0^2}\int_{-\infty}^{\infty} dx_m e^{-ik_m x_m}\int_{-\infty}^{\infty} dt\int_{-\infty}^{\infty} dx_h e^{i\omega\left[t - \frac{\sin(\theta)x_h}{c_0}\right]} D(x_m + 0.5x_h, x_m - 0.5x_h, t)\end{aligned}$$

With another change of the integration variable ($\tau = t - \frac{\sin(\theta)x_h}{c_0}$), we have :

$$\begin{aligned}&= -\frac{4q_g q_s}{\omega^2/c_0^2}\int_{-\infty}^{\infty} dx_m e^{-ik_m x_m}\int_{-\infty}^{\infty} e^{i\omega\tau} d\tau\int_{-\infty}^{\infty} dx_h D\left(x_m + 0.5x_h, x_m - 0.5x_h, \tau + \frac{\sin(\theta)x_h}{c_0}\right) \\ &= -\frac{4q_g q_s}{\omega^2/c_0^2}\int_{-\infty}^{\infty} dx_m e^{-ik_m x_m}\int_{-\infty}^{\infty} d\tau e^{i\omega\tau} D^{\tau p}(x_m, \tau)\end{aligned}$$

where $D^{\tau p}$ is simply the Radon transform of all traces within a CMP gather:

$$D^{\tau p}(x_m, t) = \int_{-\infty}^{\infty} dx_h D\left(x_m + \frac{x_h}{2}, x_m - \frac{x_h}{2}, t + x_h\frac{\sin(\theta)}{c_0}\right) \tag{32}$$

We have the expression for α_1 :

$$\widetilde{\widetilde{\alpha}}_1(k_m, k_z) = -\frac{4q_g q_s}{\omega^2/c_0^2}\int_{-\infty}^{\infty} dx_m e^{-ik_m x_m}\int_{-\infty}^{\infty} d\tau e^{i\omega\tau} D^{\tau p}(x_m, \tau) \tag{33}$$

Please notice that $D^{\tau p}(x_m, \tau)$, the last expression in the equation above, is the slant-stacking or Radon transform of the data in the data in the **CMP**-gather. The advantage of expressing data in this form is that it offers: (1) an easier cut of the direct-arrivals, and (2), very straightforward control over the amplitude and waveform.

There must be many other pre-processing procedures which can be much easily done in the $tau - p$ domain (the data after slant stacking) than in the original domain. And the computation cost can be greatly reduced since the freedom of the data is reduced.

Issues of missing spectrum

In (33), the frequency ω is calculated as in equation (30). Only in the special case of $\theta = 0$, we can sweep the data in the (k_g, k_s, ω) domain to achieve a complete spectrum of α_1 for $-\infty \leq k_m \leq \infty$, and $-\infty \leq k_z \leq \infty$. Otherwise, for $k_m \neq 0$, there is always a missing band in the spectrum.

If we require that both q_g and q_s are real, we have:

$$\left|\frac{\omega}{c_0}\right| \geq \left|\frac{\omega \sin(\theta)}{c_0} \pm \frac{k_m}{2}\right|$$

Let's consider an easy case where $\omega \geq 0$ is positive, we require:

$$\left(\begin{array}{lll} \frac{\omega}{c_0} \geq \pm\left(\frac{\omega \sin(\theta)}{c_0} + \frac{k_m}{2}\right) & \Longrightarrow & \omega \geq \frac{\pm 0.5 k_m c_0}{1 \mp \sin(\theta)} \\ \frac{\omega}{c_0} \geq \pm\left(\frac{\omega \sin(\theta)}{c_0} - \frac{k_m}{2}\right) & \Longrightarrow & \omega \geq \frac{\mp 0.5 k_m c_0}{1 \mp \sin(\theta)} \end{array} \right) \Longrightarrow \omega \geq \frac{|0.5 k_m|\, c_0}{1 - |\sin(\theta)|} = \max\left(\frac{\mp 0.5 k_m c_0}{1 \mp \sin(\theta)}, \frac{\pm 0.5 k_m c_0}{1 \mp \sin(\theta)}\right)$$

Likewise, for $\omega < 0$, we have:

$$\left(\begin{array}{lll} -\frac{\omega}{c_0} \geq \pm\left(\frac{\omega \sin(\theta)}{c_0} + \frac{k_m}{2}\right) & \Longrightarrow & \omega \leq \frac{\pm 0.5 k_m c_0}{-1 \mp \sin(\theta)} \\ -\frac{\omega}{c_0} \geq \pm\left(\frac{\omega \sin(\theta)}{c_0} - \frac{k_m}{2}\right) & \Longrightarrow & \omega \leq \frac{\mp 0.5 k_m c_0}{-1 \mp \sin(\theta)} \end{array} \right) \Longrightarrow \omega \leq \frac{-|0.5 k_m|\, c_0}{1 - |\sin(\theta)|} = \min\left(\frac{\mp 0.5 k_m c_0}{-1 \mp \sin(\theta)}, \frac{\pm 0.5 k_m c_0}{-1 \mp \sin(\theta)}\right)$$

Combining the 2 relations above, we have:

$$|\omega| \geq \frac{1}{2} \frac{|k_m|\, c_0}{1 - |\sin(\theta)|}$$

Let's denote the lower limit above as: $\omega_{\min}$

$$\omega_{\min} = \frac{1}{2} \frac{|k_m|\, c_0}{1 - |\sin(\theta)|}$$

We then consider when the lower-limit $\omega_{\min}$ is reached, what would be the corresponding k_z:

$$\left(\frac{\omega\sin(\theta)}{c_0}\pm\frac{k_m}{2}\right)^2=\left(\frac{0.5\,|k_m|\,c_0}{1-|\sin(\theta)|}\frac{\sin(\theta)}{c_0}\pm\frac{k_m}{2}\right)^2=\frac{k_m^2}{4}\left(\frac{\sin(\theta)}{1-|\sin(\theta)|}\pm 1\right)^2$$

$$=\frac{k_m^2}{4}\left(\frac{\sin(\theta)\mp|\sin(\theta)|\pm 1}{1-|\sin(\theta)|}\right)^2=\begin{pmatrix}\frac{k_m^2}{4}\left(\frac{1}{1-|\sin(\theta)|}\right)^2=\frac{\omega_{\min}^2}{c_0^2}\\ \frac{k_m^2}{4}\left(\frac{1-2|\sin(\theta)|}{1-|\sin(\theta)|}\right)^2=\frac{\omega_{\min}^2}{c_0^2}\left(1-2\,|\sin(\theta)|\right)^2\end{pmatrix}$$

$$k_z=q_g+q_s=\sqrt{\frac{\omega^2}{c_0^2}-\left(\frac{\omega\sin(\theta)}{c_0}+\frac{k_m}{2}\right)^2}+\sqrt{\frac{\omega^2}{c_0^2}-\left(\frac{\omega\sin(\theta)}{c_0}-\frac{k_m}{2}\right)^2}$$

$$=\frac{\omega_{\min}}{c_0}\sqrt{1-\{1-2\,|\sin(\theta)|\}^2}=2\frac{\omega_{\min}}{c_0}\sqrt{|\sin(\theta)|-\left|\sin^2(\theta)\right|}=|k_m|\sqrt{\frac{|\sin(\theta)|}{1-|\sin(\theta)|}}$$

$$\min(|k_z|)=|k_m|\sqrt{\frac{|\sin(\theta)|}{1-|\sin(\theta)|}} \tag{34}$$

From equation (34), it's clear that the lower-limit for k_z is proportional to k_m. The missing part of the spectrum is displayed in the shaded region of figure 14.

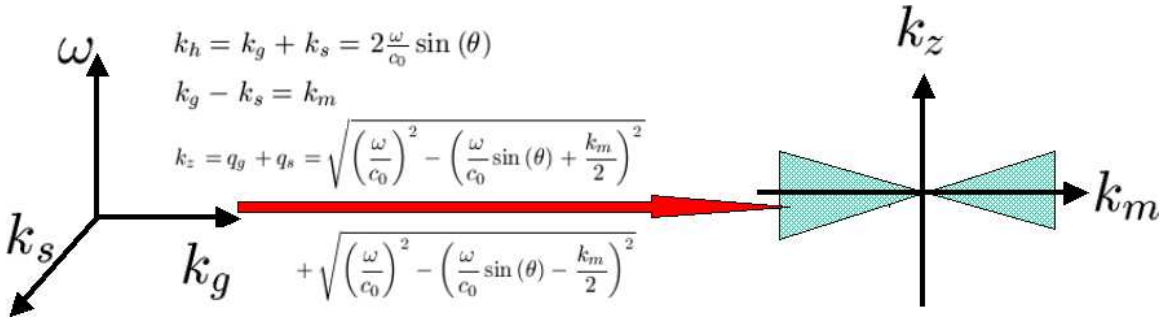

Figure 14: *In the (k_m, k_z)-plane, the spectrum is missing for the 2 shaded triangular regions.*

The slope of the shaded regions in the figure above is $\sqrt{\frac{|\sin(\theta)|}{1-|\sin(\theta)|}}$, it will be zero if $\theta = 0$. This means that for the special case of $\theta = 0$, the shaded region is empty and the spectrum is complete.

Issues of removing direct arrival

In inverse scattering series, the direct arrival (G_0) is usually assumed to be removed from the recorded data. Let's study this issue by a sample shot gather in Figure 16: for large offset, the reflection data tend to mingle with or arrive earlier than the direct arrival. The shot gather was generated by finite-difference modeling algorithm with acquisition and geological information displayed in Figure 15. The phenomena above imply that a straightforward cut of the direct wave will hurt the primaries. Ideally, the direct wave can be surgically removed by wavelet estimation followed by de-ghosting. The procedure discussed here claimed no superiority to them. The point we want to make, is that, a simple reasoning in physics, can give us a surprisingly good result compared with straightforward cut.

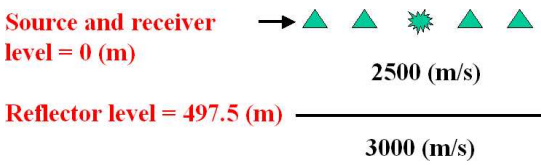

Figure 15: *A sample single-interface geological model with no lateral variation.*

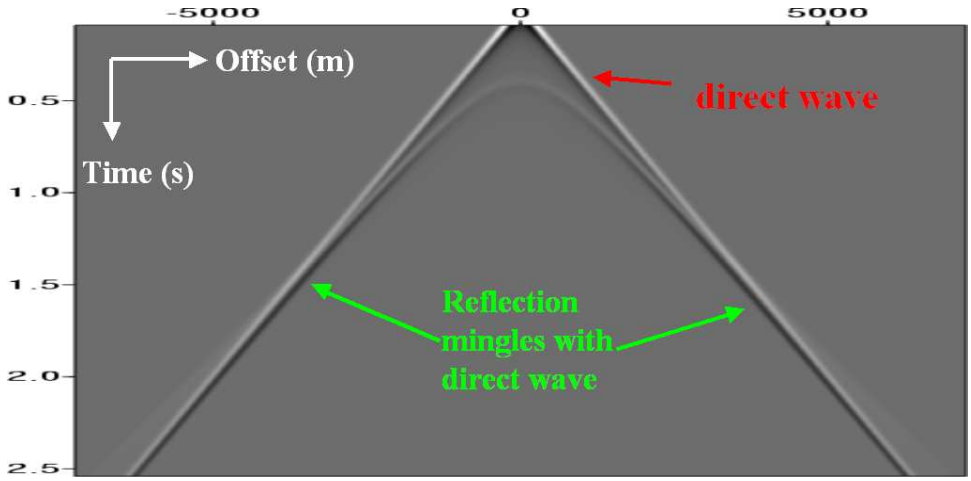

Figure 16: *A sample shot gather showing reflection data mingle direct arrivals for large offset.*

The difficulty of straightforward mute of the direct arrivals comes from the fact that the sources in the exploration seismology are very similar to point sources, which usually generate head waves. If the incident waves are plane waves, then we don't need to worry about head waves and make the cut feasible.

The procedure we discussed is the following: (1) Synthesize plane-wave experiment by slant-stack (see Figure 17). (2) Cut the direct arrivals after slant-stack. In this example, a cut from $0.2(s)$ will be an easy choice.

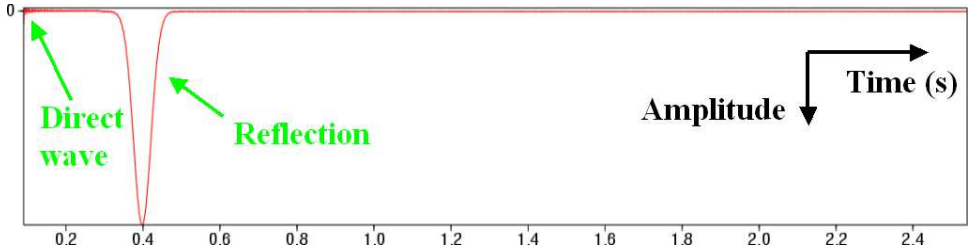

Figure 17: *The result of summing all the traces together (slant-stack with $p = 0$)in Figure 16 together. The only one reflection arrives at 0.4(s). Only very little amount of the direct arrival is visible in this example since the starting time for the seismogram is 0.09(s). It's clear that the direct arrival and reflections are well separated using a threshold $t = 0.2(s)$.*

A note on inverse scattering series based closed-forms applied to imaging

Jingfeng Zhang, Fang Liu, Kristopher Innanen, Simon Shaw and Arthur B. Weglein

Abstract

This is a detailed explanation of the intuitive leap that Liu et al. (2004) performed on the higher ordering imaging series (HOIS), except in this note the main target is the leading order imaging series (LOIS). It is shown that an altered form of the LOIS is more reasonable. For small contrast model, the difference between the outputs of the original and altered forms is almost negligible.

1 Introduction

The inverse scattering series (ISS) has been successfully employed over a full spectrum of seismic processing tasks. One such task is seismic depth imaging with a reference medium velocity which locates the Earth's reflectors. The first step of this task is to obtain $\alpha_1(z)$ which is the Stolt migration result using reference medium velocity. Secondly, more terms of the inverse scattering series are identified to improve the locations of the reflectors in α_1, without changing their amplitude/properties. To date, two closed forms of the imaging sub-series have been identified and are known in the literature as the leading order imaging series (LOIS) and the higher order imaging series (HOIS) (Shaw et al., 2003; Liu et al., 2004). In this note, through analysis of those closed forms and the work of Innanen (2005), we argue that a slightly altered form of the LOIS is more preferable.

2 Closed forms of the leading and higher order imaging series

The LOIS and HOIS closed forms are

$$\alpha^{LOIS}(z) = \alpha_1\Big(z - \frac{1}{2}\int_0^z \alpha_1(z')dz'\Big) \tag{1}$$

and

$$\alpha^{HOIS}\Big(z + \frac{1}{2}\int_0^z \frac{\alpha_1(z')}{1-\frac{1}{4}\alpha_1(z')}dz'\Big) = \alpha_1(z). \tag{2}$$

The functions $\alpha^{LOIS}(z)$ and $\alpha^{HOIS}(z)$ provide better reflector locations compared to α_1. One may notice that in Eq.1, the argument of α^{LOIS} is very simple and that of α_1 is relatively complicated, while in Eq.2, it is α^{HOIS} that has the relative complicated argument. Why this transfer of complexity? What kind of difference will it make? In this short note, we will try to answer these questions, without becoming too involved in the math or diagrams of the inverse scattering series.

3 Interpretation and alteration of the leading order imaging series

There are several ways to interpret Eq.1:

1. The value of α^{LOIS} at z equals to the value of α_1 at $z - \frac{1}{2}\int_0^z \alpha_1(z')dz' = z'_b$; or,
2. The value of α^{LOIS} at $z = z'_b + \frac{1}{2}\int_0^z \alpha_1(z')dz'$ equals to the value of α_1 at z'_b; or reversely,
3. The value of α_1 at z'_b equals to the value of α^{LOIS} at $z = z'_b + \frac{1}{2}\int_0^z \alpha_1(z')dz'$.

Imagine that there is an interface at z'_b in α_1. Then based on the third interpretation, this interface will be moved to another depth z, and the distance to be moved is determined by: $\frac{1}{2}\int_0^z \alpha_1(z')dz'$, which is an integration to depth z, *not* z'_b. So, if z is bigger than z'_b, then α_1 values from greater depths contribute to the moving of this shallower interface. This conclusion is actually a little strange since our diagram analysis only permit shallower events helping the locations of deeper events. Even from physical instincts, it seems strange that the moving of shallower events care about deeper events. What is going on here?

Actually, the higher order form for reflector location was first incorporated as part of a coupled imaging-inversion algorithm (Innanen, 2005). Through a "natural" isolation operation, the imaging part of this algorithm would seem to be

$$\alpha^{HOIS}(z) = \alpha_1\Big(z - \frac{1}{2}\int_0^z \frac{\alpha_1(z')}{1 - \frac{1}{4}\alpha_1(z')}dz'\Big), \tag{3}$$

which is very similar to Eq.2 except where the complicated argument stays.

Innanen and Liu both tested Eq.3 and found that the results were poor. Then from physical intuition, Liu et al. (2004) moved the argument to the left hand side and obtained Eq.2 which provided very good results. To understand this move, let's apply the same operation to Eq.1:

$$\alpha^{SLOIS}\Big(z + \frac{1}{2}\int_0^z \alpha_1(z')dz'\Big) = \alpha_1(z), \tag{4}$$

where SLOIS denotes "Shifted LOIS". Let's analyze its meaning in a similar way:

1. The value of α^{SLOIS} at $z + \frac{1}{2}\int_0^z \alpha_1(z')dz'$ equals to the value of α_1 at z; or, reversely,
2. The value of α_1 at z equals to the value of α^{SLOIS} at $z + \frac{1}{2}\int_0^z \alpha_1(z')dz'$; so,
3. The value of α_1 at z'_b equals to the value of α^{SLOIS} at $z'_b + \frac{1}{2}\int_0^{z'_b} \alpha_1(z')dz'$.

Clearly, if it happens that there is an interface at z'_b in α_1 then it will be moved to depth z and the distance to move is determined by an integration to depth z'_b. No deeper events will possibly contribute to the movement of shallower ones. So it seems that Eq.4 might be more reasonable compared to Eq.1, just like Eq.2 compared to Eq.3.

4 Conclusions and discussions

We briefly discussed the form of the LOIS and showed that a slightly changed form looks more reasonable, just like Fang Liu did on HOIS. For small contrast model, the difference between the outputs of the original and altered forms is almost negligible. Further efforts are needed in order to *derive* the more reasonable LOIS and HOIS closed forms, instead of just using physical intuition.

Acknowledgments

Sam Kaplan is thanked for his discussions and help in writing this note. M-OSRP sponsors are thanked for their support.

References

K. A. Innanen. Reflector location using high-order inverse scattering series terms. *M-OSRP Annual Report*, 4, 2005.

F. Liu, B. G. Nita, A. B. Weglein, and K. A. Innanen. Inverse scattering series in the presence of lateral variations. *M-OSRP Annual Report*, 3, 2004.

S. A. Shaw, A. B. Weglein, D. J. Foster, K. H. Matson, and R. G. Keys. Isolation of a leading order depth imaging series and analysis of its convergence properties. *M-OSRP Annual Report*, 2:157–195, 2003.

Approximations to direct non-linear imaging-inversion: a 1D error analysis and candidate forms for partial 2D/3D imaging

Kristopher A. Innanen

Abstract

This paper continues in the analysis and interpretation of components of the inverse scattering series, that are deemed to concern tasks of imaging and inversion (coupled and uncoupled). (1) The coupling subseries of Innanen (2003) and Innanen and Weglein (2003), at leading order, and Innanen (2005), at high order, is reviewed, and an error analysis is provided for a 1D normal incidence, single layer example. (2) The capture of velocity-independent imaging terms in multiple dimensions, by Liu et al. (2005), is extended by appealing to a 2D Taylor's series analogy. Numerical tests of the latter are presently inconclusive.

1 Introduction and terminology

This paper concerns itself with (1) a review and error analysis of the leading- and high-order versions of the coupling subseries of the inverse scattering series (Innanen, 2003; Innanen, 2005), and (2) postulation of a form for direct 2D velocity independent imaging (due to the original inverse equations formulated by Weglein et al., 2002; Weglein et al., 2003). In this section the mathematics of the inverse scattering series is briefly reviewed. Thereafter, (1) and (2) above are discussed and exemplified. Further relevant analysis and a reconciliation between the shift forms of Liu et al. (2005) is presented in this report by Zhang et al. (2006).

1.1 Terms and definitions

To briefly review the theory of inverse scattering, it is useful to temporarily resort to an operator notation, whereby, for instance, a "true" wave field satisfies the equation

$$\mathbf{LG} = \mathbf{I}, \tag{1}$$

and a "reference" wave field satisfies

$$\mathbf{L_0 G_0} = \mathbf{I}, \tag{2}$$

where $\mathbf{L}$ and $\mathbf{L_0}$ are the true and reference wave operators, and $\mathbf{G}$ and $\mathbf{G_0}$ are the true and reference Green's operators respectively. The operators are general in the sense of model, and fully 3D. Equations (1) and (2) are in the space/temporal frequency domain. The perturbation operator is given by

$$\mathbf{V} = \mathbf{L_0} - \mathbf{L}, \tag{3}$$

the scattered wave field is

$$\Psi_s = \mathbf{G} - \mathbf{G_0}, \tag{4}$$

and the Lippmann-Schwinger equation is, in this framework:

$$\Psi_s = \mathbf{G} - \mathbf{G_0} = \mathbf{G_0 V G}. \tag{5}$$

The Born series arises from equation (5) through self-substitution:

$$\begin{aligned} \Psi_s &= \mathbf{G_0 V G_0} + \mathbf{G_0 V G_0 V G_0} + \mathbf{G_0 V G_0 V G_0 V G_0} + ... \\ &= (\Psi_s)_1 + (\Psi_s)_2 + (\Psi_s)_3 + ... \ . \end{aligned} \tag{6}$$

In other words, the scattered field is represented as a series in increasing order in the scattering potential. The approach taken here (reviewing the work described completely by Weglein et al., 2003), is to represent the solution (the perturbation operator) as an infinite series:

$$\mathbf{V} = \mathbf{V_1} + \mathbf{V_2} + \mathbf{V_3} + ..., \tag{7}$$

where $\mathbf{V_j}$ is "j'th order in the data". This form is substituted into the terms of the Born series, and terms of like order in Ψ_s are equated (each term is considered to have been evaluated on the measurement surface m). This is the form of the inverse scattering series:

$$\begin{aligned} (\Psi_s)_m =& (\mathbf{G_0 V_1 G_0})_m, \\ 0 =& (\mathbf{G_0 V_2 G_0})_m + (\mathbf{G_0 V_1 G_0 V_1 G_0})_m, \\ 0 =& (\mathbf{G_0 V_3 G_0})_m + (\mathbf{G_0 V_1 G_0 V_1 G_0 V_1 G_0})_m \\ &+ (\mathbf{G_0 V_1 G_0 V_2 G_0})_m + (\mathbf{G_0 V_2 G_0 V_1 G_0})_m, \\ &... \end{aligned} \tag{8}$$

The idea is that $\mathbf{V_1}$, the component of $\mathbf{V}$ that is linear in the data, is solved for with the first equation. This result is substituted into the second equation, leaving $\mathbf{V_2}$ as the only unknown, which may then also be solved for. This continues until a sufficient set of $\mathbf{V_j}$ are known to accurately approximate the desired result $\mathbf{V}$.

The form of the operators $\mathbf{L}$, $\mathbf{G}$, $\mathbf{L_0}$, $\mathbf{G_0}$, and $\mathbf{V}$ obviously vary depending on the desired form for the wave propagation. The simplest possible case is chosen here: a 1D constant density acoustic medium, with the reference medium homogeneous. The scattering potential is confined to a finite region on one side of the source and receiver locations. This choice amounts to defining

$$\begin{aligned} \mathbf{L} &= \frac{d^2}{dz^2} + \left(\frac{\omega}{c(z)}\right)^2, \\ \mathbf{L_0} &= \frac{d^2}{dz^2} + \left(\frac{\omega}{c_0}\right)^2, \end{aligned} \tag{9}$$

in which case

$$\mathbf{V} = \left(\frac{\omega}{c_0}\right)^2 - \left(\frac{\omega}{c(z)}\right)^2 = k^2 \alpha(z), \tag{10}$$

where $k = \omega / c_0$ and $\alpha(z) = 1 - c_0^2 / c^2(z)$. This simple physical framework also permits the use of the Green's function

$$G_0(z|z_s;k) = \frac{e^{ik|z-z_s|}}{2ik} \tag{11}$$

(which becomes $\mathbf{G_0}$ when it is included as part of the kernel of the integrals of the series). In this framework equation (7) reduces to

$$k^2\alpha(z) = k^2\alpha_1(z) + k^2\alpha_2(z) + k^2\alpha_3(z) + .. \ . \tag{12}$$

Finally, following the conventional physical interpretation of the "rightmost" Green's operator in every term of equation (8) as being the incident wave field, these are replaced with incident plane-waves $\psi_0(z|z_s;k)$. The terms of equation (8) become

$$\begin{aligned}
\psi_s(z|z_s;k) &= \int_{-\infty}^{\infty} G_0(z|z';k)k^2\alpha_1(z')\psi_0(z'|z_s;k)dz', \\
0 &= \int_{-\infty}^{\infty} G_0(z|z';k)k^2\alpha_2(z')\psi_0(z'|z_s;k)dz' \\
&+ \int_{-\infty}^{\infty} G_0(z|z';k)k^2\alpha_1(z') \\
&\times \int_{-\infty}^{\infty} G_0(z'|z'';k)k^2\alpha_1(z'')\psi_0(z''|z_s;k)dz''dz', \\
&...,
\end{aligned} \tag{13}$$

in which α_n are solved for order-by-order.

2 Part I: Review and analysis of the coupled imaging-inversion subseries

The identification, manipulation, and isolation of portions (i.e., terms) of the inverse scattering series that, to some satisfactory level of approximation, operate solely on primaries is an important issue in algorithm development and analysis. I begin by appealing to the well-known linear inversion, and its "diagrammatical representation", in Figure 1a. (It is assumed that algorithms derived from such diagrams will necessarily operate on input data/linear inverse results that are free from multiples.)

The diagram, which reflects very broadly the geometry of a wave experiment with source and receiver at the same depth, say $z = 0$, and scattering interactions below, illustrates the "single-scattering" nature of the linear inverse. (These diagrams illustrate scattering geometry in the depth coordinate; the lateral extent of the diagrams are a convenience.) It is a visual representation of the mathematics in the top line of equation (8): we form a relationship between the measured wave field and a quantity involving (a) a propagation from the source to an interaction point in the reference medium, say at some depth z', via $\mathbf{G_0}$, (b) a single scattering interaction of strength $\mathbf{V_1}$ at z', followed by (c) a further propagation from interaction point to the receiver in the reference medium via $\mathbf{G_0}$.

This structure may be interpreted as a framework for interrogation of reflected primary data in the aid of imaging and inversion. The shape of the diagram indicates that the data are to be searched for contributions to an Earth model as if each and every model contribution, or discontinuity, was generated by a single interaction, a point at which a component of the wave field was deemed to change direction with respect to the preferred axis z.

All data events will be treated as primaries in this approximation, since no path consistent with a reverberation, or multiple, exists here, only a downward propagation of z', followed by an upward propagation of z', a total distance of $2z'$ in pseudo-depth. (This is held to be true even though these terms are not describing real primaries involving propagations, reflections, and transmissions, in the real medium, but rather, an inverse series analog to these, involving propagation in the reference medium and interactions of strength $\mathbf{V_1}$. Neither of these latter two quantities necessarily relate immediately to wave events in the actual Earth; rather, they describe a prescribed search and interrogation of the data as a means to process and invert.) This is a strength of the linear method, since primaries are generally considered to be the signal in a seismic experiment whereas multiples are considered noise; an accurate subsurface image is most often generated when primaries only are present. However, since all propagation occurs in the reference medium, which is in our framework held to be distinct from the true medium, the locations and amplitudes of reflectors in the single-scattering image approximation will be incorrect. Hence, this diagram/approximation has definite and well-understood weaknesses. The role of higher order image-forming and inversion terms in the series must be to correct these weaknesses – process primaries only, but to the correct depth and amplitude.

Figure 1b illustrates within this diagrammatical framework the thinking behind the choice of terms that are deemed to fulfill this role. The proposed rule is: utilize higher order terms in the series (i.e., terms with more than one scattering event), but use only those whose diagram retains the underlying form of the linear scattering diagram: cumulative reference propagation downward to some image point at z' then back up, maintaining the overall pseudo-distance $2z'$. This rule is implicit in the presentation of the inverse scattering subseries for predicting the spatial location of reflectors and subsequent developments (Weglein et al., 2002). This is in contrast to diagrams/terms in the series which involve scattering combinations of greater complexity, for instance the third-order diagram seen in Figure 1c; the early intuition and subsequent analysis and algorithm development has revealed that such a diagram corresponds to tasks associated with internal multiple attenuation (Weglein et al., 1997).

2.1 Postulating an imaging-inversion subseries

The creation of algorithms involved with imaging and inversion using the proposed "rule" above, requires the collection and computation of terms and sub-terms whose diagrams are similar to those of Figure 1b. We demonstrate how such a collection can occur using a simple 1D normal incidence milieu. The raw terms in the series are integrals over reference propagation depths. For instance, one of the third order terms of the series, after the perturbation operator is specified to the 1D acoustic case, in which $\mathbf{V} = k^2\alpha$, is

$$\begin{aligned} I_3 =& F(k) \int_{-\infty}^{\infty} e^{ikz'} \alpha_1(z') \int_{-\infty}^{\infty} e^{ik|z'-z''|} \alpha_1(z'') \\ & \times \int_{-\infty}^{\infty} e^{ik|z''-z'''|} \alpha_1(z''') e^{ikz'''} dz''' dz'' dz' \end{aligned} \tag{14}$$

where $F(k)$ is a function of wavenumber. The arguments in the exponentials describe a path of propagation from *source* $\rightarrow z''' \rightarrow z'' \rightarrow z' \rightarrow$ *receiver*. To compute this integral the absolute value

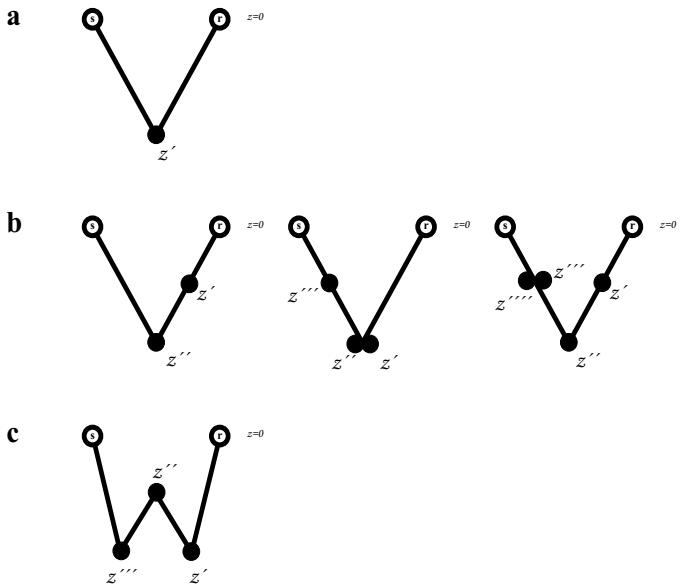

Figure 1: *Candidate and non-candidate imaging and/or inversion scattering diagrams. (a) The linear, single-scattering diagram is the prototype diagram-type for processing and inversion of primaries. (b) Examples of subsequent higher-order diagrams that involve a single direction change in depth z, i.e. that maintain a total propagation distance in pseudo-depth of $2z$; these are deemed to be involved with imaging and inversion. (c) An example of a higher-order term that mimics reverberative event paths; these are deemed to be concerned with multiple processing.*

bars are jettisoned in favor of four additive cases, amongst which are, for instance,

$$F(k)\int_{-\infty}^{\infty}\int_{-\infty}^{z'}\int_{-\infty}^{z''} e^{i2kz'}\alpha_1(z')\alpha_1(z'')\alpha_1(z''')dz'''dz''dz', \tag{15}$$

and

$$F(k)\int_{-\infty}^{\infty}\int_{-\infty}^{z'}\int_{z''}^{\infty} e^{i2k(z'-z''+z''')}\alpha_1(z')\alpha_1(z'')\alpha_1(z''')dz'''dz''dz'. \tag{16}$$

Inspection of the argument of the resultant exponential functions reveals that the former of these terms is a sum over propagations that is already consistent with the extended single-scattering idea, i.e. the total propagation distance in the reference medium is $2z'$. Meanwhile the latter involves a more complicated path and generally longer distance. It does not amount to a total distance of $2z'$ except for a few special cases, for instance when $z'' = z'''$. Notice that in equation (15) the outermost integral has the form of a Fourier transform. From here, the $F(k)$ may be interpreted as a differential operator in the spectral domain, acting on the rest of the integrand. The forms for the terms in the inverse scattering series as above are the immediate result of viewing these quantities as such in the conjugate, space, domain. The results we quote hereafter will follow this approach also, to permit comparison to previously referenced imaging/inversion algorithms.

A strategy of manipulating the integrals of the inverse scattering series and collecting the terms that mimic this single-scattering path has been followed and patterns therein analyzed. Some terms/integrals, like equation (15), need no manipulation; others, like equation (16), do. The

manipulations effectively extract the "special cases" referred to above from the integrals through integration by parts and exchange of dummy integration variables. Here a candidate generating function derived from this analysis is presented in two forms. Consider the sum:

$$\alpha_{II}(z) = \sum_{j=1}^{\infty} K_j \left(\int_0^z \alpha_1(z')dz' \right)^{(j)}, \tag{17}$$

where the superscript (j) denotes the j'th derivative with respect to z, and

$$K_{j+1} = \frac{(-1)^j}{(j+1)2^{2j}} \sum_{k=0}^{j} \frac{1}{k!(j-k)!}. \tag{18}$$

This series reproduces a subset of the terms of the inverse scattering series that conform to the diagram-rule stated above: namely, that there be one and one only direction change in z, and thus that the total propagation pseudo-depth must be $2z$ (since we have set source and receiver depths to zero). In the remainder of this section we analyze the meaning and behavior of equation (17). The subseries expressed by equation (17), and especially the coefficient K_n, may be arrived at by observing patterns in the order-by-order behavior of the coefficients of the scattering integrals; as such it retains something of the raw form of the inverse scattering series terms deemed to process primaries. We note that there are other equivalent mathematical forms. Here we quote one such expression and show that it leads to a closed-form for the 1D cases under study. The quantity α_{II} is precisely recaptured by the following expression, which, via a forward and inverse Fourier transform and the identification of a Taylor's series expansion of an exponential, collapses as also follows.

$$\begin{aligned} \alpha_{II}(z) &= \sum_{j=0}^{\infty} \frac{(-1/2)^j}{j!} \left[\alpha_1(z) \left(\int_0^z \alpha_1(z')dz' \right)^j \right]^{(j)} \\ &= \frac{1}{2\pi} \int_{-\infty}^{\infty} d\Omega e^{i\Omega z} \int_{-\infty}^{\infty} dz' e^{-i\Omega[z' + \frac{1}{2}\int_0^{z'} \alpha_1(z'')dz'']} \alpha_1(z'), \end{aligned} \tag{19}$$

in which the superscript (j) again denotes the n'th derivative with respect to z.

2.2 An analytic example

We here examine a simple analytical example of the closed-form aggregate of the primary-processing inverse scattering series terms, equation (19). The point will be to derive some insight into the underlying non-linear data activity: how do the events of a data set act upon each other to direct the re-location of reflectors and the alteration of contrast amplitudes? The leading-order component of this example is similar to that of Innanen et al. (2006); the high order component is new.

We consider models in which layers of wavespeed c_n are placed in a homogeneous background of wavespeed c_0; layer interfaces are at depths z_n, where z_1 divides the reference medium from the shallowest layer. We place the source and receiver at zero depth with no significant loss of generality: $z_s = z_g = z_0 = 0$. The reflection and transmission coefficients at interface z_n are given by

$$R_n = \frac{c_n - c_{n-1}}{c_n + c_{n-1}}, \quad T_{n-1,n} = \frac{2c_{n-1}}{c_{n-1} + c_n}, \tag{20}$$

with "effective" reflection coefficients

$$R'_n = \prod_{i=1}^{n-1}(1 - R_i^2)R_n \tag{21}$$

containing the cumulative effects of transmission down to the interface at z_n. A primary data set in the frequency domain arising from an N interface model is

$$D(\omega) = \sum_{n=1}^{N} R'_n e^{i\omega \sum_{i=1}^{n}(z_i - z_{i-1})/c_{i-1}}. \tag{22}$$

These data set types will be used for the simple analytical and numerical commentary in the remainder of this paper.

Equation (19) is here enacted upon an analytically derived linear inverse output $\alpha_1(z)$. We consider the primary reflections from a normal incidence acoustic experiment above a single layer, with interfaces at z_1 and z_2 as described in the previous section. The data and the linear inversion result, in both the depth and its conjugate (wavenumber) domains are, respectively,

$$\begin{aligned} D(\omega) &= R_1 e^{i2\omega z_1/c_0} + R'_2 e^{i2\omega z_1/c_0} e^{i2\omega(z_2 - z_1)/c_1}, \\ \alpha_1(z) &= 4R_1 H(z - \tilde{z}_1) + 4R'_2 H(z - \tilde{z}_2), \\ \alpha_1(\Omega) &= 4R_1 \frac{e^{-i\Omega\tilde{z}_1}}{i\Omega} + 4R'_2 \frac{e^{-i\Omega\tilde{z}_2}}{i\Omega}, \end{aligned} \tag{23}$$

where $H(\cdot)$ is the Heaviside function. The interfaces in α_1 are in pseudo-depth, i.e., they have been located on the assumption that waves have propagated everywhere with the reference wavespeed c_0. This means that the linearly-imaged depth of the first interface is coincident with the actual depth, $\tilde{z}_1 = z_1$, but the depth of the second, $\tilde{z}_2 = c_0\tau/2$, where $\tau = 2z_1/c_0 + 2(z_2 - z_1)/c_1$, is not. Furthermore, the amplitudes of the linear inverse are both incorrect; the actual amplitudes of $\alpha(z) = 1 - c_0^2/c^2(z)$ are non-linear in the reflection coefficients. With α_1 in hand we may begin computing analytically $\alpha_{II}(\Omega) = \int_{-\infty}^{\infty} e^{-i\Omega z}\alpha_{II}(z)dz'$:

$$\alpha_{II}(\Omega) = \int_{-\infty}^{\infty} e^{-i\Omega\left[z' + \frac{1}{2}\int_0^{z'} \alpha_1(z'')dz''\right]}\alpha_1(z')dz'. \tag{24}$$

Making use of equation (23), we have as a preliminary quantity

$$\begin{aligned} &\int_0^{z'} \alpha_1(z'')dz'' \\ &= \begin{cases} 0 & z' < \tilde{z}_1 \\ 4R_1(z' - \tilde{z}_1) & \tilde{z}_1 < z' < \tilde{z}_2 \\ 4R_1(\tilde{z}_2 - \tilde{z}_1) + [4R_1 + 4R'_2](z' - \tilde{z}_2) & \tilde{z}_2 < z'. \end{cases} \end{aligned} \tag{25}$$

Broken up into these three cases, equation (24) becomes

$$\alpha_{II}(\Omega) = I_1 + I_2 + I_3, \tag{26}$$

where

$$\begin{aligned} I_1 &= 0, \\ I_2 &= \frac{4R_1}{i\Omega(1+2R_1)}\left[e^{-i\Omega\tilde{z}_1} - e^{-i\Omega[\tilde{z}_2+2R_1(\tilde{z}_2-\tilde{z}_1)]}\right], \\ I_3 &= \frac{4(R_1+R_2')}{i\Omega(1+2(R_1+R_2'))}e^{-i\Omega[\tilde{z}_2+2R_1(\tilde{z}_2-\tilde{z}_1)]}. \end{aligned} \tag{27}$$

Summing these results in

$$\begin{aligned} \alpha_{II}(\Omega) = 4&\left[\frac{R_1}{1+2R_1}\right]\frac{e^{-i\Omega\tilde{z}_1}}{i\Omega} \\ &+ 4\left[\frac{R_1+R_2'}{1+2(R_1+R_2')} - \frac{R_1}{1+2R_1}\right]\frac{e^{-i\Omega[\tilde{z}_2+2R_1(\tilde{z}_2-\tilde{z}_1)]}}{i\Omega}. \end{aligned} \tag{28}$$

This Ω domain result, i.e., in the domain conjugate to depth z, is, like $\alpha_1(\Omega)$ in equation (23), the sum of two Heaviside functions with step locations and amplitudes that are functions of the data amplitudes R_1 and R_2'. Comparing the full result with the linear inverse output, we have

$$\begin{aligned} \alpha_1(z) &= 4R_1H(z-\tilde{z}_1) + 4R_2'H(z-\tilde{z}_2), \\ \alpha_{II}(z) &= 4A_1H(z-\tilde{z}_1) + 4A_2H(z-\tilde{Z}_2), \end{aligned} \tag{29}$$

where

$$\begin{aligned} A_1 &= \frac{R_1}{1+2R_1}, \\ A_2 &= 4\left[\frac{R_1+R_2'}{1+2(R_1+R_2')} - \frac{R_1}{1+2R_1}\right], \\ \tilde{Z}_2 &= \tilde{z}_2 + 2R_1(\tilde{z}_2-\tilde{z}_1). \end{aligned} \tag{30}$$

In essence equation (19) depicts the data (via α_1) becoming part of the kernel of a Fourier-like transformation of itself, whence derives its non-linear, "data-driven" nature. Examination of this processing mechanism begins to clarify how a specific brand of (primary data)×(primary data) multiplication can work to alter the location and magnitude of the reflectors in depth. To wit: the combined effect of these non-linear activities is (in this 1D case) to generate an exponential kernel that involves a direct integration of the data.

First consider the amplitudes. Notice that, because of the involvement of the data in the exponential argument in equation (27), when the antiderivative is taken the data amplitudes drop into the denominators of the coefficients of the steps, correcting their amplitudes. This occurs locally anywhere $\alpha_1 \neq 0$, and is in keeping with the fact that all linear contrast estimates are incorrect, even for interfaces below the known (reference) component of the overburden. Second, consider the step-locations. Step-discontinuities under a Fourier transform appear as weighted exponentials, with the location of the discontinuity fixed in the argument; for instance, $H(z-z^*)$ transforms as $e^{-i\Omega z^*}/i\Omega$. The Fourier-like transform generated by the primary-processing inverse scattering terms *allows the data to interfere with the fixing of the step location*, if there is data activity above that step. The result is that deeper reflectors are positioned at locations that are determined by the

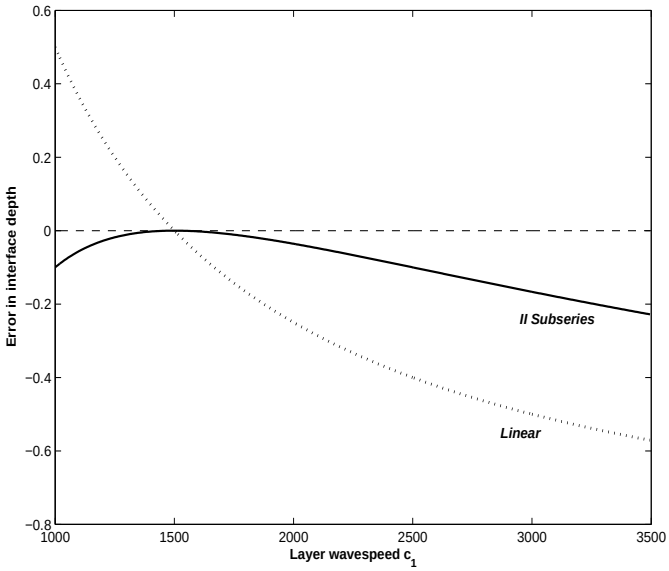

Figure 2: *Error plots for the location in depth of the second interface in the analytic single layer example; linear (dashed) vs. the non-linear II subseries (solid). The plotted values, when multiplied by the thickness of the layer, give the location error in units of depth.*

overlying reflection strengths. This can be seen in action in the last equation of (30), and is very similar to the behavior noted in the LOIS imaging algorithm (Shaw et al., 2004). Quantitatively, consider (1) the difference between the linear approximation of the depth of the second interface, $\tilde{z}_2$, and the actual depth z_2, and (2) the difference between the II approximation $\tilde{Z}_2$ and the actual depth z_2. These differences, or the errors in the linear and non-linear approximations to the depth of the second reflector, are:

$$\begin{aligned} \tilde{z}_2 - z_2 &= \left[\frac{c_0}{c_1} - 1\right](z_2 - z_1) \\ \tilde{Z}_2 - z_2 &= \left[\frac{c_0}{c_1}(1 + 2R_1) - 1\right](z_2 - z_1). \end{aligned} \tag{31}$$

Figure 2 contains a plot of the two error factors $\frac{c_0}{c_1} - 1$ and $\frac{c_0}{c_1}(1 + 2R_1) - 1$ for a fixed reference wavespeed (1500m/s) and a range of layer wavespeeds c_1. The corrective effect of the II series is notable, as is the accumulation of error in the II subseries especially at large contrast. (This II error is due to primary processing terms of the inverse scattering series *not* captured by the expressions utilized here, an issue discussed and addressed with algorithm development aimed at greater capturing of the series imaging capability by Innanen (2005) and Liu et al. (2005)). Figure 3 contains a plot of the errors in amplitude of both the linear inversion and the II subseries inversion for the layer for a range of layer wavespeeds. Again, the corrective effect of the non-linear primary processing subseries is visible.

3 The Taylor's series analogy for imaging in 1D and 2D acoustic media

The direct, non-linear, velocity-independent imaging algorithms that have arisen from the close study of the terms and behavior of the inverse scattering series, and have been led by Shaw and

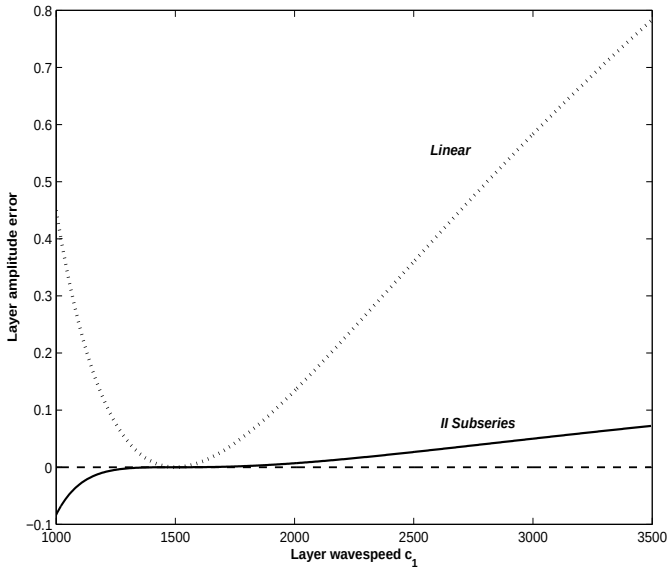

Figure 3: *Error plots for the recovered amplitude of the layer in the analytic single layer example; linear (dashed) vs. the non-linear II subseries (solid).*

Liu as discussed in the Introduction of this Annual Report, can be considered and analyzed in light of a Taylor's series analogy. In this section I will review the development and interpretation of the leading-order imaging subseries algorithm for vertically-varying media as such (Weglein et al., 2002; Shaw et al., 2004). Shaw (2005) has extended the algorithm and analysis to a pre-stack data environment over an acoustic medium that experiences perturbations in wave velocity. I will restrict my attention to the 1D normal incidence version of the algorithm for simplicity; the Taylor's series analogy at issue is unchanged by Shaw's generalization.

The "mechanistic" behavior of the imaging algorithm is straightforward. The model-space quantity $\alpha_1(z)$, that is related linearly to the data given homogeneous acoustic reference Green's operators, has interface locations that are incorrect due to the spatially-sustained discrepancy between the reference and actual media. The imaging algorithm amounts to the construction of a corrective function that re-locates these interfaces to, or close to, the actual depth. The behavior of this construction procedure is shaped and constrained by the inverse scattering series, such that (i) the information that allows it to proceed is taken directly from the measured data, and (ii) the corrective function is expressed in essence as a Taylor's series about the linear quantity.

Following the references quoted above and using the scattering-theoretic components appropriate for a 1D normal incidence acoustic experiment and depth-variations in wave velocity, the terms of

the inverse scattering series $\alpha = \alpha_1 + \alpha_2 + \alpha_3 + ...$ may be expressed up to third order as

$$\begin{aligned}
\alpha_1(z) =& 4\int_0^z D(z_r|z')dz', \\
\alpha_2(z) =& -\frac{1}{2}\alpha_1^2(z) - \frac{1}{2}\alpha_1'(z)\int_0^z \alpha_1(z')dz', \\
\alpha_3(z) =& \frac{3}{16}\alpha_1^3(z) + \frac{1}{8}\alpha_1''(z)\left(\int_0^z \alpha_1(z')dz'\right)^2 \\
&+ \frac{3}{4}\alpha_1'(z)\alpha_1(z)\int_0^z \alpha_1(z')dz' - \frac{1}{8}\alpha_1'(z)\int_0^z \alpha_1^2(z')dz' \\
&+ \text{MULTIPLE ELIMINATION TERMS.}
\end{aligned} \tag{32}$$

This is one of potentially many forms for the terms α_n, generated using an integration-by-parts strategy. It distinguishes itself by producing terms that involve weighted derivatives, and weighted powers, of the linear α_1. I focus on a portion of the former here, the sub-term type that has been identified by the originating researchers as being associated with the problem of building the corrective imaging function. The terms that involve the n'th derivative of α_1 multiplied by the n'th power of the integral of α_1 form this subseries. The expression

$$\alpha_{IM}(z) = \sum_{n=0}^{\infty} \frac{(-1/2)^n}{n!}\alpha_1^{(n)}(z)\left(\int_0^z \alpha_1(z')dz'\right)^n \tag{33}$$

reproduces it at all orders. From this point it becomes possible to discuss not only the Taylor's series analogue followed by this portion of the inverse scattering series, but to further understand how the data information is folded into the procedure. A generic 1D Taylor's series is

$$f(z+Z) = f(z) + f'(z)Z + \frac{1}{2!}f''(z)Z^2 + ..., \tag{34}$$

where a single function f is estimated at an output point $z+Z$ as a sum of weighted n'th derivatives of the function at an input point z. The weights are determined by the distance between the input and output points (Z). The imaging subseries operates in a manner very closely aligned with this Taylor's series, but with a fundamentally different set of inputs and outputs. Equation (33) can be expanded and compared to equation (34):

$$\alpha_{IM}(z) = \alpha_1(z) + \alpha_1'(z)\left(-\frac{1}{2}\int_0^z \alpha_1(z')dz'\right) + \frac{1}{2!}\alpha_1''(z)\left(-\frac{1}{2}\int_0^z \alpha_1(z')dz'\right)^2 + ... \tag{35}$$

Clearly the linear inverse α_1 is identifiable with the function f at the input point z in the standard Taylor's series, suggesting that this subseries is in some sense an expansion about the linear inverse. Equally clearly, differences arise when the outputs, or LHS, of equations (33) and (34) are compared. Whereas the straightforward Taylor's series purports to represent the same function, f, evaluated at a new output point, $z + Z$, we have not thus far had any reason to consider the output of this subseries of the inverse scattering series to act likewise; rather, it has been simply called something entirely new, $\alpha_{IM}(z)$. This analogy drawn between the terms of equation (33) and the Taylor's series, however, suggests that α_{IM} is not an entirely new function, but rather a version of the input function expressed on an altered, perhaps warped and/or shifted, coordinate system. Furthermore, the new coordinate system being apparently proffered by this subseries is defined,

not by a given/chosen distance Z from the point about which a Taylor's series is being computed, but rather directly in terms of the reflection data via α_1. Specifically, the weights Z of the Taylor's series are replaced with $-1/2\int_0^z \alpha_1(z')dz'$, a quantity that retains the dimensions of depth but does so through the incorporation of cumulative linear transmission information directly from the data.

A more compact algorithm and a framework for studying the convergence properties of the imaging subseries is presented by Shaw et al. (2004). Expressing the n'th derivative in equation (33) as an inverse Fourier transform, the portions of the algorithm that involve an n'th power are collected and summed, resulting in an overall exponential function:

$$\begin{aligned}\alpha_{IM}(z) &= \sum_{n=0}^{\infty} \frac{(-1/2)^n}{n!}\alpha_1^{(n)}(z)\left(\int_0^z \alpha_1(z')dz'\right)^n \\ &= \int_{-\infty}^{\infty} dk e^{ik\left(z-\frac{1}{2}\int_0^z \alpha_1(z')dz'\right)}\alpha_1(k) \\ &= \alpha_1\left(z-\frac{1}{2}\int_0^z \alpha_1(z')dz'\right).\end{aligned} \tag{36}$$

3.1 Closed-forms through Taylor's series analogy

The most practically compelling use of the Taylor's series analogy is its "predictive" capability. In this section the analogy is used to deduce the 1D normal incidence closed form of Shaw et al. (2004), using only second-order inverse series terms. This same approach is then applied to create something new: a postulate of a closed form for 2D and 3D direct non-linear imaging, that, similarly, requires as input only the second-order inverse series terms of Liu et al. (2004).

Let's reconsider equation (35) for a moment, and suggest that it is, in fact, acting in some ways like a classic Taylor's series. That is, through a set of derivatives of the input function at a certain z, it is creating the same function at a different z, say $z+Z$. In other words, working from equation (34), it is constructing

$$\alpha_{IM} = \alpha_1(z+Z), \tag{37}$$

using an infinite series. The Taylor's series analogy is now at its most useful: it will tell us what the series is doing, and only require of us that we have computed as far as the 2nd order term. Judging from equation (34), Z must be everything that acts as a coefficient to the first derivative of $\alpha_1(z)$. Going back to the second-order equations in (32), and collecting everything that acts as such a coefficient, we have that

$$Z = -\frac{1}{2}\int_0^z \alpha_1(z')dz'. \tag{38}$$

(There are others at higher order, but we'll stay with leading-order for the moment.) Hence the analogy leads to the summed form of the imaging operation:

$$\alpha_{IM} = \alpha_1\left(z-\frac{1}{2}\int_0^z \alpha_1(z')dz'\right), \tag{39}$$

which is the closed form leading order imaging subseries of Shaw et al. (2004). In short, the Taylor's series analogy produces nothing new in 1D. But the non-new thing it produces is produced *fast*, with a bare minimum of calculation of actual inverse scattering series terms. More compellingly, it is based on analysis that carries over in concept to 2D and 3D (to the extent that any 1D-like wave theoretic inversion scheme carries over into 2D and 3D, at any rate).

A 2D Taylor's series seeks to express a function $f(x+X, z+Z)$ at some location in terms of it and its derivatives at a different location:

$$\begin{aligned} f(x+X, z+Z) =& f(x,z) + f^x(x,z)X + f^z(x,z)Z \\ &+\frac{1}{2}\left[f^{xx}(x,z)X^2 + 2f^{xz}(x,z)XZ + f^{zz}(x,z)Z^2\right] + ..., \end{aligned} \tag{40}$$

where the superscripts denote partial derivatives. So, suppose that a component of the inverse scattering series is attempting to act in 2D the same way the full imaging attempts to act in 1D – with a shift operation. Extending the analogy, we would postulate the existence of

$$\begin{aligned} \alpha_{IM}(x,z) =& \alpha_1(x+X, z+Z) \\ =& \alpha_1(x,z) + \alpha_1^x(x,z)X + \alpha_1^z(x,z)Z + \\ &+\frac{1}{2}\left[\alpha_1^{xx}(x,z)X^2 + 2\alpha_1^{xz}(x,z)XZ + \alpha_1^{zz}(x,z)Z^2\right] + ... \quad . \end{aligned} \tag{41}$$

If there is an imaging component of the inverse scattering series that acts this way, we again should be able to characterize it to a useful extent with minor recourse to the inverse scattering series itself. In fact, the suggestion again seems to be that if we go to the second-order terms of the acoustic constant density inverse scattering series for media whose wavespeed varies in 2D, and find the coefficients of partial derivatives of α_1 with respect to x and z, we will have a leading-order approximation of our desired X and Z. Liu et al. (2005) have computed these – and more. We have

$$\alpha_{IM}(x,z) = \alpha_1\left(x + \frac{1}{2}\int_0^z \int_0^{z'} \alpha_1^x(x,z'')dz''dz', z - \frac{1}{2}\int_0^z \alpha_1(x,z')dz'\right), \tag{42}$$

an operation that has immediate extension to the second lateral dimension as well.

An expression like that of equation (42) but with no x-direction shift forms the basis for the 2D imaging tests going at present, having been derived by Liu et al. (2005). Numerical tests of the x-shift suggested by the full equation (42), done by Liu, are inconclusive at present. Empirically it seems that the double integral of the linear inverse α_1 creates a lateral shift that is far greater than that required. The relevance of equation (42) as an imaging operator, its calculation for some simple models, and its relation to the more complete 2D and 3D wave problem (see, e.g., Innanen (2006)), are matters of investigation.

4 Conclusions

This paper continues in the analysis and interpretation of components of the inverse scattering series, that are deemed to concern tasks of imaging and inversion (coupled and uncoupled). The

coupling subseries of Innanen (2003) and Innanen and Weglein (2003), at leading order, and Innanen (2005), at high order, are reviewed, and an error analysis is provided for a 1D normal incidence, single layer example. Also, the capture of velocity-independent imaging terms in multiple dimensions, by Liu et al. (2005), is extended via an approximation that involves a 2D Taylor's series analogy. Numerical tests of the latter to date are inconclusive, but suggest further terms or development are necessary of such analogy-based shift as an approximate multidimensional imaging frameworks. Further relevant analysis and a reconciliation between the shift forms of Liu et al. (2005) is presented in this report by Zhang et al. (2006).

5 Acknowledgments

The author is grateful to the sponsors and personnel of M-OSRP, and for the interaction amongst A. B. Weglein, F. Liu, J. Zhang, H. Zhang, S. Shaw, and others this year that has led to much increased understanding of non-linear direct imaging, of which this note discusses a small part. I have been partially funded by and am grateful for NSF-CMG award DMS-0327778 and DOE Basic Sciences award DE-FG02-05ER15697.

References

Innanen, K. A., Methods for the treatment of acoustic and absorptive/dispersive wave field measurements. Ph.D. Thesis, University of British Columbia, (2003).

Innanen, K. A. and Weglein, A. B., Simultaneous Imaging and Inversion with the Inverse Scattering Series. *Proceedings of the Eighth International Congress of the SBGf and Fifth Latin American Geophysical Conference, Rio de Janeiro, Brazil*, (2003).

Innanen, K. A., Two non-linear forward and inverse approximations for wave fields in the presence of sustained medium perturbations. *Proceedings of the 75th Annual Meeting of the Society of Exploration Geophysicists, Houston, TX*, (2005).

Innanen, K. A., Nita, B. G. and Weglein, A. B., Analytical and numerical aspects of the processing of reflected seismic primaries with the inverse scattering series, *Submitted to Geophysical Journal International*, (2006).

Liu, F., Weglein, A. B., Innanen, K. A. and Nita, B. G., Extension of the non-linear imaging capability of the inverse scattering series to multidimensional media: strategies and numerical results. *Proceedings of the Ninth International Congress of the SBGf and Sixth Latin American Geophysical Conference, Salvador de Bahia, Brazil*, (2005).

Shaw, S. A., Weglein, A. B., Foster, D. J., Matson, K. H., and Keys, R. G., 2004, Isolation of a leading order depth imaging series and analysis of its convergence properties for a 1D acoustic medium: *Journal of Seismic Exploration 13*, (2004): 99-120.

Shaw, S. A., An inverse scattering series algorithm for depth imaging of reflection data from a layered acoustic medium: Ph.D. Thesis, (2005): University of Houston.

Weglein, A. B., Foster, D. J., Matson, K. H., Shaw, S. A., Carvalho, P. M., Corrigan, D. Predicting the correct spatial location of reflectors without knowing or determining the precise medium and wave velocity: initial concept, and analytic and numerical example. *Journal of Seismic Exploration 10*, (2002): 367–382.

Weglein, A. B., F. V. Gasparotto, P. M. Carvalho, and R. H. Stolt, 1997, An inverse scattering series method for attenuating multiples in seismic reflection data: Geophysics, **46**, pp. 1975–1989.

Weglein, A. B., Araujo, F. V., Carvalho, P. M., Stolt, R. H., Matson, K. H., Coates, R., Corrigan, D., Foster, D. J., Shaw, S. A., and Zhang, H. Topical Review: Inverse-scattering Series and Seismic Exploration. *Inverse Problems 19*, (2003):R27–R83.

Zhang, J., Liu, F., Innanen, K. A., Shaw, S. A., and Weglein, A. B., 2006, A note on imaging closed-forms. *M-OSRP05 Annual Report*, this report.

Direct non-linear inversion of multi-parameter 1D elastic media using the inverse scattering series

Haiyan Zhang and Arthur B. Weglein

Abstract

In this report, research work on direct inversion for two parameter acoustic media is extended to the three parameter elastic case. The first direct non-linear inversion solution for 1D elastic medium (P velocity, shear velocity and density vary in depth) presented in the last annual report is corrected. The terms for moving mislocated reflectors are shown to be separated from amplitude correction terms. Although in principle this direct inversion approach requires all four components of elastic data, synthetic tests indicate that consistent value-added results may be achieved given only $\hat{D}^{PP}$ measurements. We can reasonably infer that further value would derive from actually measuring $\hat{D}^{PP}$, $\hat{D}^{PS}$, $\hat{D}^{SP}$ and $\hat{D}^{SS}$ as the method requires. For the case that all four components of data are available, we give one consistent method to solve for all of the second terms (the first terms beyond linear). The method is direct with neither a model matching nor cost function minimization.

1 Introduction

The objective of seismic processing is to predict the location (imaging) and properties (inversion) of the hydrocarbon resources in the earth using reflection data. For most of the current imaging and inversion algorithms, only primaries are considered as signal. All of the other seismic events need to be removed. So in some sense, imaging and inversion are both "inverse" process of the primaries. These two inverse processes can be performed either separately (inversion after imaging) or together (e.g., Amundsen et al., 2005a; Innanen, 2003; Weglein et al., 2003). Currently the most popular way is to do it separately. One possible advantage of doing them separately is that each task has lower ambition so that the algorithm might be more robust. The other argument is that imaging and inversion operate on the data very differently in the sense that inversion is inevitably a non-linear process of the data while imaging can either be a linear or non-linear process, depending on whether or not the actual medium velocity is required. Imaging procedures such as FK, finite difference and phase shift migration require actual medium velocity and only need linear operations of the data. The idea of these imaging techniques is essentially: depth $z = vt$. This is a simple but very robust method and is being widely used in practice. There are on-going efforts to perform imaging non-linearly in the data in which only reference medium velocity has been used (see e.g., Liu et al., 2005; Shaw, 2005; Weglein et al., 2002). A key concept of these methods is that, compared to those conventional imaging algorithms, the amplitude as well as the arrival time of signal will be used. The methods in this category are especially useful when the actual subsurface medium velocity is difficult to obtain. Inversion, on the other hand, is a guaranteed non-linear process of the data. Even for the simplest normal incidence one interface model, the relationship between the reflected data and earth property changes is non-linear. An inversion result that only involves linear

operations of the data will only give good approximation for small or smooth medium changes. The method provided in this report is a non-linear inversion of the data and only reference medium information will be used. This non-linear inversion method, together with the above mentioned imaging with reference medium velocity algorithm, are both based on inverse scattering series.

The application of inverse scattering series in seismic exploration has become very successful and well-known since the development of the algorithms to remove free surface multiples and attenuate internal multiples (Weglein et al., 1997). A very important concept that has been used to derive these two techniques is the isolated task specific series (Weglein et al., 2003). That is, instead of using the whole inverse scattering series to perform multiple removal, imaging and inversion all together, a specific subset of the series has been isolated to accomplish one task only at each step. After each task has been finished, the problem is restarted assuming that the former task doesn't exist at all. A new subset series is then pursued to address the following problem. All of the derived subseries will only need the reference medium information and no subsurface medium properties are required. The above mentioned imaging with reference medium velocity and the non-linear method in this report are the corresponding isolated task-specific imaging and inversion subseries respectively. It is also important to note that both the imaging and inversion algorithms derived from the inverse scattering series are direct methods, which means that the final results of the imaging and inversion are calculated directly step by step. There are also indirect methods that might be non-linear inversion of the data. Instead of seeking the direct solution, those methods often try to find an objective function which is assumed to be zero or minimized when the correct result is obtained. Those indirect methods certainly have values sometimes. The fundamental disadvantage of these methods is that the results or models obtained are not necessarily the correct ones. At this point, the inverse scattering series based imaging and direct non-linear inversion methods are more advantageous.

Recently, Amundsen and co-workers have written and published several papers (Amundsen et al., 2005a; Amundsen et al., 2005b) using inverse scattering formalism, and seeking non-series approximate solutions to objectives associated with primaries. Recognizing certain patterns within results for depth imaging and inversion that were derived by Simon Shaw, A Weglein, R Keys, Fang Liu, D Foster, B Nita, Kris Innanen, and H Zhang and co-workers. Amundsen et al. were cleverly able to recast and reproduce those earlier available 1D results without resorting to a series, but with an approximate single term for the scattered field. They exploit a WKBJ analytic form, available in 1D, to directly invert an approximate expression for the scattered field, for an approximate perturbation, that simultaneously resides within the WKBJ approximate to the total field, and the perturbation term within the integral itself. The Amundsen research and contribution provides new insights and understanding, and will be valuable in the campaign into imaging beneath highly complex heterogeneous media, where not only analytic WKBJ forms are not available, but even finite difference modeling has difficulty adequately capturing those complex wave responses.

The inverse scattering task specific subseries for imaging and inverting primaries is currently the only viable candidate to address that level of complexity. All of these subseries act in a certain sequence so that the total seismic data can be processed accordingly. The order of the processing is (1) free surface multiple removal (2) internal multiple removal (3) imaging and (4) inversion. The two multiple removal procedures are model type independent, i.e., they work for acoustic, elastic and anelastic medium. Taking internal multiples from attenuation to elimination is being progressed by Ramírez and Weglein (2005). Compared with model type independent multiple

removal procedures, there is a full expectation that tasks and algorithms associated with primaries will have a closer interest in model type. For example, there is no way to even imagine that medium property identification can take place without reference to a specific model type. Tasks and issues associated with structural determination, without knowing the medium, are also vastly different depending on the number of dimensions of variation in velocities that are required for imaging. Hence, a staged approach and isolation of tasks philosophy is essential in this yet tougher neighborhood, and even more in demand for seeking insights and then practical algorithms for these more complicated and daunting objectives. We adopt the staged and isolation of issues approach for primaries. The isolated task achievement plan can often spin-off incomplete but useful intermediate objectives. The test and standard is not necessarily how complete the method is but rather how does it compare to, and improve upon, current best practice.

The stages within the strategy for primaries are as follows: (1) 1D earth, with one parameter, velocity as a function of depth, and a normal incidence wave; (2) 1D earth with one parameter subsurface and offset data, one shot record; (3) 2D earth with one parameter, velocity, varying in x and z, and a suite of shot records; (4) 1D acoustic earth with two parameters varying, velocity and density, one propagation velocity, and one shot record of PP data, and (5) 1D elastic earth, two elastic isotropic parameters and density, and two wave speeds, for P and S waves, and PP, PS, SP, and SS shot records data collected. In this report we make a major step towards realism for target identification by extending the earlier work on non-linear inversion of 2D acoustic data for a two parameter 1D medium (Zhang and Weglein, 2003) to three parameter 1D elastic medium. This is the first step of direct non-linear inversion from acoustic to elastic – a more realistic world. We take these steps and learn to navigate through this complexity and steer it towards useful and powerful algorithms. However, more realism is more complicated with more issues involved. Following the task separation strategy, we ask the question what kind of tasks should we expect in this more complex, elastic, setting? In the acoustic case, for example, there is only one velocity (P wave velocity) involved and there is only one mislocation. The imaging terms only need to move the one mislocation to the correct location. When we extend our previous work on the two parameter acoustic case to the present three parameter elastic case, there will be four mislocations because of the two reference velocities (P wave velocity and S velocity). Therefore, for the non-linear elastic inversion, there will be more tasks that need to be achieved. For example, the "four mislocations", which come from linear inversion, need to be moved to one correct location.

In this report, the first non-linear inversion term for three parameter 1D elastic medium presented in last annual report is corrected. In theory, it is impossible to perform exact inversion without all four components of data. However, as you can find in the following numerical tests (got from the new corrected solution) for four models, very good inversion results can still be achieved even when only PP data measurements are available. This means that we could perform elastic inversion only using pressure measurements, i.e. towed streamer data. For the case that all four components of data are available, a consistent method is provided.

The report has the following structure: Section 2 is a brief introduction to the inverse scattering series and then presents, respectively, the derivations and numerical tests for elastic non-linear inversion when only PP data is available. A full non-linear elastic inversion method is also provided. Finally we will present some concluding remarks.

2 Background

In this section we consider the inversion problem in two dimensions for an elastic medium. For convenience, we change the basis and transform the equations of displacement space into PS space. In the PS domain, the inverse scattering series is (Weglein and Stolt, 1992; Matson, 1997; Zhang et al., 2005)

$$\hat{V} = \hat{V}_1 + \hat{V}_2 + \hat{V}_3 + \cdots . \tag{1}$$

And

$$\hat{D} = \hat{G}_0\hat{V}_1\hat{G}_0, \tag{2}$$

$$\hat{G}_0\hat{V}_2\hat{G}_0 = -\hat{G}_0\hat{V}_1\hat{G}_0\hat{V}_1\hat{G}_0, \tag{3}$$

$$\vdots$$

The perturbation is given by $\hat{V} = \begin{pmatrix} \hat{V}^{PP} & \hat{V}^{PS} \\ \hat{V}^{SP} & \hat{V}^{SS} \end{pmatrix}$, the (causal) Green's operator by $\hat{G}_0 = \begin{pmatrix} \hat{G}_0^P & 0 \\ 0 & \hat{G}_0^S \end{pmatrix}$ and the data by $\hat{D} = \begin{pmatrix} \hat{D}^{PP} & \hat{D}^{PS} \\ \hat{D}^{SP} & \hat{D}^{SS} \end{pmatrix}$.

3 Linear inversion of 1D elastic medium

Writing Eq. (2) in matrix form leads to four equations

$$\hat{D}^{PP} = \hat{G}_0^P\hat{V}_1^{PP}\hat{G}_0^P, \tag{4}$$

$$\hat{D}^{PS} = \hat{G}_0^P\hat{V}_1^{PS}\hat{G}_0^S, \tag{5}$$

$$\hat{D}^{SP} = \hat{G}_0^S\hat{V}_1^{SP}\hat{G}_0^P, \tag{6}$$

$$\hat{D}^{SS} = \hat{G}_0^S\hat{V}_1^{SS}\hat{G}_0^S. \tag{7}$$

Assuming source and receiver depths are zero, in the $(k_s, z_s; k_g, z_g; \omega)$ domain, we get respectively,

$$\widetilde{D}^{PP}(k_g, 0; -k_g, 0; \omega) = -\frac{1}{4}\left(1 - \frac{k_g^2}{\nu_g^2}\right)\widetilde{a}_\rho^{(1)}(-2\nu_g) - \frac{1}{4}\left(1 + \frac{k_g^2}{\nu_g^2}\right)\widetilde{a}_\gamma^{(1)}(-2\nu_g) + \frac{2k_g^2\beta_0^2}{(\nu_g^2 + k_g^2)\alpha_0^2}\widetilde{a}_\mu^{(1)}(-2\nu_g), \tag{8}$$

$$\widetilde{D}^{PS}(\nu_g, \eta_g) = -\frac{1}{4}\left(\frac{k_g}{\nu_g} + \frac{k_g}{\eta_g}\right)\widetilde{a}_\rho^{(1)}(-\nu_g - \eta_g) - \frac{\beta_0^2}{2\omega^2}k_g(\nu_g + \eta_g)\left(1 - \frac{k_g^2}{\nu_g\eta_g}\right)\widetilde{a}_\mu^{(1)}(-\nu_g - \eta_g), \tag{9}$$

$$\widetilde{D}^{SP}(\nu_g, \eta_g) = \frac{1}{4}\left(\frac{k_g}{\nu_g} + \frac{k_g}{\eta_g}\right)\widetilde{a}_\rho^{(1)}(-\nu_g - \eta_g) + \frac{\beta_0^2}{2\omega^2}k_g(\nu_g + \eta_g)\left(1 - \frac{k_g^2}{\nu_g\eta_g}\right)\widetilde{a}_\mu^{(1)}(-\nu_g - \eta_g), \tag{10}$$

$$\widetilde{D}^{SS}(k_g,\eta_g) = -\frac{1}{4}\left(1-\frac{k_g^2}{\eta_g^2}\right)\widetilde{a}_\rho^{(1)}(-2\eta_g) - \left[\frac{\eta_g^2+k_g^2}{4\eta_g^2} - \frac{2k_g^2}{\eta_g^2+k_g^2}\right]\widetilde{a}_\mu^{(1)}(-2\eta_g), \tag{11}$$

where $\nu_g^2 + k_g^2 = \frac{\omega^2}{\alpha_0^2},\ \eta_g^2 + k_g^2 = \frac{\omega^2}{\beta_0^2}$. Now, using $k_g^2/\nu_g^2 = \tan^2\theta$ and $k_g^2/(\nu_g^2+k_g^2) = \sin^2\theta$, where θ is the P-wave incident angle (see Fig. 1). Then, Eq. (8) becomes

$$\widetilde{D}^{PP}(\nu_g,\theta) = -\frac{1}{4}(1-\tan^2\theta)\widetilde{a}_\rho^{(1)}(-2\nu_g) - \frac{1}{4}(1+\tan^2\theta)\widetilde{a}_\gamma^{(1)}(-2\nu_g) + \frac{2\beta_0^2\sin^2\theta}{\alpha_0^2}\widetilde{a}_\mu^{(1)}(-2\nu_g). \tag{12}$$

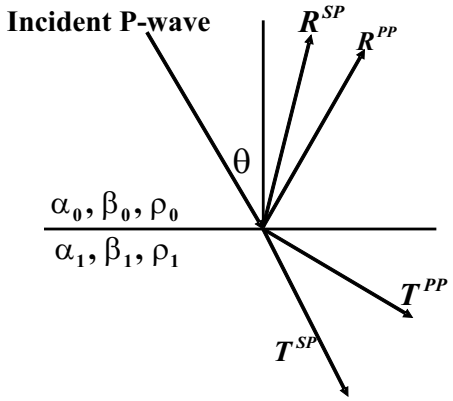

Figure 1: Response of incident compressional wave on a planar elastic interface. α_0, β_0 and ρ_0 are the compressional wave velocity, shear wave velocity and density of the upper layer, respectively; α_1, β_1 and ρ_1 denote the compressional wave velocity, shear wave velocity and density of the lower layer. R^{PP}, R^{SP}, T^{PP} and T^{SP} denote the coefficients of the reflected compressional wave, the reflected shear wave, the transmitted compressional wave and the transmitted shear wave, respectively.

4 Non-linear inversion of 1D elastic medium for 2D experiment

Writing Eq. (3) in matrix form:

$$\begin{aligned}
&\begin{pmatrix}\hat{G}_0^P & 0\\ 0 & \hat{G}_0^S\end{pmatrix}\begin{pmatrix}\hat{V}_2^{PP} & \hat{V}_2^{PS}\\ \hat{V}_2^{SP} & \hat{V}_2^{SS}\end{pmatrix}\begin{pmatrix}\hat{G}_0^P & 0\\ 0 & \hat{G}_0^S\end{pmatrix}\\
&= -\begin{pmatrix}\hat{G}_0^P & 0\\ 0 & \hat{G}_0^S\end{pmatrix}\begin{pmatrix}\hat{V}_1^{PP} & \hat{V}_1^{PS}\\ \hat{V}_1^{SP} & \hat{V}_1^{SS}\end{pmatrix}\begin{pmatrix}\hat{G}_0^P & 0\\ 0 & \hat{G}_0^S\end{pmatrix}\begin{pmatrix}\hat{V}_1^{PP} & \hat{V}_1^{PS}\\ \hat{V}_1^{SP} & \hat{V}_1^{SS}\end{pmatrix}\begin{pmatrix}\hat{G}_0^P & 0\\ 0 & \hat{G}_0^S\end{pmatrix},
\end{aligned} \tag{13}$$

leads to four equations

$$\hat{G}_0^P\hat{V}_2^{PP}\hat{G}_0^P = -\hat{G}_0^P\hat{V}_1^{PP}\hat{G}_0^P\hat{V}_1^{PP}\hat{G}_0^P - \hat{G}_0^P\hat{V}_1^{PS}\hat{G}_0^S\hat{V}_1^{SP}\hat{G}_0^P, \tag{14}$$

$$\hat{G}_0^P\hat{V}_2^{PS}\hat{G}_0^S = -\hat{G}_0^P\hat{V}_1^{PP}\hat{G}_0^P\hat{V}_1^{PS}\hat{G}_0^S - \hat{G}_0^P\hat{V}_1^{PS}\hat{G}_0^S\hat{V}_1^{SS}\hat{G}_0^S, \tag{15}$$

$$\hat{G}_0^S\hat{V}_2^{SP}\hat{G}_0^P = -\hat{G}_0^S\hat{V}_1^{SP}\hat{G}_0^P\hat{V}_1^{PP}\hat{G}_0^P - \hat{G}_0^S\hat{V}_1^{SS}\hat{G}_0^S\hat{V}_1^{SP}\hat{G}_0^P, \tag{16}$$

$$\hat{G}_0^S \hat{V}_2^{SS} \hat{G}_0^S = -\hat{G}_0^S \hat{V}_1^{SP} \hat{G}_0^P \hat{V}_1^{PS} \hat{G}_0^S - \hat{G}_0^S \hat{V}_1^{SS} \hat{G}_0^S \hat{V}_1^{SS} \hat{G}_0^S. \tag{17}$$

Since $\hat{V}_1^{PP}$ relates to $\hat{D}^{PP}$, $\hat{V}_1^{PS}$ relates to $\hat{D}^{PS}$, and so on, the four components of the data will be coupled in the non-linear elastic inversion. We cannot perform the direct non-linear inversion without knowing all components of the data. As shown above, when we extend our work on the two parameter acoustic case to the present three parameter elastic case, it is not just simply adding one more parameter, but there are more issues involved. Even for the linear case, the linear solutions found in (8) $\sim$ (11) are much more complicated than those of the acoustic case. For instance, four different sets of linear parameter estimates are produced from each component of the data. Also, three or four distinct reflector mislocations arise from the two reference velocities (P-velocity and S-velocity). However, in some situations like the towed streamer case, we don't have all components of data available. A particular non-linear approach has been chosen to side-step a portion of this complexity and address our typical lack of four components of elastic data: we use $\hat{D}^{PP}$ as our fundamental data input, and perform a reduced form of non-linear elastic inversion, concurrently asking: what beyond-linear value does this simpler framework add? This particular approach is presented in the following section.

4.1 Special approach and numerical tests with only $\hat{D}^{PP}$ available

When assuming only $\hat{D}^{PP}$ are available, first, we compute the linear solution for $a_\rho^{(1)}$, $a_\gamma^{(1)}$ and $a_\mu^{(1)}$ from Eq. (8). Then, substituting the solution into the other three Eqs. (9), (10) and (11), we synthesize the other components of data — $\hat{D}^{PS}$, $\hat{D}^{SP}$ and $\hat{D}^{SS}$. Finally, using the given $\hat{D}^{PP}$ and the synthesized data, we perform the non-linear elastic inversion, getting the following second

order (first term beyond linear) elastic inversion solution from Eq. (14),

$$
\begin{aligned}
&\left(1-\tan^2\theta\right)a_\rho^{(2)}(z)+\left(1+\tan^2\theta\right)a_\gamma^{(2)}(z)-8b^2\sin^2\theta a_\mu^{(2)}(z)\\
=&-\frac{1}{2}\left(\tan^4\theta-1\right)\left[a_\gamma^{(1)}(z)\right]^2+\frac{\tan^2\theta}{\cos^2\theta}a_\gamma^{(1)}(z)a_\rho^{(1)}(z)\\
&+\frac{1}{2}\left[\left(1-\tan^4\theta\right)-\frac{2}{C+1}\left(\frac{1}{C}\right)\left(\frac{\alpha_0^2}{\beta_0^2}-1\right)\frac{\tan^2\theta}{\cos^2\theta}\right]\left[a_\rho^{(1)}(z)\right]^2\\
&-4b^2\left[\tan^2\theta-\frac{2}{C+1}\left(\frac{1}{2C}\right)\left(\frac{\alpha_0^2}{\beta_0^2}-1\right)\tan^4\theta\right]a_\rho^{(1)}(z)a_\mu^{(1)}(z)\\
&+2b^4\left(\tan^2\theta-\frac{\alpha_0^2}{\beta_0^2}\right)\left[2\sin^2\theta-\frac{2}{C+1}\frac{1}{C}\left(\frac{\alpha_0^2}{\beta_0^2}-1\right)\tan^2\theta\right]\left[a_\mu^{(1)}(z)\right]^2\\
&-\frac{1}{2}\left(\frac{1}{\cos^4\theta}\right)a_\gamma^{(1)\prime}(z)\int_0^z dz'\left[a_\gamma^{(1)}\left(z'\right)-a_\rho^{(1)}\left(z'\right)\right]\\
&-\frac{1}{2}\left(1-\tan^4\theta\right)a_\rho^{(1)\prime}(z)\int_0^z dz'\left[a_\gamma^{(1)}\left(z'\right)-a_\rho^{(1)}\left(z'\right)\right]\\
&+4b^2\tan^2\theta a_\mu^{(1)\prime}(z)\int_0^z dz'\left[a_\gamma^{(1)}\left(z'\right)-a_\rho^{(1)}\left(z'\right)\right]\\
&+\frac{2}{C+1}\frac{1}{C}\left(\frac{\alpha_0^2}{\beta_0^2}-1\right)\tan^2\theta\left(\tan^2\theta-C\right)b^2\int_0^z dz'a_\mu^{(1)\prime}\left(\frac{(C-1)\,z'+2z}{(C+1)}\right)a_\rho^{(1)}\left(z'\right)\\
&-\frac{2}{C+1}\frac{2}{C}\left(\frac{\alpha_0^2}{\beta_0^2}-1\right)\tan^2\theta\left(\tan^2\theta-\frac{\alpha_0^2}{\beta_0^2}\right)b^4\int_0^z dz'a_\mu^{(1)\prime}\left(\frac{(C-1)\,z'+2z}{(C+1)}\right)a_\mu^{(1)}\left(z'\right)\\
&+\frac{2}{C+1}\frac{1}{C}\left(\frac{\alpha_0^2}{\beta_0^2}-1\right)\tan^2\theta\left(\tan^2\theta+C\right)b^2\int_0^z dz'a_\mu^{(1)}\left(z'\right)a_\rho^{(1)\prime}\left(\frac{(C-1)z'+2z}{(C+1)}\right)\\
&-\frac{2}{C+1}\frac{1}{2C}\left(\frac{\alpha_0^2}{\beta_0^2}-1\right)\tan^2\theta\left(\tan^2\theta+1\right)\int_0^z dz'a_\rho^{(1)}\left(z'\right)a_\rho^{(1)\prime}\left(\frac{(C-1)\,z'+2z}{(C+1)}\right),
\end{aligned}
\tag{18}
$$

where $a_\rho^{(1)\prime}\left(\frac{(C-1)z'+2z}{(C+1)}\right)=d\left[a_\rho^{(1)}\left(\frac{(C-1)z'+2z}{(C+1)}\right)\right]/dz$, $b=\frac{\beta_0}{\alpha_0}$ and $C=\frac{\eta_g}{\nu_g}=\frac{1}{b}\frac{\sqrt{1-b^2\sin^2\theta}}{\sqrt{1-\sin^2\theta}}$.

The first five terms on the right side of the Eq. (18) are inversion terms, i.e., contribute to amplitude correction. The other terms on the right side of the equation are imaging terms. Both the inversion terms and the imaging terms (especially the imaging terms) become much more complicated with the extension to elastic media from acoustic. The integrand of the first three integral terms is the first order approximation of the relative change in P-wave velocity. The derivatives $a_\gamma^{(1)\prime}$, $a_\rho^{(1)\prime}$ and $a_\mu^{(1)\prime}$ in front of those integrals are acting to correct the wrong locations caused by the inaccurate reference P-wave velocity. The other four terms with integrals will be zero as $\beta_0\to 0$ since in this case $C\to\infty$. In the following, we test this approach numerically.

For one interface 1D elastic medium case, as shown in Fig. 1, the reflection R^{PP} coefficient has the following form (Foster et al., 1997)

$$R^{PP}=\frac{N}{D}. \tag{19}$$

Here we have

$$\begin{aligned} N =& -(1+2kx^2)^2 b\sqrt{1-c^2x^2}\sqrt{1-d^2x^2} - (1-a+2kx^2)^2 bcdx^2 \\ &+ (a-2kx^2)^2 cd\sqrt{1-x^2}\sqrt{1-b^2x^2} \\ &+ 4k^2x^2\sqrt{1-x^2}\sqrt{1-b^2x^2}\sqrt{1-c^2x^2}\sqrt{1-d^2x^2} - ad\sqrt{1-b^2x^2}\sqrt{1-c^2x^2} \\ &+ abc\sqrt{1-x^2}\sqrt{1-d^2x^2}. \end{aligned} \tag{20}$$

$$\begin{aligned} D =& (1+2kx^2)^2 b\sqrt{1-c^2x^2}\sqrt{1-d^2x^2} + (1-a+2kx^2)^2 bcdx^2 \\ &+ (a-2kx^2)^2 cd\sqrt{1-x^2}\sqrt{1-b^2x^2} \\ &+ 4k^2x^2\sqrt{1-x^2}\sqrt{1-b^2x^2}\sqrt{1-c^2x^2}\sqrt{1-d^2x^2} + ad\sqrt{1-b^2x^2}\sqrt{1-c^2x^2} \\ &+ abc\sqrt{1-x^2}\sqrt{1-d^2x^2}. \end{aligned} \tag{21}$$

$$a = \rho_1/\rho_0,\ b = \beta_0/\alpha_0,\ c = \alpha_1/\alpha_0,\ d = \beta_1/\alpha_0,\ k = ad^2 - b^2 \ and\ x = \sin\theta,$$

where the subscripts "0" and "1" denote the reference medium and actual medium respectively. Using perfect data (Clayton and Stolt, 1981; Weglein et al., 1986)

$$\widetilde{D}^{PP}(\nu_g, \theta) = R^{PP}(\theta)\frac{e^{2i\nu_g a}}{4\pi i\nu_g}, \tag{22}$$

and substituting Eq.(22) into Eq.(12), Fourier transform Eq.(12) over $2\nu_g$, for $z > a$ and fixed θ, we have

$$(1-\tan^2\theta)a_\rho^{(1)}(z) + (1+\tan^2\theta)a_\gamma^{(1)}(z) - 8\frac{\beta_0^2}{\alpha_0^2}\sin^2\theta a_\mu^{(1)}(z) = 4R^{PP}(\theta)H(z-a). \tag{23}$$

In this report, we numerically test the direct inversion approach on the following same four models used in the last annual report:

Model 1: shale (0.20 porosity) over oil sand (0.10 porosity).

$$\rho_0 = 2.32g/cm^3, \rho_1 = 2.46g/cm^3; \alpha_0 = 2627m/s, \alpha_1 = 4423m/s; \beta_0 = 1245m/s, \beta_1 = 2939m/s.$$

Model 2: shale over oil sand, 0.20 porosity.

$$\rho_0 = 2.32g/cm^3, \rho_1 = 2.27g/cm^3; \alpha_0 = 2627m/s, \alpha_1 = 3251m/s; \beta_0 = 1245m/s, \beta_1 = 2138m/s.$$

Model 3: shale (0.20 porosity) over oil sand (0.30 porosity).

$$\rho_0 = 2.32g/cm^3, \rho_1 = 2.08g/cm^3; \alpha_0 = 2627m/s, \alpha_1 = 2330m/s; \beta_0 = 1245m/s, \beta_1 = 1488m/s.$$

Model 4: oil sand over wet sand, 0.20 porosity.

$$\rho_0 = 2.27g/cm^3, \rho_1 = 2.32g/cm^3; \alpha_0 = 3251m/s, \alpha_1 = 3507m/s; \beta_0 = 2138m/s, \beta_1 = 2116m/s.$$

To test and compare methods, the top of sand reflection was modeled for oil sands with porosities of 10, 20, and 30%. The three models used the same shale overburden. An oil/water contact model was also constructed for the 20% porosity sand.

The low porosity model (10%) represents a deep, consolidated reservoir sand. Pore fluids have little effect on the seismic response of the reservoir sand. It is difficult to distinguish oil sands from brine sands on the basis of seismic response. Impedance of the sand is higher than impedance of the shale.

The moderate porosity model (20%) represents deeper, more compacted reservoirs. Pore fluids have a large impact on seismic response, but the fluid effect is less than that of the high porosity case. The overlying shale has high density compared to the reservoir sand, but the P-wave velocity of the oil sand exceeds that of the shale. As a result, impedance contrast is reduced, and shear wave information becomes more important for detecting the reservoir.

The high porosity model (30%) is typical of a weakly consolidated, shallow reservoir sand. Pore fluids have a large impact on the seismic response. Density, P-wave velocity, and the α/β ratio of the oil sand are lower than the density, P-wave velocity, and α/β ratio of the overlying shale. Consequently, there is a significant decrease in density and P-bulk modulus and an increase in shear modulus at the shale/oil sand interface.

The fourth model denotes an oil/water contact in a 20% porosity sand. At a fluid contact, both density and P-wave velocity increase in going from the oil zone into the wet zone. Because pore fluids have no effect on shear modulus, there is no change in shear modulus.

Using these four models, we can find the corresponding R^{PP} from Eq. (19). Then, choosing three different angles θ_1, θ_2 and θ_3, we can get the linear solutions for $a_\rho^{(1)}$, $a_\gamma^{(1)}$ and $a_\mu^{(1)}$ from Eq. (23), and then get the solutions for $a_\rho^{(2)}$, $a_\gamma^{(2)}$ and $a_\mu^{(2)}$ from Eq. (18).

There are two plots in each figure. The left ones are the results for the first order, while the right ones are the results for the first order plus the second order. The red lines denote the corresponding actual values. In the figures, we illustrate the results corresponding to different sets of angles θ_1 and θ_2. The third angle θ_3 is fixed at zero.

The numerical results indicate that all the second order solutions provide improvements over the linear for all of the four models. When the second term is added to the linear order, the results become much closer to the corresponding exact values and the surfaces become flatter in a larger range of angles. But the degree of those improvements are different for different models. How accurately $\hat{D}^{PP}$ effectively synthesize $\hat{D}^{PS}$, $\hat{D}^{SP}$ and $\hat{D}^{SS}$ determined the degree of benefit provided by the non-linear elastic inversion.

Elastic non-linear inversion in 2D requires all four components of data. In this paper we present the first direct non-linear elastic equations, and analyze an algorithm which requires only $\hat{D}^{PP}$ and approximately synthesizes the other required components. Value-added results are obtained. Although $\hat{D}^{PP}$ can itself provide useful non-linear direct inversion results, the implication of this research is that further value would derive from actually measuring $\hat{D}^{PP}$, $\hat{D}^{PS}$, $\hat{D}^{SP}$ and $\hat{D}^{SS}$, as the method requires. In the following section, we give a consistent method with all four components of data available.

4.2 Full non-linear elastic inversion of all four components of data

Using four components of data, one consistent method to solve for the second terms is, first, using the linear solutions as shown in Eqs. (8), (9), (10) and (11), we can get the linear solution for $a_\rho^{(1)}$, $a_\gamma^{(1)}$ and $a_\mu^{(1)}$ in terms of $\hat{D}^{PP}, \hat{D}^{PS}, \hat{D}^{SP}$and $\hat{D}^{SS}$ through the following way

$$\begin{pmatrix} a_\rho^{(1)} \\ a_\gamma^{(1)} \\ a_\mu^{(1)} \end{pmatrix} = (O^T O)^{-1} O^T \begin{pmatrix} \hat{D}^{PP} \\ \hat{D}^{PS} \\ \hat{D}^{SP} \\ \hat{D}^{SS} \end{pmatrix}, \tag{24}$$

where the matrix O is

$$\begin{pmatrix} -\frac{1}{4}\left(1-\frac{k_g^{PP2}}{\nu_g^{PP2}}\right) & -\frac{1}{4}\left(1+\frac{k_g^{PP2}}{\nu_g^{PP2}}\right) & \frac{2\beta_0^2 k_g^{PP2}}{\alpha_0^2\left(\nu_g^{PP2}+k_g^{PP2}\right)} \\ -\frac{1}{4}\left(\frac{k_g^{PS}}{\nu_g^{PS}}+\frac{k_g^{PS}}{\eta_g^{PS}}\right) & 0 & -\frac{\beta_0^2}{2\omega^2}k_g^{PS}\left(\nu_g^{PS}+\eta_g^{PS}\right)\left(1-\frac{k_g^{PS2}}{\nu_g^{PS}\eta_g^{PS}}\right) \\ \frac{1}{4}\left(\frac{k_g^{SP}}{\nu_g^{SP}}+\frac{k_g^{SP}}{\eta_g^{SP}}\right) & 0 & \frac{\beta_0^2}{2\omega^2}k_g^{SP}\left(\nu_g^{SP}+\eta_g^{SP}\right)\left(1-\frac{k_g^{SP2}}{\nu_g^{SP}\eta_g^{SP}}\right) \\ -\frac{1}{4}\left(1-\frac{k_g^{SS2}}{\eta_g^{SS2}}\right) & 0 & -\left[\frac{k_g^{SS2}+\eta_g^{SS2}}{4\eta_g^{SS2}}-\frac{2k_g^{SS2}}{k_g^{SS2}+\eta_g^{SS2}}\right] \end{pmatrix}, \tag{25}$$

and O^T is the transpose of matrix O, the superscript -1 denotes the inverse of the matrix $O^T O$. Then, we can get the solution for $a_\rho^{(2)}$, $a_\gamma^{(2)}$ and $a_\mu^{(2)}$ in terms of $a_\rho^{(1)}$, $a_\gamma^{(1)}$ and $a_\mu^{(1)}$ through the following similar way

$$\begin{pmatrix} a_\rho^{(2)} \\ a_\gamma^{(2)} \\ a_\mu^{(2)} \end{pmatrix} = (O^T O)^{-1} O^T Q, \tag{26}$$

Where the matrix Q is in terms of $a_\rho^{(1)}$, $a_\gamma^{(1)}$ and $a_\mu^{(1)}$.

Given θ^{PP}, as shown in Figure 2, we can find the corresponding angles θ^{PS}, θ^{SP} and θ^{SS} which appear in O and Q (Details in Appendix A).

$$\begin{aligned} \theta^{PS} &= \cos^{-1}\left[\frac{4b^2\cos^2\theta^{PP}+1-b^2}{4b\cos\theta^{PP}}\right], \\ \theta^{SP} &= \cos^{-1}\left[\frac{4b^2\cos^2\theta^{PP}-1+b^2}{4b^2\cos\theta^{PP}}\right], \\ \theta^{SS} &= \cos^{-1}\left(b\cos\theta^{PP}\right), \end{aligned}$$

where $b = \frac{\beta_0}{\alpha_0}$.

Based on this idea, we get the following non-linear solutions for Eqs. (14), (15), (16) and (17) respectively.

The form of the solution for Eq. (14), i.e.,

$$\hat{G}_0^P \hat{V}_2^{PP} \hat{G}_0^P = -\hat{G}_0^P \hat{V}_1^{PP} \hat{G}_0^P \hat{V}_1^{PP} \hat{G}_0^P - \hat{G}_0^P \hat{V}_1^{PS} \hat{G}_0^S \hat{V}_1^{SP} \hat{G}_0^P,$$

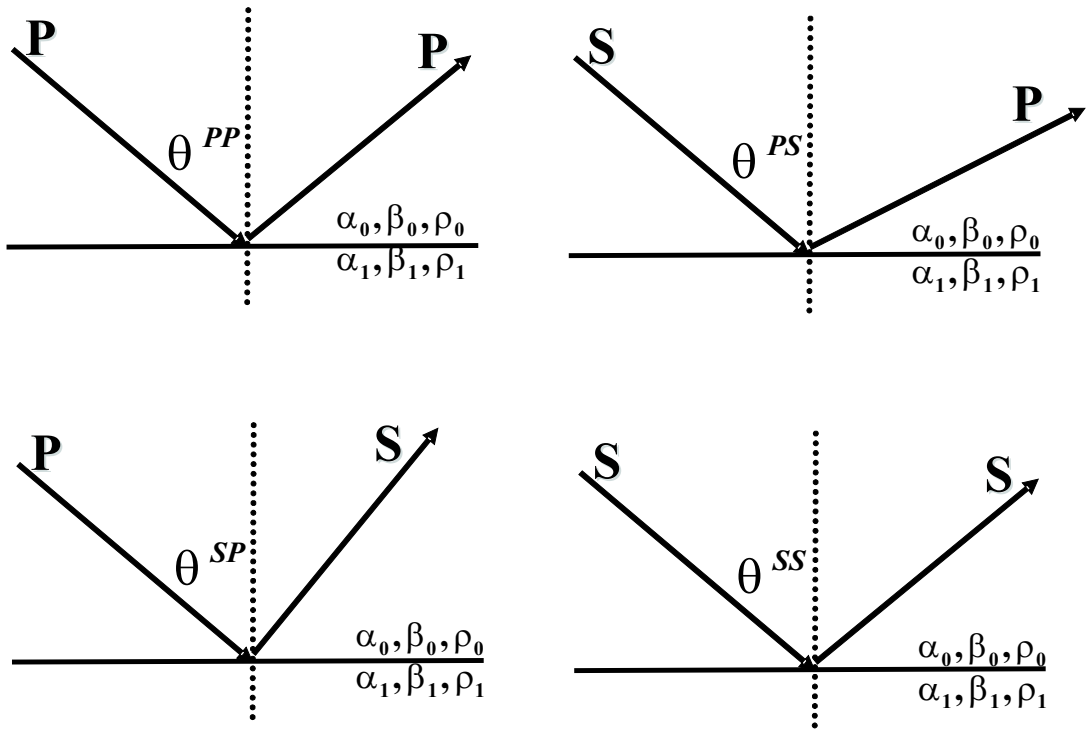

Figure 2: Different incident angles.

is the same as Eq. (18). In the $(k_s, z_s; k_g, z_g; \omega)$ domain, we get the the other three solutions respectively, for Eqs. (15), (16) and (17).

The solution for Eq. (15), i.e.,

$$\hat{G}_0^P \hat{V}_2^{PS} \hat{G}_0^S = -\hat{G}_0^P \hat{V}_1^{PP} \hat{G}_0^P \hat{V}_1^{PS} \hat{G}_0^S - \hat{G}_0^P \hat{V}_1^{PS} \hat{G}_0^S \hat{V}_1^{SS} \hat{G}_0^S,$$

is

$$
\begin{aligned}
&-\frac{1}{4}\left(\frac{k_g}{\nu_g}+\frac{k_g}{\eta_g}\right)a_\rho^{(2)}(z)-\frac{\beta_0^2}{2\omega^2}k_g\left(\nu_g+\eta_g\right)\left(1-\frac{k_g^2}{\nu_g\eta_g}\right)a_\mu^{(2)}(z)\\
=&-\left[\left(\frac{1}{2}+\frac{1}{C+1}\right)\frac{1}{\eta_g\nu_g^2}\left(\frac{\beta_0^4}{\alpha_0^4}Ck_g^3-3\frac{\beta_0^2}{\alpha_0^2}Ck_g^5\frac{\beta_0^2}{\omega^2}-k_g^3\nu_g^2\frac{\beta_0^2}{\omega^2}+2k_g^5\nu_g^2\frac{\beta_0^4}{\omega^4}+2Ck_g^7\frac{\beta_0^4}{\omega^4}\right)\right.\\
&+\left(\frac{1}{2}-\frac{1}{C+1}\right)\frac{1}{\eta_g\nu_g^2}\left(\frac{\beta_0^2}{\alpha_0^2}Ck_g^3\nu_g^2\frac{\beta_0^2}{\omega^2}+2\frac{\beta_0^2}{\alpha_0^2}k_g^5\frac{\beta_0^2}{\omega^2}-2Ck_g^5\nu_g^2\frac{\beta_0^4}{\omega^4}-\frac{\beta_0^2}{\alpha_0^2}k_g^3+k_g^5\frac{\beta_0^2}{\omega^2}-2k_g^7\frac{\beta_0^4}{\omega^4}\right)\\
&+\left(\frac{1}{2C}+\frac{1}{C+1}\right)\frac{1}{4\eta_g^2\nu_g}\left(6k_g^3-12k_g^5\frac{\beta_0^2}{\omega^2}-k_g\frac{\omega^2}{\beta_0^2}+8k_g^7\frac{\beta_0^4}{\omega^4}+8C^3\nu_g^2k_g^5\frac{\beta_0^4}{\omega^4}-4\frac{\beta_0^2}{\alpha_0^2}C^3\nu_g^2k_g^3\frac{\beta_0^2}{\omega^2}\right)\\
&-\left(\frac{1}{2C}-\frac{1}{C+1}\right)\frac{1}{4\eta_g\nu_g^2}\left(4\frac{\beta_0^2}{\alpha_0^2}k_g^3-8k_g^5\frac{\beta_0^2}{\omega^2}-k_g\frac{\omega^2}{\alpha_0^2}+2k_g^3-4C\nu_g^2k_g^3\frac{\beta_0^2}{\omega^2}+8C\nu_g^2k_g^5\frac{\beta_0^4}{\omega^4}-4\frac{\beta_0^2}{\alpha_0^2}k_g^5\frac{\beta_0^2}{\omega^2}\right.\\
&\left.\left.+8k_g^7\frac{\beta_0^4}{\omega^4}\right)-\frac{\beta_0^2}{\alpha_0^2}\frac{k_g^3}{\nu_g}\frac{\beta_0^2}{\omega^2}+\frac{k_g}{2\eta_g}\left(2k_g^2\frac{\beta_0^2}{\omega^2}-1\right)\right]a_\mu^{(1)}(z)a_\mu^{(1)}(z)\\
&-\left[\left(\frac{1}{2}+\frac{1}{C+1}\right)\frac{k_g}{8\eta_g\nu_g^2}\left(Ck_g^2+\nu_g^2\right)-\left(\frac{1}{2}-\frac{1}{C+1}\right)\frac{k_g}{8\eta_g\nu_g^2}\left(k_g^2+C\nu_g^2\right)\right.\\
&\left.+\left(\frac{1}{2C}+\frac{1}{C+1}\right)\frac{k_g}{8\eta_g^2\nu_g}\left(C^3\nu_g^2+k_g^2\right)-\left(\frac{1}{2C}-\frac{1}{C+1}\right)\frac{k_g}{8\eta_g\nu_g^2}\left(k_g^2+C\nu_g^2\right)\right]a_\rho^{(1)}(z)a_\rho^{(1)}(z)\\
&-\left[\left(\frac{1}{2}+\frac{1}{C+1}\right)\frac{\beta_0^2}{\alpha_0^2}\frac{1}{4\nu_g^3}k_g\left(k_g^2-\nu_g^2\right)+\left(\frac{1}{2}-\frac{1}{C+1}\right)\frac{1}{4\eta_g\nu_g^2}\left(k_g\frac{\omega^2}{\alpha_0^2}-2\frac{\beta_0^2}{\alpha_0^2}k_g^3\right)+\frac{\beta_0^2}{\alpha_0^2}\frac{k_g}{2\nu_g}\right]\\
&\times a_\mu^{(1)}(z)a_\gamma^{(1)}(z)
\end{aligned}
$$

$$
\begin{aligned}
&+\left[\left(\frac{1}{2}+\frac{1}{C+1}\right)\frac{k_g\left(k_g^2+\nu_g^2\right)}{8\nu_g^3}-\left(\frac{1}{2}-\frac{1}{C+1}\right)\frac{k_g\left(k_g^2+\nu_g^2\right)}{8\eta_g\nu_g^2}\right]a_\rho^{(1)}(z)a_\gamma^{(1)}(z)\\
&-\left[\left(\frac{1}{2}+\frac{1}{C+1}\right)\frac{1}{4\eta_g\nu_g^2}\left(3\frac{\beta_0^2}{\alpha_0^2}Ck_g^3+\nu_g^2k_g-4Ck_g^5\frac{\beta_0^2}{\omega^2}-4k_g^3\nu_g^2\frac{\beta_0^2}{\omega^2}\right)\right.\\
&\left.-\left(\frac{1}{2}-\frac{1}{C+1}\right)\frac{1}{4\eta_g\nu_g^2}\left(\frac{\beta_0^2}{\alpha_0^2}C\nu_g^2k_g+k_g^3-4k_g^5\frac{\beta_0^2}{\omega^2}-4Ck_g^3\nu_g^2\frac{\beta_0^2}{\omega^2}+2\frac{\beta_0^2}{\alpha_0^2}k_g^3\right)\right.\\
&+\left(\frac{1}{2C}+\frac{1}{C+1}\right)\frac{1}{4\eta_g^2\nu_g}\left(k_g^3-2k_g^5\frac{\beta_0^2}{\omega^2}+\frac{\beta_0^2}{\alpha_0^2}C^3\nu_g^2k_g-4C^3\nu_g^2k_g^3\frac{\beta_0^2}{\omega^2}-\frac{1}{2}k_g\frac{\omega^2}{\beta_0^2}+2C^2\nu_g^2k_g^3\frac{\beta_0^2}{\omega^2}\right)\\
&-\left(\frac{1}{2C}-\frac{1}{C+1}\right)\frac{1}{4\eta_g\nu_g^2}\left(C\nu_g^2k_g-2C\nu_g^2k_g^3\frac{\beta_0^2}{\omega^2}+\frac{\beta_0^2}{\alpha_0^2}k_g^3-2k_g^5\frac{\beta_0^2}{\omega^2}+2C^2\nu_g^2k_g^3\frac{\beta_0^2}{\omega^2}-2C\nu_g^2k_g^3\frac{\beta_0^2}{\omega^2}\right.\\
&\left.\left.-\frac{1}{2}k_g\frac{\omega^2}{\beta_0^2}\right)\right]\times a_\rho^{(1)}(z)a_\mu^{(1)}(z)\\
&-\frac{1}{\eta_g\nu_g^2}\left(\frac{\beta_0^4}{\alpha_0^4}Ck_g^3-3\frac{\beta_0^2}{\alpha_0^2}Ck_g^5\frac{\beta_0^2}{\omega^2}-k_g^3\nu_g^2\frac{\beta_0^2}{\omega^2}+2k_g^5\nu_g^2\frac{\beta_0^4}{\omega^4}+2Ck_g^7\frac{\beta_0^4}{\omega^4}\right)\\
&\times\left[\frac{1}{2}\int_0^z dz' a_\mu^{(1)}{}_z\left(\frac{(C+1)z-(C-1)\,z'}{2}\right)a_\mu^{(1)}\left(z'\right)+\frac{1}{C+1}a_\mu^{(1)'}(z)\int_0^z dz' a_\mu^{(1)}(z')\right]\\
&-\frac{1}{\eta_g\nu_g^2}\left(\frac{\beta_0^2}{\alpha_0^2}Ck_g^3\nu_g^2\frac{\beta_0^2}{\omega^2}+2\frac{\beta_0^2}{\alpha_0^2}k_g^5\frac{\beta_0^2}{\omega^2}-2Ck_g^5\nu_g^2\frac{\beta_0^4}{\omega^4}-\frac{\beta_0^2}{\alpha_0^2}k_g^3+k_g^5\frac{\beta_0^2}{\omega^2}-2k_g^7\frac{\beta_0^4}{\omega^4}\right)\\
&\times\left[\frac{1}{2}\int_0^z dz' a_\mu^{(1)}{}_z\left(\frac{(C+1)z-(C-1)\,z'}{2}\right)a_\mu^{(1)}\left(z'\right)-\frac{1}{C+1}a_\mu^{(1)'}(z)\int_0^z dz' a_\mu^{(1)}(z')\right]\\
&-\frac{1}{4\eta_g^2\nu_g}\left(6k_g^3-12k_g^5\frac{\beta_0^2}{\omega^2}-k_g\frac{\omega^2}{\beta_0^2}+8k_g^7\frac{\beta_0^4}{\omega^4}+8C^3\nu_g^2k_g^5\frac{\beta_0^4}{\omega^4}-4\frac{\beta_0^2}{\alpha_0^2}C^3\nu_g^2k_g^3\frac{\beta_0^2}{\omega^2}\right)\\
&\times\left[\frac{1}{2C}\int_0^z dz' a_\mu^{(1)}{}_z\left(\frac{(C+1)z+(C-1)\,z'}{2C}\right)a_\mu^{(1)}\left(z'\right)+\frac{1}{C+1}a_\mu^{(1)'}(z)\int_0^z dz' a_\mu^{(1)}(z')\right]\\
&+\frac{1}{4\eta_g\nu_g^2}\left(4\frac{\beta_0^2}{\alpha_0^2}k_g^3-8k_g^5\frac{\beta_0^2}{\omega^2}-k_g\frac{\omega^2}{\alpha_0^2}+2k_g^3-4C\nu_g^2k_g^3\frac{\beta_0^2}{\omega^2}+8C\nu_g^2k_g^5\frac{\beta_0^4}{\omega^4}-4\frac{\beta_0^2}{\alpha_0^2}k_g^5\frac{\beta_0^2}{\omega^2}+8k_g^7\frac{\beta_0^4}{\omega^4}\right)\\
&\times\left[\frac{1}{2C}\int_0^z dz' a_\mu^{(1)}{}_z\left(\frac{(C+1)z+(C-1)\,z'}{2C}\right)a_\mu^{(1)}\left(z'\right)-\frac{1}{C+1}a_\mu^{(1)'}(z)\int_0^z dz' a_\mu^{(1)}(z')\right]\\
&-\frac{k_g\left(Ck_g^2+\nu_g^2\right)}{8\eta_g\nu_g^2}\left[\frac{1}{2}\int_0^z dz' a_\rho^{(1)}{}_z\left(\frac{(C+1)z-(C-1)\,z'}{2}\right)a_\rho^{(1)}\left(z'\right)+\frac{1}{C+1}a_\rho^{(1)'}(z)\int_0^z dz' a_\rho^{(1)}(z')\right]
\end{aligned}
$$

$$
\begin{aligned}
&+\frac{k_g\left(k_g^2+C\nu_g^2\right)}{8\eta_g\nu_g^2}\left[\frac{1}{2}\int_0^z dz' a_\rho^{(1)}{}_z\left(\frac{(C+1)z-(C-1)\,z'}{2}\right)a_\rho^{(1)}\left(z'\right)-\frac{1}{C+1}a_\rho^{(1)'}(z)\int_0^z dz' a_\rho^{(1)}(z')\right]\\
&-\frac{C^3k_g\nu_g^2+k_g^3}{8\eta_g^2\nu_g}\left[\frac{1}{2C}\int_0^z dz' a_\rho^{(1)}{}_z\left(\frac{(C+1)z+(C-1)\,z'}{2C}\right)a_\rho^{(1)}\left(z'\right)+\frac{1}{C+1}a_\rho^{(1)'}(z)\int_0^z dz' a_\rho^{(1)}(z')\right]\\
&+\frac{k_g\left(k_g^2+C\nu_g^2\right)}{8\eta_g\nu_g^2}\left[\frac{1}{2C}\int_0^z dz' a_\rho^{(1)}{}_z\left(\frac{(C+1)z+(C-1)\,z'}{2C}\right)a_\rho^{(1)}\left(z'\right)-\frac{1}{C+1}a_\rho^{(1)'}(z)\int_0^z dz' a_\rho^{(1)}(z')\right]\\
&-\frac{\beta_0^2}{\alpha_0^2}\frac{k_g\left(k_g^2-\nu_g^2\right)}{4\nu_g^3}\left[\frac{1}{2}\int_0^z dz' a_\gamma^{(1)}{}_z\left(\frac{(C+1)z-(C-1)\,z'}{2}\right)a_\mu^{(1)}\left(z'\right)+\frac{1}{C+1}a_\mu^{(1)'}(z)\int_0^z dz' a_\gamma^{(1)}(z')\right]\\
&-\frac{1}{4\eta_g\nu_g^2}\left(k_g\frac{\omega^2}{\alpha_0^2}-2\frac{\beta_0^2}{\alpha_0^2}k_g^3\right)\left[\frac{1}{2}\int_0^z dz' a_\gamma^{(1)}{}_z\left(\frac{(C+1)z-(C-1)\,z'}{2}\right)a_\mu^{(1)}\left(z'\right)\right.\\
&\left.-\frac{1}{C+1}a_\mu^{(1)'}(z)\int_0^z dz' a_\gamma^{(1)}(z')\right]\\
&+\frac{k_g\left(k_g^2+\nu_g^2\right)}{8\nu_g^3}\left[\frac{1}{2}\int_0^z dz' a_\gamma^{(1)}{}_z\left(\frac{(C+1)z-(C-1)\,z'}{2}\right)a_\rho^{(1)}\left(z'\right)+\frac{1}{C+1}a_\rho^{(1)'}(z)\int_0^z dz' a_\gamma^{(1)}(z')\right]\\
&-\frac{k_g\left(k_g^2+\nu_g^2\right)}{8\eta_g\nu_g^2}\left[\frac{1}{2}\int_0^z dz' a_\gamma^{(1)}{}_z\left(\frac{(C+1)z-(C-1)\,z'}{2}\right)a_\rho^{(1)}\left(z'\right)-\frac{1}{C+1}a_\rho^{(1)'}(z)\int_0^z dz' a_\gamma^{(1)}(z')\right]\\
&-\frac{1}{4\eta_g\nu_g^2}\left(\frac{\beta_0^2}{\alpha_0^2}Ck_g^3+\nu_g^2k_g-2Ck_g^5\frac{\beta_0^2}{\omega^2}-2k_g^3\nu_g^2\frac{\beta_0^2}{\omega^2}\right)\\
&\times\left[\frac{1}{2}\int_0^z dz' a_\rho^{(1)}{}_z\left(\frac{(C+1)z-(C-1)\,z'}{2}\right)a_\mu^{(1)}\left(z'\right)+\frac{1}{C+1}a_\mu^{(1)'}(z)\int_0^z dz' a_\rho^{(1)}(z')\right]\\
&-\frac{1}{4\eta_g\nu_g^2}\left(2\frac{\beta_0^2}{\alpha_0^2}Ck_g^3-2Ck_g^5\frac{\beta_0^2}{\omega^2}-2k_g^3\nu_g^2\frac{\beta_0^2}{\omega^2}\right)\\
&\times\left[\frac{1}{2}\int_0^z dz' a_\mu^{(1)}{}_z\left(\frac{(C+1)z-(C-1)\,z'}{2}\right)a_\rho^{(1)}\left(z'\right)+\frac{1}{C+1}a_\rho^{(1)'}(z)\int_0^z dz' a_\mu^{(1)}(z')\right]
\end{aligned}
$$

$$
\begin{aligned}
&+\frac{1}{4\eta_g\nu_g^2}\left(\frac{\beta_0^2}{\alpha_0^2}C\nu_g^2k_g+k_g^3-2k_g^5\frac{\beta_0^2}{\omega^2}-2Ck_g^3\nu_g^2\frac{\beta_0^2}{\omega^2}\right)\\
&\times\left[\frac{1}{2}\int_0^z dz' a_\rho^{(1)}{}_z\left(\frac{(C+1)z-(C-1)\,z'}{2}\right)a_\mu^{(1)}\left(z'\right)-\frac{1}{C+1}a_\mu^{(1)'}(z)\int_0^z dz' a_\rho^{(1)}(z')\right]\\
&+\frac{1}{4\eta_g\nu_g^2}\left(2\frac{\beta_0^2}{\alpha_0^2}k_g^3-2k_g^5\frac{\beta_0^2}{\omega^2}-2Ck_g^3\nu_g^2\frac{\beta_0^2}{\omega^2}\right)\\
&\times\left[\frac{1}{2}\int_0^z dz' a_\mu^{(1)}{}_z\left(\frac{(C+1)z-(C-1)\,z'}{2}\right)a_\rho^{(1)}\left(z'\right)-\frac{1}{C+1}a_\rho^{(1)'}(z)\int_0^z dz' a_\mu^{(1)}(z')\right]\\
&-\frac{1}{4\eta_g^2\nu_g}\left(k_g^3-2k_g^5\frac{\beta_0^2}{\omega^2}+\frac{\beta_0^2}{\alpha_0^2}C^3\nu_g^2k_g-2C^3\nu_g^2k_g^3\frac{\beta_0^2}{\omega^2}\right)\\
&\times\left[\frac{1}{2C}\int_0^z dz' a_\rho^{(1)}{}_z\left(\frac{(C+1)z+(C-1)\,z'}{2C}\right)a_\mu^{(1)}\left(z'\right)+\frac{1}{C+1}a_\mu^{(1)'}(z)\int_0^z dz' a_\rho^{(1)}(z')\right]\\
&-\frac{1}{4\eta_g^2\nu_g}\left(-2C^3\nu_g^2k_g^3\frac{\beta_0^2}{\omega^2}-\frac{1}{2}k_g\frac{\omega^2}{\beta_0^2}+2C^2\nu_g^2k_g^3\frac{\beta_0^2}{\omega^2}\right)\\
&\times\left[\frac{1}{2C}\int_0^z dz' a_\mu^{(1)}{}_z\left(\frac{(C+1)z+(C-1)\,z'}{2C}\right)a_\rho^{(1)}\left(z'\right)+\frac{1}{C+1}a_\rho^{(1)'}(z)\int_0^z dz' a_\mu^{(1)}(z')\right]\\
&+\frac{1}{4\eta_g\nu_g^2}\left(C\nu_g^2k_g-2C\nu_g^2k_g^3\frac{\beta_0^2}{\omega^2}+\frac{\beta_0^2}{\alpha_0^2}k_g^3-2k_g^5\frac{\beta_0^2}{\omega^2}\right)\\
&\times\left[\frac{1}{2C}\int_0^z dz' a_\rho^{(1)}{}_z\left(\frac{(C+1)z+(C-1)\,z'}{2C}\right)a_\mu^{(1)}\left(z'\right)-\frac{1}{C+1}a_\mu^{(1)'}(z)\int_0^z dz' a_\rho^{(1)}(z')\right]\\
&+\frac{1}{4\eta_g\nu_g^2}\left(2C^2\nu_g^2k_g^3\frac{\beta_0^2}{\omega^2}-2C\nu_g^2k_g^3\frac{\beta_0^2}{\omega^2}-\frac{1}{2}k_g\frac{\omega^2}{\beta_0^2}\right)\\
&\times\left[\frac{1}{2C}\int_0^z dz' a_\mu^{(1)}{}_z\left(\frac{(C+1)z+(C-1)\,z'}{2C}\right)a_\rho^{(1)}\left(z'\right)-\frac{1}{C+1}a_\rho^{(1)'}(z)\int_0^z dz' a_\mu^{(1)}(z')\right],
\end{aligned}
$$

the solution for Eq. (16), i.e.,

$$\hat{G}_0^S\hat{V}_2^{SP}\hat{G}_0^P=-\hat{G}_0^S\hat{V}_1^{SP}\hat{G}_0^P\hat{V}_1^{PP}\hat{G}_0^P-\hat{G}_0^S\hat{V}_1^{SS}\hat{G}_0^S\hat{V}_1^{SP}\hat{G}_0^P,$$

is

$$
\begin{aligned}
&\frac{1}{4}\left(\frac{k_g}{\nu_g}+\frac{k_g}{\eta_g}\right)a_\rho^{(2)}(z)+\frac{\beta_0^2}{2\omega^2}k_g\left(\nu_g+\eta_g\right)\left(1-\frac{k_g^2}{\nu_g\eta_g}\right)a_\mu^{(2)}(z)\\
=&\Bigg\{-\frac{1}{2\eta_g\nu_g^2}\left[2(C-1)\nu_g^2k_g^5\frac{\beta_0^4}{\omega^4}+\left(1-\frac{\beta_0^2}{\alpha_0^2}C\right)\nu_g^2k_g^3\frac{\beta_0^2}{\omega^2}\right]-\frac{\beta_0^2}{\alpha_0^2}\frac{k_g^3}{\nu_g}\frac{\beta_0^2}{\omega^2}+\frac{k_g}{2\eta_g}\left(2k_g^2\frac{\beta_0^2}{\omega^2}-1\right)\\
&+\left(\frac{1}{2C}+\frac{1}{C+1}\right)\frac{1}{4\eta_g^2\nu_g}\left(6k_g^3-12k_g^5\frac{\beta_0^2}{\omega^2}-k_g\frac{\omega^2}{\beta_0^2}+8k_g^7\frac{\beta_0^4}{\omega^4}+8C^3\nu_g^2k_g^5\frac{\beta_0^4}{\omega^4}-4\frac{\beta_0^2}{\alpha_0^2}C^3\nu_g^2k_g^3\frac{\beta_0^2}{\omega^2}\right)\\
&-\left(\frac{1}{2C}-\frac{1}{C+1}\right)\frac{1}{4\eta_g\nu_g^2}\left(4\frac{\beta_0^2}{\alpha_0^2}k_g^3-8k_g^5\frac{\beta_0^2}{\omega^2}-k_g\frac{\omega^2}{\alpha_0^2}+2k_g^3-4C\nu_g^2k_g^3\frac{\beta_0^2}{\omega^2}+8C\nu_g^2k_g^5\frac{\beta_0^4}{\omega^4}-4\frac{\beta_0^2}{\alpha_0^2}k_g^5\frac{\beta_0^2}{\omega^2}\right.\\
&\left.+8k_g^7\frac{\beta_0^4}{\omega^4}\right)\Bigg\}a_\mu^{(1)}(z)a_\mu^{(1)}(z)\\
&+\left[\left(\frac{1}{2}+\frac{1}{C+1}\right)\frac{k_g}{8\eta_g\nu_g^2}\left(Ck_g^2+\nu_g^2\right)-\left(\frac{1}{2}-\frac{1}{C+1}\right)\frac{k_g}{8\eta_g\nu_g^2}\left(k_g^2+C\nu_g^2\right)\right.\\
&\left.+\left(\frac{1}{2C}+\frac{1}{C+1}\right)\frac{k_g}{8\eta_g^2\nu_g}\left(C^3\nu_g^2+k_g^2\right)-\left(\frac{1}{2C}-\frac{1}{C+1}\right)\frac{k_g}{8\eta_g\nu_g^2}\left(k_g^2+C\nu_g^2\right)\right]a_\rho^{(1)}(z)a_\rho^{(1)}(z)\\
&+\left[\left(\frac{1}{2}+\frac{1}{C+1}\right)\frac{\beta_0^2}{\alpha_0^2}\frac{1}{4\nu_g^3}k_g\left(k_g^2-\nu_g^2\right)+\left(\frac{1}{2}-\frac{1}{C+1}\right)\frac{1}{4\eta_g\nu_g^2}\left(k_g\frac{\omega^2}{\alpha_0^2}-2\frac{\beta_0^2}{\alpha_0^2}k_g^3\right)\right.\\
&\left.+\frac{\beta_0^2}{\alpha_0^2}\frac{k_g}{2\nu_g}\right]a_\mu^{(1)}(z)a_\gamma^{(1)}(z)\\
&-\left[\left(\frac{1}{2}+\frac{1}{C+1}\right)\frac{k_g\left(k_g^2+\nu_g^2\right)}{8\nu_g^3}-\left(\frac{1}{2}-\frac{1}{C+1}\right)\frac{k_g\left(k_g^2+\nu_g^2\right)}{8\eta_g\nu_g^2}\right]a_\rho^{(1)}(z)a_\gamma^{(1)}(z)\\
&-\left[\left(\frac{1}{2}+\frac{1}{C+1}\right)\frac{1}{4\eta_g\nu_g^2}\left(2\nu_g^2k_g^3\frac{\beta_0^2}{\omega^2}-\nu_g^2k_g+2Ck_g^5\frac{\beta_0^2}{\omega^2}-\frac{\beta_0^2}{\alpha_0^2}Ck_g^3\right)\right.\\
&-\left(\frac{1}{2}-\frac{1}{C+1}\right)\frac{1}{4\eta_g\nu_g^2}\left(2C\nu_g^2k_g^3\frac{\beta_0^2}{\omega^2}-\frac{\beta_0^2}{\alpha_0^2}C\nu_g^2k_g+2k_g^5\frac{\beta_0^2}{\omega^2}-k_g^3\right)\\
&-\left(\frac{1}{2C}+\frac{1}{C+1}\right)\frac{1}{4\eta_g^2\nu_g}\left(3k_g^3+\frac{\beta_0^2}{\alpha_0^2}C^3\nu_g^2k_g-4C^3\nu_g^2k_g^3\frac{\beta_0^2}{\omega^2}-4k_g^5\frac{\beta_0^2}{\omega^2}-\frac{1}{2}k_g\frac{\omega^2}{\beta_0^2}\right)\\
&+\left(\frac{1}{2C}-\frac{1}{C+1}\right)\frac{1}{4\eta_g\nu_g^2}\left(C\nu_g^2k_g+2k_g^3+\frac{\beta_0^2}{\alpha_0^2}k_g^3-4k_g^5\frac{\beta_0^2}{\omega^2}-4C\nu_g^2k_g^3\frac{\beta_0^2}{\omega^2}-\frac{1}{2}k_g\frac{\omega^2}{\beta_0^2}\right)\\
&\left.-(C-1)\frac{k_g^3}{2\eta_g}\frac{\beta_0^2}{\omega^2}\right]a_\rho^{(1)}(z)a_\mu^{(1)}(z)
\end{aligned}
$$

$$
\begin{aligned}
&- \frac{1}{2\eta_g\nu_g^2}\left[2(C-1)\nu_g^2k_g^5\frac{\beta_0^4}{\omega^4}+\left(1-\frac{\beta_0^2}{\alpha_0^2}C\right)\nu_g^2k_g^3\frac{\beta_0^2}{\omega^2}\right]\int_0^z dz' {a_\mu^{(1)}}_z\left(\frac{(C+1)z-(C-1)\,z'}{2}\right)a_\mu^{(1)}\left(z'\right)\\
&+ \frac{1}{4\eta_g^2\nu_g}\left(6k_g^3-12k_g^5\frac{\beta_0^2}{\omega^2}-k_g\frac{\omega^2}{\beta_0^2}+8k_g^7\frac{\beta_0^4}{\omega^4}+8C^3\nu_g^2k_g^5\frac{\beta_0^4}{\omega^4}-4\frac{\beta_0^2}{\alpha_0^2}C^3\nu_g^2k_g^3\frac{\beta_0^2}{\omega^2}\right)\\
&\times\left[\frac{1}{2C}\int_0^z dz' {a_\mu^{(1)}}_z\left(\frac{(C+1)z+(C-1)\,z'}{2C}\right)a_\mu^{(1)}\left(z'\right)+\frac{1}{C+1}a_\mu^{(1)'}(z)\int_0^z dz' a_\mu^{(1)}(z')\right]\\
&- \frac{1}{4\eta_g\nu_g^2}\left(4\frac{\beta_0^2}{\alpha_0^2}k_g^3-8k_g^5\frac{\beta_0^2}{\omega^2}-k_g\frac{\omega^2}{\alpha_0^2}+2k_g^3-4C\nu_g^2k_g^3\frac{\beta_0^2}{\omega^2}+8C\nu_g^2k_g^5\frac{\beta_0^4}{\omega^4}-4\frac{\beta_0^2}{\alpha_0^2}k_g^5\frac{\beta_0^2}{\omega^2}+8k_g^7\frac{\beta_0^4}{\omega^4}\right)\\
&\times\left[\frac{1}{2C}\int_0^z dz' {a_\mu^{(1)}}_z\left(\frac{(C+1)z+(C-1)\,z'}{2C}\right)a_\mu^{(1)}\left(z'\right)-\frac{1}{C+1}a_\mu^{(1)'}(z)\int_0^z dz' a_\mu^{(1)}(z')\right]\\
&+ \frac{k_g\left(Ck_g^2+\nu_g^2\right)}{8\eta_g\nu_g^2}\left[\frac{1}{2}\int_0^z dz' {a_\rho^{(1)}}_z\left(\frac{(C+1)z-(C-1)\,z'}{2}\right)a_\rho^{(1)}\left(z'\right)+\frac{1}{C+1}a_\rho^{(1)'}(z)\int_0^z dz' a_\rho^{(1)}(z')\right]\\
&- \frac{k_g\left(k_g^2+C\nu_g^2\right)}{8\eta_g\nu_g^2}\left[\frac{1}{2}\int_0^z dz' {a_\rho^{(1)}}_z\left(\frac{(C+1)z-(C-1)\,z'}{2}\right)a_\rho^{(1)}\left(z'\right)-\frac{1}{C+1}a_\rho^{(1)'}(z)\int_0^z dz' a_\rho^{(1)}(z')\right]\\
&+ \frac{C^3k_g\nu_g^2+k_g^3}{8\eta_g^2\nu_g}\left[\frac{1}{2C}\int_0^z dz' {a_\rho^{(1)}}_z\left(\frac{(C+1)z+(C-1)\,z'}{2C}\right)a_\rho^{(1)}\left(z'\right)+\frac{1}{C+1}a_\rho^{(1)'}(z)\int_0^z dz' a_\rho^{(1)}(z')\right]\\
&- \frac{k_g\left(k_g^2+C\nu_g^2\right)}{8\eta_g\nu_g^2}\left[\frac{1}{2C}\int_0^z dz' {a_\rho^{(1)}}_z\left(\frac{(C+1)z+(C-1)\,z'}{2C}\right)a_\rho^{(1)}\left(z'\right)-\frac{1}{C+1}a_\rho^{(1)'}(z)\int_0^z dz' a_\rho^{(1)}(z')\right]\\
&+ \frac{\beta_0^2}{\alpha_0^2}\frac{k_g\left(k_g^2-\nu_g^2\right)}{4\nu_g^3}\left[\frac{1}{2}\int_0^z dz' {a_\gamma^{(1)}}_z\left(\frac{(C+1)z-(C-1)\,z'}{2}\right)a_\mu^{(1)}\left(z'\right)+\frac{1}{C+1}a_\mu^{(1)'}(z)\int_0^z dz' a_\gamma^{(1)}(z')\right]
\end{aligned}
$$

$$
\begin{aligned}
&+\frac{1}{4\eta_g\nu_g^2}\left(k_g\frac{\omega^2}{\alpha_0^2}-2\frac{\beta_0^2}{\alpha_0^2}k_g^3\right)\left[\frac{1}{2}\int_0^z dz' a_\gamma^{(1)}{}_z\left(\frac{(C+1)z-(C-1)\,z'}{2}\right)a_\mu^{(1)}\left(z'\right)\right.\\
&\left.-\frac{1}{C+1}a_\mu^{(1)'}(z)\int_0^z dz' a_\gamma^{(1)}(z')\right]\\
&-\frac{k_g\left(k_g^2+\nu_g^2\right)}{8\nu_g^3}\left[\frac{1}{2}\int_0^z dz' a_\gamma^{(1)}{}_z\left(\frac{(C+1)z-(C-1)\,z'}{2}\right)a_\rho^{(1)}\left(z'\right)+\frac{1}{C+1}a_\rho^{(1)'}(z)\int_0^z dz' a_\gamma^{(1)}(z')\right]\\
&+\frac{k_g\left(k_g^2+\nu_g^2\right)}{8\eta_g\nu_g^2}\left[\frac{1}{2}\int_0^z dz' a_\gamma^{(1)}{}_z\left(\frac{(C+1)z-(C-1)\,z'}{2}\right)a_\rho^{(1)}\left(z'\right)-\frac{1}{C+1}a_\rho^{(1)'}(z)\int_0^z dz' a_\gamma^{(1)}(z')\right]\\
&-\frac{1}{4\eta_g\nu_g^2}\left(2\nu_g^2k_g^3\frac{\beta_0^2}{\omega^2}-\nu_g^2k_g+2Ck_g^5\frac{\beta_0^2}{\omega^2}-\frac{\beta_0^2}{\alpha_0^2}Ck_g^3\right)\\
&\times\left[\frac{1}{2}\int_0^z dz' a_\rho^{(1)}{}_z\left(\frac{(C+1)z-(C-1)\,z'}{2}\right)a_\mu^{(1)}\left(z'\right)+\frac{1}{C+1}a_\mu^{(1)'}(z)\int_0^z dz' a_\rho^{(1)}(z')\right]\\
&+\frac{1}{4\eta_g\nu_g^2}\left(2C\nu_g^2k_g^3\frac{\beta_0^2}{\omega^2}-\frac{\beta_0^2}{\alpha_0^2}C\nu_g^2k_g+2k_g^5\frac{\beta_0^2}{\omega^2}-k_g^3\right)\\
&\times\left[\frac{1}{2}\int_0^z dz' a_\rho^{(1)}{}_z\left(\frac{(C+1)z-(C-1)\,z'}{2}\right)a_\mu^{(1)}\left(z'\right)-\frac{1}{C+1}a_\mu^{(1)'}(z)\int_0^z dz' a_\rho^{(1)}(z')\right]\\
&+(C-1)\frac{k_g^3}{2\eta_g}\frac{\beta_0^2}{\omega^2}\int_0^z dz' a_\mu^{(1)}{}_z\left(\frac{(C+1)z-(C-1)\,z'}{2}\right)a_\rho^{(1)}\left(z'\right)
\end{aligned}
$$

$$
\begin{aligned}
&-\frac{1}{4\eta_g^2\nu_g}\left(-2k_g^3+2C^3\nu_g^2k_g^3\frac{\beta_0^2}{\omega^2}+2k_g^5\frac{\beta_0^2}{\omega^2}+\frac{1}{2}k_g\frac{\omega^2}{\beta_0^2}\right)\\
&\times\left[\frac{1}{2C}\int_0^z dz' a_\mu^{(1)}{}_z\left(\frac{(C+1)z+(C-1)\,z'}{2C}\right)a_\rho^{(1)}\left(z'\right)+\frac{1}{C+1}a_\rho^{(1)'}(z)\int_0^z dz' a_\mu^{(1)}(z')\right]\\
&-\frac{1}{4\eta_g^2\nu_g}\left(-k_g^3-\frac{\beta_0^2}{\alpha_0^2}C^3\nu_g^2k_g+2C^3\nu_g^2k_g^3\frac{\beta_0^2}{\omega^2}+2k_g^5\frac{\beta_0^2}{\omega^2}\right)\\
&\times\left[\frac{1}{2C}\int_0^z dz' a_\rho^{(1)}{}_z\left(\frac{(C+1)z+(C-1)\,z'}{2C}\right)a_\mu^{(1)}\left(z'\right)+\frac{1}{C+1}a_\mu^{(1)'}(z)\int_0^z dz' a_\rho^{(1)}(z')\right]\\
&-\frac{1}{4\eta_g\nu_g^2}\left(2k_g^3-2k_g^5\frac{\beta_0^2}{\omega^2}-2C\nu_g^2k_g^3\frac{\beta_0^2}{\omega^2}-\frac{1}{2}k_g\frac{\omega^2}{\beta_0^2}\right)\\
&\times\left[\frac{1}{2C}\int_0^z dz' a_\mu^{(1)}{}_z\left(\frac{(C+1)z+(C-1)\,z'}{2C}\right)a_\rho^{(1)}\left(z'\right)-\frac{1}{C+1}a_\rho^{(1)'}(z)\int_0^z dz' a_\mu^{(1)}(z')\right]\\
&-\frac{1}{4\eta_g\nu_g^2}\left(C\nu_g^2k_g+\frac{\beta_0^2}{\alpha_0^2}k_g^3-2k_g^5\frac{\beta_0^2}{\omega^2}-2C\nu_g^2k_g^3\frac{\beta_0^2}{\omega^2}\right)\\
&\times\left[\frac{1}{2C}\int_0^z dz' a_\rho^{(1)}{}_z\left(\frac{(C+1)z+(C-1)\,z'}{2C}\right)a_\mu^{(1)}\left(z'\right)-\frac{1}{C+1}a_\mu^{(1)'}(z)\int_0^z dz' a_\rho^{(1)}(z')\right],
\end{aligned}
$$

and the solution for Eq. (17), i.e.,

$$\hat{G}_0^S\hat{V}_2^{SS}\hat{G}_0^S=-\hat{G}_0^S\hat{V}_1^{SP}\hat{G}_0^P\hat{V}_1^{PS}\hat{G}_0^S-\hat{G}_0^S\hat{V}_1^{SS}\hat{G}_0^S\hat{V}_1^{SS}\hat{G}_0^S,$$

is

$$
\begin{aligned}
&-\frac{1}{4}\left(1-\frac{k_g^2}{\eta_g^2}\right)a_\rho^{(2)}(z)-\left[\frac{k_g^2+\eta_g^2}{4\eta_g^2}-\frac{2k_g^2}{k_g^2+\eta_g^2}\right]a_\mu^{(2)}(z)\\
=&-\left\{\frac{1}{8\eta_g^4}\left(8k_g^2\eta_g^2-\frac{\omega^4}{\beta_0^4}\right)-\frac{1}{4\eta_g^2}\left(\frac{\omega^2}{\beta_0^2}-4\frac{\beta_0^2}{\omega^2}\eta_g^2k_g^2\right)-\frac{\beta_0^2}{\alpha_0^2}k_g^2\frac{\beta_0^2}{\omega^2}\right.\\
&\left.+\frac{1}{\eta_g^2(C+1)}\left[k_g^2\left(\frac{\beta_0^4}{\alpha_0^4}C^2-1\right)-4k_g^4\frac{\beta_0^2}{\omega^2}\left(\frac{\beta_0^2}{\alpha_0^2}C^2-1\right)+4k_g^6\frac{\beta_0^4}{\omega^4}(C^2-1)\right]\right\}a_\mu^{(1)}(z)a_\mu^{(1)}(z)\\
&-\left[\frac{1}{8\eta_g^4}\left(\eta_g^4-k_g^4\right)+\frac{1}{4\eta_g^2}k_g^2(C-1)\right]a_\rho^{(1)}(z)a_\rho^{(1)}(z)\\
&+\left\{\frac{k_g^2}{\eta_g^2}-\frac{1}{\eta_g^2(C+1)}\left[k_g^2\left(\frac{\beta_0^2}{\alpha_0^2}C^2-1\right)-2\frac{\beta_0^2}{\omega^2}k_g^4\left(C^2-1\right)\right]\right\}a_\mu^{(1)}(z)a_\rho^{(1)}(z)\\
&-\frac{1}{8\eta_g^4}\left(8k_g^2\eta_g^2-\frac{\omega^4}{\beta_0^4}\right)a_\mu^{(1)'}(z)\int_0^z dz'a_\mu^{(1)}(z')\\
&-\frac{1}{8\eta_g^4}\left(\eta_g^4-k_g^4\right)a_\rho^{(1)'}(z)\int_0^z dz'a_\rho^{(1)}(z')\\
&+\frac{k_g^2}{2\eta_g^2}\left[a_\mu^{(1)'}(z)\int_0^z dz'a_\rho^{(1)}(z')+a_\rho^{(1)'}(z)\int_0^z dz'a_\mu^{(1)}(z')\right]\\
&-\frac{1}{8\eta_g^2}\left(\eta_g^2-3k_g^2\right)\left[a_\mu^{(1)'}(z)\int_0^z dz'a_\rho^{(1)}(z')-a_\rho^{(1)'}(z)\int_0^z dz'a_\mu^{(1)}(z')\right]\\
&-\frac{1}{\eta_g^2(C+1)}\left[k_g^2\left(\frac{\beta_0^4}{\alpha_0^4}C^2-1\right)-4k_g^4\frac{\beta_0^2}{\omega^2}\left(\frac{\beta_0^2}{\alpha_0^2}C^2-1\right)+4k_g^6\frac{\beta_0^4}{\omega^4}(C^2-1)\right]\\
&\times\int_0^z dz'a_\mu^{(1)}{}_z\left(\frac{2Cz-(C-1)\,z'}{(C+1)}\right)a_\mu^{(1)}\left(z'\right)\\
&-\frac{1}{4\eta_g^2}k_g^2(C-1)\int_0^z dz'a_\rho^{(1)}{}_z\left(\frac{2Cz-(C-1)\,z'}{(C+1)}\right)a_\rho^{(1)}\left(z'\right)\\
\\
&-\frac{1}{2\eta_g^2(C+1)}\left[k_g^2\left(\frac{\beta_0^2}{\alpha_0^2}C^2-1\right)-2\frac{\beta_0^2}{\omega^2}k_g^4\left(C^2-1\right)\right]\\
&\times\left[\int_0^z dz'a_\mu^{(1)}{}_z\left(\frac{2Cz-(C-1)\,z'}{(C+1)}\right)a_\rho^{(1)}\left(z'\right)+\int_0^z dz'a_\rho^{(1)}{}_z\left(\frac{2Cz-(C-1)\,z'}{(C+1)}\right)a_\mu^{(1)}\left(z'\right)\right]\\
&+\frac{Ck_g^2}{2(C+1)\eta_g^2}\left(\frac{\beta_0^2}{\alpha_0^2}-1\right)\\
&\times\left[\int_0^z dz'a_\mu^{(1)}{}_z\left(\frac{2Cz-(C-1)\,z'}{(C+1)}\right)a_\rho^{(1)}\left(z'\right)-\int_0^z dz'a_\rho^{(1)}{}_z\left(\frac{2Cz-(C-1)\,z'}{(C+1)}\right)a_\mu^{(1)}\left(z'\right)\right],
\end{aligned}
$$

where $\eta_g = C\nu_g, k_g^2+\nu_g^2=\omega^2/\alpha_0^2$ and $k_g^2+\eta_g^2=\omega^2/\beta_0^2$.

5 Figures

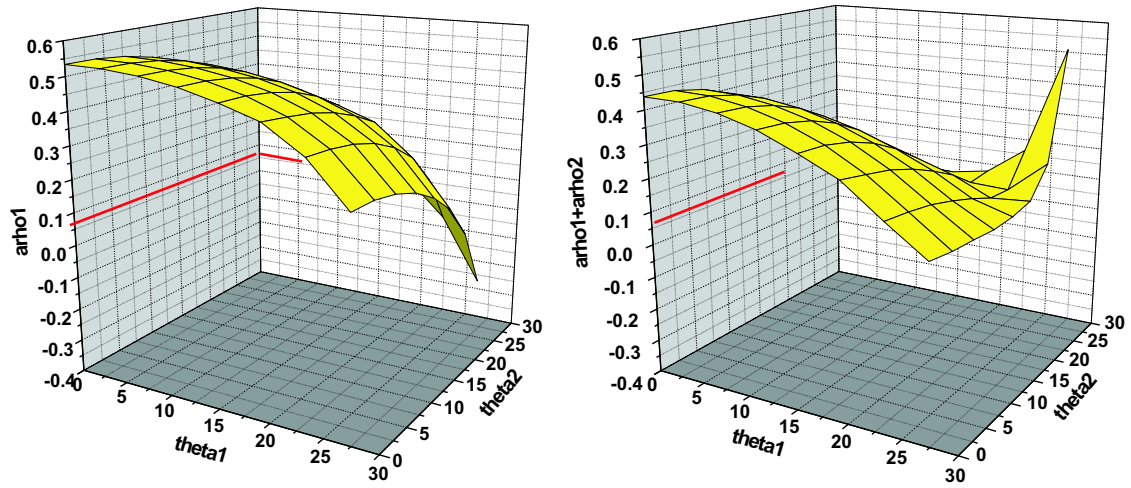

Figure 3: Model 1: shale (0.20 porosity) over oil sand (0.10 porosity). $\rho_0 = 2.32 g/cm^3, \rho_1 = 2.46 g/cm^3; \alpha_0 = 2627 m/s, \alpha_1 = 4423 m/s; \beta_0 = 1245 m/s, \beta_1 = 2939 m/s$. For this model, the exact value of a_ρ is 0.06. The linear approximation $a_\rho^{(1)}$ (left) and the sum of linear and first non-linear $a_\rho^{(1)} + a_\rho^{(2)}$ (right).

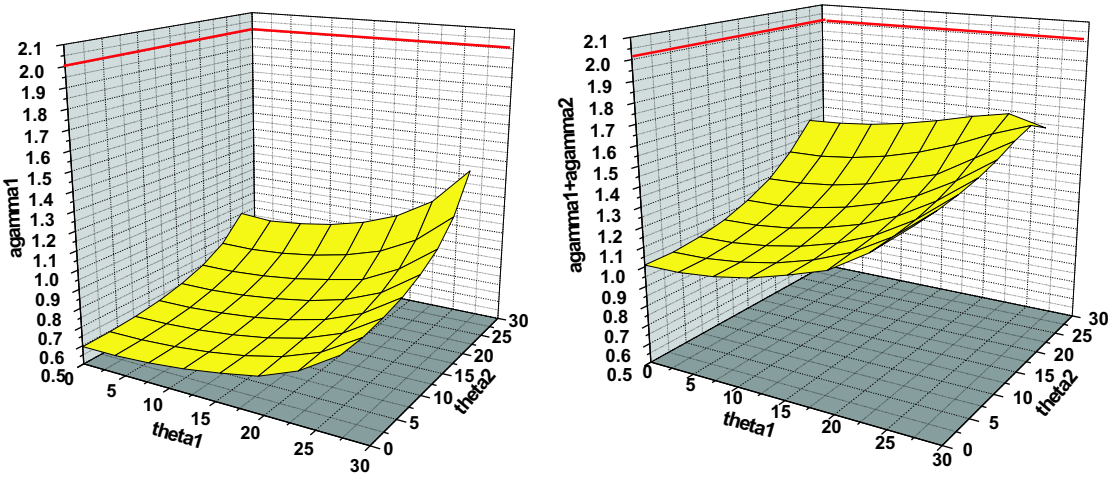

Figure 4: Model 1: shale (0.20 porosity) over oil sand (0.10 porosity). $\rho_0 = 2.32 g/cm^3, \rho_1 = 2.46 g/cm^3; \alpha_0 = 2627 m/s, \alpha_1 = 4423 m/s; \beta_0 = 1245 m/s, \beta_1 = 2939 m/s$. For this model, the exact value of a_γ is 2.01. The linear approximation $a_\gamma^{(1)}$ (left) and the sum of linear and first non-linear $a_\gamma^{(1)} + a_\gamma^{(2)}$ (right).

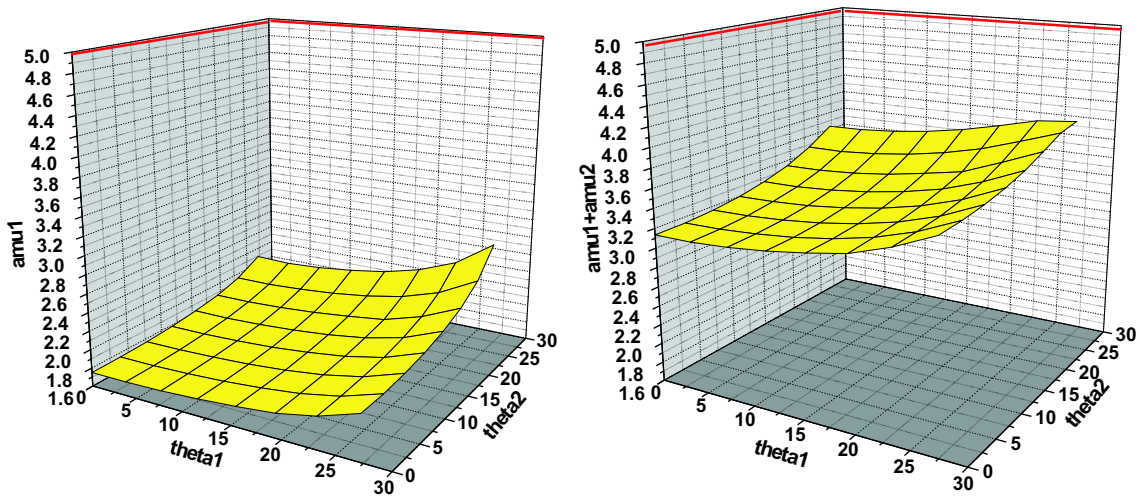

Figure 5: Model 1: shale (0.20 porosity) over oil sand (0.10 porosity). $\rho_0 = 2.32g/cm^3, \rho_1 = 2.46g/cm^3; \alpha_0 = 2627m/s, \alpha_1 = 4423m/s; \beta_0 = 1245m/s, \beta_1 = 2939m/s$. For this model, the exact value of a_μ is 4.91. The linear approximation $a_\mu^{(1)}$ (left) and the sum of linear and first non-linear $a_\mu^{(1)} + a_\mu^{(2)}$ (right).

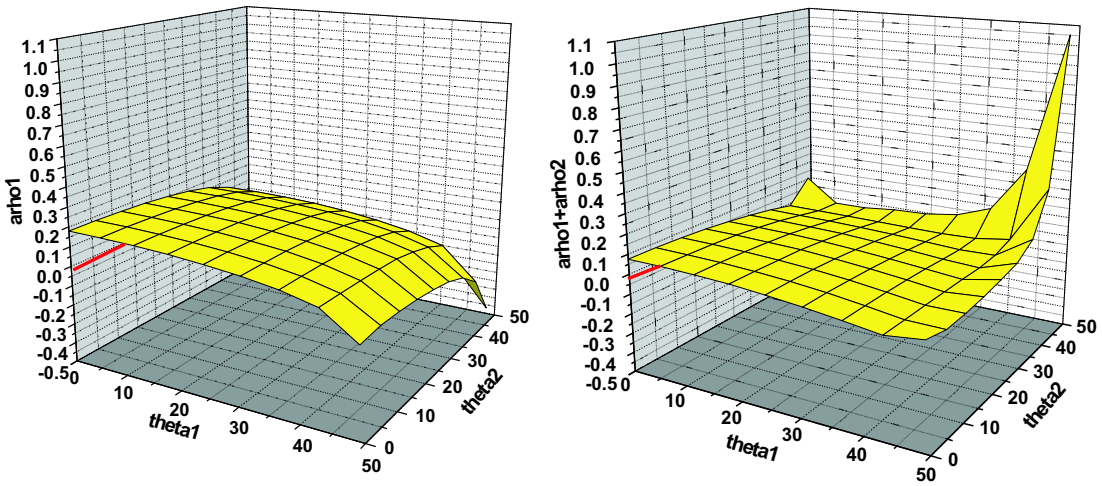

Figure 6: Model 2: shale over oil sand, 0.20 porosity. $\rho_0 = 2.32g/cm^3, \rho_1 = 2.27g/cm^3; \alpha_0 = 2627m/s, \alpha_1 = 3251m/s; \beta_0 = 1245m/s, \beta_1 = 2138m/s$. For this model, the exact value of a_ρ is -0.022. The linear approximation $a_\rho^{(1)}$ (left) and the sum of linear and first non-linear $a_\rho^{(1)} + a_\rho^{(2)}$ (right).

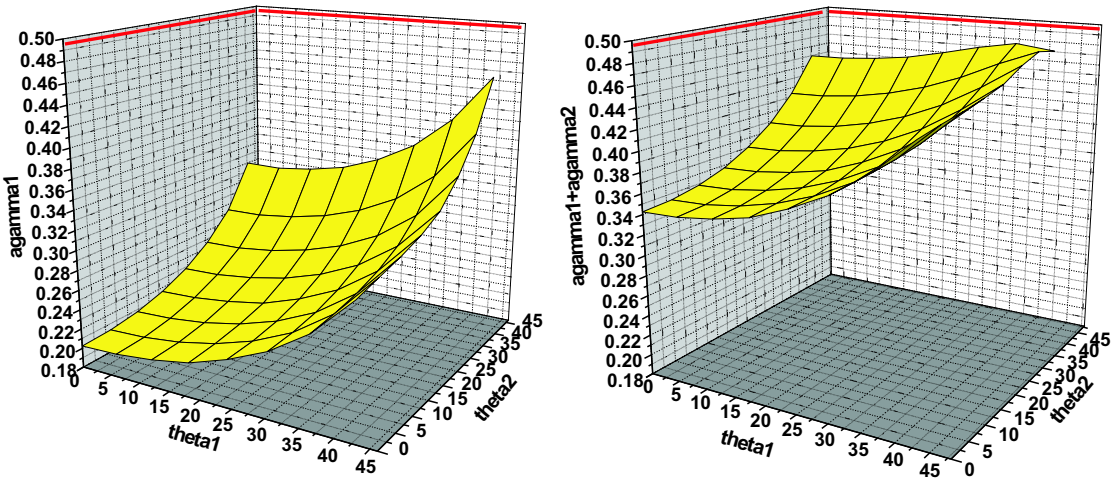

Figure 7: Model 2: shale over oil sand, 0.20 porosity. $\rho_0 = 2.32g/cm^3, \rho_1 = 2.27g/cm^3; \alpha_0 = 2627m/s, \alpha_1 = 3251m/s; \beta_0 = 1245m/s, \beta_1 = 2138m/s$. For this model, the exact value of a_γ is 0.498. The linear approximation $a_\gamma^{(1)}$ (left) and the sum of linear and first non-linear $a_\gamma^{(1)} + a_\gamma^{(2)}$ (right).

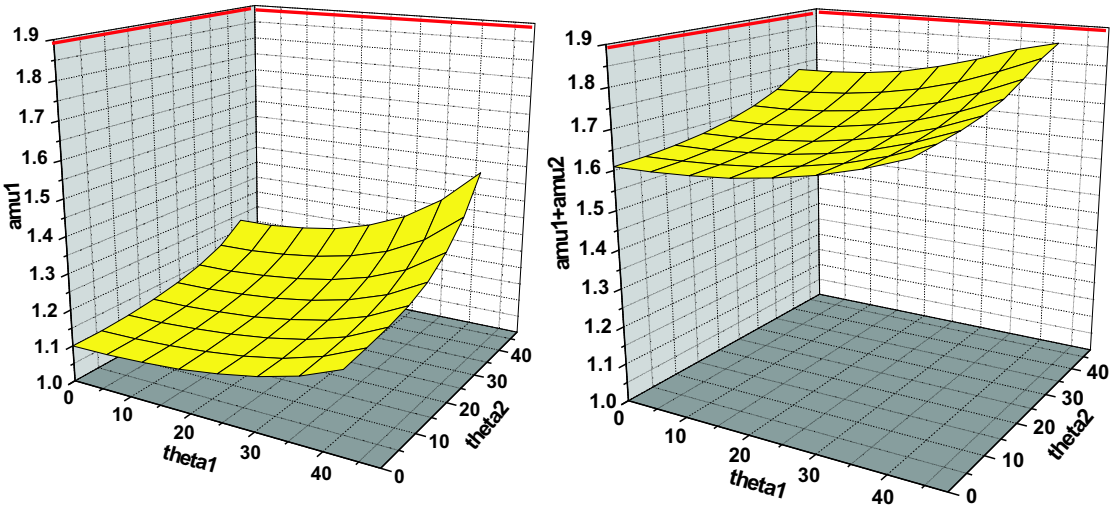

Figure 8: Model 2: shale over oil sand, 0.20 porosity. $\rho_0 = 2.32g/cm^3, \rho_1 = 2.27g/cm^3; \alpha_0 = 2627m/s, \alpha_1 = 3251m/s; \beta_0 = 1245m/s, \beta_1 = 2138m/s$. For this model, the exact value of a_μ is 1.89. The linear approximation $a_\mu^{(1)}$ (left) and the sum of linear and first non-linear $a_\mu^{(1)} + a_\mu^{(2)}$ (right).

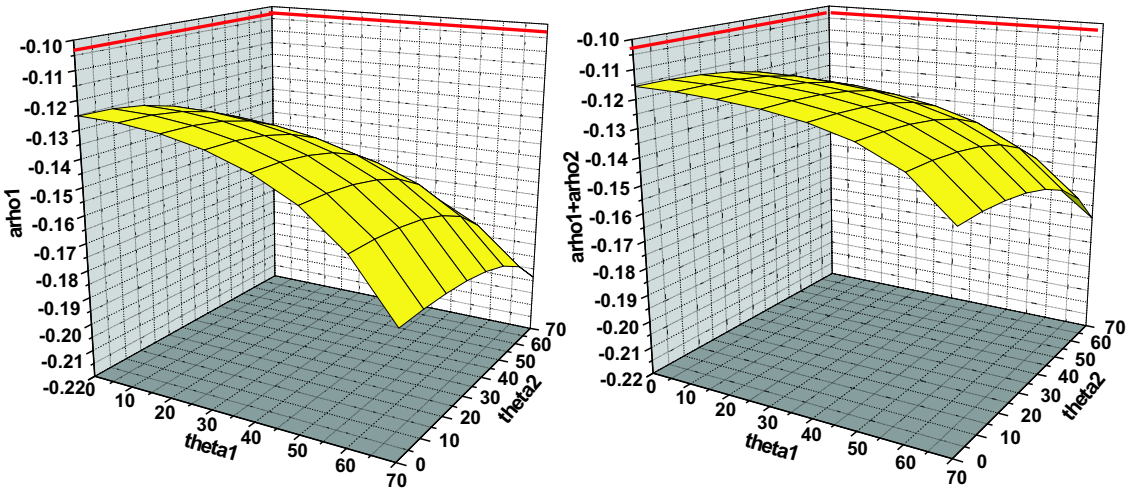

Figure 9: Model 3: shale (0.20 porosity) over oil sand (0.30 porosity). $\rho_0 = 2.32g/cm^3, \rho_1 = 2.08g/cm^3; \alpha_0 = 2627m/s, \alpha_1 = 2330m/s; \beta_0 = 1245m/s, \beta_1 = 1488m/s$. For this model, the exact value of a_ρ is -0.103. The linear approximation $a_\rho^{(1)}$ (left) and the sum of linear and first non-linear $a_\rho^{(1)} + a_\rho^{(2)}$ (right).

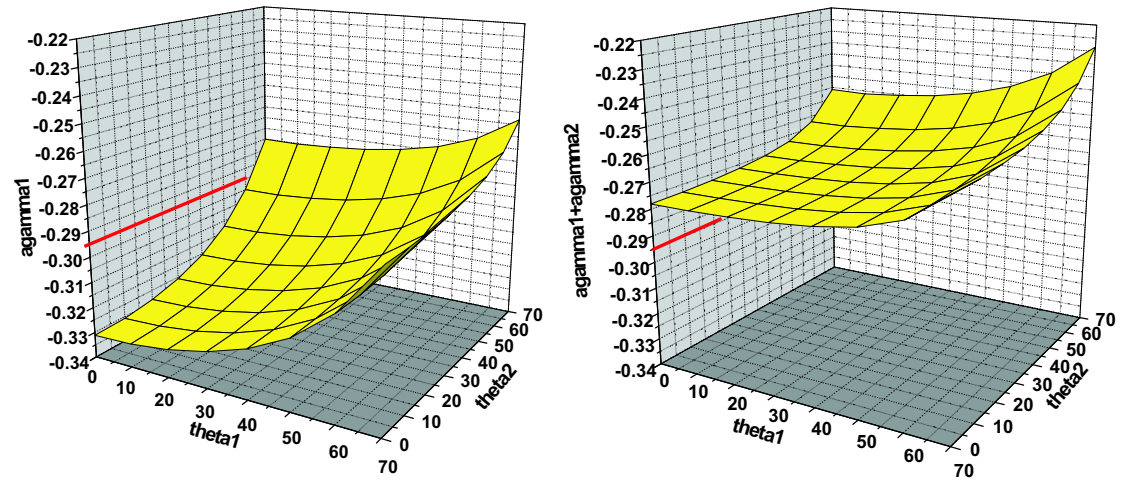

Figure 10: Model 3: shale (0.20 porosity) over oil sand (0.30 porosity). $\rho_0 = 2.32g/cm^3, \rho_1 = 2.08g/cm^3; \alpha_0 = 2627m/s, \alpha_1 = 2330m/s; \beta_0 = 1245m/s, \beta_1 = 1488m/s$. For this model, the exact value of a_γ is -0.295. The linear approximation $a_\gamma^{(1)}$ (left) and the sum of linear and first non-linear $a_\gamma^{(1)} + a_\gamma^{(2)}$ (right).

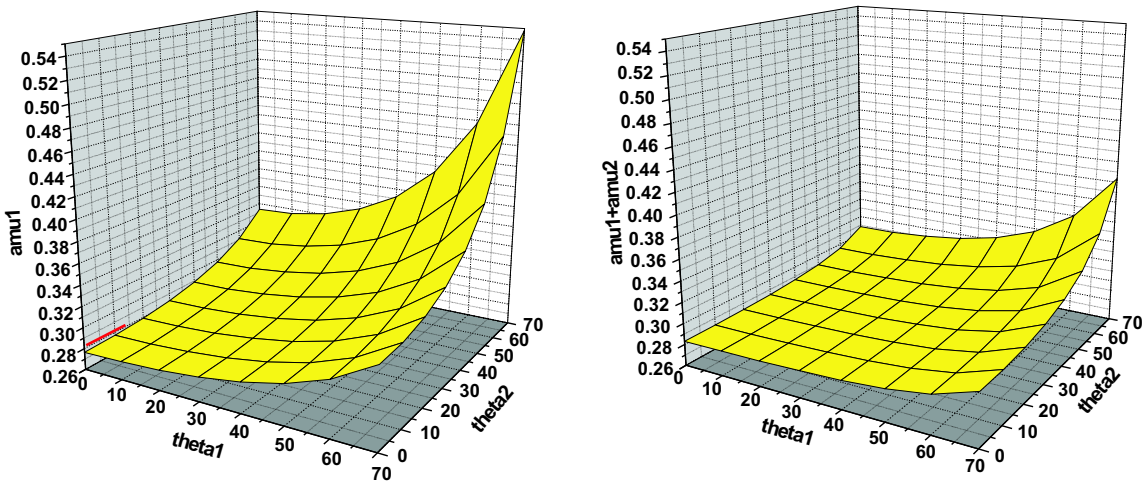

Figure 11: Model 3: shale (0.20 porosity) over oil sand (0.30 porosity). $\rho_0 = 2.32g/cm^3, \rho_1 = 2.08g/cm^3; \alpha_0 = 2627m/s, \alpha_1 = 2330m/s; \beta_0 = 1245m/s, \beta_1 = 1488m/s$. For this model, the exact value of a_μ is 0.281. The linear approximation $a_\mu^{(1)}$ (left) and the sum of linear and first non-linear $a_\mu^{(1)} + a_\mu^{(2)}$ (right).

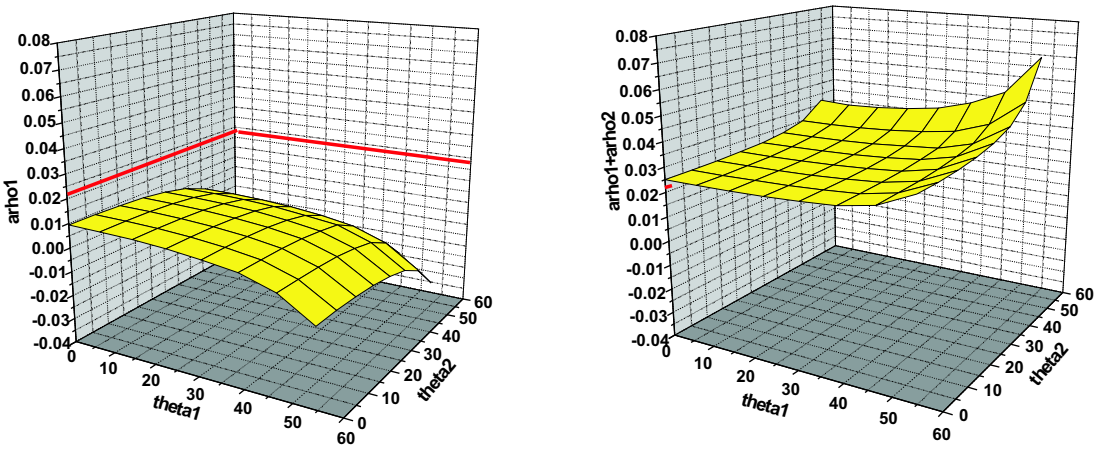

Figure 12: Model 4: oil sand over wet sand, 0.20 porosity. $\rho_0 = 2.27g/cm^3, \rho_1 = 2.32g/cm^3; \alpha_0 = 3251m/s, \alpha_1 = 3507m/s; \beta_0 = 2138m/s, \beta_1 = 2116m/s$. For this model, the exact value of a_ρ is 0.022. The linear approximation $a_\rho^{(1)}$ (left) and the sum of linear and first non-linear $a_\rho^{(1)} + a_\rho^{(2)}$ (right).

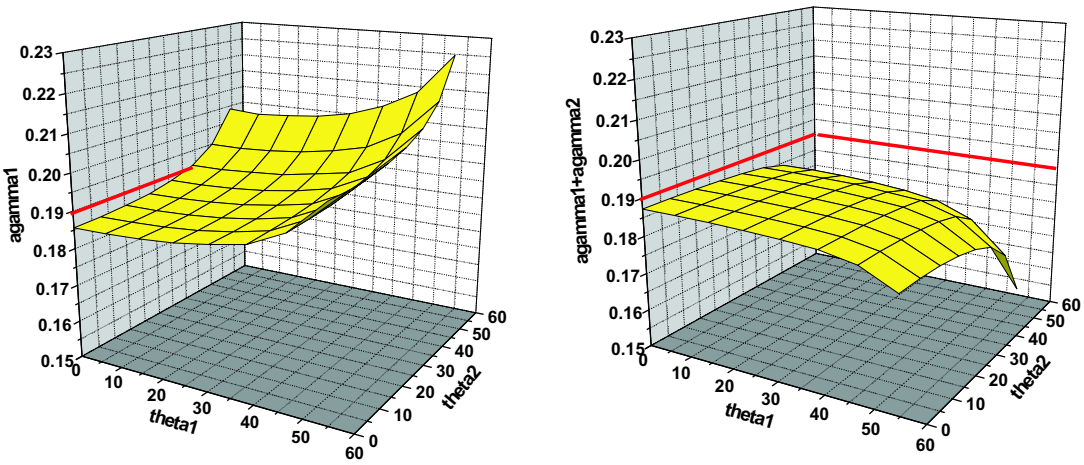

Figure 13: Model 4: oil sand over wet sand, 0.20 porosity. $\rho_0 = 2.27g/cm^3, \rho_1 = 2.32g/cm^3; \alpha_0 = 3251m/s, \alpha_1 = 3507m/s; \beta_0 = 2138m/s, \beta_1 = 2116m/s$. For this model, the exact value of a_γ is 0.19. The linear approximation $a_\gamma^{(1)}$ (left) and the sum of linear and first non-linear $a_\gamma^{(1)} + a_\gamma^{(2)}$ (right).

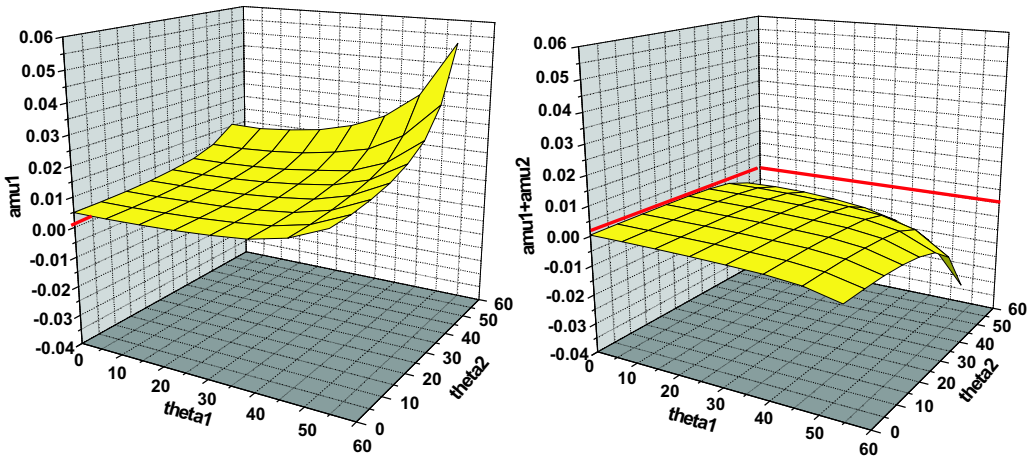

Figure 14: Model 4: oil sand over wet sand, 0.20 porosity. $\rho_0 = 2.27g/cm^3, \rho_1 = 2.32g/cm^3; \alpha_0 = 3251m/s, \alpha_1 = 3507m/s; \beta_0 = 2138m/s, \beta_1 = 2116m/s$. For this model, the exact value of a_μ is 0.001. The linear approximation $a_\mu^{(1)}$ (left) and the sum of linear and first non-linear $a_\mu^{(1)} + a_\mu^{(2)}$ (right).

6 Conclusion

In this report, a framework and algorithm have been developed for more accurate target identification. The elastic non-linear inversion requires all four components of data, but in this report we analyzed an algorithm which inputs only $\hat{D}^{PP}$. Although $\hat{D}^{PP}$ can itself provide useful non-linear direct inversion results, the implication of this research is that further value would derive from actually measuring $\hat{D}^{PP}$, $\hat{D}^{PS}$, $\hat{D}^{SP}$ and $\hat{D}^{SS}$, as the method requires. For the case that all four components of data available, we also provided a consistent method to solve for all of the second terms. Further plan is the numerical test on this consistent full non-linear elastic inversion method.

Acknowledgements

The M-OSRP sponsors are thanked for supporting this research. We are grateful to Robert Keys and Douglas Foster for useful comments and suggestions. We have been partially funded by and are grateful for NSF-CMG award DMS-0327778 and DOE Basic Sciences award DE-FG02-05ER15697.

Appendix A

In this Appendix, we give the different coefficients before every linear quantity $(a_\gamma^{(1)}, a_\rho^{(1)}, a_\mu^{(1)})$ — different incidence angle θ. For P to P case, we have

$$k_g^{PP} = \frac{\omega}{\alpha_0}\sin\theta^{PP},$$
$$\nu_g^{PP} = \frac{\omega}{\alpha_0}\cos\theta^{PP},$$

For S to P case,

$$k_g^{PS} = \frac{\omega}{\beta_0}\sin\theta^{PS},$$
$$\nu_g^{PS} = \frac{\omega}{\alpha_0}\sqrt{1-\frac{\alpha_0^2}{\beta_0^2}\sin^2\theta^{PS}}$$
$$\eta_g^{PS} = \frac{\omega}{\beta_0}\cos\theta^{PS},$$

For P to S case,

$$k_g^{SP} = \frac{\omega}{\alpha_0}\sin\theta^{SP},$$
$$\nu_g^{SP} = \frac{\omega}{\alpha_0}\cos\theta^{SP}$$
$$\eta_g^{SP} = \frac{\omega}{\beta_0}\sqrt{1-\frac{\beta_0^2}{\alpha_0^2}\sin^2\theta^{SP}},$$

For S to S case,

$$k_g^{SS} = \frac{\omega}{\beta_0}\sin\theta^{SS},$$
$$\eta_g^{SS} = \frac{\omega}{\beta_0}\cos\theta^{SS},$$

Let the arguments of $a_\rho^{(1)}$ and $a_\mu^{(1)}$ in Eqs. (8), (9), (10) and (11) equal, we need

$$-2\nu_g^{PP} = -\nu_g^{PS} - \eta_g^{PS} = -\nu_g^{SP} - \eta_g^{SP} = -2\eta_g^{SS},$$

which leads to

$$2\frac{\omega}{\alpha_0}\cos\theta^{PP} = \frac{\omega}{\alpha_0}\sqrt{1-\frac{\alpha_0^2}{\beta_0^2}\sin^2\theta^{PS}} + \frac{\omega}{\beta_0}\cos\theta^{PS} = \frac{\omega}{\alpha_0}\cos\theta^{SP} + \frac{\omega}{\beta_0}\sqrt{1-\frac{\beta_0^2}{\alpha_0^2}\sin^2\theta^{SP}} = 2\frac{\omega}{\beta_0}\cos\theta^{SS},$$

From the expression above, given θ^{PP}, we can find the corresponding θ^{PS}, θ^{SP} and θ^{SS}.

$$\theta^{PS} = \cos^{-1}\left[\frac{4b^2\cos^2\theta^{PP} + 1 - b^2}{4b\cos\theta^{PP}}\right],$$
$$\theta^{SP} = \cos^{-1}\left[\frac{4b^2\cos^2\theta^{PP} - 1 + b^2}{4b^2\cos\theta^{PP}}\right],$$
$$\theta^{SS} = \cos^{-1}\left(b\cos\theta^{PP}\right),$$

where $b = \frac{\beta_0}{\alpha_0}$.

References

L. Amundsen, A. Reitan, and B. Arntsen. Geometric analysis of data-driven inversion/depth imaging. *Journal of Seismic Exploration*, 14:51–62, 2005a.

L. Amundsen, A. Reitan, H. K. Helgesen, and B. Arntsen. Data-driven inversion/depth imaging derived from approximations to one-dimensional inverse acoustic scattering. *Inverse Problems*, 21:1823–1850, 2005b.

R. W. Clayton and R. H. Stolt. A Born-WKBJ inversion method for acoustic reflection data. *Geophysics*, 46(11):1559–1567, 1981.

D. J. Foster, R. G. Keys, and D. P. Schmitt. *Detecting subsurface hydrocarbons with elastic wavefields*. Springer-In Inverse Problems in Wave Progagation, Volume 90 of The IMA Volumes in Mathematics and its Applications, 1997.

Kristopher. A. Innanen. *Methods for the treatment of acoustic and absorptive/dispersive wave field measurements*. PhD thesis, University of British Columbia, 2003.

F. Liu, A. B. Weglein K. A. Innanen, and B. G. Nita. Extension of the non-linear depth imaging capability of the inverse scattering series to multidimensional media: strategies and numerical results. In *9th Ann. Cong. SBGf, Expanded Abstracts*. SBGf, 2005.

K. H. Matson. *An inverse-scattering series method for attenuating elastic multiples from multi-component land and ocean bottom seismic data*. PhD thesis, University of British Columbia, 1997.

Adriana C. Ramírez and Arthur B. Weglein. An inverse scattering internal multiple elimination method: Beyond attenuation, a new algorithm and initial tests. In *75th Annual Internat. Mtg., Soc. Expl. Geophys., Expanded Abstracts*, pages 2115–2118. Soc. Expl. Geophys., 2005.

S. A. Shaw. *An inverse scattering series algorithm for depth imaging of reflection data from a layered acoustic medium with an unknown velocity model*. PhD thesis, University of Houston, 2005.

A. B. Weglein, F. V. Araújo, P. M. Carvalho, R. H. Stolt, K. H. Matson, R. T. Coates, D. Corrigan, D. J. Foster, S. A. Shaw, and H. Zhang. Inverse scattering series and seismic exploration. *Inverse Problems*, 19:R27–R83, 2003.

A. B. Weglein, D. J. Foster, K. H. Matson, S. A. Shaw, P. M. Carvalho, and D. Corrigan. Predicting the correct spatial location of reflectors without knowing or determining the precise medium and wave velocity: initial concept, algorithm and analytic and numerical example. *Journal of Seismic Exploration*, 10(4):367–382, 2002.

A. B. Weglein, F. A. Gasparotto, P. M. Carvalho, and R. H. Stolt. An inverse-scattering series method for attenuating multiples in seismic reflection data. *Geophysics*, 62(6):1975–1989, 1997.

A. B. Weglein and R. H. Stolt. Approaches on linear and non-linear migration-inversion, 1992. Personal Communication.

A. B. Weglein, P. B. Violette, and T. H. Keho. Using multiparameter born theory to obtain certain exact multiparameter inversion goals. *Geophysics*, 51:1069–1074, 1986.

H. Zhang and A. B. Weglein. Target identification using the inverse scattering series: inversion of large-contrast, variable velocity and density acoustic media. *M-OSRP Annual Report*, 2, 2003.

H. Zhang, A. B. Weglein, and R. G. Keys. Velocity independent depth imaging and non-linear direct target identification for 1D elastic media: testing and evaluation for application to non-linear AVO, using only PP data. *M-OSRP Annual Report*, 4, 2005.

Discrimination between pressure and fluid saturation using direct non-linear inversion method: an application to time-lapse seismic data

Haiyan Zhang, Arthur B. Weglein, Robert G. Keys[+*], Douglas J. Foster[+*] and Simon A. Shaw[*]
[*] ConocoPhillips
[+] Adjunct Professor, Physics Dept., M-OSRP, UH

Abstract

The inverse scattering series based direct non-linear inversion method has shown positive results on its application to multi-parameter 1D acoustic and elastic media (see, e.g., Weglein et al., 2003; Zhang et al., 2005; Zhang and Weglein, 2005). In this paper, we present another application of this method to time-lapse seismic data aiming to distinguish pressure changes from reservoir fluid changes. Two elastic parameters (Shear modulus and velocity ratio) are chosen to discriminate the two changes. Synthetic tests indicate that these two parameters are very useful in mapping the pressure and fluid changes; and, the direct non-linear inversion method gives closer and more reliable parameter predictions compared to conventional linear order approximation.

1 Introduction

Time-lapse seismic data can be defined as those seismic data acquired at different times over the same area to assess changes in the subsurface with time, such as fluid movement or the fraction of hydrocarbons that can be or has been produced from a well, reservoir or field. Optimizing the reservoir development requires precise and timely information on those changes like reservoir pressure change and fluid change. But distinguishing pressure changes from reservoir fluid changes is difficult with conventional seismic time-lapse attributes. Some works on studying the sensitivities and/or discrimination of these two changes have been presented by, e.g., Tura and Lumley (1999); Landrø (2001); Landrø et al. (2003); Landrø and Duffaut (2004); Stovas and Landrø (2005); Kvam and Landrø (2005). In this paper, we choose two parameters — relative changes in shear modulus and velocity ratio V_p/V_s (V_p is the acoustic P velocity and V_s is the elastic shear velocity) which may be useful for separating pressure changes from fluid changes. The reason for choosing these two parameters is that V_p/V_s is sensitive to changes in fluid/water saturation, but insensitive to changes in pressure; while, shear modulus is sensitive to changes in pore pressure but unaffected by changes in fluid. These two parameters can help to indicate either a pressure or a fluid changed in the reservoir. Hence, if these two parameters can be more accurately predicted/estimated using the direct non-linear inversion method, it would be easier to accomplish this goal.

The direct non-linear inversion method is based on the inverse scattering series, and it uses the measured scattered wave field, i.e., data D, to predict the earth property changes in space. Over here, the baseline survey is considered as the reference wave field G_0 in the inverse scattering series, and the monitor survey as the actual wave field G. The initial reservoir condition is considered

as the background and the reservoir property changes in TIME are related to the earth property changes in SPACE in the inverse scattering series, and the monitor survey minus the baseline survey is related to the scattered field. The relationship between the inverse scattering series and the time-lapse seismic monitoring is illustrated in the following table:

Inverse scattering series	**Time-lapse seismic monitoring**
Reference medium L_0	Initial reservoir condition
Actual medium L	Current reservoir condition
Earth property changes in space $V = L_0 - L$	Reservoir property changes in time
Reference wave field G_0	Baseline survey
Actual wave field G	Monitor survey
Scattered wave field $D = G - G_0$	Monitor − Baseline

In the following sections, we show the numerical tests of the first and second order algorithms to estimate shear modulus and V_p/V_s contrasts with only $\hat{D}^{PP}$ (PP data). The applications are on the core data (Gregory, 1976) and Heidrun well log data, respectively. The tests are similar to those numerical tests described in our previous work (e.g., Zhang et al., 2005; Zhang and Weglein, 2005) with reference medium over actual medium replaced by baseline over monitor; and the parameters require modification from a_γ, a_ρ and a_μ to a_R, a_ρ and a_μ, where a_R is the relative change in the velocity ratio V_p/V_s. The detail derivations of writing $a_R^{(1)}$ and $a_R^{(2)}$ in terms of $a_\gamma^{(1)}$, $a_\gamma^{(2)}$, $a_\mu^{(1)}$ and $a_\mu^{(2)}$ are in the Appendix.

2 Core data tests

In this section, we numerically test the direct non-linear inversion approach and compare the effects of pressure and fluid changes on the elastic properties in the following two cases: (1) Fixing the fluid as 100% water saturation, while the pressure changes from 1000 to 9000psi. The measurement at pressure = 5000psi presents the baseline and the measurements at the other different pressures are respectively considered as monitors (Gregory, 1976, Table 3). (2) Fixing the pressure at 5000psi, while the fluid changes from 0 to 100 percent. The measurement at 100% saturation is the baseline and the other cases with different water saturations are monitors, respectively (Gregory, 1976, Table 4).

The numerical results are shown in the figures at the end of this paper. As illustrated in Figs. 1 and 2, when pressure changes, shear modulus has the most variation and V_p/V_s has the least variation; while when only water saturation changes, shear modulus has the least variation and V_p/V_s has bigger variation. So shear modulus is very sensitive to pressure changes while relatively not sensitive to the fluid changes, and V_p/V_s is very sensitive to the fluid changes, but is relatively insensitive to the pressure changes. These two parameters would be very useful in indicating/mapping pressure and fluid changes. The P impedance has very big variation in both cases. So it is very sensitive to each of the two kinds of changes and can't discriminate fluid changes from pressure changes.

From Figs. $3 \sim 6$, we show the comparison of first and second order approximation of the relative changes in shear modulus and V_p/V_s in the two cases as stated above. Among all of the examples tested, because the contrast here is relatively small, both the first and second order approximation

give good approximations, and the second order approximation does an ever better job, especially for lager contrasts, the improvements are more obvious. Here, it is worth noting that the objective of the direct non-linear inversion method (see, e.g., Weglein et al., 2003) is trying to predict more reliable property changes for more complex, larger contrast targets where the error coming from the linear approximation would be significant.

3 Heidrun well log data tests

In this section, well log data tests are performed on the Heidrun synthetic well log A-52 (Fig. 7). From the year 1986 to the year 2001, at the first layer of the reservoir, oil is replaced by gas, and at the second layer, oil is replaced by water. Throughout the interval, the pore pressure decreased. The baseline is the log data in 1986 and the monitor is the log data in 2001. In the numerical tests, the inputs are analytically calculated reflection coefficients $R_1, R_2, \cdots, R_i, \cdots$ and the corresponding actual changes are, respectively, $\frac{M_1}{B_1} - 1, \frac{M_2}{B_2} - 1, \cdots, \frac{M_i}{B_i} - 1, \cdots$ (As shown in Fig. 8).

From Fig. 9, we can see that, in the interval from about 3150 $\sim$ 3185m, oil goes to gas, and V_p/V_s decreases; while in the interval from about 3200 $\sim$ 3220m, oil is replaced by water, and V_p/V_s increases. Throughout this area, the pore pressure decreases a little bit, so the shear modulus increase in a small amount. The numerical results agree with the given well log A-52, and also indicate that the shear modulus is not sensitive to fluid changes since it has very small changes throughout the interval because the pressure change is small. Figure 10 is the comparison of the first order and second order approximation for the relative changes in the shear modulus. In this case, the second order approximation provides significant improvements beyond the linear results. It is much closer to the actual values. Figure 11 shows that both the first and second order approximation give very good results for the relative changes in V_p/V_s. The error from the first approximation is smaller and hence the first order approximation is more reliable compared with shear modulus (Fig. 10). But when we zoom in on Fig. 11, say from about 3150 $\sim$ 3590m, the results can be re-illustrated in Fig. 12, and we can see that the second order approximation does give better results compared with the first order approximation.

4 Conclusion and further discussions

Numerical tests indicate that the second order approximation provides improvements in the earth property predictions. The second order approximation is more helpful for predicting shear modulus. The results are very encouraging. In the next step, we expect to apply this method to the synthetic data and real seismic data.

Acknowledgements

We'd like to thank ConocoPhillips for permission to publish this paper. The M-OSRP sponsors are thanked for supporting this research. The authors also like to thank Baishali Roy (ConocoPhillips)

for kindly providing the schematic of synthetic well log A-52 and well log data. We have been partially funded by and are grateful for NSF-CMG award DMS-0327778 and DOE Basic Sciences award DE-FG02-05ER15697.

Appendix

The following is the derivation of expressing $a_R^{(1)}$ and $a_R^{(2)}$ in terms of $a_\gamma^{(1)}$, $a_\gamma^{(2)}$, $a_\mu^{(1)}$ and $a_\mu^{(2)}$.

Since

$$a_\gamma = \frac{\gamma}{\gamma_0} - 1 = \frac{\rho\alpha^2}{\rho_0\alpha_0^2} - 1,$$

$$a_\mu = \frac{\mu}{\mu_0} - 1 = \frac{\rho\beta^2}{\rho_0\beta_0^2} - 1,$$

and

$$a_R = \frac{\alpha/\beta}{\alpha_0/\beta_0} - 1,$$

then we have

$$(a_R + 1)^2 = \frac{a_\gamma + 1}{a_\mu + 1},$$

then

$$a_R^2 + 2a_R + 1 = (a_\gamma + 1)(1 - a_\mu + a_\mu^2 - \cdots),$$

where the series expansion is valid for $|a_\mu| < 1$.

Expanding the relative changes, we have

$$\begin{aligned} a_\gamma &= a_\gamma^{(1)} + a_\gamma^{(2)} + a_\gamma^{(3)} + \cdots, \\ a_\mu &= a_\mu^{(1)} + a_\mu^{(2)} + a_\mu^{(3)} + \cdots, \\ a_R &= a_R^{(1)} + a_R^{(2)} + a_R^{(3)} + \cdots, \end{aligned}$$

then after substitutions, we obtain

$$\begin{aligned} a_R^{(1)} &= \frac{1}{2}\left(a_\gamma^{(1)} - a_\mu^{(1)}\right), \\ a_R^{(2)} &= \frac{1}{2}\left(a_\gamma^{(2)} - a_\mu^{(2)} + a_\mu^{(1)^2} - a_R^{(1)^2} - a_\gamma^{(1)} a_\mu^{(1)}\right). \end{aligned}$$

References

A. R. Gregory. Fluid saturation effects on dynamic elastic properties of sedimentary rocks. *Geophysics*, 41(5):895–921, 1976.

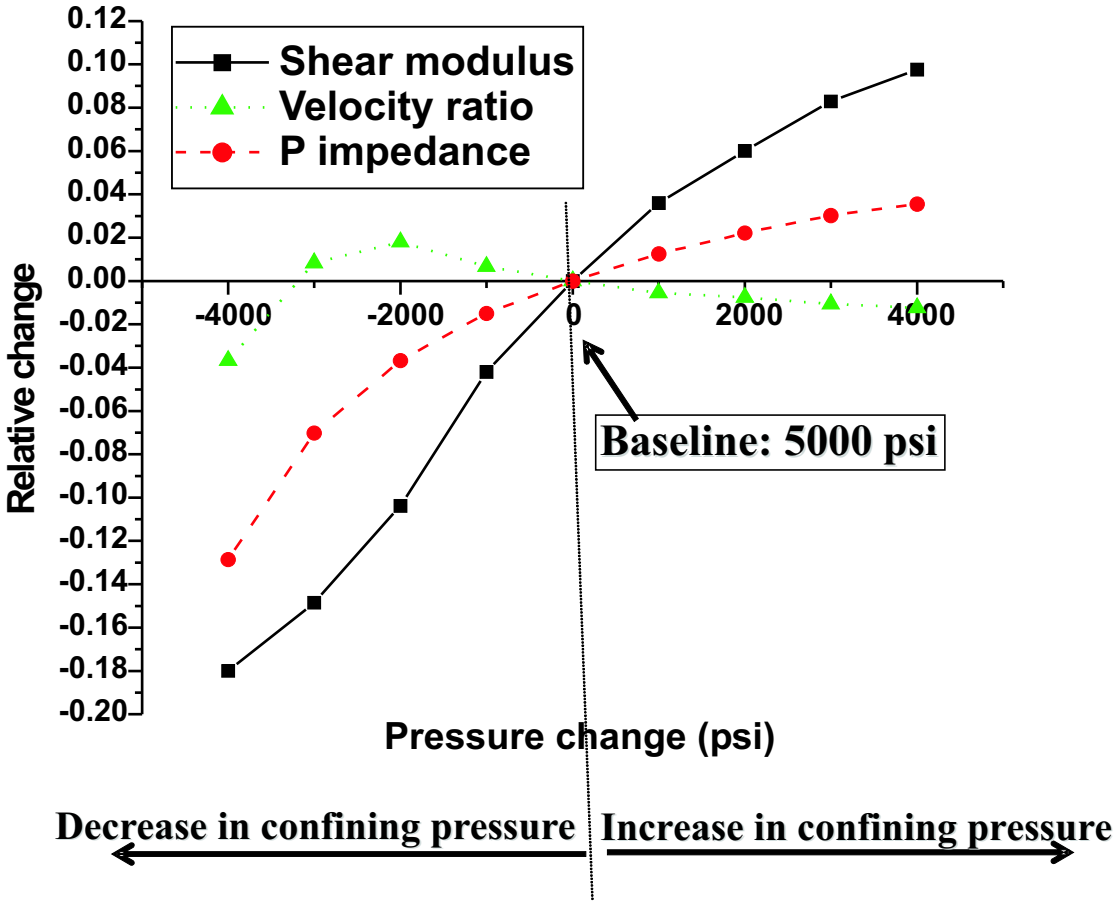

Figure 1: Comparison of attributes for pressure changes, fluid fixed (100 percent water saturation). Gregory (1976), Table 3.

Ø. Kvam and M. Landrø. Pore-pressure detection sensitivities tested with time-lapse seismic data. *Geophysics*, 70(6):O39–O50, 2005.

M. Landrø. Discrimination between pressure and fluid saturation changes from time-lapse seismic data. *Geophysics*, 66(3):836–844, 2001.

M. Landrø and K. Duffaut. Vp-vs ratio versus effective pressure and rock consolidation – a comparison between rock models and time-lapse avo studies. In *74th Annual Internat. Mtg., Soc. Expl. Geophys., Expanded Abstracts*. Soc. Expl. Geophys., 2004.

M. Landrø, H. H. Veire, K. Duffaut, and N. Najjar. Discrimination between pressure and fluid saturation changes from marine multicomponent time-lapse seismic data. *Geophysics*, 68(5): 1592–1599, 2003.

A. Stovas and M. Landrø. Fluid-pressure discrimination in anisotropic reservoir rocks — a sensitivity study. *Geophysics*, 70(3):O1–O11, 2005.

A. Tura and D. E. Lumley. Estimating pressure and saturation changes from time-lapse avo data.

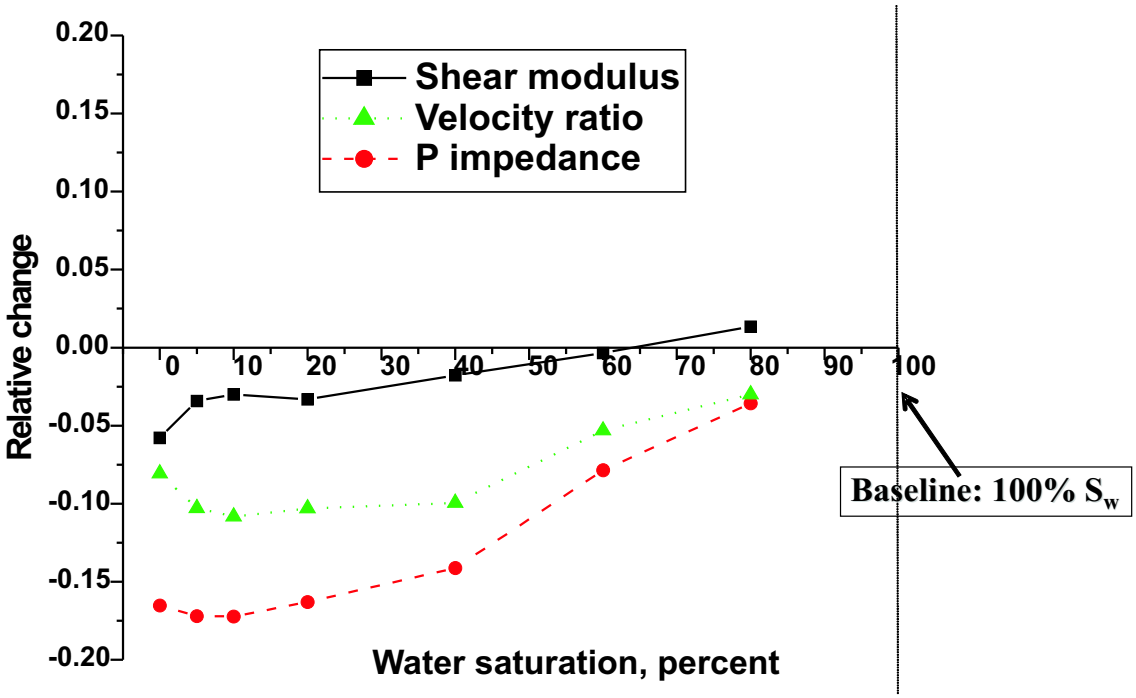

Figure 2: Comparison of attributes for fluid changes, pressure fixed (5000psi). Gregory (1976), Table 4.

In *69th Annual Internat. Mtg., Soc. Expl. Geophys., Expanded Abstracts*. Soc. Expl. Geophys., 1999.

A. B. Weglein, F. V. Araújo, P. M. Carvalho, R. H. Stolt, K. H. Matson, R. T. Coates, D. Corrigan, D. J. Foster, S. A. Shaw, and H. Zhang. Inverse scattering series and seismic exploration. *Inverse Problems*, 19:R27–R83, 2003.

H. Zhang and A. B. Weglein. The inverse scattering series for tasks associated with primaries: Depth imaging and direct non-linear inversion of 1d variable velocity and density acoustic media. In *75th Annual Internat. Mtg., Soc. Expl. Geophys., Expanded Abstracts*, pages 1705–1708. Soc. Expl. Geophys., 2005.

H. Zhang, A. B. Weglein, and R. G. Keys. Velocity independent depth imaging and non-linear direct target identification for 1D elastic media: testing and evaluation for application to non-linear AVO, using only PP data. *M-OSRP Annual Report*, 4, 2005.

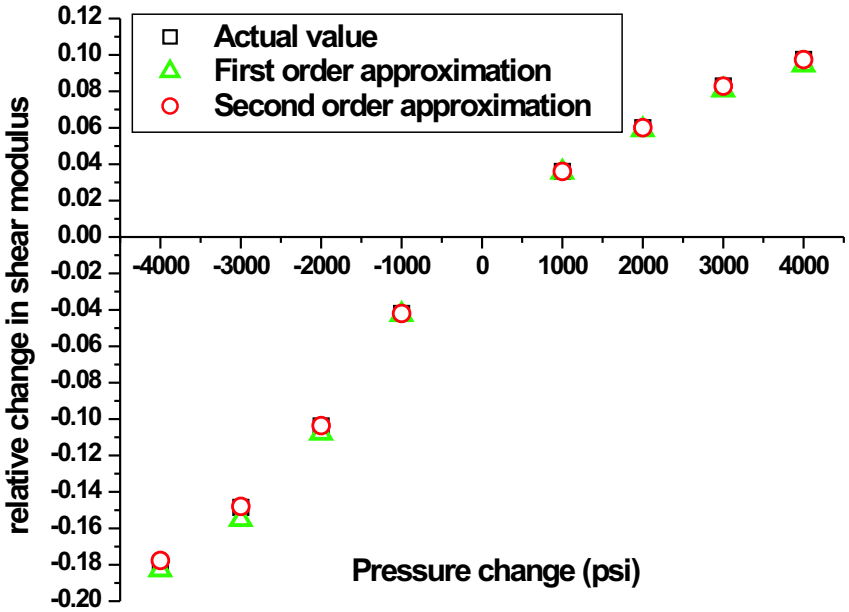

Figure 3: Comparison of first and second order approximation of relative change in shear modulus for pressure changes, fluid fixed (100 percent water saturation). Gregory (1976), Table 3.

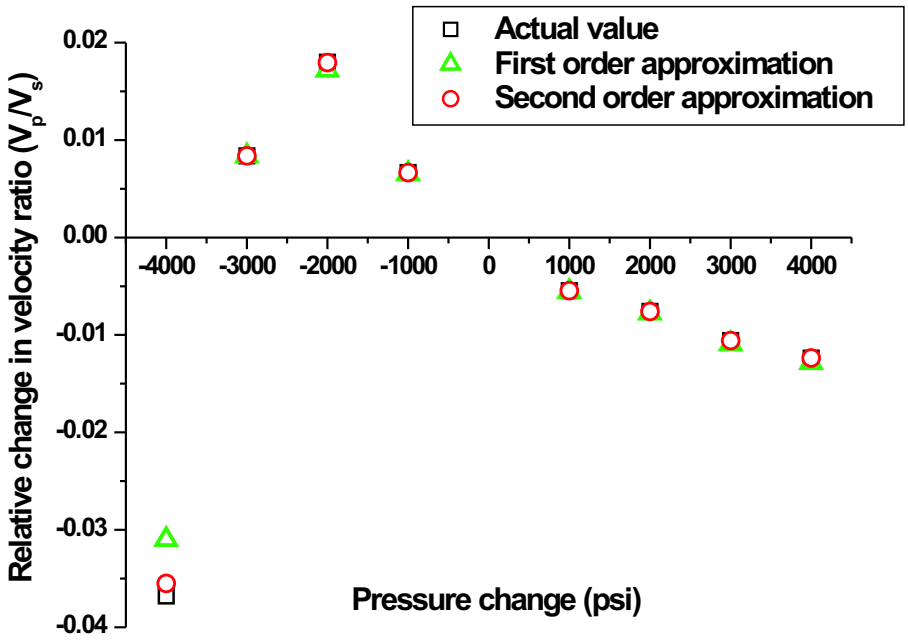

Figure 4: Comparison of first and second order approximation of relative change in V_p/V_s (See Appendix) for pressure changes, fluid fixed (100 percent water saturation). Gregory (1976), Table 3.

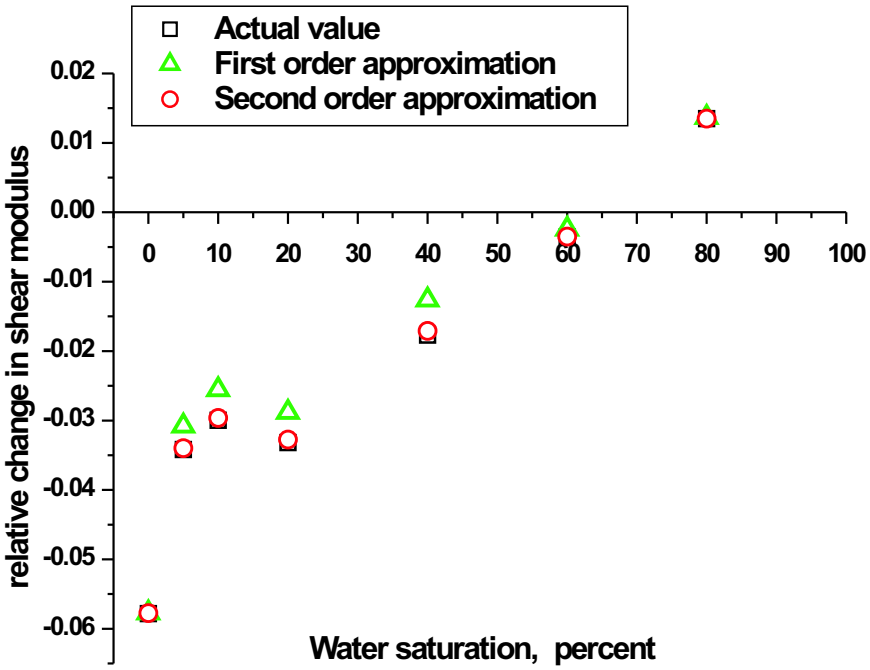

Figure 5: Comparison of first and second order approximation of relative change in shear modulus for fluid changes, pressure fixed (5000psi). Gregory (1976), Table 4.

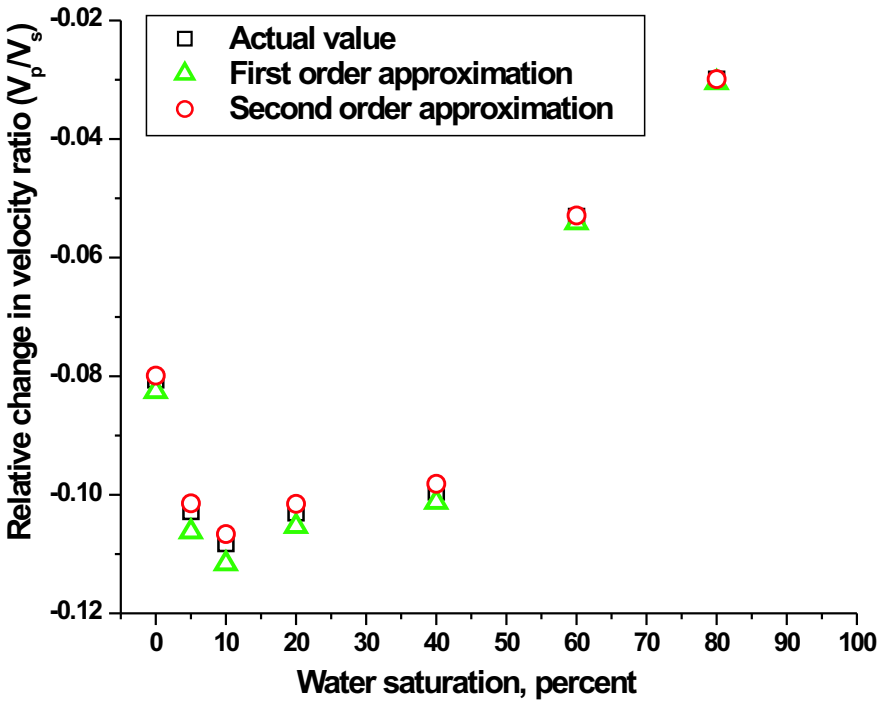

Figure 6: Comparison of first and second order approximation of relative change in V_p/V_s for fluid changes, pressure fixed (5000psi). Gregory (1976), Table 4.

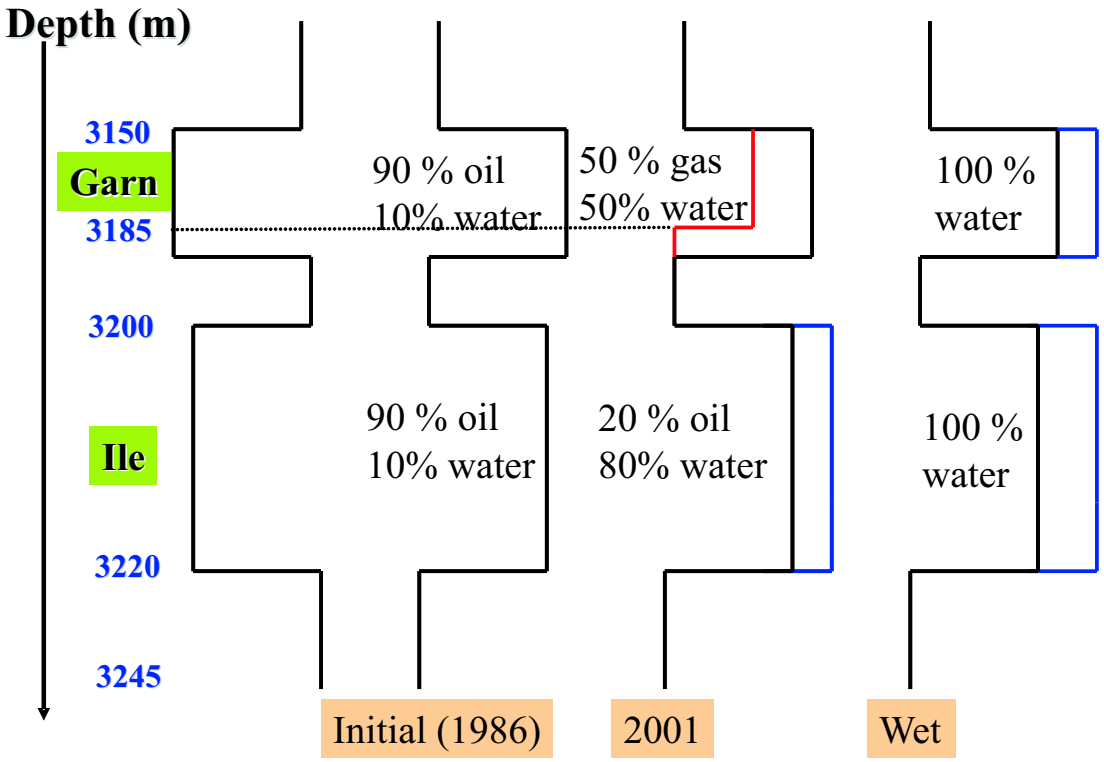

Figure 7: Schematic of the synthetic well log A-52.

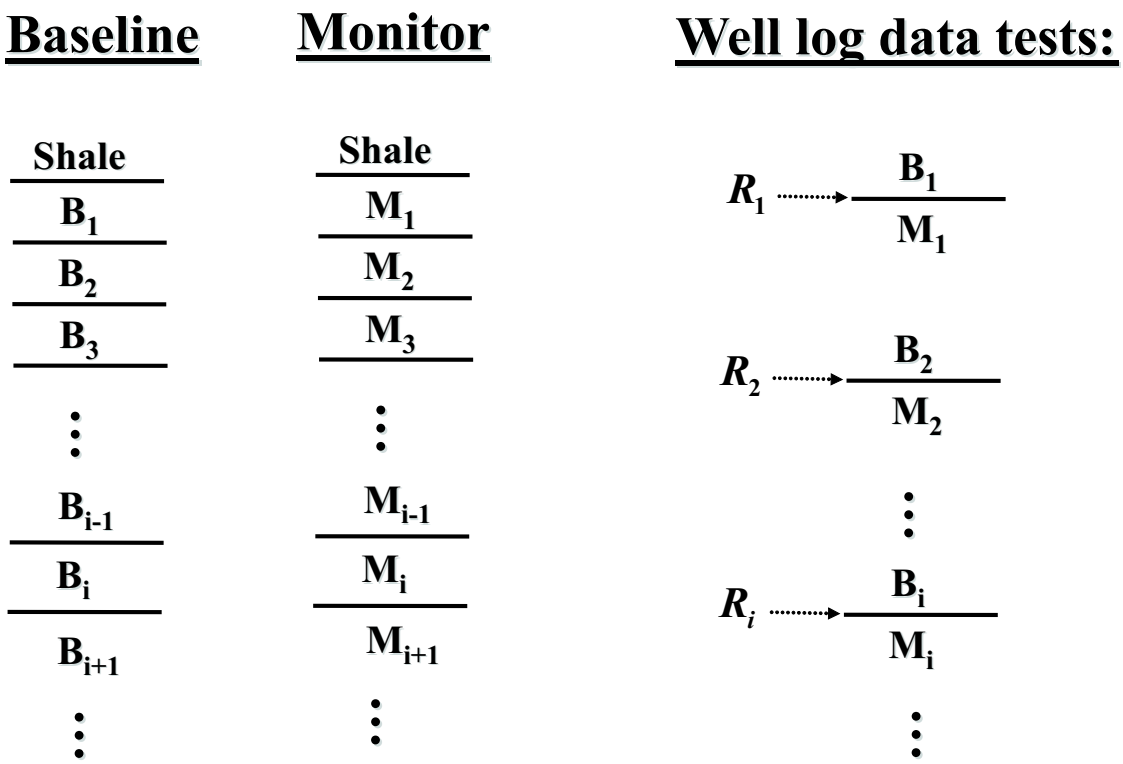

Figure 8: Schematic of the baseline, monitor and input reflection coefficients.

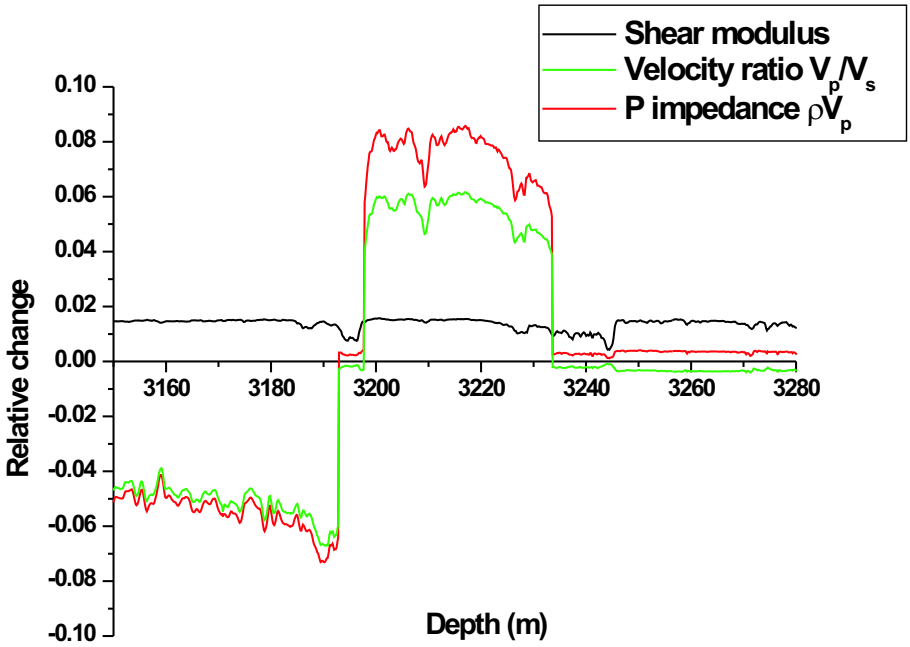

Figure 9: Comparison of actual changes in shear modulus, P-impedance and velocity ratio V_p/V_s. The baseline is the log data in 1986 and the monitor is the log data in 2001.

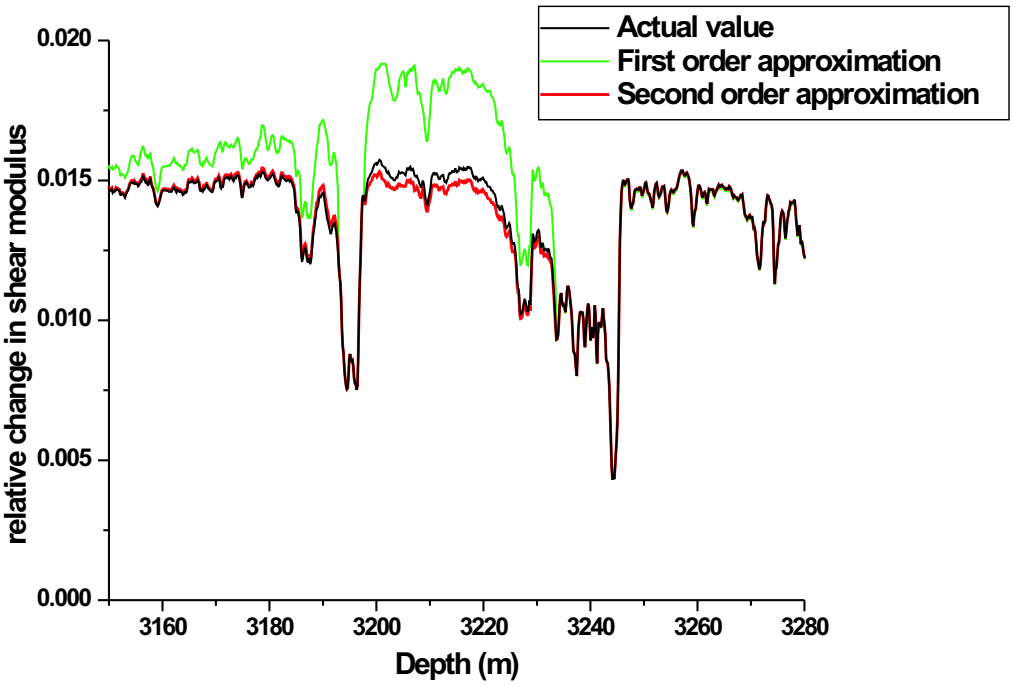

Figure 10: Comparison of first and second order approximation of relative change in shear modulus. The baseline is the log data in 1986 and the monitor is the log data in 2001.

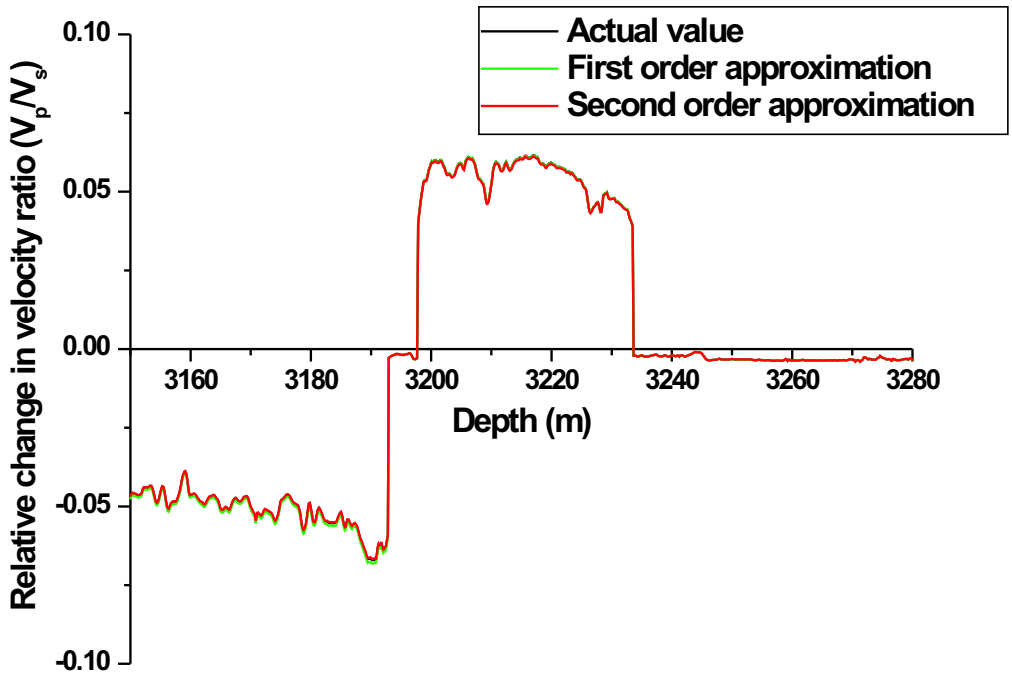

Figure 11: Comparison of first and second order approximation of relative change in V_p/V_s. The baseline is the log data in 1986 and the monitor is the log data in 2001.

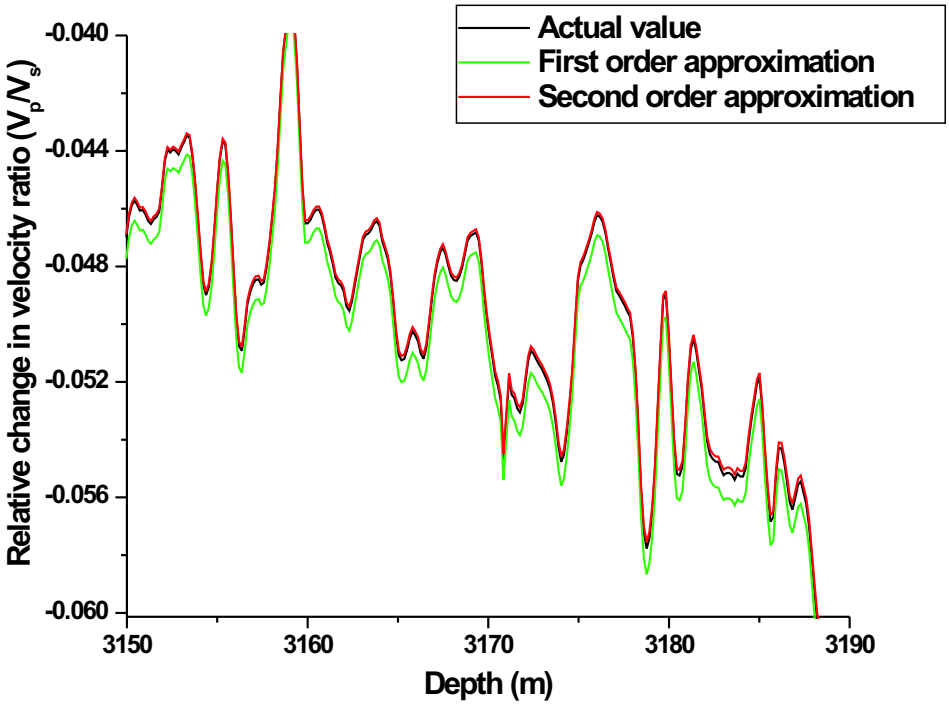

Figure 12: Zoomed in comparison of first and second order approximation of relative change in V_p/V_s. The baseline is the log data in 1986 and the monitor is the log data in 2001.

Theoretical developments in direct non-linear Q-compensation and a strategy for achieving task-separated multiparameter inversion algorithms

Kristopher A. Innanen and Arthur B. Weglein

Abstract

We present developments in the theory and application of inverse scattering series (ISS) methods for the direct non-linear processing of attenuated primaries. The motivation is to provide differential capability in improving the resolution of seismic images within the direct, non-linear inversion milieu, such that no medium information is required a priori. We begin by discussing the linear inversion of a reflected seismic data set over a layered 2-parameter viscoacoustic medium, and the basic means for construction of the complex frequency-dependent linear scattering potential from the angle- and frequency-dependence of reflected data events. We then show that the equations for coupled imaging and inversion of acoustic primaries (e.g., Innanen et al., 2004) may be extended to accommodate the viscoacoustic model, providing an approximate solution of the non-linear 2-parameter direct inverse problem. We then use these equations (which are themselves a potential stopping point) and a new strategy, in which the data is processed linearly in one parameter and non-linearly in the other as the basis from which to propose a set of task-separated Q-processing algorithms.

1 Introduction

In this paper we present a theory for linear and non-linear processing of primary reflections from a seismic experiment over a one-dimensional visco-acoustic medium, i.e., a medium that has the intrinsic capacity to dissipate wave energy as it propagates. We refer to such media as having absorptive-dispersive (hereafter A-D) properties.

We fit this theory into the developing framework for "task-separated" processing based on the inverse scattering series (ISS), which confers on its methods – when posed and investigated correctly – the ability to proceed in the absence of accurate prior knowledge of medium parameters. As is discussed in detail elsewhere (Weglein et al., 2002; Weglein et al., 2003; Shaw et al., 2004; Shaw, 2005; Innanen, 2003; Liu et al., 2005; Zhang and Weglein, 2005; Innanen, 2005) when applied to problems of primary processing, as opposed to multiples (Weglein et al., 1997; Weglein et al., 2003; Ramirez and Weglein, 2005; Nita and Weglein, 2006), a large number of ISS terms are often necessary, and in some cases closed forms have been available in problems of limited dimensionality. Some groundwork has been laid for the investigation of the non-linear ISS primary processing capability for dissipative media (Innanen and Weglein, 2003; Innanen and Weglein, 2004; Innanen and Weglein, 2005) and will be discussed further as needed here.

Some important issues are not addressed technically in this paper, primarily those centering on strategies for dealing with the finite, discrete and inaccurate nature of a field data set, the first

and third of which in particular will have consequences for a processing framework involving non-linear methods and some flavor of Q compensation. The "aperture" problems of a seismic data set when integral methods are applied is aggravated in non-linear schemes, and is of particular interest in the case of lateral aperture of sources and receivers and the effective aperture in the temporal frequency domain (i.e., the problem of band-limitation). "Data reconstruction", the handle given to a class of methods that address specifically the former of those two issues, is of course a community-wide research effort whose success benefits all corners of seismic processing; even a broad perspective on that literature is beyond the scope of this introduction and we will not attempt it. The problem of band-limitation is of particular interest to a smaller community, however there is a literature beyond our own that directly addresses the problem. "Band-limited impedance inversion" (Wiggins and Miller, 1972; Walker and Ulrych, 1983; Oldenburg et al., 1983; Ulrych, 1984; Oldenburg, 1984; Ulrych, 1989), in which a model with a full spectrum (including DC component) is estimated from a bandlimited data set, is functionally identical to the problem of computing, for ISS primary methods, the requisite linear input to higher order terms from a bandlimited data set. Shaw (2005) and Innanen (2003) have discussed aspects of this relationship. A broad result of these investigations is to recommend for any application of methods like those described in this paper is to take the data as completely as is possible, especially in the regimes of low temporal frequency. Beyond that, if it is necessary, we may employ such methods as described above and import as they do low-level a priori assumptions into the methodology.

Beyond the utility of a method that estimates and compensates for attenuation without a prior determination of Q, the novelty of the methods in this paper lies in: (*i*) it being the first instance of a closed-form non-linear processing theory for a multi-parameter medium (Shaw et al. (2004) and Innanen (2005) present closed-form non-linear processing theories for a single parameter, while Zhang and Weglein (2005) present the second-order corrections available from two-parameter acoustic model); (*ii*) it being an example of far more extensive separation of tasks than previously considered, in particular, a mapping of fully attenuated-dispersed data to data that has had only the dispersion compensated for is presented; and (*iii*) the suggestion, for a multi-parameter system, that an "unprocessed data-to-processed data" mapping may be accomplished through non-linear manipulation of one or more of the parameters, but only linear manipulation of others. Parameters that are processed but which themselves remain linear in the data are ideally suited to be mapped (often trivially) back to data space.

We begin with a description of the physical and experimental framework within which we will form the processing theory, and the math-physics quantities, Green's functions and scattering integrals, that are the basis for the current research; following this we review and provide a new analysis and comparison between various levels of complexity of the visco-acoustic linear problem. Next the non-linear problem is tackled using the previously-developed viscous linear inverse and commentary based on the non-linear imaging and inversion procedures previously developed for a single parameter problem. Task-separation of the inversion equations is discussed and synthetic examples are produced and analyzed.

1.1 Physical-experimental framework

In this research we proceed assuming certain kinds of Earth structure and make-up are in place beneath certain kinds of reflection seismic experiments. Furthermore we develop methods for

primary processing only that behave well if all other kinds of reflection event are absent; this presupposes the successful application of methods to (1) estimate the source wavelet, (2) remove source and receiver ghosts, (3) remove free-surface multiples, and (4) remove internal multiples.

Fig. 1a illustrates some of the key details of the wave experiment as we cast it in the theory to follow. We consider a homogeneous whole-space (of water, say) as a reference medium in which resides the source and receiver; all explicit wave quantities we utilize in this paper are associated with propagation in this reference medium. All perturbations upon this reference are assumed to occur at depths below the source and receiver, which for convenience we collocate in depth at $z_g = z_s = 0$. We assume a line-source/line-receiver experiment expressed in the x_g, k_s domain, that is, with a receiver point at the lateral coordinate x_g, and source characterized by a suite of plane waves with varying lateral wavenumber k_s. Processing is conceived of here, in the standard terminology of the seismic reflection processing, as occurring to a receiver-gather having been Fourier-transformed in the lateral coordinate and in the time coordinate. We assume a medium that varies in the depth direction only, and so a single receiver-record is sufficient to characterize the medium-wave field response.

We specify to the simple case of a plane wave normally-incident upon a single interface at the outset to provide a simple heuristic on the behavior of the linear component of the full inverse problem; see Fig. 1b.

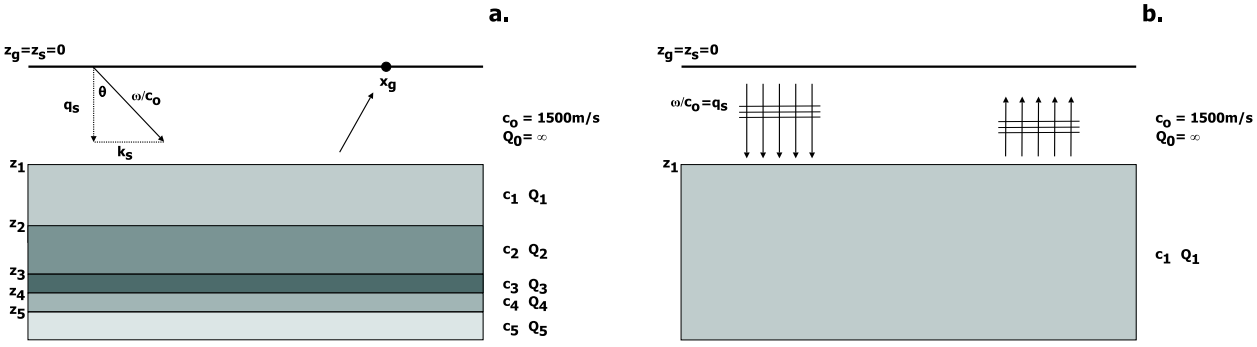

Figure 1: *Two frameworks for modelling and processing data acquired over a 2-parameter layered visco-acoustic medium. (a) An incident plane wave characterized by $k = \omega/c_0$ and lateral/depth wavenumbers k_s/q_s propagates into the layered medium and is measured at the receiver point x_g; (b) A plane wave at normal incidence propagates downward and interacts with a single-interface.*

1.2 Green's functions for homogeneous constant-density acoustic media

We consider propagation in a homogeneous constant density acoustic medium characterized by wavespeed c_0 (no absorptive-dispersive effects are modelled in the reference medium); both 1D normal incidence experiments (i.e., 1D medium, and horizontal plane source) and 1.5D experiments (i.e., 1D medium, and line source) are considered. We utilize the following Green's functions. A 1D normal incidence Green's function for a source at z_s and a receiver at z_g for frequency $\omega = kc_0$ is

$$G_0(z_g|z_s;k) = \frac{e^{ik|z_g - z_s|}}{i2k}. \tag{1}$$

A 2D Green's function for a receiver at x_g, $z_g = 0$ and a source at x', z' is

$$G_0(x_g, 0|x', z'; k) = \frac{1}{2\pi} \int_{-\infty}^{\infty} dk' e^{ik'(x_g - x')} \frac{e^{iq'z'}}{i2q'}, \tag{2}$$

where $q'^2 = k^2 - k'^2$; more generally, a 2D Green's function for a receiver at x', z' and a source at x'', z'' is

$$G_0(x', z'|x'', z''; k) = \frac{1}{2\pi} \int_{-\infty}^{\infty} dk' e^{ik'(x' - x'')} \frac{e^{iq'|z' - z''|}}{i2q'}. \tag{3}$$

Finally, a 2D Green's function for a receiver at x'', z'', and a source at lateral wavenumber k_s and source depth $z_s = 0$ is

$$G_0(x'', z''|k_s, 0; k) = e^{ik_s x'} \frac{e^{iq_s z''}}{i2q_s}, \tag{4}$$

where $q_s^2 = k^2 - k_s^2$. Eqns. (1)–(4) represent the only explicit propagation relationships used in the developments to follow; all account of propagation outside of the known homogeneous reference medium will be taken by high-order non-linear interactions of these acoustic, non-attenuating Green's functions with the requisite perturbation operator.

1.3 Scattering in an absorptive-dispersive medium

The inverse methods (and the forward methods they are based upon) come about from a specific characterization of the field variables and coefficients of two partial differential equations describing waves in a reference and in an actual medium. The basic equation governing the propagation we consider is

$$\left[\nabla^2 + K^2\right] G(x', z'|x_s, z_s, K) = -\delta(x' - x_s, z' - z_s), \tag{5}$$

in which differences arise from the definitions of K for the two media. We consider the reference medium to be a homogeneous constant density acoustic medium, characterized by wavespeed c_0, in which case $K^2 \equiv k^2 = \omega^2/c_0^2$. We consider the actual medium to correspond to one that has both variable wavespeed and variable Q, the latter being a parameter that governs absorption and dispersion, in which case:

$$K^2 \equiv \frac{\omega^2}{c^2(z)} \left[1 + 2\frac{F(k)}{Q(z)}, \right] \tag{6}$$

is an appropriate form provided terms quadratic and higher in $\frac{F(k)}{Q(z)}$ are small. If A-D models similar to those discussed by Aki and Richards (2002), due to, for instance, Futterman (1962), and similar at seismic frequencies to that of Kjartansson (1979) are utilized, then the function $F(k)$ is defined to be

$$F(k) = \frac{i}{2} - \frac{1}{\pi} \ln\left(\frac{k}{k_0}\right), \tag{7}$$

where k_0 is a reference quantity $k_0 = \omega_{max}/c_0$, in which ω_{max} is often chosen to be the largest frequency in the experiment. Notice that the function of $F(k)$ is to produce both imaginary and frequency dependent components in the propagation wavenumber K. Provided we assume a model-type for A-D behavior, this function is generally assumed to be known; we assume that here.

This form for propagation leads to altered descriptions of medium impedance, and hence reflection and transmission coefficients, the former of which will be of some importance. A reflection coefficient for an acoustic-viscoacoustic interface such as that illustrated in Fig. 1b is

$$\begin{aligned} R(k) &= \frac{k-K}{k+K} \\ &= \frac{1-\frac{c_0}{c_1}\left(1+\frac{F(k)}{Q_1}\right)}{1+\frac{c_0}{c_1}\left(1+\frac{F(k)}{Q_1}\right)}, \end{aligned} \tag{8}$$

and hence, like the propagation wavenumber, is both complex and frequency-dependent by virtue of the A-D behavior of the actual medium.

Expressing eqn. (5) in operator form for both the reference and actual cases respectively, we straightforwardly form the standard quantities of scattering theoretic modelling and inversion – two wave equations (reference and actual), and the difference between the associated wave operators and Green's operators; respectively

$$\begin{aligned} &\mathbf{L_0 G_0} = -\mathbf{I}, \qquad \mathbf{LG} = -\mathbf{I}, \\ &\mathbf{V} = \mathbf{L} - \mathbf{L_0}, \qquad \psi = \mathbf{G} - \mathbf{G_0}. \end{aligned} \tag{9}$$

These operators may be related by the identity referred to in scattering theory as the Lippmann-Schwinger, or Scattering equation, which further may be expanded in series to form the Born series, i.e.,

$$\begin{aligned} \psi &= \mathbf{G_0 V G}, \\ &= \mathbf{G_0 V G_0} + \mathbf{G_0 V G_0 V G_0} + \mathbf{G_0 V G_0 V G_0 V G_0} + ... \end{aligned} \tag{10}$$

The inverse scattering series is a series expansion of the scattering potential/perturbation operator $\mathbf{V}$, in which the n'th term is considered to be "n'th order in measurements of the scattered field". The order-by-order prescription for computation of $\mathbf{V}$ is attained by [1] substituting the series form for $\mathbf{V}$ into eqn. (10), and [2] restricting the wave field quantities to a measurement surface. We proceed assuming [2]. Substituting $\mathbf{V} = \mathbf{V_1} + \mathbf{V_2} + \mathbf{V_3} + ...$ into the Born series and equating like orders gives

$$\begin{aligned} \psi &= \mathbf{G_0 V_1 G_0}, \\ 0 &= \mathbf{G_0 V_2 G_0} + \mathbf{G_0 V_1 G_0 V_1 G_0}, \\ 0 &= \mathbf{G_0 V_3 G_0} + \mathbf{G_0 V_1 G_0 V_2 G_0} + \mathbf{G_0 V_2 G_0 V_1 G_0} \\ &\quad + \mathbf{G_0 V_1 G_0 V_1 G_0 V_1 G_0}, \end{aligned} \tag{11}$$

etc. For the two wave equations we have fixed upon in this research, we may write down specific

forms for the scattering quantity $\mathbf{V}$:

$$\begin{aligned}\mathbf{V} &= \mathbf{L} - \mathbf{L_0} \\ &= \left[\nabla^2 + \left(\frac{\omega}{c_0}\right)^2\right] - \left[\nabla^2 + K^2\right] \\ &= k^2 - K^2 \\ &= \left(\frac{\omega}{c_0}\right)^2 - \frac{\omega^2}{c^2(\vec{x})}\left[1 + 2\frac{F(k)}{Q(\vec{x})}\right] \\ &\approx \left(\frac{\omega}{c_0}\right)^2 \left[\alpha(\vec{x}) - 2F(k)\beta(\vec{x})\right].\end{aligned} \tag{12}$$

The last line is the result of expressing the coefficients of the actual wave equation in terms of perturbations on the coefficients on the reference wave equation:

$$\begin{aligned}\alpha(\vec{x}) &= 1 - \frac{c_0^2}{c^2(\vec{x})}, \\ \beta(\vec{x}) &= \frac{1}{Q(\vec{x})},\end{aligned} \tag{13}$$

and the assumption that $\alpha\beta$ is small. This form may be substituted into the forward scattering series in eqn. (10) to approximate to any level of accuracy an absorptive-dispersive wave field in terms of non-linear interactions of wave fields that are purely acoustic (Innanen, 2003; Innanen and Weglein, 2003). The inverse scattering series for such a two-parameter acoustic and absorptive-dispersive problem then arises by setting

$$\begin{aligned}\mathbf{V_1} &= \left(\frac{\omega}{c_0}\right)^2 \left[\alpha_1(\vec{x}) - 2F(k)\beta_1(\vec{x})\right], \\ \mathbf{V_2} &= \left(\frac{\omega}{c_0}\right)^2 \left[\alpha_2(\vec{x}) - 2F(k)\beta_2(\vec{x})\right],\end{aligned} \tag{14}$$

etc., and solving directly for α_n and β_n in terms of the measured data. We proceed in this analysis as is becoming standard for task-separated/velocity independent non-linear primary processing, that is by solving carefully the linear problem and casting the higher order terms as operations acting on this preliminary output.

2 Linear processing of primaries over a multiparameter c/Q medium

Some effort has been expended in casting and determining the nature of the linear 2-parameter absorptive-dispersive inverse problem given a layered medium and acoustic reference (Innanen, 2003; Innanen and Weglein, 2004). The resulting methodology resembles (1) the acoustic theories of Raz (1981) and Clayton and Stolt (1981), in its strategy for handling multiple parameters, and (2) the work of Carrion and VerWest (1987) in its devising and solution for a viscous scattering potential. The present theory differs from the latter work in that it is not a single-parameter profile inversion that assumes a prior knowledge of the medium wavespeed, but rather a formalism in which

both parameter profiles are concurrently estimated; nevertheless in many aspects of the detailed handling of the scattering potential the two linear theories bear a resemblance. Most importantly, we do, to some extent, come here to bury linear Q inversion and not to praise it; the failure of the linear approximation for reflectors embedded in the viscous part of the medium is the primary motivation for a view to extend to non-linear methods. The goal of this section is to review the linear theory and illustrate its basic behavior as a prelude to discussing the nonlinear problem and its manipulation for processing attenuated primaries.

2.1 For a normal incidence plane source over a single interface

Here we carry out the linear A-D inversion for the simplest possible case, a normal incident experiment over a single viscous interface; in spite of its simplicity, it will be seen to illustrate conceptually and mechanically very clearly the process of extracting multi-parameter information from an A-D data set. To explore an experiment and linear inverse procedure like that illustrated in Fig. 1b, we relate the linear component of the perturbation operator (the first line of eqn. 14) to the measured data via the first line of eqn. (11), allowing the now unknown parameters α_1 and β_1 to vary in depth z only:

$$\begin{aligned} D(z_g = 0|z_s = 0, k) &= \int_{-\infty}^{\infty} dz' G_0(0|z'; k) k^2 \left[\alpha_1(z') - 2F(k)\beta_1(z')\right] \psi_0(z'|0; k) \\ &= -\frac{1}{2} ik \int_{-\infty}^{\infty} dz' e^{i2kz'} \left[\alpha_1(z') - 2F(k)\beta_1(z')\right] \\ &= -\frac{i2k}{4} \left[\alpha_1(-2k) - 2F(k)\beta_1(-2k)\right], \end{aligned} \tag{15}$$

where we have impelled the data to be "spike-like" rather than "step-like" by using an incident plane wave, $\psi_0(z'|0; k) = \exp(ikz')$, rather than an incident Green's function. This is not a well-posed problem for two parameters with arbitrary spectra in the depth-wavenumber; however if we further impose a single interface (as in Fig. 1b) at depth z_1 on the problem, then these spectra and that of the resulting data have straightforward analytic forms:

$$\begin{aligned} D(k) &= -\frac{1}{4} \left[\alpha_1(-2k) - 2F(k)\beta_1(-2k)\right] \\ R(k)e^{i2kz_1} &= -\frac{i2k}{4} \left[\alpha_1 \frac{e^{i2kz_1}}{i2k} - 2F(k)\beta_1 \frac{e^{i2kz_1}}{i2k}\right] \\ -4R(k) &= \alpha_1 - 2F(k)\beta_1. \end{aligned} \tag{16}$$

The problem, which now amounts to solving for two scalar quantities, the interface linear perturbation values for c and Q, is then well-posed and in principle requires only two input frequencies in the data, or measured reflection coefficient $R(k) = R(f)$. With two input frequencies two independent linear equations are produced, and the unknowns may be solved for as

$$\begin{aligned} \alpha_1(f_1, f_2) &= 4\frac{R(f_2)F(f_1) - R(f_1)F(f_2)}{F(f_1) - F(f_2)}, \\ \beta_1(f_1, f_2) &= 2\frac{R(f_2) - R(f_1)}{F(f_1) - F(f_2)}. \end{aligned} \tag{17}$$

This expression speaks to the manner in which a linear inverse scattering formalism demands that A-D wave field behavior be detectable in the data. Clearly the dispersion (that generates frequency-dependence in the reflection coefficient) is paramount. If the variability of the reflection coefficient from frequency to frequency is not detectable in the data, the linear Q perturbation parameter β_1 will be zero. (Furthermore, the linear c perturbation parameter will lapse to $4R$, which is the expected linear inverse result for the single parameter wavespeed problem at normal incidence.) Although it is a simple, and perhaps none-to-striking result, the form expressed in equation (17) will recur in all forthcoming instances of A-D inversion and processing, both as the experiment/medium become more complicated, and as we move from linear to non-linear processing.

2.2 For a line source over a layered medium

In the previous section, an ill-posedness in the two-parameter normal incidence problem was overcome by assuming a single interface medium structure and analytic form for the data. Ideally the problem should be cast such that an arbitrary profile of both $\beta_1(z)$ and $\alpha_1(z)$ is obtainable. This turns out to be possible in a pre-stack milieu. The linear relationship for the two parameter, depth varying problem with source and receiver depths fixed at $z = 0$ is

$$\begin{aligned} D(x_g|k_s;k) &= \int_{-\infty}^{\infty} dz' \int_{-\infty}^{\infty} dx' G_0(x_g,0|x,'z';k) k^2 \left[\alpha_1(z') - 2F(k)\beta_1(z')\right] G_0(x',z'|k_s,0;k) \\ &= \int_{-\infty}^{\infty} dz' \int_{-\infty}^{\infty} dx' \left[\frac{1}{2\pi}\int_{-\infty}^{\infty} dk' e^{ik'(x_g-x')} \frac{e^{iq'z'}}{i2q'}\right] k^2 \left[\alpha_1(z') - 2F(k)\beta_1(z')\right] \left[e^{ik_s x'} \frac{e^{iq_s z'}}{i2q_s}\right] \\ &= \frac{k^2}{2\pi(i2q_s)} \int_{-\infty}^{\infty} dz' \int_{-\infty}^{\infty} dk' \frac{e^{i(q'+q_s)z'}}{i2q'} e^{ik'x_g} \left[\alpha_1(z') - 2F(k)\beta_1(z')\right] \delta(k_s - k') \\ &= -\frac{e^{ik_s x_g}}{4\cos^2\theta} \int_{-\infty}^{\infty} dz' e^{i2q_s z'} \left[\alpha_1(z') - 2F(k)\beta_1(z')\right]. \end{aligned} \tag{18}$$

The angle of the incident plane wave (θ) arises, in the last line, from the plane wave geometry illustrated in Fig. 1a. The depth integral in equation (18) is a Fourier transform, leading to an equation relating the temporal frequency components of the data to the spatial frequency components of the linear part of the model; the model reconstruction proceeds as such. To see specifically how the presence of offset, or multiple incidence angles θ, renders the two-parameter problem well-posed, we carry out the Fourier transform, and replace (i) the k dependence in the A-D function $F(k)$, and (ii) the k_s, k dependence of the data, by again looking to the plane wave geometry of Fig. 1a. We then have

$$D(x_g|q_s;\theta) = -\frac{e^{ik_s x_g}}{4\cos^2\theta} \left[\alpha_1(-2q_s) - 2F(\theta,q_s)\beta_1(-2q_s)\right]. \tag{19}$$

The situation has reverted to something similar to the 1D normal incidence single interface problem in eqn. (15), in other words for any member q_s of the model spectra we may solve for $\alpha_1(-2q_s)$

and $\beta_1(-2q_s)$ given the data at at least two angles of incidence θ_1 and θ_2. From

$$\begin{aligned} D(x_g|q_s;\theta_1) &= -\frac{e^{ik_s x_g}}{4\cos^2\theta_1}\left[\alpha_1(-2q_s) - 2F(\theta_1,q_s)\beta_1(-2q_s)\right], \\ D(x_g|q_s;\theta_2) &= -\frac{e^{ik_s x_g}}{4\cos^2\theta_2}\left[\alpha_1(-2q_s) - 2F(\theta_2,q_s)\beta_1(-2q_s)\right], \end{aligned} \tag{20}$$

we may solve for the two linear components as

$$\begin{aligned} \alpha_1(-2q_s;\theta_1,\theta_2) &= 4e^{-ik_s x_g}\frac{D(x_g|q_s;\theta_2)\cos^2\theta_2 F(\theta_1,q_s) - D(x_g|q_s;\theta_1)\cos^2\theta_1 F(\theta_2,q_s)}{F(\theta_1,q_s) - F(\theta_2,q_s)} \\ \beta_1(-2q_s;\theta_1,\theta_2) &= 2e^{-ik_s x_g}\frac{D(x_g|q_s;\theta_2)\cos^2\theta_2 - D(x_g|q_s;\theta_1)\cos^2\theta_1}{F(\theta_1,q_s) - F(\theta_2,q_s)}. \end{aligned} \tag{21}$$

Notice that the form is in essence the same as that of the simpler problem. With regard to the Q perturbation β_1, the data is corrected, by $\cos^2\theta$, for its expected acoustic angle dependence, and the difference is taken at the two angles. If a difference still exists after this correction, that difference is attributed to dispersion and used to estimate β_1. If there is no difference, (1) β_1 will clearly be zero, and (2) the factors F in the α_1 expression will cancel such that it lapses to its expected single-parameter acoustic value.

This form, which is sufficiently general (in comparison with that of section 2.1) to be considered an inverse algorithm, has strengths and weaknesses. Like other linear multi-dimensional methods (Clayton and Stolt, 1981; Raz, 1981) it generalizes to multiple dimensions in short order, given multiple receiver gathers. Furthermore, given more than two angles of incidence the problem is over-determined, allowing a weighted estimation of the two parameters to take place, via, for instance, a least-squares scheme. However, it is well established that the error in this linear inverse method is increased for reflectors embedded in perturbed regions of the medium, that is, where the difference between the reference and actual medium above the structure of interest is large. This error (attributable to the cumulative transmission coefficient down to the structure of interest) is strongly aggravated in an A-D medium, in which attenuation and dispersion joins transmission in decaying amplitudes. In the next section the development of methods to overcome some of these issues is addressed.

3 Non-linear processing of primaries over a multiparameter medium

Innanen and Weglein (2004) report on encouraging synthetic results being obtained with the linear inverse for a single interface overlain by the reference medium – that is, provided the overburden is known, the linear inverse produces results that are more than acceptable. However, for a medium in which recorded events have propagated through unknown A-D structures, i.e., those that are not included in the reference medium, and hence are distorted and smoothed, linear results are highly degraded. The usual choice is at hand: spend more effort to characterize the medium structure and include it in the reference medium, or face the non-linearity of the current problem. Since we are motivated to create methods that act in the absence of detailed, or in any case adequate, prior knowledge of the medium structure, we proceed in the latter vein.

To do this we will express the higher-order terms similarly to the first order term as in the previous section, but retain only those terms and term components that are adjudged to be concerned with the processing and inversion of primaries. These terms have been derived and discussed as such in several of the previously-referenced papers on imaging and inversion with the inverse scattering series by Weglein et al. (2002), Weglein et al. (2003), Shaw et al. (2004), Liu et al. (2005), as well as in several theses (Innanen, 2003; Shaw, 2005). Innanen (2005) discusses the symmetry of a forward/inverse scattering subseries pair, the former of which is argued and demonstrated to accurately approximate primaries in high-contrast and high-variability 1.5D media given a homogeneous acoustic reference; the symmetry suggests further that these types of series term work to process primaries under conditions of highly-simplified reference media. In the remainder of this paper we proceed on the assumption that certain identifiable and straightforwardly expressible inverse scattering series term behave as such.

3.1 A series expression for processing primaries over a c/Q medium

The formalism of eqns. (11) translate to explicit forms for second and higher order in much the same way as occurs in the linear term. Let us begin by considering the second order relationship:

$$\mathbf{G_0 V_2 G_0} = -\mathbf{G_0 V_1 G_0 V_1 G_0}. \tag{22}$$

Making use of the forms for the Green's operators and perturbation operator components defined in the first section, the LHS of this second-order relation behaves in exactly the same way as the RHS of the linear expression does, to wit:

$$\text{LHS}_2 = -\frac{e^{ik_s x_g}}{4\cos^2\theta}\int_{-\infty}^{\infty} dz' e^{i2q_s z'}\left[\alpha_2(z') - 2F(\theta,q_s)\beta_2(z')\right]. \tag{23}$$

The RHS begins to show evidence of the increasing levels of complexity of the high orders:

$$\begin{aligned}\text{RHS}_2 = &-\int_{-\infty}^{\infty} dx' \int_{-\infty}^{\infty} dz' G_0(x_g|x',z';k)k^2\left[\alpha_1(z') - 2F(\theta,q_s)\beta_1(z')\right] \\ &\times \int_{-\infty}^{\infty} dx'' \int_{-\infty}^{\infty} dz'' G_0(x',z'|x'',z'';k)k^2\left[\alpha_1(z'') - 2F(\theta,q_s)\beta_1(z'')\right] G_0(x'',z''|k_s;k).\end{aligned} \tag{24}$$

Making substitutions of the Green's functions given in the first section, simplifications arise due to the lack of dependence of the perturbations on the lateral coordinate, resulting in

$$\begin{aligned}\text{RHS}_2 = &-\frac{e^{ik_s x_g}}{16\cos^4\theta}\int_{-\infty}^{\infty} dz'(i2q_s)e^{iq_s z'}\left[\alpha_1(z') - 2F(\theta,q_s)\beta_1(z')\right] \\ &\times \int_{-\infty}^{\infty} dz'' e^{iq_s|z'-z''|}\left[\alpha_1(z'') - 2F(\theta,q_s)\beta_1(z'')\right] e^{iq_s z''},\end{aligned} \tag{25}$$

or

$$\text{RHS}_2 = -\frac{e^{ik_s x_g}}{8\cos^4\theta}\int_{-\infty}^{\infty} dz' e^{i2q_s z'}\left\{(i2q_s)\left[\alpha_1(z') - 2F(\theta,q_s)\beta_1(z')\right]\int_0^{z'} dz''\left[\alpha_1(z'') - 2F(\theta,q_s)\beta_1(z'')\right]\right\}. \tag{26}$$

This second-order relationship, like the first-order relationship, works only on primaries, since it takes at least three scattering interactions to begin to process (or create, in the forward scattering series) multiples (e.g., Matson, 1996; Weglein et al., 2003). At third-order and higher, it is necessary in developing primary-processing methods to invoke the strategy of task-separation, and identify and isolate terms that, to an acceptable level of approximation, work to process primaries as if multiples were absent. Indeed, it will therefore be necessary as a preliminary processing step to attenuate multiples from the data to be treated by here-generated algorithms.

To collect and use only such primary-processing terms, we find it convenient in this particular two-parameter case to follow the development of the single-parameter processing equations of Innanen (2003), Innanen and Weglein (2003) and Innanen (2005). (This is as opposed to the single-parameter Q processing results described by Innanen and Weglein (2005), in which it was convenient to follow the task-separated imaging equations of Weglein et al. (2002), Shaw et al. (2004), and Shaw (2005).) Doing so results in a relationship between the inverse scattering series equations' LHS and RHS at $(n+1)$'th order, in which the RHS retains only the portion of the full inverse scattering series terms that are deemed to process primaries:

$$\text{LHS}_{n+1} = -\frac{e^{ik_s x_g}}{4\cos^2\theta}\int_{-\infty}^{\infty} dz' e^{i2q_s z'}\left[\alpha_{n+1}(z') - 2F(\theta,q_s)\beta_{n+1}(z')\right], \tag{27}$$

and

$$\begin{aligned}\text{RHS}_{n+1} = &-\frac{e^{ik_s x_g}}{(-2)^n n!\cos^{2n}\theta} \\ &\times \int_{-\infty}^{\infty} dz' e^{i2q_s z'}\left\{(i2q_s)^n\left[\alpha_1(z') - 2F(\theta,q_s)\beta_1(z')\right]\left(\int_0^{z'} dz''\left[\alpha_1(z'') - 2F(\theta,q_s)\beta_1(z'')\right]\right)^n\right\}.\end{aligned} \tag{28}$$

Equations (27) and (28) may be summed and equated, i.e.,

$$\sum_{n=0}^{\infty}\text{LHS}_{n+1} = \sum_{n=0}^{\infty}\text{RHS}_{n+1}, \tag{29}$$

or, explicitly,

$$\begin{aligned}&\sum_{n=0}^{\infty}\int_{-\infty}^{\infty} dz' e^{i2q_s z'}\left[\alpha_{n+1}(z') - 2F(\theta,q_s)\beta_{n+1}(z')\right] \\ =&\sum_{n=0}^{\infty}\frac{(-1/2)^n}{n!\cos^{2n}\theta}\int_{-\infty}^{\infty} dz' e^{i2q_s z'}\left\{(i2q_s)^n\left[\alpha_1(z') - 2F(\theta,q_s)\beta_1(z')\right]\left(\int_0^{z'} dz''\left[\alpha_1(z'') - 2F(\theta,q_s)\beta_1(z'')\right]\right)^n\right\},\end{aligned} \tag{30}$$

such that, defining the summed portions of the LHS to be

$$\alpha_P \equiv \sum_{n=0}^{\infty}\alpha_{n+1}, \quad \text{and} \quad \beta_P \equiv \sum_{n=0}^{\infty}\beta_{n+1},$$

portions of the model perturbations that are, in a specifically chosen way, non-linear in the data, we have:

$$\begin{aligned}&\int_{-\infty}^{\infty} dz' e^{i2q_s z'} \left[\alpha_P(z') - 2F(\theta, q_s)\beta_P(z')\right] \\ &= \sum_{n=0}^{\infty} \frac{(-1/2)^n}{n! \cos^{2n}\theta} \int_{-\infty}^{\infty} dz' e^{i2q_s z'} \left\{ (i2q_s)^n \left[\alpha_1(z') - 2F(\theta, q_s)\beta_1(z')\right] \left(\int_0^{z'} dz'' \left[\alpha_1(z'') - 2F(\theta, q_s)\beta_1(z'')\right] \right)^n \right\}.\end{aligned} \tag{31}$$

Two incidence angles, and two versions of eqn. (31) that involve α_1 and β_1 *constructed from data at those incidence angles*, can again lead to a well-posed set of expressions for the high order quantities α_P and β_P, which are by assumption accurate approximations of the actual perturbations α and β even for a homogeneous and inaccurate reference medium. We defer this activity to the next section, in which a more compact and simply computable form of the RHS is devised. However, since this computable and elegant form is the only part of this development that entirely relies on the assumption of a layered medium, we hardly advocate ignoring series forms similar to equation (31). At present it seems likely that they will, by necessity, be used in an extension to fully 2D and 3D frameworks.

3.2 A closed-form expression for processing primaries over a c/Q medium

We have utilized the same patterns in the inverse scattering series that have elsewhere been determined to approximately solve the full imaging-inversion problem for primaries, now in a multi-parameter A-D milieu. In this section we use a simple argument to express that series in closed form, thus in a single computation produce the numerical/analytical effect of having summed a potentially large number of terms in equation (31). Starting at that equation, we have

$$\begin{aligned}&\int_{-\infty}^{\infty} dz' e^{i2q_s z'} \left[\alpha_P(z') - 2F(\theta, q_s)\beta_P(z')\right] \\ &= \int_{-\infty}^{\infty} dz' e^{i2q_s z'} \sum_{n=0}^{\infty} \frac{1}{n!} \left\{ \frac{(-1/2)}{\cos^2\theta} (i2q_s) \int_0^{z'} dz'' \left[\alpha_1(z'') - 2F(\theta, q_s)\beta_1(z'')\right] \right\}^n \left[\alpha_1(z') - 2F(\theta, q_s)\beta_1(z')\right] \\ &= \int_{-\infty}^{\infty} dz' e^{-i2q_s \left\{ z' + \frac{1}{2cos^2\theta} \int_0^{z'} dz'' [\alpha_1(z'') - 2F(\theta, q_s)\beta_1(z'')] \right\}} \left[\alpha_1(z') - 2F(\theta, q_s)\beta_1(z')\right].\end{aligned} \tag{32}$$

Let us render this closed form more compact by defining:

$$\Delta(q_s, \theta) \equiv \int_{-\infty}^{\infty} dz' e^{-i2q_s \left\{ z' + \frac{1}{2cos^2\theta} \int_0^{z'} dz'' [\alpha_1(z'') - 2F(\theta, q_s)\beta_1(z'')] \right\}} \left[\alpha_1(z') - 2F(\theta, q_s)\beta_1(z')\right]. \tag{33}$$

Now, performing the Fourier transform on the left-hand side, and utilizing equation (33), equation (32) can be expressed twice, once for each of two input incident angles θ_1 and θ_2:

$$\begin{aligned}\alpha_P(-2q_s) - 2F(\theta_1, q_s)\beta_P(-2q_s) &= \Delta(q_s, \theta_1) \\ \alpha_P(-2q_s) - 2F(\theta_2, q_s)\beta_P(-2q_s) &= \Delta(q_s, \theta_2),\end{aligned} \tag{34}$$

in which case a solution exists for these non-linear processed quantities that is remarkably similar to both the prestack and normal-incidence linear solutions:

$$\begin{aligned}\alpha_P(-2q_s;\theta_1,\theta_2) &= \frac{\Delta(q_s,\theta_1)F(\theta_2,q_s)-\Delta(q_s,\theta_2)F(\theta_1,q_s)}{F(\theta_1,q_s)-F(\theta_2,q_s)}\\ \beta_P(-2q_s;\theta_1,\theta_2) &= \frac{1}{2}\frac{\Delta(q_s,\theta_1)-\Delta(q_s,\theta_2)}{F(\theta_1,q_s)-F(\theta_2,q_s)}.\end{aligned} \tag{35}$$

Eqns. (33) and (49) form the basis for the herein-presented theory for non-linear processing of primaries above an unknown and undetermined layered c/Q medium. Comparing equation (49) to equations (21) and (17) it is clear that, again, in a two parameter A-D system, if solved-for in angle-pairs, exactly the same form of data-interrogation appears. The variability of the quantity $\Delta(q_s,\theta)$ is measured, through differencing over angle, to estimate β_P; if there is no angle dependence of this quantity the Q perturbation construction is zero, i.e., the same interrogation technique used in the linear two-parameter case, now with the quantity Δ (which is a non-linear quantity that works to take account for transmission through the unknown A-D overburden) in place of the raw data.

4 Task-separation I: absorption-dispersion compensation without a Q-estimate

Eqns. (33) and (49) are the basis for non-linear estimation of the actual c/Q medium in terms of only a reflected data set over a layered medium, and a homogeneous reference wavespeed model (characterized by c_0) that the actual Earth necessarily obeys only at and above the source and receiver. This is at the outset already a task-separated processing regimen, in the sense of Weglein et al. (2003), in that only primaries and not multiples are meant to be processed with it; however, within these relationships lies an opportunity for much more focused task-separation. We explore that opportunity in this section.

A convenience of form in the key quantity of these equations, which we have referred to as $\Delta(q_s,\theta)$, allows both (1) the activity of the non-linear operations and (2) the part of the data/linear models that are operated upon, to be isolated from one another. Let us take a closer look at $\Delta(q_s,\theta)$, and make several new definitions. Writing the original $\Delta(q_s,\theta)$ as

$$\Delta(q_s,\theta)=\int_{-\infty}^{\infty}dz'e^{-i2q_s\left[z'+Z^{\alpha}(\theta,z')+Z^{\beta}(q_s,\theta,z')\right]}\left[\alpha_1(z')-2F(\theta,q_s)\beta_1(z')\right], \tag{36}$$

we consider the two variants

$$\begin{aligned}\Delta^{(\alpha)}(q_s,\theta)&\equiv\int_{-\infty}^{\infty}dz'e^{-i2q_s[z'+Z^{\alpha}(\theta,z')]}\left[\alpha_1(z')-2F(\theta,q_s)\beta_1(z')\right],\\ \Delta^{(\beta)}(q_s,\theta)&\equiv\int_{-\infty}^{\infty}dz'e^{-i2q_s\left[z'+Z^{\beta}(q_s,\theta,z')\right]}\left[\alpha_1(z')-2F(\theta,q_s)\beta_1(z')\right],\end{aligned} \tag{37}$$

where

$$\begin{aligned}Z^{\alpha}(\theta,z')&\equiv-\frac{1}{2\cos^2\theta}\int_0^{z'}\alpha_1(z'')dz'',\\ Z^{\beta}(q_s,\theta,z')&\equiv\frac{F(q_s,\theta)}{\cos^2\theta}\int_0^{z'}\beta_1(z'')dz''.\end{aligned} \tag{38}$$

The definitions are relatively straightforward: the terms in the argument of the exponential are in dimensions of depth but are sensitive to size and duration of the linear estimates α_1 and β_1 down to the output point of the integration variable z', as well as the current angle of incidence and reference depth wavenumber. This simply emphasizes the fact that the portion of the operator embodied in $\Delta(q_s, \theta)$, i.e., the Fourier-like transform being enacted upon α_1 and β_1, is clearly concerned with the impact of β_1 on the data, and the other is clearly concerned with the impact of α_1 on the data. Since in the absence of an A-D element in the data (in which case $\beta_1 = 0$) these equations reduce to the single-parameter acoustic case involving α_1, α_P and α, it is reasonable to ascribe to the Z^α component of the operator the "task" of undoing the effects of sustained perturbations on the P-wave velocity of the medium. It follows then that we ascribe to the Z^β component of the operator the task of undoing the effects of sustained perturbations on the attenuation parameter of the medium – Q processing. The similarity of this operator to that studied in isolation by Innanen and Weglein (2005) is testament to this assumption if that is needed. Hence to carry out one of these joint tasks of c/Q processing and not the other is to set one or other of these operator components to unity, or depth-like quantities to zero. This is the meaning of the variant quantities in equation (37).

The sum total of the non-linear activity of the data in these inversion equations (which represent a portion of the full inversion capability of the inverse scattering series) is to generate the operators described above. Hence, to set the operator component associated with one of the parameters to zero is to negate the accumulated non-linearity of the series in that parameter – to process linearly in that parameter. Doing so, furthermore, clearly means that we may either (1) form an accurate depth image without knowing or determining the actual velocity model of the medium and leave all attenuation aspects intact and unchanged, or (2) perform Q compensation without knowing or determining the actual Q model of the medium and leave all reflector locations at their linear depths and amplitudes. Mapping this latter quantity back (trivially) to data space with the reference Green's functions will create a data set corresponding to the changes in P-wave velocity and contain no imprint of Q – a processing regimen with a strong flavor of Q-compensation.

Remaining selectively linear in one or more parameters in a multiparameter non-linear direct problem, in other words, makes available far more focused opportunities for task-separation.

The spectrum of the linearly-imaged, Q-compensated wavespeed perturbation, which we will call $\alpha_Q(z)$, is computed using a variant of the full processing equations (33) and (49), namely:

$$\alpha_Q(-2q_s; \theta_1, \theta_2) = \frac{\Delta^{(\beta)}(q_s, \theta_1)F(\theta_2, q_s) - \Delta^{(\beta)}(q_s, \theta_2)F(\theta_1, q_s)}{F(\theta_1, q_s) - F(\theta_2, q_s)} \tag{39}$$

for two input angles of incidence, at which point linear single parameter acoustic data equations may be used with this output to estimate the associated data set. Put into a single algorithm, the Q compensated data set $D^{\text{A-D}}$, in terms of the linear parameters α_1 and β_1 computed at two incidence angles, is

$$\begin{aligned} D^{\text{A-D}}(x_g, q_s, \theta; \theta_1, \theta_2) &= -\frac{e^{ik_s x_g}}{4\cos^2\theta}\alpha_Q(-2q_s; \theta_1, \theta_2) \\ &= -\frac{e^{ik_s x_g}}{4\cos^2\theta}\frac{\Delta^{(\beta)}(q_s, \theta_1)F(\theta_2, q_s) - \Delta^{(\beta)}(q_s, \theta_2)F(\theta_1, q_s)}{F(\theta_1, q_s) - F(\theta_2, q_s)}, \end{aligned} \tag{40}$$

where

$$\begin{aligned}
\Delta^{(\beta)}(q_s,\theta) &= \int_{-\infty}^{\infty} dz' e^{-i2q_s\left[z'+Z^{\beta}(q_s,\theta,z')\right]}\left[\alpha_1(z') - 2F(\theta,q_s)\beta_1(z')\right], \\
Z^{\beta}(q_s,\theta,z) &= \frac{F(q_s,\theta)}{\cos^2\theta}\int_0^z \beta_1(z')dz', \\
F(\theta,q_s) &= \frac{i}{2} - \frac{1}{\pi}\ln\left(\frac{q_s}{k_0\cos\theta}\right).
\end{aligned} \tag{41}$$

4.1 Non-linear correction of dispersion

A potentially valuable separability of the non-linear inversion tasks associated with primaries above an A-D medium is available and visible in equations (40) and (41). The additive nature of the linear and full perturbations is such that either the Q-based operator or the c-based operator (those acting to correct attenuation and mis-location issues respectively) may be individually enacted upon either the Q-based input or the c-based input (i.e., β_1 or α_1 respectively). In equations (40) and (41) that separability is used to propose a means to compute an equivalent un-attenuated data set; here we find that, due to the – again – additive nature of the problem, a further task separability is available, similar to one that is often accomplished in standard Q-based processing.

The operator

$$e^{-i2q_s\left[z'+Z^{\beta}(q_s,\theta,z')\right]} \tag{42}$$

gains the wherewithal to both correct absorptive and dispersive effects through the appearance in $Z^{\beta}(q_s,\theta,z')$ of the Q model-type function

$$F(\theta,q_s) = \frac{i}{2} - \frac{1}{\pi}\ln\left(\frac{q_s}{k_0\cos\theta}\right). \tag{43}$$

This function renders and separates the production of absorptive and dispersive effects; suppressing $i/2$ for instance would leave a function that concerned itself solely with dispersion effects:

$$F_D(\theta,q_s) = -\frac{1}{\pi}\ln\left(\frac{q_s}{k_0\cos\theta}\right). \tag{44}$$

In the presence of noisy data often the removal of the dispersion is the only level of Q compensation attempted; in quarters of the geophysical community this is considered to be in any case the Q problem of importance, there being other means to "compensate for high-frequency loss" of late-arriving signals (Hargreaves and Calvert, 1991). Forming an operator based on F_D of the form

$$e^{-i2q_s\left[z'+Z_D^{\beta}(q_s,\theta,z')\right]}, \tag{45}$$

where

$$Z_D^{\beta}(q_s,\theta,z) = \frac{F_D(q_s,\theta)}{\cos^2\theta}\int_0^z \beta_1(z')dz', \tag{46}$$

we may re-form the equations of the full A-D problem to administer only to the dispersive component:

$$D^{\mathrm{D}}(x_g,q_s,\theta;\theta_1,\theta_2) = -\frac{e^{ik_s x_g}}{4\cos^2\theta}\frac{\Delta_D^{(\beta)}(q_s,\theta_1)F(\theta_2,q_s) - \Delta_D^{(\beta)}(q_s,\theta_2)F(\theta_1,q_s)}{F(\theta_1,q_s) - F(\theta_2,q_s)}, \tag{47}$$

where

$$\begin{aligned}
\Delta_D^{(\beta)}(q_s,\theta) &= \int_{-\infty}^{\infty} dz' e^{-i2q_s\left[z'+Z_D^{\beta}(q_s,\theta,z')\right]}\left[\alpha_1(z') - 2F(\theta,q_s)\beta_1(z')\right], \\
Z_D^{\beta}(q_s,\theta,z) &= \frac{F_D(q_s,\theta)}{\cos^2\theta}\int_0^z \beta_1(z')dz', \\
F(\theta,q_s) &= \frac{i}{2} - \frac{1}{\pi}\ln\left(\frac{q_s}{k_0\cos\theta}\right), \\
F_D(\theta,q_s) &= -\frac{1}{\pi}\ln\left(\frac{q_s}{k_0\cos\theta}\right).
\end{aligned} \tag{48}$$

Notice that the model-type function F is only changed to F_D when it appears in the operator. As a weight "explaining" the angle/frequency dependence of reflection coefficients, it is left in its original fully complex and frequency-dependent form.

5 Task-separation II: acoustic velocity processing with visco-acoustic data

The approach used in the previous section, in which a deliberate choice was made to "process" the data non-linearly in one parameter (Q) and linearly in the other (c), left us with the ability in principle to estimate an equivalent non-attenuated data set. The data set is, by definition, that which is linear in α_1 alone. The practical upshot is a Q-compensation scheme. In this section we mention (briefly) that the mirror image of this process, in which we choose to process the data non-linearly in the wavespeed parameter, could also be of interest.

We take as our basic equations

$$\begin{aligned}
\alpha_{\mathrm{Ac}}(-2q_s;\theta_1,\theta_2) &= \frac{\Delta^{(\alpha)}(q_s,\theta_1)F(\theta_2,q_s) - \Delta^{(\alpha)}(q_s,\theta_2)F(\theta_1,q_s)}{F(\theta_1,q_s) - F(\theta_2,q_s)} \\
\beta_{\mathrm{Ac}}(-2q_s;\theta_1,\theta_2) &= \frac{1}{2}\frac{\Delta^{(\alpha)}(q_s,\theta_1) - \Delta^{(\alpha)}(q_s,\theta_2)}{F(\theta_1,q_s) - F(\theta_2,q_s)}.
\end{aligned} \tag{49}$$

which differ from those of eqn. (49) in their use of the $\Delta^{(\alpha)}$ defined in eqn. (37). The point is that both parameters – in particular the velocity parameter α has been processed non-linearly in velocity only. In other words the non-linear problem of location has been dealt with, but the non-linear problem of attenuation has not. And, as a result, no ill-conditioned problem has been attempted.

This instance of the multiparameter task-separated idea, in other words, permits attenuation to be accounted-for but not used. It is worth contrasting this with a problem in which the same data (let us assume a data set that has non-negligible A-D effects in the phase and amplitude of the events) is being processed *assuming they are due to velocity contrasts only.* The latter incorrectly explains amplitude and phase as wavespeed alterations and mislocates reflectors*. In this case we do not process the Q aspects of the data non-linearly, but we correctly incorporate them, such that the now well-posed velocity processing regimen can move forward.

*A simple "reductio" argument will serve to explain. We could imagine a medium consisting of only Q contrasts, so that the reflected data (i.e., in which Q-contrasts alone produce reflections, a la Kjartansson (1979)) is correctly

6 Towards numerical examples: a layered viscoacoustic model of primaries

At present we are working towards a suite of numerical examples to illustrate the behaviour of these multi-parameter task-separated processing strategies. To create synthetic data suitable for testing of this theory and algorithm, we consider a stratified medium involving layers of constant wavespeed and Q. The data may therefore be expressed analytically in the frequency domain, and numerically transformed into the space-time domain. Figures 2–6 illustrate.

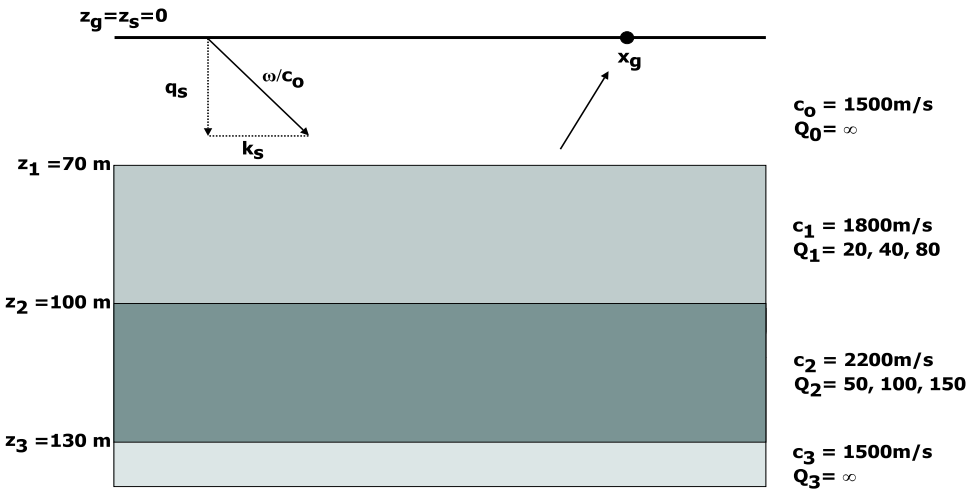

Figure 2: *A layered 2-parameter viscoacoustic medium model.*

7 Conclusions

The issue of resolution of seismic images is impacted by a potentially large set of phenomena which act on a pulse during its propagation history in the unknown medium, referred to collectively as "attenuation". Included within this blanket category are the so-called "intrinsic attenuation" effects, those which can be modelled to some adequate level with a viscoelastic continuum model. A matter of ongoing interest are the obstacles faced by, and opportunities afforded to, direct non-linear primary processing algorithms when the recorded data contain a non-negligible degree of such attenuation.

The most recent previous discussions on the subject (Innanen and Weglein, 2005) have discerned (1) an imaging-analogous set of inverse scattering series terms whose purpose appears from analytic study to be geared towards reinstatement of attenuated high frequencies, and (2) the salutary effect of this subseries on a specially contrived attenuated synthetic data set.

The current effort has involved moving toward a theory that permits concurrent contrasts in two parameters, and has viewed this extension as an opportunity to explore further the changes to

imaged with the reference wavespeed. If we process this non-linearly using a single parameter acoustic imaging theory the reflectors will be moved, since within such a theory an event can only have arisen due to a deviation of wavespeed away from reference. The move can only be away from correct and toward incorrect. This is the cost of non-linear, model-type dependent processing with the incorrect model.

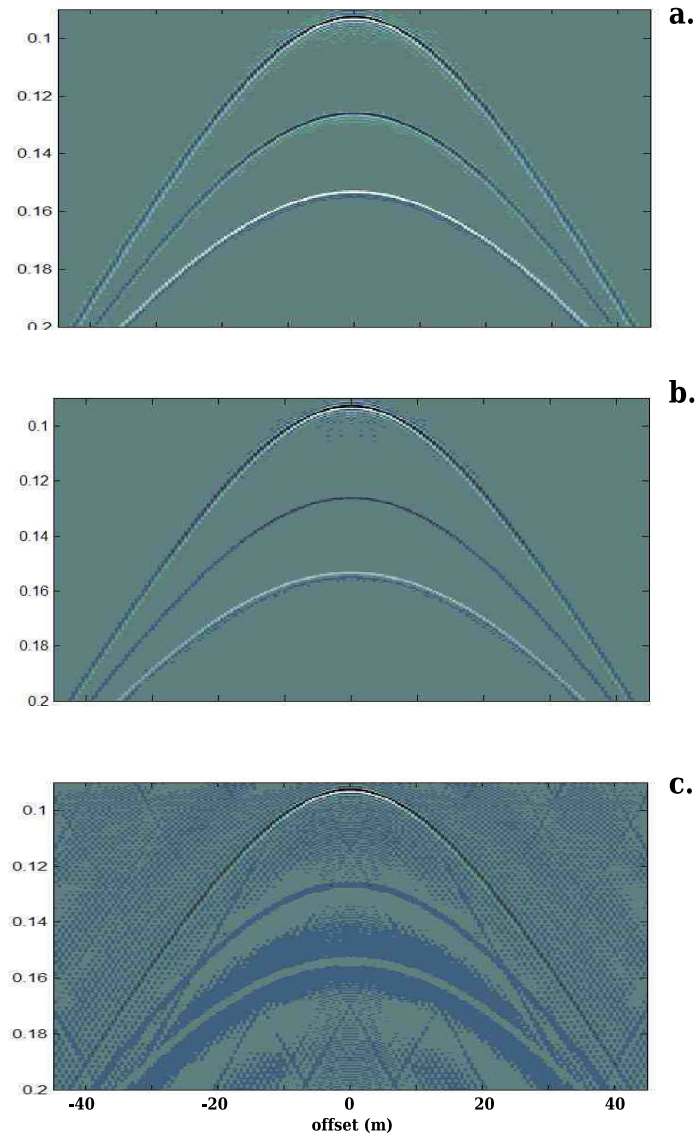

Figure 3: *Three primaries-only shot records created over the three interface model. Layer velocities are fixed and Q values are altered.*

a direct non-linear theory of processing that come about in the presence of a multi-parameter medium. The patterns that elsewhere (e.g., Innanen et al., 2004) have been used to generate direct coupled imaging-inversion equations for a single parameter medium are retained in this 2-parameter model, hence the closed-forms derivable in the former are available also in the latter for 1D media. These forms, furthermore, have led to a straightforward application of a multi-parameter strategy for task-separated processing, in which the data are processed non-linearly in a particular chosen parameter, and linearly in another (or others). Doing so permits, for instance, the estimation of an unattenuated data set from only non-linear operations on an attenuated data set, i.e., Q compensation without a determination of Q. Lastly, we still withhold the claim that we have produced an *algorithm*, as we are yet putting effort into creating numerical results to be

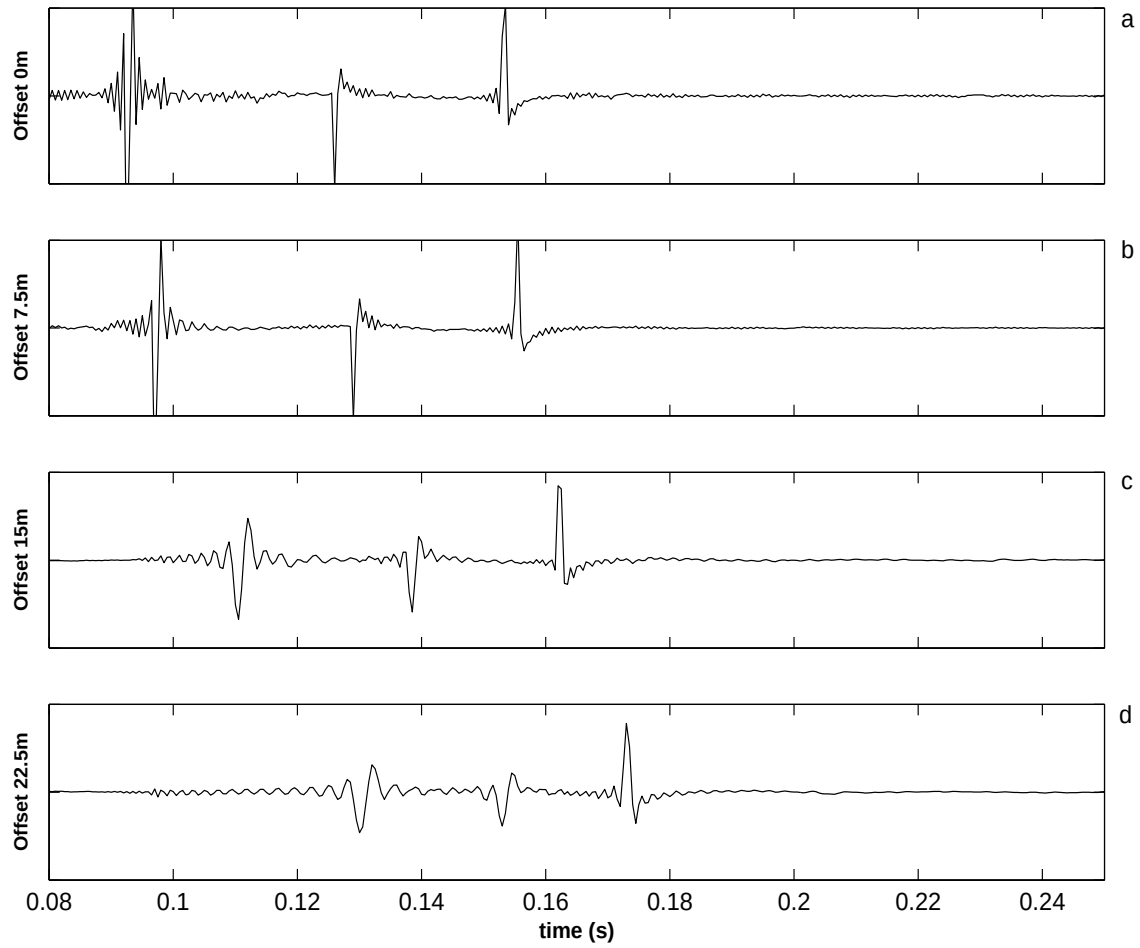

Figure 4: *Three trace detail of synthetic data over the 2-parameter viscoacoustic medium with large Q values.*

validated and analyzed, nevertheless results remain encouraging. The real question to be answered is: can we measure the variability needed to drive this theory in field data?

Acknowledgements

The authors are grateful for the support and help of the M-OSRP sponsors and personnel. We have been partially funded by and are grateful for NSF-CMG award DMS-0327778 and DOE Basic Sciences award DE-FG02-05ER15697.

References

Aki, K., and Richards, P., 2002: Quantitative Seismology, 2nd Ed. *University Science Books.*

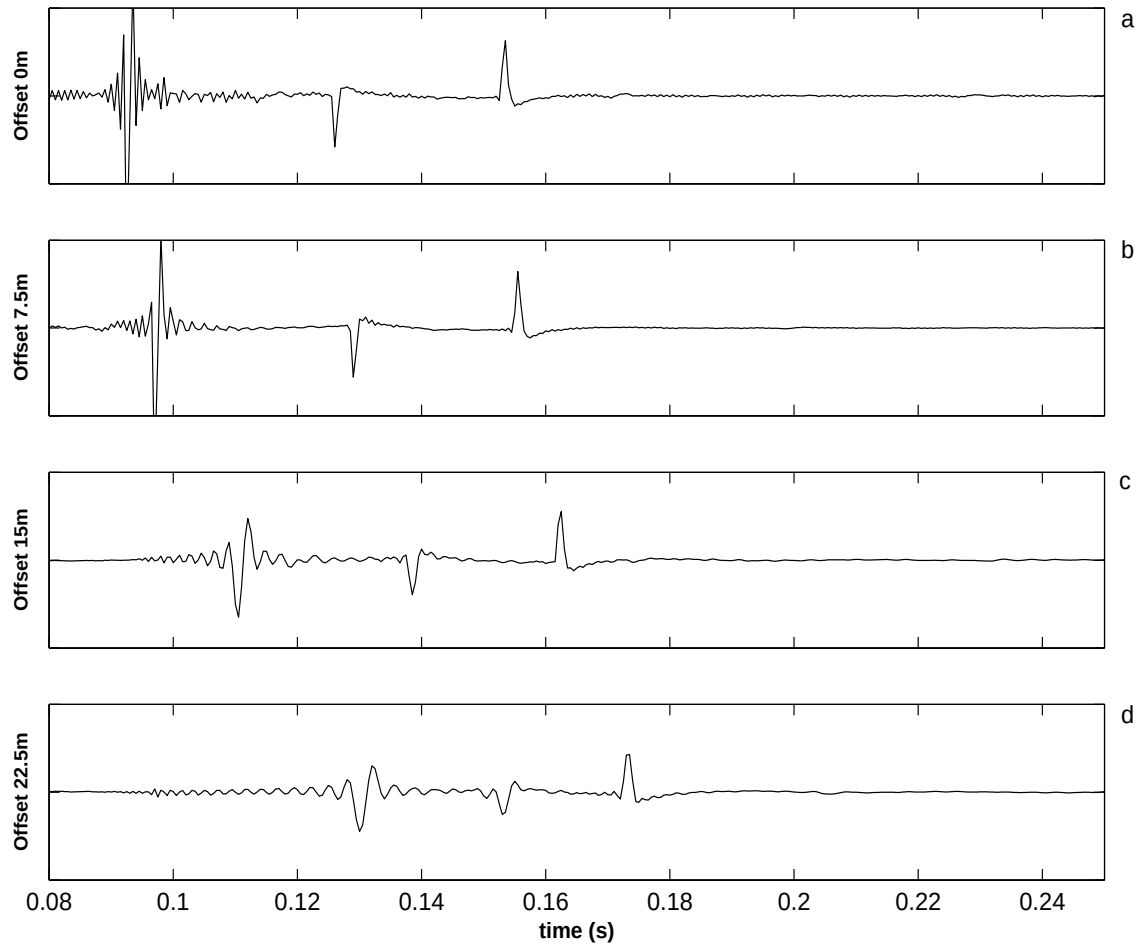

Figure 5: *Three trace detail of synthetic data over the 2-parameter viscoacoustic medium with mid-range Q values.*

Carrion, P. M. and VerWest, B., 1987: A procedure for inverting seismic data to obtain Q profiles. *Inverse Problems 3*, 65–71.

Clayton, R. and Stolt, R. H., A Born-WKBJ Inversion Method for Acoustic Reflection Data. *Geophysics*, **46** (1981).

Futterman, W. I., Dispersive body waves. *Journal of Geophysical Research*, **67** (1962).

Hargreaves, N. and Calvert, A. J., 1991, Inverse Q-filtering by Fourier transform. *Geophysics 56*, 519–527.

Innanen, K. A., Methods for the treatment of acoustic and absorptive/dispersive wave field measurements. Ph.D. Thesis, University of British Columbia, (2003).

Innanen, K. A. and A. B. Weglein, 2003, Construction of absorptive/dispersive wave fields with

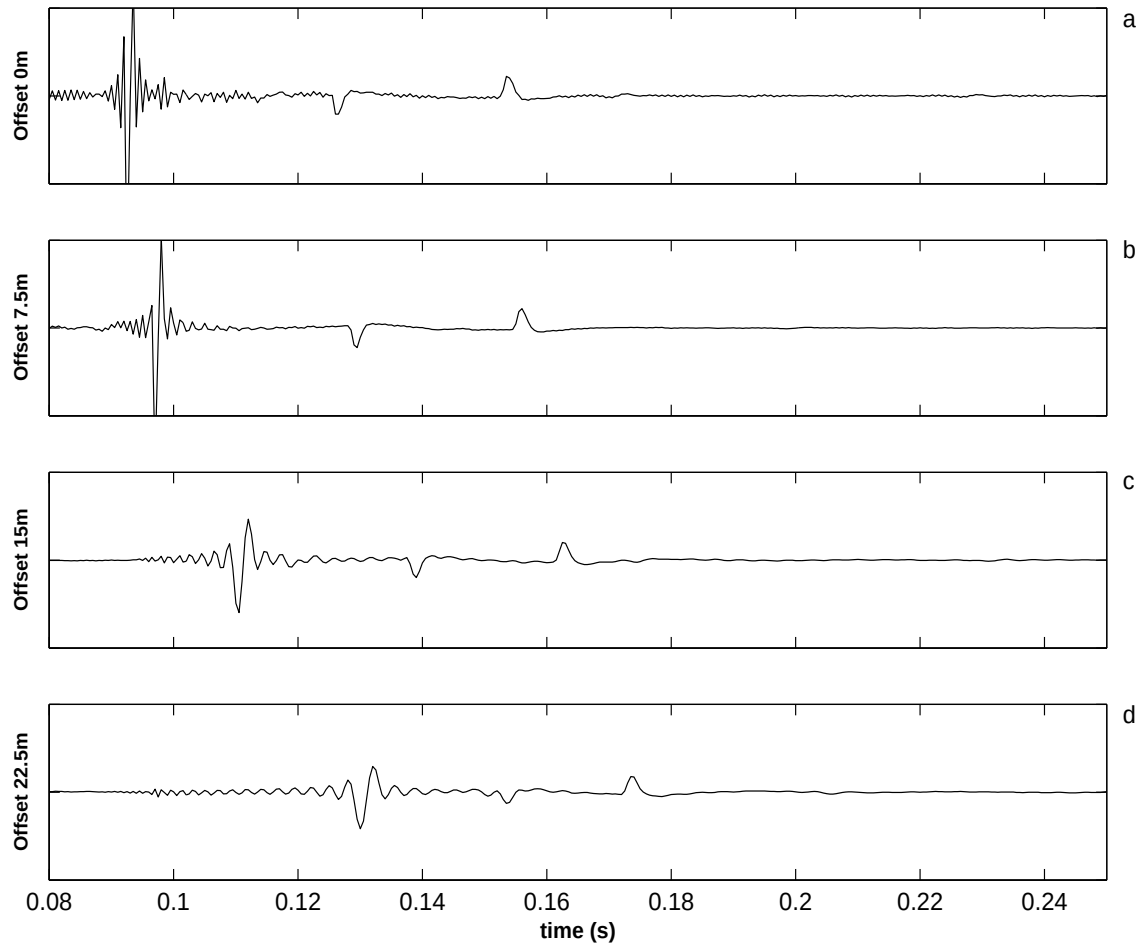

Figure 6: *Three trace detail of synthetic data over the 2-parameter viscoacoustic medium with small Q values.*

the forward scattering series: *Journal of Seismic Exploration*, **12** 259–282.

Innanen, K. A., Nita, B. G. and A. B. Weglein, 2004, Investigating the grouping of inverse scattering series terms: simultaneous imaging and inversion: *M-OSRP03 Annual Report.*

Innanen, K. A., 2004, Linear inversion for absorptive/dispersive medium parameters: *74th Ann. Internat. Mtg. Soc. Expl. Geophys.*

Innanen, K. A., 2005, Two non-linear forward and inverse approximations for wavefields in the presence of sustained medium perturbations: *75th Ann. Internat. Mtg. Soc. Expl. Geophys.*

Innanen, K. A., and Weglein, A. B. 2005, Towards non-linear construction of a Q-compensation operator directly from seismic reflection data: *75th Ann. Internat. Mtg. Soc. Expl. Geophys.*

Kjartansson, E., Constant-Q wave propagation and attenuation. *Journal of Geophysical Research*,

84 (1979).

Liu, F., Weglein, A. B., Innanen, K. A. and Nita, B. G., 2005, Extension of the non-linear imaging capability of the inverse scattering series to multidimensional media: strategies and numerical results: *Proceedings of the Ninth International Congress of the SBGf and Sixth Latin American Geophysical Conference, Salvador de Bahia, Brazil.*

Matson, K. H., 1996, The relationship between scattering theory and the primaries and multiples of seismic data: *Journal of Seismic Exploration*, **5** 63–78.

Nita, B. G., and Weglein, A. B., 2006, Pseudo-depth/intercept-time monotonicity requirements in the inverse scattering algorithm for predicting internal multiple reflections: *Submitted to Inverse Problems.*

Oldenburg, D. W., Scheuer, T., and Levy, S., 1983, Recovery of the acoustic impedance from reflection seismograms. *Geophysics 48*, 1318–1337.

Oldenburg, D. W., 1983, An introduction to linear inverse theory. *IEEE Transactions on geoscience and remote sensing GE-22*, 665–674.

Ramirez, A. C., and Weglein, A. B., 2005, An inverse scattering internal multiple elimination method: beyond attenuation, a new algorithm, and initial tests: *M-OSRP04 Annual Report.*

Raz, S., Direct reconstruction of velocity and density profiles from scattered field data. *Geophysics*, **46** (1981).

Shaw, S. A., Weglein, A. B., Foster, D. J., Matson, K. H., and Keys, R. G., 2004, Isolation of a leading order depth imaging series and analysis of its convergence properties for a 1D acoustic medium: *Journal of Seismic Exploration 13*, (2004): 99-120.

Shaw, S. A., 2005: An inverse scattering series algorithm for depth imaging of reflection data from a layered acoustic medium: Ph.D. Thesis, University of Houston.

Ulrych, T. J., 1989, Minimum relative entropy and inversion. *In: Geophysical Inversion, SIAM, J. B. Bednar, L. R. Lines, R. H. Stolt, A. B. Weglein eds.*, 158.

Walker, C., and Ulrych, T. J., 1984, On a modified algorithm for the autoreggressive recovery of the acoustic impedance. *Geophysics 48*, 2190–2192.

Weglein, A. B., F. A. Gasparotto, P. M. Carvalho, and R. H. Stolt, 1997, An inverse scattering series method for attenuating multiples in seismic reflection data: Geophysics, **46**, pp. 1975–1989.

Weglein, A. B., Foster, D. J., Matson, K. H., Shaw, S. A., Carvalho, P. M., and Corrigan, D., 2002, Predicting the correct spatial location of reflectors without knowing or determining the precise medium and wave velocity: initial concept, algorithm and analytic and numerical example: *Journal of Seismic Exploration*, **10**,.

Weglein, A. B., Araujo, F. A., Carvalho, P. M., Stolt, R. H., Matson, K. H., Coates, R., Corrigan, D., Foster, D. J., Shaw, S. A., and Zhang, H. 2003, Topical Review: Inverse-scattering Series and Seismic Exploration. *Inverse Problems 19*, R27–R83.

Wiggins, R. A. and Miller, S. P., 1972, New noise reduction techniques applied to long period oscillations of the Alaskan earthquake. *BSSA 62*, 417–479.

Zhang, H., and Weglein, A. B., 2005, The inverse scattering series for tasks associated with primaries: depth imaging and direct non-linear imaging of 1D variable velocity and density acoustic media: *75th Ann. Internat. Mtg. Soc. Expl. Geophys.*